C 55.2 :C61/2/978

PENNSYLVANIA STATE UNIVERSITY
MAY 14 1979
DOCUMENTS COLLECTION

Proceedings of the Third Annual Climate Diagnostics Workshop

Cooperative Institute for
Marine and Atmospheric Studies
University of Miami
Miami, Florida

October 31 - November 2, 1978

U.S. DEPARTMENT OF COMMERCE
National Oceanic and Atmospheric Administration

Digitized by the Internet Archive
in 2012 with funding from
LYRASIS Members and Sloan Foundation

http://archive.org/details/proceedingsofann00clim

Foreword

Dr. Edward S. Epstein
Director, National Climate Program Office
National Oceanic and Atmospheric Administration

The occasion of the Third Climate Diagnostics Workshop signaled as well the beginning of the National Climate Program under Public Law 95-367. The National Climate Program Act, signed into law on September 17, 1978, encourages development of national applications and services of climate information -- information derived from active research. These annual Workshops serve both research and services in this program. They are, first and foremost, intended to review the climate of the preceding year and examine particularly unusual recent climatic events. This review affords, too, an opportunity to examine diagnostic tools and techniques, to exchange current impressions on the mechanisms behind short-term climate variations, and to introduce more scientists and institutions to the study of climate.

Of perhaps particular interest to those who assembled in Miami and those who will find these Proceedings useful, 1978 also marked the establishment of the NOAA Climate Analysis Center in the National Weather Service; some of the concepts of tasks for this Center came from previous Workshops, and conversely, some Workshop concepts from early planning for the Center. The Climate Analysis Center should become a major bridge between research and services under the National Program. The CAC has been established to: maintain awareness of current climate and weather anomalies and fluctuations; produce climate projections and extended range outlooks; disseminate climate information to support applications, including impact assessments and research; and develop and test improved diagnostic and climate projection techniques and products.

Thus, these Workshops have provided those of us planning the National program with an idea of the limits of our abilities and what is needed to improve them. Views expressed by participants of previous Workshops have improved our plans and helped develop National Program concepts. As the National Climate Program continues to evolve, planners will draw upon these Workshops again for guidance, for information and for furthering cooperative looks at the global climate. I hope other participants will find these meetings even more advantageous, and that individual and collective research aims are advanced accordingly.

I wish to take this opportunity to thank Dr. Eric Kraus, Director of the Cooperative Institute for Marine and Atmospheric Sciences, and officials of the University of Miami, for hosting the meeting in such excellent

U.S. Depository Copy

facilities and for helping to organize the Workshop. My appreciation is extended to Ms. Josie Sanchez of CIMAS who served ably as the key for local arrangements and logistical support. Of course, the success of a meeting depends on those who come to participate. I have had an opportunity to review the contents of these Proceedings and find this collection a stimulating reminder of the excellent work that is being done and of the science we can look forward to. My thanks to all participants for their contributions which have made this a valuable and successful meeting.

Preface

The "notes" which comprise these Proceedings are to guide the reader to current, ongoing research, or to notions, questions or problems that beg elaboration or solution. Some editorial license has been taken where a few papers have been moved out of the sequence in which they were given at the Workshop; this to improve continuity. Notes on a study by Quiroz have been added to augment information on the most recent climate and to follow up on many participants' interests in the unusual 1976-77 winter, as expressed during both 1977 and 1978 Workshops. Interest in the winter season continues (Wagner, p. 1-1; Diaz and Quayle, p. 3-1; Dickson, P. 4-1; Quiroz, p. 5-1; Namias, p. 6-1; Seckel, Bakun, and Parrish, p. 7-1; Winston and Krueger, p. 8-1, Berg and Matson, p. 10-1; Douglas, p. 28-1, and Barnett, p. 33-1) because of the potentially great impact on human activities and because it is an extreme within the annual cycle which serves as an important point of calibration in testing hypotheses of climate variability.

Data for 1978 have been examined by several of the group assembled, providing views of the most recent seasonal climate: Wagner (p. 1-1); Angell (p. 2-1); Diaz and Quayle (p. 3-1); Dickson (p. 4-1); Quiroz (p. 5-1); Namias (p. 6-1); Seckel, Bakun and Parrish (p. 7-1); Winston and Krueger (p. 8-1); Kukla and Gavin (p. 9-1); Berg and Matson (p. 10-1); Douglas (p. 28-1) and Ernst and Sherman (p. 36-1). Other analyses of atmospheric data reveal a biennial variation in surface temperatures over the U.S. (Rasmusson, et. al. p. 22-1) and suggestions of latitudinal, interannual continuity in 700 mb anomalies (Hanson, p. 23-1). Large-scale atmospheric moisture fluxes are examined by Rosen (p. 24-1).

Considerable attention was given during the Workshop to ocean-related climate characteristics. Miyakoda and Rosati, prompted by last year's Workshop discussions of incomparability between sea surface temperature data sets, analyzed ship and satellite derived data over Pacific regions in an attempt to clarify differences (p. 11-1). Variability of sea surface temperature was examined by Merle (p. 12-1); Thang and Lamb (p. 13-1); Brown and Evans, who also compared ship and satellite measurements, (p. 14-1); Steiner, who has looked for possible interrelationships between SST, wind and clouds (p. 25-1); Fletcher (p. 26-1); Starr, Bryson and Kutzbach (p. 27-1); Douglas (p. 28-1), and Barnett (p. 33-1). Heat transport in the oceans was reviewed by Oort (p. 18-1), estimated by Hastenrath in relation to large-scale atmosphere and ocean heat budgets (p. 21-1), and examined through modeling by Bryan (p. 19-1) and Schopf (p. 20-1). Heat exchanges at the ocean-atmosphere interface were calculated by Clark (p. 16-1) and Bunker (p. 17-1).

Connections between terrestrial hydrology and ocean thermodynamics and the potential for affecting regional climate were discussed by Rooth (p. 15-1). A hydrologic model used to examine moisture exchanges within the climate system was discussed by Eagleson (p. 29-1), and Schaake (p. 31-1) outlined the state-of-the-art in hydrologic modeling for streamflow predictions using climate outlooks prepared by the National Weather Service. Although not formally presented, a paper has been added to the proceedings (submitted for the meeting by Kurilova, et. al., P. 30-1) in response to a view of many participants that insufficient attention has been placed on understanding the hydrologic cycle as part of the climate variability problem. Robert Hirsch, in material presented during the poster session (not formatted for inclusion in the Proceedings) discussed activities of the U.S. Geological Survey and the monthly publication of "Water Resources Review," which reports (among other items) streamflow and ground-water conditions in the U.S. and parts of Canada; the "Review" is free on application to the Water Resources Review, U.S. Geological Survey, Reston, Virginia 22092.

Development of credible climate prediction techniques is an aim of the National Climate Program, and an aim of several of the Workshop participants. Among those who addressed the prediction aspects of climate research were Schaake (p. 31-1), Dittberner (32-1), Barnett (33-1), and Schofield and Barnett (34-1), while Pittock (p. 35-1) ably demonstrated why caution is required.

As a final note, the assistance of Drs. D. Gilman, R. Harnack, S. Hastenrath, E. Kraus, C. Rooth and J. Winston as discussion leaders is gratefully acknowledged. Thanks are extended to all Workshop participants for their excellent presentations, lively discussions and timely insights into climate processes and prediction research.

William A. Sprigg
November 1978

List of Participants
Climate Diagnostics Workshop
October 31 - November 3, 1978

James K. Angell	NOAA/NWS
Timothy P. Barnett	Scripps/University of California
Craig P. Berg	NOAA/NESS/ESG
Otis B. Brown	University of Miami
Reid A. Bryson	University of Wisconsin
Andrew F. Bunker	WHOI
Nathan E. Clark	Scripps/University of California
Curtis A. Collins	National Science Foundation
Henry F. Diaz	NOAA/NCC
Robert R. Dickson	NOAA/NWS/CAC
Gerald J. Dittberner	USAF/ETAC
Arthur V. Douglas	University of Nebraska
Peter S. Eagleson	MIT
John A. Ernst	NOAA/NESS
Joseph O. Fletcher	NOAA/ERL
Donald L. Gilman	NOAA/NWS/CAC
Kent Groninger	NOAA/ERL
Donald V. Hansen	NOAA/AOML
Kirby J. Hanson	NOAA
William S. Harley	Atmospheric Environment Service/Canada
Robert Harnack	Rutgers University
Stefan Hastenrath	University of Wisconsin
Robert Hirsch	U.S. Department of Interior, USGS
Michael Kelly	Climatic Research Unit/UK
Eric P. Kraus	University of Miami, CIMAS
Arthur F. Krueger	NOAA/NESS/MSL
George Kukla	Lamont-Doherty
Gennadii P. Kurbatkin	NOAA/GFDL/Visiting Scientist/Soviet Union
Peter J. Lamb	University of Miami, CIMAS
Dudley McConnell	NOAA/NCPO
Jacq Merle	University of Miami, Visiting Prof./France
Jerome Namias	Scripps/University of California
Abraham H. Oort	Princeton University, GFDL
Barry Pittock	University of Arizona and CSIRO, Australia
Robert G. Quayle	NOAA/EDS
Eugene M. Rasmusson	NOAA/EDIS
Mitchell Roffer	RSMAS - BLR
Claes Rooth	University of Miami, CIMAS
Anthony Rosati	NOAA/GFDL
Richard D. Rosen	Environmental Research & Technology, Inc.
John C. Schaake, Jr.	NOAA/NWS

James G. Schofield	USAF/ETAC
Paul Schopf	Goddard Space Flight Center, NASA
Gunter R. Secket	NOAA/NMFS/PEG
William A. Sprigg	NOAA/NCPO
Ellen J. Steiner	CIRES, University of Colorado
James Wagner	NOAA/NWS/CAC
James Weinman	Goddard Space Flight Center, NASA
Jay S. Winston	NOAA/NESS/MSL
Stanley Woronko	Atmospheric Environment Service/Canada

TABLE OF CONTENTS

		Page
Foreword		i
Preface		iii
List of Participants		v
Contributed Papers:		
A Review of the Seasonal Circulation and Weather from Fall 1977 Through Summer 1978	A.J. Wagner	1-1
An Update of Temperature and Vortex-Area Data Through the Winter of 1977-78	J.K. Angell	2-1
A Comparative Analysis of the 1977-78 Winter Season in the United States	H.F. Diaz R.G. Quayle	3-1
The Low Index Winter 1977-78 vs the High Index Winter 1975-76: A Comparison of Energetics	R.R. Dickson	4-1
A Hemispheric View of the Troposphere and Stratosphere During the Winters 1975-76, 1976-77, and 1977-78	R.S. Quiroz	5-1
1978 Break in the West Coast Drought	J. Namias	6-1
Large-scale Atmospheric Circulation and the West Coast Upwelling Regime in 1976/77 and 1977/78	G.R. Seckel A. Bakun R. Parrish	7-1
Tropical Circulation and Radiation Fluctuations: Interactions with Mid-Latitude Circulations During 1976-1978	J.S. Winston A.R. Krueger	8-1
Snow and Sea Ice Cover Fluctuations in 1977-78	G. Kukla J. Gavin	9-1
The 12-year Satellite Snowcover Record and the Record Winter Snowcover of 1977-78	C.P. Berg M. Matson	10-1

TABLE OF CONTENTS
(continued)

		Page
The Variation of Sea Surface Temperature in 1976 and 1977: The Data Analysis	K. Miyakoda A. Rosati	11-1
Annual and Interannual Variability of SST in the Eastern Tropical Atlantic Ocean	J. Merle	12-1
Recent Variability of the Gulf Stream Extension Front	C.P. Thang P.J. Lamb	13-1
Interannual Variability of Arabian Sea Sea Surface Temperature	O.B. Brown R.H. Evans	14-1
Salinity Fluctuations in the Labrador Sea, and their Implications for High Latitude Oceanic Climate Feedback	C. Rooth	15-1
Characteristics of Interannual Variations of Large-Scale Heat Exchange Across the Air/Sea Interface in the Mid-Latitude North Pacific	N.E. Clark	16-1
A 25-year Oceanic Flux Data Set of the Atlantic Ocean and Analyses	A.F. Bunker	17-1
Short Review of the Evidence for a Large Poleward Transport of Heat by the Oceans	A.H. Oort	18-1
The Heat Balance of a Diagnostic Model of the Northern Atlantic	K. Bryan	19-1
Low-Latitude Seasonal Ocean Heat Transport	P.S. Schopf	20-1
On the Heat Budget of the Tropical Atmosphere and Oceans	S. Hastenrath	21-1
Biennial Variations in Surface Temperatures over the United States as Revealed by Singular Decomposition	E.M. Rasmusson J.B. Jalickee P.A. Arkin Wen-Yuan Chen	22-1

TABLE OF CONTENTS
(Continued)

		Page
Summary of Northern Hemisphere 700 MB Height Departures from Normal, 1966-1969	K.J. Hanson	23-1
Variability in the Annual Fields of Large-Scale Atmospheric Water Vapor Transport	R.D. Rosen	24-1
A Comparison of Surface Wind Parameters, Cloud Amount, and Sea Surface Temperature in the Tropical Pacific	E.J. Steiner	25-1
Ocean and Climate Variability Over the Last Century	J.O. Fletcher	26-1
Sea-Air Interaction at the Pole-tide Frequency: A Preliminary Report	T.B. Starr R.A. Bryson J.E. Kutzbach	27-1
Interannual Sea Surface Temperature Variations as Related to Severe North American Winters	A.V. Douglas	28-1
Sensitivity Study of the Annual Water Balance	P.S. Eagleson	29-1
Study of the Hydrological Cycle Based on Satellite and Surface Information	Yu.V. Kurilova P.A. Kolosov E.L. Muzylev L.K. Poplavskaya	30-1
Extended Streamflow Prediction Techniques: Description and Applications During 1977	J.C. Schaake	31-1
Application of the University of Wisconsin Model to Climate Prediction	G.J. Dittberner	32-1
Predictability of Air Temperature over North America - A Progress Report	T.P. Barnett	33-1
A Sea Level Pressure Analog Model for Predicting Temperature over the Northern Hemisphere	J.G. Schofield T.P. Barnett	34-1

TABLE OF CONTENTS
(Continued)

		Page
Solar Variations and Weather/Climate	A.B. Pittock	35-1
Status Report on the Geophysical Data Processing of the Seasat Microwave Sensors	J.A. Ernst J.W. Sherman, III	36-1

A REVIEW OF THE SEASONAL CIRCULATION AND WEATHER FROM FALL 1977 THROUGH SUMMER 1978

A. James Wagner
National Weather Service, NOAA

FALL 1977 - Except for a small area of weak blocking north of Siberia, 700 mb heights were generally below normal at high latitudes, and fast zonal westerlies prevailed at middle latitudes around most of the hemisphere. An exception was eastern North America, where there was a tendency for recurrent blocking.

The negative height anomaly near Vancouver Island was associated with frequent storminess in the area and the advection of cool maritime air from the Gulf of Alaska into the Pacific Northwest and adjacent areas of Canada. Most of the southern two-thirds of the United States had warmer than normal temperatures, a continuation of the previous summer pattern. The temperature anomaly of +4°F in west Texas was due in part to a heat wave which produced record temperatures well in excess of 100°F during the last third of September.

Precipitation was above normal over much of the country, the only exceptions being part of the Southwest, where a severe drought continued, and the western portions of the southern and central Great Plains. The severe summer drought over much of the Southeast was relieved. Heavy rains from Hurricane Babe during the second week of September fell from the Louisiana Coast northward and eastward to the Tennessee Valley and lower Appalachians. The drought in the mid-Atlantic states was not relieved until October, however.

WINTER 1977-78 - Many aspects of the mean circulation were similar to that of the previous record cold winter, although subtle differences between the two patterns led to most of the records in the 1977-78 season being due to heavy snow rather than cold. A large area of negative height anomaly again covered much of the north-central Pacific, and an extensive area of blocking was centered over Canada. A deep trough over the eastern United States was associated with frequent and often intense storminess contributing to record and near-record snowfall totals over the eastern third of the United States.

One of the important differences between the past two winters is that the strongest westerlies were farther south in 1977-78, with the low latitude portion of the western North American ridge weaker than normal. Instead of being deflected northward toward Alaska as in the previous winter, Pacific storms entered California, giving more than twice the normal winter precipitation to much of the Southwest. The drought was decisively broken, but at the cost of flooding and mudslides in southern California. The main positive 700 mb height anomaly was centered over northern Canada instead of British Columbia as in the previous winter. Easterly anomalous flow over the northern Great Plains contributed to upslope flow of Arctic air, with the result that cold and snowy conditions prevailed, in sharp contrast to generally mild, dry weather the previous winter.

Mild Pacific air dominated all areas west of the Continental Divide, where storm-related cloudiness also prevented the normal nocturnal cooling over the Plateau. All areas east of the Divide were colder than normal, but east of the Mississippi River it was not quite as cold as the previous winter. Much of the Great Plains was considerably colder in 1977-78. This was due in part to the eastern North American trough being farther west in the more recent winter. This position also brought more moisture into the East, where the previous winter had been quite dry. Extensive areas had two to more than three times their normal winter snowfall in 1977-78. Record-breaking blizzards paralyzed the Midwest in January and southern New England in February.

SPRING 1978 - A wave number two pattern at high latitudes was associated with blocking over the Beaufurt Sea and Northern Scandinavia while an intense vortex was located over Baffin Island. A weak area of blocking was centered just north of Minnesota. This feature, together with the absence of appreciable troughing in the West, produced a generally milder than normal spring over much of the West. Fast mid-latitude westerlies prevailed over both oceans, with deeper than normal Aleutian and Icelandic lows. A stronger than normal trough over Europe contributed to an unusually cold and wet spring there.

In contrast to the fast mid-latitude westerlies over the oceans, below normal heights across the southern United States and the Canadian block meant weak westerlies in that area. Storms crossing the U.S. moved slowly and produced large quantities of precipitation. Pacific storms continued to produce more than twice the normal seasonal rainfall along the California coast. The only noticeably dry area was in Texas and Louisiana, where some areas had less than half the normal precipitation.

SUMMER 1978 - The strong polar low persisted over northern Canada into the summer, moving slightly westward from its spring position. It was surrounded by a ring of positive height anomalies, south of which an active storm track prevailed across northern Eurasia. The area of positive height anomalies broadened to include middle latitudes from the central Pacific to the central Atlantic, with several moderately strong anomaly centers across the United States from lower California to the mid-Atlantic States. Each was associated with a center of positive temperature anomaly and at times, drought.

The overall temperature anomaly pattern was similar to that of the preceding summer, although areas of heat and drought were for the most part much less severe. The seasonal mean maps do not, however, reflect the fact that parts of central Texas had a record-breaking heat wave during July, with readings as high as 114°F at Wichita Falls. During the first week of August, torrential rains from moisture brought inland from Tropical Storm Amelia at the end of July caused widespread flooding along a north-south line through central Texas. Some totals were in excess of 20 inches. By the end of the summer, rather severe drought conditions existed over Oklahoma, northeast Texas, and portions of adjacent states. Sections of the Southeast and Southwest were also dry, but drought conditions in these areas were less severe than during the previous summer because fairly good rains had fallen in the preceding months of 1978.

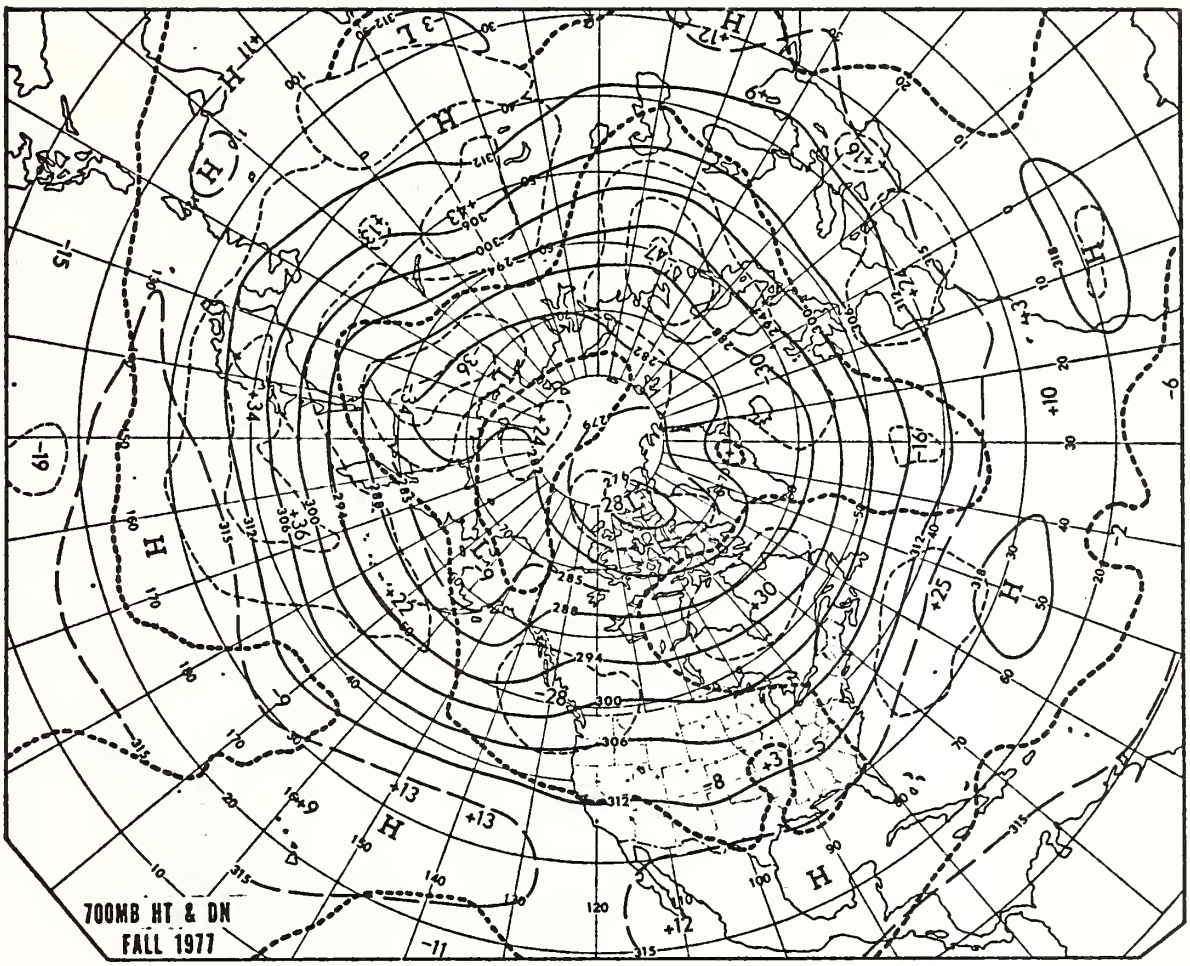
700MB HT & DN
FALL 1977

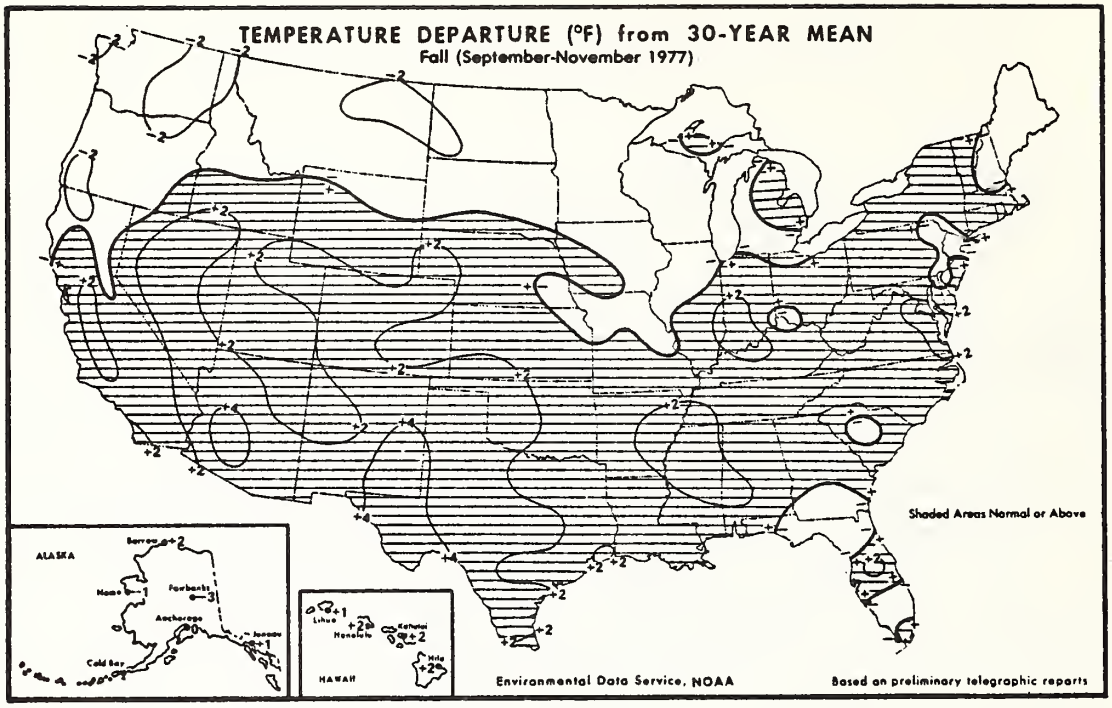
TEMPERATURE DEPARTURE (°F) from 30-YEAR MEAN
Fall (September-November 1977)
Shaded Areas Normal or Above
ALASKA
HAWAII
Environmental Data Service, NOAA
Based on preliminary telegraphic reports

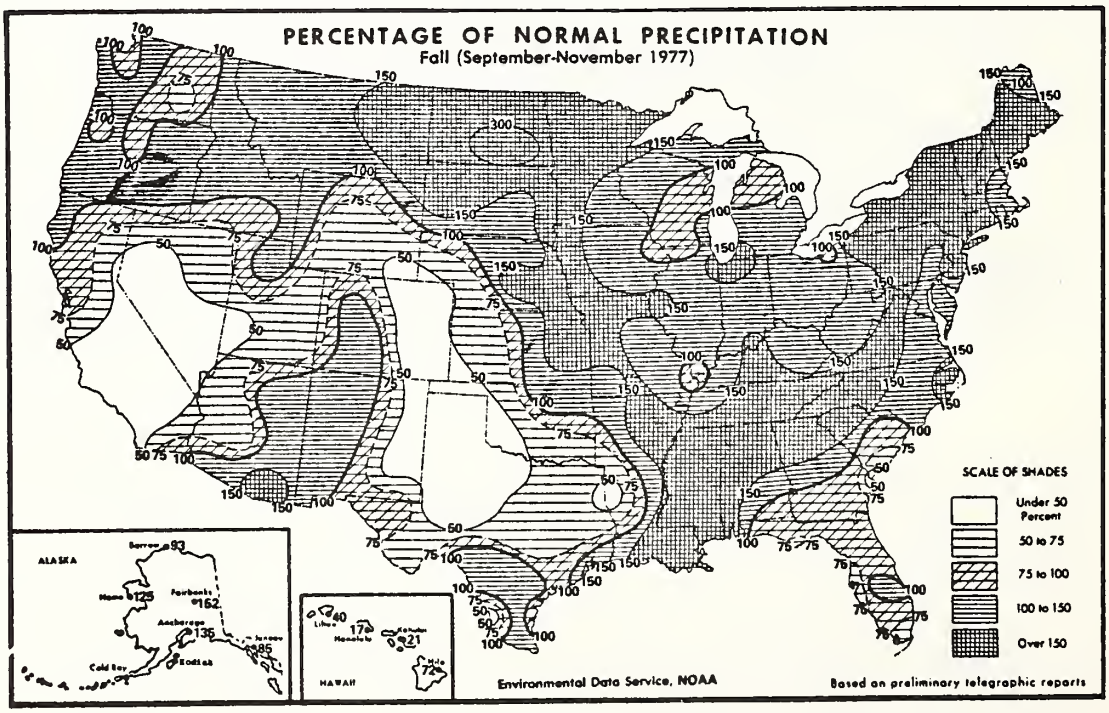
PERCENTAGE OF NORMAL PRECIPITATION
Fall (September-November 1977)
SCALE OF SHADES
Under 50 Percent
50 to 75
75 to 100
100 to 150
Over 150
ALASKA
HAWAII
Environmental Data Service, NOAA
Based on preliminary telegraphic reports

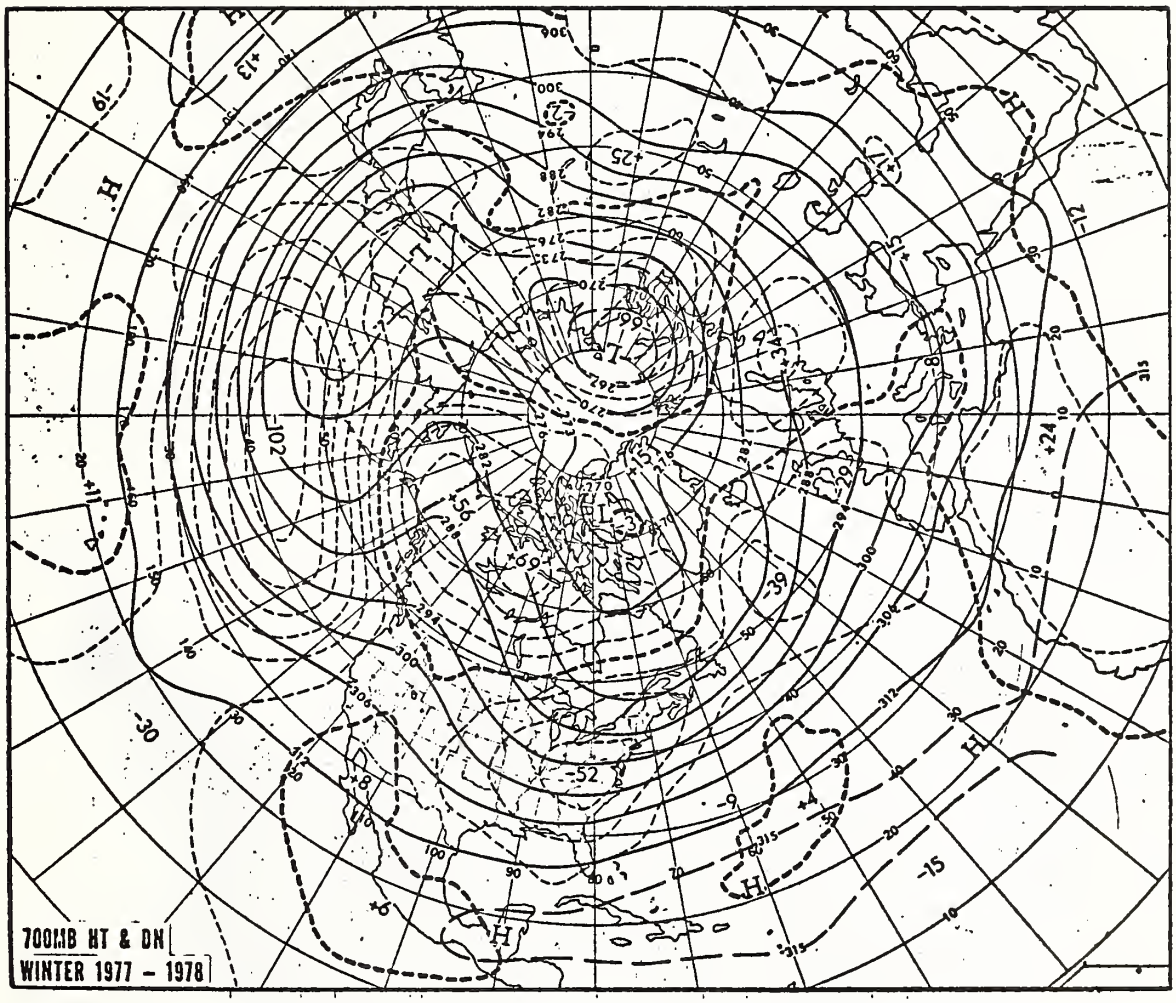
700MB HT & DN
WINTER 1977 - 1978

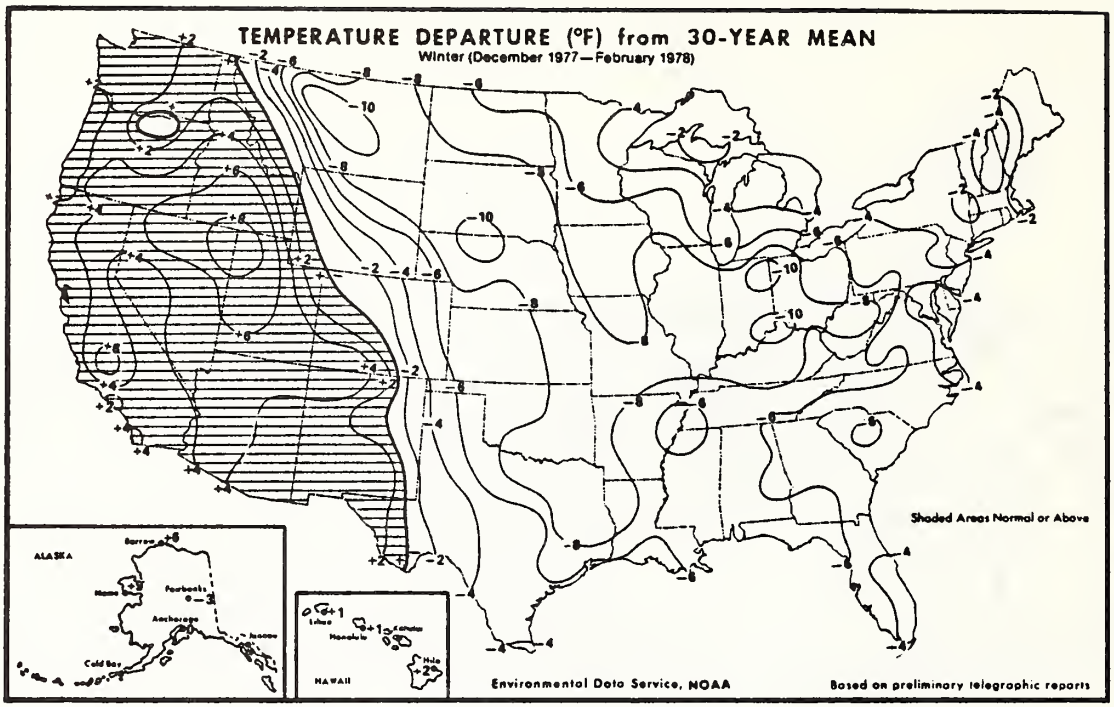
TEMPERATURE DEPARTURE (°F) from 30-YEAR MEAN
Winter (December 1977—February 1978)
Shaded Areas Normal or Above
ALASKA
HAWAII
Environmental Data Service, NOAA
Based on preliminary telegraphic reports

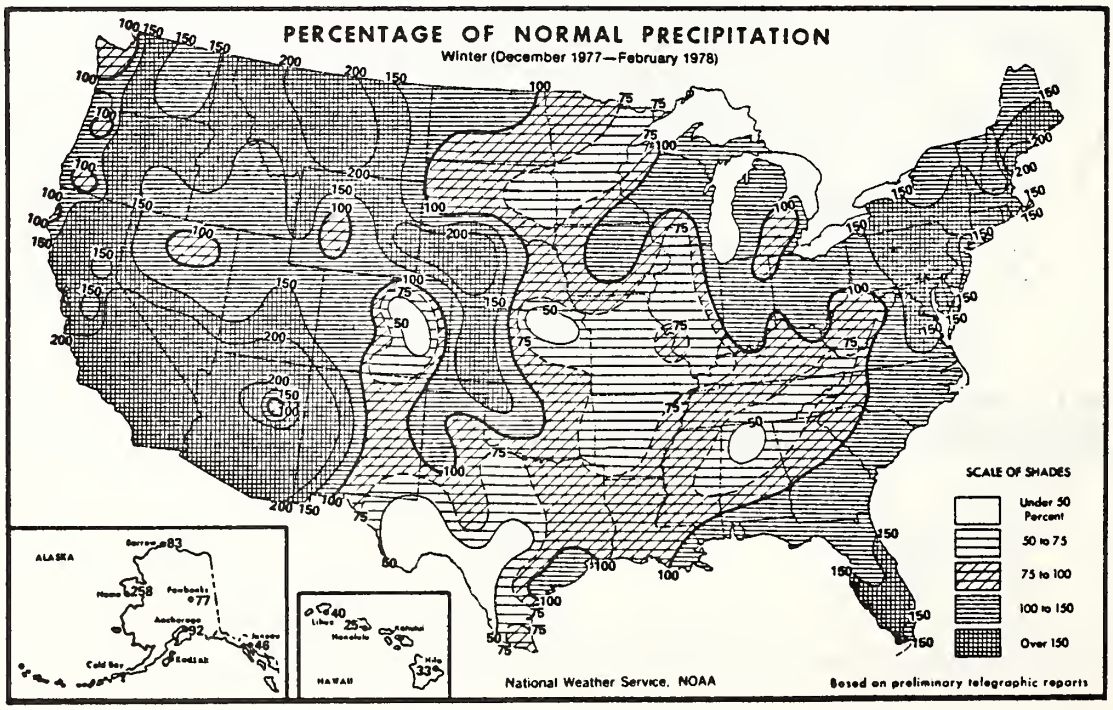
PERCENTAGE OF NORMAL PRECIPITATION
Winter (December 1977—February 1978)
SCALE OF SHADES
Under 50 Percent
50 to 75
75 to 100
100 to 150
Over 150
ALASKA
HAWAII
National Weather Service, NOAA
Based on preliminary telegraphic reports

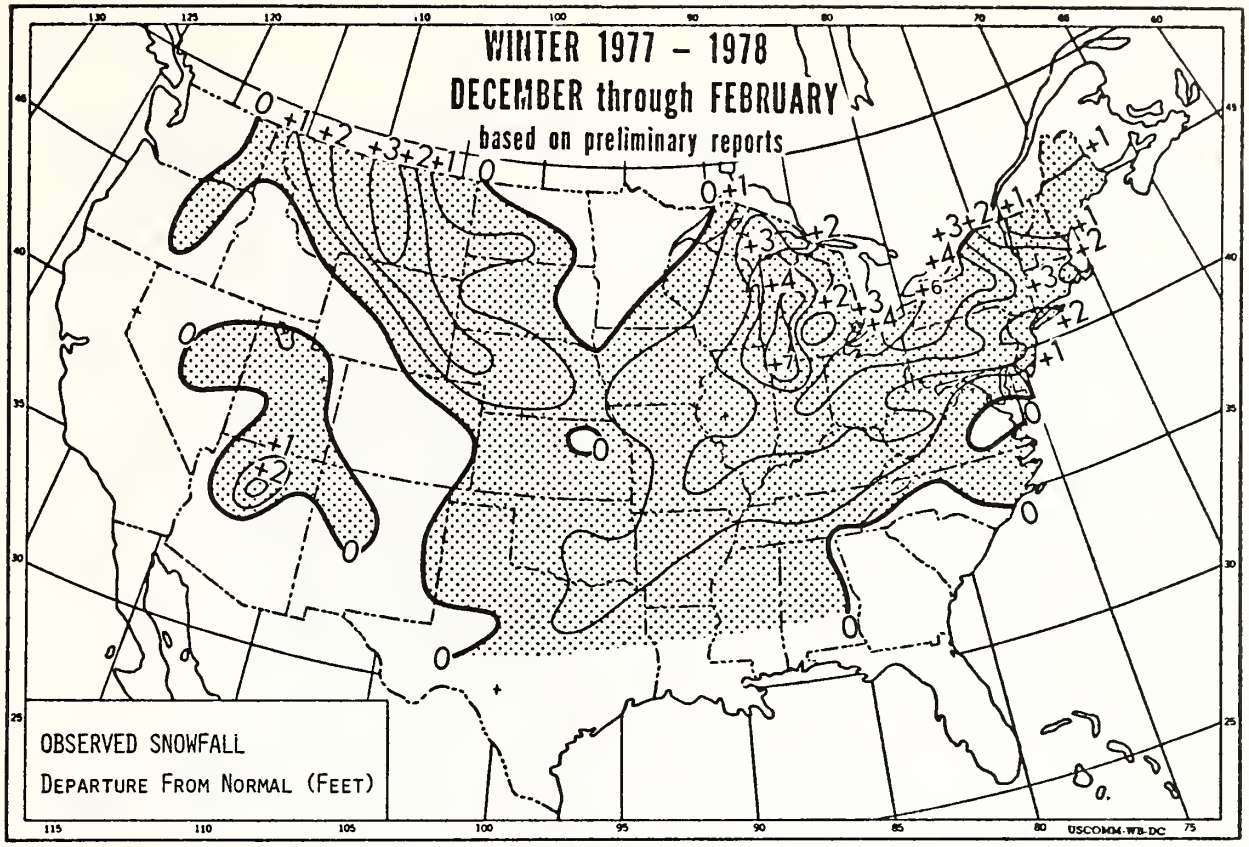
WINTER 1977 - 1978
DECEMBER through FEBRUARY
based on preliminary reports
OBSERVED SNOWFALL
DEPARTURE FROM NORMAL (FEET)
USCOMM-WB-DC

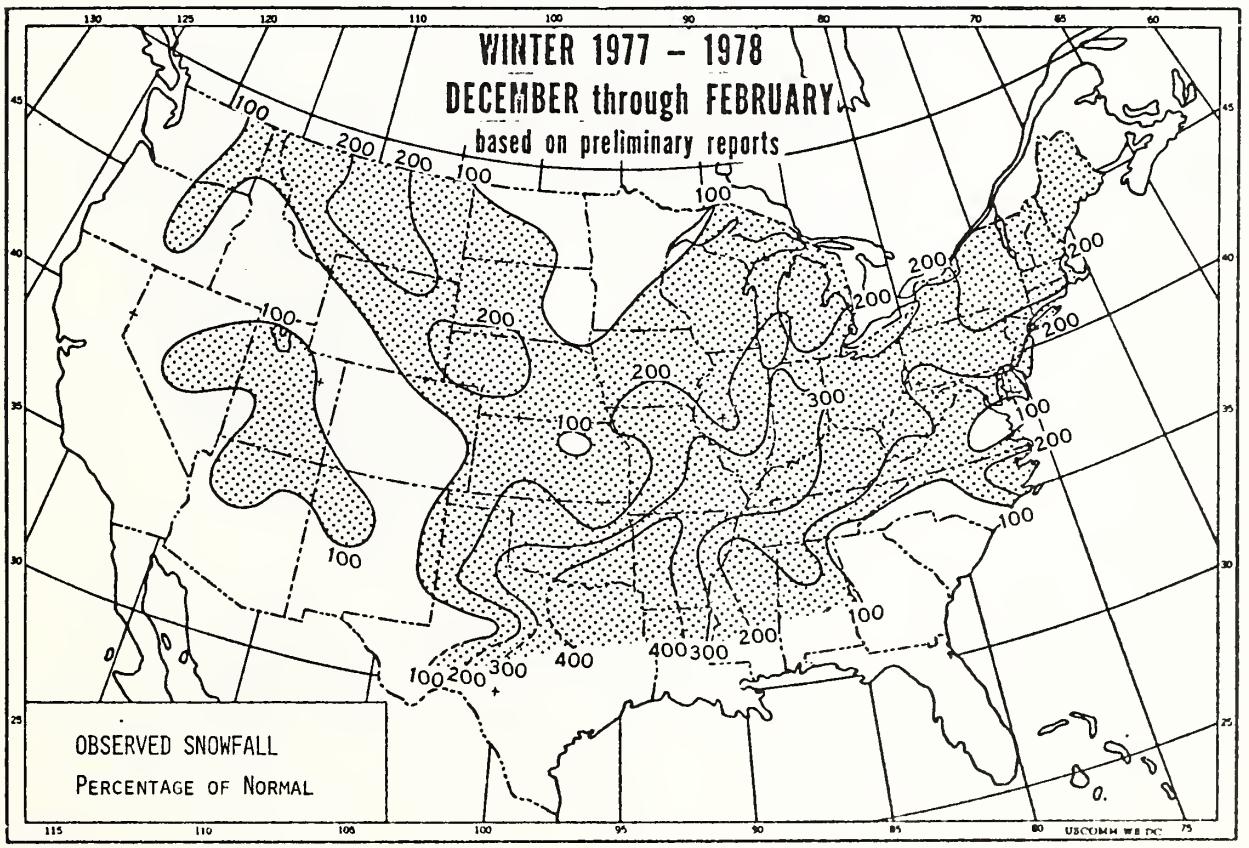
WINTER 1977 - 1978
DECEMBER through FEBRUARY
based on preliminary reports
OBSERVED SNOWFALL
PERCENTAGE OF NORMAL

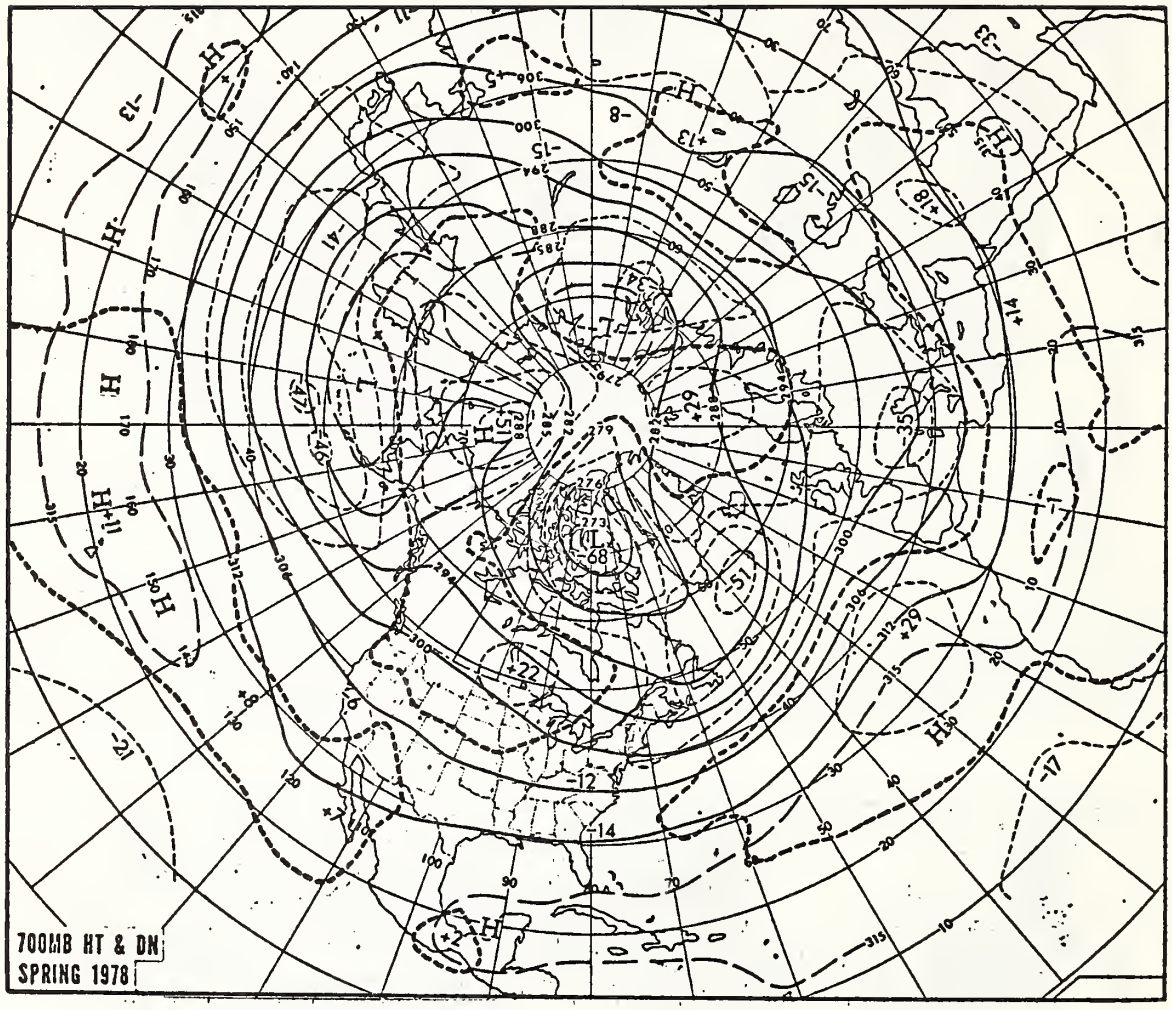
700MB HT & DN
SPRING 1978

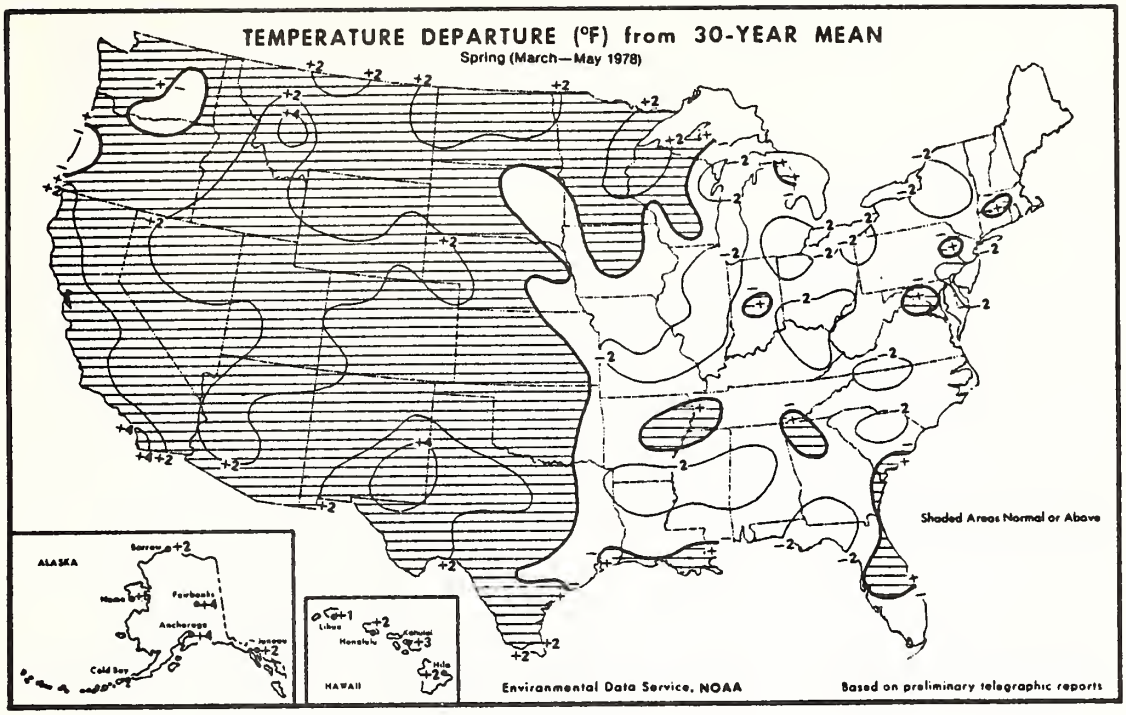
TEMPERATURE DEPARTURE (°F) from 30-YEAR MEAN
Spring (March—May 1978)
Shaded Areas Normal or Above
ALASKA
HAWAII
Environmental Data Service, NOAA
Based on preliminary telegraphic reports

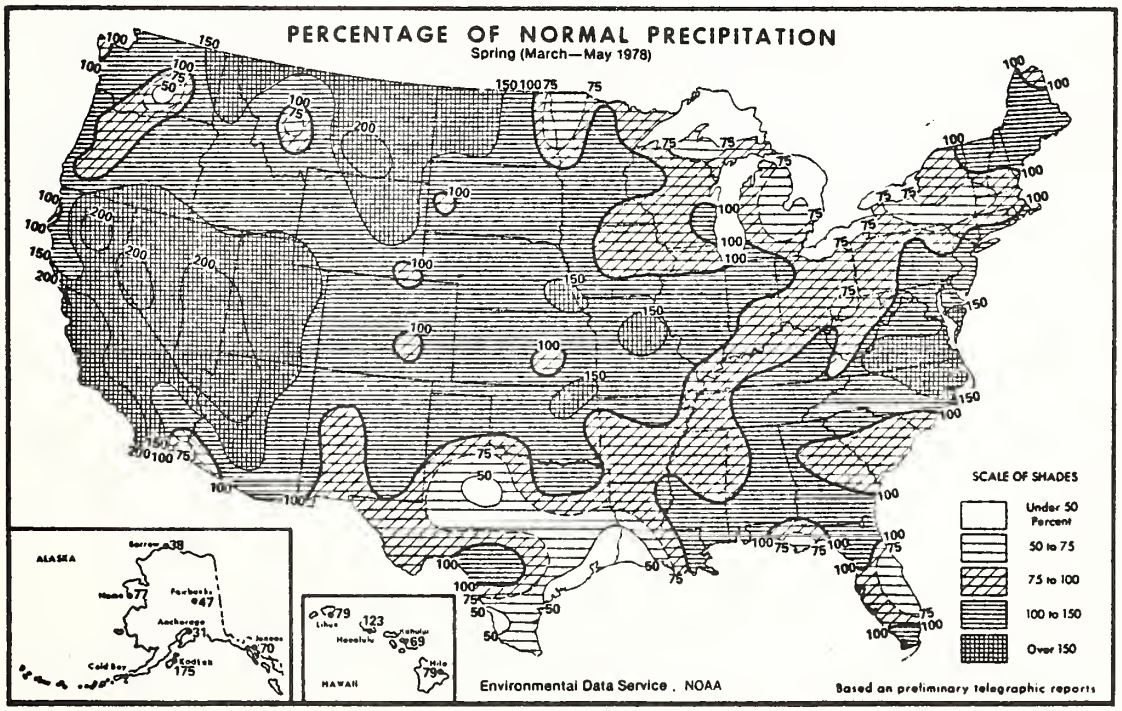
PERCENTAGE OF NORMAL PRECIPITATION
Spring (March—May 1978)
SCALE OF SHADES
Under 50 Percent
50 to 75
75 to 100
100 to 150
Over 150
ALASKA
HAWAII
Environmental Data Service , NOAA
Based on preliminary telegraphic reports

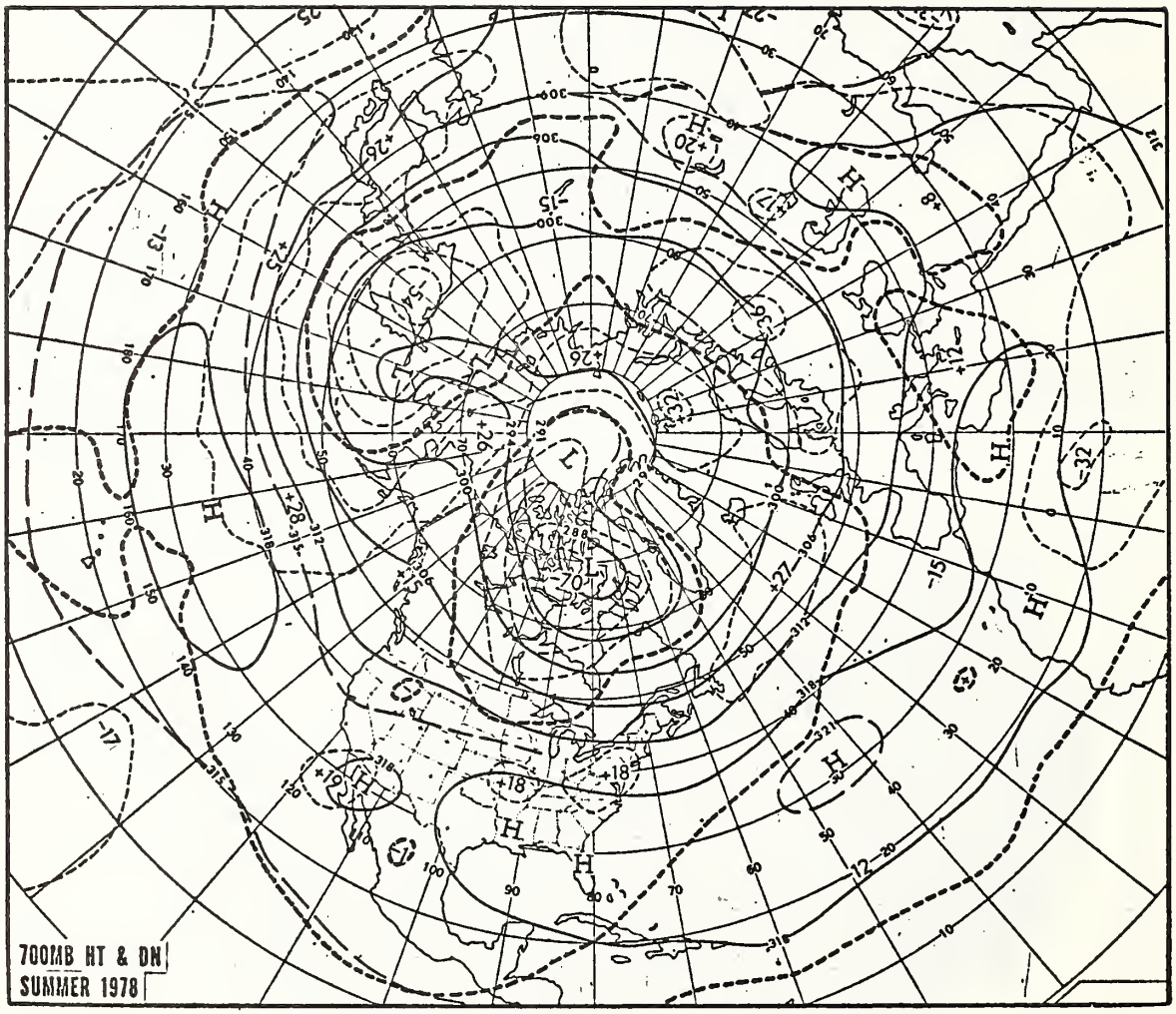
700MB HT & DN
SUMMER 1978

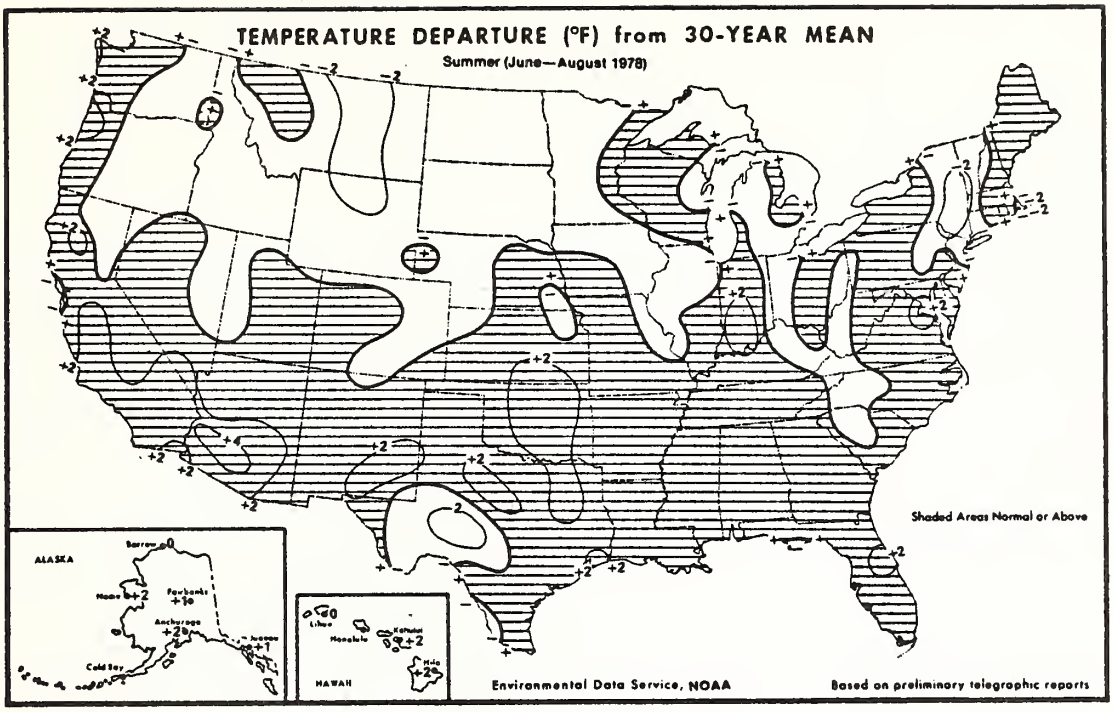
TEMPERATURE DEPARTURE (°F) from 30-YEAR MEAN
Summer (June—August 1978)
Shaded Areas Normal or Above
ALASKA
HAWAII
Environmental Data Service, NOAA
Based on preliminary telegraphic reports

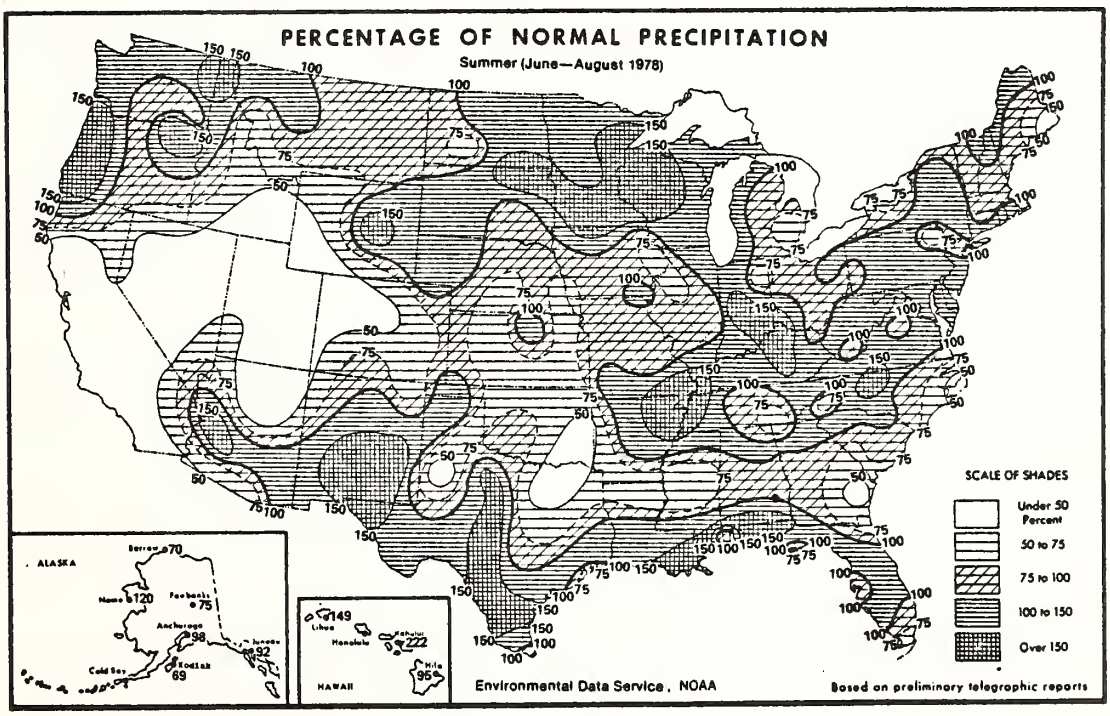
PERCENTAGE OF NORMAL PRECIPITATION
Summer (June—August 1978)
SCALE OF SHADES
Under 50 Percent
50 to 75
75 to 100
100 to 150
Over 150
ALASKA
HAWAII
Environmental Data Service, NOAA
Based on preliminary telegraphic reports

An Update of Temperature and Vortex-Area Data Through the Winter of 1977-78

J.K. Angell
Air Resources Labs, ERL, NOAA
Silver Spring, MD 20910

The following are the main results obtained from an update, through the northern winter of 1977-78, of global temperature variations at the surface and in surface-100 mb and 100-30 mb layers, as well as from an update of the size and location of the 300 mb north circumpolar vortex. Some other points of interest are also recorded. Figure 1 shows the global distribution of radiosonde stations used initially for the temperature analysis. In recent years some substitutions have had to be made in the equatorial zone.

1. The large 3-yearly temperature oscillations in the tropics, apparently related to El Nino (EN) occurrences, have recently decreased in amplitude and become less uniform (Figs. 2 and 3).

2. There is evidence of a similar 3-yearly temperature oscillation in the surface-100 mb layer of north polar latitudes, almost in phase with the oscillation in the tropics (Fig. 3).

3. In recent years there has been a greater temperature decrease in north temperate latitudes than in north subtropics, resulting in an increase in meridional temperature gradient between the two zones (Figs. 2 and 3).

4. In north temperate latitudes the overall decrease in temperature has been associated with an overall increase in total ozone. On the shorter time scale there is evidence of a lag, i.e., the relatively high total ozone values in 1977 appear to be related to the cold year 1976 (Fig. 3).

5. In the Northern Hemisphere since about 1965 the surface temperature has tended to increase slightly while the surface-100 mb temperature has tended to decrease slightly, implying an increase in lapse rate (Fig. 4).

6. In the 100-30 mb layer of the Northern Hemisphere, the temperatures were relatively high following the eruptions of Agung and Fuego (Fig. 4), but for the world as a whole the temperatures were much higher following Agung (Fig. 5).

7. The surface temperature decrease following Agung was larger in the Northern Hemisphere than for the world, but note that in both cases the decrease was not unique (Figs. 4 and 5).

8. The large interannual variability of temperature in recent years is shown by the observation that 1976 (X) was a record cold year globally, whereas 1977 (XX) was a relatively warm year globally (Fig. 6). This alteration was worldwide, being found in the tropics and both extratropical regions.

9. In north temperate latitudes the winter of 1977-78 (XX) was indicated to be not as cold as the winter of 1976-77 (Fig. 7), even though the area of the 300 mb north circumpolar vortex was indicated to be greater in the winter of 1977-78 (Fig. 8).

10. As perhaps a contributing factor to the discrepancy in 9 above, it has been found from the 70-year Historical Weather Map Series that the central latitude of the subpolar low-pressure belt and subtropical high-pressure belt have averaged about 1 degree of latitude less at the time of 11-year sunspot maximum than sunspot minimum (Fig. 9). There is evidence also of a 22-year cycle in the central pressure of subpolar low and subtropical high (Fig. 9).

11. The eccentricity of the north circumpolar vortex was the smallest of record (vortex-center nearest the North Pole) during 1977 Fig. 8).

12. In the 25-55 km layer of the western hemisphere the temperature is indicated to have decreased by about 3°C between sunspot maximum in 1969 and sunspot minimum in 1976 in polar (P), subtropical (S) and equatorial (E) latitudes (Fig. 10). It will be of interest to see if this temperature increases again with the recent upsurge in solar activity.

13. There is evidence of about a 2-season lag between the 3-yearly temperature oscillation in the equatorial zone and in both temperate latitudes (Fig. 11). Hence, if the tropical oscillation persists, there would appear to be some possibility of foreshadowing seasonal temperatures in the extratropics. On the basis of the somewhat limited data record, summer temperatures are better foreshadowed than winter temperatures in this way.

14. The warm periods in the 3-yearly tropical temperature oscillation have been associated with enhancements in the rate of increase of carbon dioxide (Fig. 12).

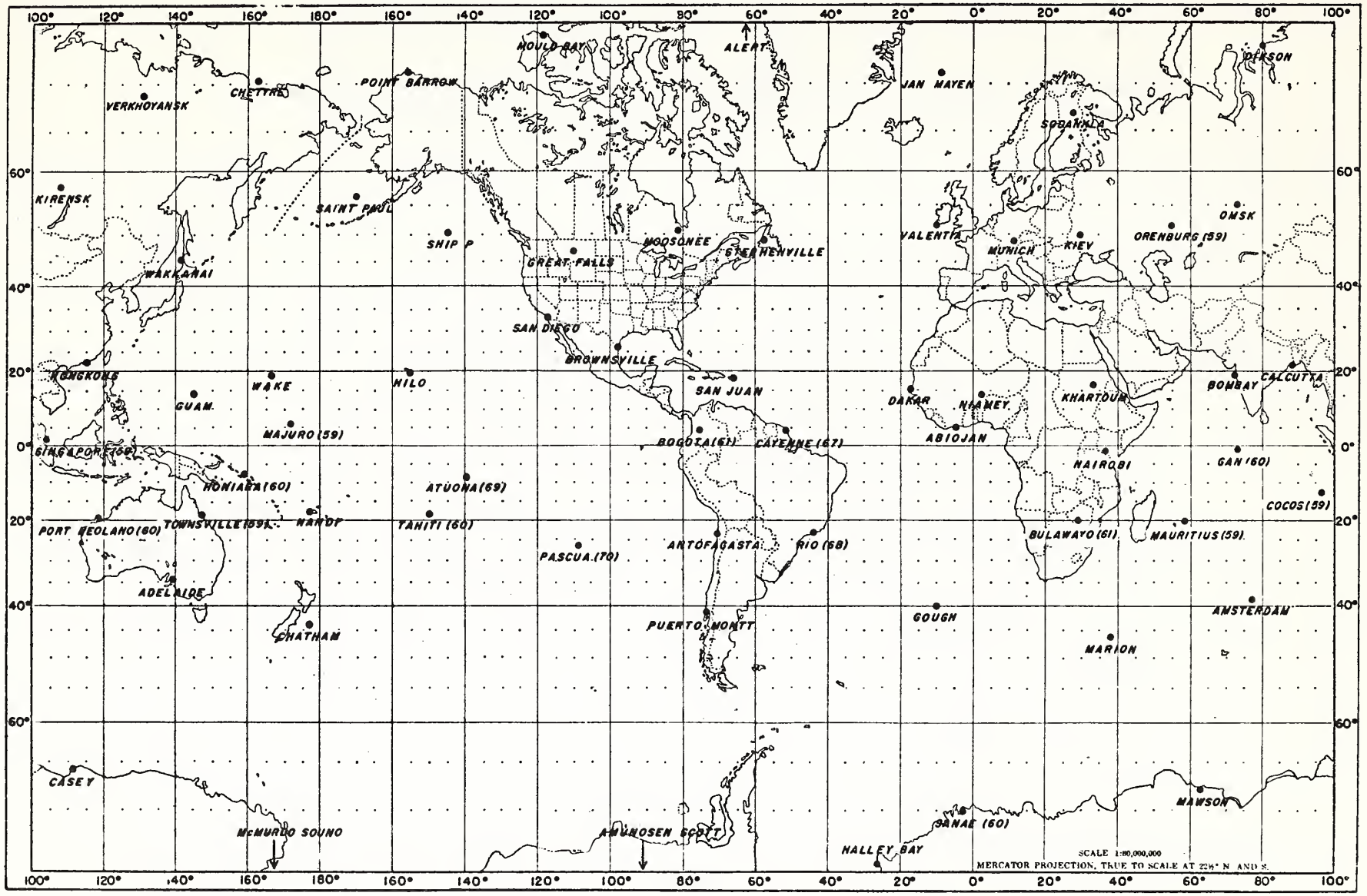

Fig. 1. Distribution of radiosonde stations used for the global temperature analysis. In recent years a few substitutions have had to be made in the equatorial zone.

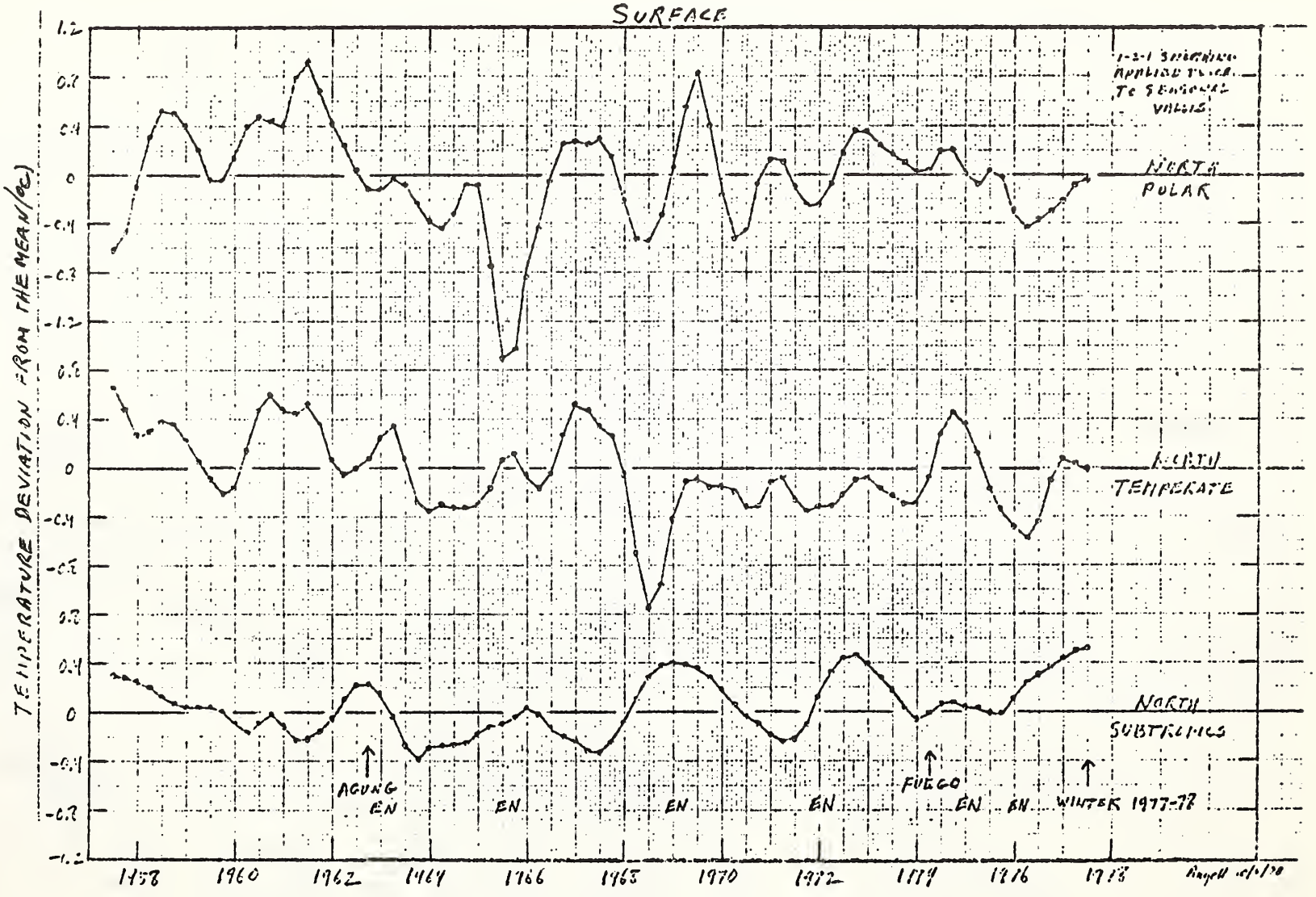

Fig. 2. Surface-temperature variations in the three Northern Hemisphere climatic zones. A 1-2-1 smoothing (1-1 at beginning and end of record) has been applied twice to successive seasonal values (annual variation eliminated). Indicated at bottom are the volcanic eruptions of Agung and Fuego, and the years of El Nino (EN) phenomena. Tick marks are in summer of the given year.

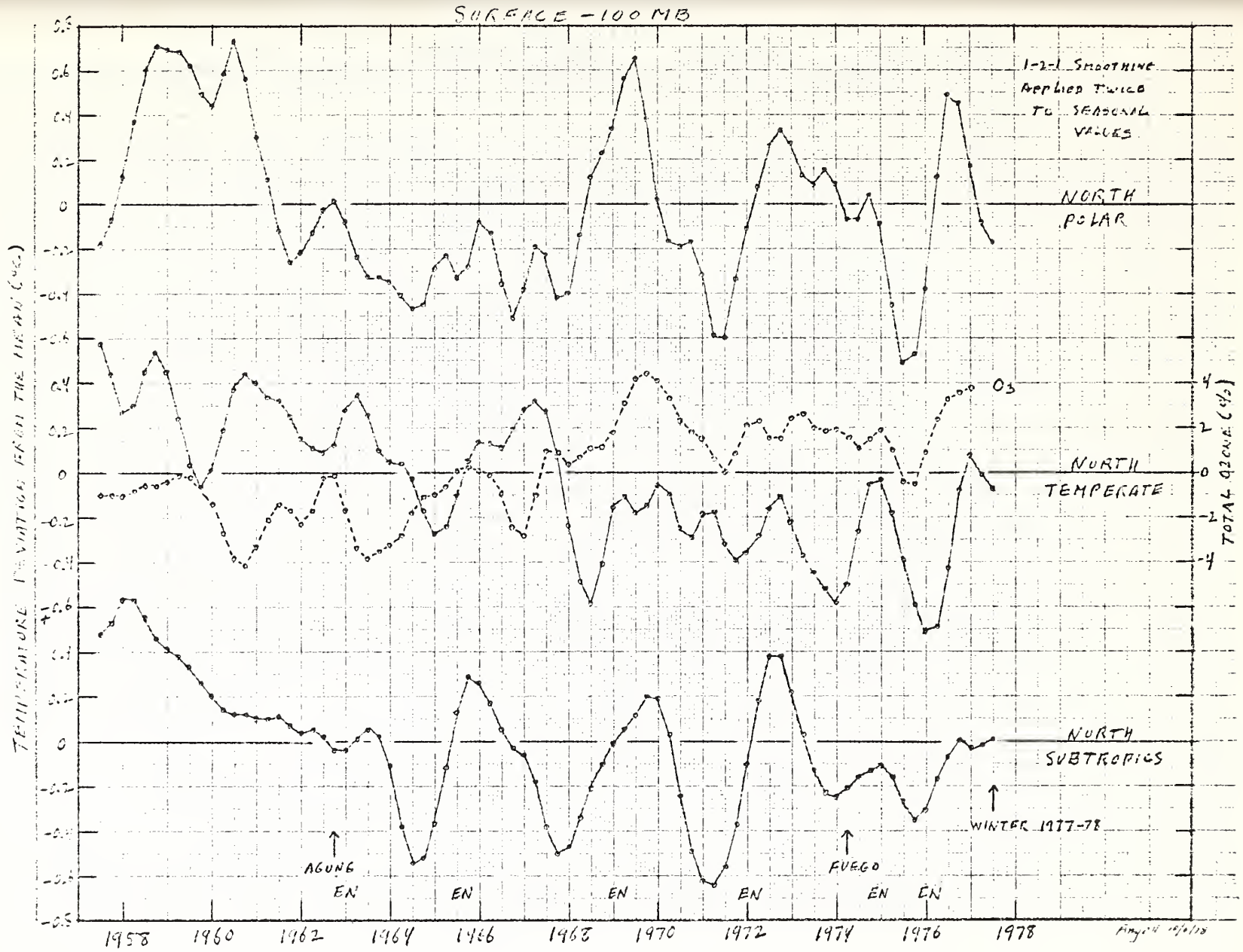

Fig. 3. Same as Fig. 2 for the surface–100 mb layer. The dashed line at center shows the derived variation in total ozone in north temperate latitudes.

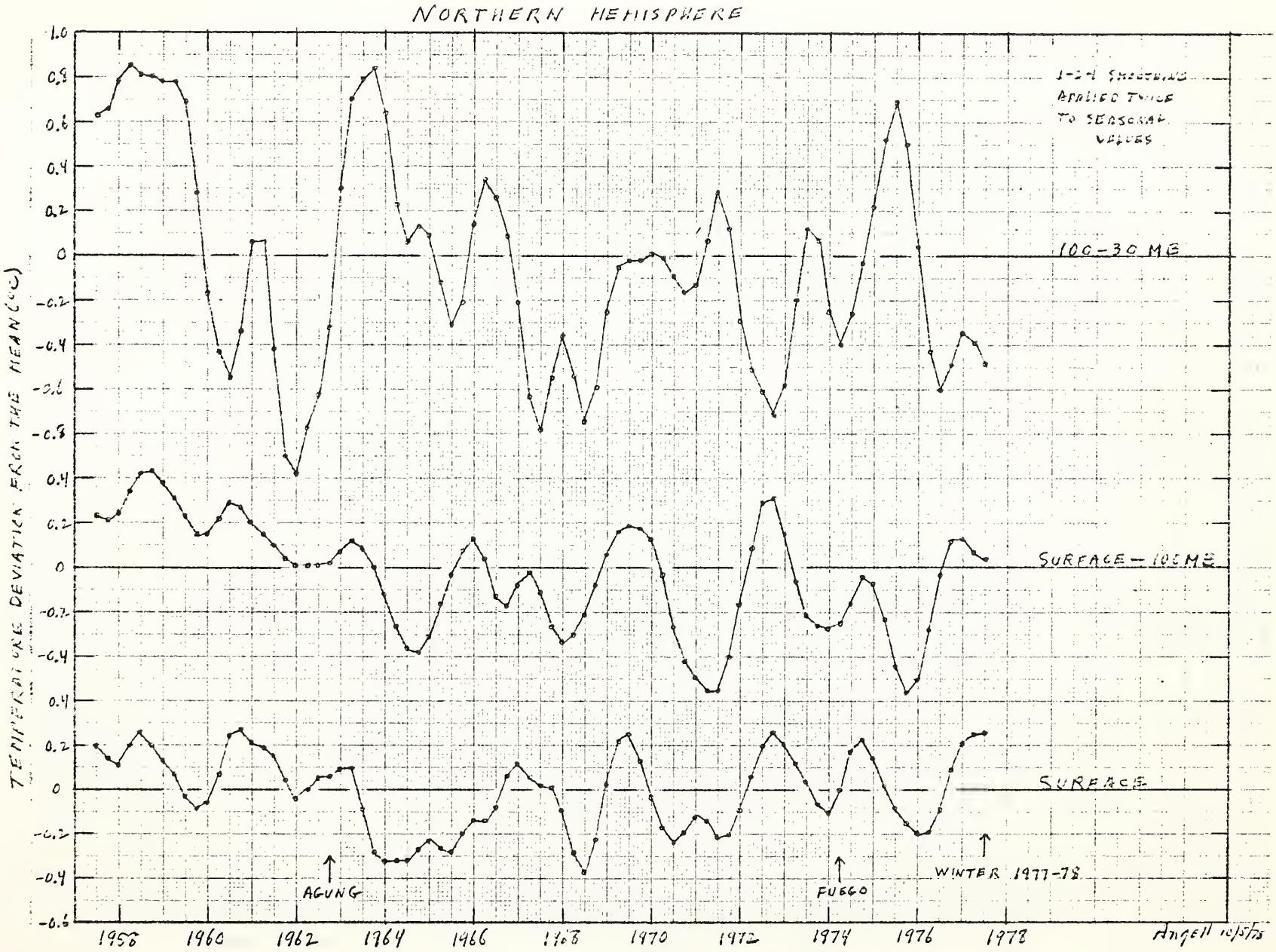

Fig. 4. Northern Hemisphere temperature variation at the surface and in surface-100 mb and 100-30 mb layers. Otherwise, see Fig. 2 legend.

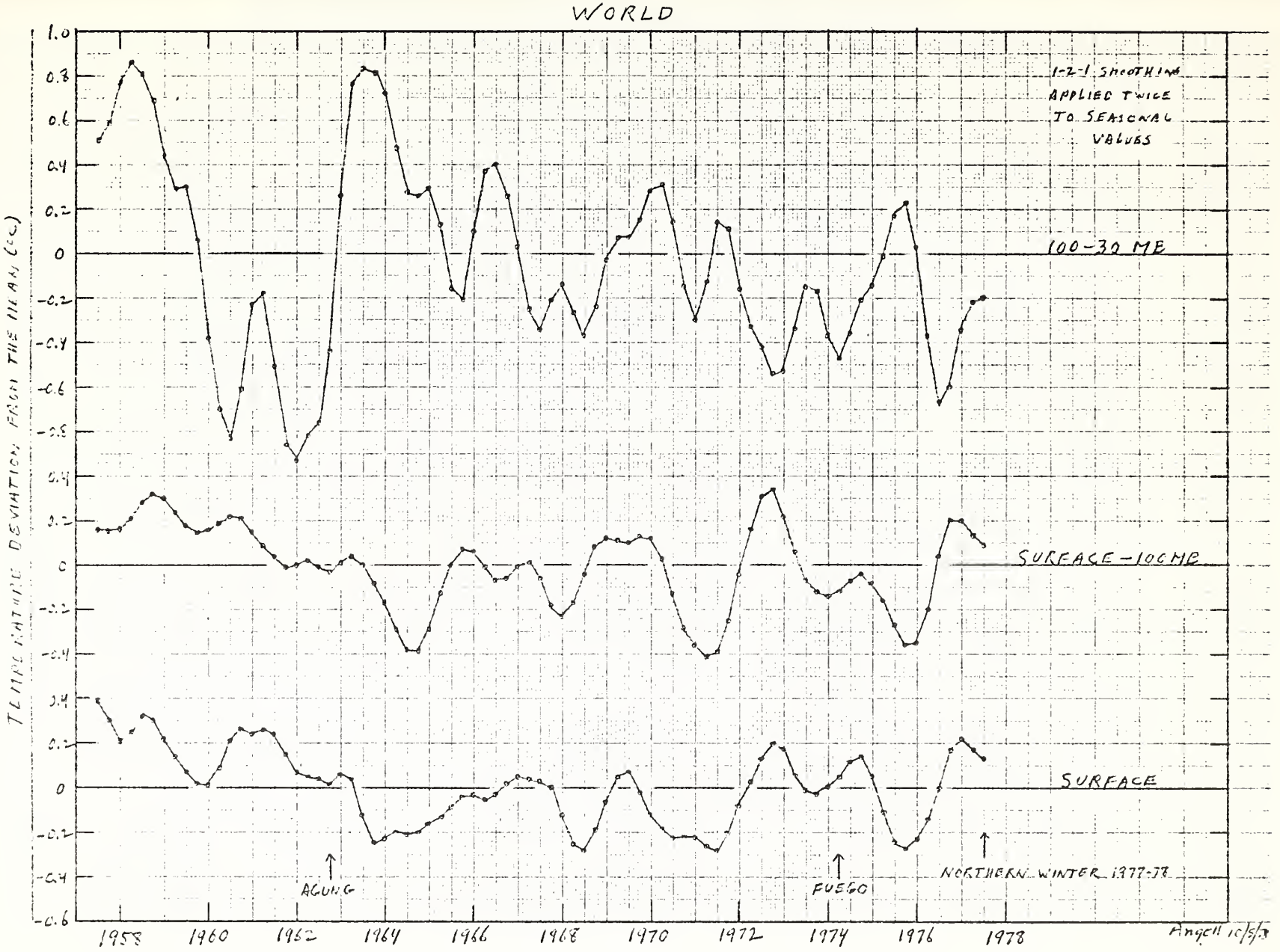

Fig. 5. Same as Fig. 4, but for the world.

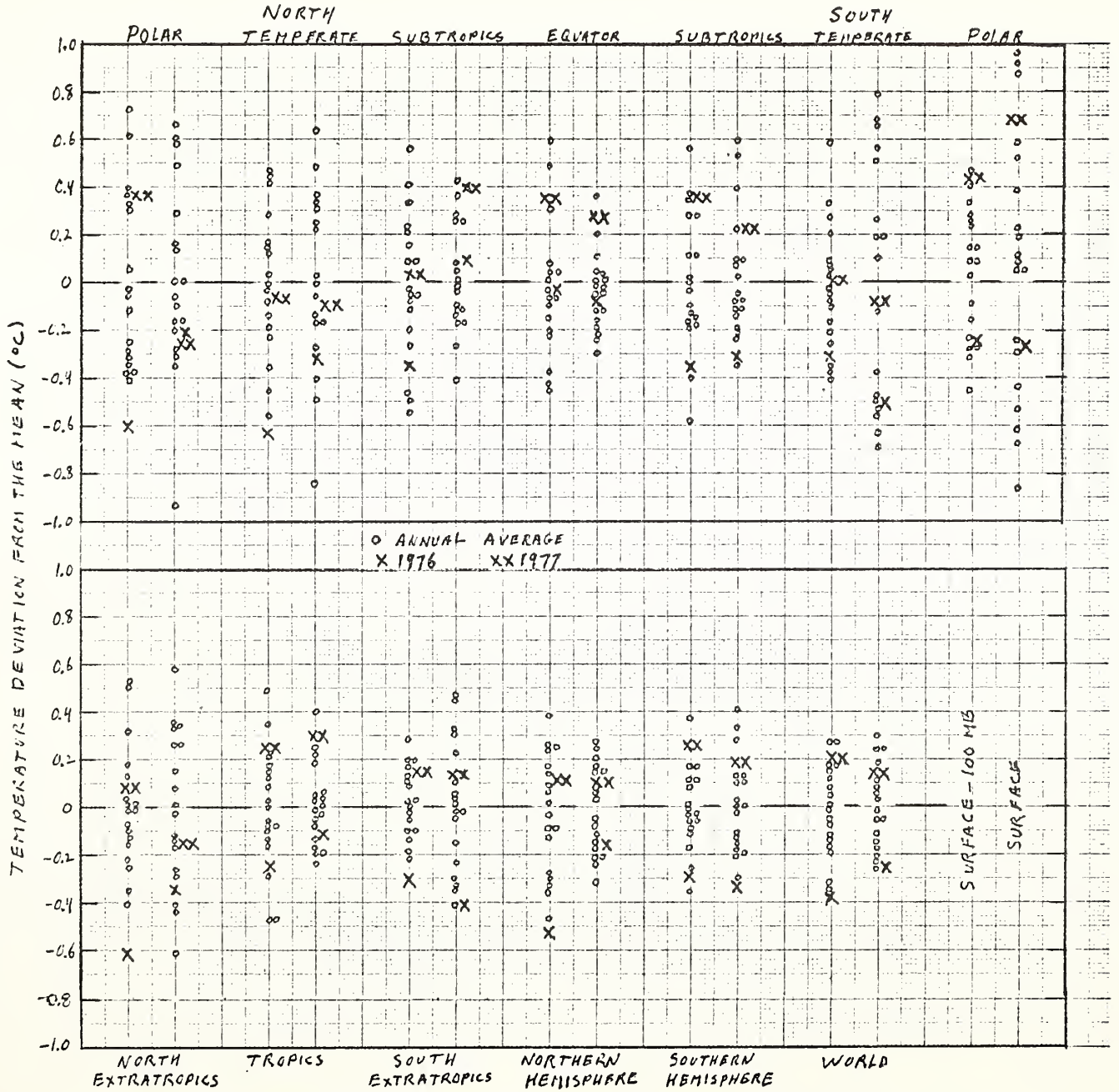

Fig. 6. Comparison of the mean annual temperature in 1976 (X) and 1977 (XX) with the temperature of previous years (circles). Note that for each region the left-hand distribution represents the surface-100 mb temperature, the right-hand distribution the surface temperature.

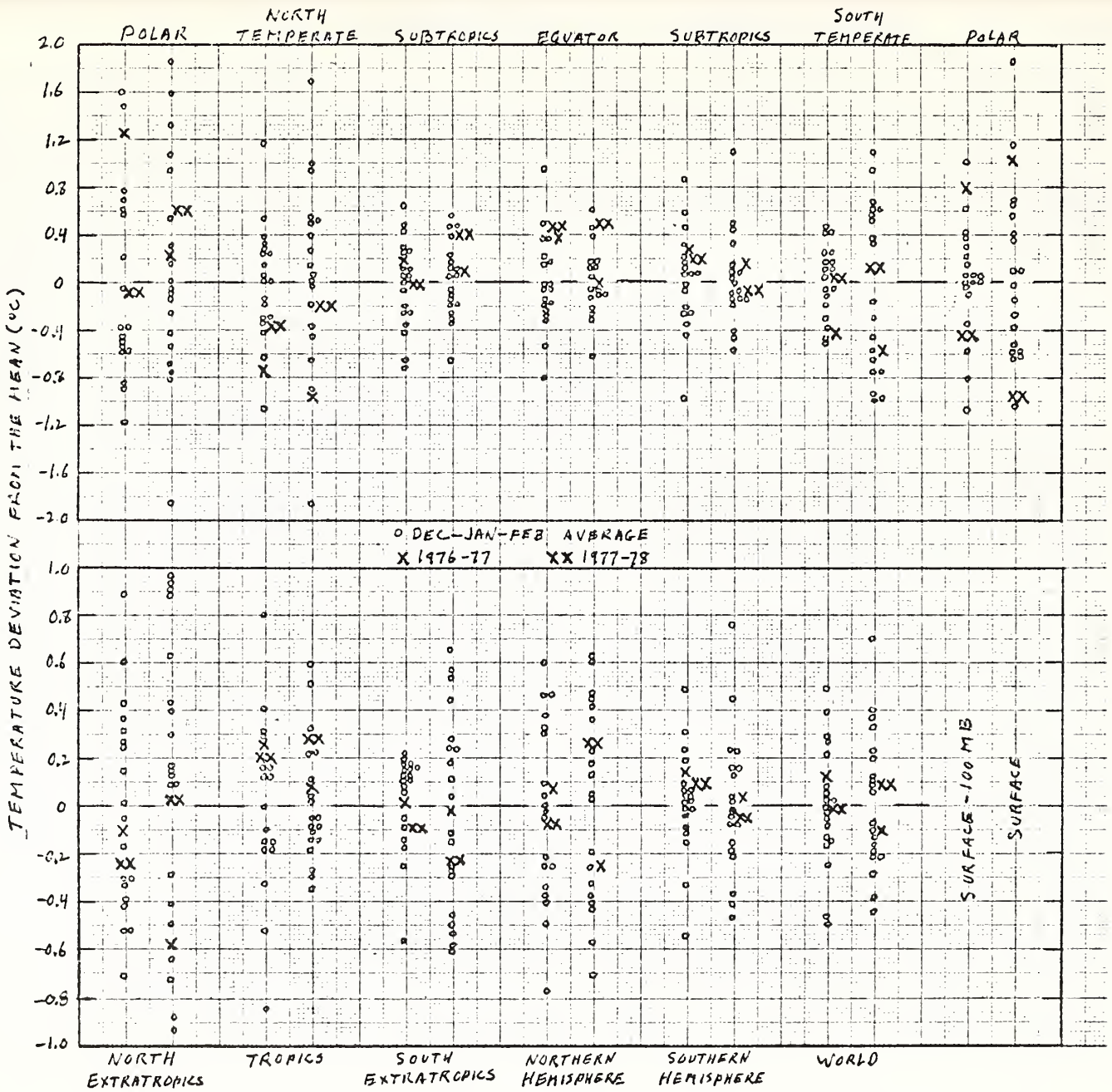

Fig. 7. Comparison of the northern winters of 1976-77 (X) and 1977-78 (XX) with previous northern winters. Otherwise, see Fig. 6 legend.

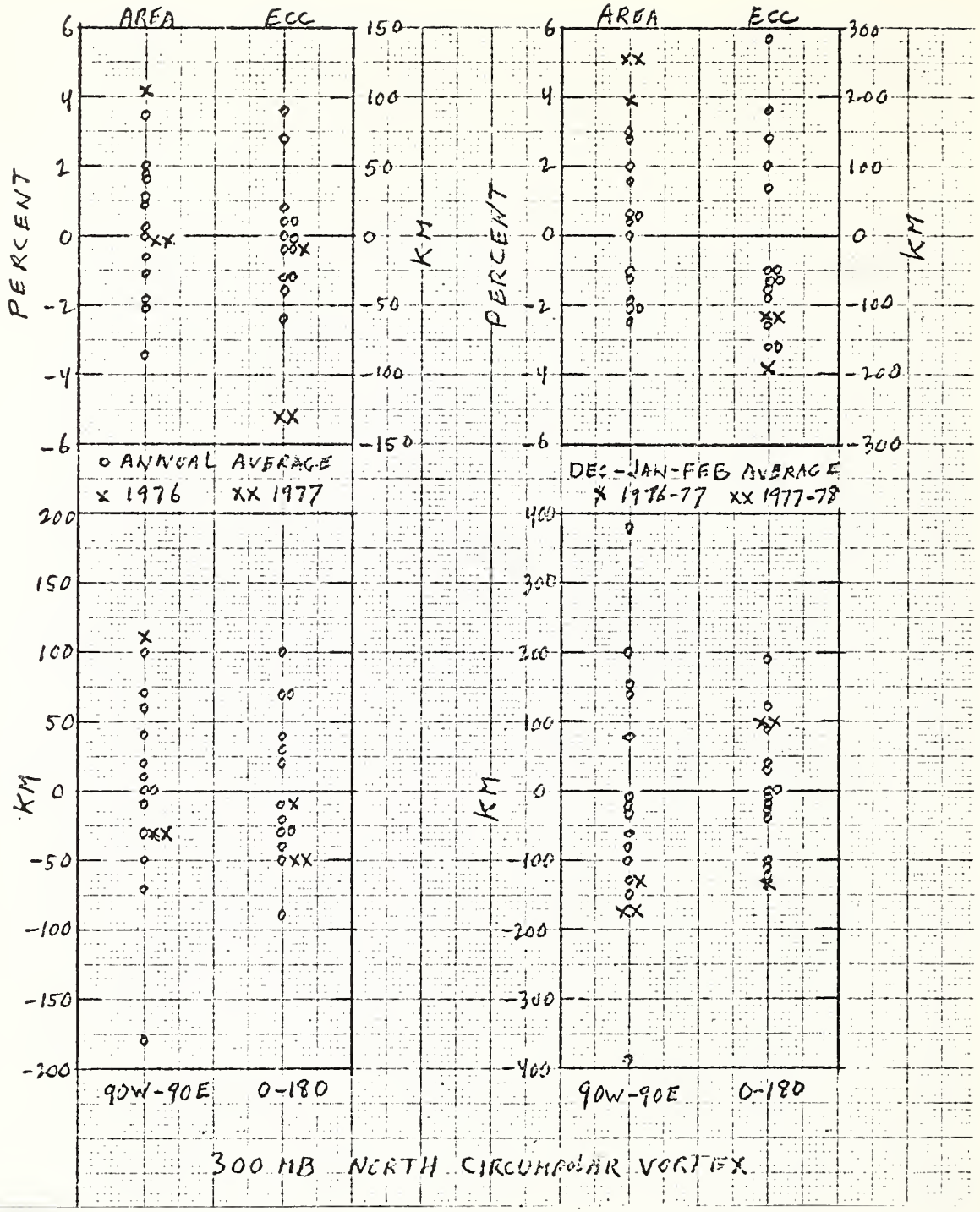

Fig. 8. Comparison with other years of the area, eccentricity, and displacement along axes 90°W-90°E and 0°-180° of the 300 mb north circumpolar vortex during 1976 (X) and 1977 (XX), and at right the comparisons for the northern winter of 1976-77 (X) and 1977-78 (XX). A positive eccentricity signifies that the vortex center is further from the North Pole than average and similarly, for the bottom diagrams, that the vortex-center is displaced further in the direction of 90°E and 180° than average.

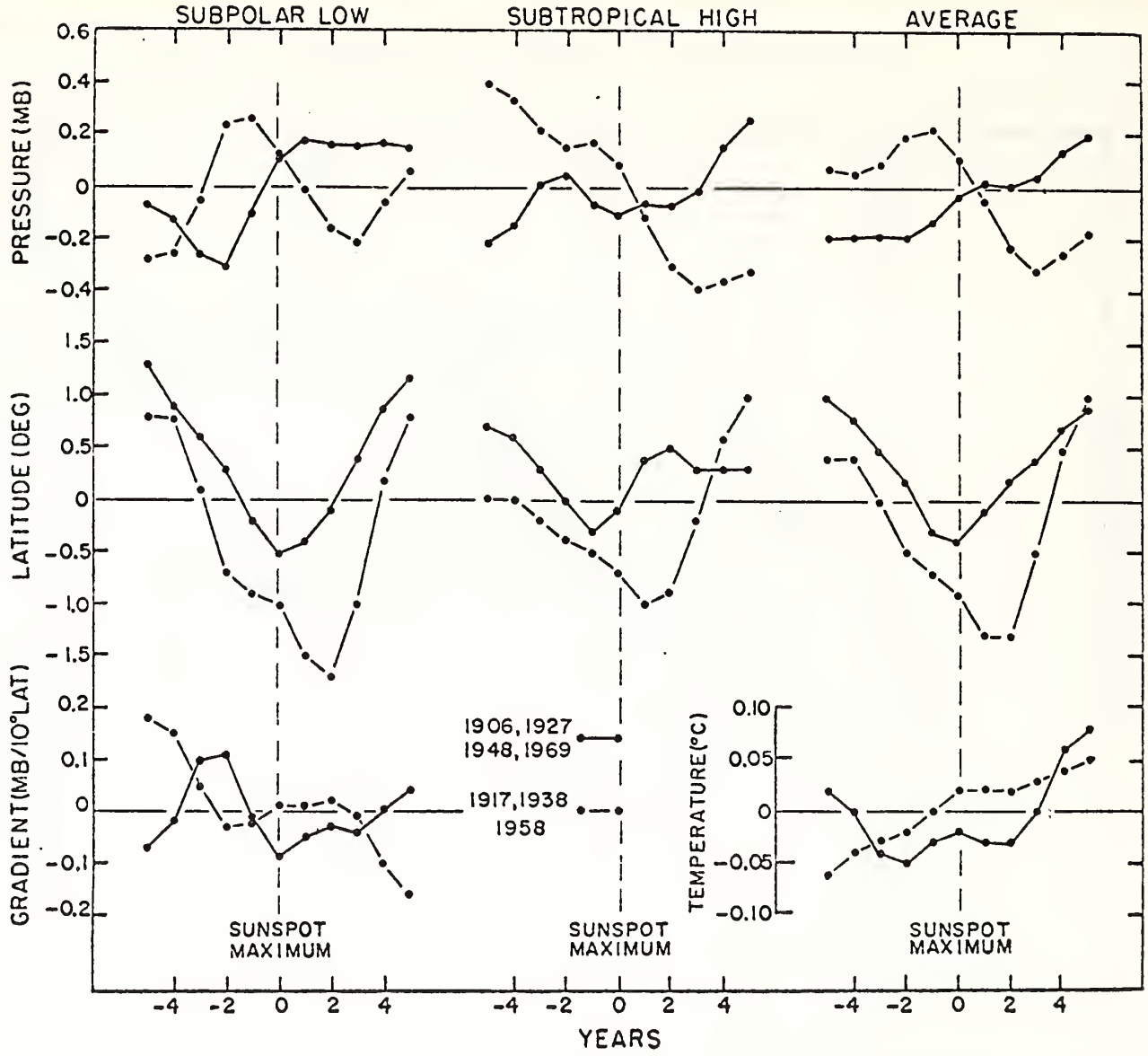

Fig. 9. Variation of the central latitude and central pressure of the subpolar low pressure belt and subtropical high pressure belt with alternate 11-year sunspot cycles. An opposition in trend implies a 22-year cycle. At bottom is shown the variation with sunspot number of the pressure gradient between subtropical high and subpolar low, and of the Northern Hemisphere surface temperature.

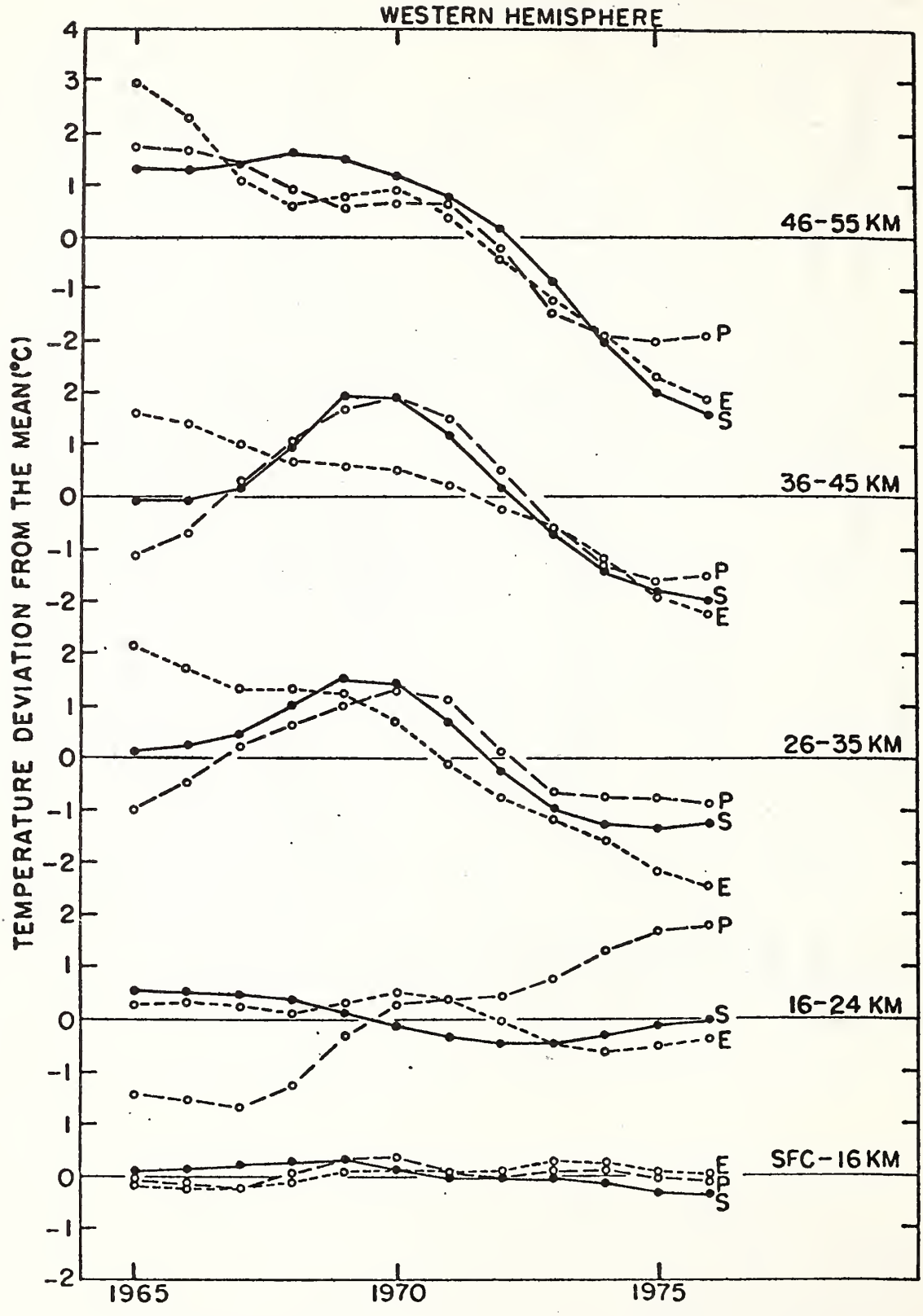

Fig. 10. Temperature trends as a function of height for north polar (P), north subtropical (S) and equatorial (E) zones of the western hemisphere. A 1-2-1 smoothing (1-1 at beginning and end of record) has been applied twice to successive year-average values.

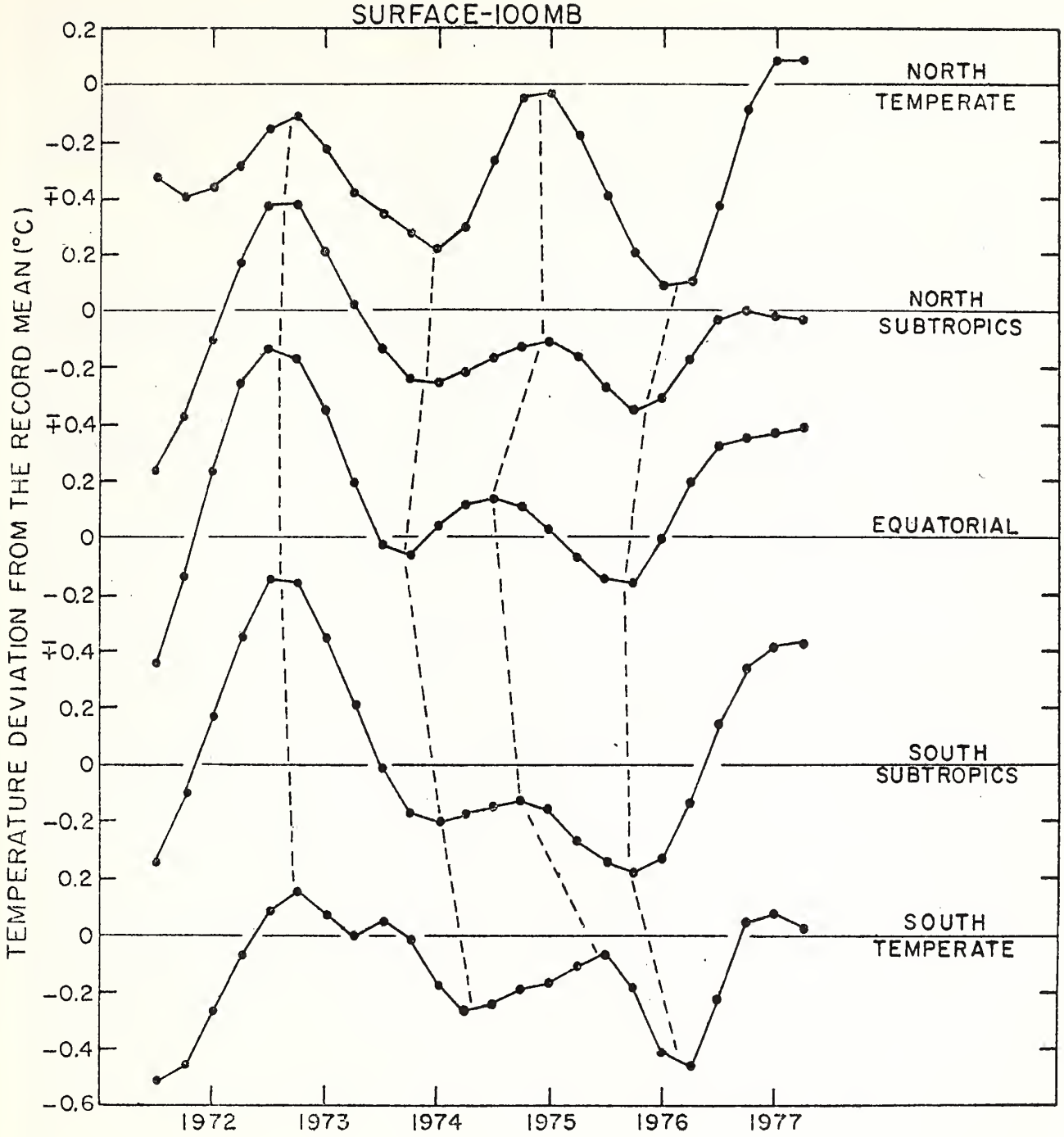

Fig. 11. Recent temperature variations, for the surface-100 mb layer, in tropical and north and south temperate latitudes, where again a 1-2-1 smoothing has been applied twice to successive seasonal values. The dashed lines connect corresponding temperature maxima and minima.

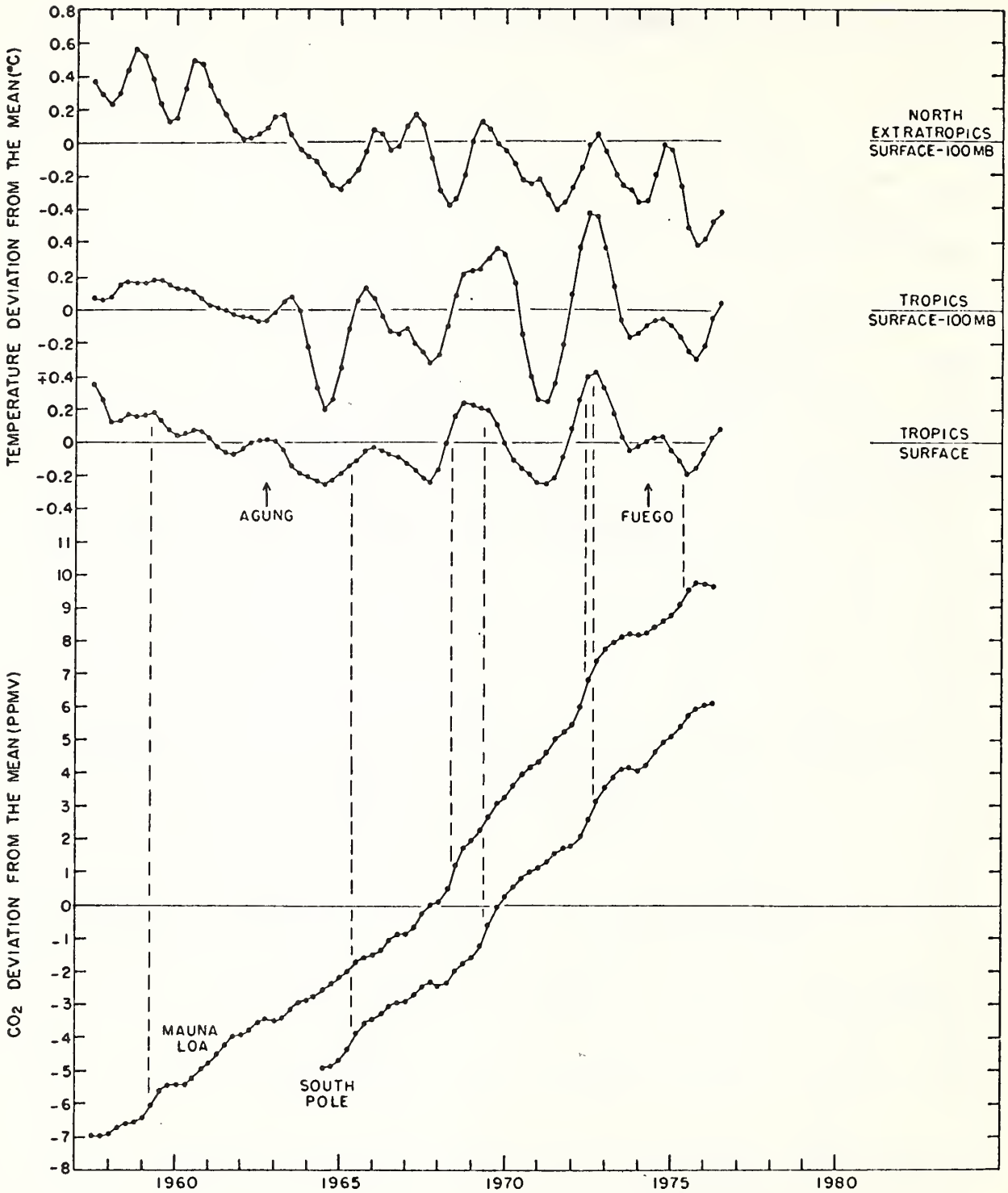

Fig. 12. Comparison of the rate of increase of carbon dioxide at Mauna Loa and the South Pole with the temperature variations in tropics and extratropics. Smoothing as in Fig. 2.

Contribution to the 1978 Climate Diagnostics Workshop

A Comparative Analysis of the 1977-78 Winter Season in the United States

Henry F. Diaz and Robert G. Quayle
National Climatic Center
Asheville, N. C. 28801

The record-setting winter of 1977-78 was unusual in a number of ways. On the temperature side, record cold weather prevailed in the Nation's midsection from the Ohio valley westward to the Central Plains. It followed on the heels of the severe winter of 1976-77 which had set many records for prolonged cold, and had produced one of the coldest months in the Nation's history (January). The occurrence of such extreme back-to-back winter seasons has had only two or three precedents in the instrumental meteorological record: 1903-04 & 1904-05; 1855-56 & 1856-57 and to a lesser degree of severity a series of cold winters from 1884-85 to 1887-88.

Several low monthly and seasonal temperature records were set in winter of 1977-78. It was the coldest February on record in six states and the second or third coldest in an additional sixteen. It was the coldest December-February period in twelve states and the second or third coldest in another eight. The January-February mean was the lowest on record in 19 states and second or third coldest in four more states.

On the precipitation side, the extreme 2-year drought in the far West was decisively broken with accumulations in some areas exceeding twice the normal seasonal precipitation amounts. The Northeast also experienced heavy precipitation, as record snowfall exceeding 40 inches in parts of southern New England occurred in February. January 1978 was one of the wettest on record in the Northeast.

Population-weighted heating degree days are commonly used as an index of fuel demand for heating purposes. Because of a westward shift of the region of largest negative anomalies, the 1977-78 heating degree day season did not exceed the 1976-77 season, finishing a close second in an 81-year period of record.

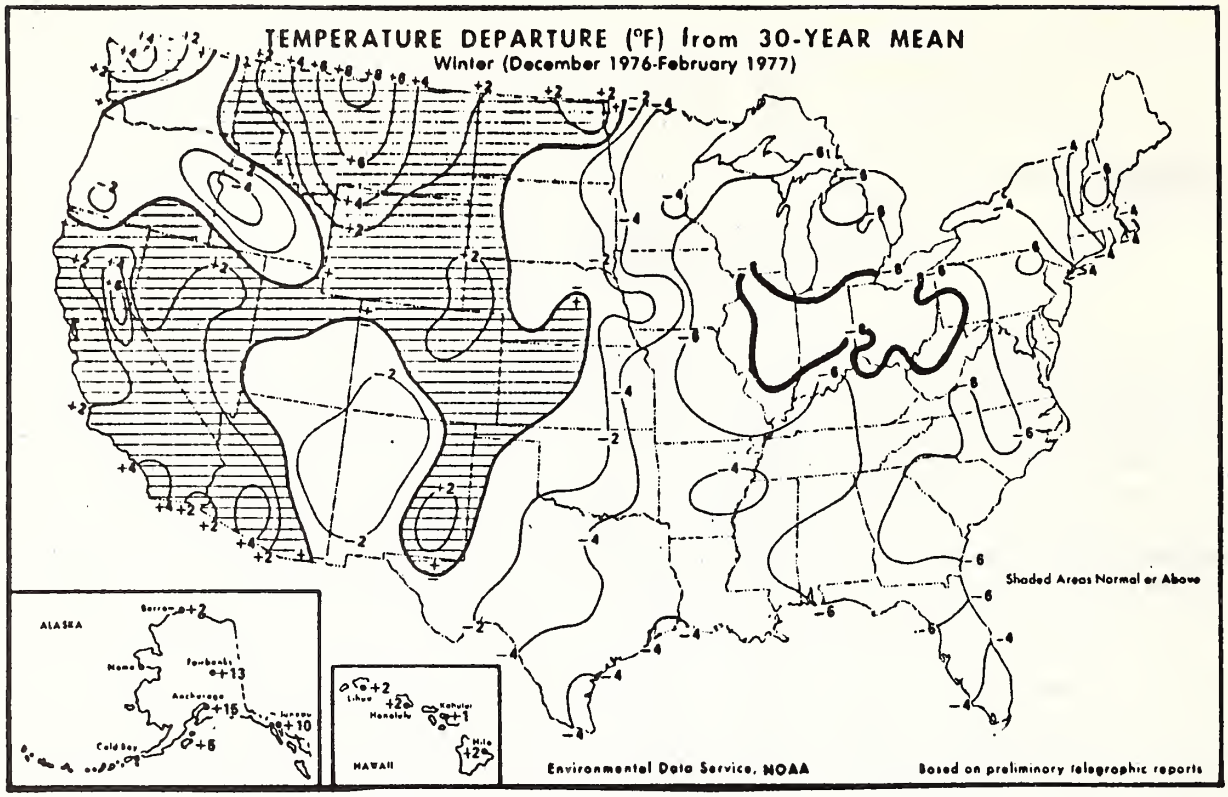

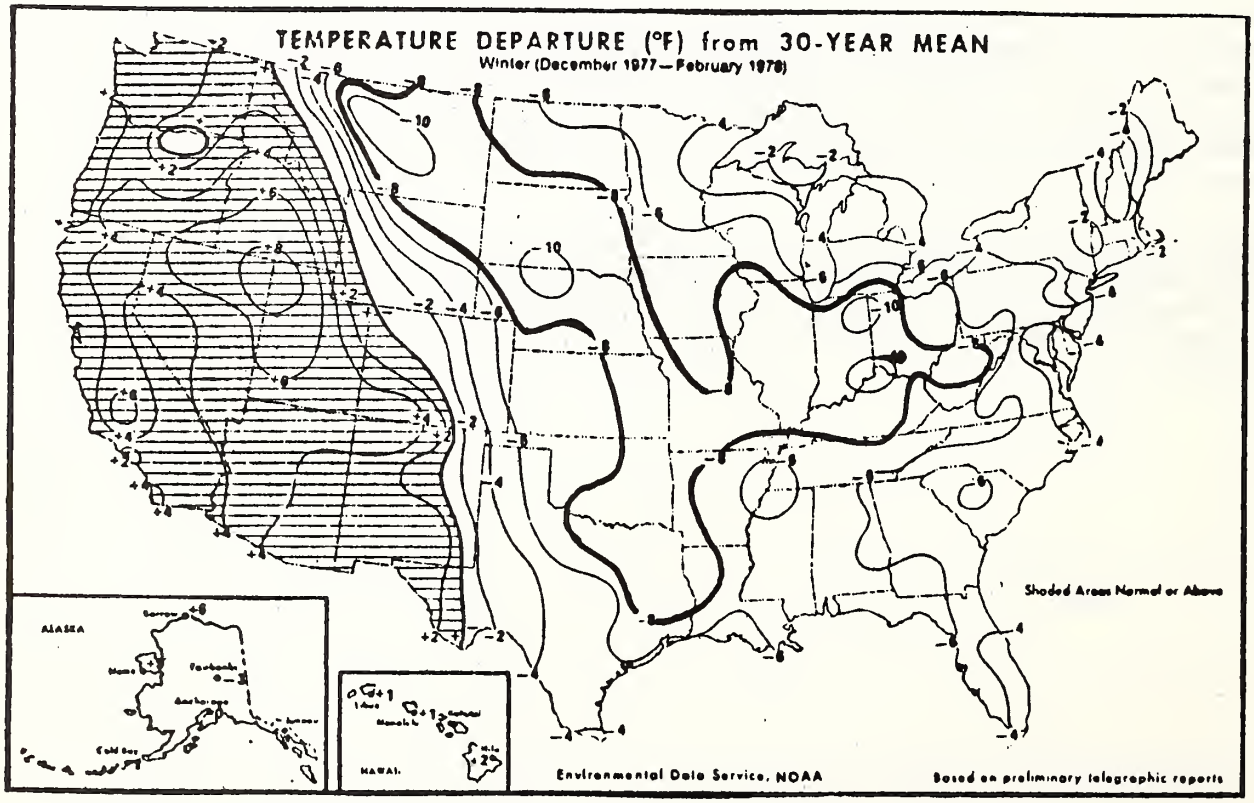

Winter temperature departure (°F) from 1941-70 normal in 1976-77 season (Top Map) and 1977-78 season.

OCTOBER-MARCH NATIONAL POPULATION-WEIGHTED HEATING DEGREE DAYS (1897-98 — 1977-78)

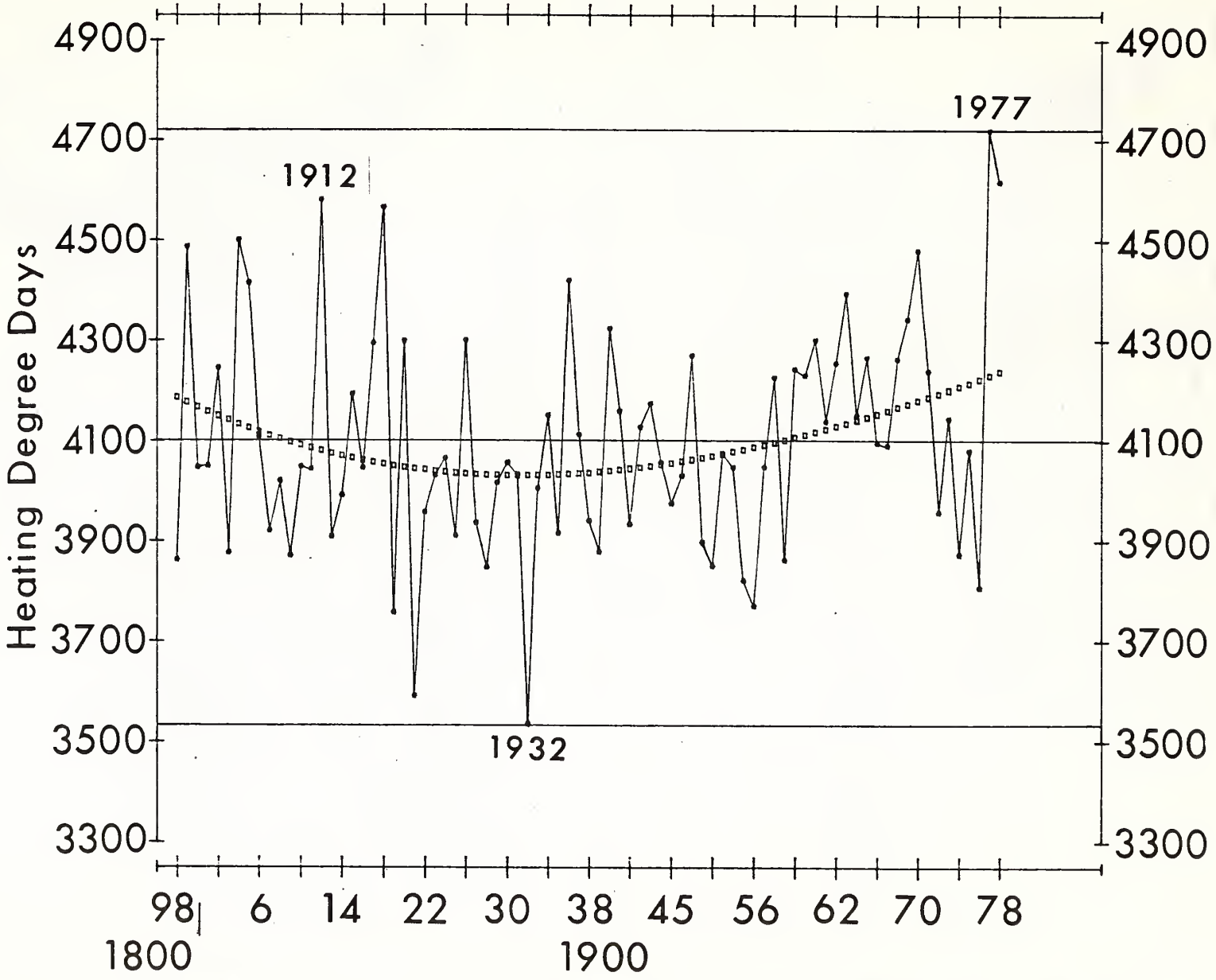

The trend line is a 3rd order polynomial least-squares fit.

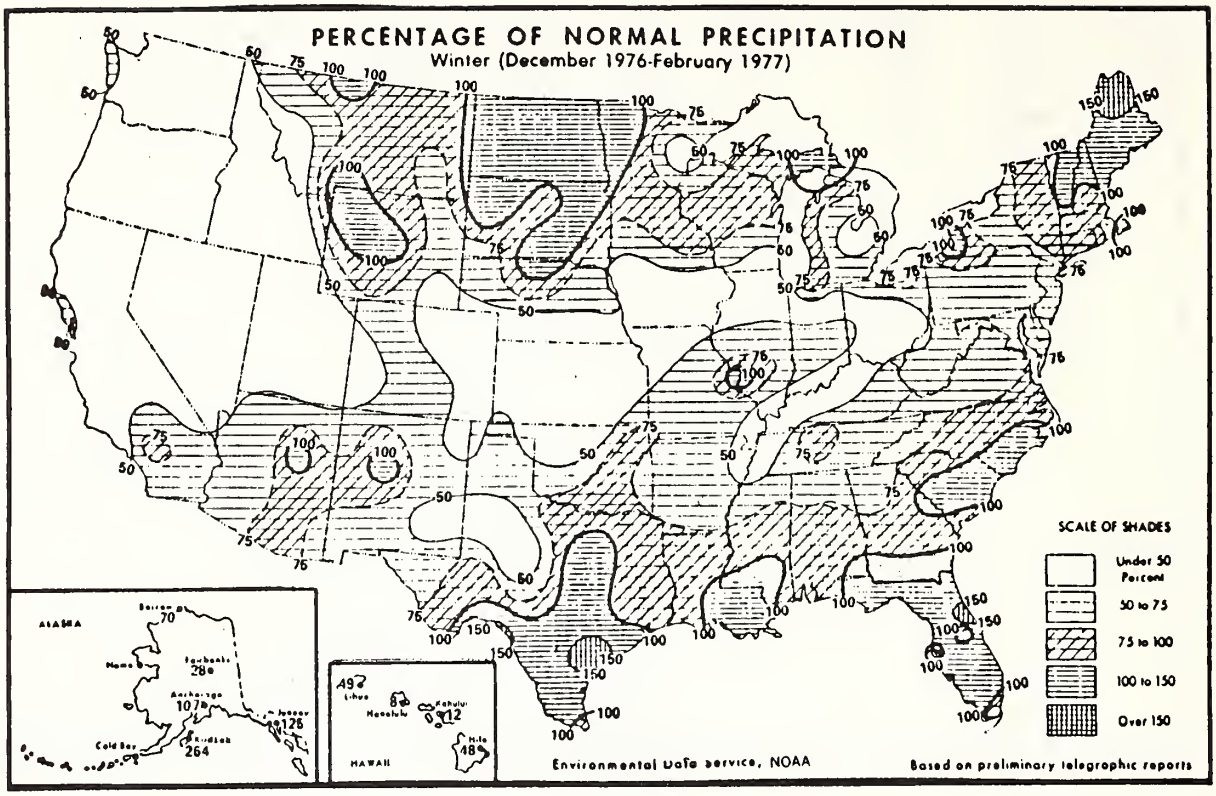

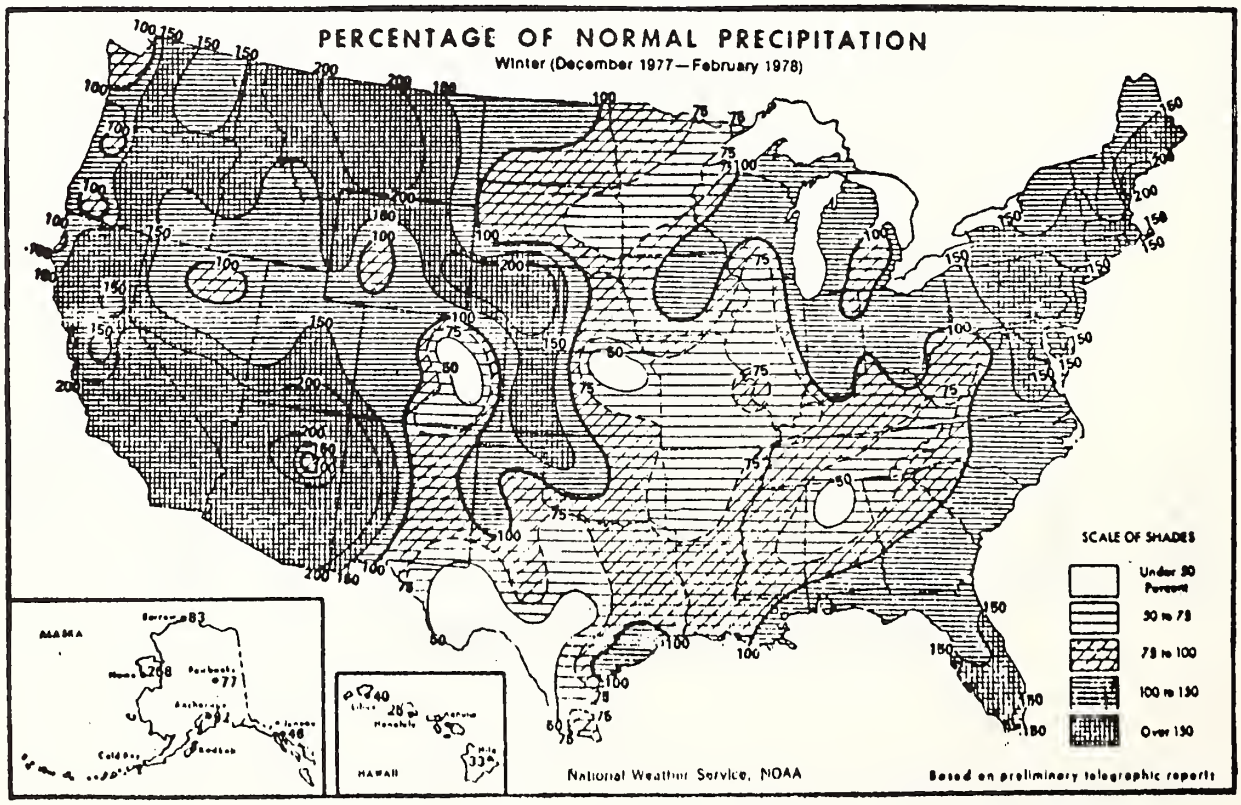

Percentage of normal winter precipation for 1976-77 season (Top Map)

and 1977-78 season

TABLE 1

	December-February Total Precipitation (inches)			Percent of Normal Precipitation (1897-1976)			October-March Total Precipitation (inches)			Percent of Normal Precipitation (1897-1976)		
STATE	1975-76	1976-77	1977-78	1975-76	1976-77	1977-78	1975-76	1976-77	1977-78	1975-76	1976-77	1977-78
CALIFORNIA	4.74	3.68	18.75	39.6	30.7	156.6	9.78	6.50	26.87	51.4	34.2	141.3
OREGON	11.40	3.37	12.67	102.5	30.3	113.8	21.00	7.70	20.73	106.1	38.9	104.7
WASHINGTON	19.71	7.02	16.04	131.7	46.9	107.1	36.12	14.50	27.79	134.1	53.8	103.2

Table 1. Areally weighted total precipitation and percent of normal (based on the 1897-1976 mean) for December-February and October-March.

TABLE 2
RANKING OF MONTHLY AND SEASONAL TEMPERATURE EXTREMES

		1977			1978			
STATE	YRS. OF REC.	JAN	DEC-FEB	JAN-FEB	JAN	FEB	DEC-FEB	JAN-FEB
AL	(95)	COLDEST				*2ND COLDEST	COLDEST	COLDEST
AR	(88)	3RD COLDEST				3RD COLDEST	COLDEST	COLDEST
CT	(83)	3RD COLDEST						
DE	(84)	2ND COLDEST				2ND COLDEST		*COLDEST
FL	(86)	2ND COLDEST	3RD COLDEST	3RD COLDEST		2ND COLDEST	COLDEST	2ND COLDEST
GA	(87)	COLDEST	COLDEST	3RD COLDEST		2ND COLDEST	2ND COLDEST	COLDEST
IL	(89)	COLDEST	2ND COLDEST	3RD COLDEST		COLDEST	COLDEST	COLDEST
IN	(92)	COLDEST	2ND COLDEST	2ND COLDEST		COLDEST	COLDEST	COLDEST
KS	(92)			2ND COLDEST		3RD COLDEST	COLDEST	COLDEST
KY	(89)	COLDEST	*2ND COLDEST	2ND COLDEST		COLDEST	COLDEST	COLDEST
LA	(87)	COLDEST				3RD COLDEST	COLDEST	COLDEST
MA	(83)	*COLDEST						
MD	(83)	2ND COLDEST				*3RD COLDEST		3RD COLDEST
MI	(91)	3RD COLDEST						
MN	(87)							
MS	(90)	2ND COLDEST	2ND COLDEST		3RD COLDEST	2ND COLDEST	COLDEST	COLDEST
MO	(90)	3RD COLDEST				3RD COLDEST	COLDEST	COLDEST
MT	(83)							
NE	(102)					*3RD COLDEST		*3RD COLDEST
NV	(89)							
NJ	(93)	COLDEST				2ND COLDEST		
NM	(86)							
NY	(88)	COLDEST	3RD COLDEST			2ND COLDEST		
NC	(91)	COLDEST	COLDEST				2ND COLDEST	
ND	(86)	COLDEST						
OH	(95)	COLDEST	COLDEST	2ND COLDEST		COLDEST	2ND COLDEST	COLDEST
OK	(86)				3RD COLDEST	3RD COLDEST	3RD COLDEST	COLDEST
PN	(90)	COLDEST	COLDEST	2ND COLDEST		2ND COLDEST	COLDEST	

STATE	YRS. OF REC.	1977 JAN	1977 DEC-FEB	1977 JAN-FEB	1978 JAN	1978 FEB	1978 DEC-FEB	1978 JAN-FEB
RI	(83)	*2ND COLDEST						
SC	(91)	COLDEST	COLDEST			*2ND COLDEST	2ND COLDEST	COLDEST
SD	(88)				2ND COLDEST		2ND COLDEST	2ND COLDEST
TN	(95)	COLDEST	2ND COLDEST	2ND COLDEST	2ND COLDEST	COLDEST	COLDEST	COLDEST
TX	(90)	3RD COLDEST			2ND COLDEST		COLDEST	COLDEST
VA	(87)	COLDEST	*3RD COLDEST	3RD COLDEST			2ND COLDEST	COLDEST
WV	(87)	COLDEST	COLDEST	2ND COLDEST		COLDEST	2ND COLDEST	COLDEST
WI	(87)	COLDEST						

*TIED WITH OTHER YEAR(S)

TABLE 3
RANKING OF MONTHLY AND SEASONAL PRECIPITATION EXTREMES

		1977				1978			
STATE	YRS. OF REC.	JAN	FEB	DEC-FEB	JAN-FEB	JAN	FEB	DEC-FEB	JAN-FEB
DE	(83)			3RD DRIEST			2ND DRIEST		
ID	(85)	DRIEST	3RD DRIEST	DRIEST	DRIEST				
IN	(91)			3RD DRIEST			3RD DRIEST		
MD	(84)				DRIEST	2ND WETTEST	3RD DRIEST		
AZ									2ND WETTEST
CA	(82)			DRIEST	3RD DRIEST				
IA	(106)			3RD DRIEST					
MT	(84)		3RD DRIEST						
NV	(90)			DRIEST					
NJ	(94)					WETTEST			
NY	(89)					WETTEST	2ND DRIEST	WETTEST	
NC	(92)					3RD WETTEST	3RD WETTEST		
OH	(96)			DRIEST	3RD DRIEST		DRIEST		
OR	(89)	DRIEST		DRIEST	2ND DRIEST				
PA	(91)			*DRIEST	*3RD DRIEST	WETTEST			
TN	(95)			3RD DRIEST			3RD DRIEST		
UT	(87)			DRIEST					
VA	(88)			3RD DRIEST	DRIEST		2ND DRIEST		
WA	(89)			DRIEST	3RD DRIEST				
WV	(88)			2ND DRIEST	DRIEST		3RD DRIEST		
WY	(87)		2ND DRIEST	2ND DRIEST					

*TIED WITH OTHER YEAR(S)

The Low Index Winter 1977-78 Vs. The High Index Winter 1975-76: A Comparison of Energetics

Robert R. Dickson
National Weather Service, NOAA

For many years it has been common to characterize the large-scale atmospheric circulation in terms of the strength of the westerlies at middle latitudes--i.e. the zonal index. A high index situation involves fast westerlies at middle latitudes and the enhanced transport of maritime air across the continents. A low index regime, on the other hand, displays weak mid-latitude westerlies, blocking ridges at high latitudes and increased meridional transport of air masses.

In the brief interval from winter 1975-76 to that of 1977-78 the atmosphere has fluctuated from a well developed high index situation to a pronounced low index pattern in the Western Hemisphere (Figures 1-3). Over the United States this has produced a change from widespread warmth in winter 1975-76 to extreme temperature contrasts--warm in the west, cold in the east--during the 1977-78 winter (Fig. 4).

The Energy Analysis Program of the National Meteorological Center (Miller et al, 1975) provides data by which the average energetics behavior of these two "opposite" types of winter can be viewed. The time variation of available energetic parameters preceding, during and following the two winters is shown in Figure 5. These quantities are integrated over the Northern Hemisphere from 1000 to 100 mb, and averaged over monthly and mid-month to mid-month periods. It should be noted at the outset that the zonal kenetic energy (K_z) of the "low index" winter, 1977-78, exceeded that of the "high index" winter 1975-76--by as much as 25% in February. Beginning in fall and continuing through most of the winter to spring, 1977-78 was a greater converter of zonal to eddy available potential energy and eddy to zonal kinetic energy (C_A and C_K) and K_Z was higher. During winter 1977-78, zonal available potential energy (A_z) remained greater despite generally stronger conversions through the energy cycle to sustain the stronger zonal flow. Factors involved in this replenishment of A_z probably included radiative effect of the late winter snow cover (Fig. 6), as well as the insolation- excluding effects of the extensive cloud cover which must have occurred at mid-latitudes.

The latitudinal distribution of vertically integrated values of the various energy parameters and the northward eddy momentum transport for February (Krueger 1978), month of peak K_z in the two winters under study, is given in Figures 7 and 8. The excess in Northern Hemisphere K_Z during winter 1977-78 (Fig. 5) is now seen to be highly concentrated in a latitudinal sense with a peak value in February 1978 more than twice that of February 1976. This concentration was supported by increased energy conversions south of 45°N latitude (Figs. 7C and D). The low latitude maximum in the

conversion from eddy to zonal kinetic energy involves an augmented eddy momentum transport out of the tropics (Fig. 8). Eddy kinetic energy in February 1978 (Fig. 7B) was concentrated just north of the K_Z max where kinetic energy was fed from the zonal flow to eddies (negative CK, Fig. 7D). In contrast, in February 1976, utilization of available potential energy was displaced northward and momentum transport out of the tropics and the associated contribution to zonal kinetic energy were reduced.

Thus the low index winter is seen as one with a concentration of zonal kinetic energy at relatively low latitudes due to the cooperative effect of a southward displaced mid-latitude baroclinic zone and accompanying energy conversions together with the enhanced export of kinetic energy from the tropics. The two events, futhermore, are not independent. An initial substantial displacement of the winter mid-latitude westerlies south of normal at appropriate longitudes brings westerly troughs into the tropics. As pointed out by Riehl (1969) such troughs in the upper troposphere are a significant means for momentum transport out of the tropics with maximum transport possible at those longitudes where,jointly, the subtropical jet stream reaches fartherest north and the polar troughs intrude fartherest south--i.e. near the east coasts of Asia and North America and, to a lesser extent, over the Near East. Reference to the mean 700 mb height maps for the two winters (Figs. 2 and 3) reveals an increased opportunity for such interactions in the low index winter of 1977-78 and a diminished opportunity, in the high index winter of 1975-76.

REFERENCES

Krueger, A.F. Personal communication, August 1978.

Miller, A.J., W. Collins and D. Dubofski, 1975: The NMC Operational Global Energy Program, National Meteorological Center, Office Note 109, 16 pp.

Riehl, H., 1969: On the Role of the Tropics in the General Circulation of the Atmosphere, Weather, 24, 288-308.

LEGEND TO FIGURES

Fig. 1 700 mb mean geostrophic wind speed profiles for the Western Hemisphere during the winters of 1975-76 and 1977-78.

Fig. 2 Mean 700 mb height (dam) and DN (m) for winter 1975-76.

Fig. 3 Mean 700 mb height (dam) and DN (m) for winter 1977-78.

Fig. 4 Mean surface air temperature DN categories for winters of 1975-76 and 1977-78.

Fig. 5 Time variation of monthly (and mid-month to mid-month) mean values of energetics parameters for the Northern Hemisphere, 1000 to 100 mb, for portions of 1975-76 and 1977-78.

Fig. 6 Snow and ice boundaries for February 9-15, 1976 and February 13-19, 1978.

Fig. 7 Latitudinal profiles of February mean values of vertically integrated energetics parameters, 1000 to 50 mb, for 1976 and 1978.

Fig. 8 Latitudinal profiles of vertically integrated northward transport of eddy angular momentum, 1000 to 50 mb, for February 1976 and 1978.

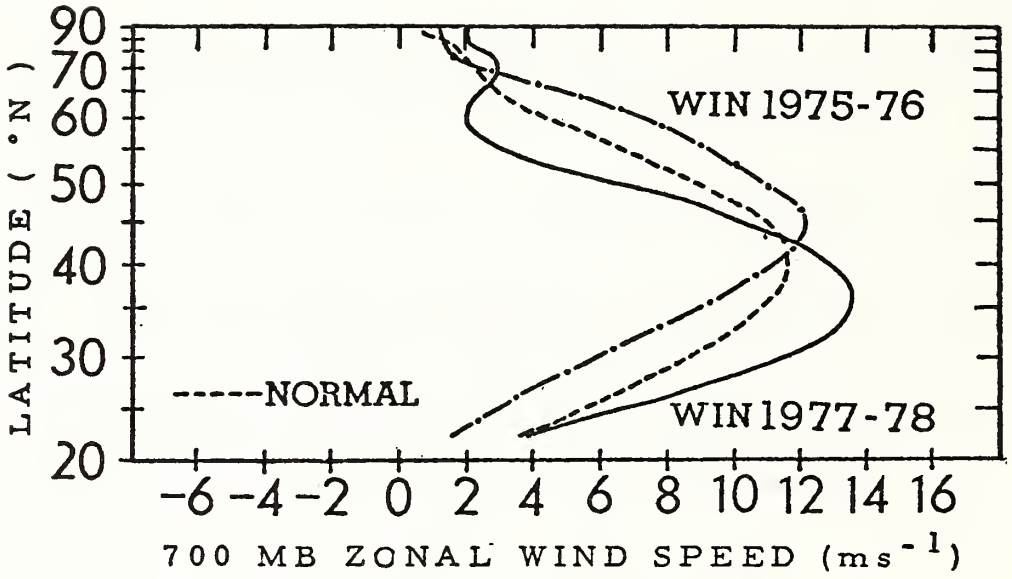

Fig. 1 700 mb mean geostrophic wind speed profiles for the Western Hemisphere during the winters of 1975-76 and 1977-78.

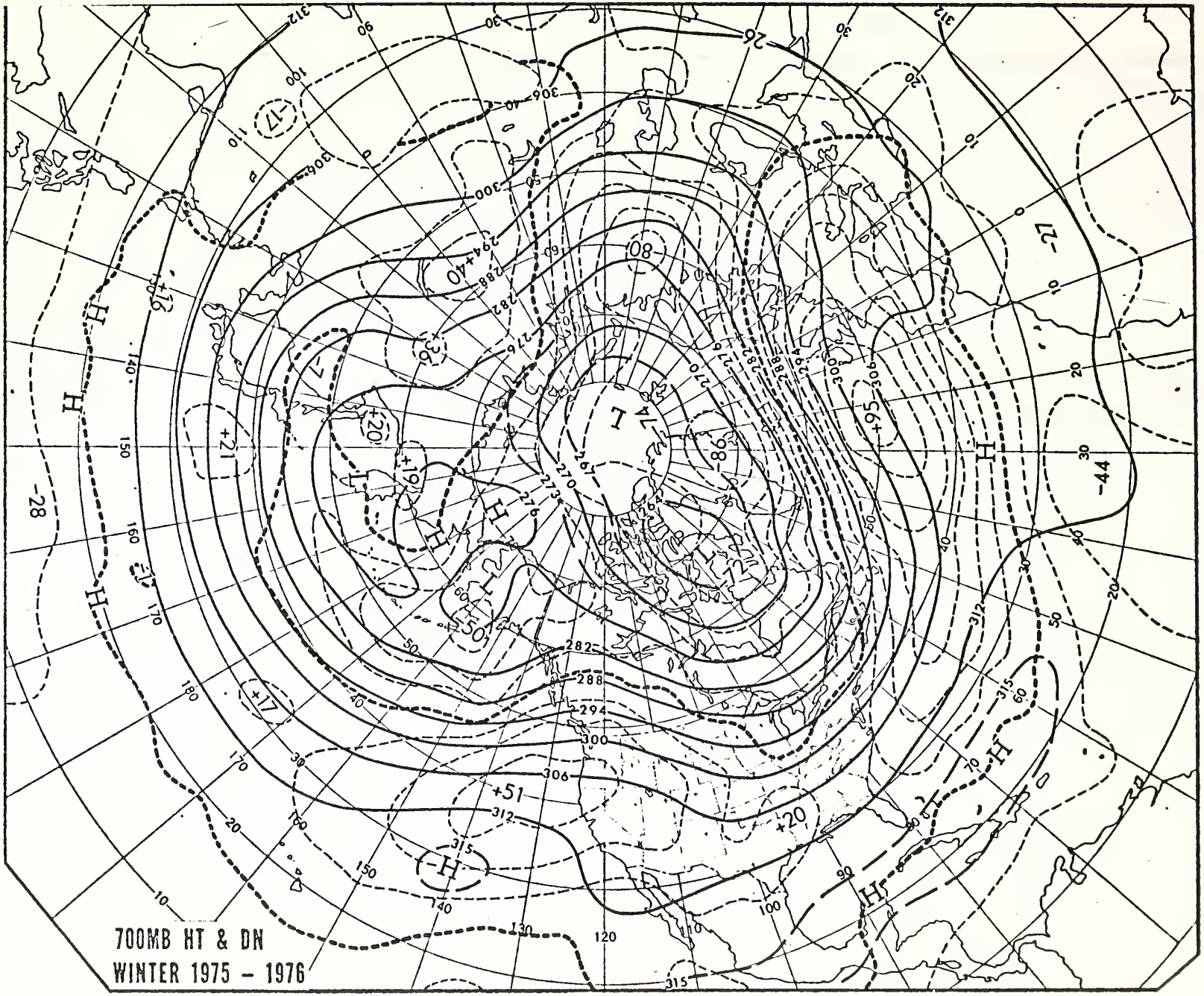

Fig. 2 Mean 700 mb height (dam) and DN (m) for winter 1975-76.

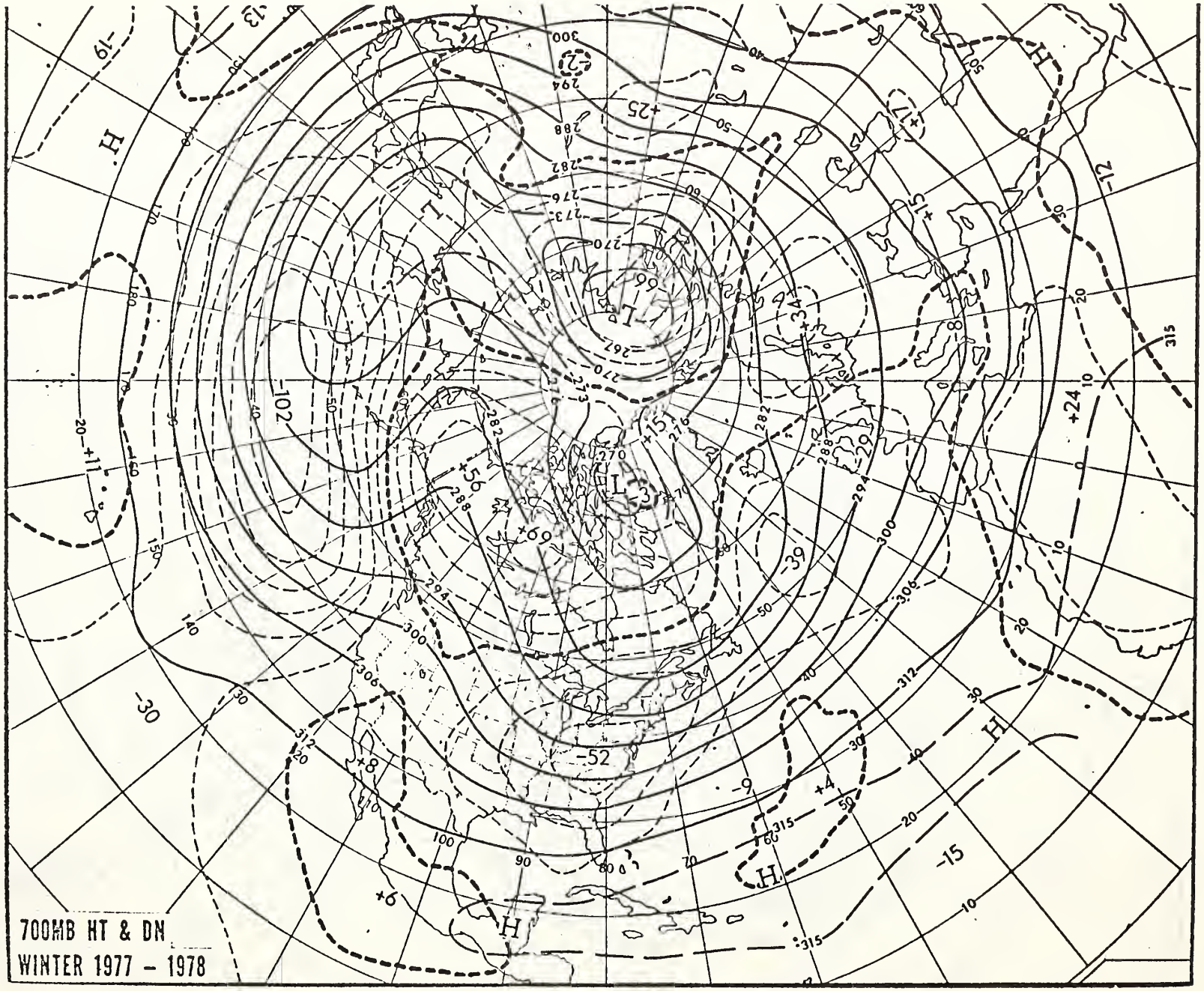

Fig. 3 Mean 700 mb height (dam) and DN (m) for winter 1977-78.

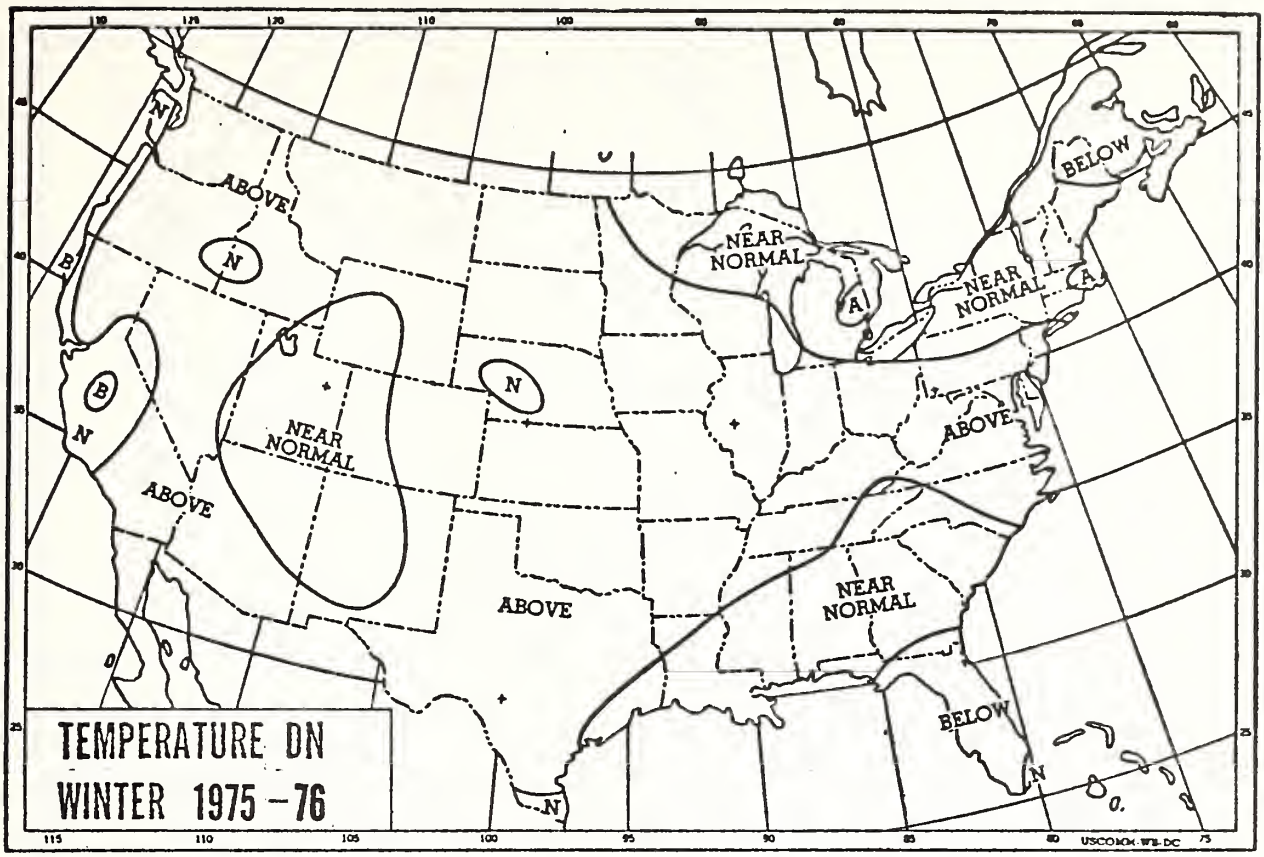

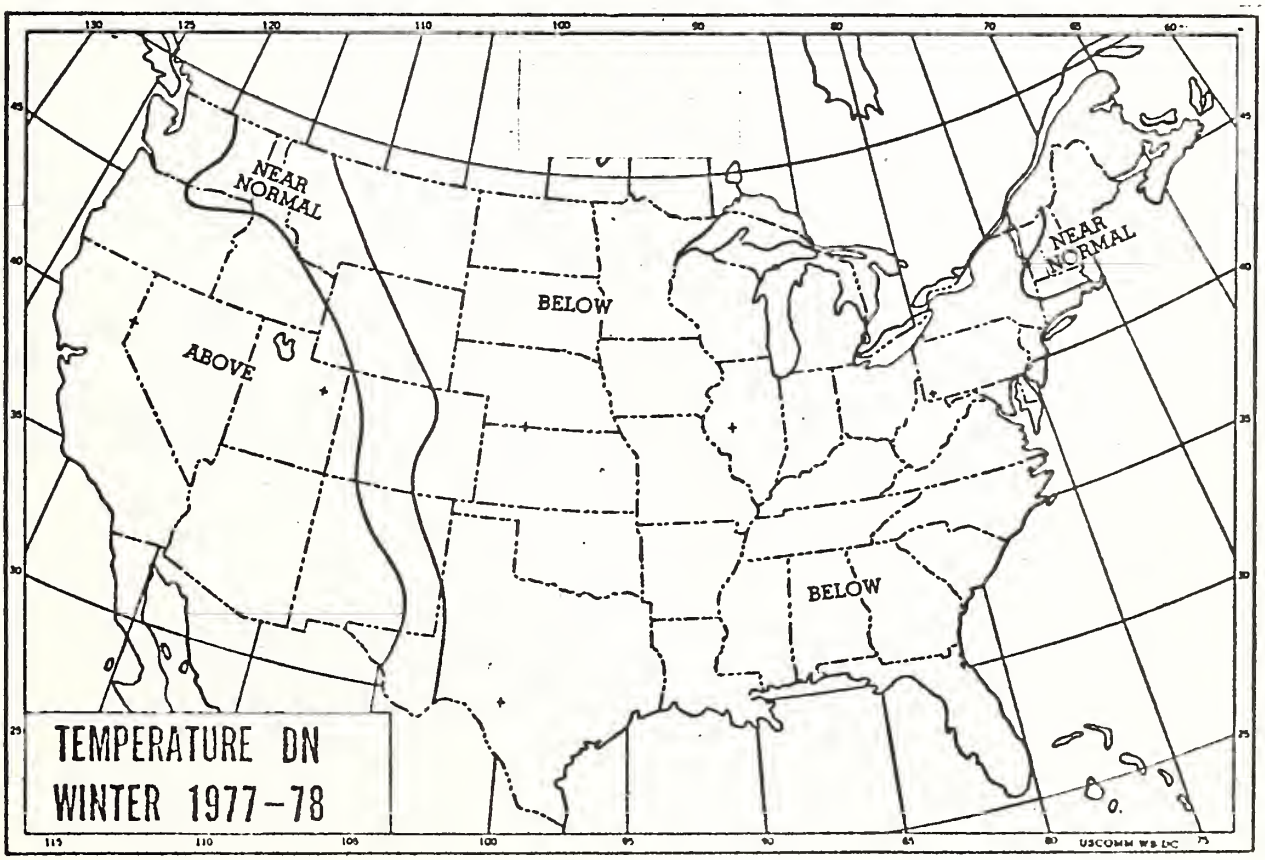

Fig. 4 Mean surface air temperature DN categories for winters of 1975-76 and 1977-78.

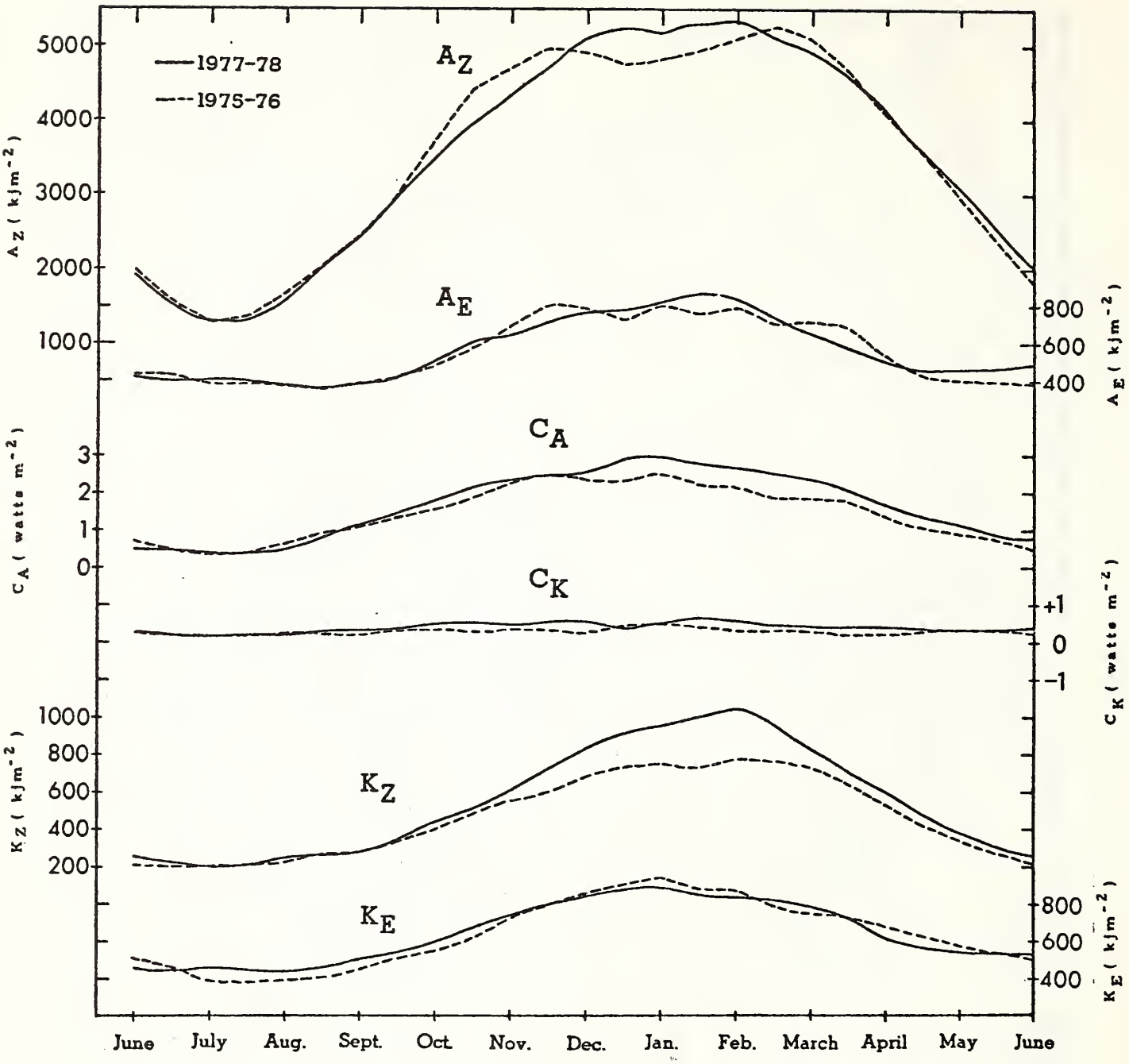

Fig. 5 Time variation of monthly (and mid-month to mid-month) mean values of energetics parameters for the Northern Hemisphere, 1000 to 100 mb, for portions of 1975-76 and 1977-78.

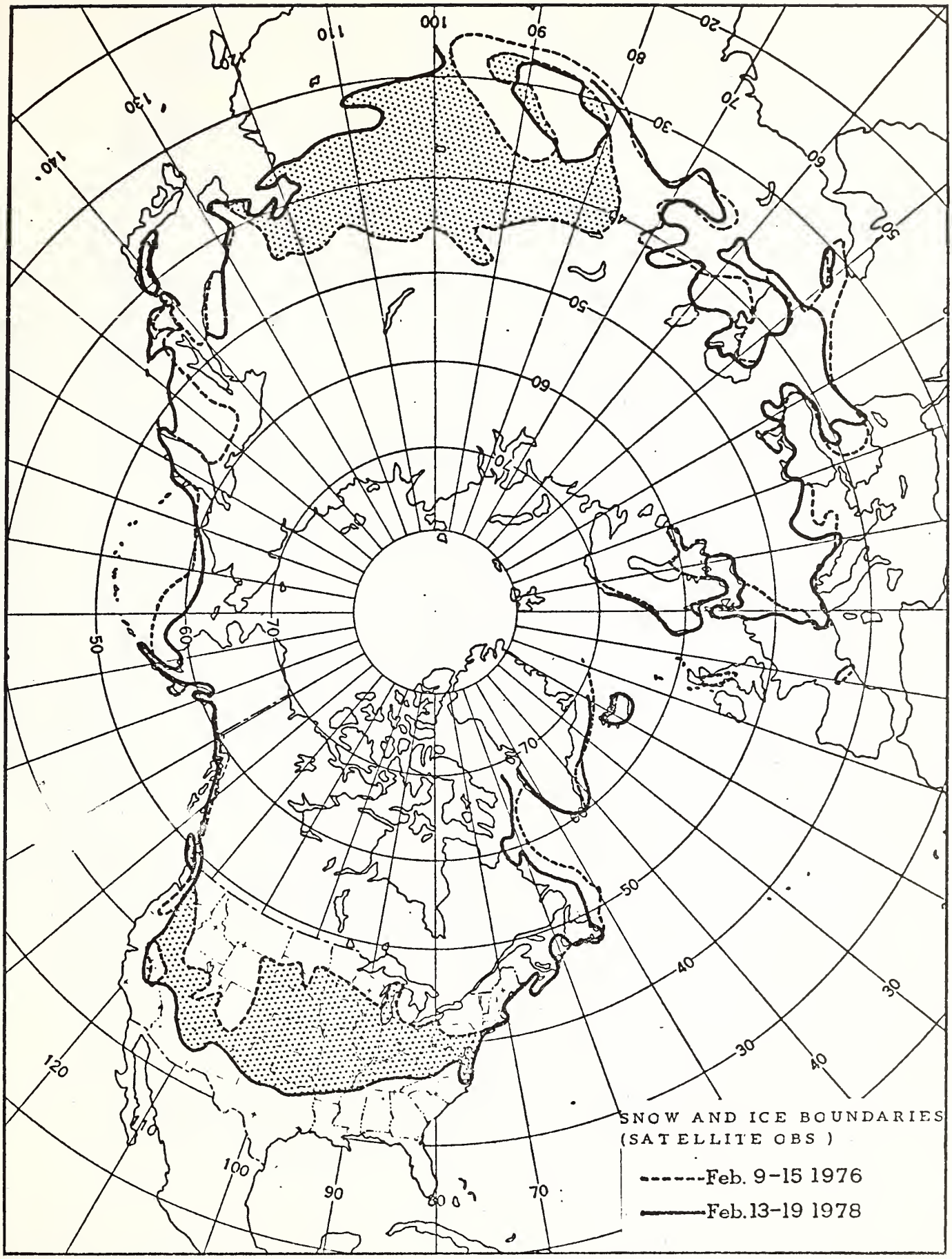

Fig. 6 Snow and ice boundaries for February 9-15, 1976 and February 13-19, 1978.

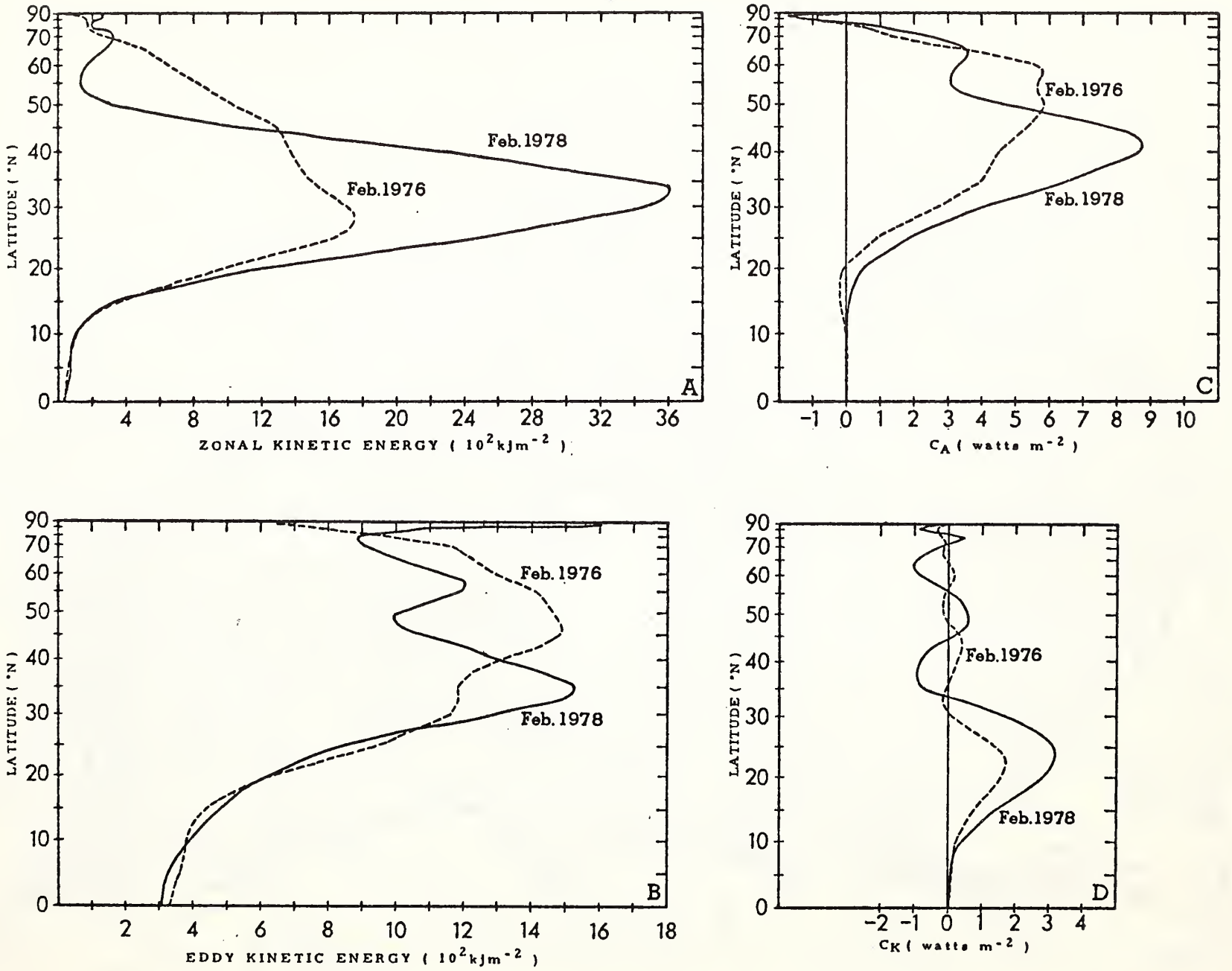

Fig. 7 Latitudinal profiles of February mean values of vertically integrated energetics parameters, 1000 to 50 mb, for 1976 and 1978.

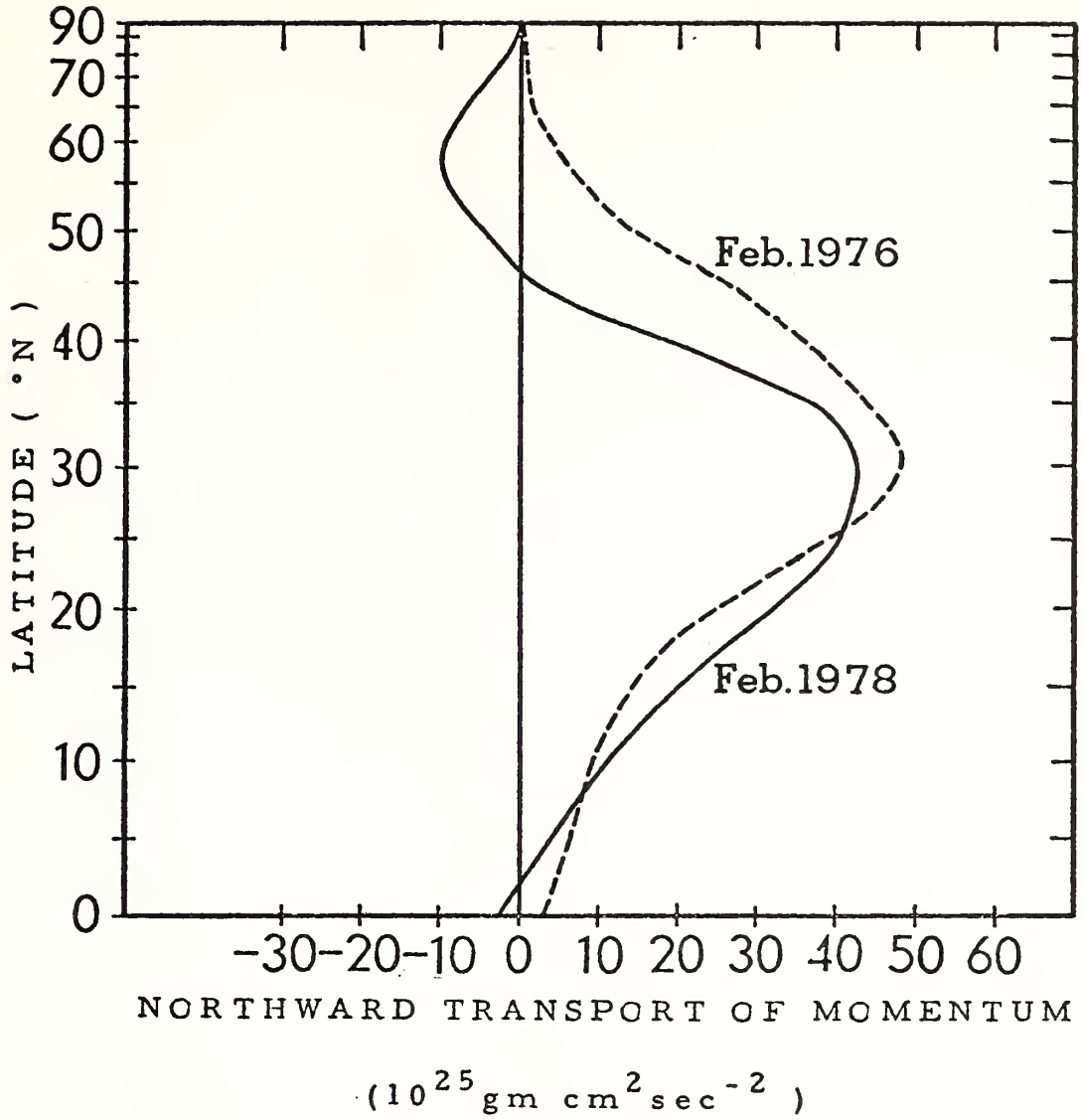

Fig. 8 Latitudinal profiles of vertically integrated northward transport of eddy angular momentum, 1000 to 50 mb, for February 1976 and 1978.

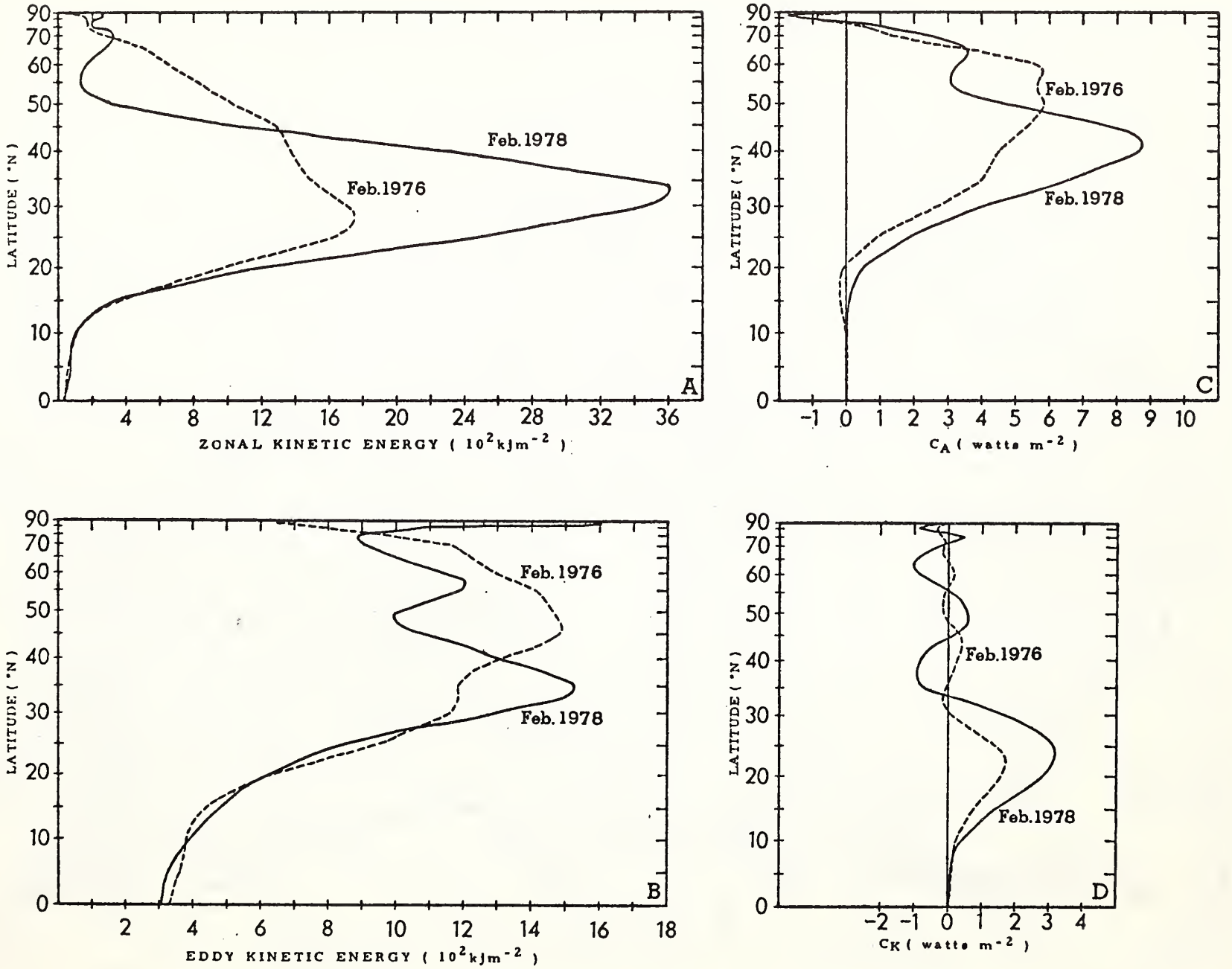

Fig. 7 Latitudinal profiles of February mean values of vertically integrated energetics parameters, 1000 to 50 mb, for 1976 and 1978.

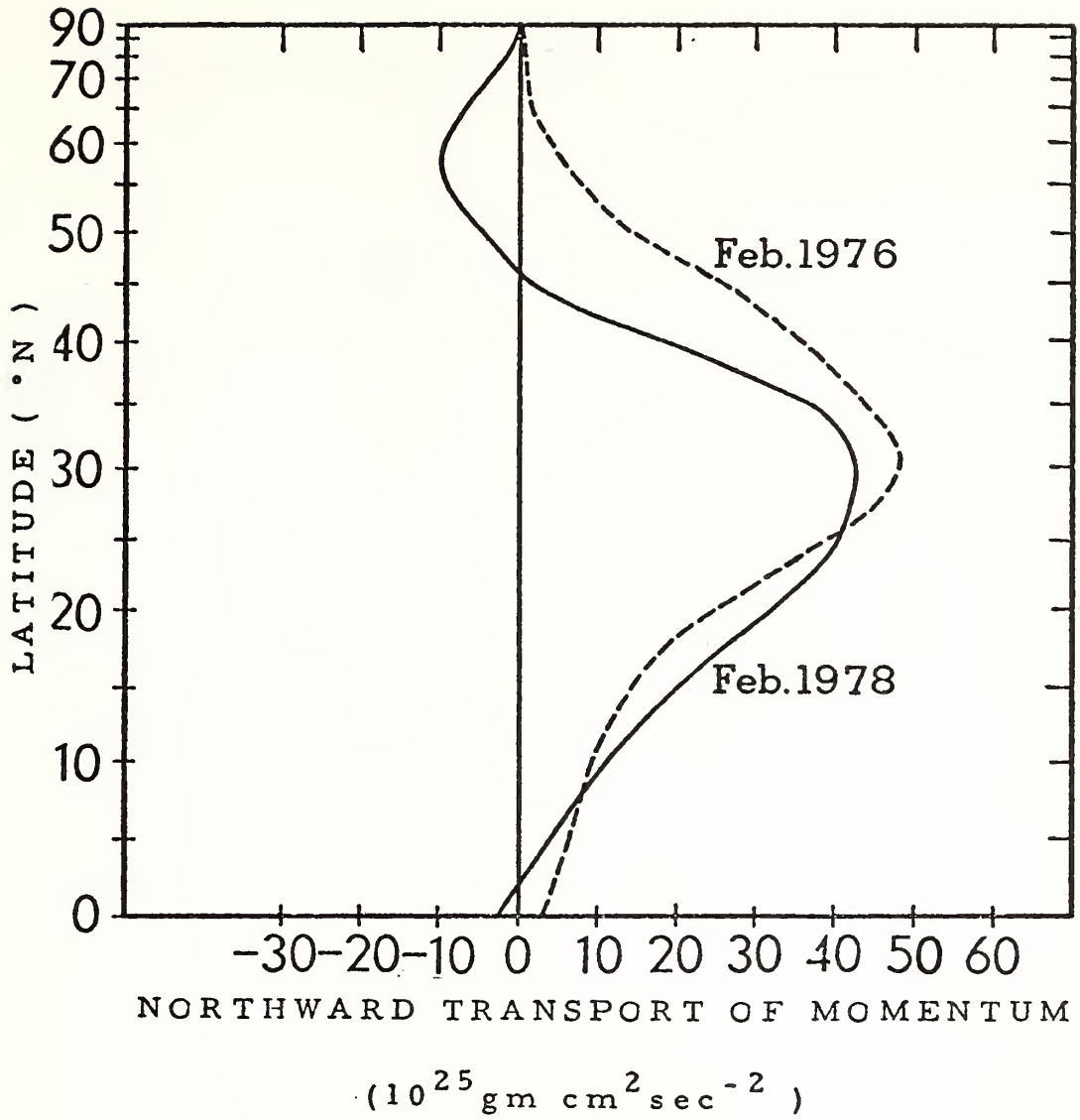

Fig. 8 Latitudinal profiles of vertically integrated northward transport of eddy angular momentum, 1000 to 50 mb, for February 1976 and 1978.

A HEMISPHERIC VIEW OF THE TROPOSPHERE AND STRATOSPHERE DURING THE WINTERS 1975-76, 1976-77, AND 1977-78

R. S. Quiroz

National Meteorological Center, NOAA, Washington, D.C. 20233

ABSTRACT

Zonal averages of temperature, height, and mean zonal wind are portrayed for selected altitudes and latitudes of the stratosphere and troposphere for the last 3 winters. From these data the following findings are presented: (1) Coupling in the stratospheric thermal fields at low and high latitudes was strongest in 1976-77, with a negative correlation of 0.92 between low- and high-latitude oscillations. (2) Coupling in the tropospheric thermal fields in middle and high latitudes, as indicated by 100-mb height data, was also strongest in 1976-77. (3) Tropospheric jet stream and stratospheric polar night jet strengths were inversely related in the 3 winters, with a delay of maximum winds in the troposphere (minimum winds in the stratosphere) from January in 1976-77 to February in 1977-78. (4) In 1976-77 and 1977-78, strong high-latitude stratospheric warmings were succeeded by polar tropospheric warming and mid-latitude tropospheric cooling, with a delay of about one month in these occurrences in winter 1977-78 relative to 1976-77. The negative temperature anomaly defined by 40^{o}N zonal mean temperatures (compared to normal) and integrated over the periods of significant cooling in December-February is about two-thirds as great in 1977-78 as in 1976-77. No physical interpretation of these results is attempted here; it is meanwhile evident that meriodional heat transports were important in both the troposphere and stratosphere.

"1978 Break in the West Coast Drought"

Jerome Namias

Scripps Institution of Oceanography
La Jolla, California 92093

This paper describes how two years of back-to-back drought in California and the Far West, during the winters of 1976 and 1977, abruptly changed to an anomalously wet winter in 1978. After first describing some of the conditions of the general circulation and the sea-surface temperatures preceding and during the 1977 drought, the differing patterns antecedent and during the winter of 1978 are detailed.

These differences were largely associated with a strong low latitude westerly flow pattern in 1978 in contrast to a strong meridional ridge in the preceding year, and also a different SST anomaly distribution. These striking differences began to show up as early as September 1977 over much of the Northern Hemisphere as well as over the North Pacific. Specifications and predictions of upper level heights from sea-surface temperatures strongly indicate the break in the drought regime, and many charts are shown objectively relating precipitation to pressure patterns and to teleconnections.

Some physical explanations of the above material are offered.

"1978 BREAK IN THE WEST COAST DROUGHT"

CLIMATE DIAGNOSTICS WORKSHOP - OCTOBER 31 - NOVEMBER 2, 1978

MIAMI, FLORIDA

JEROME NAMIAS

LEGENDS TO FIGURES

Fig. 1 Percentage of normal precipitation over the West for the past three winters.

Fig. 2 700 mb height and departures (Broken Lines) from the long term mean for Winter 1977.

Fig. 3 Sea level pressure and anomalies (Broken) in mb for Winter 1977.

Fig. 4 700 mb mean height patterns for the Winters of 1977 and 1978.

Fig. 5 700 mb height anomalies and sea-surface temperature (SST) anomalies (Shaded) for the Winters of 1977 and 1978. Slant shading indicates Below Normal Temperatures, Stippling—Above Normal.

Fig. 6 700 mb height and standardized anomalies for the Winter 1977-78.

Fig. 7 Mean sea-level pressure for January, 1978.

Fig. 8 Correlations between precipitation in the North,Central and Southern California Water Sheds (Boxes) and the mean sea-level pressure elsewhere. Correlations are for 26 years of data.

Fig. 9 Sea-surface temperature anomalies for the Septembers of 1976 and 1977.

Fig. 10 Sea-surface temperature anomalies for the Falls of 1976 and 1977.

Fig. 11 700 mb height and standardized departures from normal for Sept., 1977.

Fig. 12 700 mb height standardized anomalies for the Falls of 1976 & 1977.

Fig. 13 Winter 1978 700 mb anomalies specified from the contemporary sea-surface temperature anomalies.

Fig. 14 Predicted 700 mb anomalies for the 1977-78 Winter made at the end of the preceding Sept., Oct., and November.

Fig. 15 700 mb height and anomalies for the Winter of 1977-78 predicted assuming that the standardized anomalies of Fall 1977 are conserved.

LEGENDS TO FIGURES

J. Namias

Fig. 16 Winter teleconnections (cross correlations) of 700 mb anomalies from a center at 40°N-140°W.

Fig. 17 Winter teleconnections of 700 mb anomalies from a center at 65°N-115°W.

Fig. 18 Winter teleconnections of 700 mb anomalies from a center at 45°N-125°W.

PERCENTAGE OF NORMAL PRECIPITATION

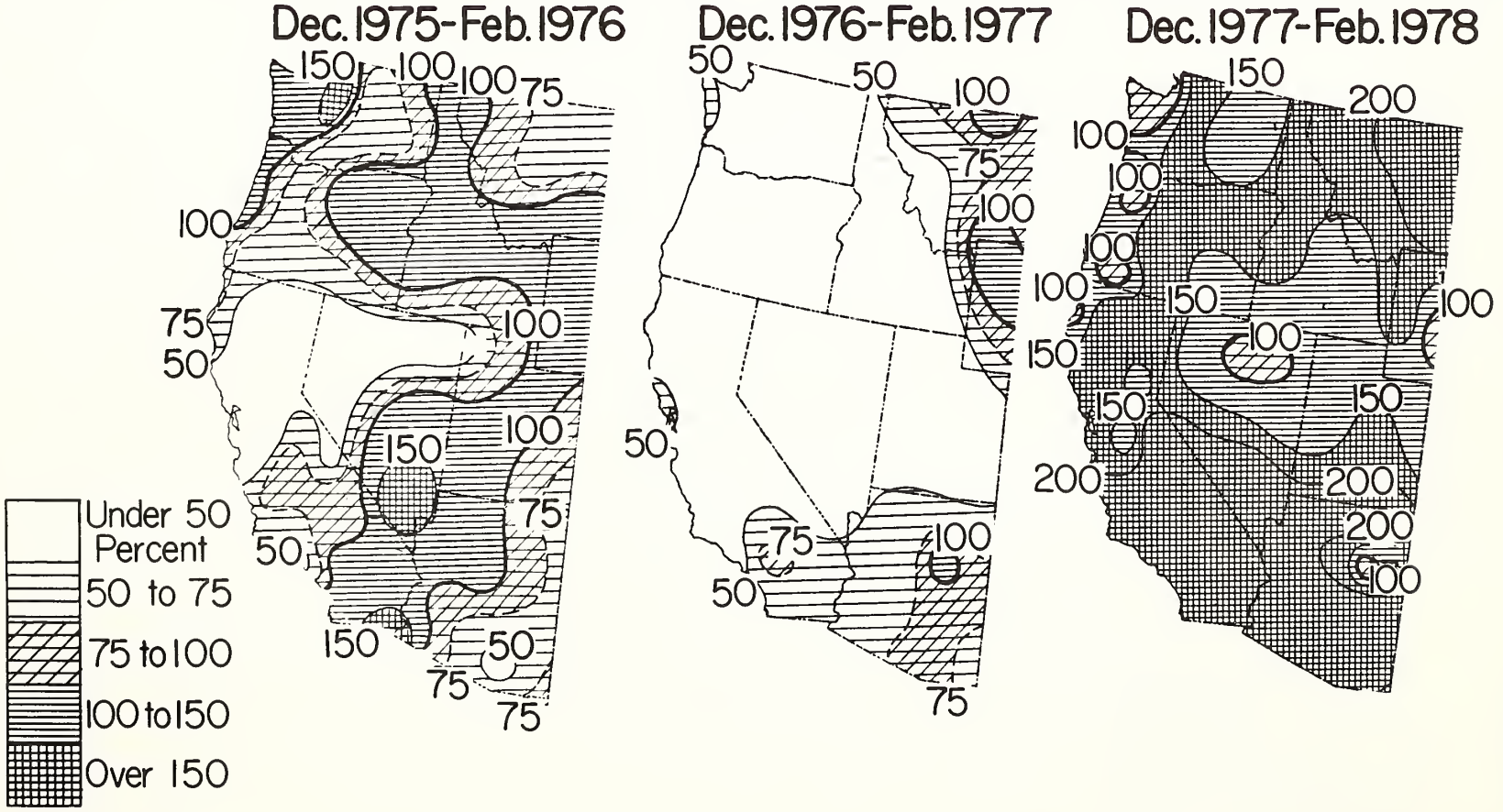

700 mb HT and DM
WINTER 1977
(tens of feet)

SLP and DM
WINTER 1977

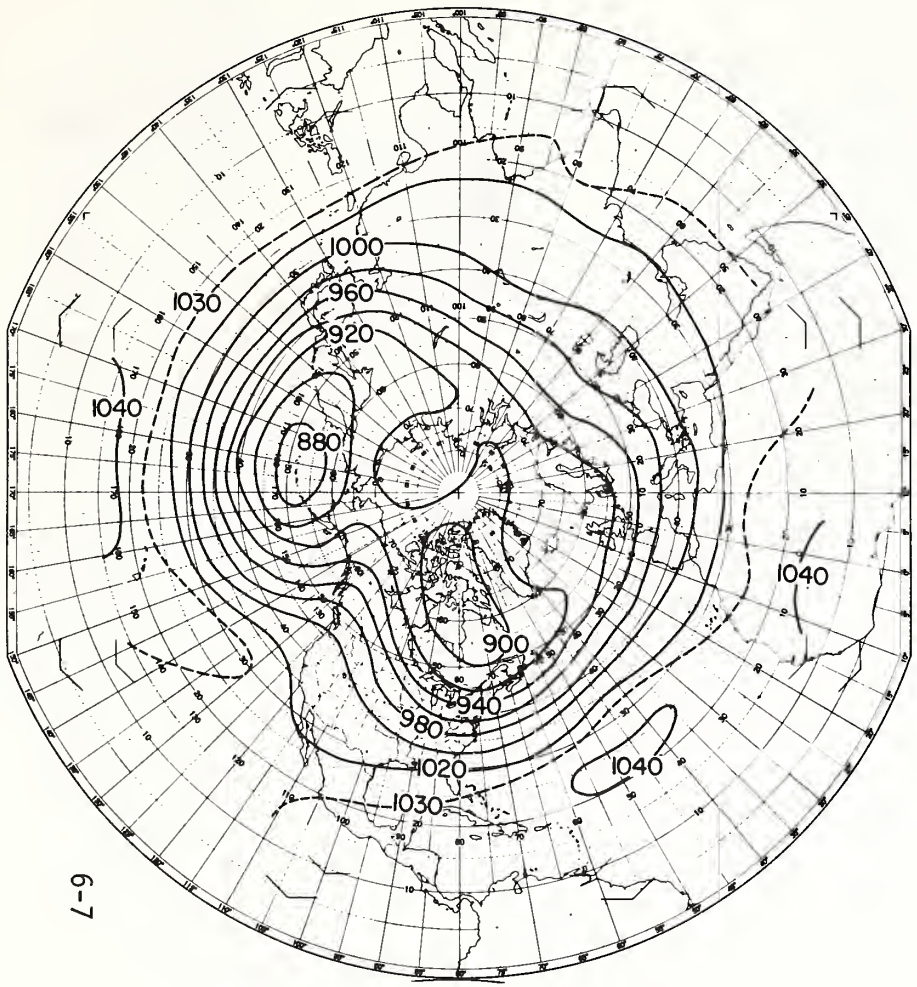

700mb HEIGHT WINTER 1977
(TENS OF FEET)

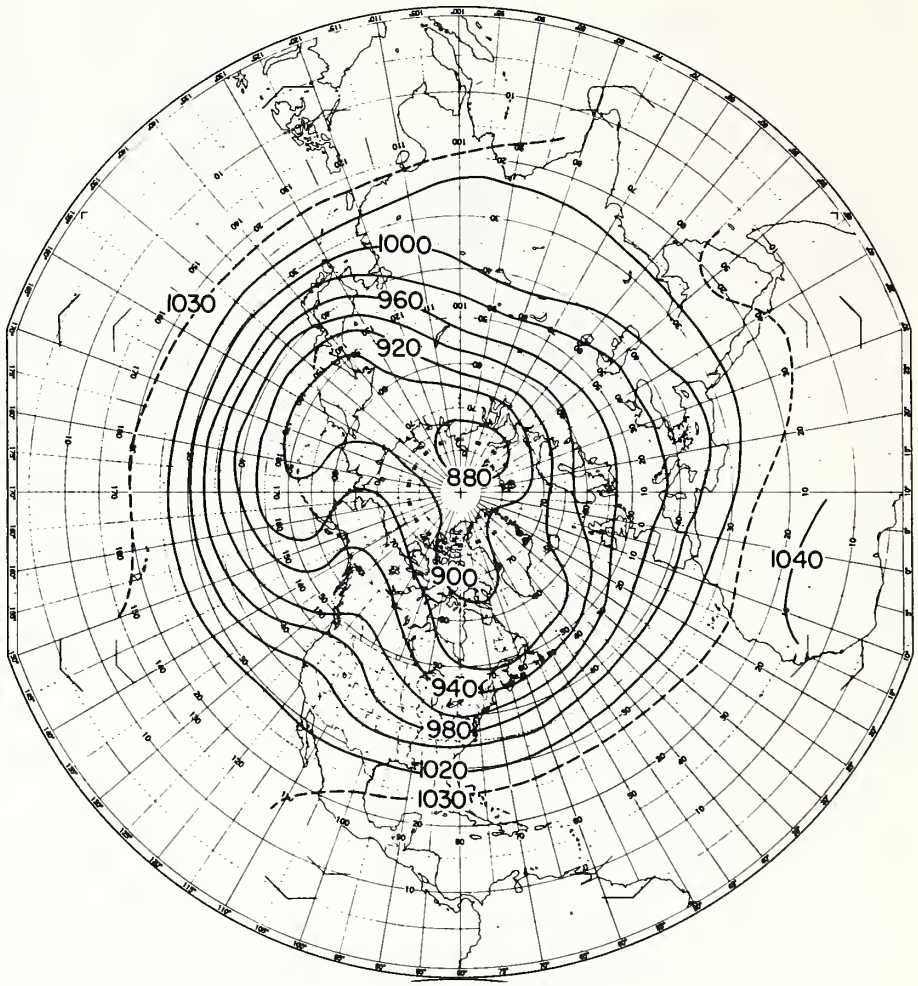

700mb HEIGHT WINTER 1978
(TENS OF FEET)

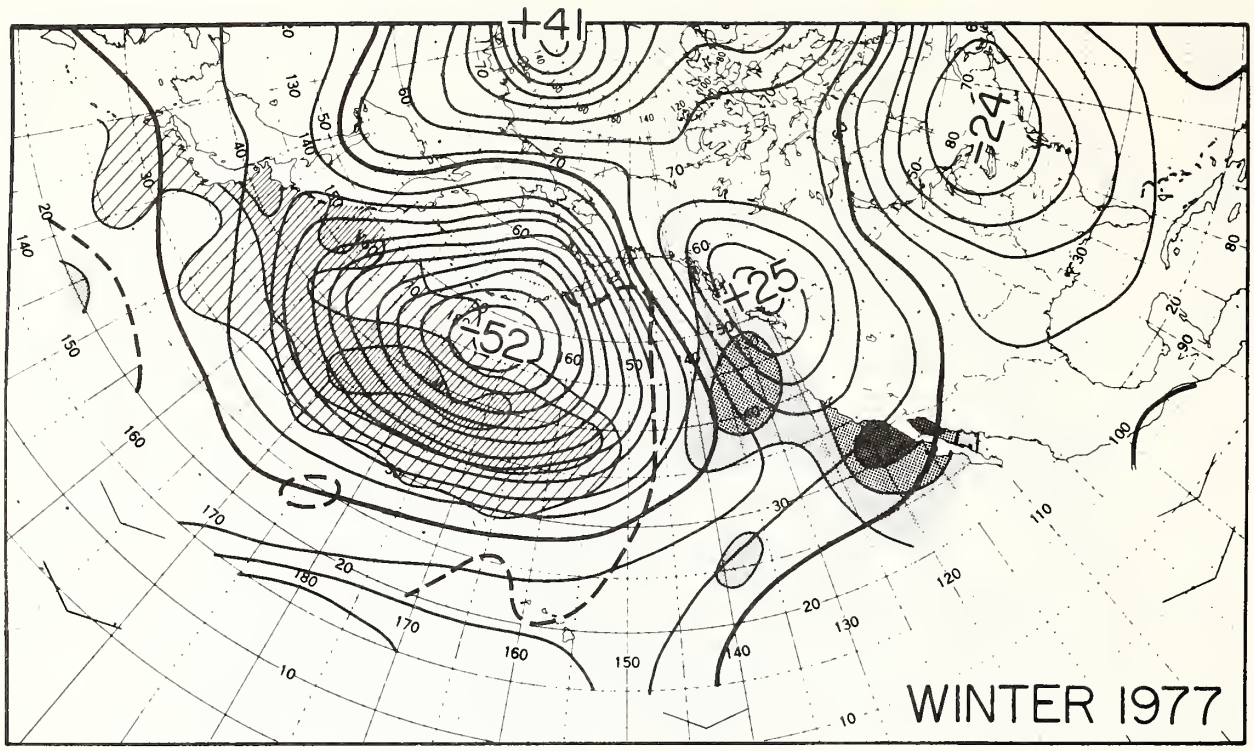

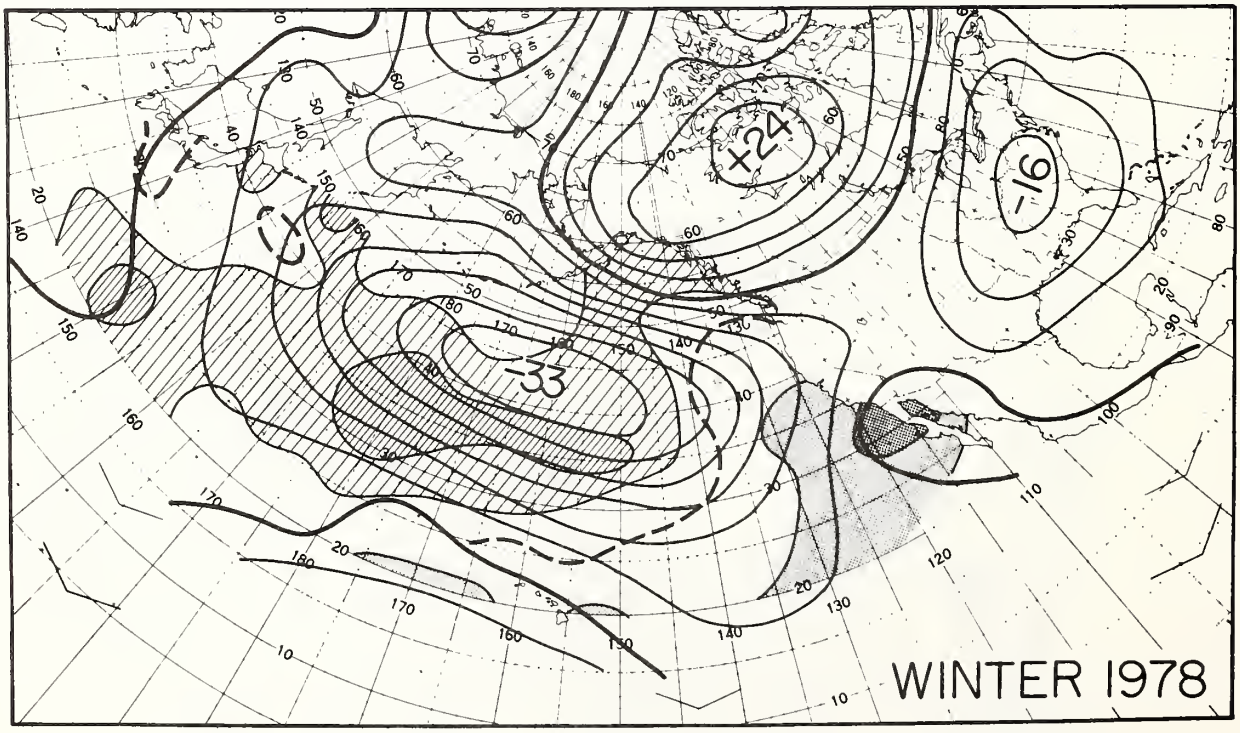

700 mb HT_{DM} ANALYZED TO 50 ft.)
SST_{DM} (ANALYZED TO 1°F)

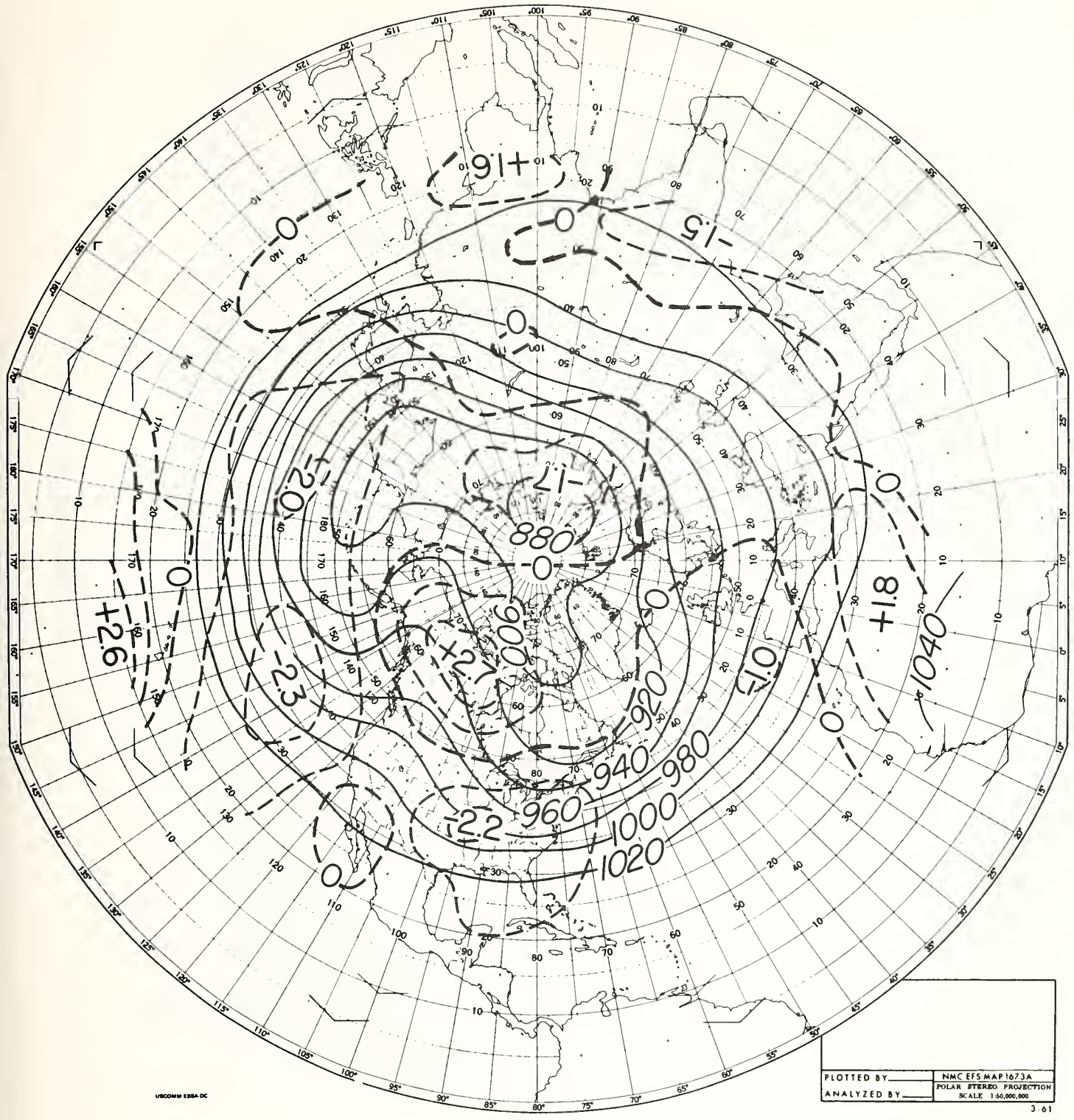

700mb HT. & DM/σ, WINTER 1977-'78

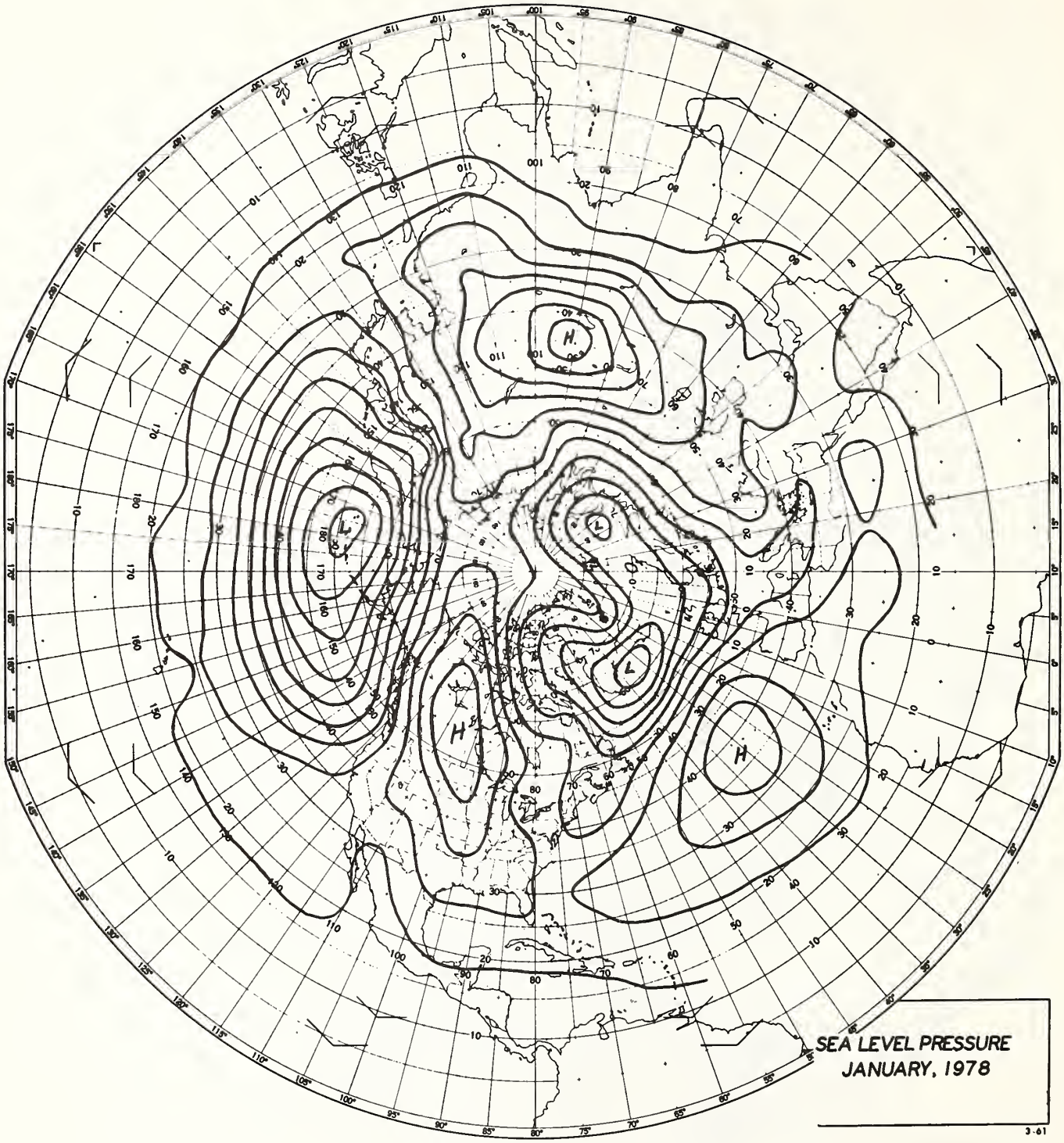
SEA LEVEL PRESSURE
JANUARY, 1978
3-61

DECEMBER, r PRECIPITATION vs. SLP

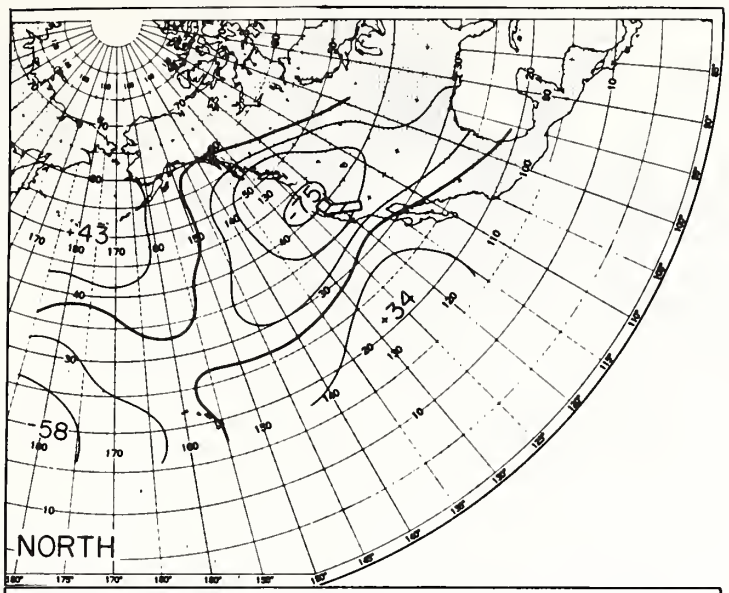

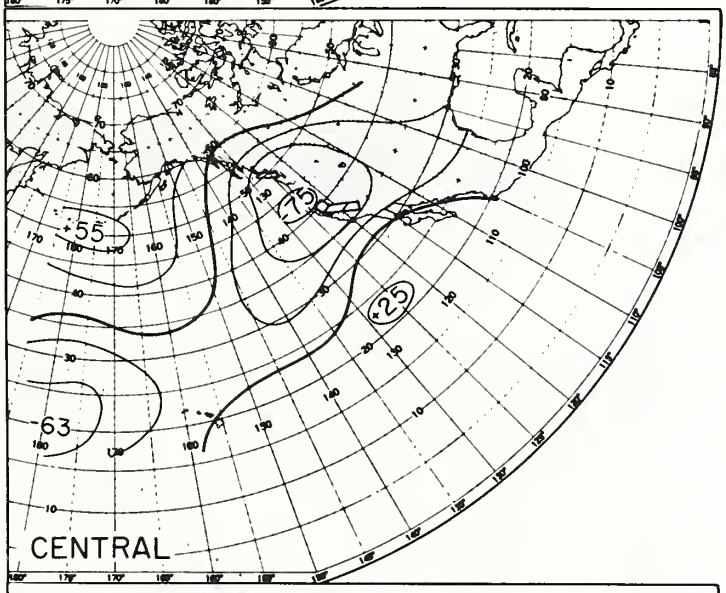

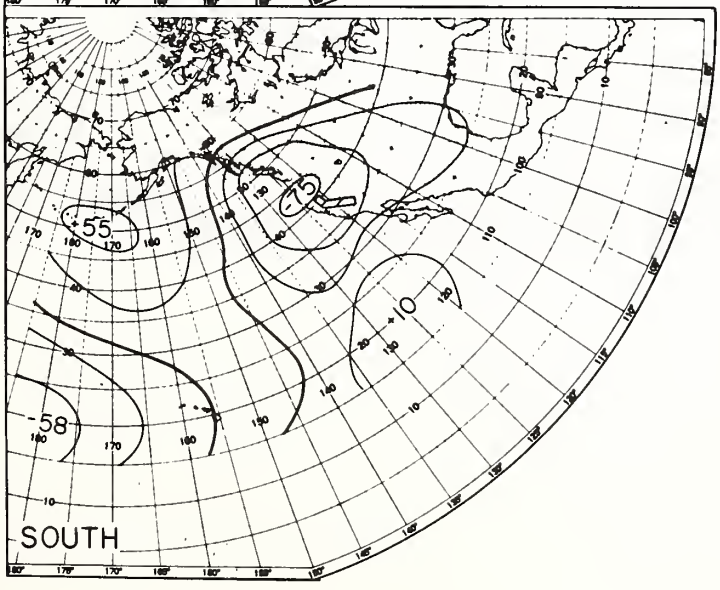

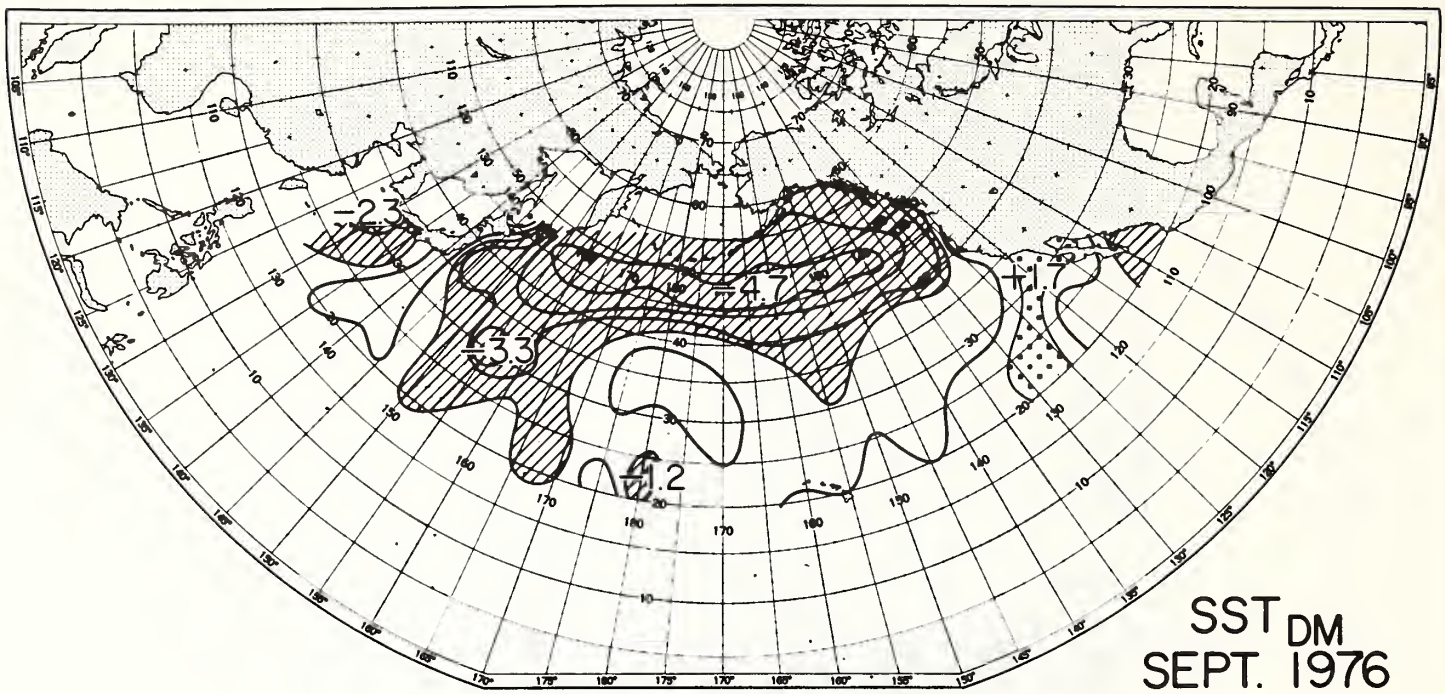

SST_{DM}
SEPT. 1976

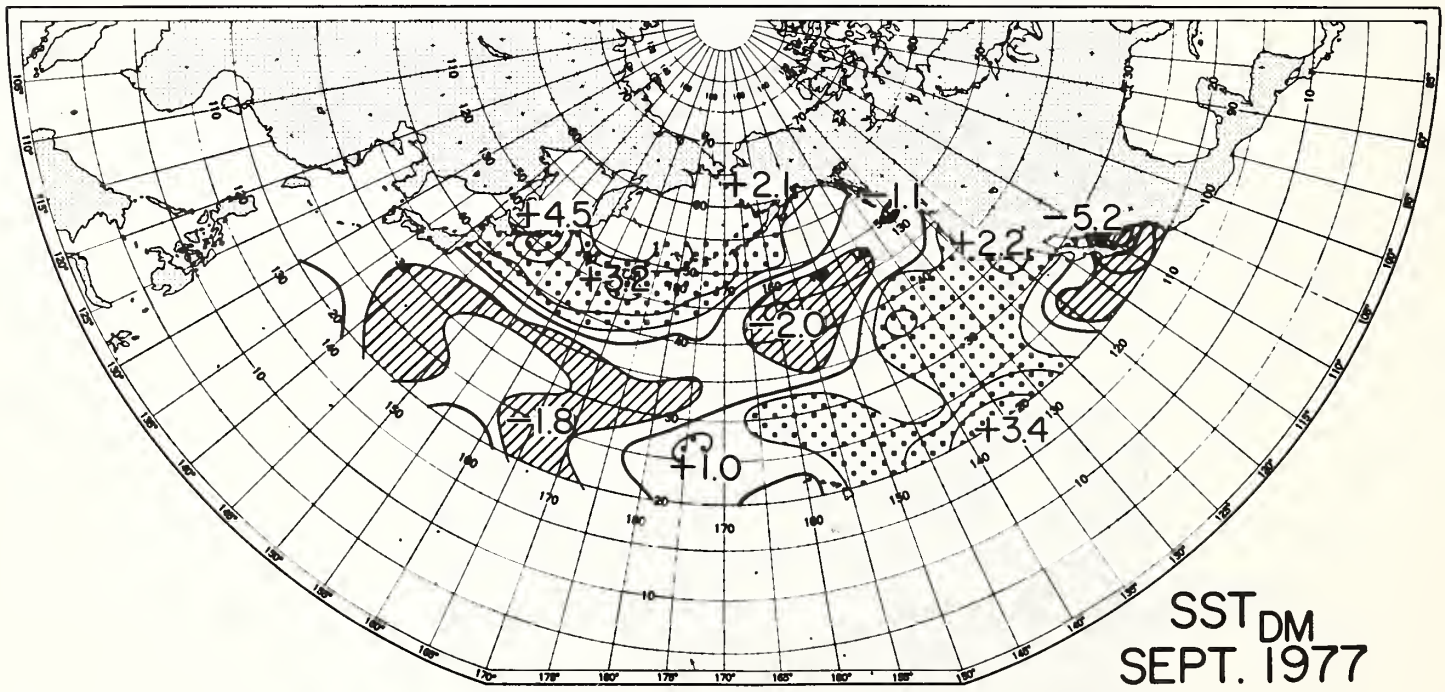

SST_{DM}
SEPT. 1977

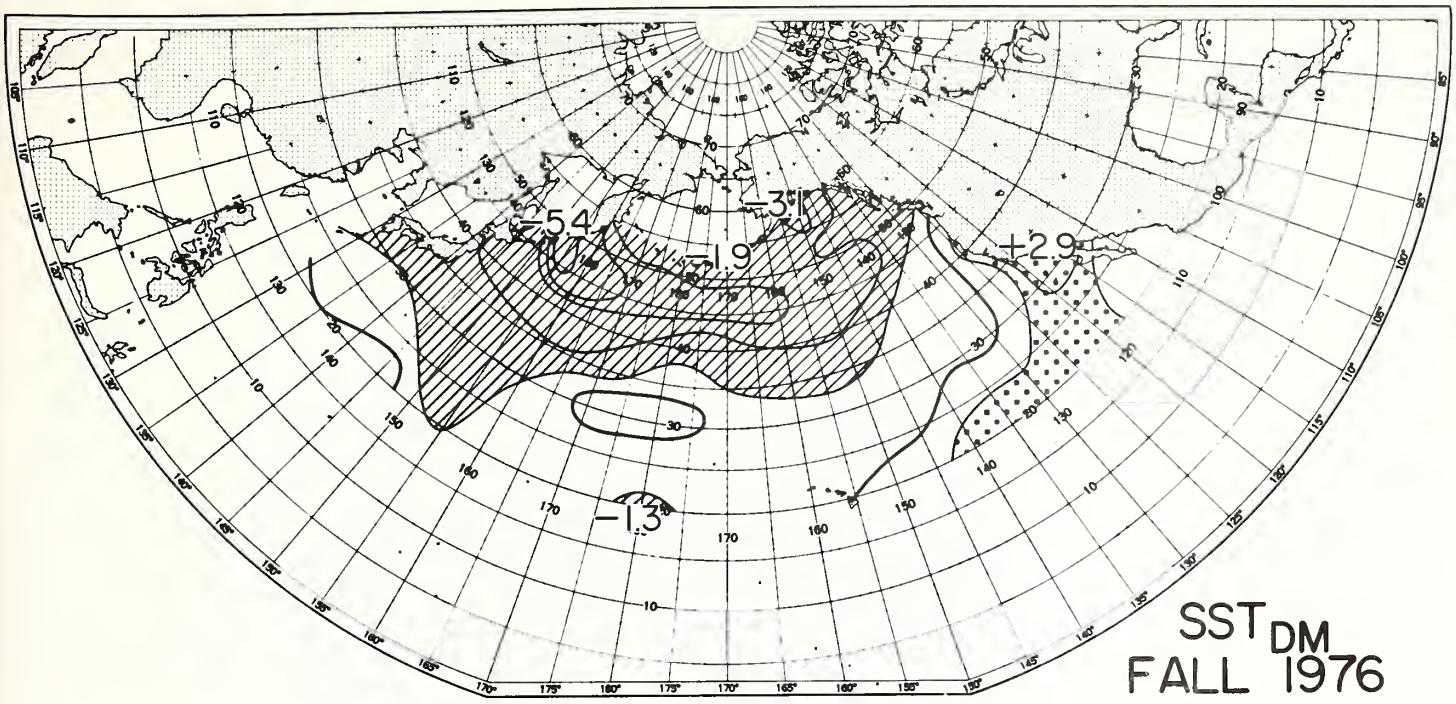

SST DM
FALL 1976

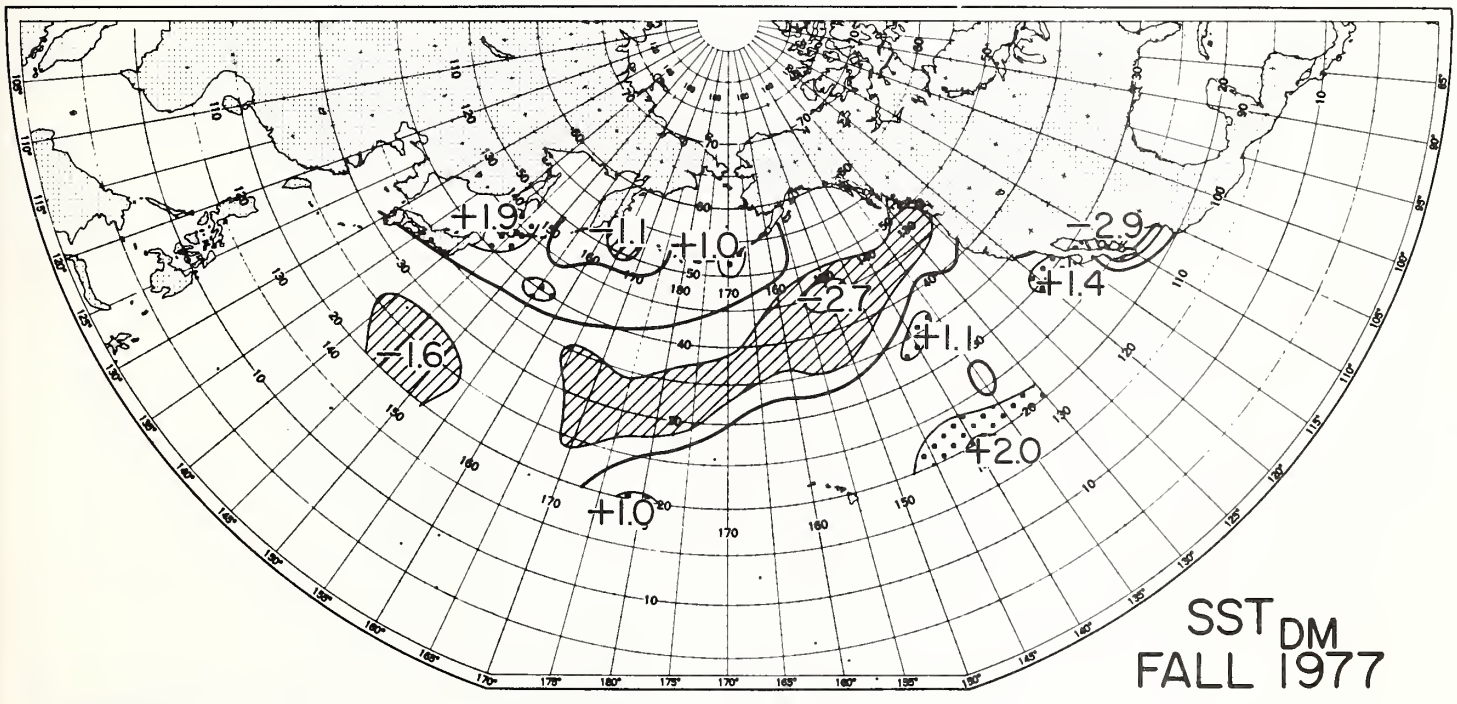

SST DM
FALL 1977

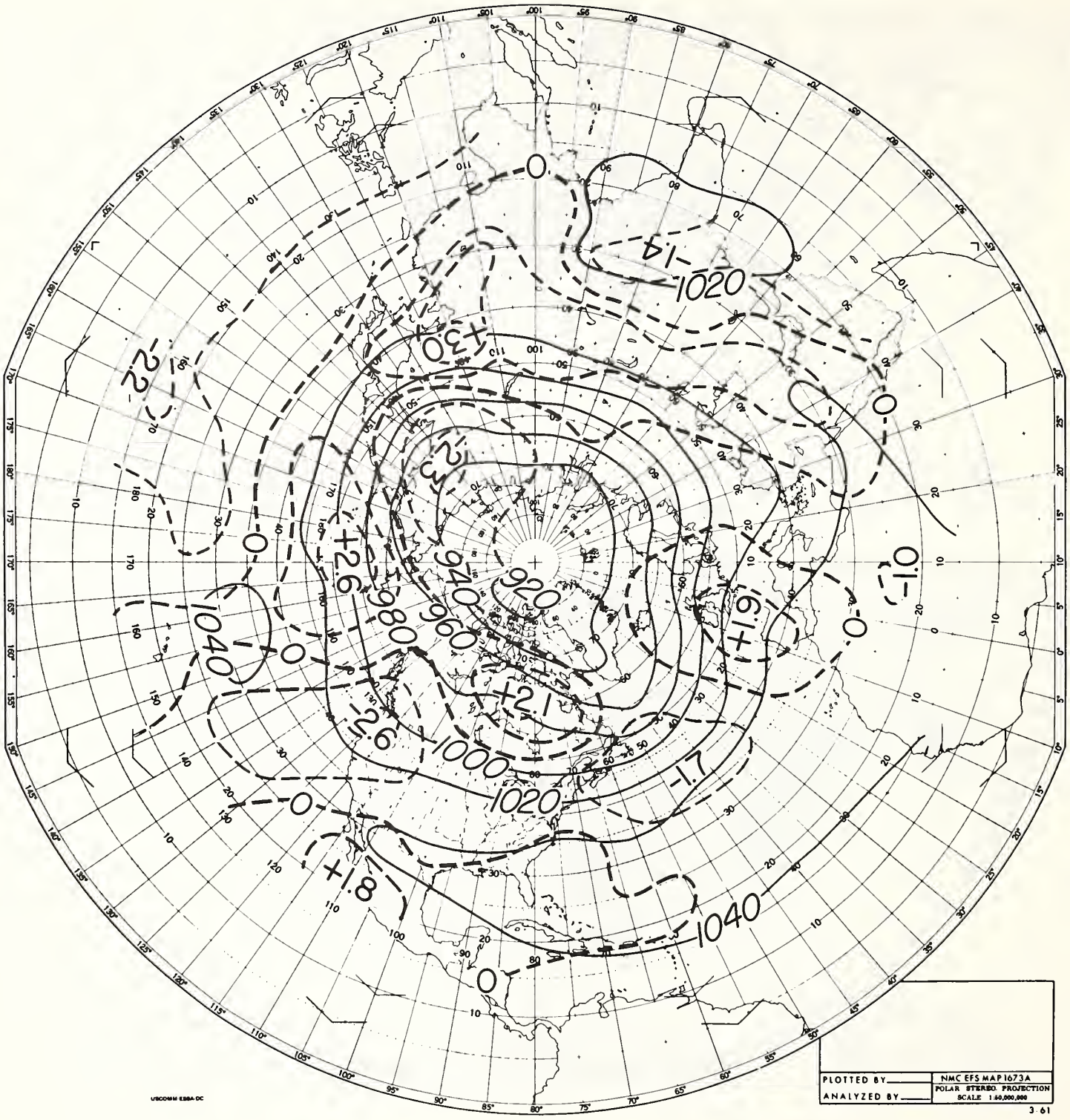

700mb HT. & DM/σ, SEPTEMBER 1977

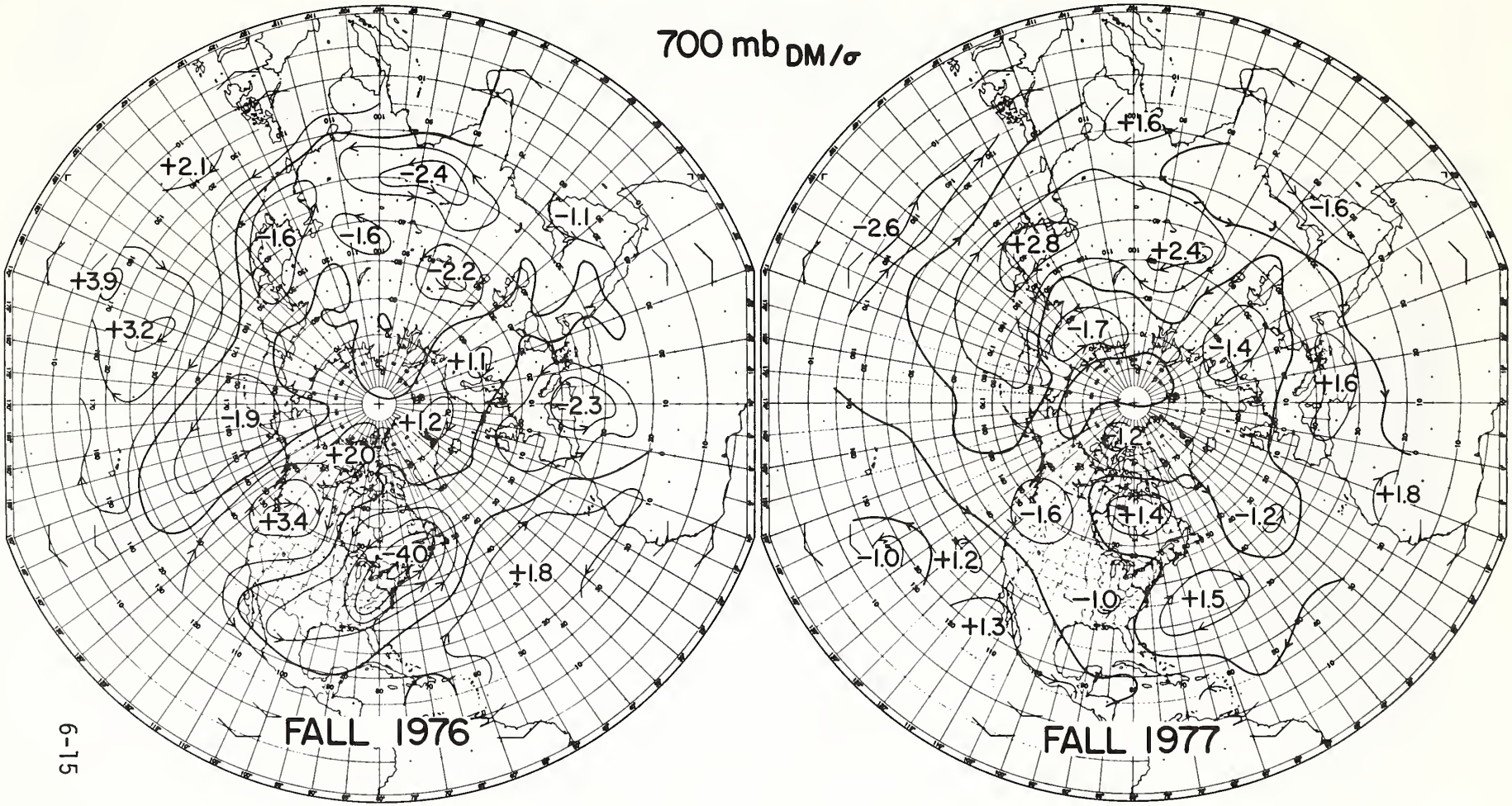
700 mb DM/σ
+2.1
-2.4
-1.1
-1.6
-1.6
-2.2
+3.9
+3.2
+1.1
-2.3
-1.9
+1.2
+2.0
+3.4
-4.0
+1.8
FALL 1976
+1.6
-1.6
-2.6
+2.8
+2.4
-1.7
-1.4
+1.6
1.2
+1.8
-1.6
+1.4
-1.2
-1.0
+1.2
-1.0
+1.5
+1.3
FALL 1977

WINTER 1978 700mb$_{DM}$ SPECIFIED FROM CONTEMPORANEOUS SST$_{DM}$

700 mb DM SPECIFICATIONS FROM PREDICTED SST (1977-78 WINTER)

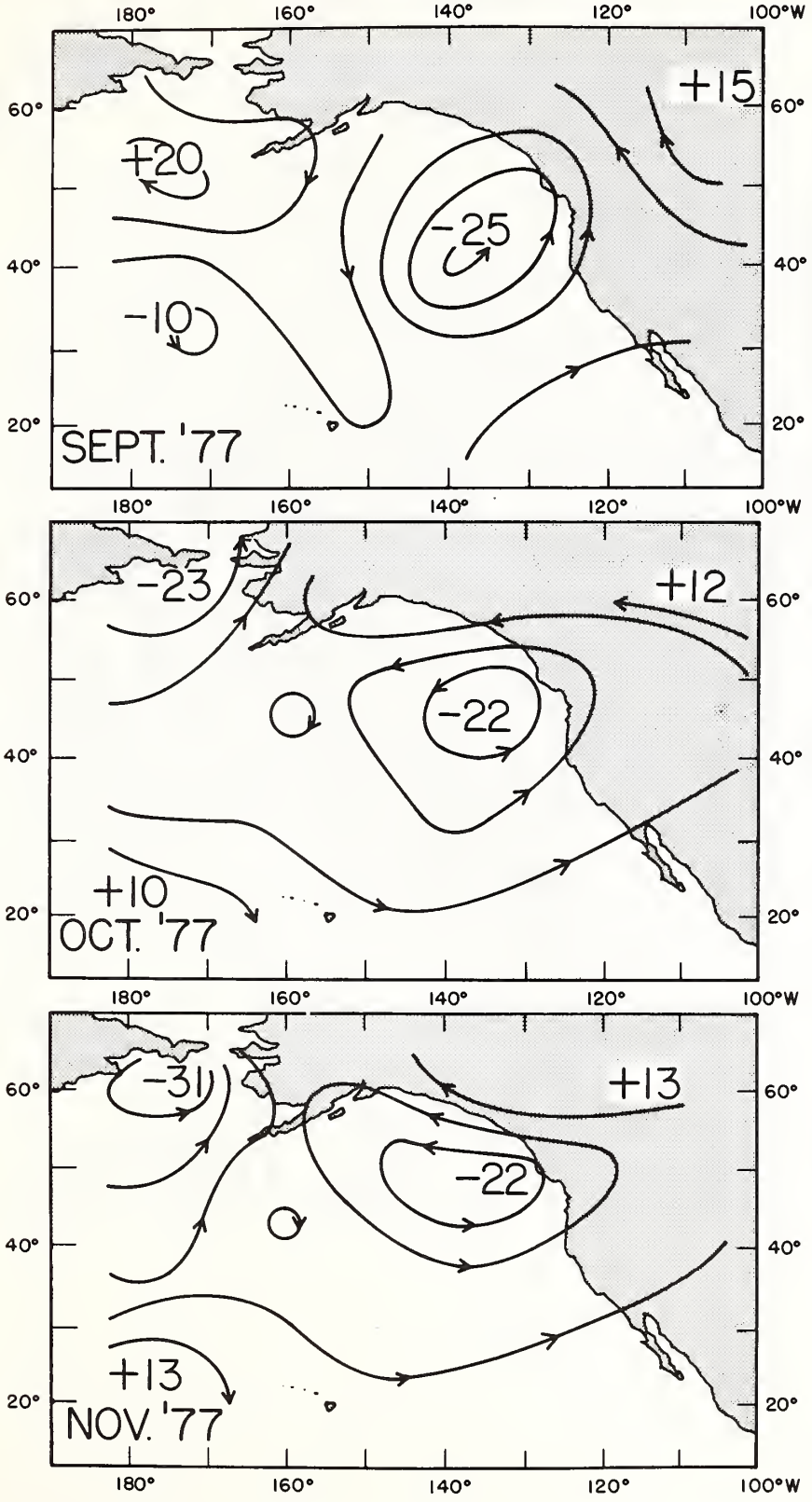

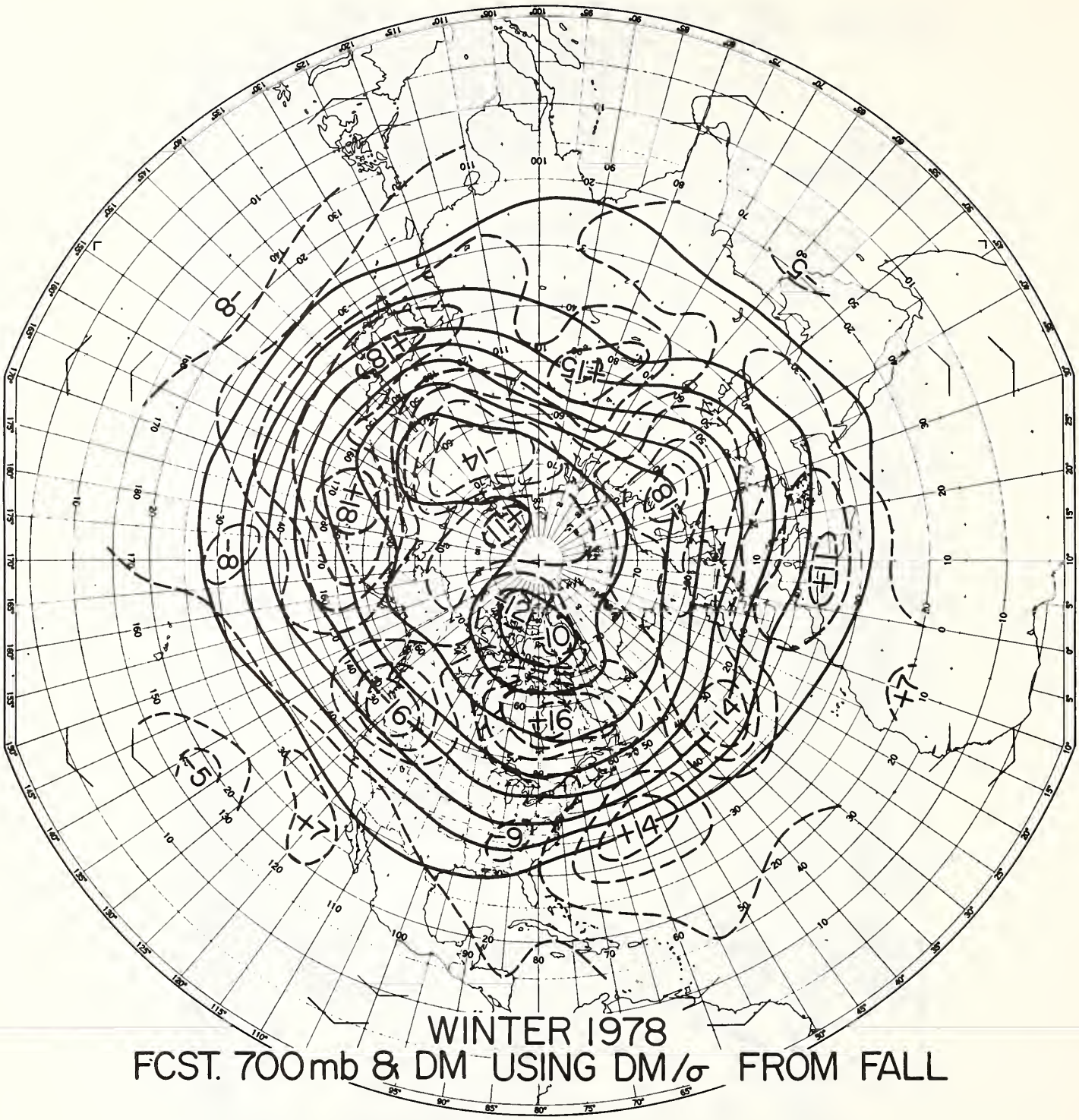

WINTER 1978
FCST. 700mb & DM USING DM/σ FROM FALL

TELECONNECTIONS OF 700 DM

TELECONNECTIONS OF 700 DM
65N-115W WINTER

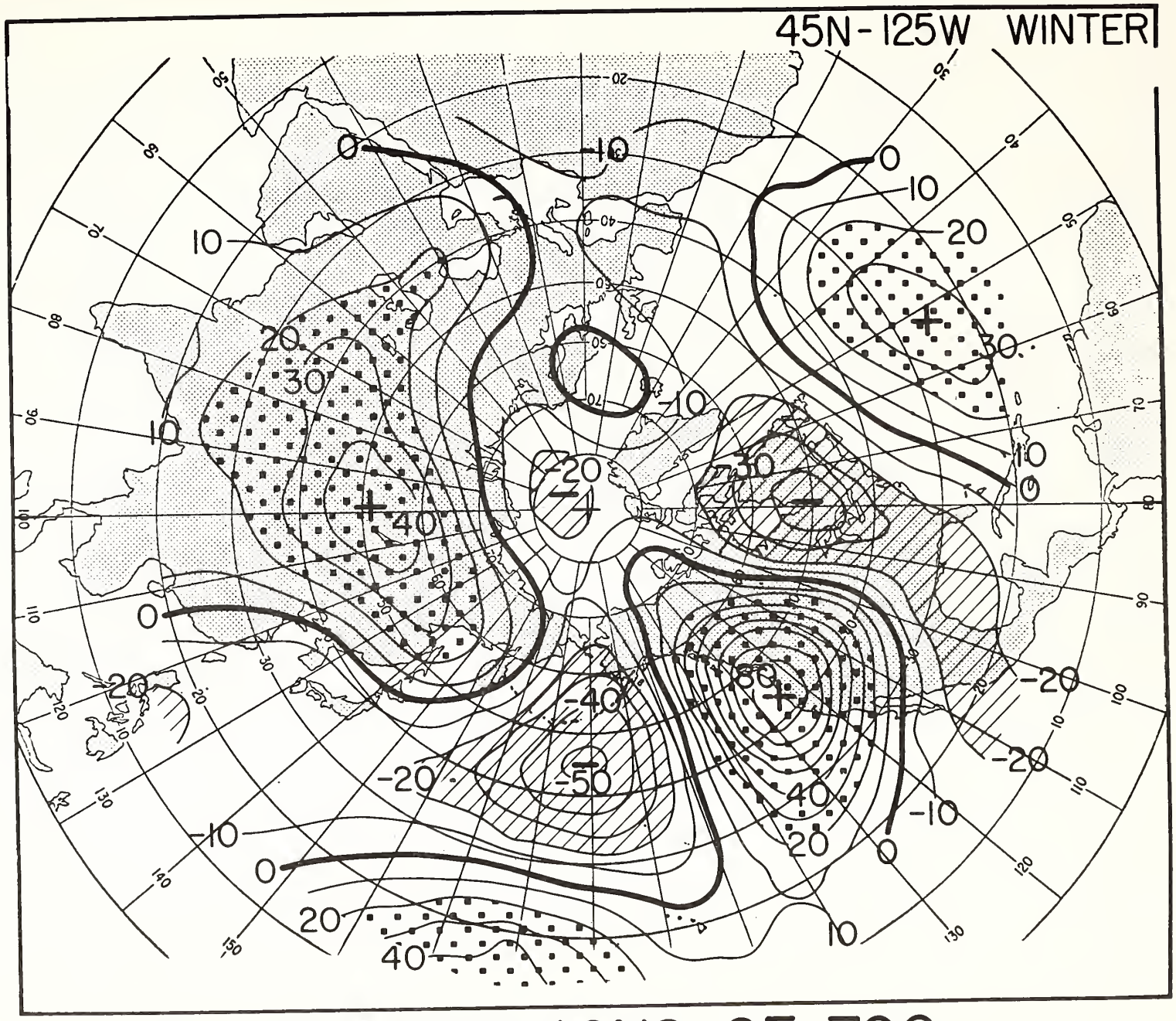

TELECONNECTIONS OF 700 DM

Large-scale Atmospheric Circulation and the West Coast Upwelling Regime in 1976/77 and 1977/78

Gunter R. Seckel, Andrew Bakun and Richard Parrish

Pacific Environmental Group, SWFC
National Marine Fisheries Service, NOAA
Monterey, California 93940

Anomalies in the large-scale atmospheric circulation affect the upwelling regime off the west coast of North America. In turn, these anomalies affect the stocks of valuable fishery resources in the U.S. 200 mile fisheries management zone.

THE UPWELLING REGIME

During spring and summer the North Pacific High and the Continental Low pressure systems produce prevailing northwesterlies over the offshore region of North America. During fall and winter the Aleutian Low and a pressure ridge extending from the continent over central California and westward over the eastern Pacific produce prevailing southwesterlies off Oregon and Washington and northwesterlies off southern California. The wind stress climatology (Fig. 1, 2, 3, 4) (Nelson, 1977) shows that maximum northwesterlies begin to strengthen off southern California early in the year. In April maximum northwesterlies occur off central California and in summer they are found off northern California. During summer the entire offshore region from Canada to Baja California is under the influence of the prevailing northwesterlies. From October to April southwesterlies prevail off Oregon and Washington.

Northwesterlies off the west coast produce an offshore component of surface flow (Ekman transport). This water is replaced in part with colder, nutrient rich "upwelled" water from below the surface layer. Southwesterlies produce an onshore component of surface flow, "piling up" warm surface water against the coast. This process can be termed "downwelling."

The upwelling regime also affects the along shore California and Davidson currents. Upwelling during spring and summer changes the baroclinicity in such a manner as to increase the southward flow of the California Current. Onshore surface flow and downwelling would tend to increase the northward flowing Davidson current.

The offshore or onshore Ekman transport has been computed from sea-level atmospheric pressure distributions. These transports are used as coastal divergence or upwelling indices (Bakun, 1973, 1975). Daily upwelling indices based on 6-hourly pressure analyses are computed at three-degree latitude intervals along the west coast from Baja California to the Gulf of Alaska. Examples for 1975 are shown in Figure 5 and illustrate the upwelling regime associated with the prevailing wind systems described above.

FALL AND WINTER 1976/77 and 1977/78

The winter atmospheric circulation during 1976/77 and 1977/78 (Fig. 6, 7) produced upwelling regimes that are distinct from the more usual pattern that occurred in 1975. The anomolous patterns are most distinct off central California, lat. 36°N (Fig. 8).

Anomalously low wind speeds and, therefore, low index values prevailed during the fall of 1976 through February 1977. In October and November 1977 stronger than normal upwelling persisted. However, from December 1977 through the winter of 1978, the pattern for Central California resembled that normally found off Oregon and Washington with recurring strong downwelling events. The strong downwelling events also occurred off southern California at lat. 33°N.

FISHERIES IMPLICATIONS

The biological significance of upwelling in terms of sea surface temperature and biological productivity is well known. Other aspects of the upwelling system may be particularly important during the egg and larvae stages of fishery resources (Parrish, Bakun and Nelson, manuscript).

An offshore component of surface flow would tend to disperse eggs and larvae into areas remote from the favorable coastal environment. Onshore surface flow would act to hold them in the near-coastal environment in which they were spawned. We observe striking conformities between fish reproduction strategies and the seasonality and geography of onshore-offshore transport. Off Oregon and Washington, important species of fish spawn during the winters when onshore wind driven flow prevails rather than during the more productive upwelling season. In the southern California Bight, where a closed gyral circulation provides favorable drift conditions, these types of species are much reduced and the fauna is dominated by spring spawners. In the region of vigorous upwelling off

Northern California which is characterized by strong offshore surface transport through most of the year there is a paucity of locally spawning species. Rather, the fish stocks which harvest the massive productivity of that region are mainly migrating species which spawn in the Southern California Bight.

During the slack wind conditions from November 1976 to February 1977 organisms were subjected to much lower than normal levels of onshore and offshore excursions of surface waters and to turbulent mixing and related dispersion of planktonic aggregations. The dominant winter spawners of the central California coast are the rockfishes. Several species apparently had excellent spawning success as unusually large numbers of juvenile rockfishes were reported by personnel of the California Department of Fish and Game. In marked contrast, the recurring strong storm events during 1977/78 with onshore-offshore excursions of wind-driven surface flow would have made it difficult for planktonic larvae to remain in favorable bathymetric ranges. Strong turbulent mixing would have tended to destroy patch structure in the plankton. Anomalous coastal convergence or piling of surface waters against the coast throughout the California region would tend to induce northward alongshore flow and anomalously warm advection. The onshore Ekman transport events at 30°N are without precedent in the 1967-1978 data base. This anomalous onshore transport during the northern anchovy's spawning season may have concentrated both anchovy larvae and forage near the coast with resulting good spawning success in relation to spawning stock size. The large numbers of young-of-the-year fish in southern California waters as well as the unusually large concentrations of young fish as far north as Monterey Bay during the summer and fall of 1978 appear to support this hypothesis.

REFERENCES

Bakun, A.

1973. Coastal upwelling indices, west coast of North America, 1946-71. U.S. Dep. Commer., NOAA Tech. Rep. NMFS SSRF-671, 103 p.

1975. Daily and weekly upwelling indices, west coast of North America, 1967-73. U.S. Dep. Commer., NOAA Tech. Rep. NMFS SSRF-693, 114 p.

Nelson, C.S.

1977. Wind stress and wind stress curl over the California Current. U.S. Dep. Commer., NOAA Tech. Rep. NMFS SSRF-714, 87 p.

Parrish, R.H., C.S. Nelson, and A. Bakun

manuscript. Larval transport mechanisms and reproductive success of fishes in the California Current.

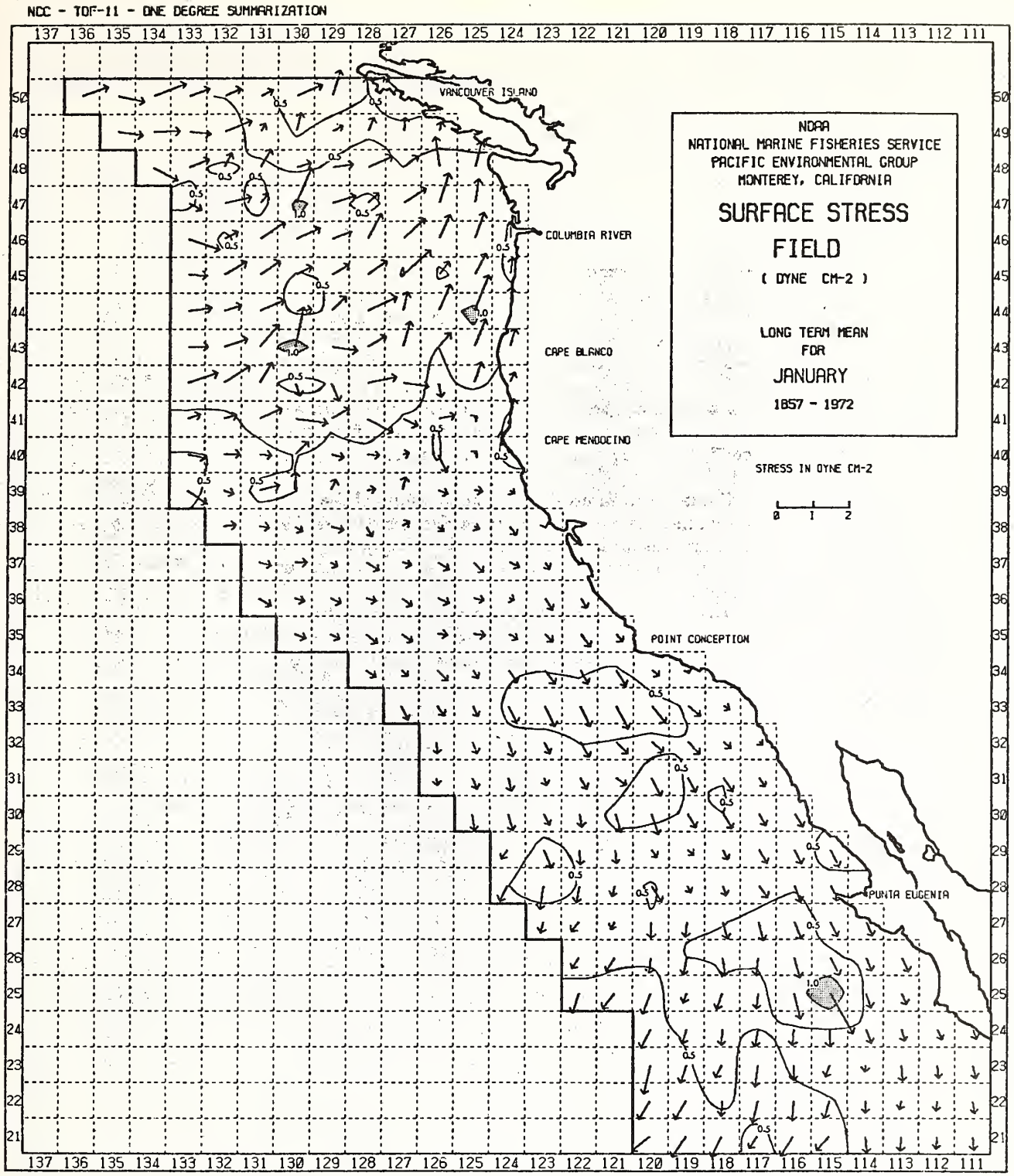

Figure 1. Resultant surface wind stress vectors for January. Stresses off Oregon and Washington reflect the prevailing southwesterly winds to be expected from the atmospheric pressure distribution. South of Point Conception stress vectors reflect relatively weak northwesterlies, with maximum stress occurring off Baja California.

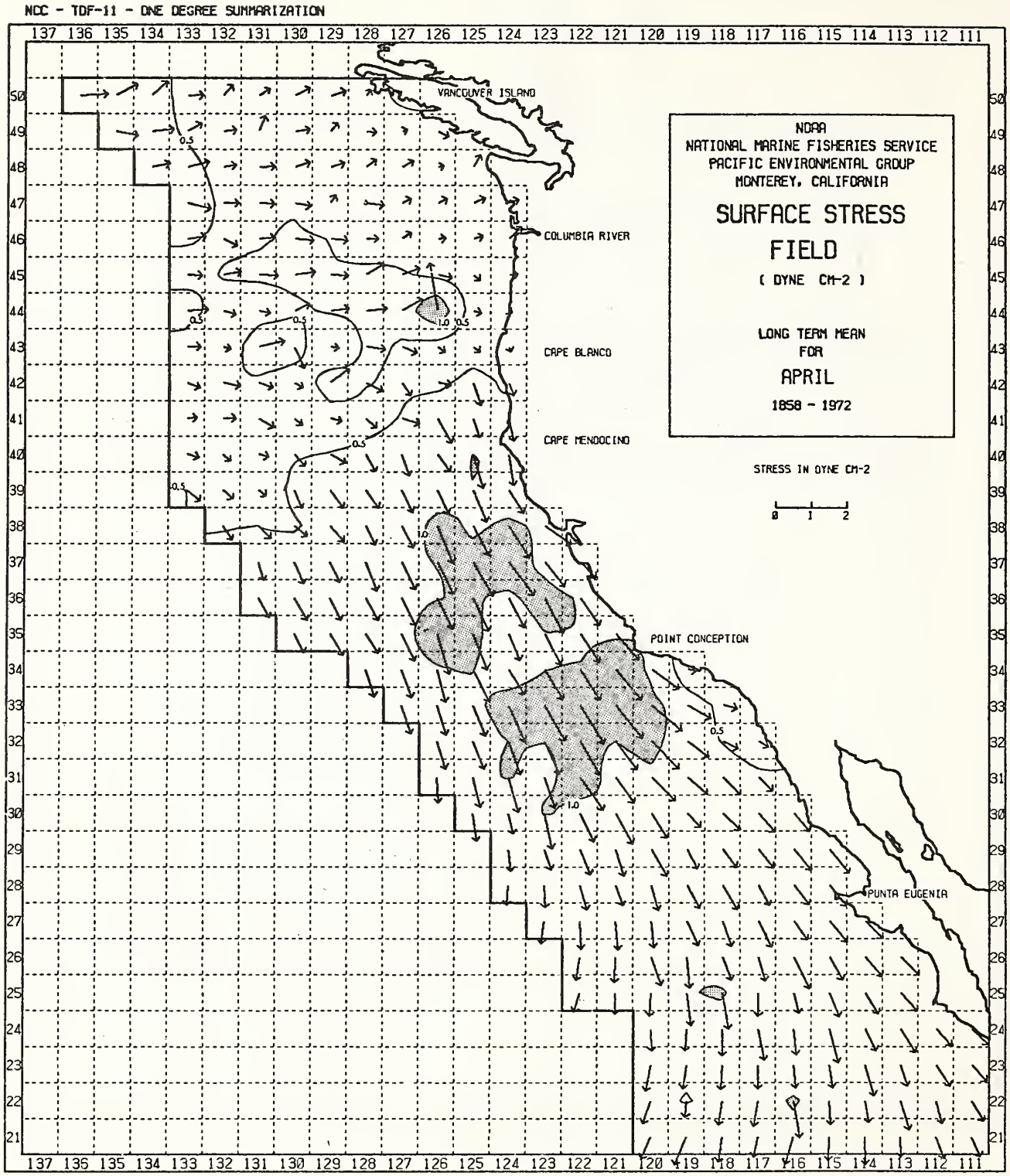

Figure 2. Resultant surface wind stress vectors for April. The prevailing winter stress pattern off Oregon and Washington is beginning to weaken while northwesterlies off California continue to strengthen with highest stress occurring off central California.

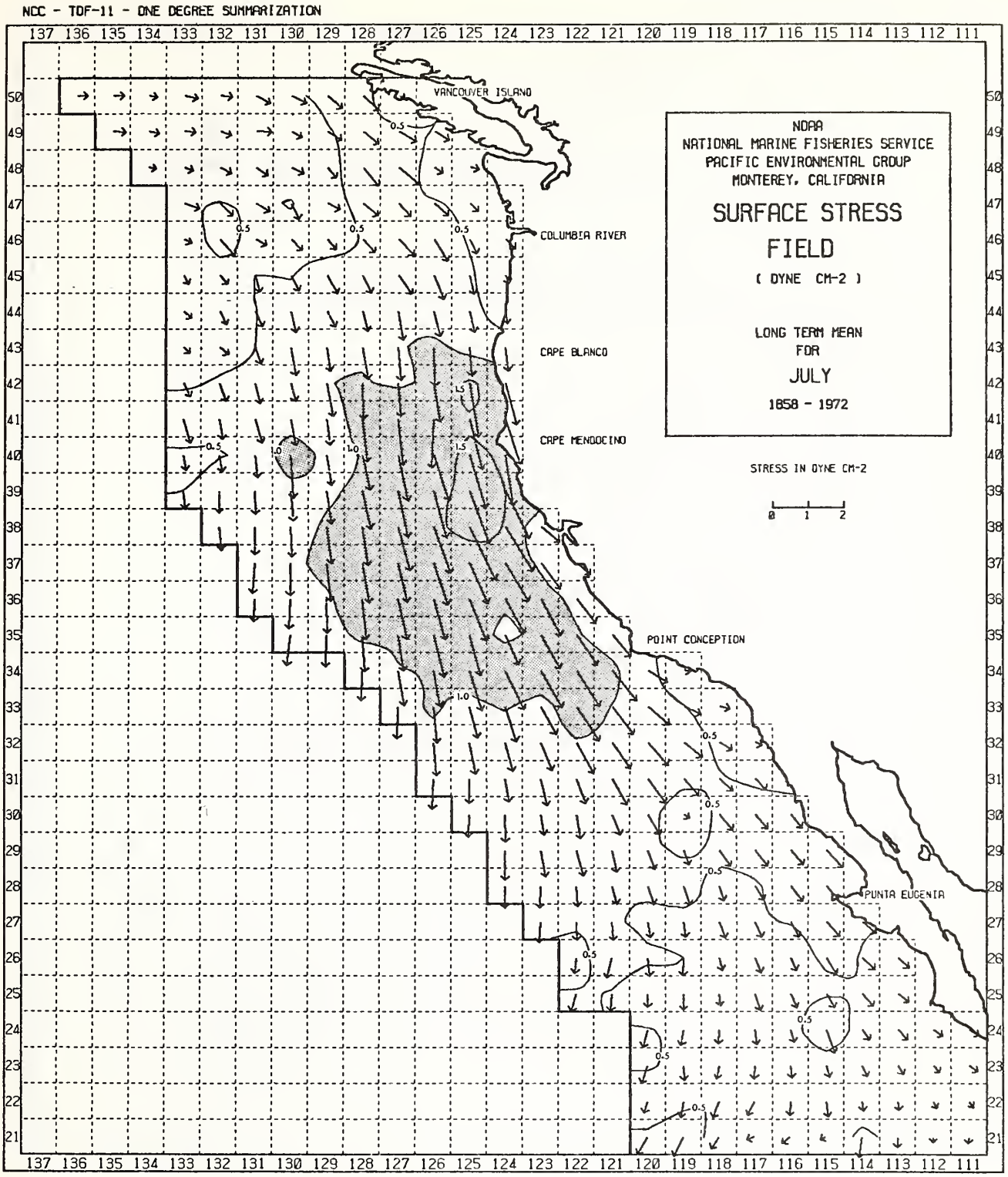

Figure 3. Resultant surface wind stress vectors for July. The entire west coast is dominated by northwesterlies. The area of high stresses extends from Point Conception to Oregon with highest stresses occurring off northern California near Cape Mendocino.

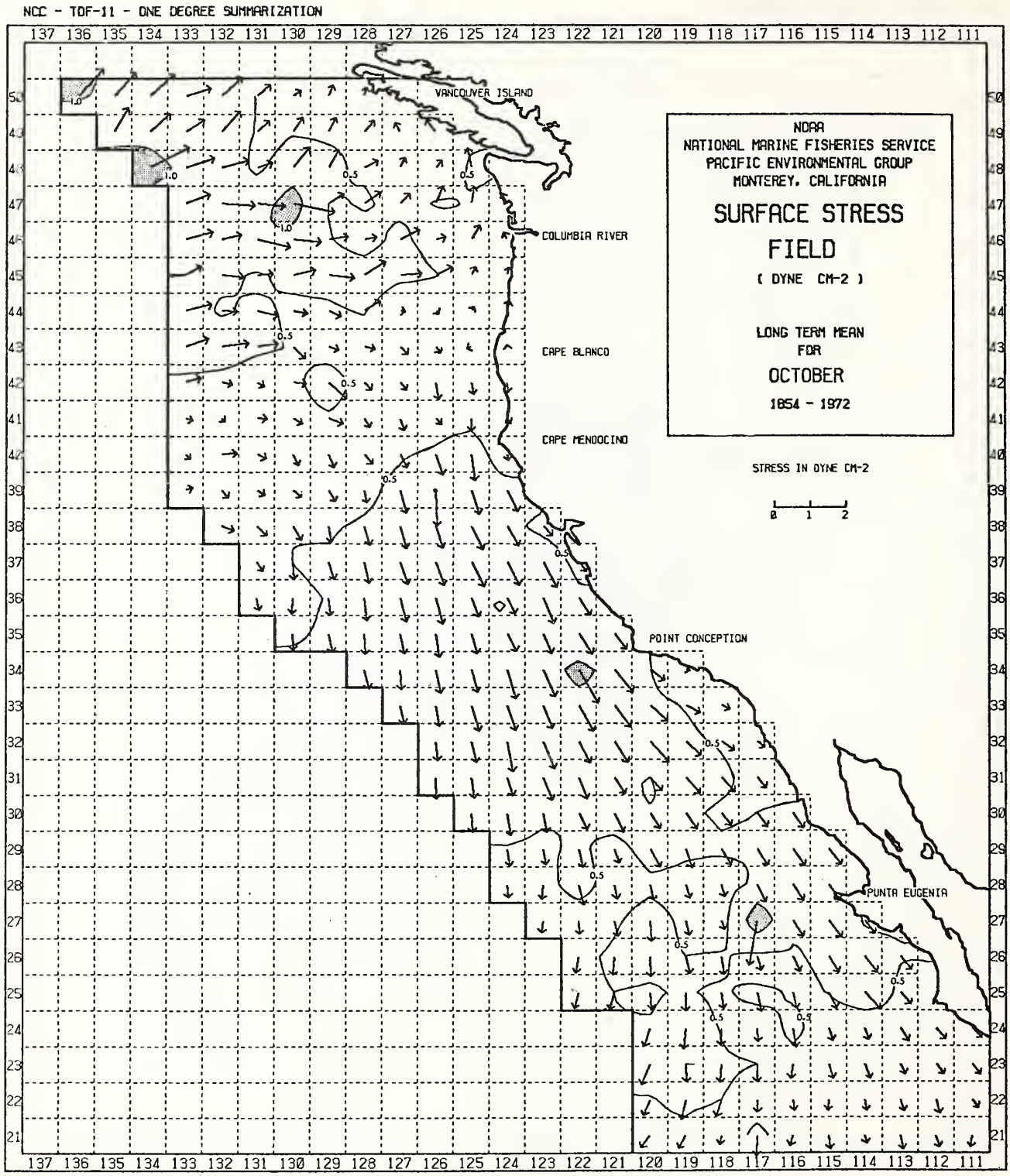

Figure 4. Resultant surface wind stress vectors for October. Off Oregon and Washington the winter stress distribution pattern is beginning to set in. Off California stress magnitudes continue the decrease that began in September.

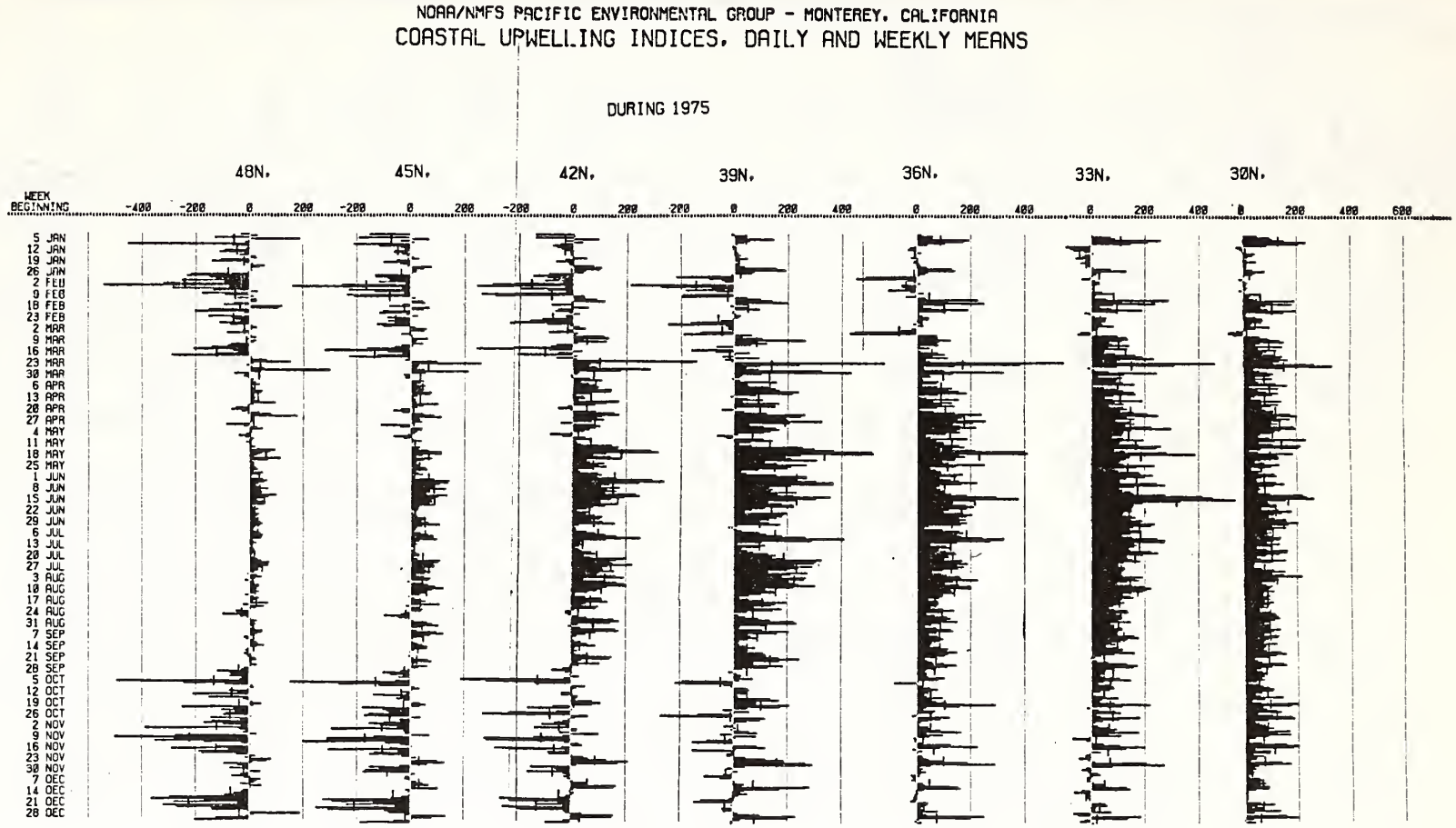

Figure 5. Daily upwelling indices for 1975 at 3 degree intervals from Washington to Baja California computed from 6-hourly sea-level pressure analyses. The magnitude is indicated by the length of the bar with the scale in units of metric tons per second per 100 m length of coast. Bars extending to the right indicate offshore Ekman transport (upwelling). Bars extending to the left indicate onshore Ekman transport (downwelling).

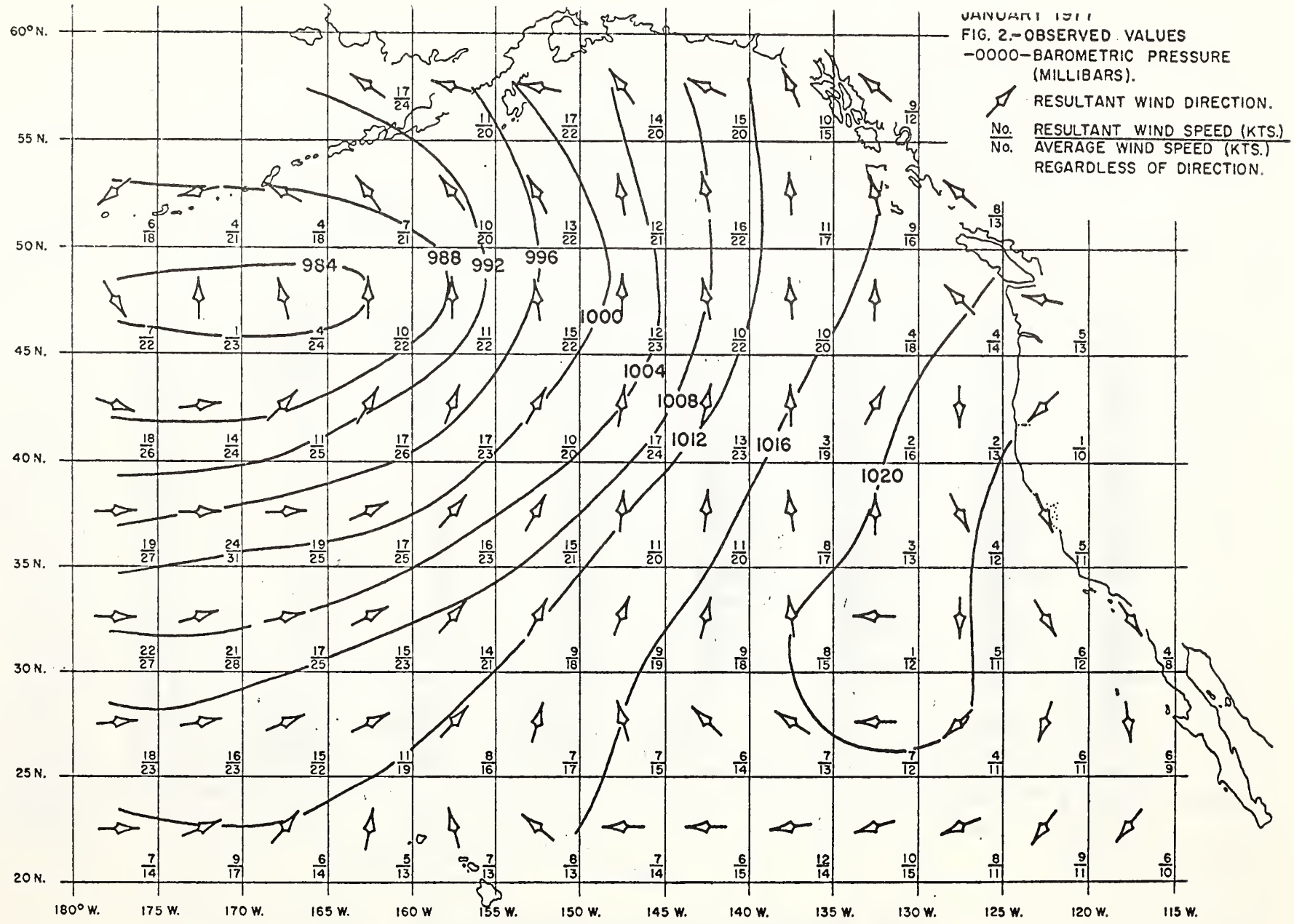

Figure 6. Sea-level atmospheric pressure eastern North Pacific January 1977.

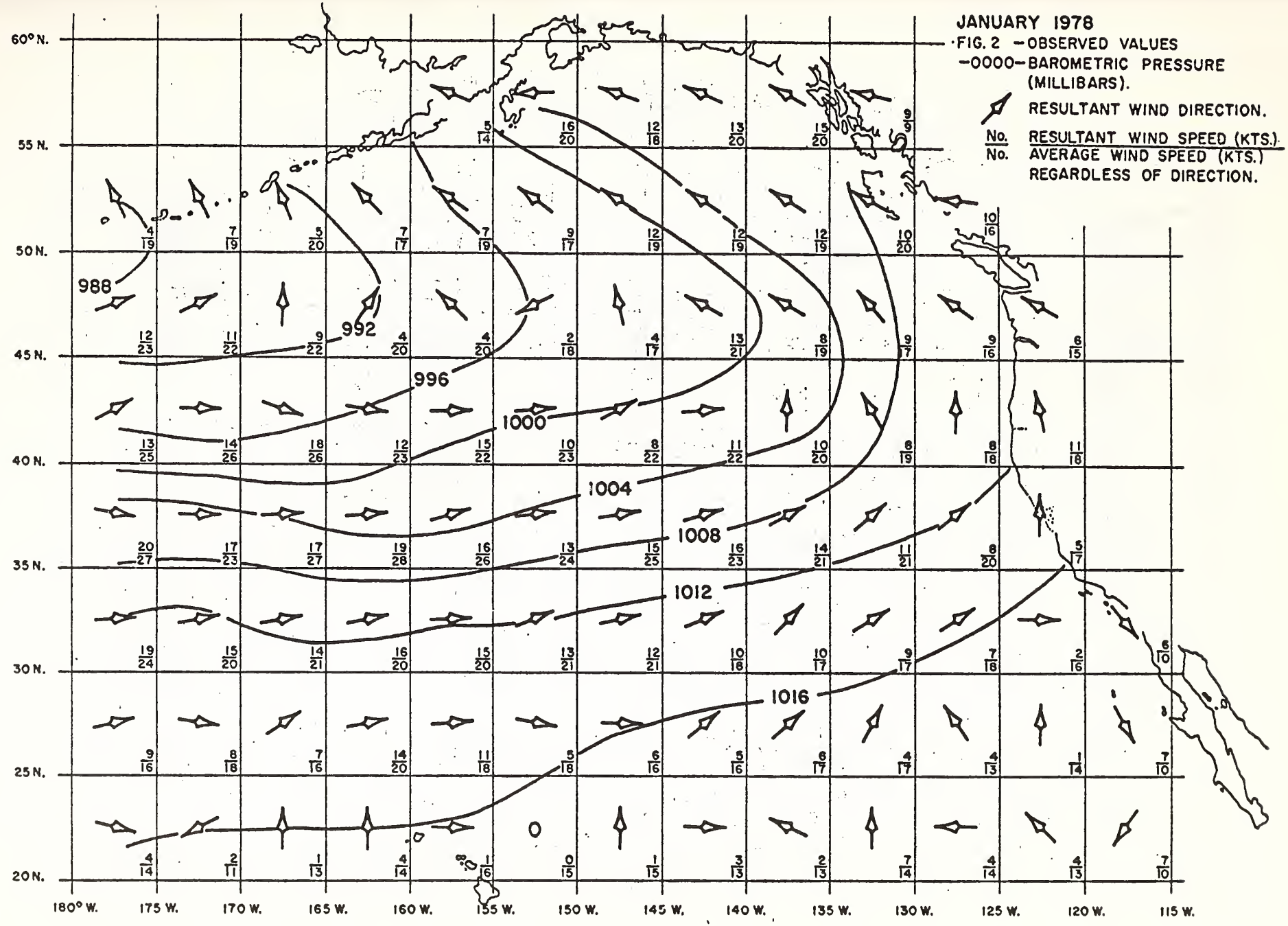

Figure 7. Sea-level atmospheric pressure eastern North Pacific January 1978.

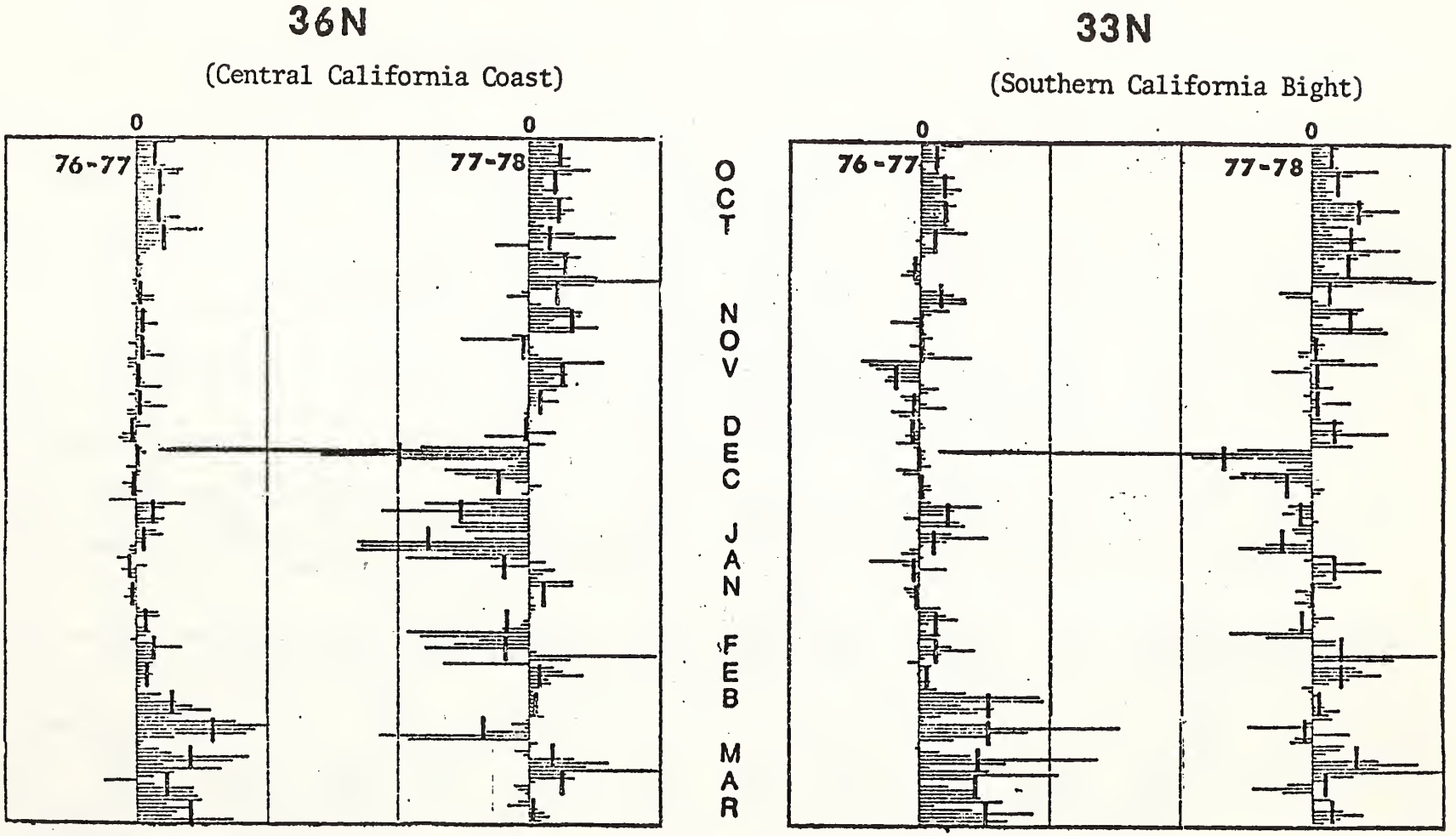

Figure 8. Upwelling (downwelling) patterns at lat. 30° and 33°N, fall 1976/winter 1977 and fall 1977/winter 1978. Bars have the same meaning as in Figure 5.

Tropical Circulation and Radiation Fluctuations: Interactions with Mid-Latitude Circulations During 1976-1978

Jay S. Winston and Arthur F. Krueger
NOAA-NESS, Washington, D. C.

1. Summary

The remarkable displacement of westerlies toward the equator during the past two Northern Hemisphere winters was associated with a weakening of the large scale standing eddies over the tropics and an eastward displacement of major convective cloudiness and rainfall in the tropical Pacific. These events in turn appear to have contributed to a stronger Hadley circulation. The changes in the tropics were first noted during the 1976 southern winter when the South Pacific anticyclone and tradewinds weakened and equatorial sea surface temperatures increased. In much of the tropical central Pacific the cloudiness regime was even more intense in the 1977-78 (northern) winter than in 1976-77.

2. Relevant zonally averaged features of the circulation

Zonal kinetic energy distributions for the last three Januaries are shown in Fig. 1 (top). Note in particular the very high kinetic energy between 25N and 35N during these past two winters in contrast to 1976. This was accompanied by a larger meridional temperature gradient in these latitudes (Fig. 2). This expansion of the westerlies and temperature gradient equatorward was accompanied by a similar shift of the subtropical anticyclones and also the baroclinic instability. The baroclinic activity can be monitored with the conversion of zonal to eddy available potential energy (C_A) which is shown in the upper part of Fig. 3. Note the larger values in 1977 and 1978 extending from 40N to about 15N in contrast to 1976. Larger conversions from eddy to zonal kinetic energy (C_K) also occurred these past two winters in the subtropics (lower part of Fig. 3). While the westerlies were receiving larger amounts of kinetic energy on their southern flanks they were losing energy on their northern flanks. Note in particular the larger negative values of C_K near 40N in association with large positive values of C_A, indicating that the eddies in middle latitudes grew in response to both baroclinic and barotropic processes. The stronger eddy processes occurring at lower latitudes these past two winters may have played a role in reducing the amplitude of the large standing eddies over the tropics. This loss in tropical eddy kinetic energy is shown in the lower part of Fig. 1. To a large extent this reflects a loss of kinetic energy of the lowest two wave numbers as shown in Fig. 4 and represents a weakening of the Walker circulation.

These events occurring in the wintertime circulations appear to signify a stronger Hadley circulation occurring during these last two

years. There is indirect evidence of this in the outgoing longwave radiation shown on the left side of Fig. 5. Note in particular the low values between 5S and 5N during the last two Januaries in contrast to January 1976. Since this parameter is largely modulated by major cloudiness over the tropics this suggests increased cloudiness, rainfall, and upward motion during the past two winters. In contrast, at 15N increased values in longwave cooling occurred the last two winters suggesting decreased cloudiness and greater subsidence. Also note the generally higher temperatures over the tropics and subtropics in contrast to 1976 (right side of Fig. 5). This increased temperature (or total potential energy) very likely results from the increased release of heat of condensation suggested by the decreased longwave radiation.

The eddy momentum flux has also been used to infer the strength of the mean meridional circulation. In particular an approximate balance between the Coriolis term and horizontal eddy flux has been noted in the upper troposphere by Newell and his colleagues. Assuming this balance we have made estimates of 200 mb meridional flow (Fig. 6). Note the three cell structure and also the stronger northward motion at low latitudes these past two winters.

3. Regional fluctuations in longwave radiation (cloudiness) and circulation over the tropics

Examination of patterns of radiation and circulation over the past few years has revealed that the major fluctuations in the tropics have occurred over the Pacific region. By the southern winter of 1976 the South Pacific anticyclone and tradewinds had weakened substantially. This is shown by several of the time series in Fig. 7. Note the Easter-Darwin pressure anomaly difference which is a simple measure of the Southern Oscillation. This peaked during 1975, then declined slowly, dropping below normal during 1976 where it has essentially remained except for several short upward excursions. Variations in the strength of the tradewinds for two points along the equator are shown just below with the scale reversed - i.e. easterlies above the axis. Note the strong trades during 1975 and 1976. At 170E they declined to near zero during 1976 and even became westerly during this past northern winter. Since strong southern tradewinds accompany a well-defined equatorial dry zone extending well west of 180 we can also use satellite observations to monitor this. Two such time series in longwave cooling are shown at the top of Fig. 7. At the equator and 180 the decline in cooling (increased major cloudiness) set in by June 1976. South of the equator, towards French Polynesia (10S, 160W), it set in late in 1976.

The spatial variation of this outgoing longwave radiation over the Pacific for the past three winters is shown in Fig. 8. Note the eastward spread of lower values (e.g., below 250 W m^{-2}) between 10N and 10S from (northern) winter of 1976 (Dec. 1975-Feb. 1976) to winter of 1977 and the further eastward spread by winter of 1978.

These lower values signify substantial increases in major cloudiness through the heart of the central tropical Pacific. Note also the accompanying major eastward retreat of the equatorial dry zone. Taking the 280 W m^{-2} contour as an indicator of the extent of a nearly unadulterated dry zone we see that its western edge retreated from near 175W in winter 1976 to 160W in 1977, and then to near 145W in 1978. Fig. 9 illustrates the patterns of year-to-year differences in these longwave radiation values. The eastward shift of the large area of decreases is striking. Note that much of the central Pacific region (roughly from 150W to 165E) experienced falls in longwave cooling for two consecutive years. Accompanying the eastward march of the falls is a large area of rises over the western Pacific in 1978-77 signifying substantial decreases in the major cloudiness over the normally convectively active "maritime continent".

The 200 mb circulation anomalies for the past three winters are shown in Fig. 10.* In many respects the last two are similar and quite different from that for 1975-76. Note the relative easterly flow over the equatorial Pacific, with anticyclonic anomalous flow both north and south in contrast to the equatorial westerly flow and cyclonic anomalous flow north and south during the 1975-76 winter. Interestingly, westerly anomalous flow appeared over the equatorial Atlantic the past two winters. Another feature worth noting is the anomalous flow from the eastern tropical Pacific toward the north in all three years. In the past two winters this flow penetrated into southern and southeastern United States, suggesting frequent incursions of deep tropical air into the subtropical edge of the southward-displaced westerlies over the United States and the Atlantic.

The type of shorter-period activity that contributed to the anomalous seasonal mean patterns of radiation and circulation of the past few winters is illustrated in Figs. 11 and 12. The GOES infrared imagery for February 19, 1978 (Fig. 11) shows large clusters of convective activity south of the equator in the central Pacific. (Three tropical cyclones were located in the southern intertropical convergence zone just north of Polynesia.) High level outflow from this region could be seen in the GOES imagery to extend across the equator to join up with the Northern Hemisphere's subtropical jet stream. Note the long cirrostratus - altostratus band extending from the South Pacific,across Mexico out over the Atlantic, a distance of 12,000 km! Six day mean patterns of circulation and longwave radiation for February 16-21, 1978 (Fig. 12) illustrate the abnormal eastward displacement of the southern ITCZ and the associated flow patterns. The west-east axis of very low outgoing longwave radiation extending from about 160E to 150W is located generally near the east-west 1000 mb trough (indicated by the H labels) extending from Indonesia to French Polynesia. The 200 mb flow over this major

---

* The anomalies represent departures from 6 year mean seasonal values based on data from 1968-74. H refers to centers of clockwise circulation, L refers to centers of counterclockwise circulation.

cloudiness and low level convergence is anticyclonic. At the eastern end of this active cloud region the 200 mb flow is most strongly anticyclonic and there is a concentrated flow from the ITCZ northward across the equator. North of the equator this flow divides, one branch continuing mainly eastward into the subtropical jet stream over Mexico, while the other branch returns to the south circulating about the pronounced low latitude trough south of the equator.

Figure 1

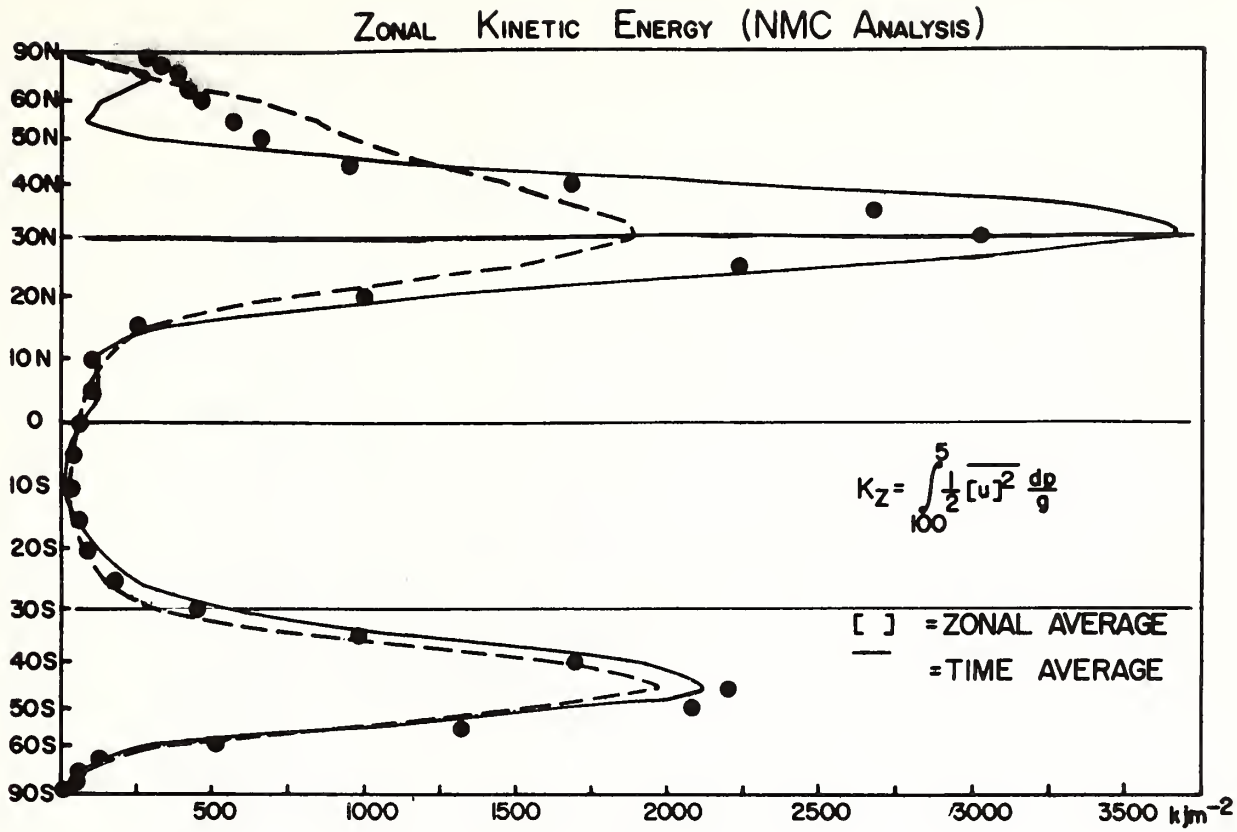
ZONAL KINETIC ENERGY (NMC ANALYSIS)
90N
60N
50N
40N
30N
20N
10N
0
10S
20S
30S
40S
50S
60S
90S
500
1000
1500
2000
2500
3000
3500 kjm-2
$K_Z = \int_{100}^{5} \frac{1}{2} \overline{[u]^2} \frac{dp}{g}$
[ ] =ZONAL AVERAGE
— =TIME AVERAGE

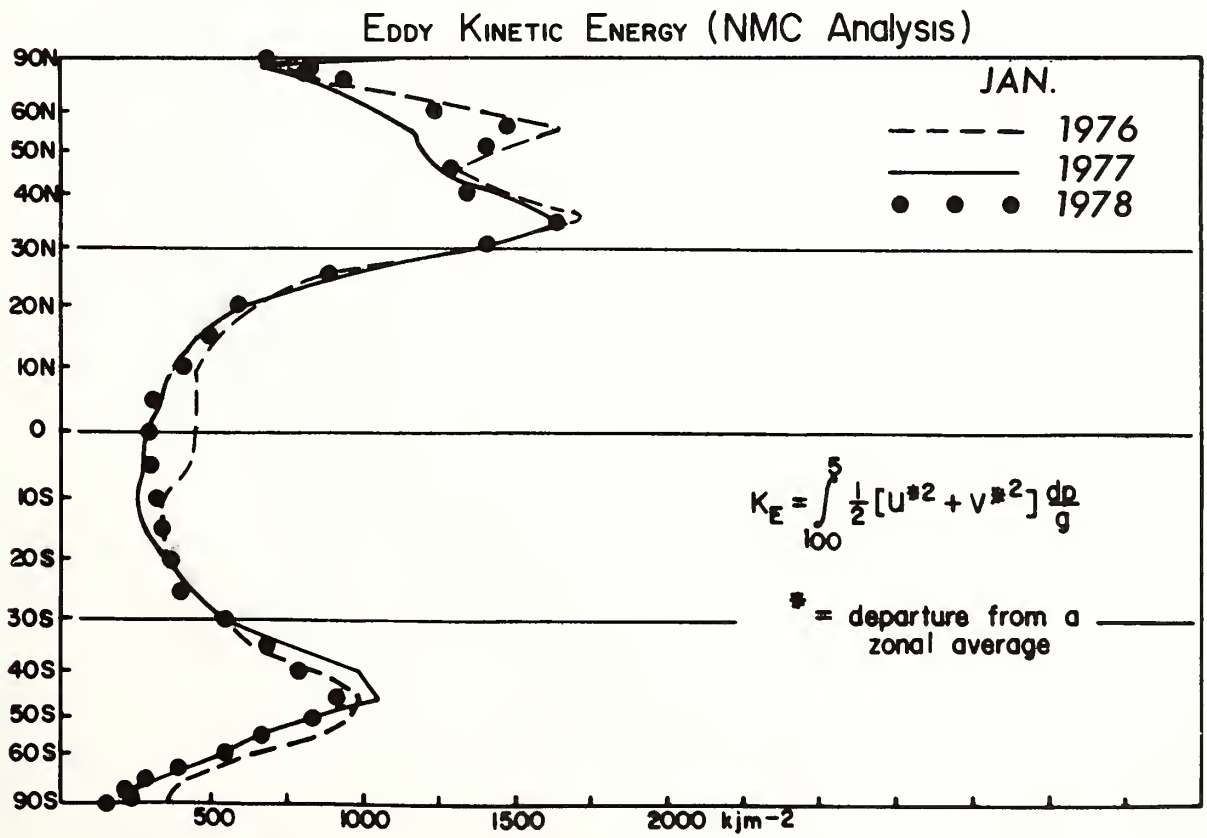
EDDY KINETIC ENERGY (NMC Analysis)
90N
60N
50N
40N
30N
20N
10N
0
10S
20S
30S
40S
50S
60S
90S
500
1000
1500
2000 kjm-2
JAN.
1976
1977
1978
$K_E = \int_{100}^{5} \frac{1}{2} [u^{*2} + v^{*2}] \frac{dp}{g}$
* = departure from a zonal average

Figure 2

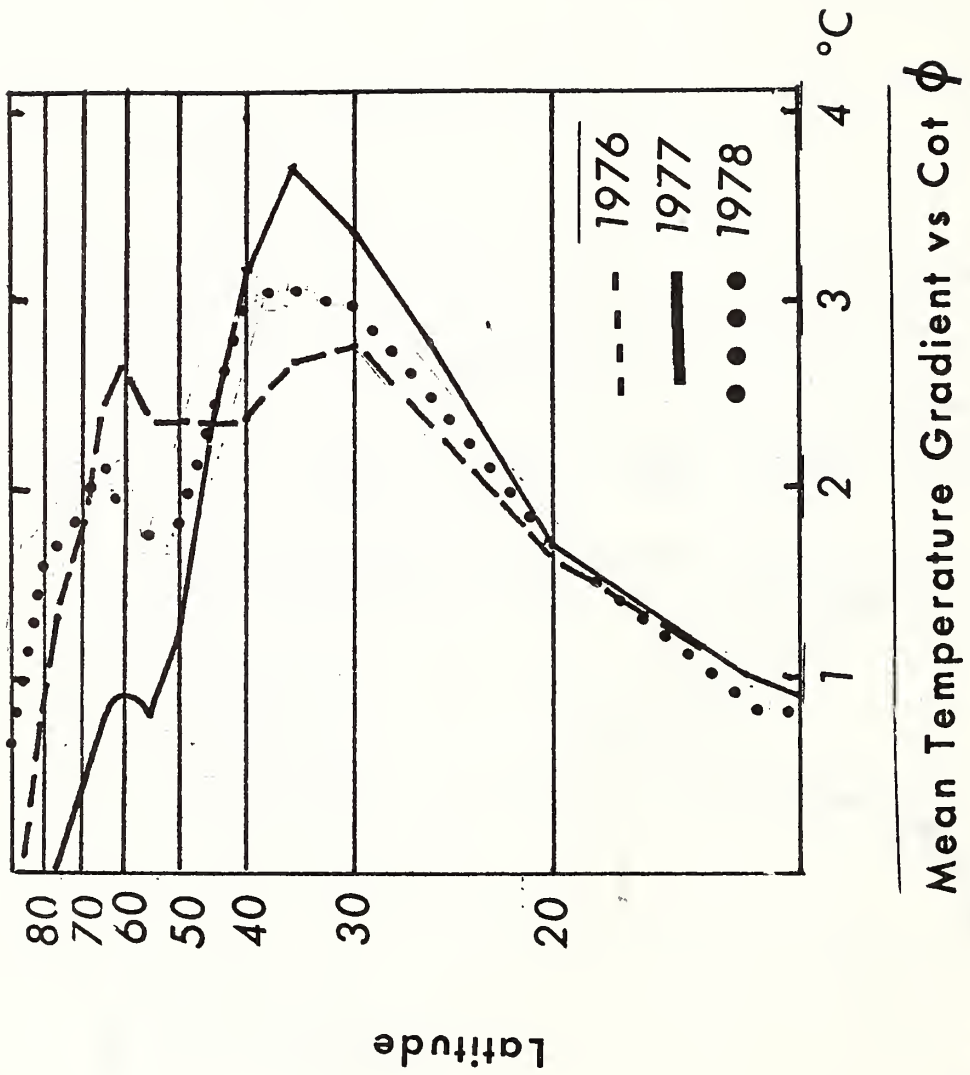
Mean Temperature Gradient vs Cot ϕ
°C
1
2
3
4
1976
1977
1978
Latitude
80
70
60
50
40
30
20

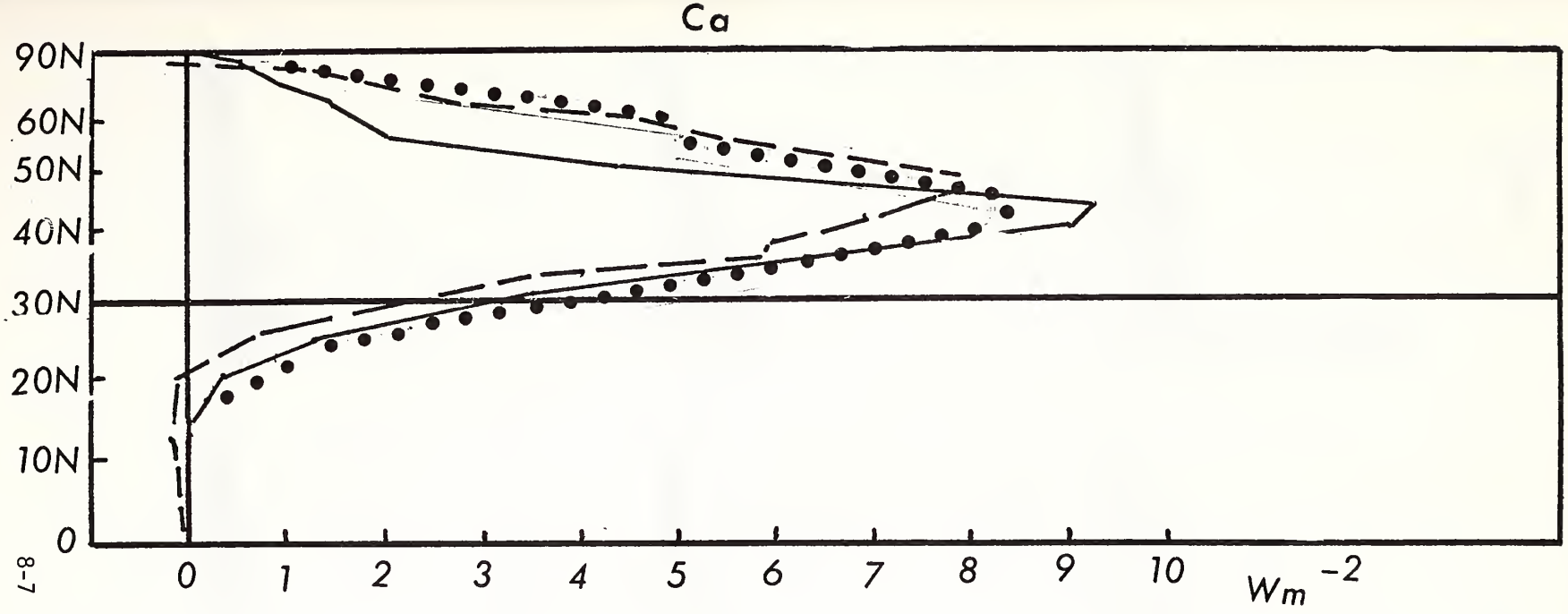
Ca
90N
60N
50N
40N
30N
20N
10N
0
0 1 2 3 4 5 6 7 8 9 10
Wm -2

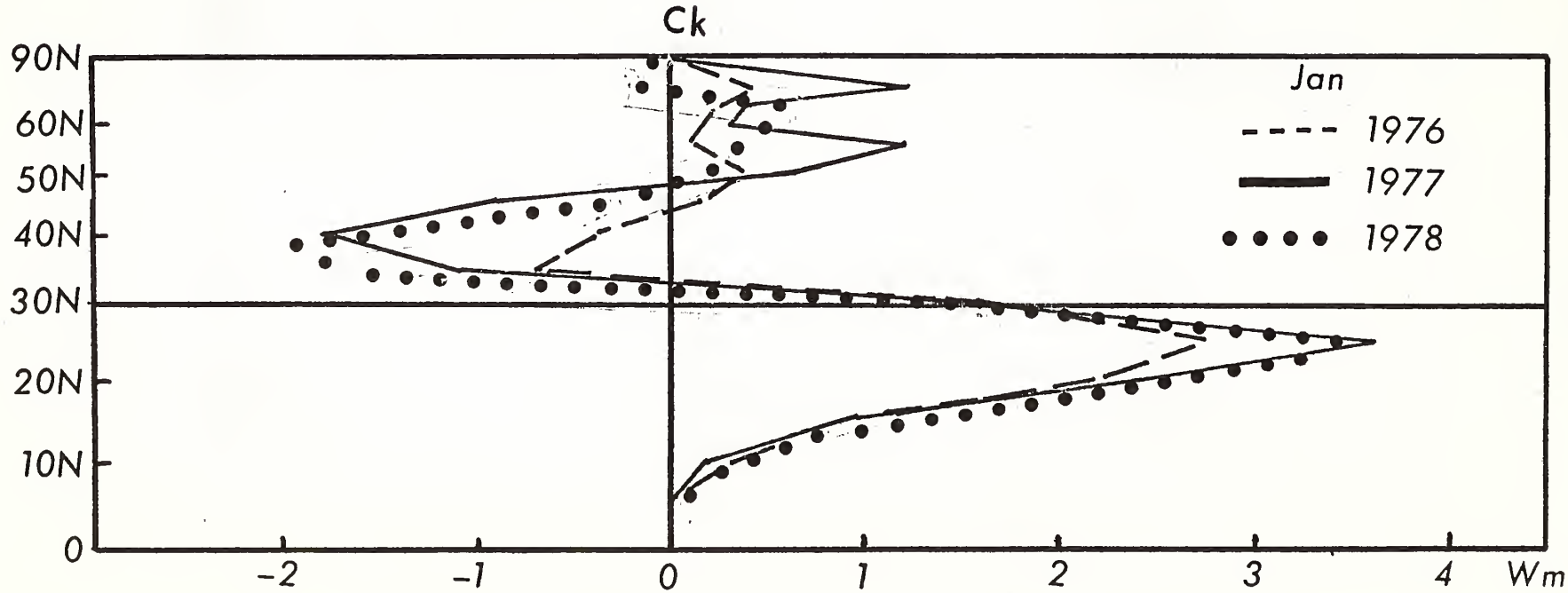
Ck
90N
60N
50N
40N
30N
20N
10N
0
-2 -1 0 1 2 3 4
Wm -2
Jan
1976
1977
1978

Figure 3

Figure 4

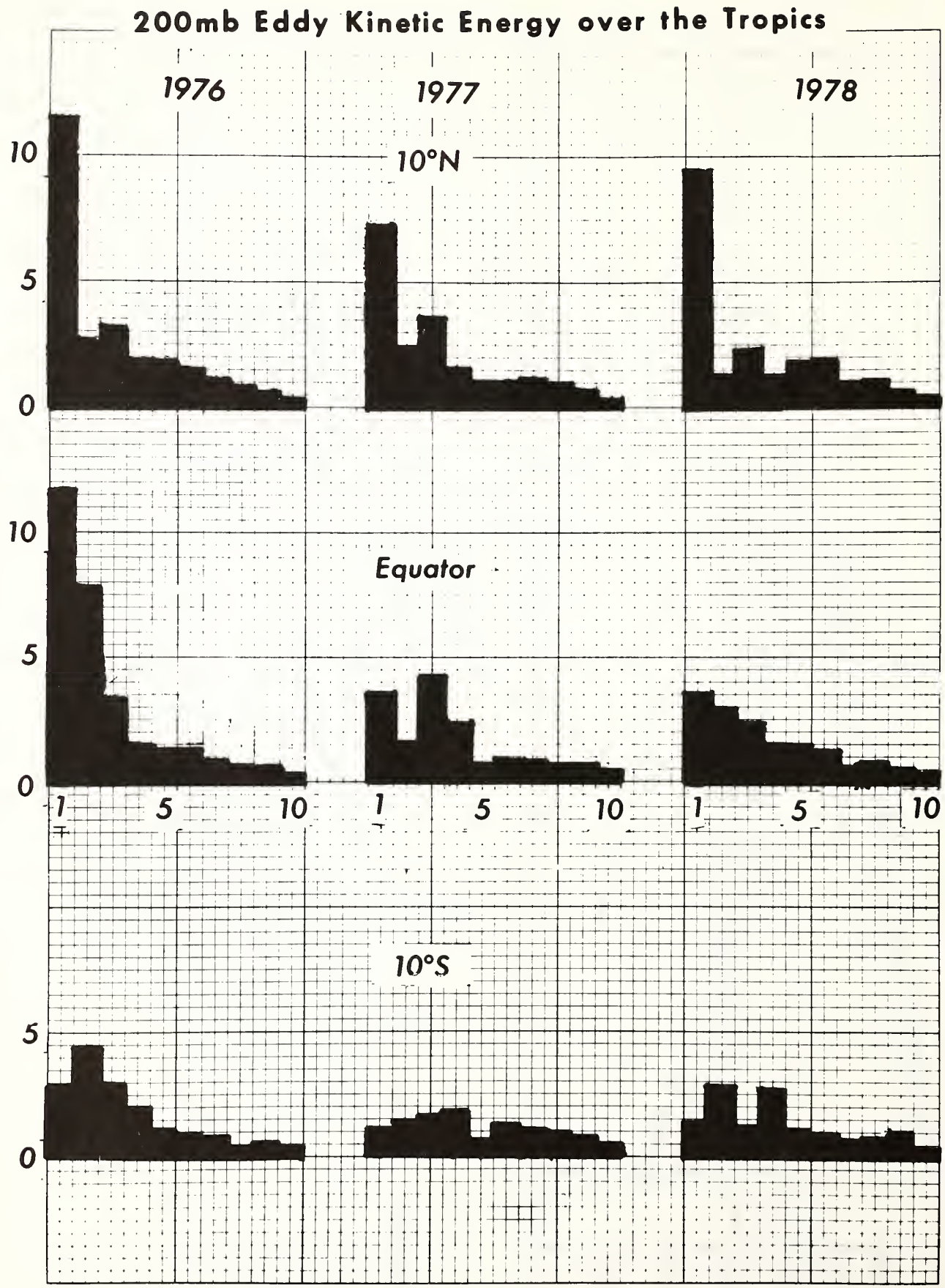
200mb Eddy Kinetic Energy over the Tropics
1976
1977
1978
10°N
Equator
10°S
10
5
0
1
5
10

Figure 5

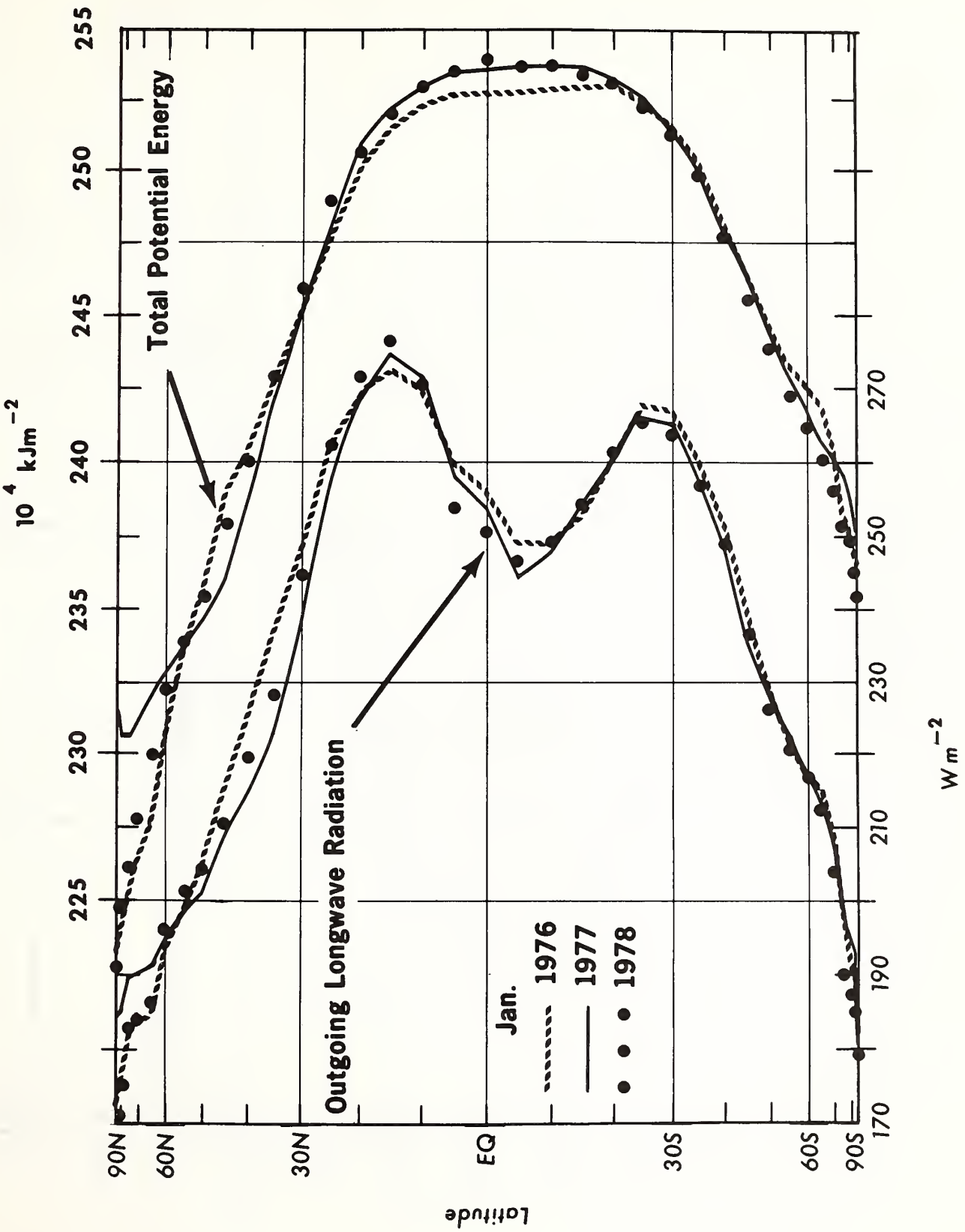
Total Potential Energy
Outgoing Longwave Radiation
Jan.
1976
1977
1978
10^4 kJm^{-2}
W m^{-2}
Latitude
90N
60N
30N
EQ
30S
60S
90S
225
230
235
240
245
250
255
170
190
210
230
250
270

Figure 6

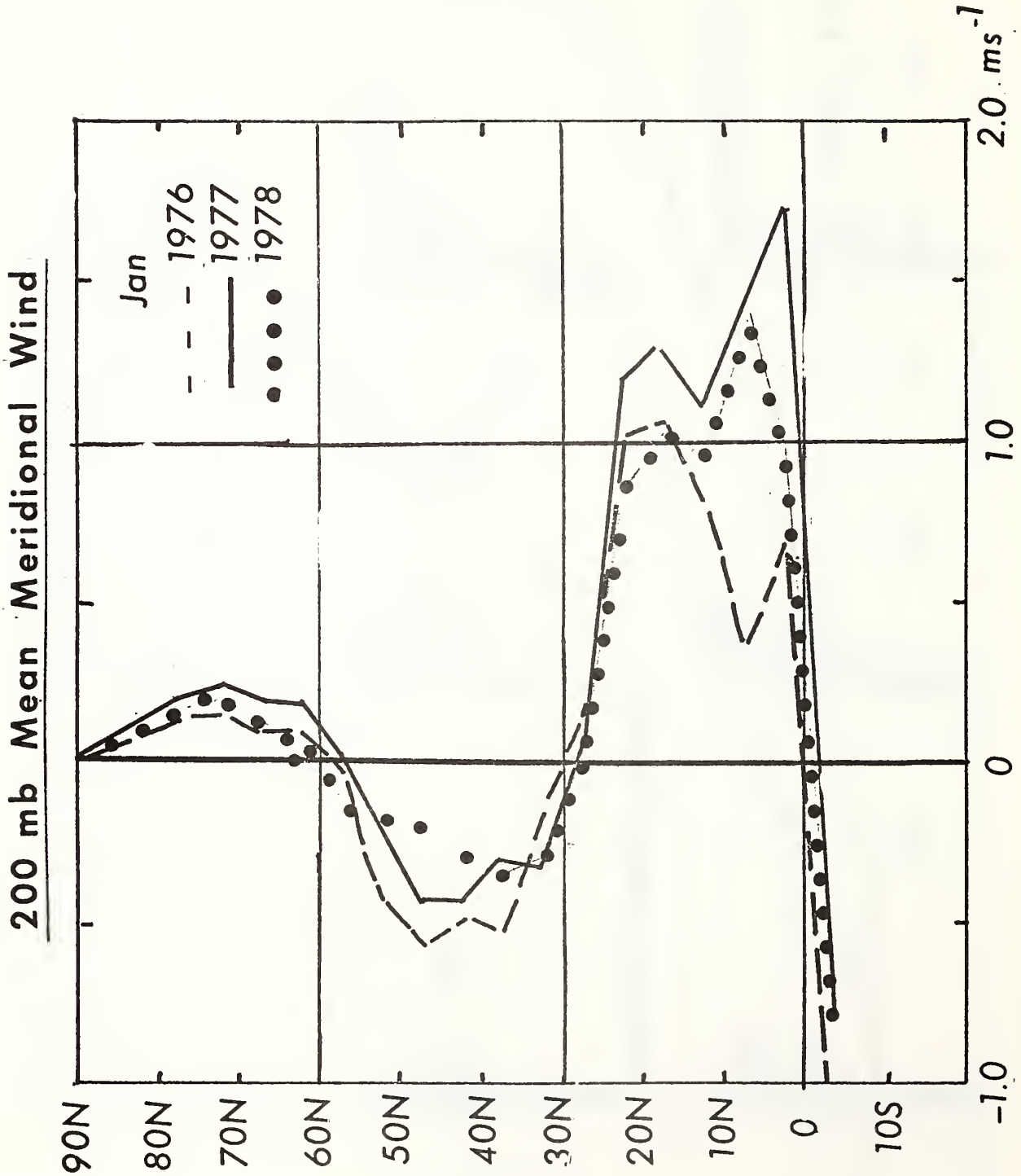
200 mb Mean Meridional Wind
Jan
1976
1977
1978
90N
80N
70N
60N
50N
40N
30N
20N
10N
0
10S
-1.0
0
1.0
2.0 ms-1

Figure 7

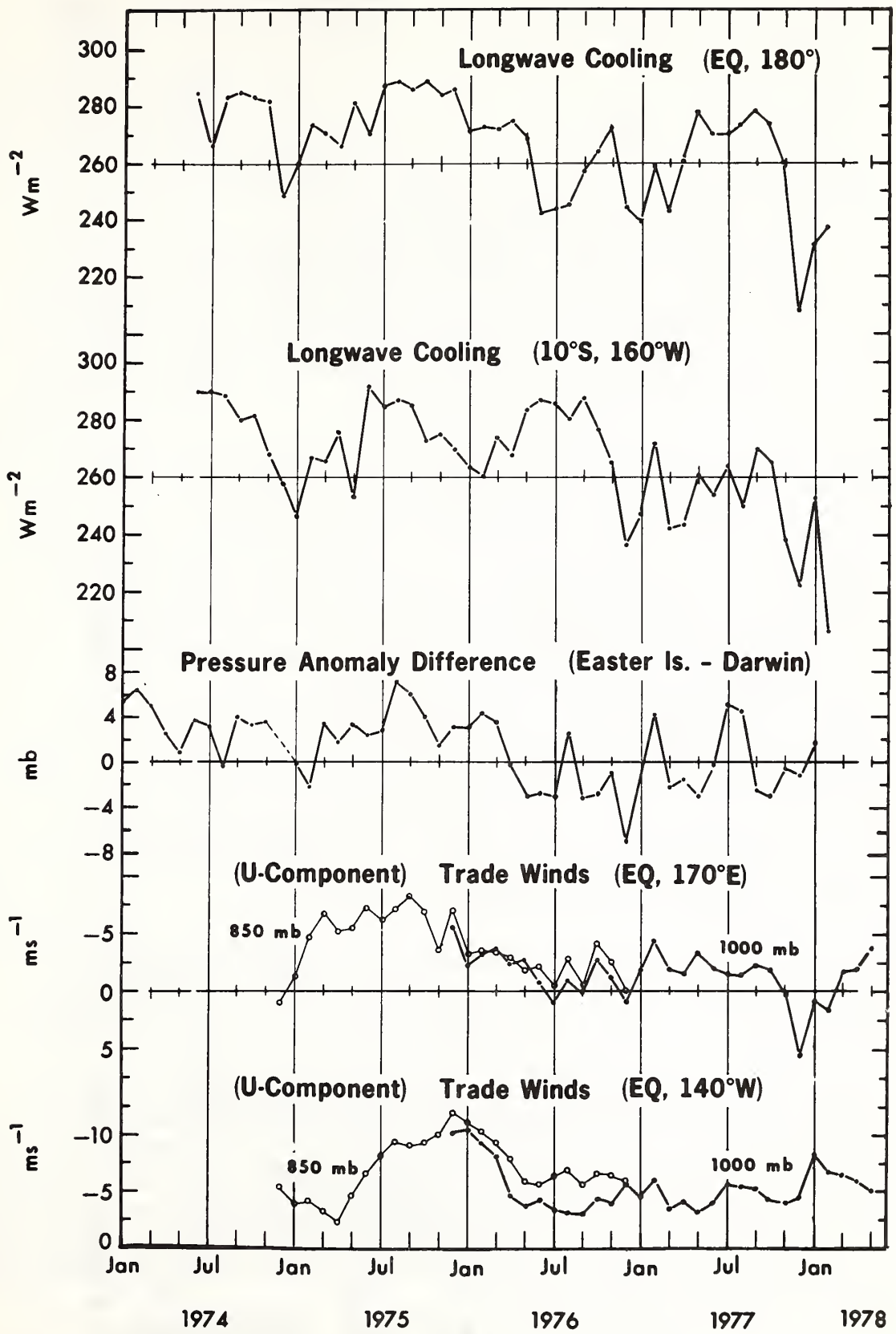
Longwave Cooling (EQ, 180°)
Wm⁻²
300
280
260
240
220
Longwave Cooling (10°S, 160°W)
Wm⁻²
300
280
260
240
220
Pressure Anomaly Difference (Easter Is. - Darwin)
mb
8
4
0
−4
−8
(U-Component) Trade Winds (EQ, 170°E)
ms⁻¹
850 mb
1000 mb
−5
0
5
(U-Component) Trade Winds (EQ, 140°W)
ms⁻¹
−10
−5
0
850 mb
1000 mb
Jan
Jul
Jan
Jul
Jan
Jul
Jan
Jul
Jan
1974
1975
1976
1977
1978

Figure 8

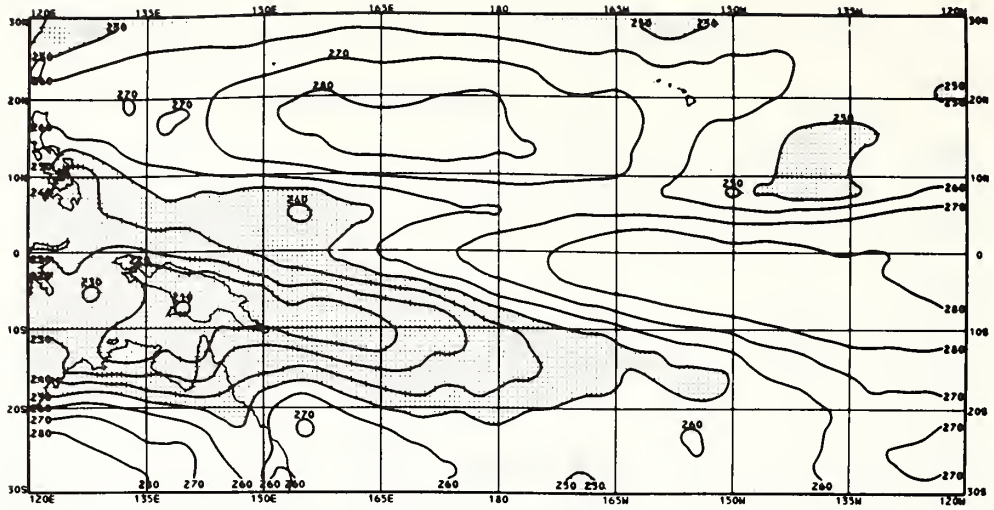

OUTGOING LONGWAVE RADIATION (WM^{-2})
WINTER 1976

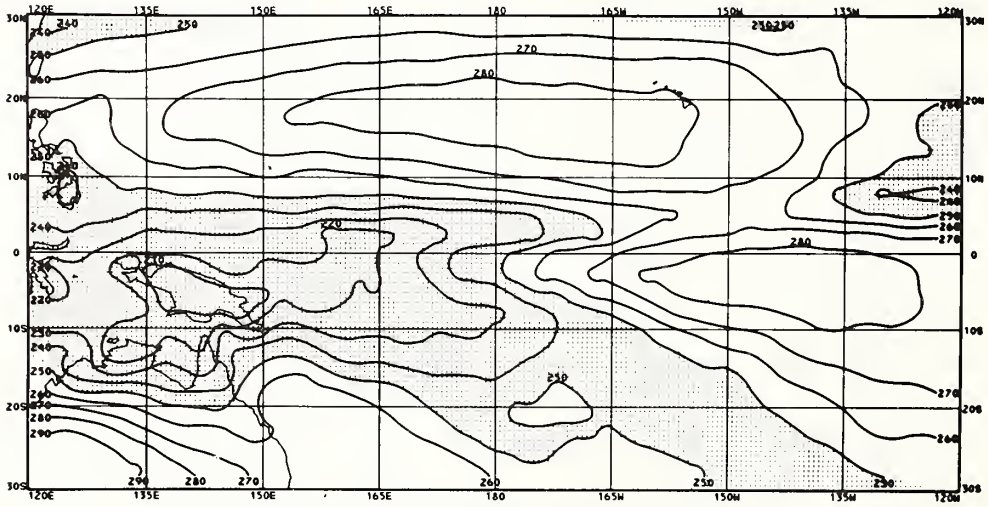

OUTGOING LONGWAVE RADIATION (WM^{-2})
WINTER 1977

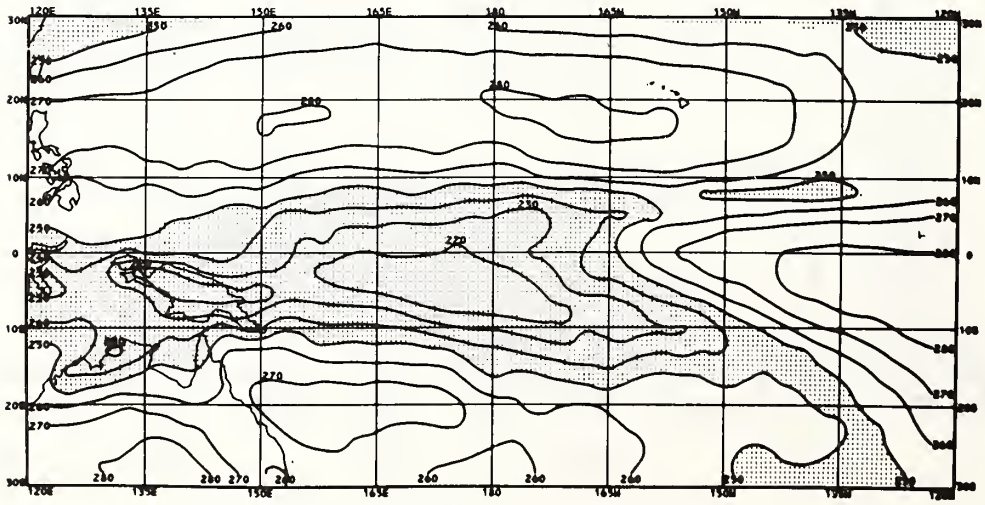

OUTGOING LONGWAVE RADIATION (WM^{-2})
WINTER 1978

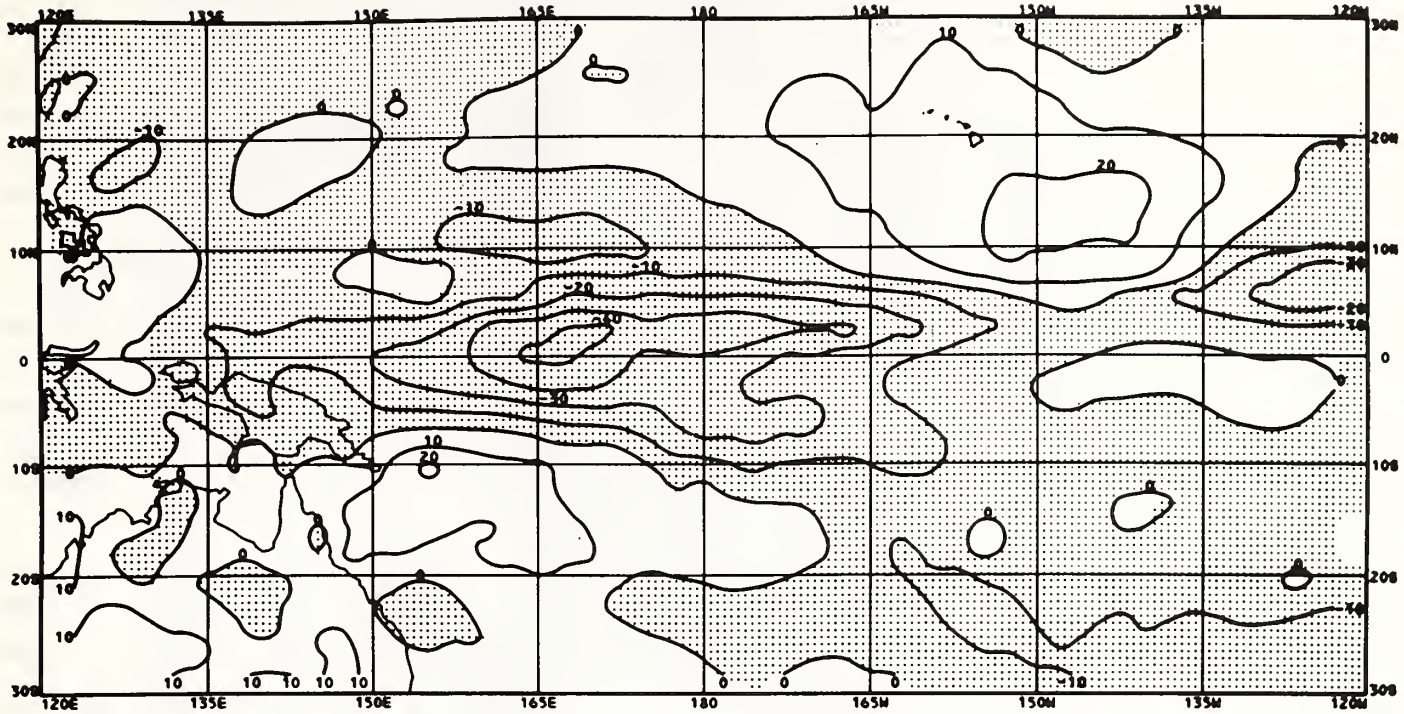

OUTGOING LONGWAVE RADIATION (WM^{-2})
DIFFERENCE WINTER 1977-1976

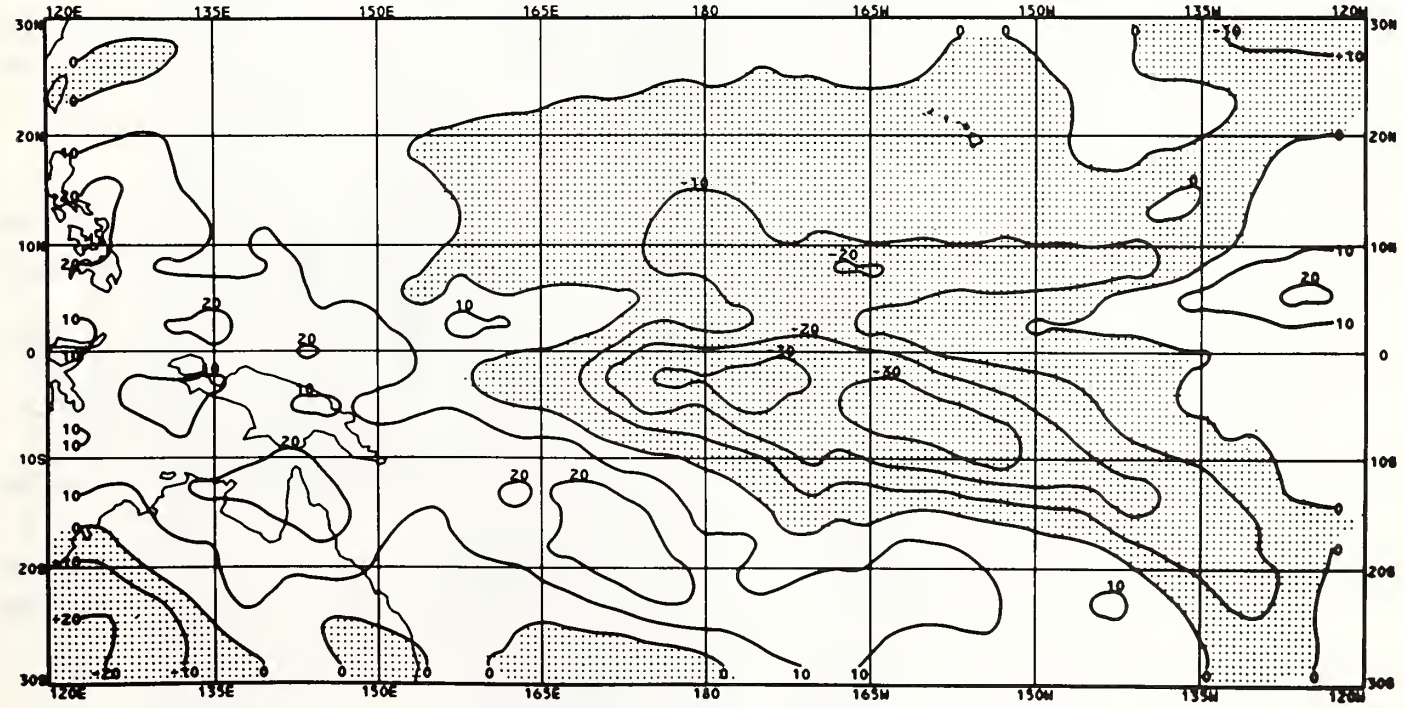

OUTGOING LONGWAVE RADIATION (WM^{-2})
DIFFERENCE WINTER 1978-1977

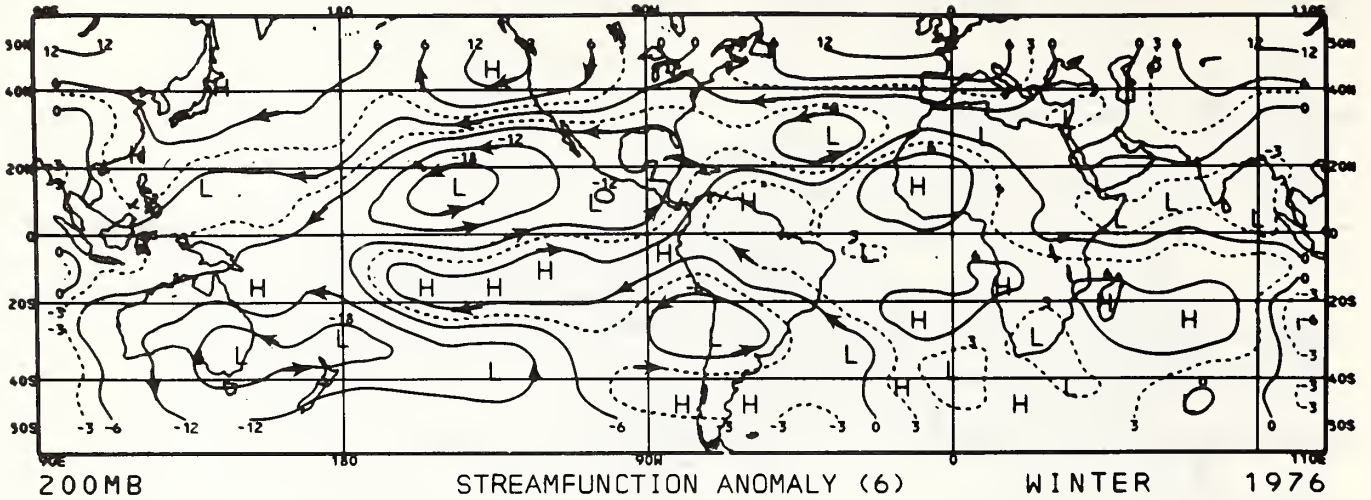
200MB
STREAMFUNCTION ANOMALY (6)
WINTER
1976

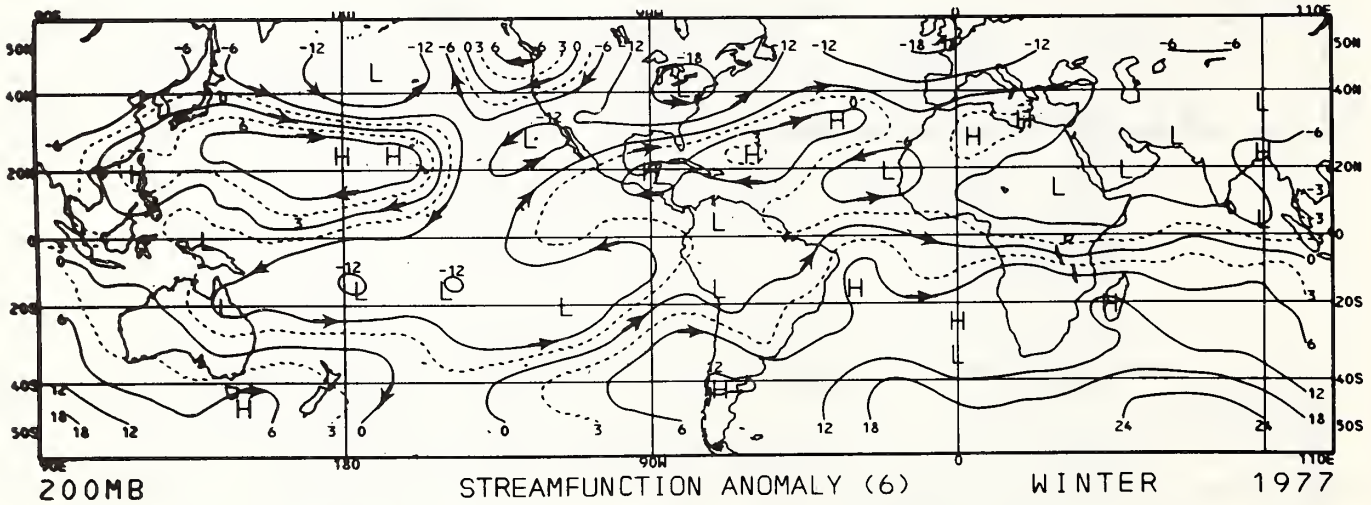
200MB
STREAMFUNCTION ANOMALY (6)
WINTER
1977

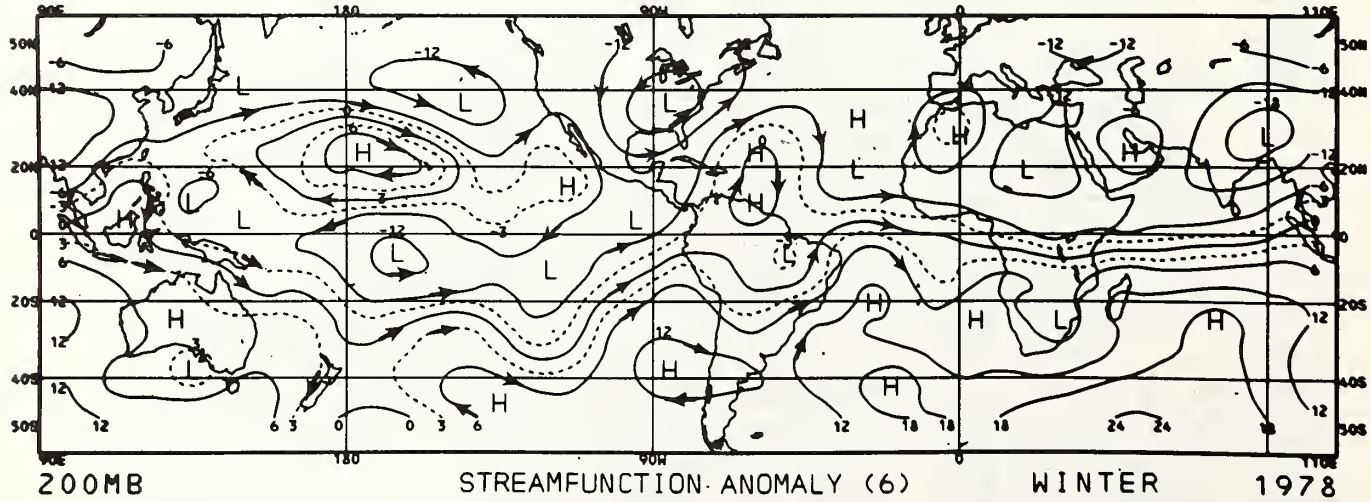
200MB
STREAMFUNCTION ANOMALY (6)
WINTER
1978

↑ 11:45 19FE78 32A-Z 0006-1640 FULL DISC IR
↑ 12:00 19FE78 14A-Z 0006-1640 FULL DISC IR

Figure 11

Figure 12

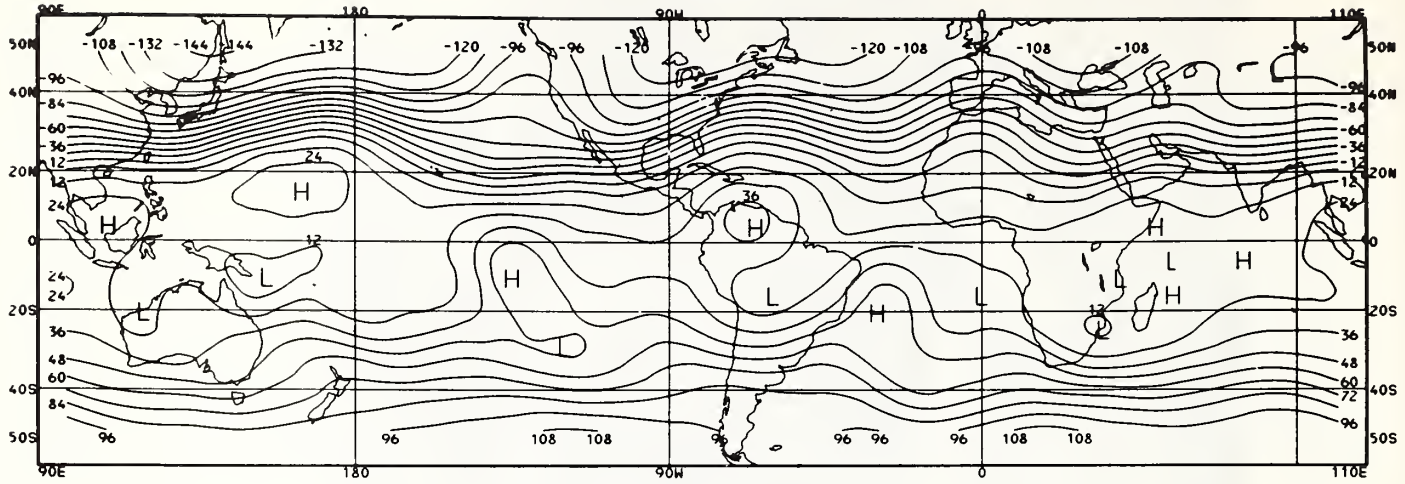

200MB STREAMFUNCTION FEBRUARY (16-21) 1978

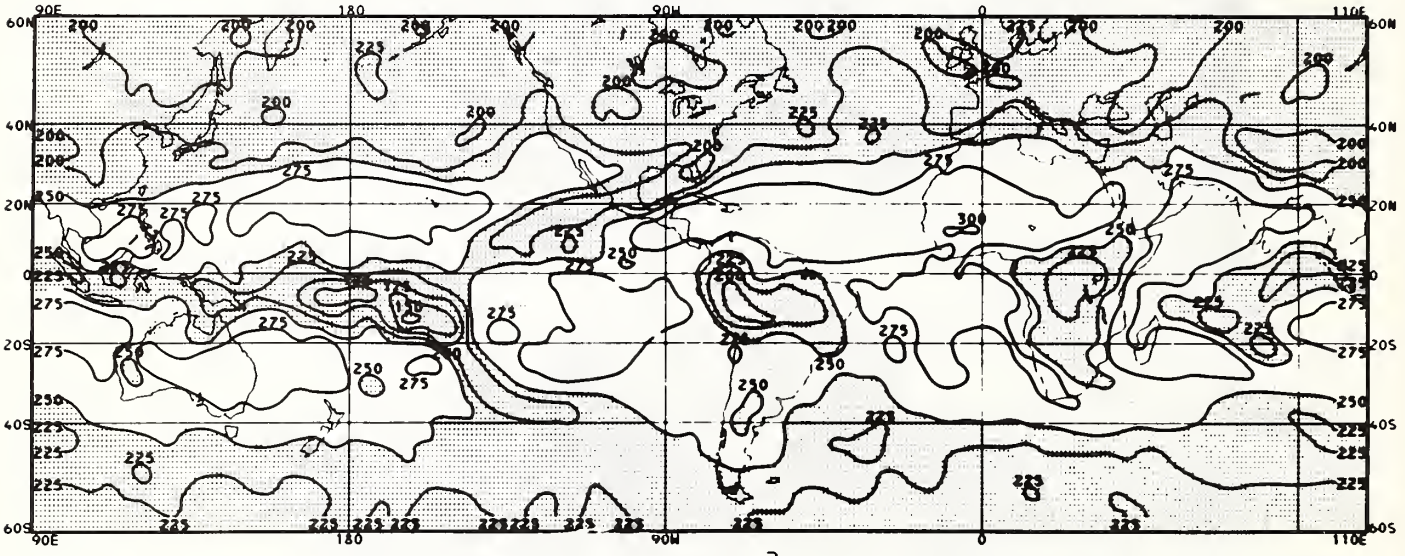

OUTGOING LONGWAVE RADIATION (WM^{-2}) FEBRUARY (16-21) 1978

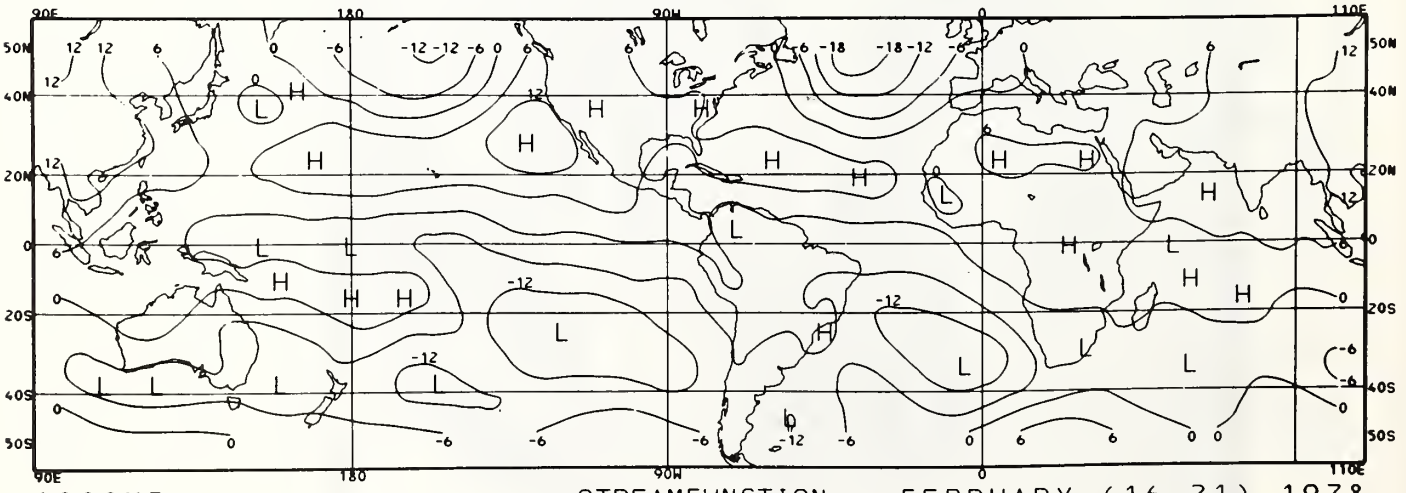

1000MB STREAMFUNCTION FEBRUARY (16-21) 1978

SNOW AND SEA ICE COVER FLUCTUATIONS IN 1977-78

G. Kukla and J. Gavin

Lamont-Doherty Geological Observatory
Palisades, New York 10964

Variation of snow and pack-ice in both hemispheres was measured from U.S. Navy and NOAA charts separately for various geographic segments (Figs. 1 and 2). The methodology used is described in detail elsewhere (Kukla and Gavin, 1978).

NOAA charts were occasionally cross-checked and complemented by information from Air Force charts and DMSP satellite images. The continued improvement in the quality of the snow charts through 1978 should be noted. Data checks are made on a continual basis by exchanging results with that generated by another method (Wiesnet and Matson, 1975).

The northern hemisphere snow charts were incomplete for the spring of 1978 due to instrument failure. Air Force photographs were analysed in order to complete the set. The charts have been made available to NOAA for further distribution.

Snow and ice coverage during 1977 was on the heavy side in the northern hemisphere, but light in the southern one. In February 1978 the largest average monthly snow and ice extent in the northern hemisphere observed over the past decade was reached. The largest 12 month running average was reached in the interval ending August 1978. (Figs. 3 and 4).

Compared to the 1973-77 seasonal means, Arctic ice was above normal in winter and spring but below in summer and autumn. Snow was below normal in spring and summer but above average in autumn and winter. (Fig.10)

Large year to year regional Arctic ice variations can be observed. (Fig. 7). Note the opposite trends between the Bering Sea (BER) and the North Atlantic sector (NAT) which includes the Barents, Norwegian and Greenland Seas.

.....

Kukla, G. and Gavin, J. 1978. Proc. of the Intern. Workshop on World Glacier Inventory, 17-22 Sept., 1978,Switzerland.

Wiesnet, D. R. and Matson, M. 1975. Monthly Weather Review, 104, 323-835.

FIGURE 1: Geographic segments analysed by grid count for both the northern and southern hemisphere.

FIGURE 2: Geographic segments for the northern hemisphere (planimetered)

FIGURE 3: 12 month running means of snow and ice cover in the northern hemisphere(NH-SIC); of sea ice in concentration $\geq$4 octas plus the Antarctic continent in the southern hemisphere (SH-SIC). Plotted on terminal date. Also shown Antarctic sea ice and land ice extent at the end of November (SH-NOV). Scale in million km^2. Dots mark annual average.

FIGURE 4: Mean monthly snow and sea ice covers in the Northern Hemisphere from 1967-78. Ice $\geq$4 octas, large polynyas excluded, Greenland included. Scale in million km^2.

FIGURE 5: Mean monthly snow and ice cover in the Northern Hemisphere from 1972-78 for individual segments.(Jan-Jun)

FIGURE 6: Same as Fig. 5 (Jul-Aug) Scale in million km^2.

FIGURE 7: Mean monthly Arctic ice cover from 1972-78 for BER, LAB, and NAT. Ice $\geq$ 4 octas. Scale in 0.1 million km^2

FIGURE 8: Mean monthly sea ice extent in Antarctic segments ANR and ANW from 1973-78. Minimum concentration 4 octas. Units in millions of square kilometers.

FIGURE 9: 12 month running means of Antarctic sea ice for 5 segments. Plotted at terminal date. Upper curves show ice over 1 octa and polynyas, lower curves show sea ice $\geq$4 octas and exclude polynyas. Lines mark beginning of the year. Scale in million km^2.

FIGURE 10: Seasonal difference in percent from the 1973-77 mean shown for Arctic ice and northern hemisphere snow and ice combined. Winter(Dec-Feb);Spring(Mar-May);Summer (June-Aug);Autumn(Sept-Nov).

FIGURE 11: Difference in percent from the 1973-77 mean for northern hemisphere snow and ice for individual segments. Units in 5% increments.

FIG. 1

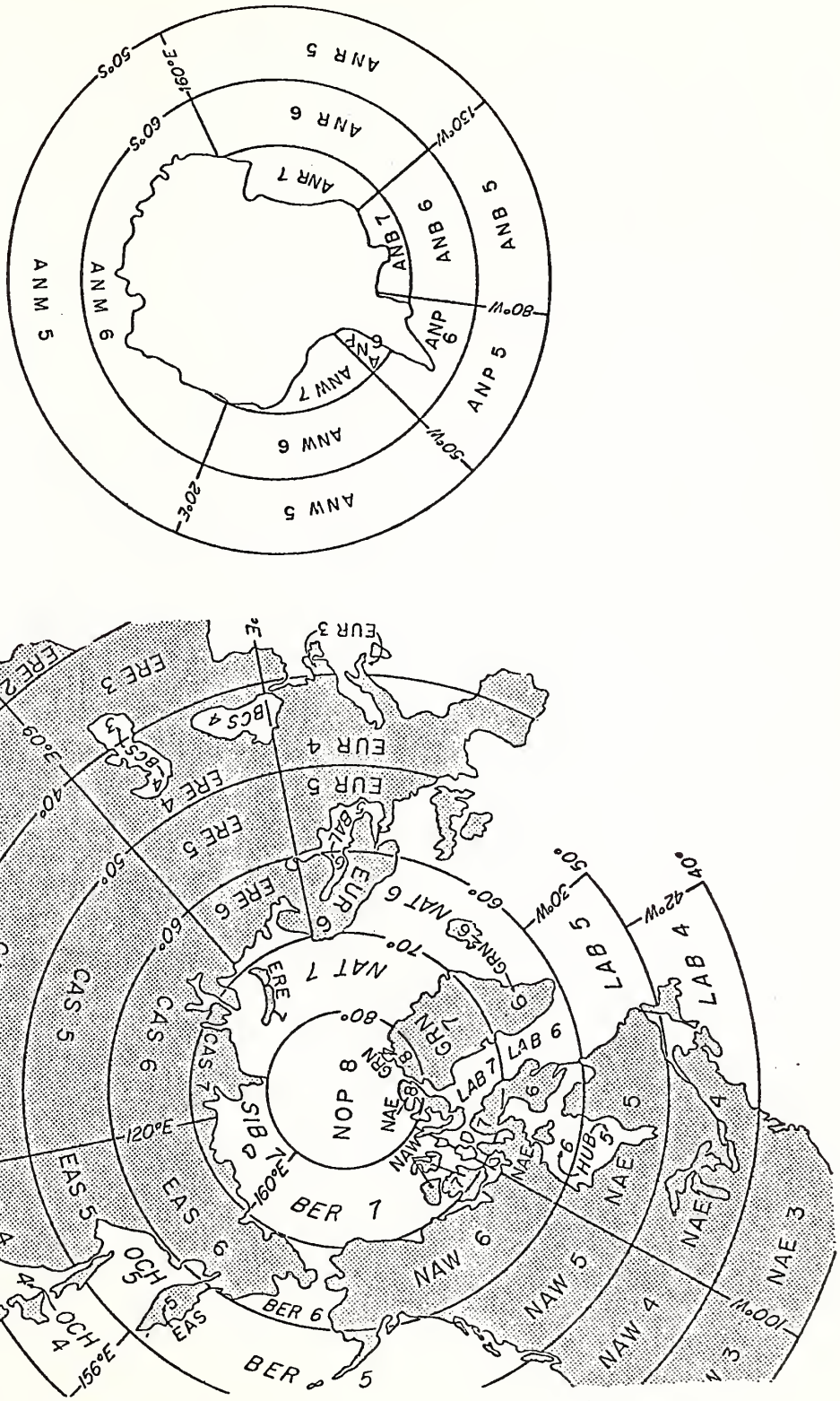
ANR 5
ANR 6
ANR 7
ANB 7
ANB 6
ANB 5
ANP 6
ANP 5
ANW 7
ANW 6
ANW 5
ANM 6
ANM 5
50°S
60°S
160°E
130°W
80°W
50°W
20°E
EUR 3
EUR 4
EUR 5
EUR 6
ERE 2
ERE 3
ERE 4
ERE 5
ERE 6
BCS 4
BCS 3
BAL 5
GRN 6
GRN 7
GRN 8
NAT 6
NAT 7
ERE
CAS 2
CAS 3
CAS 4
CAS 5
CAS 6
CAS 7
SIB 7
SIB 6
EAS 3
EAS 4
EAS 5
EAS 6
OCH 4
OCH 5
BER 5
BER 6
BER 7
NOP 8
NAE
NAW
LAB 4
LAB 5
LAB 6
LAB 7
HUB
NAE 3
NAE 4
NAE 5
NAE 6
NAW 4
NAW 5
NAW 6
30°
40°
50°
60°
70°
80°
3.09
120°E
160°E
156°E
60°W
30°W
42°W
100°W

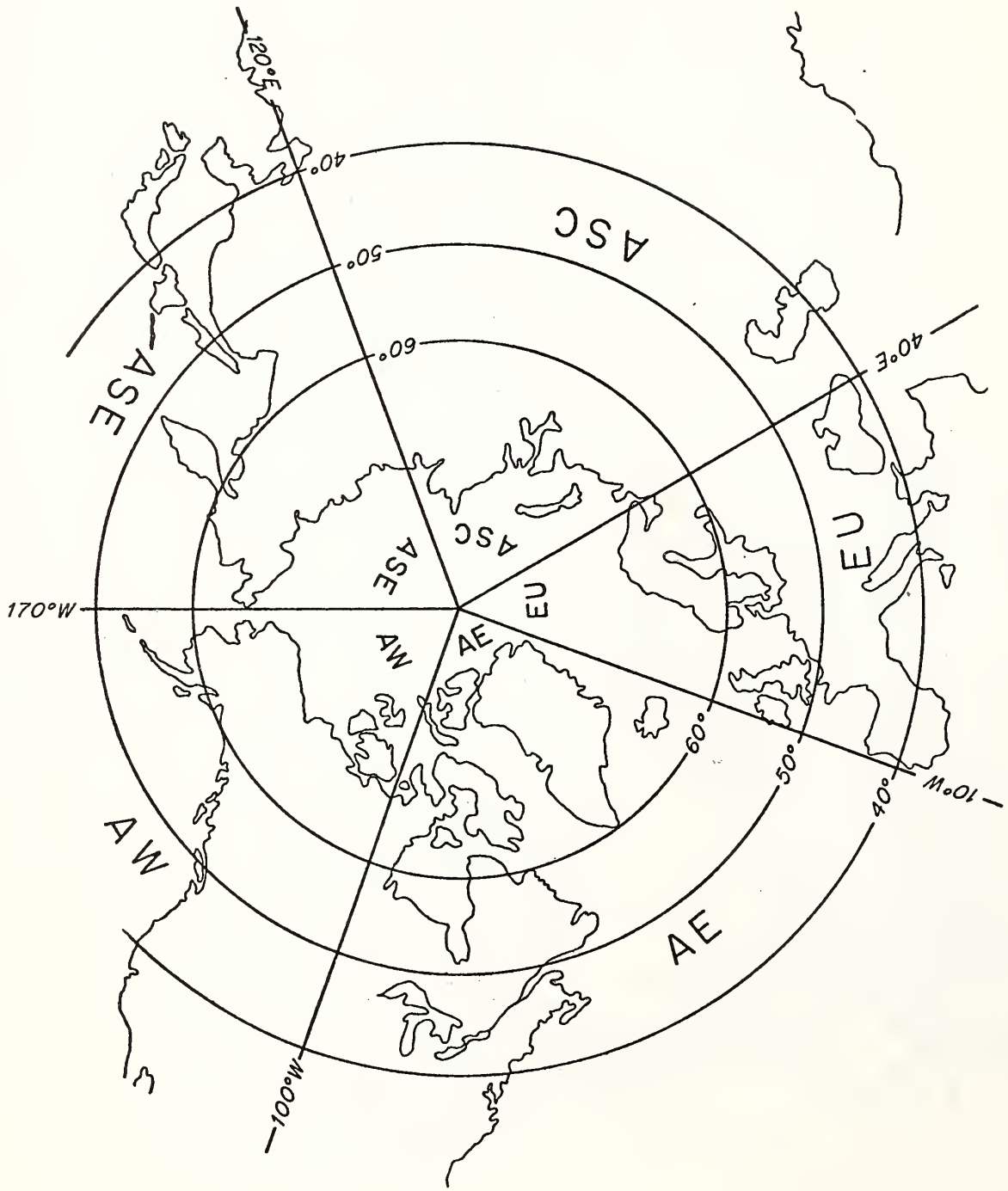
120°E
40°
50°
60°
40°E
ASC
ASE
EU
170°W
AW
AE
10°W
100°W

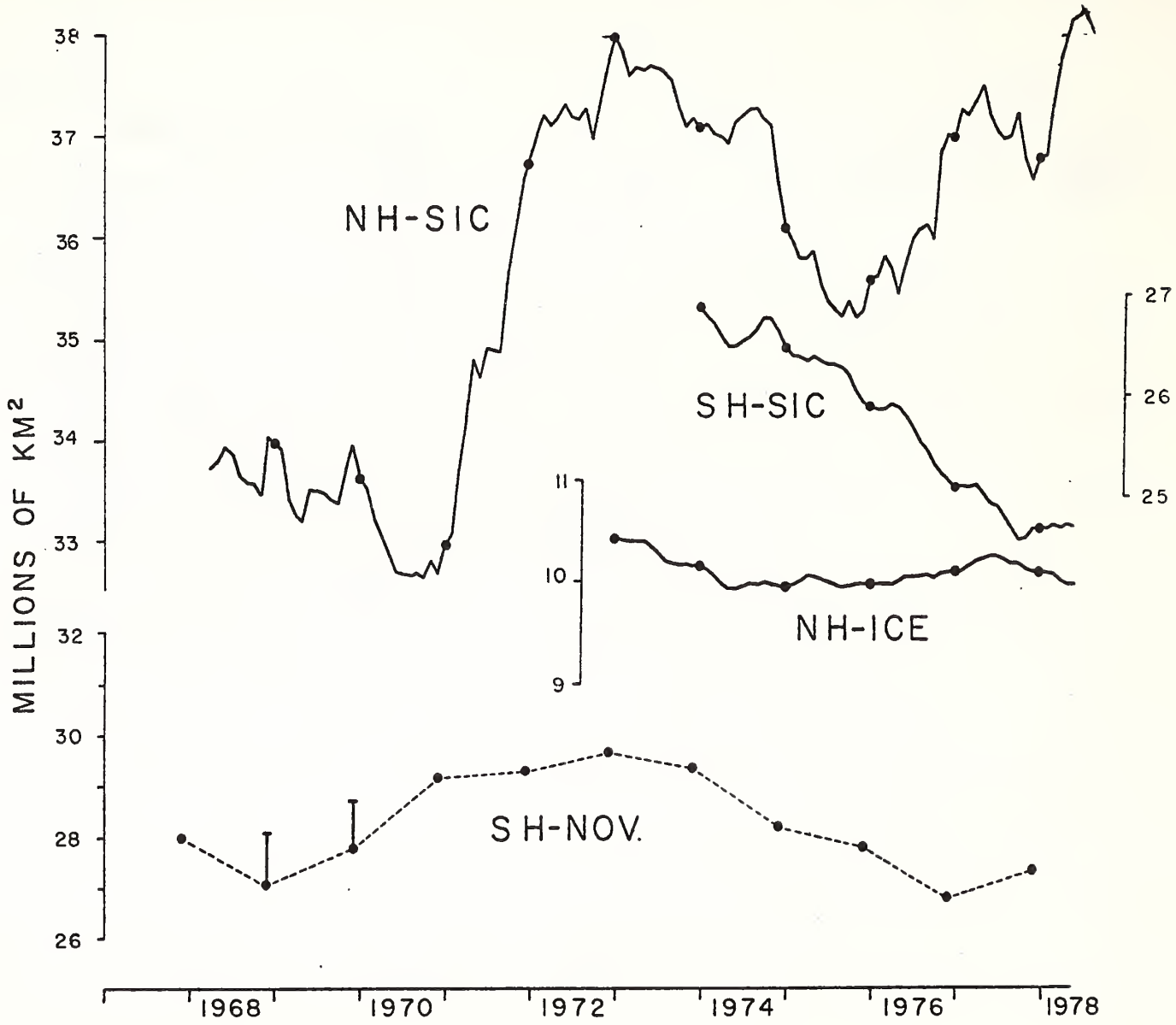
MILLIONS OF KM²
38
37
36
35
34
33
32
30
28
26
NH-SIC
SH-SIC
27
26
25
11
10
9
NH-ICE
SH-NOV.
1968
1970
1972
1974
1976
1978

FIG 4

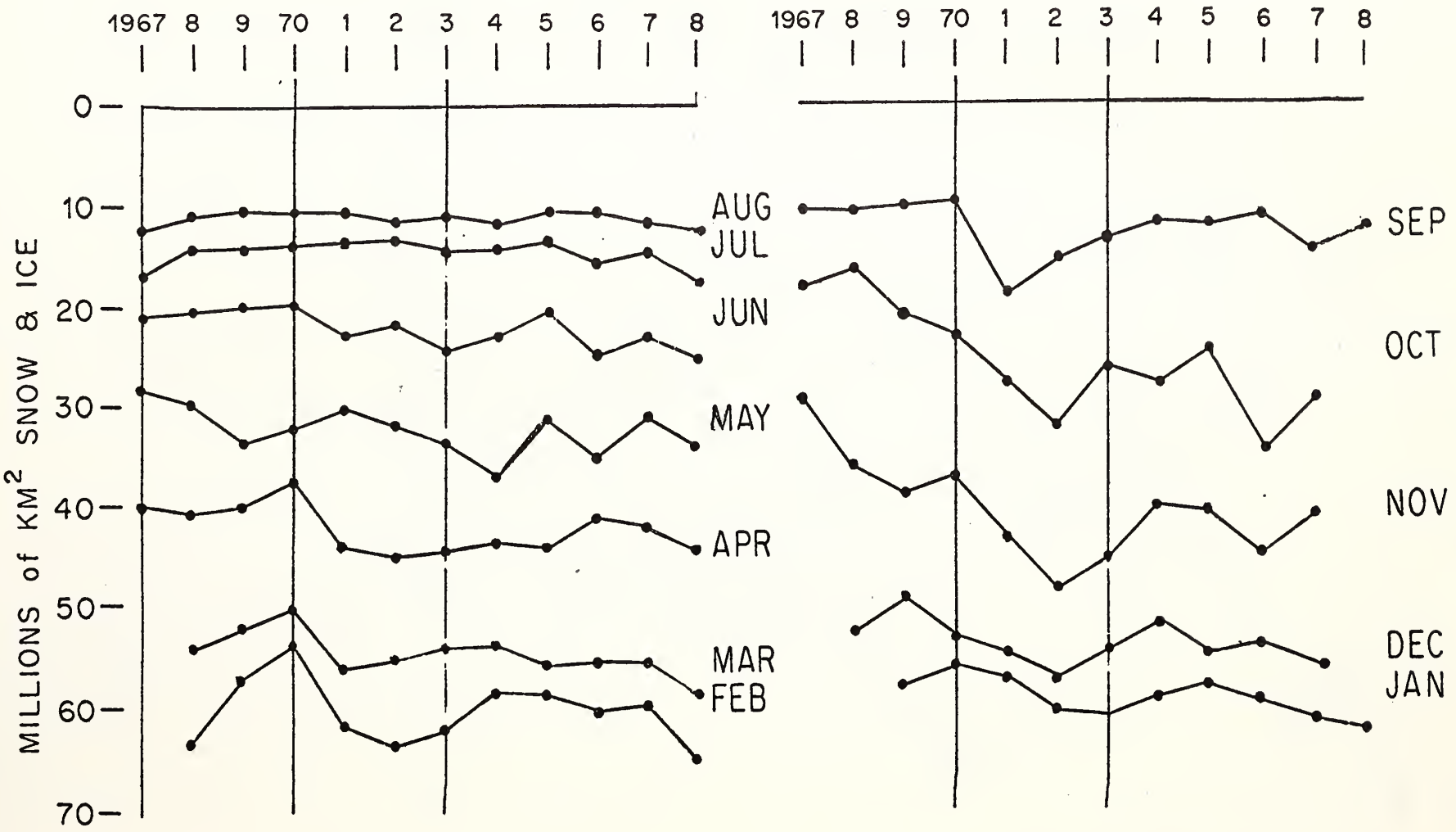
1967 8 9 70 1 2 3 4 5 6 7 8
1967 8 9 70 1 2 3 4 5 6 7 8
0
10
20
30
40
50
60
70
MILLIONS of KM2 SNOW & ICE
AUG
JUL
JUN
MAY
APR
MAR
FEB
SEP
OCT
NOV
DEC
JAN

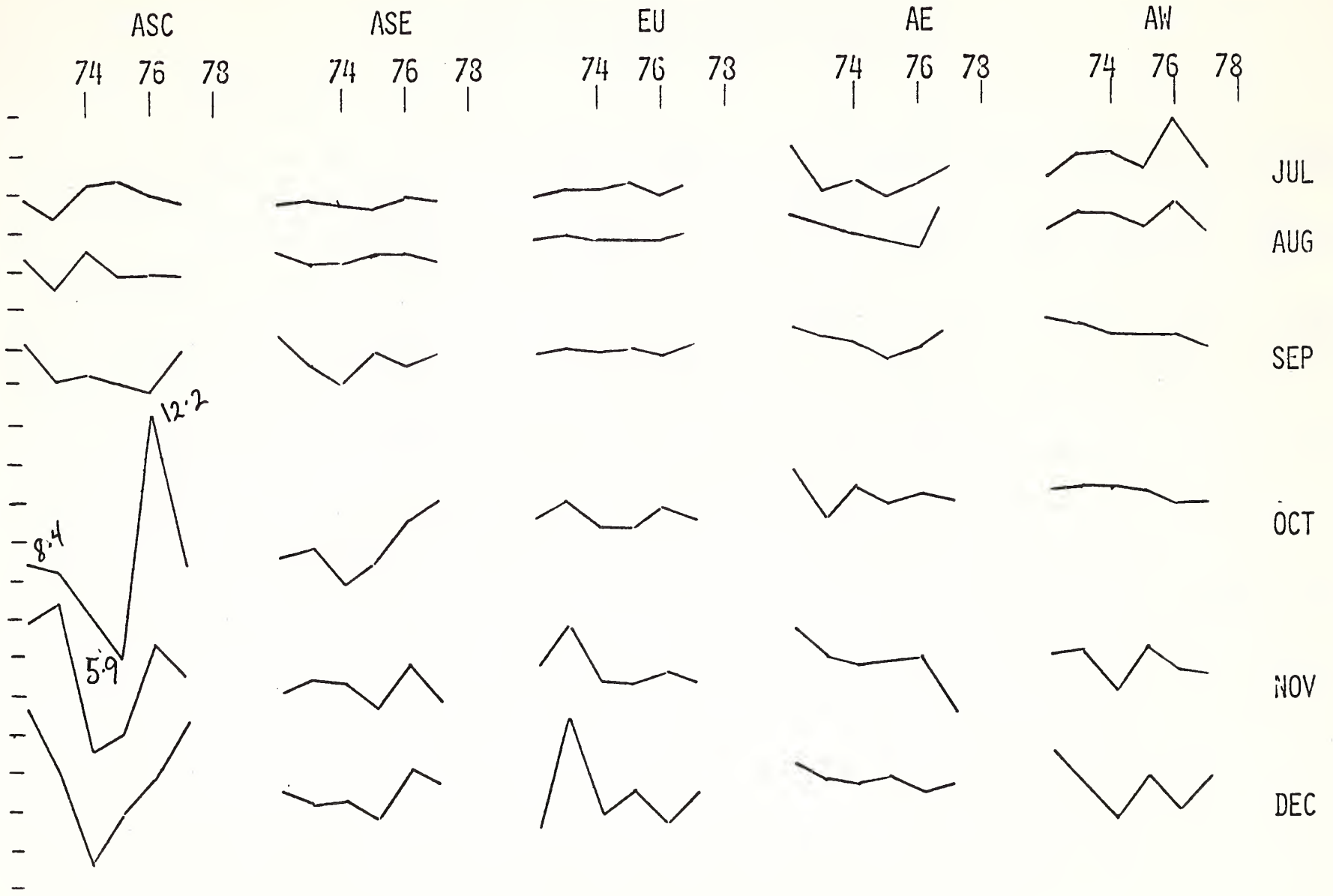

MEAN MONTHLY SNOW AND ICE EXTENTS

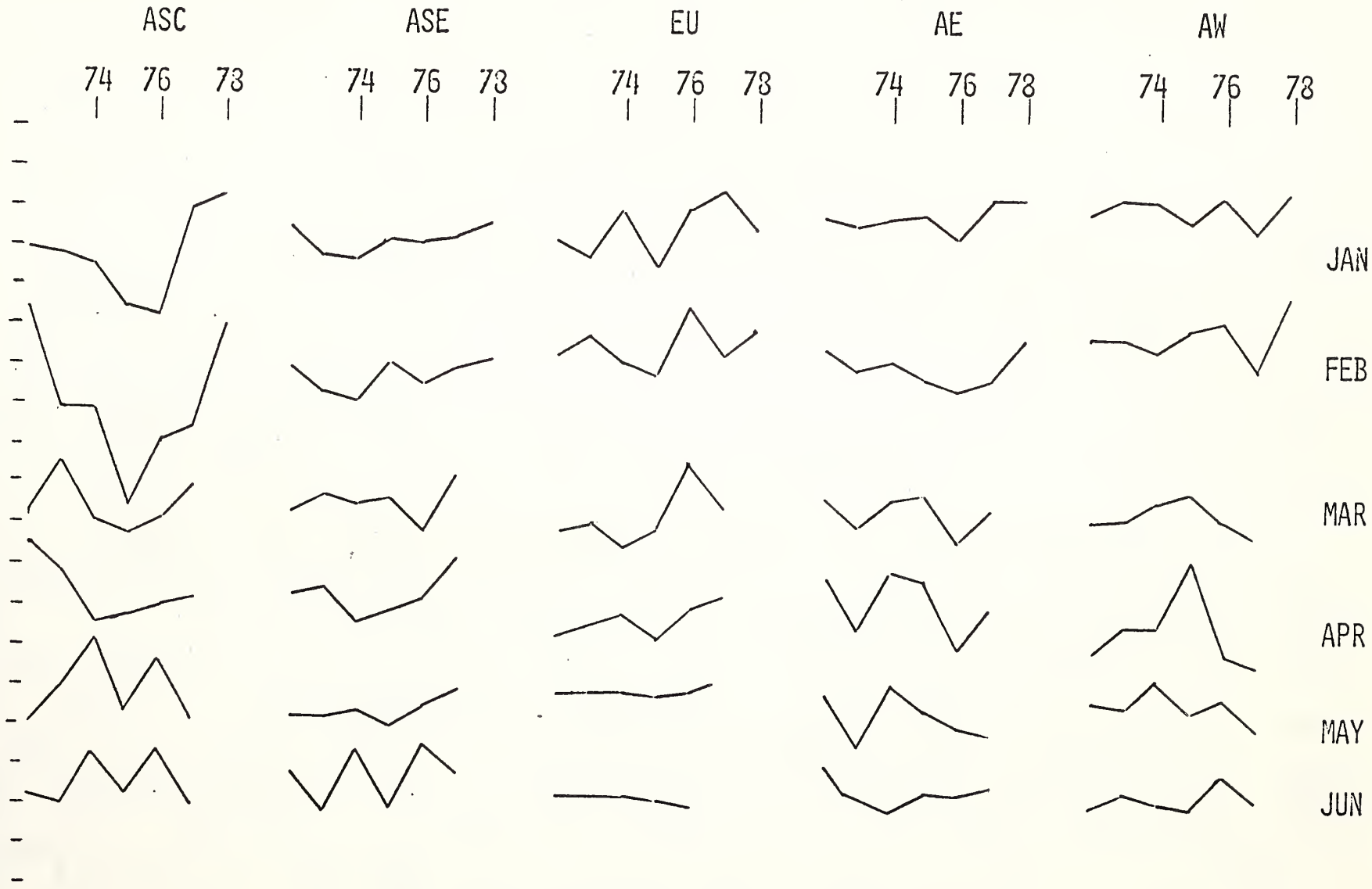

MEAN MONTHLY SNOW AND ICE EXTENTS

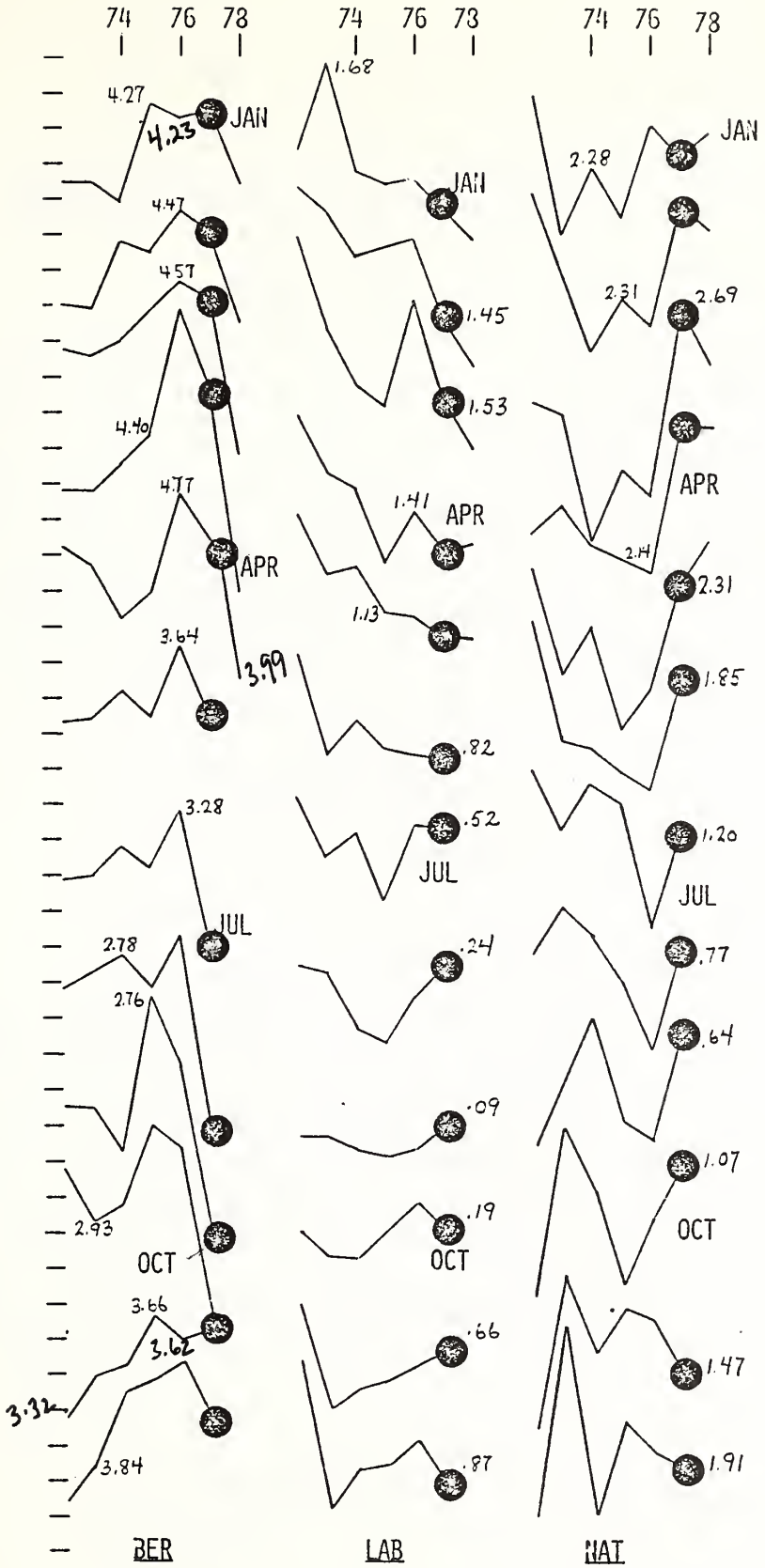

MEAN MONTHLY ICE EXTENTS

ARCTIC

MONTHLY MEAN [2-5]

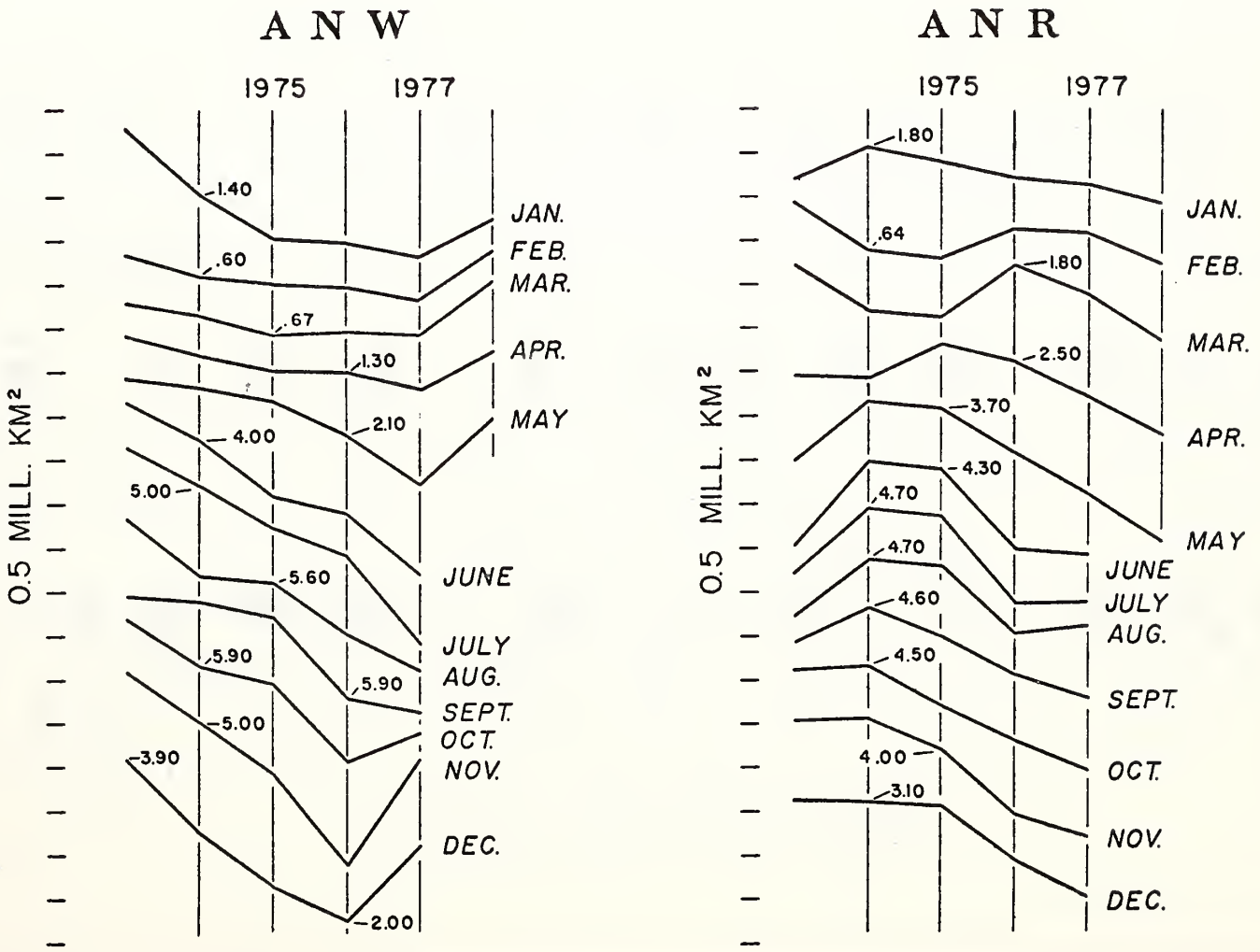

12 MONTH RUNNING MEANS

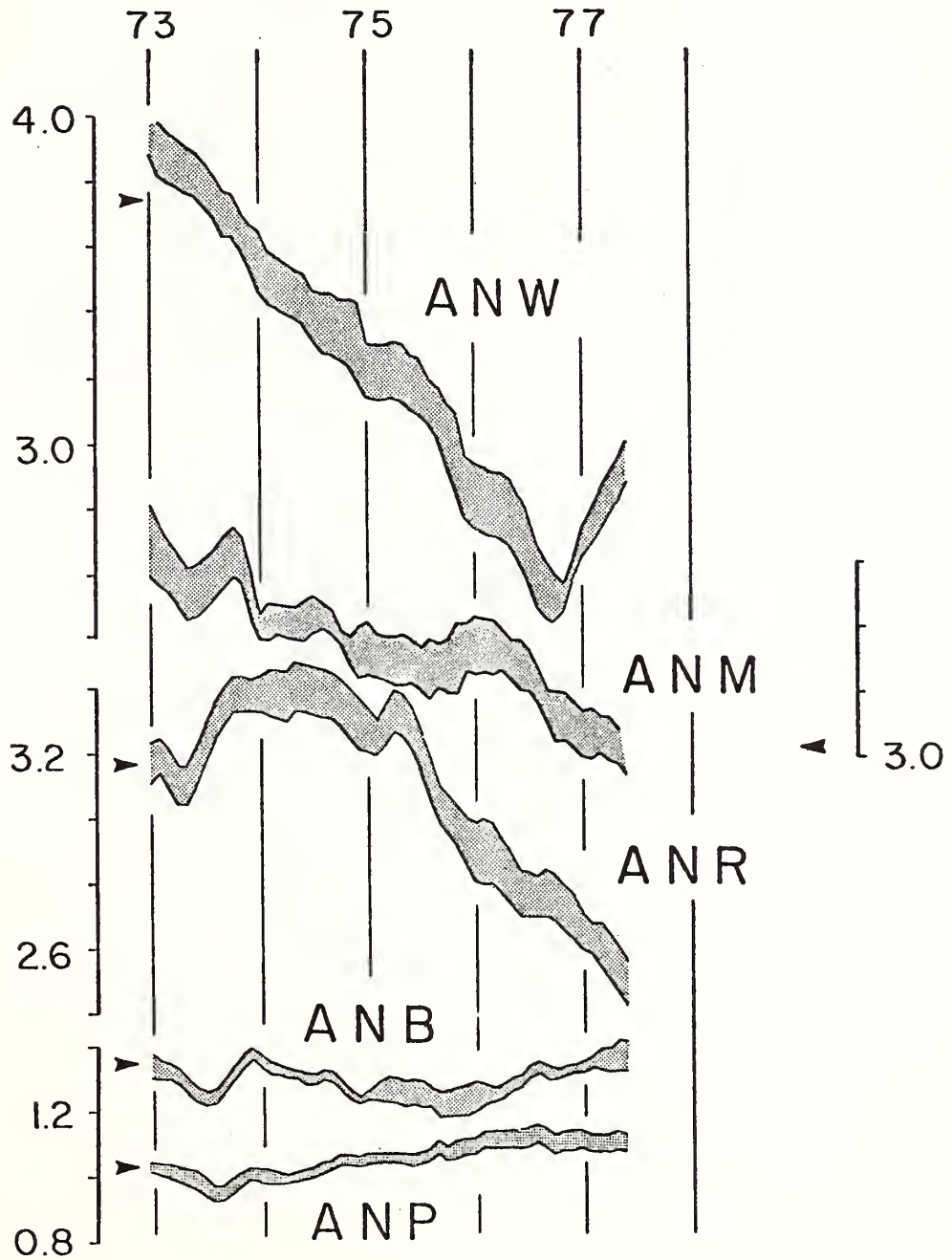

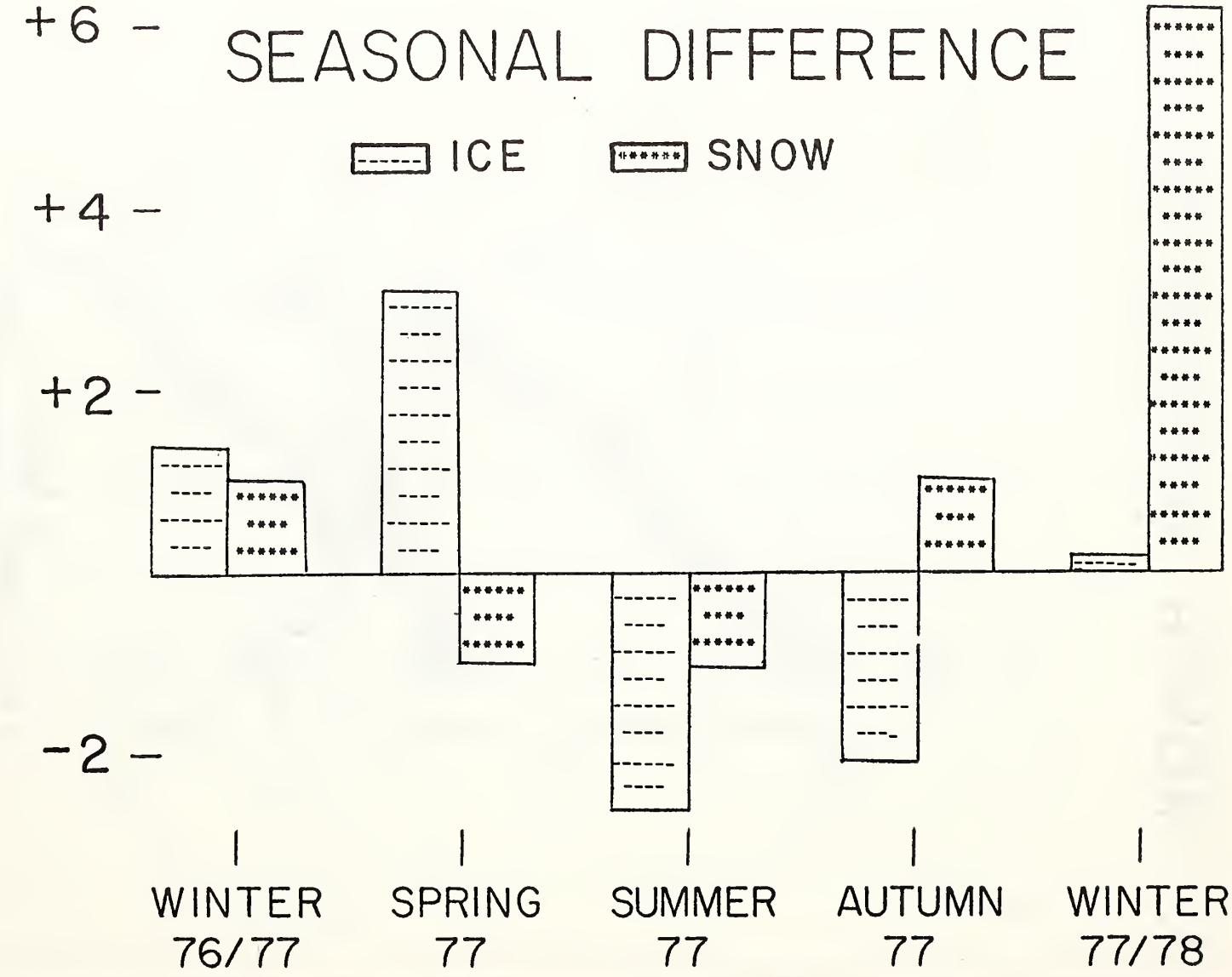
SEASONAL DIFFERENCE
ICE
SNOW
+6
+4
+2
-2
WINTER 76/77
SPRING 77
SUMMER 77
AUTUMN 77
WINTER 77/78

FIG 11

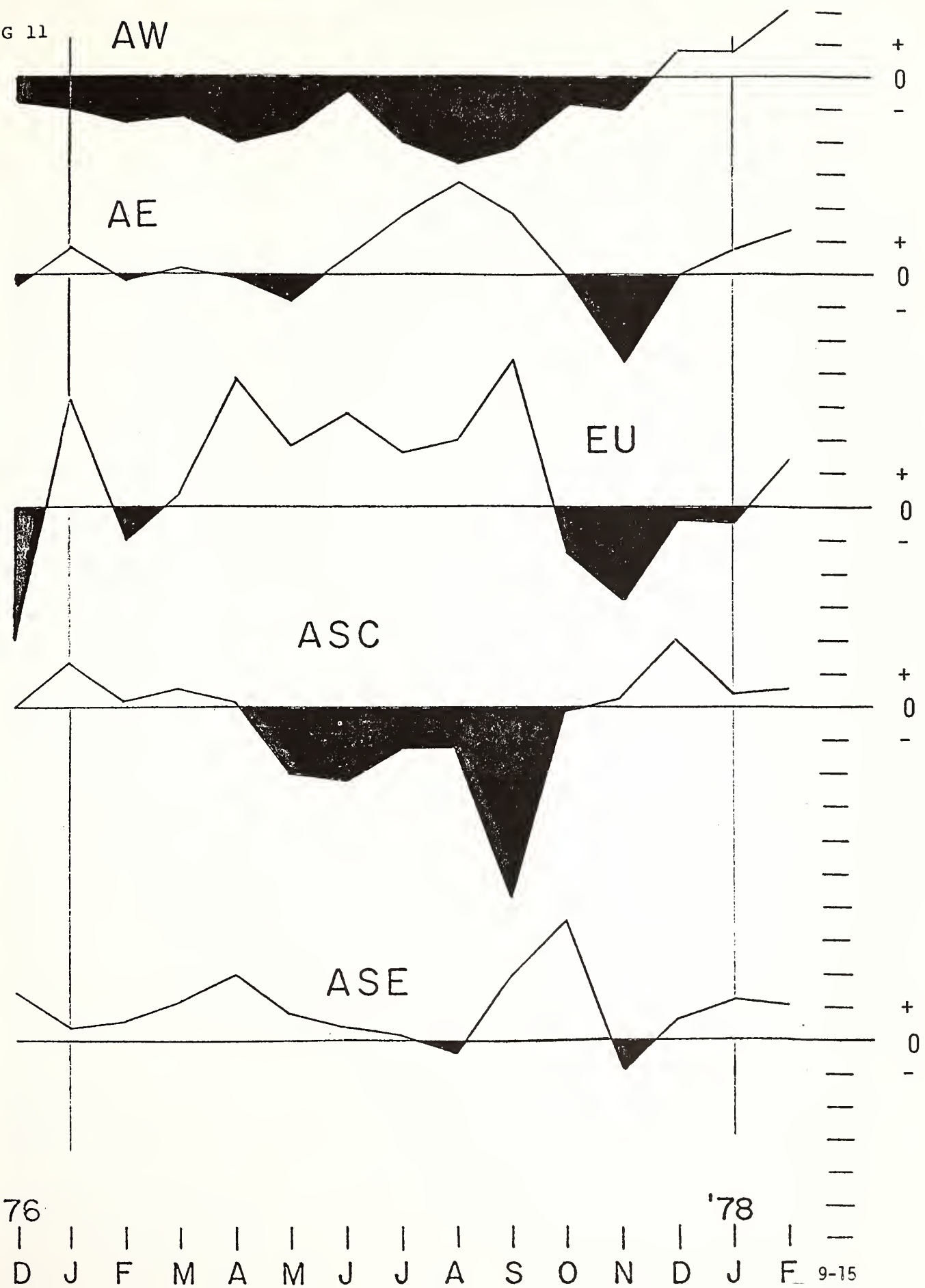

The 12-year Satellite Snowcover Record and the Record Winter Snowcover of 1977-78

Craig P. Berg[1] and Michael Matson[2]

The winter of 1977-78 was the second consecutive year of record-breaking winter snowcover in North America according to NOAA/NESS satellite-derived measurements. February 1978, in particular, had the maximum snowcover on record for the 12-year North American data set from 1967-1978.

The data set, now complete from November 1966 through September 1978, consists of monthly mean snowcover maps and their corresponding areal snowcover values. The snowcover data have been corrected to correspond to true surface area (Matson, 1977). December 1967 and January 1968 imagery from the ESSA Series satellites was previously missing making the monthly maps for these two months unavailable (Wiesnet and Matson, 1976). Through the courtesy of Sea Ice Consultants, new images were obtained and the monthly mean snowcover maps and snowcover area were derived.

The updated plot of the 12-month running mean (figure 1) shows an upward trend due to the record winter snowcover of 1977-78. The Eurasian running mean snowcover, though declining in 1977, now shows a slight upward trend.[3] The Northern Hemispheric running mean snowcover, also declining in 1977, likewise shows an upward trend as a result of the extensive snowcover during the winter of 1977-78.

---

[1]Lieutenant, NOAA Corps

[2]Physical Scientist, NOAA/NESS

[3]The Scanning Radiometer on the NOAA-5 satellite failed on 16 MAR 78. During the months of March and April 1978, limited Defense Meteorological Satellite Program (DMSP) data, supplemented with the 10-year mean monthly snowline, were used to derive the Eurasian weekly snowline.

North American and Eurasian winter satellite snowcover values for the twelve-year period are graphically illustrated in figure 2. February 1978 snowcover in North America was the highest and January 1978 snowcover the second highest for any month in the 12-year snowcover record. Eurasian winter snowcover in 1977-78 remained about the same as the 1977 Eurasian winter snowcover.

Figure 3 permits a comparison of the snow lines of the record February 1978 Northern Hemispheric snowcover with the 10-year (1967-76) mean February snowcover. The February 1978 snow line in the southern and midwestern regions of the U.S. is generally 500 to 1000 kilometers south of the 10-year satellite-derived mean snow line; whereas, in the West the snow line differed insignificantly from its 10-year mean. Eurasian February 1978 snowcover, when compared to the 10-year mean, shows large areas of more extensive snowcover in Eastern Europe, Central Asia, Korea, and Japan.

Table 1 contains the 10-year mean monthly winter continental snowcover and the 1976-77 and 1977-78 winter snowcovers. January February, and March 1978 winter snowcover values in North America are greater than those for 1976-77. December snowcover in both winters was within the expected limits.

Table 1 also shows that December and January of both winters were unusual snowcover months in Eurasia, whereas February and March of both winters were within the expected limits of snowcover extent. The 1977-78 Eurasian snowcover was more extensive in December, February, and March than in 1976-77, with the peak February snowcover of 1978 being less extensive than the peak January snowcover of 1977.

Figures 4-7 show the monthly mean snowcover maps for the Northern Hemisphere for the winter of 1977-78 for comparison to the 10-year mean monthly snowcover maps for the Northern Hemisphere. Note the extensive snowcover in North America during January, February, and March.

Several statistical relationships between snowcover data of the winter months in Eurasia and the Northern Hemisphere, as first reported by Wiesnet and Matson (1976), have been updated to include eleven data points. Figures 8-10 are the 11-point updates of these linear regression relationships. The snowcover estimates for Eurasia and Northern Hemisphere shown in Table 2 were derived using the updated regression equations based on the 1977-78 snowcover data. In figure 11, we compare these estimates with the measured snowcover values. North American snowcover estimates are the arithmetic difference of Eurasian from Northern Hemispheric snowcover values, i.e., $e_{NA} = e_{NH} - e_E$, where e is the snowcover estimate.

References

Matson, M., 1977: The Satellite Snowcover Record: Status, Trends, and Relationships, Proceed. Second Annual NOAA Climate Diagnostics Workshop, pp. 10-1 to 10-16.

Wiesnet, D.R. and M. Matson, 1976: A possible Forecasting Technique for Winter Snowcover in the Northern Hemisphere and Eurasia, Monthly Weather Rev., V. 104, pp. 828-835.

Fig. 1. 12-month running mean of monthly mean snowcover for North America, Eurasia, and the Northern Hemisphere for the period 1966-1978.

Fig. 2. Monthly mean winter snowcover of North America and Eurasia for the period 1966-1978.

Fig. 3. Comparison of the satellite-derived mean snow line for February 1978 and the 10-year satellite-derived mean snow line.

Fig. 4. Comparison of December 1977 mean snow line and 10-year mean snow line, 1966-1975.

Fig. 5. Comparison of January 1978 mean snow line and 10-year snow line, 1967-1976.

Fig. 6. Comparison of February 1978 mean snow line and 10-year mean snow line, 1967-1976.

Fig. 7. Comparison of March 1978 mean snow line and 10-year mean snow line, 1967-1976.

Fig. 8. Regression analysis of January snowcover vs. December snowcover for Eurasia and the Northern Hemisphere.

Fig. 9. Regression analysis of February snowcover vs. December plus January snowcover for Eurasia and the Northern Hemisphere.

Fig. 10. Regression analysis of January through March snowcover vs. December snowcover for Eurasia and the Northern Hemisphere.

Fig. 11. Winter 1978 snowcover estimates compared to winter 1978 snowcover measurements.

THE 12-YEAR SATELLITE SNOWCOVER RECORD AND THE RECORD WINTER SNOWCOVER OF 1977-78

Craig P. Berg (LT, NOAA Corps) and Michael Matson

ABSTRACT

The winter 1977-78 satellite-derived snowcover data were examined and compared to the 12-year records to determine possible trends and relationships. Winter 1977-78 was the second consecutive year of record-breaking continental winter snowcover in North America as reflected in graphical analysis of both winter snowcover and the upward trend in the 12-month running mean. The regression analysis equations have been updated and now include eleven data points; correlation coefficients remain significant for possible continental snowcover estimates.

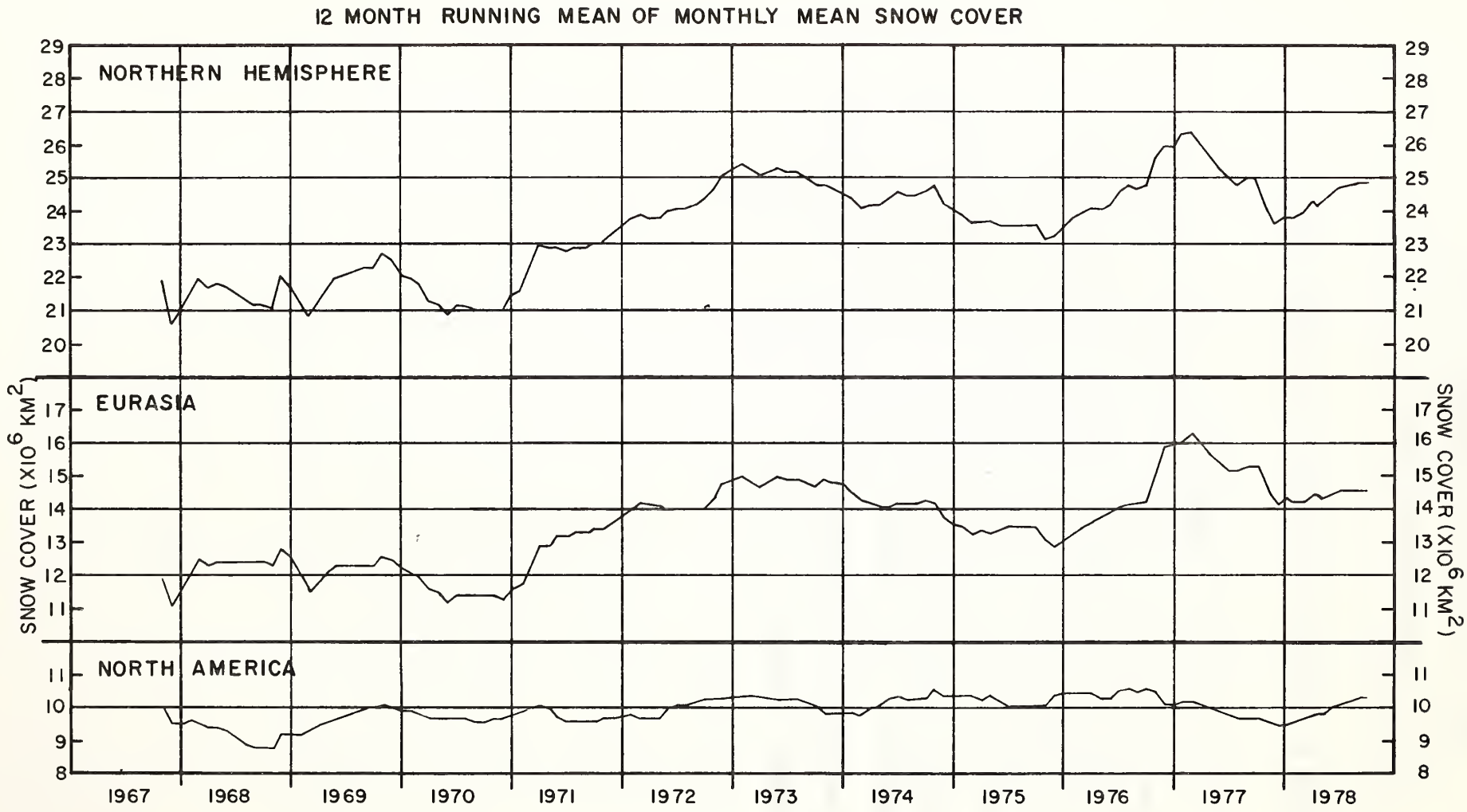
12 MONTH RUNNING MEAN OF MONTHLY MEAN SNOW COVER
NORTHERN HEMISPHERE
EURASIA
NORTH AMERICA
SNOW COVER (X10^6 KM^2)
SNOW COVER (X10^6 KM^2)
29
28
27
26
25
24
23
22
21
20
17
16
15
14
13
12
11
10
9
8
1967
1968
1969
1970
1971
1972
1973
1974
1975
1976
1977
1978

10-6

Fig. 1

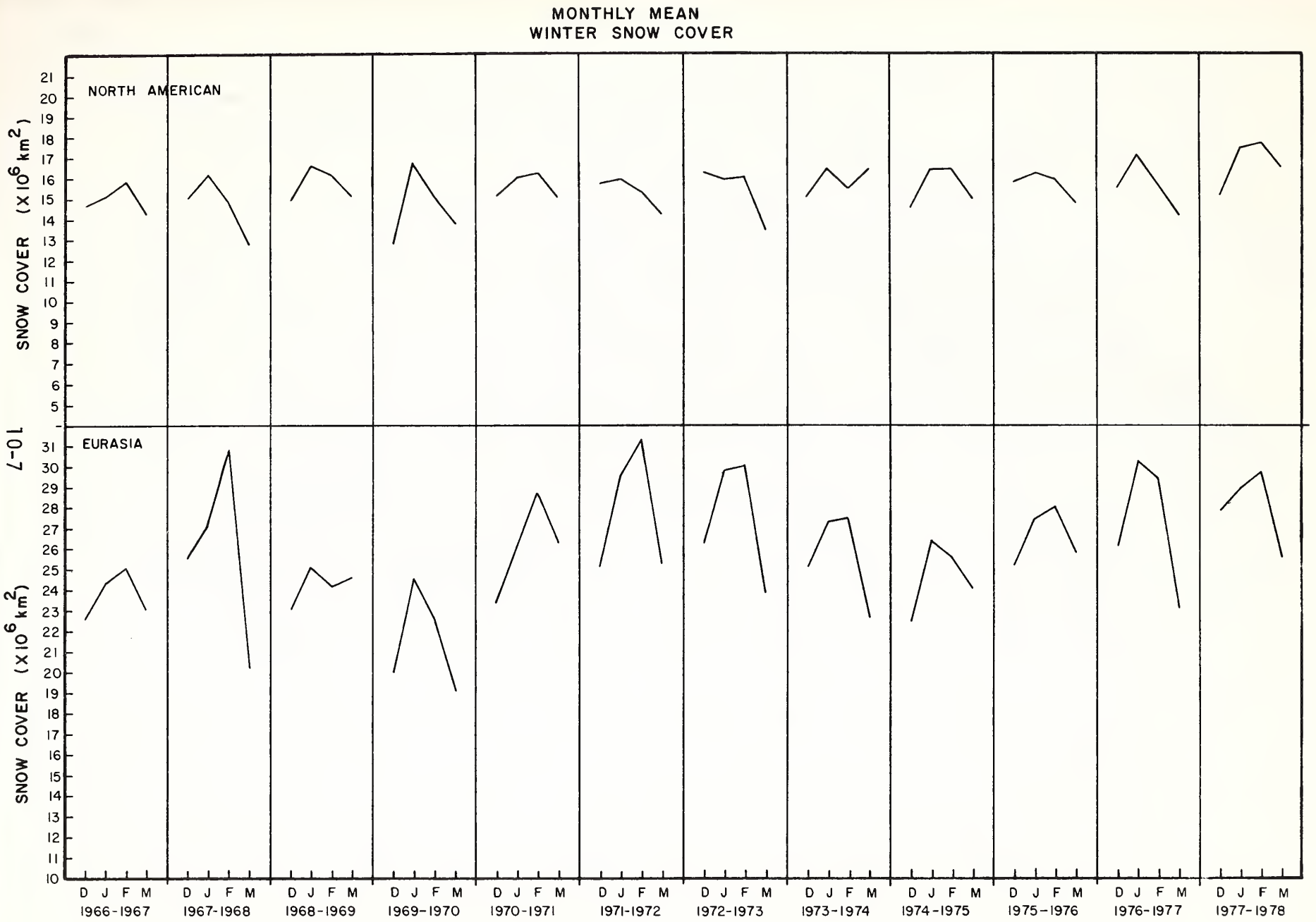
MONTHLY MEAN
WINTER SNOW COVER
NORTH AMERICAN
EURASIA
SNOW COVER (X10^6 km^2)
SNOW COVER (X10^6 km^2)
D J F M
1966-1967
1967-1968
1968-1969
1969-1970
1970-1971
1971-1972
1972-1973
1973-1974
1974-1975
1975-1976
1976-1977
1977-1978

Fig. 2

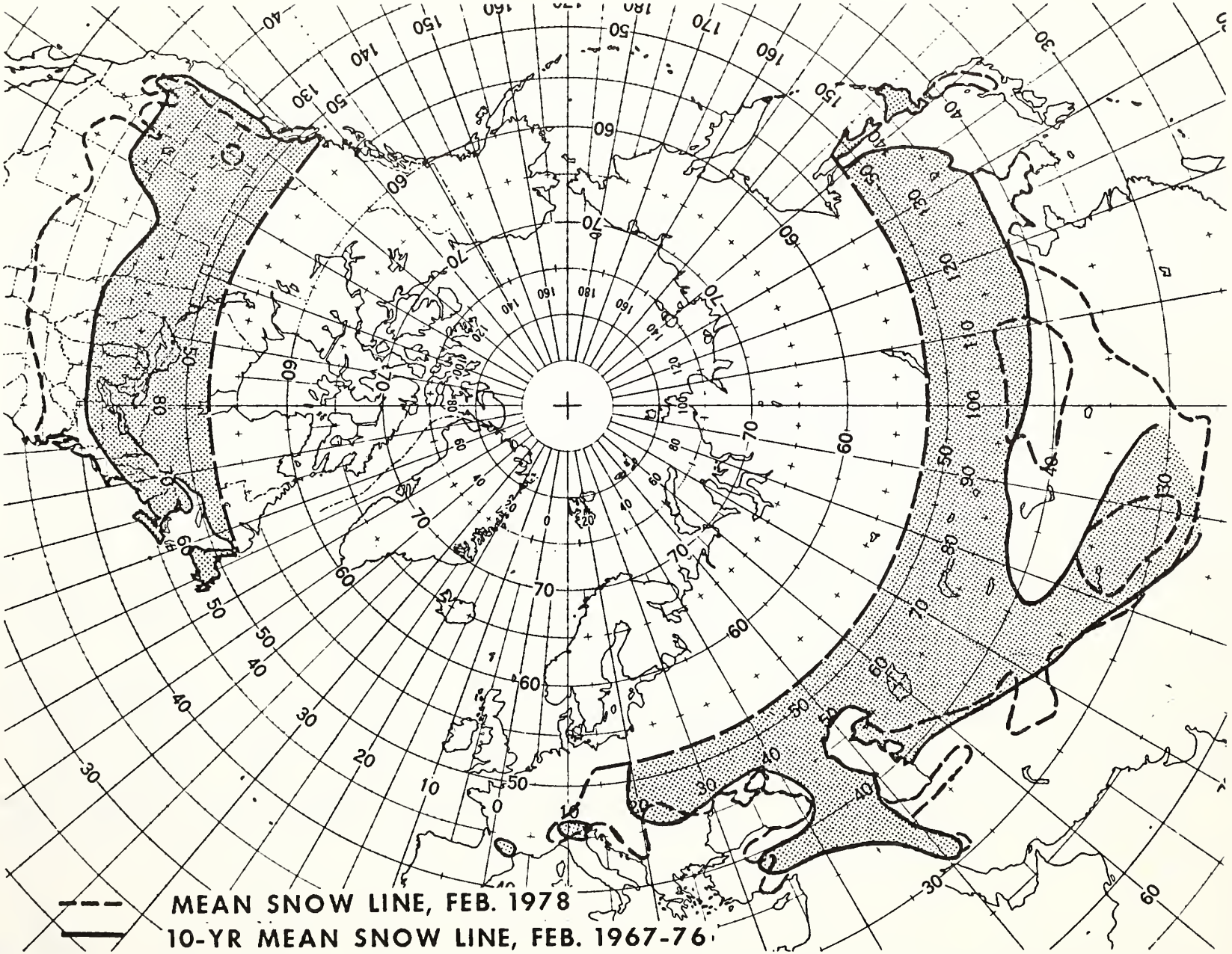

Fig. 3

Table 1. 10-year (1967-1976) Mean of Monthly Winter Continental Snowcover and Comparison with 1976-1977 and 1977-1978 Winter Snowcover.

Continent	Month	Number of Data Points	10-year Mean Snowcover ($x10^6 km^2$)	Standard Deviation ($x10^6 km^2$)	10-year Range of Snowcover Data ($x10^6 km^2$)	1976-77 Snowcover ($x10^6 km^2$)	1977-78 Snowcover ($x10^6 km^2$)
Eurasia	DEC	10	23.9	1.9	20.0 - 26.2	26.1	27.8*
Eurasia	JAN	10	26.8	1.9	24.3 - 29.8	30.2*	28.9
Eurasia	FEB	10	27.4	3.0	22.5 - 31.3	29.3	29.7
Eurasia	MAR	10	23.5	2.3	19.1 - 26.2	23.0	25.5
N. America	DEC	10	14.9	1.0	12.8 - 16.2	15.4	15.1
N. America	JAN	10	16.1	0.5	15.1 - 16.7	17.1	17.4*
N. America	FEB	10	15.7	0.5	14.8 - 16.2	15.7	17.6*
N. America	MAR	10	14.4	1.0	12.7 - 16.4	14.1	15.6

*Highest of Record

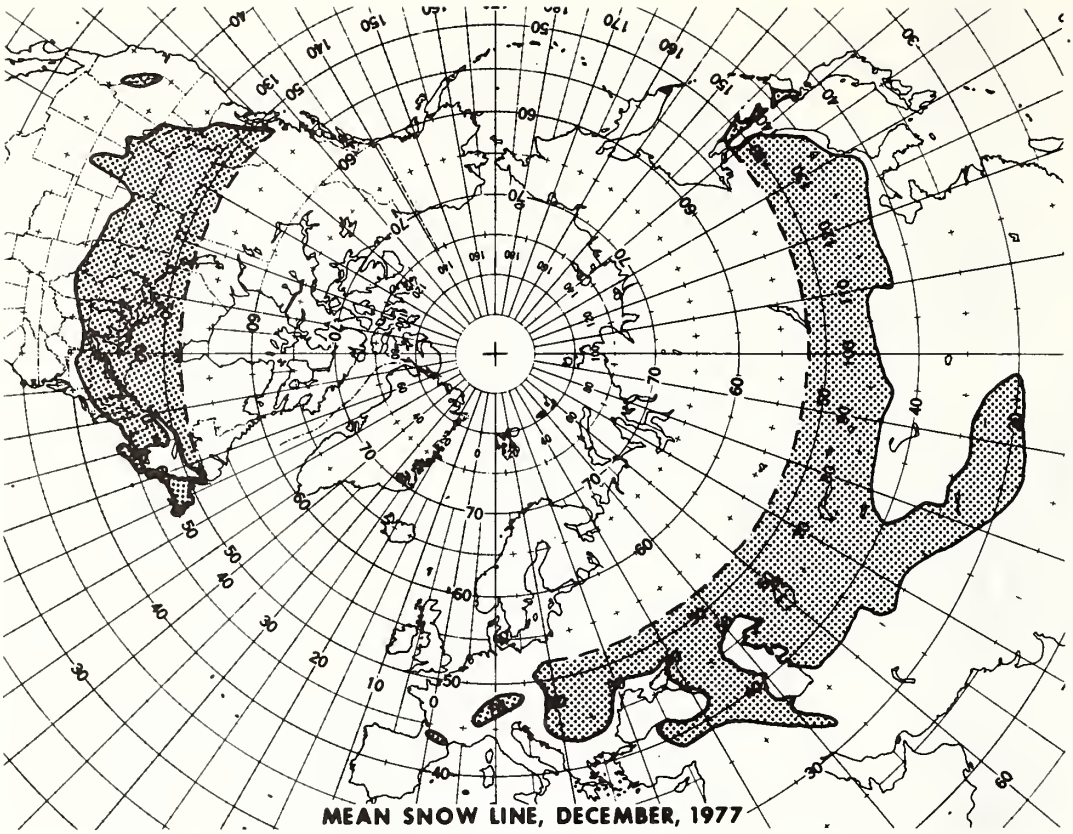

MEAN SNOW LINE, DECEMBER, 1977

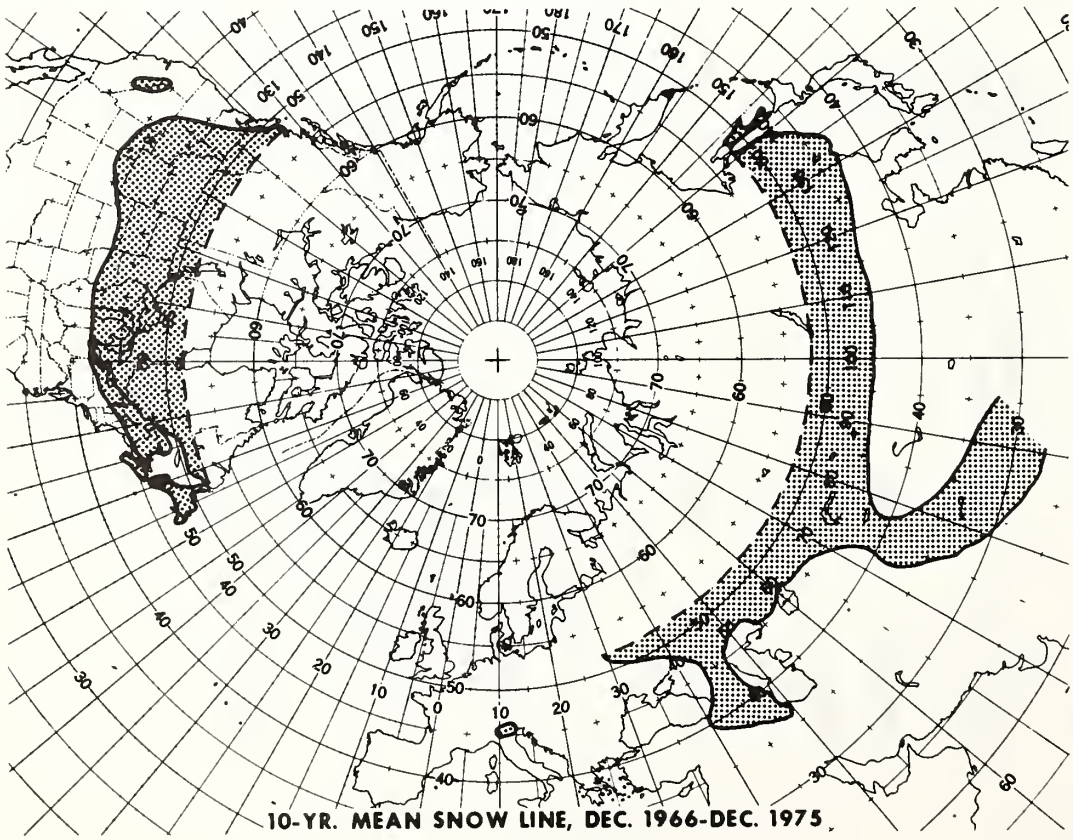

10-YR. MEAN SNOW LINE, DEC. 1966-DEC. 1975

Fig. 4

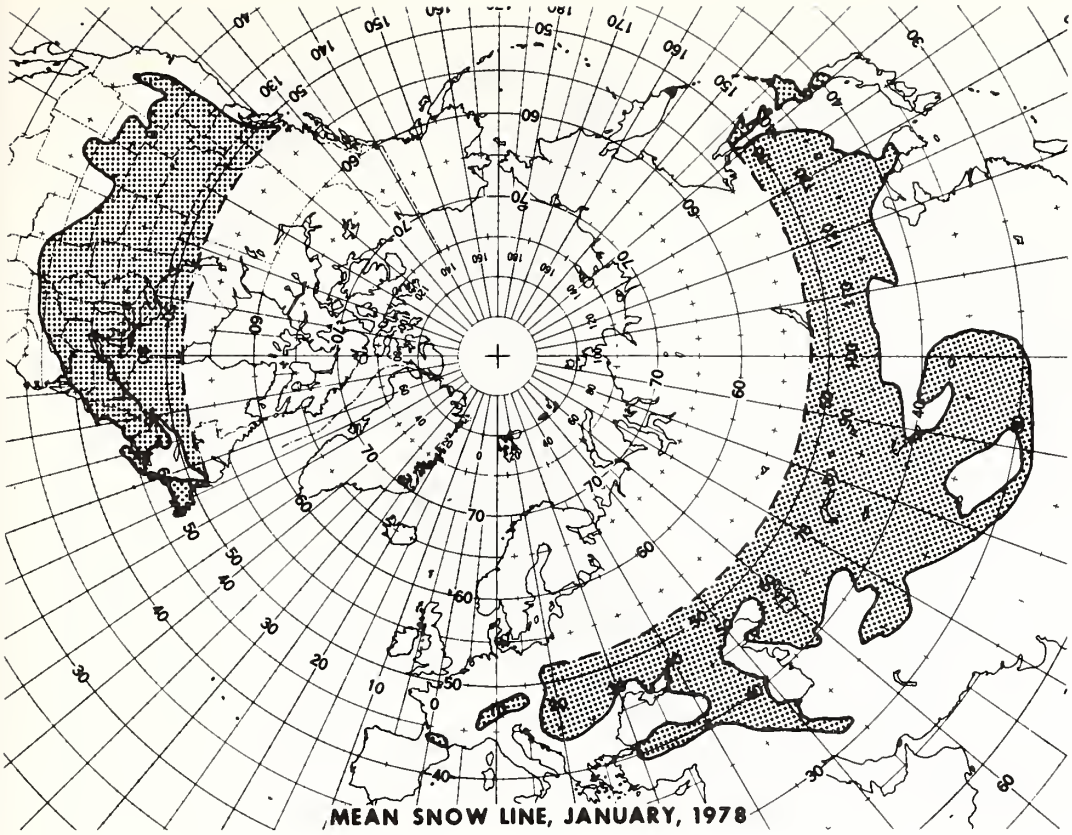

MEAN SNOW LINE, JANUARY, 1978

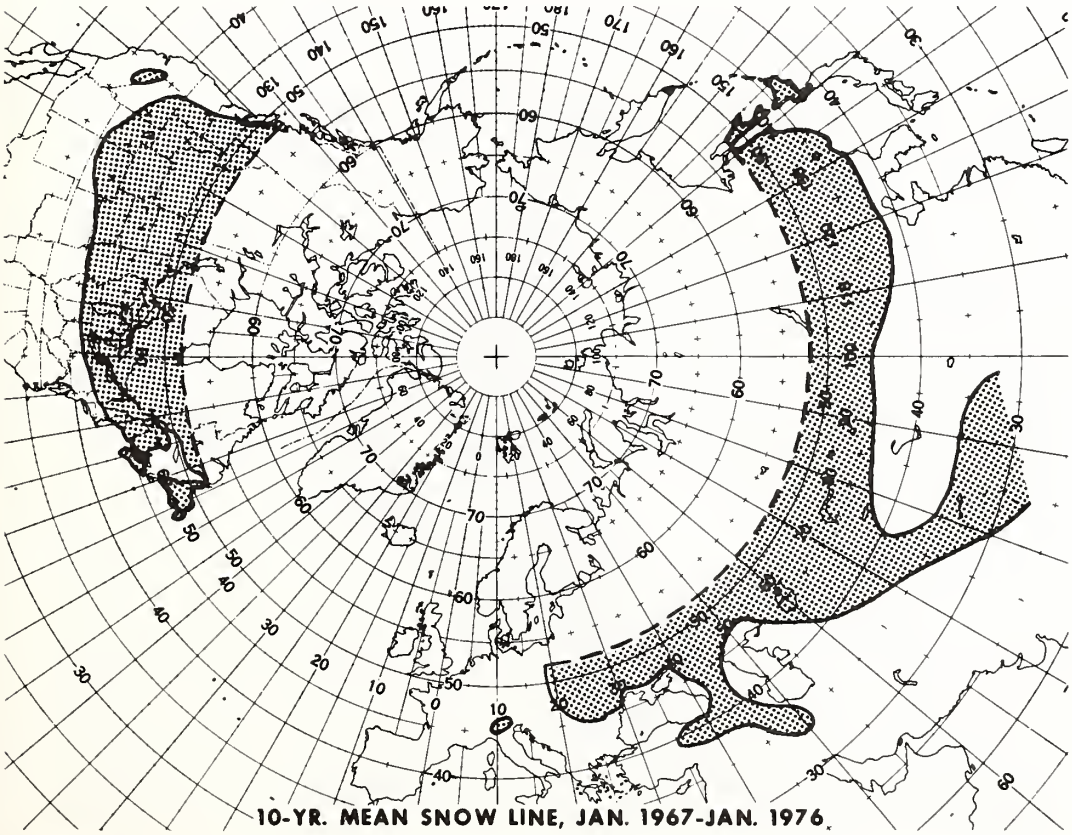

10-YR. MEAN SNOW LINE, JAN. 1967-JAN. 1976

Fig. 5

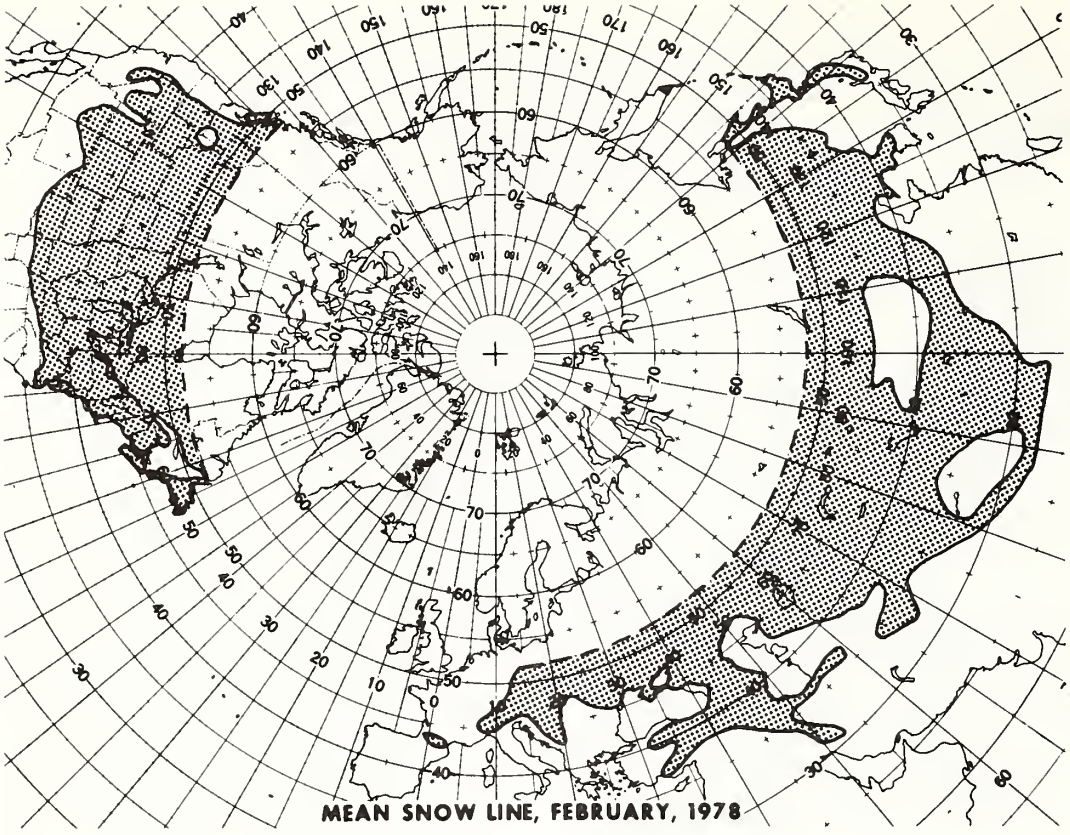

MEAN SNOW LINE, FEBRUARY, 1978

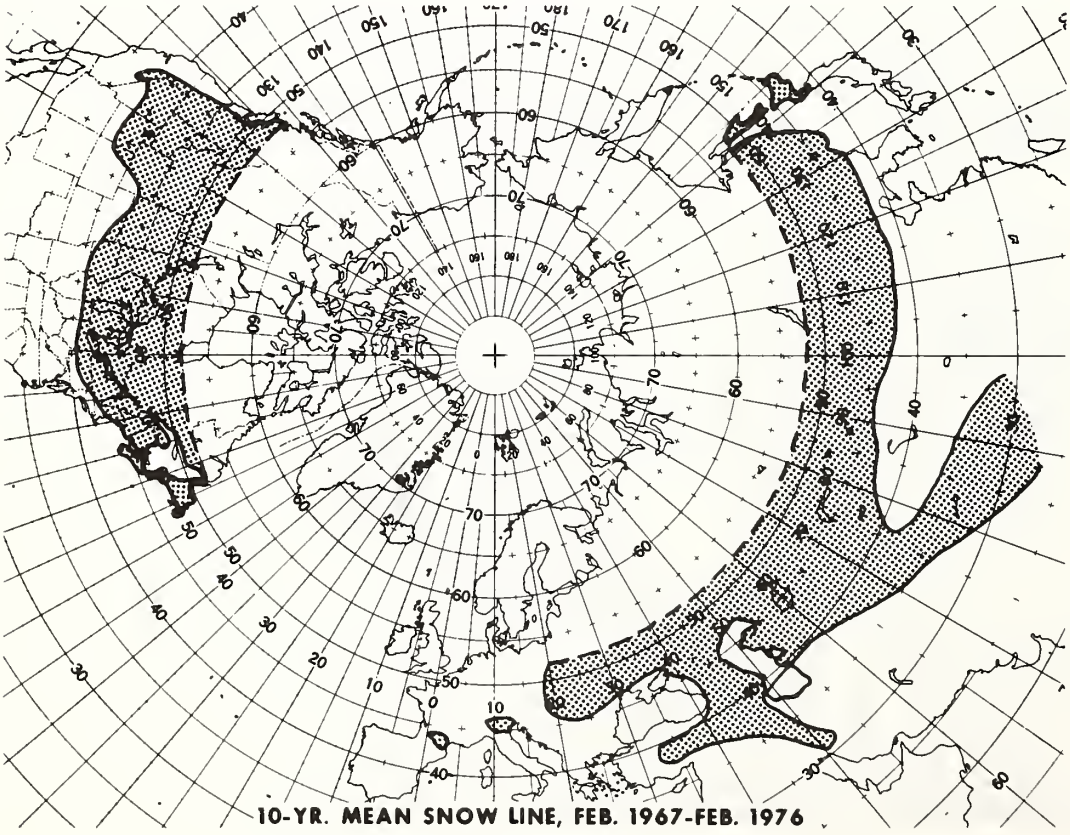

10-YR. MEAN SNOW LINE, FEB. 1967-FEB. 1976

Fig. 6

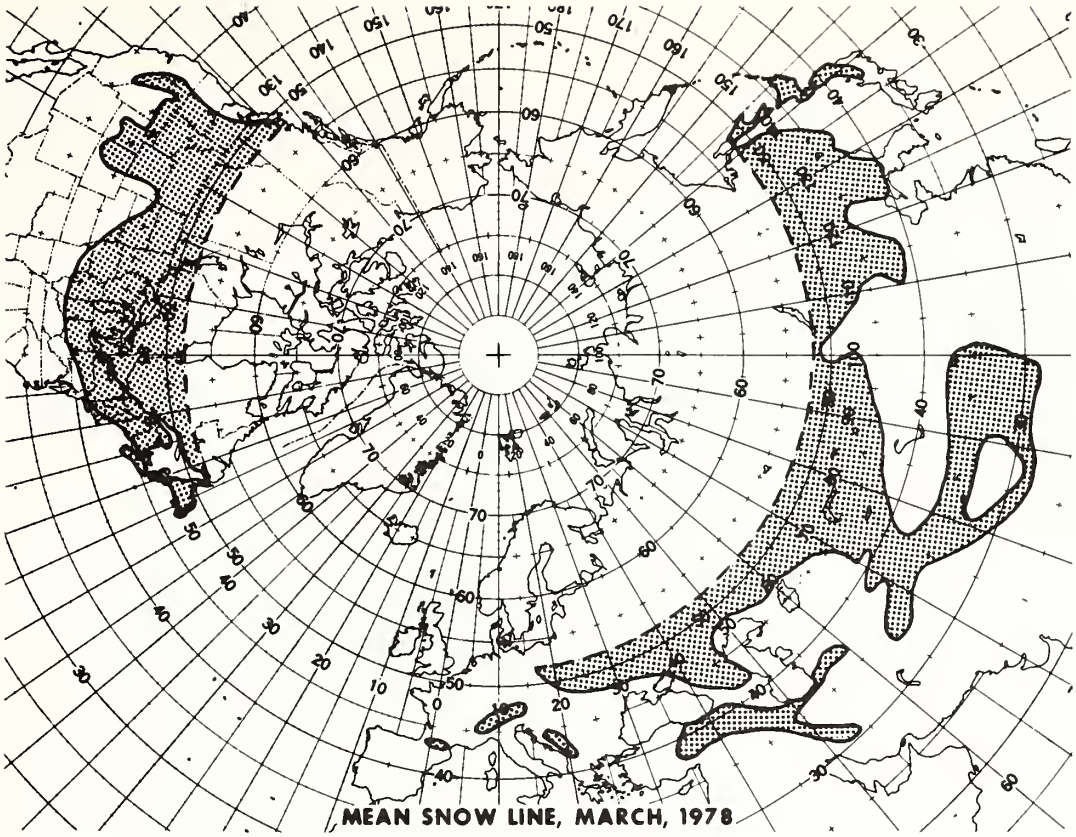
MEAN SNOW LINE, MARCH, 1978

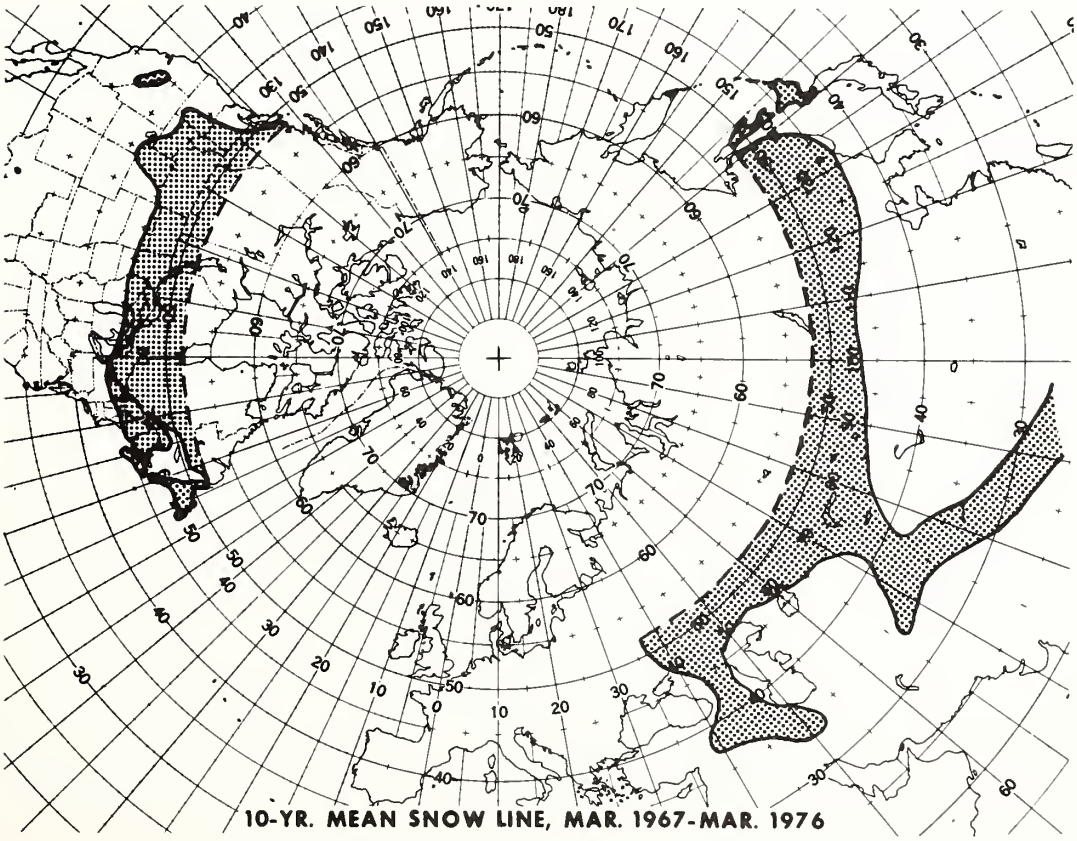
10-YR. MEAN SNOW LINE, MAR. 1967-MAR. 1976

Fig. 7

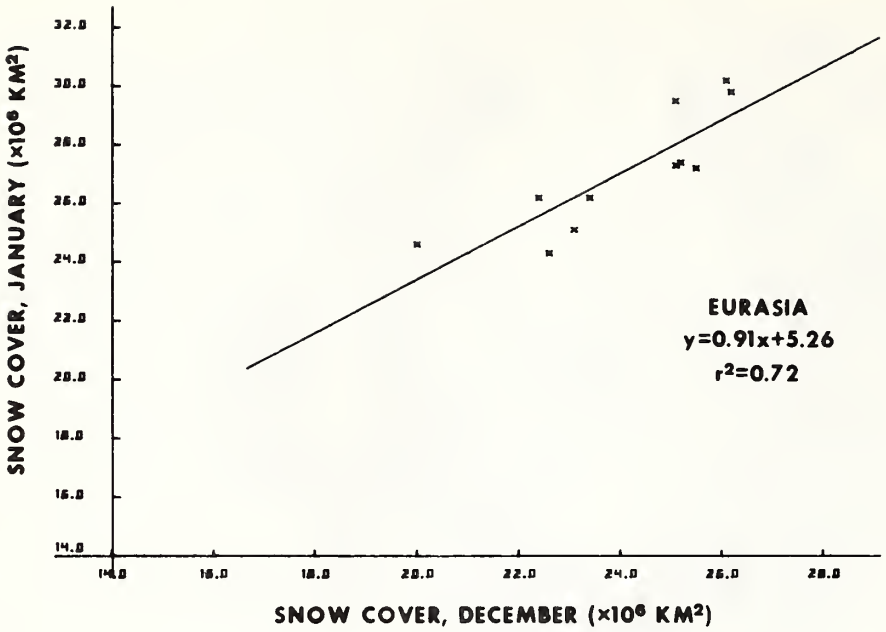
SNOW COVER, JANUARY (×10⁶ KM²)
32.0
30.0
28.0
26.0
24.0
22.0
20.0
18.0
16.0
14.0
14.0
16.0
18.0
20.0
22.0
24.0
26.0
28.0
SNOW COVER, DECEMBER (×10⁶ KM²)
EURASIA
y=0.91x+5.26
r²=0.72

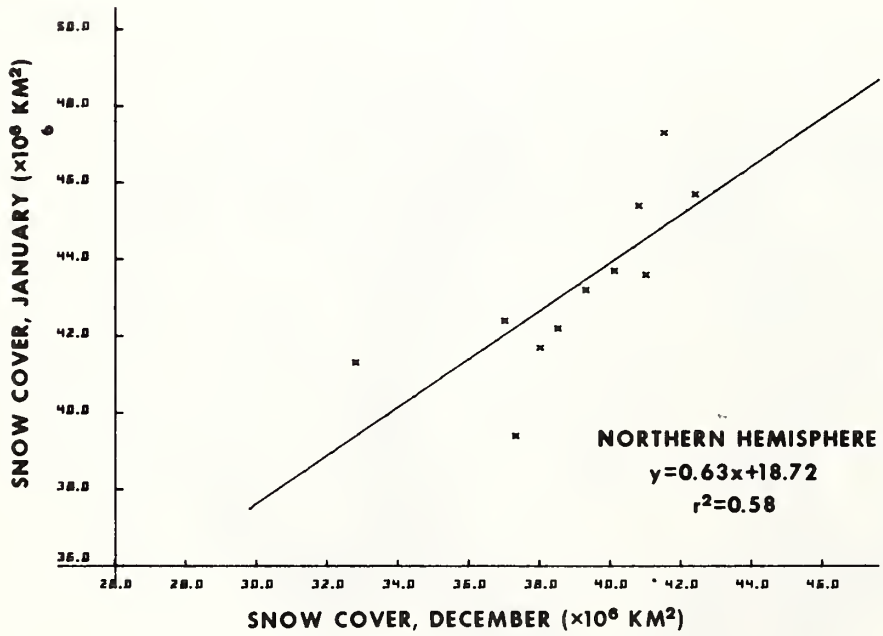
SNOW COVER, JANUARY (×10⁶ KM²)
50.0
48.0
46.0
44.0
42.0
40.0
38.0
36.0
26.0
28.0
30.0
32.0
34.0
36.0
38.0
40.0
42.0
44.0
46.0
SNOW COVER, DECEMBER (×10⁶ KM²)
NORTHERN HEMISPHERE
y=0.63x+18.72
r²=0.58

Fig. 8

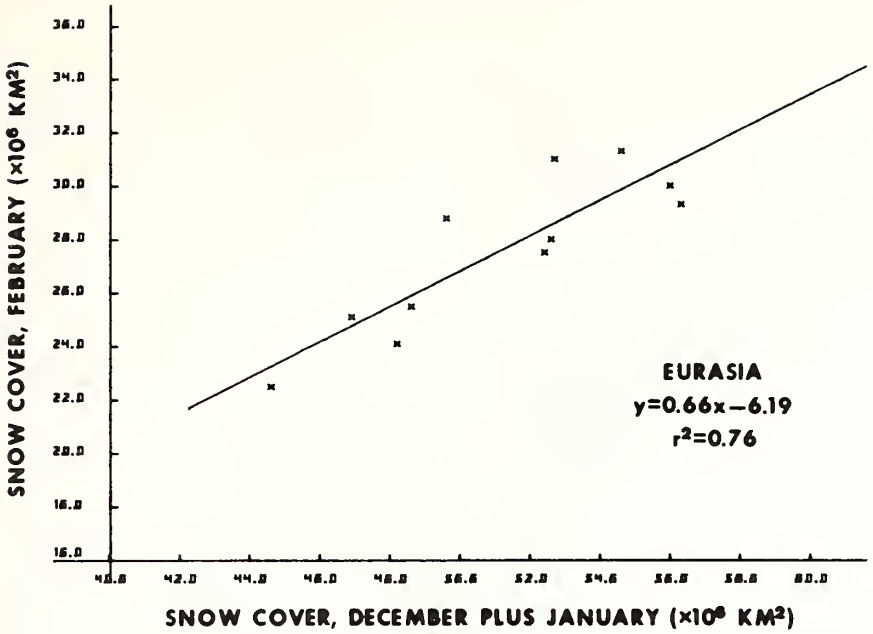
SNOW COVER, FEBRUARY (×10⁶ KM²)
EURASIA
y=0.66x−6.19
r²=0.76
SNOW COVER, DECEMBER PLUS JANUARY (×10⁶ KM²)

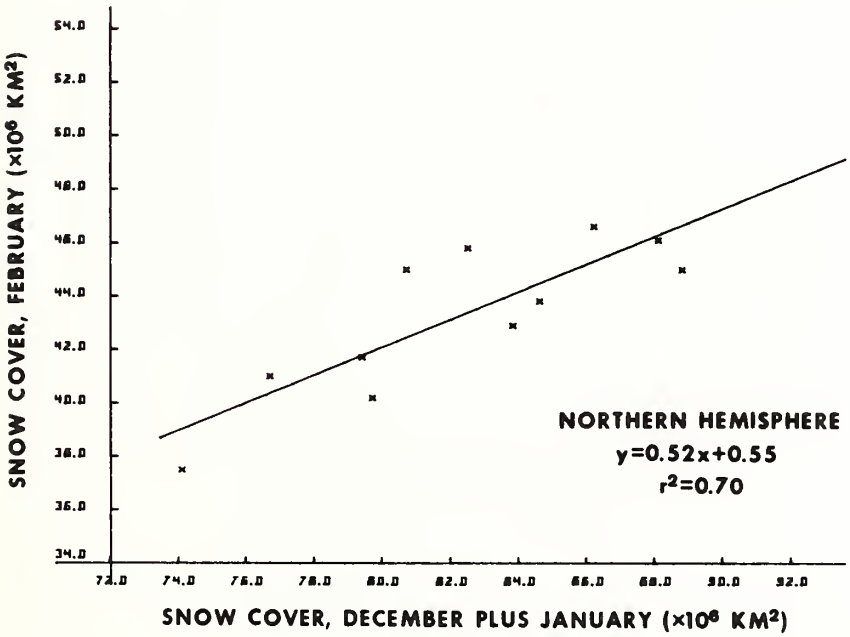
SNOW COVER, FEBRUARY (×10⁶ KM²)
NORTHERN HEMISPHERE
y=0.52x+0.55
r²=0.70
SNOW COVER, DECEMBER PLUS JANUARY (×10⁶ KM²)

Fig. 9

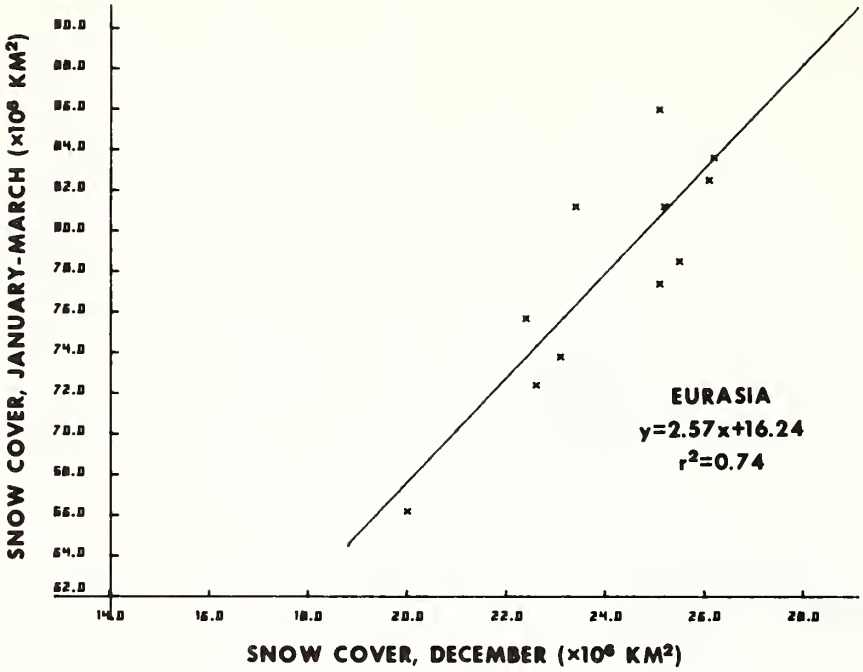
SNOW COVER, JANUARY-MARCH (×10⁶ KM²)
SNOW COVER, DECEMBER (×10⁶ KM²)
EURASIA
y=2.57x+16.24
r²=0.74

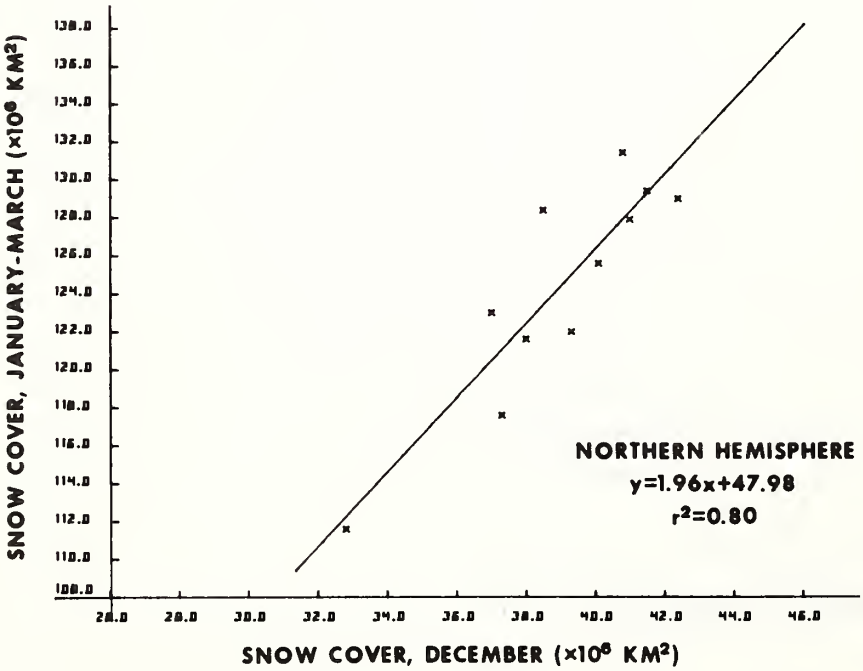
SNOW COVER, JANUARY-MARCH (×10⁶ KM²)
SNOW COVER, DECEMBER (×10⁶ KM²)
NORTHERN HEMISPHERE
y=1.96x+47.98
r²=0.80

Fig. 10

Table 2. Winter Snow Cover Estimate Data in the Northern Hemisphere and Eurasia from Regression Analysis

Snowcover Period	Estimate ($x10^6 km^2$)	Measured ($x10^6 km^2$)	Percent Difference	Standard Error of Estimate ($x10^6 km^2$)
		NORTHERN HEMISPHERE		
JAN 78	45.8	46.4	-1.3	1.58
FEB 78	47.0	47.3	-0.6	1.60
JAN-MAR 78	132.1	134.8	-2.0	2.80
		EURASIA		
JAN 78	30.6	28.9	+5.9	1.16
FEB 78	31.2	29.7	+5.1	1.51
JAN-MAR 78	87.7	84.1	+4.3	3.09

COMPARISON OF WINTER 1978 SNOW COVER ESTIMATES VERSUS WINTER 1978 SNOW COVER MEASUREMENTS

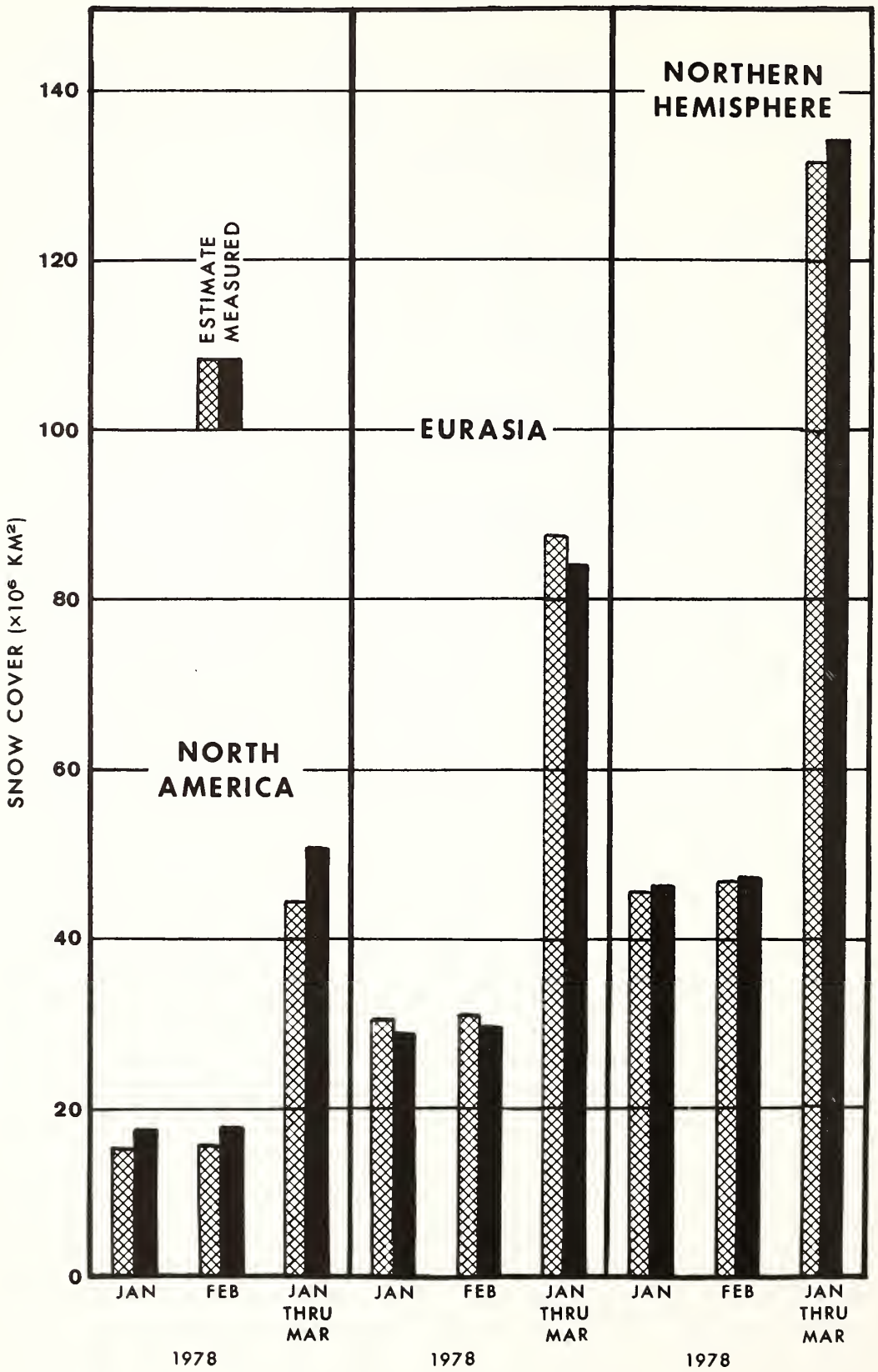

Fig. 11

The Variation of Sea Surface Temperature in 1976 and 1977
The Data Analysis

K. Miyakoda and A. Rosati

The objective of this paper is to investigate the variation of SST over the world's oceans for the years of 1976 and 1977. In order to study the spacial distribution of the SST, ship and satellite data at 1° quadrangles were collected. Two points were investigated; (i) the difference of monthly mean SST data between the two sources; and (ii) map analysis over the world ocean. The SST charts were then compared with independent analyses.

Using monthly mean SST data derived from NOAA-5 soundings, the quality of the data was examined relative to the observations of ships of opportunity. Table 1 shows the month-to-month variations for two regions in the North Pacific. Concerning the difference of the spatial mean SST, negative values are dominating at the high latitudes, 40°-60°N, implying that the satellite data are cooler than ship data, probably due to cloud coverage. On the other hand, in the lower latitudes, 20°-40°N, the differences are more positive. The standard deviation ranges from ± 1.18° to ± 2.3°C, ± 1.49°C being the arithmetic average for the entire period and domain. Any systematic seasonal variation in the satellite data deviation was hardly detectable.

Figure 1 shows the statistics over the domains of the North Pacific (20°-60°N, 120°E-120°W) and the North Atlantic (20°-60°N, 70°W-10°W) for the annual averages of 1976 and 1977 separately. The numbers are the mean differences and the standard deviation, and sample numbers are shown in parenthesis. In April 1977, a new method to detect clouds and improve atmospheric attenuation correction was introduced into the satellite retrievals. This resulted in a reduction of the sample size but, supposedly improved the quality of the data. The mean difference ranges from -1.3°C to +.8°C, and the standard deviation ranges from ± 1.43°C, which is not small in view of ± 2.3°C as the root-mean-square of the monthly mean SST anomaly.

We understand that the quality of the satellite SST and the data processing techniques are still under continuing development. In years to come, we have to rely on satellite data over a wide area of the ocean. Yet there seems to exist a fundamental difference between the satellite and the ship observations; one is a skin temperature while the other is the temperature at a depth 3 ∿ 6 meters. It is essential to develop an improved technique by which one can only extract the benefits from satellite data, and assimilate or amalgamate it properly with ship data.

Adopting an analysis program of Levitus and Oort and using ship and satellite data, we produced monthly mean SST charts of 1°x1° grid over the world ocean for 1976 and 1977. Figure 2 shows an amalgamation of satellite and ship analysis for Jan. 1977.

The charts agreed well with the independent analysis at Fleet Numerical Weather Central, Monterey, so far as the large scale features are concerned. However, GFDL's analysis contained a great deal of small-scale irregularities, whereas, the other was considerably smoother. It would appear that screening the data is very important in the analysis, and a proper judgement has to be made as to whether a datum is the reflection of an eddy or an error. It is hoped that satellite data will give some insight in this regard.

FIGURE CAPTIONS

Fig. 1. The mean difference and the standard deviations of the difference between the satellite and ship SST for the Pacific Ocean and the Atlantic Ocean in 1976 (upper) and 1977 (lower). The geography is shown to indicate the locations.

Fig. 2. The Amalgamated SST anomaly (°C) for January 1977. The negative anomalies are shaded.

Table 1.

$(T_{SAT} - T_{SHP}) \pm$ Standard Deviation

	middle latitude 40°-60°N, 160°E-160°W	lower latitude 20°-40°N, 160°E-160°W
1976 Jan	-1.85 ± 1.35	.84 ± 1.47
Feb	-1.75 ± 1.55	.04 ± 1.17
Mar	-1.30 ± 1.25	.19 ± 1.17
Apr	-1.20 ± 1.2	.79 ± 1.4
May	- .97 ± 1.5	.94 ± 1.2
June	-1.19 ± 1.85	1.22 ± 1.3
July	- .8 ± 1.5	1.01 ± 1.43
Aug	- .35 ± 1.8	.7 ± 1.18
Sept	- .71 ± 1.45	- .58 ± 1.25
Oct	-1. ± 1.35	.46 ± 1.31
Nov	-1.4 ± 1.6	.91 ± 1.49
Dec	-1.08 ± 1.5	.99 ± 1.23
1977 Jan	-2.1 ± 1.45	+ .12 ± 1.23
Feb	-2.5 ± 1.3	- .56 ± 1.27
Mar	-1.9 ± 1.4	- .34 ± 1.33
Apr	-1.95 ± 1.95	- .38 ± 1.53
May	- .585 ± 1.75	- .07 ± 1.43
June	+ .385 ± 2.05	+ .54 ± 1.83
July	+2.7 ± 2.3	+ .74 ± 1.77
Aug	+ .38 ± 1.7	- .6 ± 1.33
Sept	- .32 ± 1.5	- .55 ± 1.27
Oct	- .95 ± 1.9	- .27 ± 1.43
Nov	- .67 ± 1.8	+ .18 ± 1.43
Dec	-1. ± 1.6	+ .35 ± 1.5
1978 Jan	-1.65 ± 1.55	- .33 ± 1.3

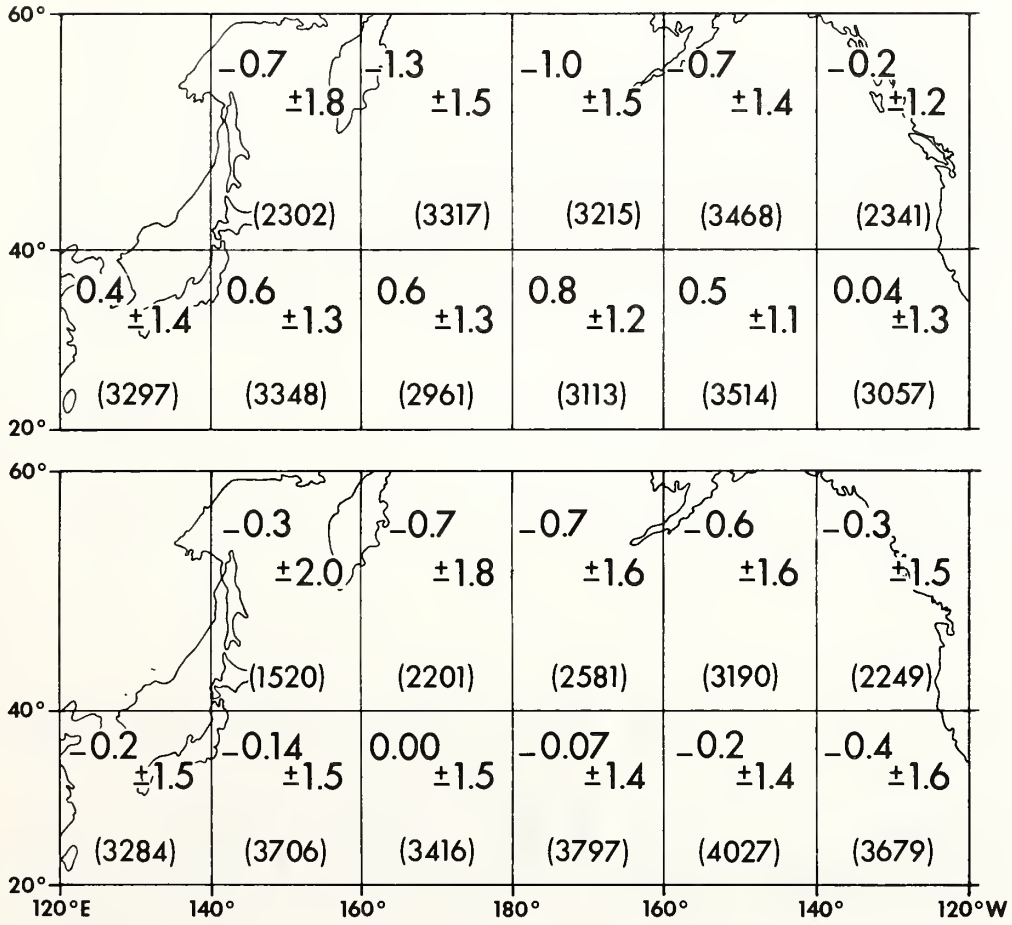
60°
40°
20°
-0.7 ±1.8 (2302)
-1.3 ±1.5 (3317)
-1.0 ±1.5 (3215)
-0.7 ±1.4 (3468)
-0.2 ±1.2 (2341)
0.4 ±1.4 (3297)
0.6 ±1.3 (3348)
0.6 ±1.3 (2961)
0.8 ±1.2 (3113)
0.5 ±1.1 (3514)
0.04 ±1.3 (3057)
-0.3 ±2.0 (1520)
-0.7 ±1.8 (2201)
-0.7 ±1.6 (2581)
-0.6 ±1.6 (3190)
-0.3 ±1.5 (2249)
-0.2 ±1.5 (3284)
-0.14 ±1.5 (3706)
0.00 ±1.5 (3416)
-0.07 ±1.4 (3797)
-0.2 ±1.4 (4027)
-0.4 ±1.6 (3679)
120°E
140°
160°
180°
160°
140°
120°W

1976

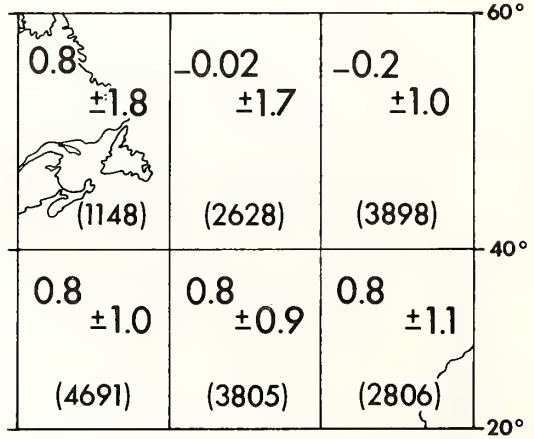
60°
40°
20°
0.8 ±1.8 (1148)
-0.02 ±1.7 (2628)
-0.2 ±1.0 (3898)
0.8 ±1.0 (4691)
0.8 ±0.9 (3805)
0.8 ±1.1 (2806)

1977

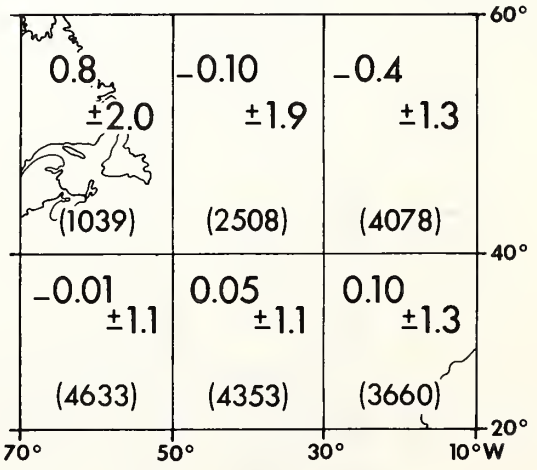
60°
40°
20°
0.8 ±2.0 (1039)
-0.10 ±1.9 (2508)
-0.4 ±1.3 (4078)
-0.01 ±1.1 (4633)
0.05 ±1.1 (4353)
0.10 ±1.3 (3660)
70°
50°
30°
10°W

AMALGAMATED ANOMALY JAN 77

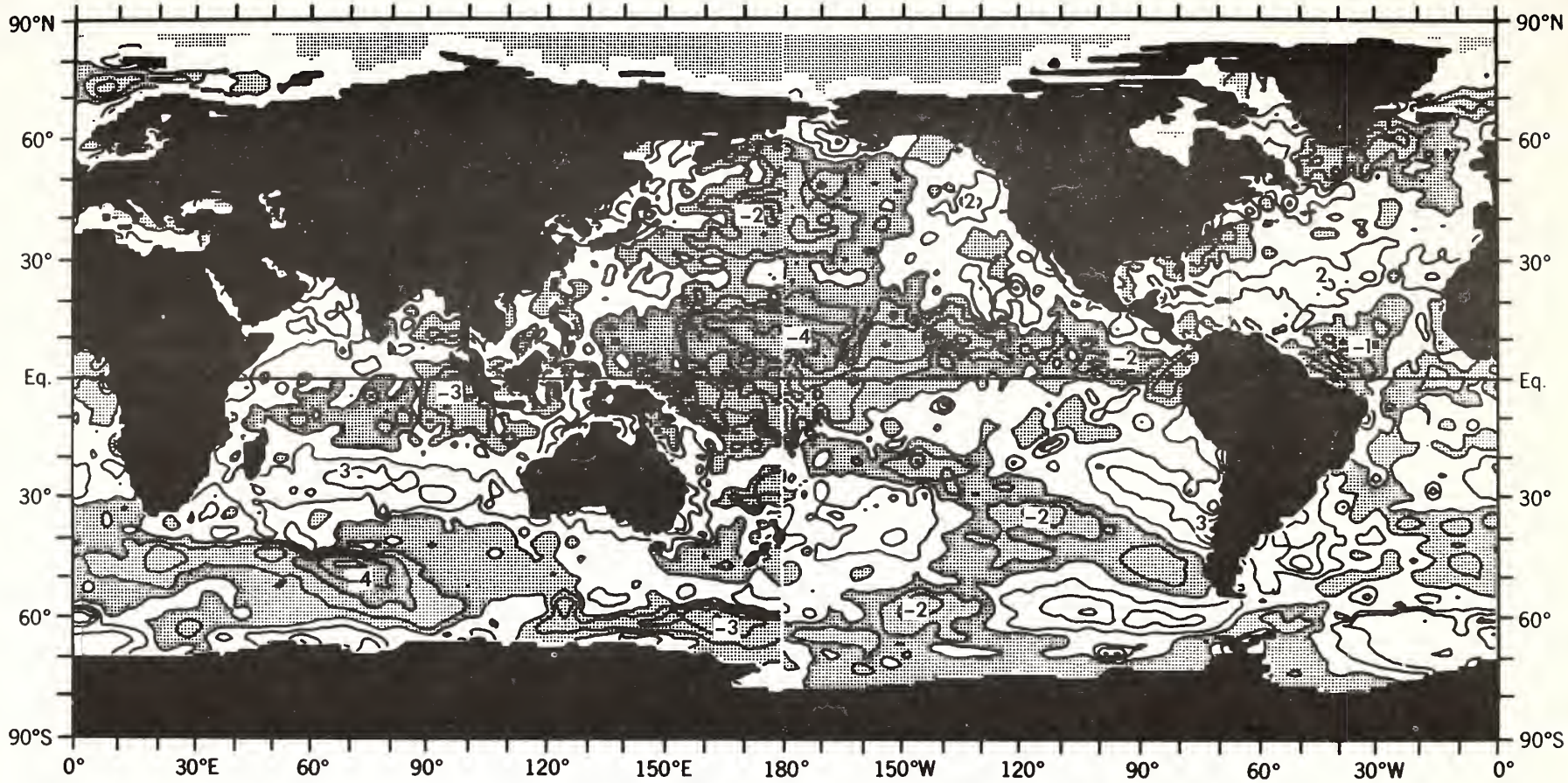

ANNUAL AND INTERANNUAL VARIABILITY OF SST IN THE EASTERN TROPICAL ATLANTIC OCEAN

J. Merle

CIMAS, University of Miami
4600 Rickenbacker Causeway, Miami, FL 33149

In the eastern equatorial Atlantic Ocean the annual signal is larger than the interannual anomalies but its characteristics have important spatial variations (Fig. 1). Two regions are specially affected by large amplitude both of the annual signal (Fig. 2) and of the interannual anomalies: south of the Equator (from 0 to 4°S) and E.W. coast. In these areas the thermocline shallows and even surfaces in summer lowering suddenly the SST. During the other months a thin low saline and warm mixed layer covers the whole Gulf of Guinea giving a long warm season only cut by a slight secondary cold season in December-January. This warm superficial layer call to our mind a kind of El Nino phenomenon. This warm season is possibly due to an eastward warm advection and its local consequences: rains and run off of the great rivers. This advection could be complex involving the three branches of the counter-current system in an alternative northern and southern influence explaining the strong superficial semi-annual component responsible of a bimodal temperature cycle. This warm and low saline surface layer appears to be the leading factor of the SST variability in the annual and interannual time scale whatever the dynamic process conducting its motion and the motion of the sub-surface layers.

Interannual anomalies, as in the equatorial region of the Pacific Ocean, have a large spatial extension at the scale of the basin and affects the region for several months, sometimes more than a year (Fig. 4). The magnitude of these anomalies is intensified both at the Equator and near the E-W coast. A long-term trend shows an increase of SST from the beginning of the century to the sixties and a decrease until now. This trend is similar to the one observed by Fieux and Stommel (1975, 1976) both in the North Atlantic Ocean and in the Arabian Sea (Fig. 3).

Fig. 1. Annual variability and interannual variability (SD) of SST along a ship line crossing the Eastern Tropical Atlantic from 20°S-10°E to 10°N -20°W. Interannual variability is found to be 5 times smaller than the annual variability except in the North-South transition area (8°N) where the annual signal is minimum (see Fig. 2).

Fig. 2. Amplitude in degree C of the annual component of the SST annual signal in the Tropical Atlantic.

Fig. 3. Long-term trend of SST anomalies in MSQ300 (0=10W-0-10S) compared with the one found in the North Atlantic and Arabian Sea (Fieux and Stommel).

Fig. 4. Interannual anomalies of SST in several areas of the Eastern Tropical Atlantic including a coastal station. The coherence of the anomalies seem remarkable.

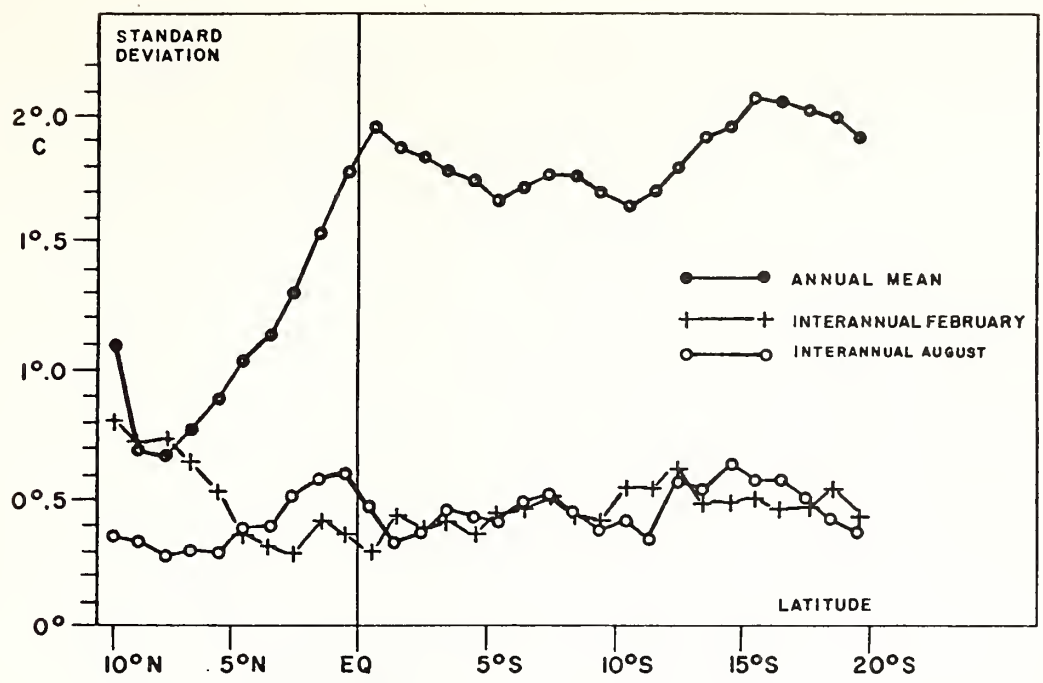
STANDARD DEVIATION
2°.0 C
1°.5
1°.0
0°.5
0°
ANNUAL MEAN
INTERANNUAL FEBRUARY
INTERANNUAL AUGUST
LATITUDE
10°N
5°N
EQ
5°S
10°S
15°S
20°S

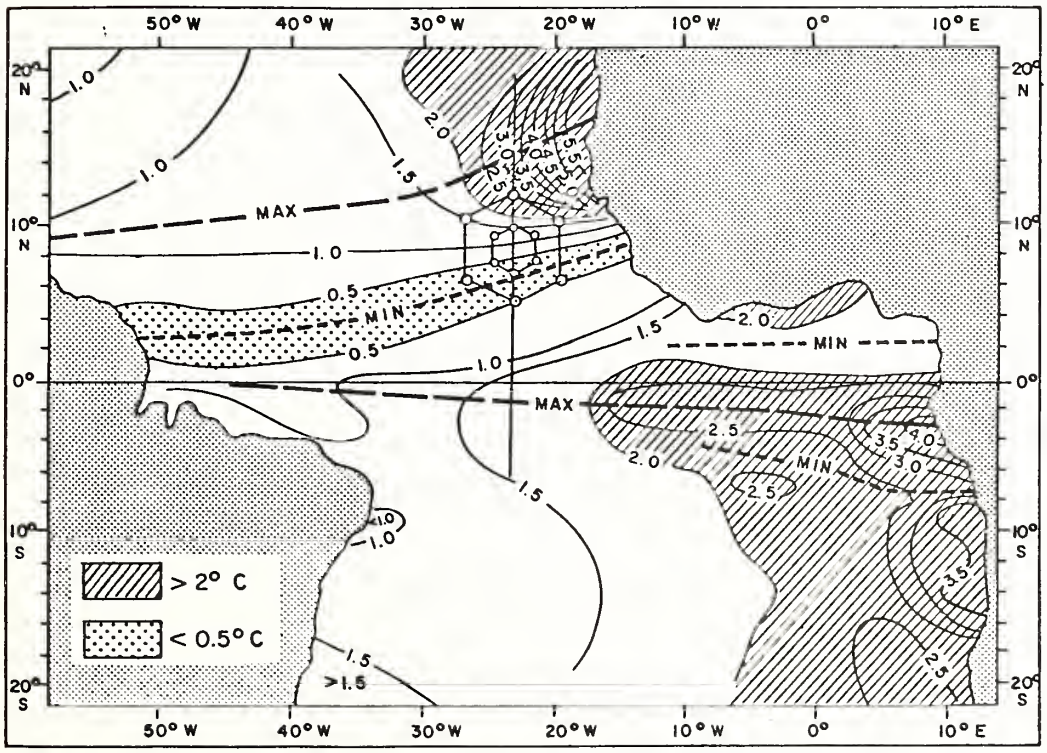
50° W
40° W
30° W
20° W
10° W
0°
10° E
20° N
10° N
0°
10° S
20° S
MAX
MIN
1.0
0.5
1.5
2.0
2.5
3.0
3.5
4.0
> 2° C
< 0.5° C
>1.5

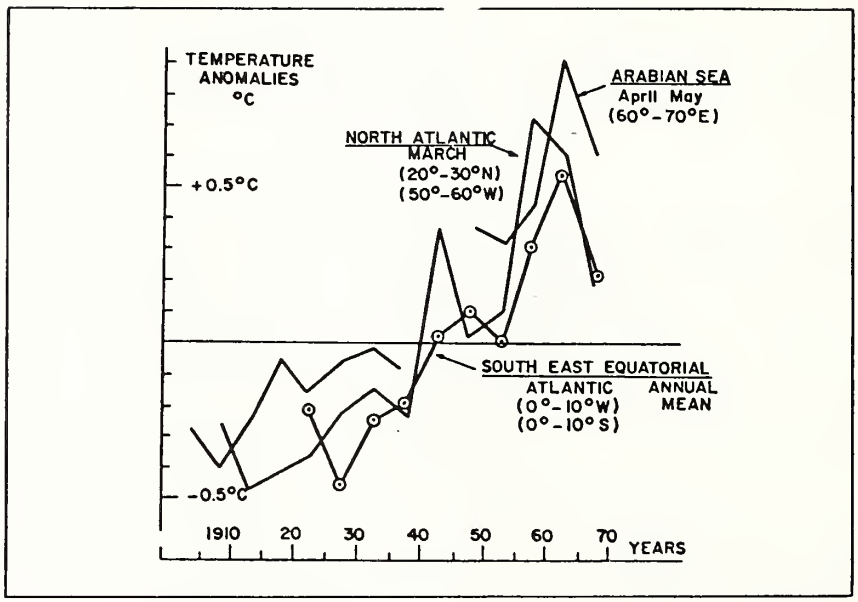
TEMPERATURE
ANOMALIES
°C
+0.5°C
-0.5°C
ARABIAN SEA
April May
(60°-70°E)
NORTH ATLANTIC
MARCH
(20°-30°N)
(50°-60°W)
SOUTH EAST EQUATORIAL
ATLANTIC
(0°-10°W)
(0°-10°S)
ANNUAL
MEAN
1910
20
30
40
50
60
70
YEARS

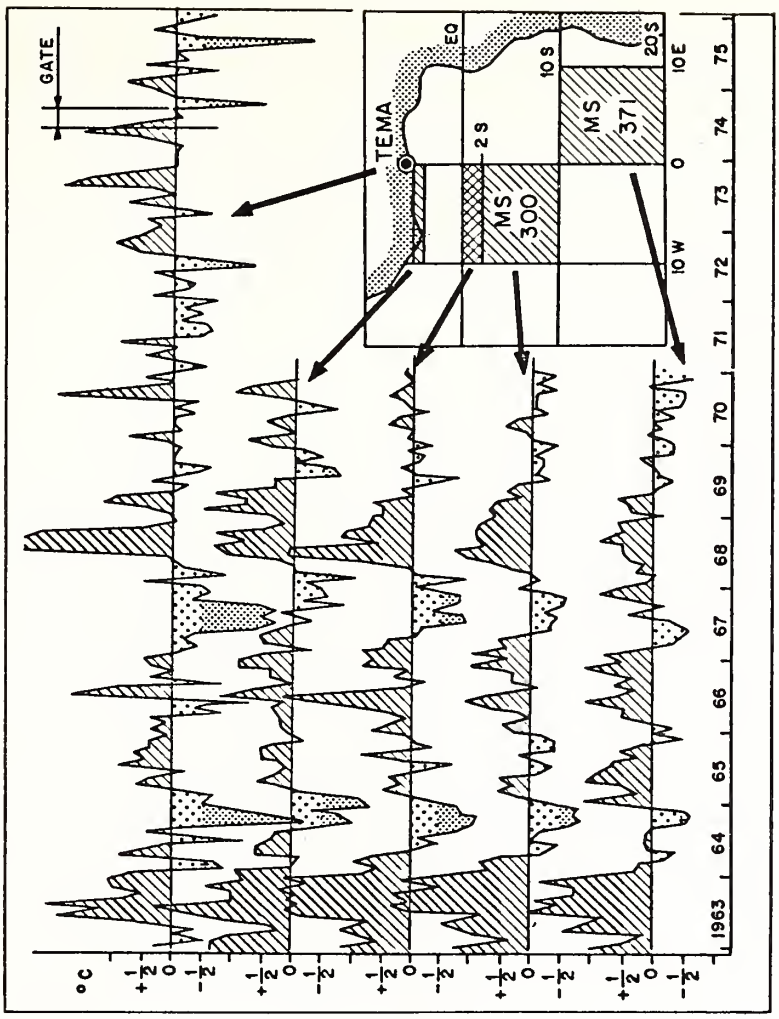
GATE
°C
TEMA
EQ
2 S
10 S
20 S
10 W
0
10 E
MS
300
MS
371
1963
64
65
66
67
68
69
70
71
72
73
74
75

RECENT VARIABILITY OF THE GULF STREAM EXTENSION FRONT

C.-P. Thang and Peter J. Lamb

Cooperative Institute for Marine and Atmospheric Studies
University of Miami/NOAA
Miami, Florida 33149

Sea surface temperature (SST) variations in the vicinity of the boundary between the Gulf Stream Extension and Labrador current waters during 1962-76 have been identified from a preliminary analysis of individual monthly data for 2.5° latitude-longitude grid intersections. This area to the south and east of Newfoundland experienced the maximum SST variance and strongest average meridional SST gradients in the Atlantic north of the Equator during 1962-76. The present note focuses on the variability of the winter SST field; variations characteristic of other seasons appear less pronounced and systematic.

Time series of the yearly minimum SST were established at 2.5° latitude intervals along five separate meridional transects in the region between 35°-65°N and 25°-60°W. To the south of Newfoundland, and immediately to its east, two principal trends are evident (Figs. 1-3). Along the equatorward side of the transects (37.5°-42.5°N), warming of up to 3.5°C occurred between 1969 and 1975 or 1976. Its magnitude decreased eastward. From 1970-1974, this warming coincided with cooling of similar magnitudes along the poleward side of the transects (45°-52.5°N). As a result, the maximum meridional SST gradient was strengthened by up to 50%, but little if any change occurred in its latitudinal position. At the more poleward latitudes 50°N and 52.5°N, the aforementioned cooling commenced as early as 1966.

Further east (Figs. 4-5), the two mid-Atlantic transects (longitudes 28.75°W and 38.75°W) reveal smaller changes. There is only very limited evidence of post-1969 warming along the equatorward side of these transects, with the values barely reaching 1°C. Cooling of up to 1.5°C occurred after 1968 at most latitudes from 42.5°N poleward, with more pronounced SST decreases being confined to extreme northern latitudes. The latter produced a marked poleward displacement of the maximum meridional SST gradient after 1970.

In contrast to the post-1966 trends described above, the earlier years of the study period were characterized by more irregular variation (Figs. 1-5).

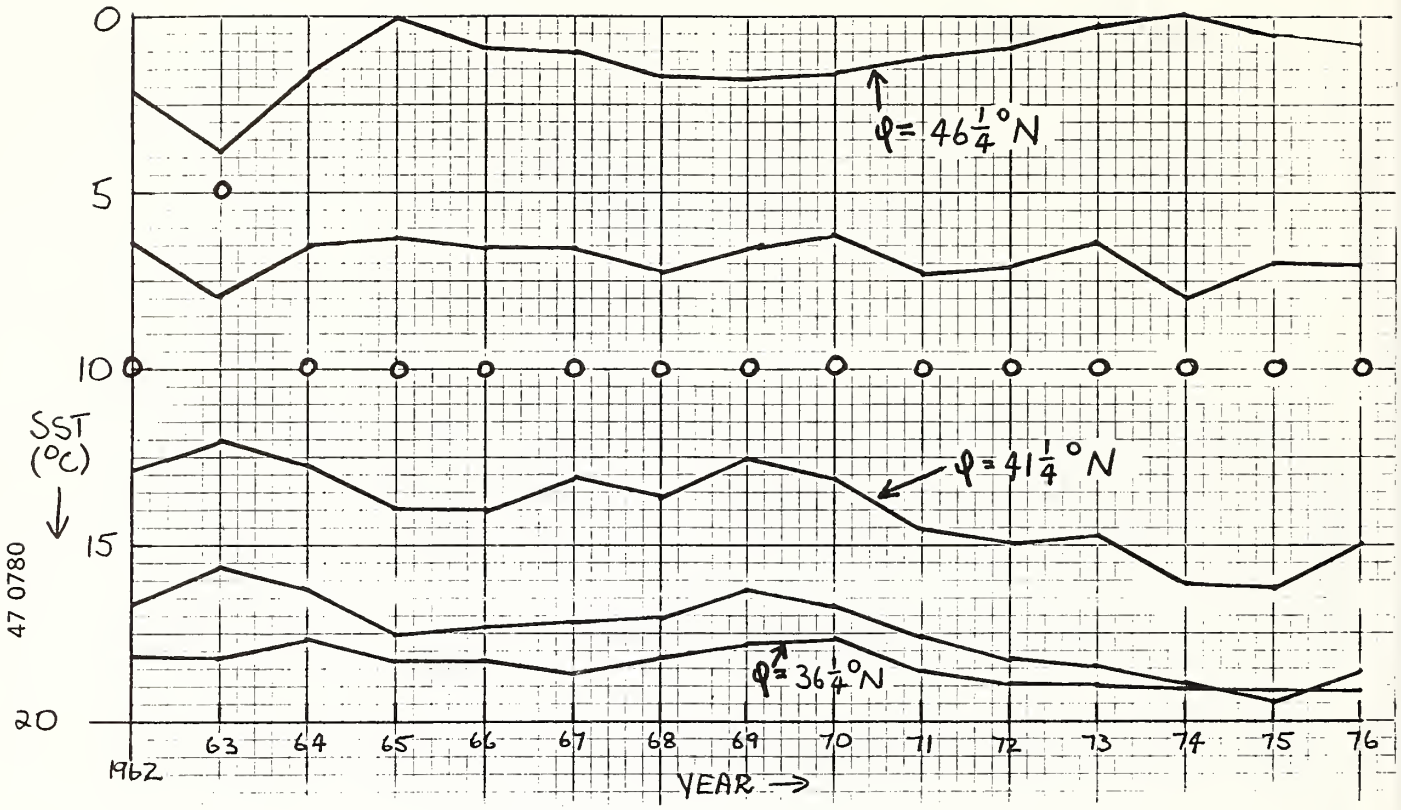

FIG. 1: TRANSECT ALONG 58¾° W: YEARLY MINIMUM SST AT 46¼° N AND CONCURRENT SSTs FURTHER SOUTH OPEN CIRCLES INDICATE GRID INTERVAL OF MAXIMUM MERIDIONAL SST DECREASE

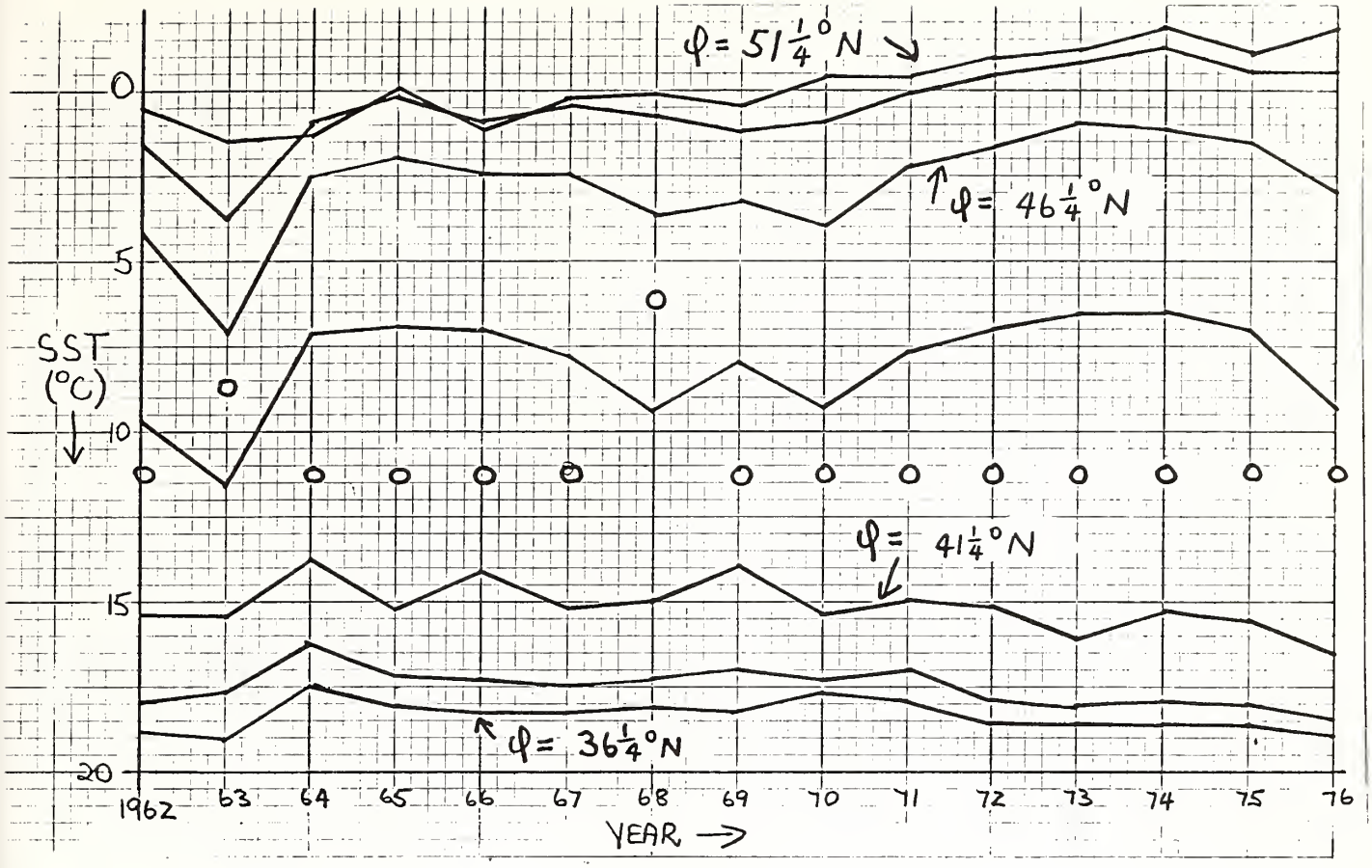

FIG 2: TRANSECT ALONG 51¼°W : YEARLY MINIMUM SST AT 46¼°N AND CONCURRENT SSTs FURTHER NORTH AND SOUTH. OPEN CIRCLES INDICATE GRID INTERVAL OF MAXIMUM MERIDIONAL SST DECREASE

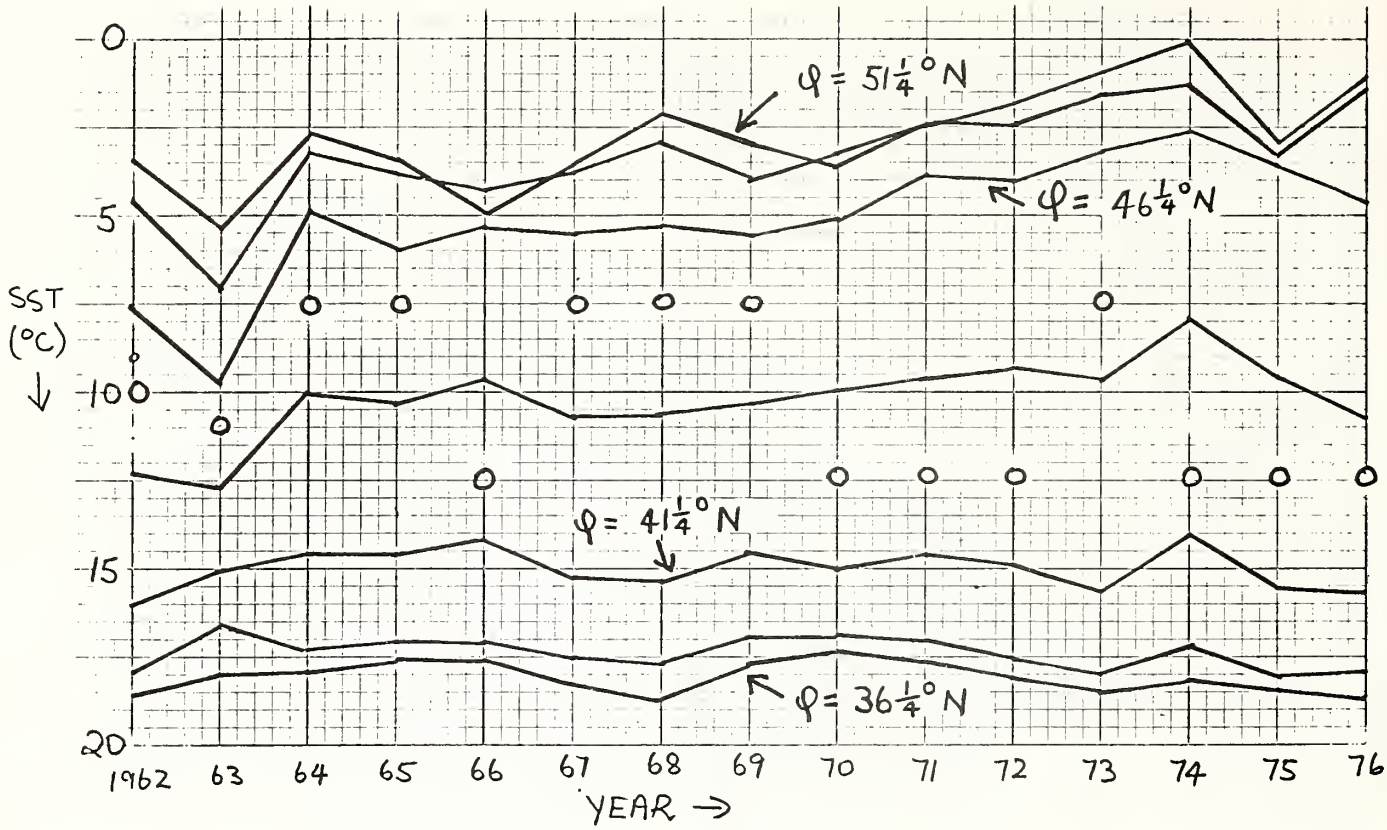

FIG. 3 TRANSECT ALONG $46\frac{1}{4}^{\circ}$ W: YEARLY MINIMUM SST AT $46\frac{1}{4}^{\circ}$ N AND CONCURRENT SSTs FURTHER SOUTH. OPEN CIRCLES INDICATE GRID INTERVAL OF MAXIMUM MERIDIONAL SST DECREASE

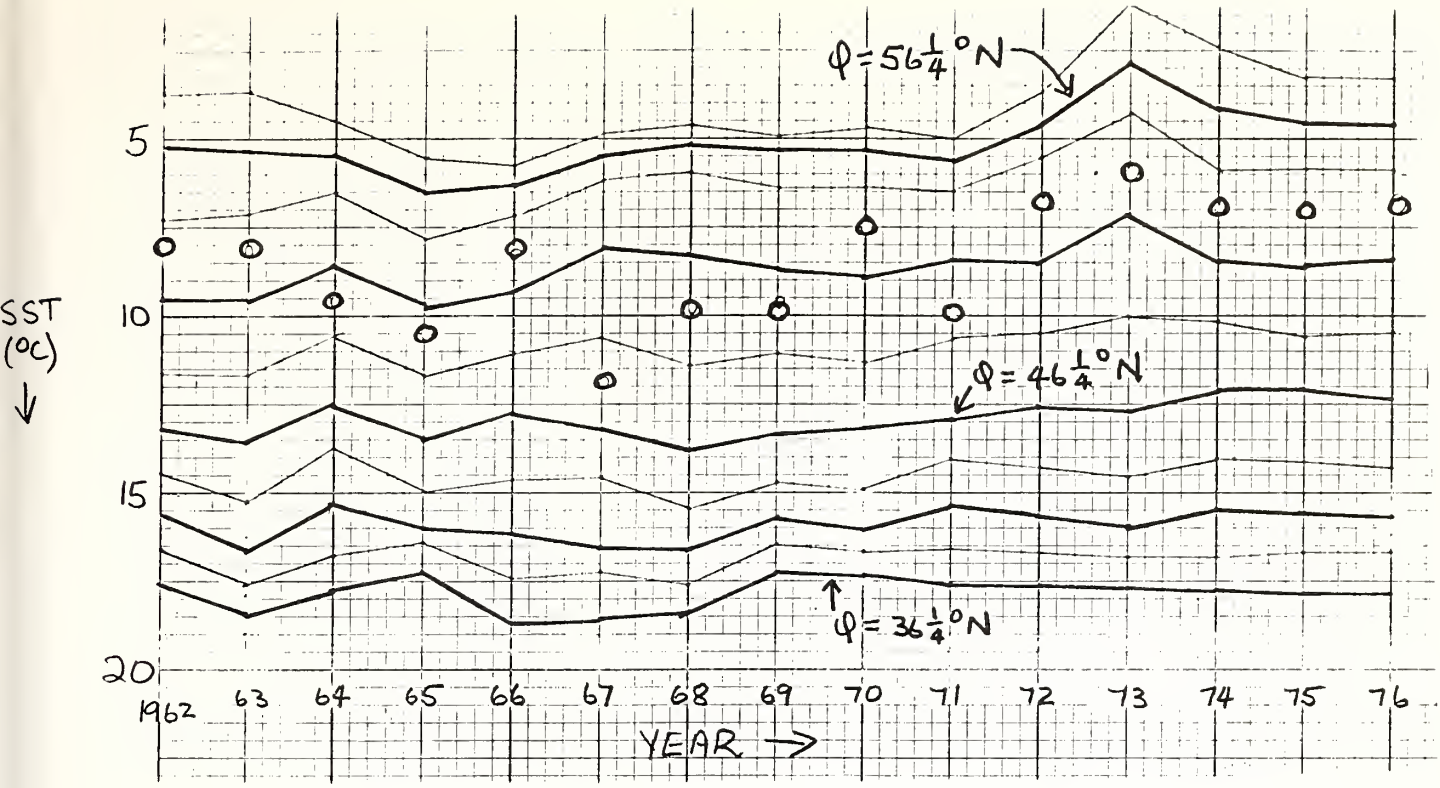

FIG. 4: TRANSECT ALONG 38¾° W: YEARLY MINIMUM SST AT 53¾°N AND CONCURRENT SSTs NORTH AND SOUTH. OPEN CIRCLES INDICATE GRID INTERVAL OF MAX. MERIDIONAL SST DECREASE

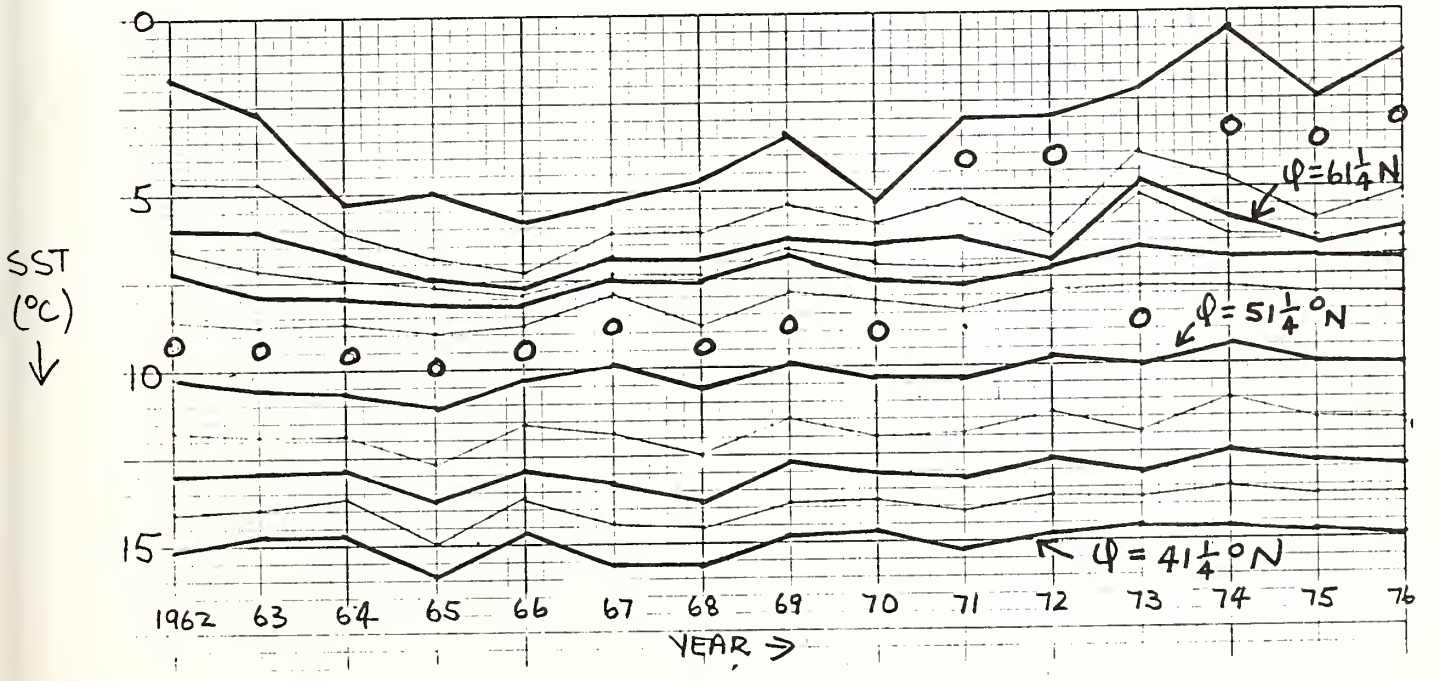

FIG. 5: TRANSECT ALONG 28¾°N: YEARLY MINIMUM SST AT 53¾°N AND CONCURRENT SSTs NORTH AND SOUTH. OPEN CIRCLES INDICATE GRID INTERVAL OF MAX MERIDIONAL SST DECREASE

INTERANNUAL VARIABILITY OF ARABIAN SEA SEA SURFACE TEMPERATURE

by

Otis B. Brown

and

Robert H. Evans

University of Miami
Division of Meteorology and
Physical Oceanography
Rosenstiel School of Marine and Atmospheric Science

Arabian Sea Summer Cooling

This study is focused on the large scale interannual variability of the western Indian Ocean's response to the Summer Monsoon. Saha (1974) and Shukla (1976) have investigated the role of SST in modulating the monsoonal rainfall over western India. Other work (Duing and Leetmaa, 1978) has studied the overall upper mixed layer heat budget in this region. We wish to determine the extent and variability of the monsoon induced ocean thermal contrast.

We utilize satellite remotely sensed surface temperatures in this study, hence validation experiments between various satellite data products and available ship observations are an integral part. The work involves most aspects of remotely sensed data acquisition and processing. In the following discussion we shall concentrate on the analysis aspects.

The discussion is broken into two sections: data preparation and analyses in Appendix A and a discussion of pertinent results in the present section. We shall freely abstract results from the Appendix; the reader is urged to study the technique outlined in Appendix A.

Four sources of SST observations are used in this study: 100 year ship means, ship of opportunity results, NESS First Guess Field (FGF), Scanning Radiometer (SR), and NESS GOSSTCOMP SR retrievals. Our intention is to use ship measurements as a verification of satellite retrievals while also (in the case of 100 year means) providing long-term mean monsoon SST response patterns. The study spans the months of April through September for the years 1975-1977. Problems exist due to variation in data density from year to year within a source of observations and also between different sources. (Examples of data density variation are examined in Appendix A for ship and FGF retrieval percentages). To minimize difficulties due to the diversity in data density, monthly mean fields were calculated and uniform optimal interpolation techniques were applied by month to each data set.

Validation of the satellite observations with ship measurements consisted of comparing the interpolated monthly maps of ship and satellite observations. Two types of satellite observations are used: the FGF are connoted as "monthly" in Table 1, GOSSTCOMP as noted.

Table 1 presents a comparison between ship and satellite SST observations for 1977. The preparation of the data sets is discussed in Appendix A. The standard deviation of the satellite and ship observations averages approximately 1.5 C. Mean differences are approximately 1 C. This should be compared with Brower et al. (1975) who show XMS variability between ship of opportunity temperatures to be ∿1.5 C. Hence in the Indian Ocean satellite observations appear to be a reasonable method of monitoring SST (or at least they are no worse than ships of opportunity).

A common grid has been defined for the area 93 x 67 elements (46.5° longitude x 33.5° latitude, 0.5 degree square). The upper left-hand corner is located at 38°E, 23°N. Ship and satellite-acquired data of various types must be mapped onto this basis set. Experience shows that due to sampling vagaries it will be difficult to densely fill such a grid with the ship observations. Interpolation of unequally-spaced observations to the regular grid is accomplished by an optimal interpolation scheme (Gandin, 1963).

A 100 year compilation of ship temperature (Navy Atlas Project: Indian Ocean, 1976) has been used as a climatic mean temperature set. These temperatures (1° x 1° grid) are interpolated two-dimensionally with a Bessel interpolation scheme to 0.5° x 0.5° resolution. The results are shown in Figure 1 and the interpolation technique is discussed in detail in Appendix A.

Figure 1 presents the climatic, i.e., 100 year ship mean temperatures for the months April through September. Upwelling along the African coast at 8°N to 12°N is well resolved, starting in May and reaching a maximum in August along Somali and Arabia. The cooling in the central part of the western Indian Ocean is well resolved with the relative high temperatures being constrained to a region southwest of India. Upwelling along the Indian West Coast is found also. An abrupt transition between seasonal warming and monsoon-induced cooling is observed. These results compare very well with the satellite observations we have previously shown for 1976. The maximum thermal contrast occurs between the months of April and August in the climatic data. Therefore we shall limit the discussions of the multi-year satellite observations to monthly differences between April and August.

Figure 2a shows the climatic mean result for the April-August differences. Figures 2b, c, and d illustrate the April minus August differences for the raw composite satellite retrievals for the years 1975, 1976 and 1977. Duing, in the previous section, presents results for 1963. Although the general pattern does not change from year to year, the absolute magnitude and areal extent of given isotherms show large variation. A relative low exists southwest of India in all years with a similar isotherm spreading to the south and west. This can be inferred from the climatic patterns in Figure 1 by noticing the development during the summer months of the large scale cooling. Marked changes occur in the northwestern quadrant yearly and from climatology. Examination of the +2.0 C isotherm shows greater than a factor of 2 areal variation over the time period studied.

The interannual differences of Arabian Sea summer cooling are large, both in amplitude and area. In fact, they are large enough to substantially alter the heat budget calculations presented by Duing and Leetmaa (1978).

As a consequence, we may speculate that the two main contributors to summer cooling, i.e., cross-equatorial advection by the Somali Current and coastal upwelling, also undergo substantial interannual variation. We are planning to intercompare the interannual cooling results with precipitation data from the Indian Subcontinent between 1975 and 1977 in order to test the model predictions of Shukla, 1975.

Table 1

MONTH	GOSSTCOMP - SHIP Mean (C * 10)	GOSSTCOMP - SHIP σ (C * 10)	MONTHLY - SHIP Mean (C * 10)	MONTHLY - SHIP σ (C * 10)	GOSSTCOMP - MONTHLY Mean (C * 10)	GOSSTCOMP - MONTHLY σ (C * 10)
April	-6.15	15.9	13.71	13.9	-6.96	10.00
May	-9.02	13.55	13.38	11.69	-4.35	9.91
June	-13.04	14.4	16.56	13.76	-2.65	9.29
July	-10.8	15.58	13.35	15.82	-2.55	10.05
August	-8.7	13.3	9.16	13.44	-.60	9.85

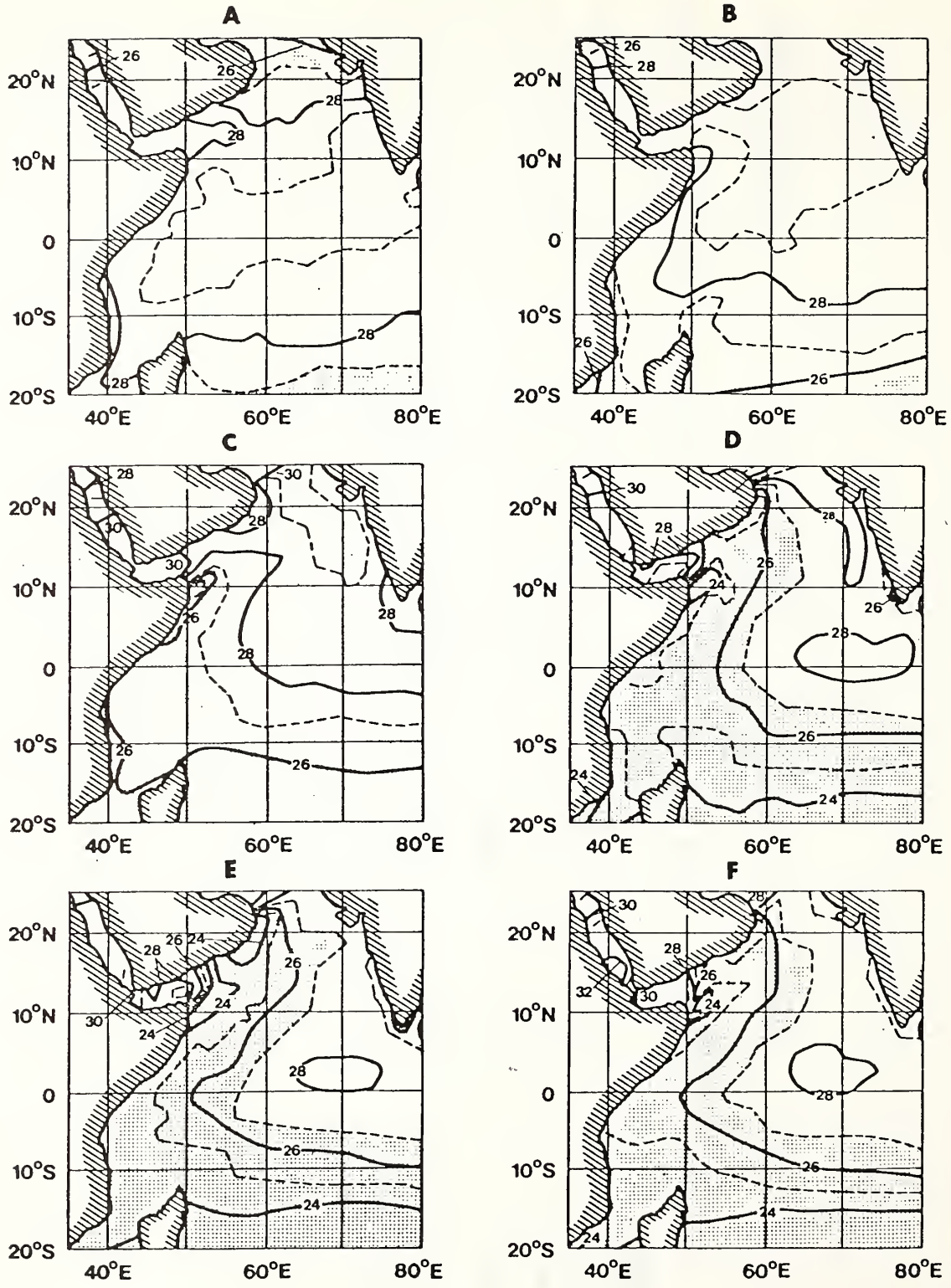

Figure 1. Long-term variability for the months April-September based on 100 means of ship observations: a,b,c,d,e,f refer to monthly means for April, May, June, July, August and September, respectively.

APPENDIX A
(Arabian Sea Cooling)

Data sources and subsequent processing are presented. Emphasis is placed on deriving an appropriate interpolation algorithm which can be used on ship and satellite SST observations. Observations are discussed and followed by a delineation of the interpolation procedure.

Ship Observations

World Meterological Organization Temperature Daily File (TDF11) ship observations for the grid area were obtained from the National Climatic Center (NCC) for the months April through September in the years 1975, 1976 and 1977. These observations were sorted, checked for gross discrepancies, and mapped to the common grid. Retrievals by month and year for the grid are shown in Table A.1.

TDF11 observations are mostly intake or, rarely, bucket measurements. The statistics are highly variable; Brower et al. (1975) show that the standard deviation between ships approaches 1.5 C. Other work (Barnett, private communication) in the central Pacific has shown these measurements are generally warmer than the surroundings, highly ship dependent, and are biased by $\sim$ 0.4 C.

Satellite Observations

NOAA Scanning Radiometer (SR) infrared observations were chosen as the data source for this aspect of the analysis. The retrievals are mapped to 0.5° x 0.5° grids and have been archived daily for the entire study period. Two types of satellite observations are analyzed: raw and "analyzed". Both products are produced by NESS from the SR data. The first comprise the "First Guess Field" from which NESS calculates the latter, GOSSTCOMP product.

The First Guess Field is generated on a daily basis from the SR and Vertical Temperature Profiling Radiometer (VTPR) results. Clear areas of image are identified and a 10 x 10 (100 km. x 100 km.) matrix extracted about grid points. VTPR water vapor correction and cloud contamination corrections are applied and a boxcar average is calculated to produce a corrected SST estimate. FGF algorithms have changed several times since the field's inception. The algorithm is documented by Leese et al. (1971a). These changes represent another bias which must be removed. Retrievals by month are given in Table A.2.

GOSSTCOMP (Global Operational SST Composite) derivation is discussed by Leese et al. (1971a). Essentially, the FGF is combined with previous day's observations, constraints on maximum spatial gradient and allowable daily changes are applied and the resultant field is interpolated to produce a dense mapped SST grid. The constraints have also been subject to change over the period of interest and represent unknown biases. Leese et al. (1971b) give reliability estimates for GOSSTCOMP. Since all grid points are filled there always exists 100% retrieval. We have discarded data more than one day old in the monthly mean generation in order to reduce biases due to the interpolation of old data by NESS.

The goal of this study is the understanding of the larger scale, seasonally varying signatures in the SST field. Monthly mean data sets are constructed for each of the three data types by year. A total of 54 data matrices, many of them sparsely populated, now must be interpolated for map making and analysis purposes.

Interpolation

Removal of the long-term mean does not produce a non-zero mean data set. For the three years under study the mean Indian Ocean temperature differs from the 100 year mean by 0.2 C to 1.0 C depending on the month and geographical location. Subsequently a mean square difference plane is removed from the remaining anomaly and the remaining field has zero mean.

Gandin (1963), Thiebaux (1973), have developed optimal interpolation in which the mean square error of the interpolated value is a minimum. Such an interpolation utilizes an auto-covariance matrix of the data points to compute a set of weights with which a new value is computed from it's nearest neighbors. Functionally we define the interpolation as:

$$Y = BX \qquad \text{A.1.A}$$

where

$$B = C_{oi}\, C^{-1}_{ij} \qquad \text{A.1.B}$$

with C the covariance matrix of the item with respect to its neighbors, C a covariance matrix for the X items, X a vector of the surrounding observations and Y the interpolated value. We make an assumption of field homogeneity, but not isotropy. That is, we assert that the covariance matrix is independent of position in the data field, but that the elements have covariances dependent on the vector orientation of the point set (the covariance matrix is independent of field position, however the value for a given element may depend on the relative orientation between two points as well as their relative separation: interested readers are referred to Gandin, (1963) for a complete discussion).

Ideally the covariance matrix should always be computed from the data set to be interpolated. The long-term and satellite data set densities are high enough for this approach to succeed. However, the ship observation sets are quite sparse with monthly composite minima and maxima of 11% and 28% occupation, respectively. The lack of observations precludes a reasonable (i.e. low variance) estimate of the monthly auto-covariance matrices in the Indian Ocean. Months taken by year could be averaged together or yearly averages computed. This approach was rejected on the basis of expected and observed high interannual variability in the SST data fields and their respective auto-covariance matrices.

Obvious alternative candidates for the ship auto-covariance fields are matrices computed from the long-term or ship data sets. Sample covariance matrices, normalized to 1 at zero lag, so they are auto-correlation functions, for the climatic and satellite observations are presented in Figure A.1 for June, 1977. They are quite different with the rapid fall off of the long-term auto-correlation function ascribed to the monthly averaging over many (>100) realizations destroying the inherent fine

structure. Due to this we believe the satellite observations are more relavent to the ship measurements and we shall use the satellite covariance matrices to interpolate the ship observations.

The data set (54 matrices + 6 100 year mean matrices) has been uniformly mapped and interpolated. A two-dimensional Gaussian smoothing function is uniformly applied to the data sets to damp out high frequency spatial variability. For these cases the function has an "E" folding length of 1.5 grid elements (165 km.).

A number of non-physical biases with annual time scale exists in the data sets; ship population statistics vary, and satellite sensing systems and retrieval and analysis algorithms change. To compensate for these changes (only at the zero order) all data sets are referenced to the pre-summer monsoon condition by removing the April observation grid. The resultant data sets cover the period May-September, 1975, 1976 and 1977. We will concentrate on the August differences for the data types.

Table A.1

Ship SST Retrievals (%)

Year/Month	April	May	June	July	August	September
1975	11.5	11.6	14.4	14.5	15.0	17.7
1976	17.2	17.3	18.9	19.1	17.8	17.5
1977	18.4	19.3	25.5	27.9	25.7	21.7

Table A.2

Satellite SST Retrievals (%)

Year/Month	April	May	June	July	August	September
1975	51.8	49.2	28.7	34.4	34.7	37.1
1976	81.7	91.7	84.5	73.2	75.5	90.0
1977	95.4	95.1	91.5	80.5	90.5	94.8

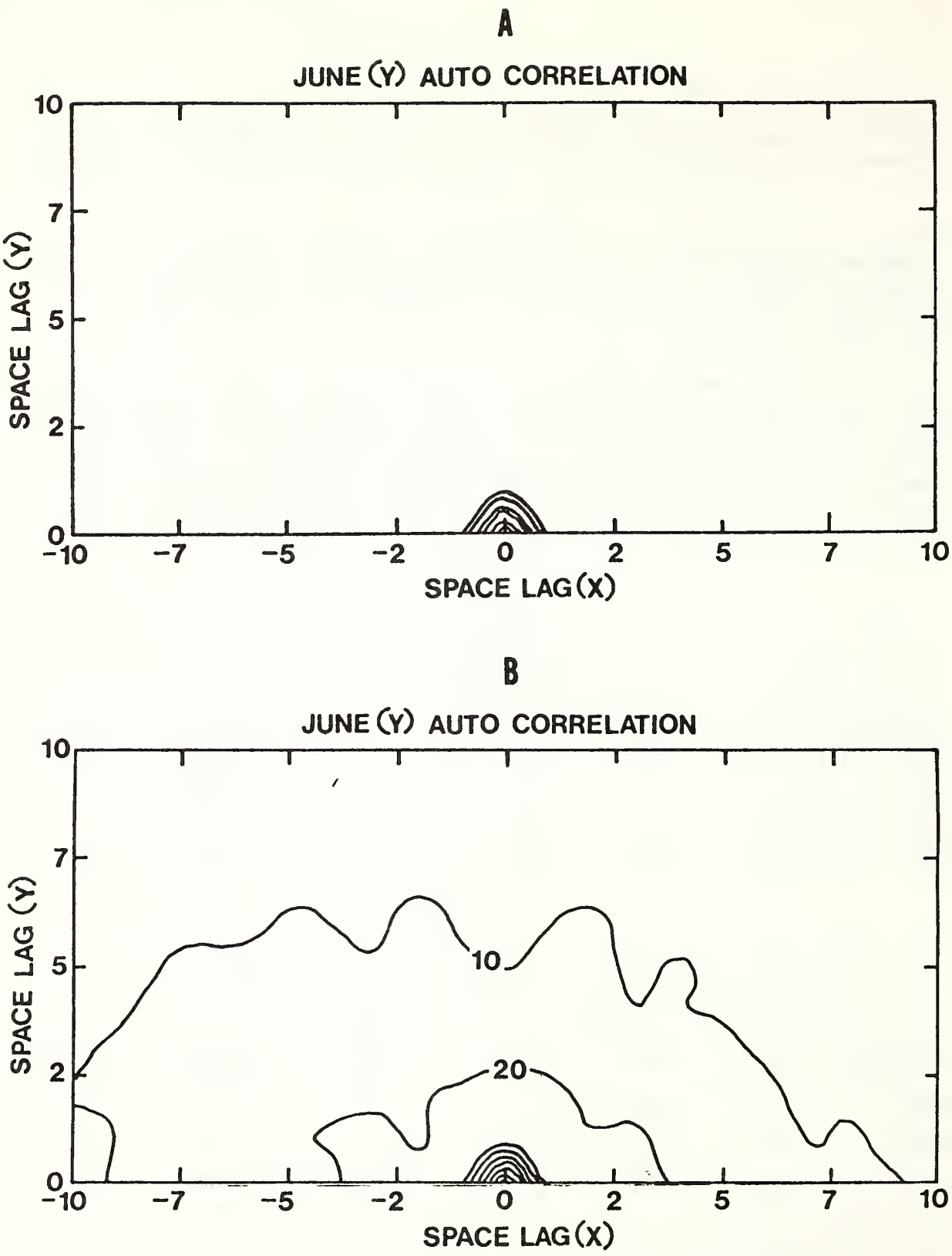

Figure A.1. June covariance matrices for a) climatic mean and b) raw satellite data for June, 1977.

References

Brower, R.L., W.G. Pichel, C.C. Walter and T.L. Signore. 1975. Current status and quality of global operational sea surface temperatures from satellite infrared data. NESS International report, 10 pp.

Duing, W. and A. Leetmaa. 1978. Arabian Sea Cooling; a preliminary heat budget.

Gandin, L.S. 1963. Objective Analysis of Meteorological Fields. Israel Program for Scientific Translations, Jerusalem, 1965. 242 pp.

Leese, J.W., W. Pichel, B. Goddard and R. Brower. 1971a. An experimental model for automated detection, measurement, and quality control of sea surface temperature from ITOS-SR data. Proceedings of the Seventh International Symposium on Remote Sensing of the Environment, March 1971, Ann Arbor, Michigan, Willow Run Laboratories, University of Michigan. pp. 625-646.

Leese, J.W., W. Pichel, B. Goddard and R. Brower. 1971b. Factors affecting the accuracy of sea surface temperature measurements from ITOS-SR data. Conference Preprint No. 90 on Propagation Limitation in Remote Sensing, June 1971, NATO Advisory Group for Aerospace Research and Development, Paris, France, NATO, Paris, France. 13 pp.

Saha, K. 1974. Some aspects of the Arabian Sea summer monsoon. Tellus, 26: 464-476.

Shukla, J. 1975. Effect of Arabian Sea surface temperature anomaly on Indian summer monsoon: a numerical experiment with the GFDL model. J. Atmos. Sci., 32: 503-511

Thiebaux, H.J. 1973. Maximally stable estimation of meteorological parameters at gridpoints. J. Atmos. Sci., 30: 1710-1714.

SALINITY FLUCTUATIONS IN THE LABRADOR SEA, AND THEIR IMPLICATIONS FOR HIGH LATITUDE OCEANIC CLIMATE FEEDBACK

Claes Rooth
CIMAS, University of Miami

SUMMARY: Hydrographic data time series from Ocean Station Bravo suggest that over a five year period from 1967 to 1971, the normal winter time convection in the Labrador Sea was shut off due to low surface salinities. Two models of seasonal heat cycles interacting with a steady fresh water supply suggest that bimodal state distributions (intransitivity) is possible in some parameter range. Large differences in the severity of ice conditions occur between regimes.

BACKGROUND: John Lazier[1] of the BIO in Canada has processed the hydrographic data time series from Ocean Station Bravo. Figure 1, produced by him, shows a pronounced transient in surface conditions in the Labrador Sea, where for several years in sequence surface salinities were too low to allow deep convective mixing at freezing point temperatures. This period coincided with a period of extreme ice conditions around Iceland and in the Davis Straits, and terminated in thewinter 1971-72, just ahead of the Atlantic leg of the GEOSECS, a benchmark survey of ocean chemistry and tracer distributions. As was shown by Dorsy and Peterson[2] concentrations of tritium in surface waters of the East Greenland Current (1972) were anomalously high compared to expectations based on stationary Arctic Circulation. Derived from thermonuclear tests, but also from various aspects of nuclear technology applications, tritium in the Arctic is completely dominated by USSR activities. It is of interest here, that testing of devices in the atmosphere ceased in 1964. It has been accepted since the drift of the FRAM, that sea ice drift from the Siberian coast line to the Greenland Sea takes a couple of years, suggesting that near zone fallout cannot be invoked as an explanation of the observed tritium anomaly. A third suggestive coincidence was brought up at this meeting by Kukla[3], who finds in satellite observations of snow cover a substantial negative anomaly in the late sixties, abruptly terminated in 1971. According to Kukla, the anomaly is due to late snow cover onset in fall, suggestive of an elongated runoff season, and perhaps implying enhanced supply of fresh water and terrestrial fallout tritium previously tied up in "permanent" snow on the North Siberian slopes.

The significance of fresh water supply in the Arctic for the maintenance of the ice regime has been long appreciated, c.f. review by Weyl[4]. The seasonal variations in the near surface halocline caused by freezing out of salt in the formation of sea ice are thought in many instances to limit the extent of the latter. What is explored here is the effect of the mean annual transport processes of heat and salt in a basin where convection may be switched off by the fresh water supply.

MODEL PHYSICS AND RESULTS. My basic model is that of a two-layer isolated basin, which is in diffusive lateral exchange with a large reservoir (ocean) of heat flow (not necessarily of zero mean) and to a fresh water inflow, and may be forced

either by fluctuations in the latter, or in the surface salinity of the outer basin. The analysis concerns itself with possible forms of the stationary annual cycle, and intransitivity of the mean state, and is thus applicable to both types of climatic forcing. The use of a non-linear equation of state is essential, since it allows the generation of available potential energy by the onset of convection. It is indeed found that for a range of parameter combinations, either a seasonally convective state with small salinity anomaly in the basin may exist, or alternatively a permanent halocline.

Provided that these box model results can be shown to realistically represent the first order effects in real world marginal seas, an interaction pathway between high latitude terrestrial hydrology and ocean thermodynamics has been demonstrated which has a potential for controlling regional climatic anomalies on time scales of several years and larger[5].

REFERENCES AND NOTES

[1] John Lazier, Bedford Institute of Oceanography. Personal communication.

[2] Dorsy, H.G. and Peterson, W.H.: Tritium in the Arctic Ocean and East Greenland Current. Earth Planet. Sci. Let., 32, 1976, pp. 342-350.

[3] Kukla, G.: Snow and Ice Covers in 1977. Proceedings, Climate Diagnostics Workshop, Miami, 1978.

[4] Weyl, P.: The Role of the Oceans in Climate Change: A Theory of the Ice Ages, Met. Monographs, 8, 30, 1968, pp. 32-62.

I plan to submit a more detailed account to Geophysical Research Letters.

FIGURE 1

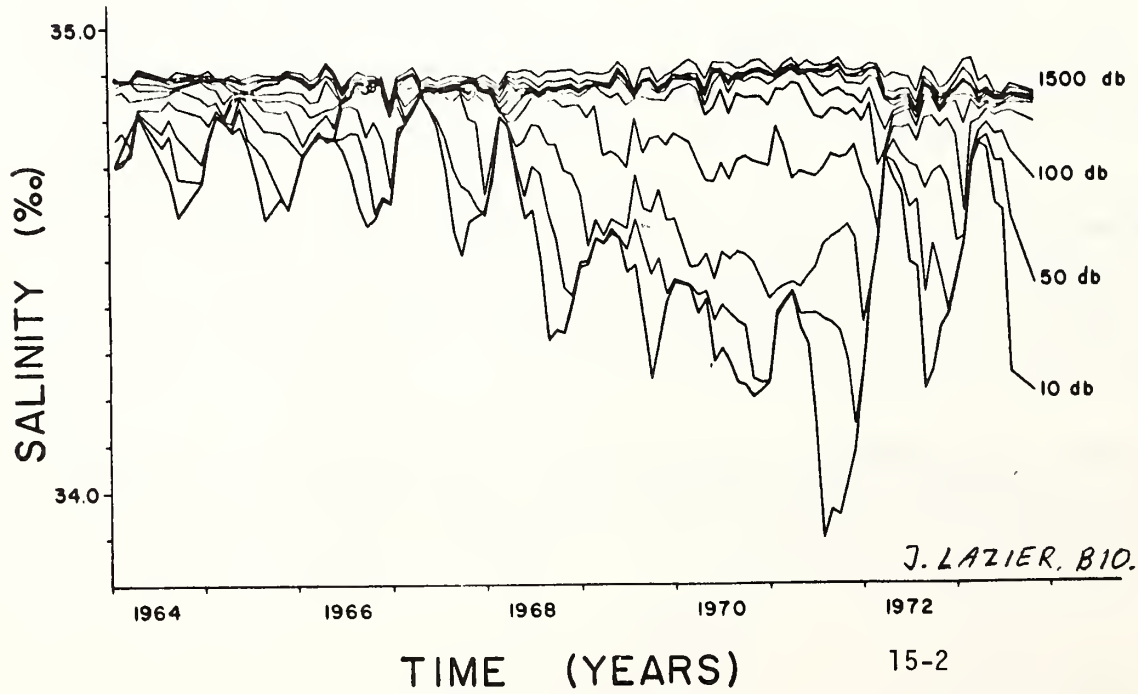

CHARACTERISTICS OF INTERANNUAL VARIATIONS OF LARGE-SCALE HEAT EXCHANGE ACROSS THE AIR/SEA INTERFACE IN THE MID-LATITUDE NORTH PACIFIC

by

N. E. Clark

SIO-NORPAX A-030
La Jolla, CA 92093

The interannual variability of heat exchange across the air-sea interface has been investigated using 9 years of data collected by ships-of-opportunity operating in the North Pacific.

Figures 1 and 2 show the seasonal values of standard deviations and ranges, respectively, for the total heat flux across the interface, the evaporative flux, and the solar insolation. These graphs reveal several interesting aspects of heat flux interannual variability:

1) The largest standard deviation and range values occur in spring and fall, while the lowest values occur in summer.

2) The increase in total heat flux variability from winter to spring is due to an increase in insolation variability, while that of evaporative heat flux has decreased.

3) The decrease in total heat flux variability from spring to summer is due to a decrease in the variability of both insolation and evaporation.

4) The increase in interannual variability of total heat flux from summer to fall is due to an increase in the variability of both insolation and evaporation.

5) The decrease in variability of total heat flux from fall to winter is due to a decrease in the variability of insolation.

6) The maximum interannual variability occurs in the western North Pacific in all seasons except summer when it is equivalent in both the eastern and western Pacific.

The interannual variability of heat exchange between ocean and atmosphere can also be studied by looking at monthly departures from long-term means (anomalies) of the various heat flux terms. Figures 3 through 6 show graphs of area averages of anomalous values of total heat transfer between ocean and atmosphere, latent and sensible heat transfer and insolation from December 1975 through May 1977. On each graph, the left panel shows the time sequence of the anomalous heat flux averaged over the area 30-50°N and 150-170°W, the center panel shows the time sequence of the anomalous flux averaged over 30-50°N and 130-150°W, and the right panel shows the difference between the center (eastern area) and left (western area) values. Figure 7 shows the areas over which the heat flux anomalies were averaged outlined on the sea surface temperature anomaly map for February 1977. Several interesting features are indicated by these graphs:

1) The western area received or lost heat at near-normal rates, while the eastern area exchanged heat with the atmosphere at near-normal rates until October 1976; it then began losing heat at below-normal rates (anomalies of 40-80 cal/cm /day) through February 1977. The differential anomalous cooling between the two areas during this period is reflected in both surface and sub-surface ocean thermal data.

2) The area averages of total heat flux (Q_T) are predominantly related to those of latent heat flux (Q_e) and somewhat less to those of sensible heat flux (Q_s). (Correlation coefficients between time sequences of Q_T and Q_e and Q_s are 0.99 and 0.97, respectively.) Fluctuations in the solar insolation (Q_i) had little effect on the total heat flux anomalies for these two open ocean areas.

3) The fluctuating nature of heat exchange in the western area reflects the variations in position of the upper level trough and storm tracks throughout the period (the most intense anomalous ocean cooling occurred to the west of 180° on the western flank of the intense Aleutian low).

4) In the eastern area, the almost total absence of storm tracks after September 1976 caused below-normal latent and sensible heat loss and led to above-normal temperatures in the ocean surface layer down to 60 meters.

FIGURES

Figure 1 Seasonal values of the standard deviations for total heat flux (Q_T), evaporative heat flux (Q_e) and insolation (Q_i) for the western and eastern mid-latitude North Pacific. Seasonal values were computed over the 9-year period 1969-1977.

Figure 2 Seasonal values of the ranges for total heat flux (Q_T), evaporative heat flux (Q_e) and insolation (Q_i) for the western and eastern mid-latitude North Pacific. Seasonal values were computed over the 9-year period 1969-1977.

Figure 3 Area averages of anomalous total heat flux (Q_T) between ocean and atmosphere. Areas 1 and 2 are shown in Figure 7.

Figure 4 Area averages of anomalous evaporative heat flux (Q_e) between ocean and atmosphere. Areas 1 and 2 are shown in Figure 7.

Figure 5 Area averages of anomalous sensible heat flux (Q_s) between ocean and atmosphere. Areas 1 and 2 are shown in Figure 7.

Figure 6 Area averages of anomalous insolation (Q_i). Areas 1 and 2 are shown in Figure 7.

Figure 7 Areas 1 and 2 over which the heat flux anomalies in Figures 3 through 6 were averaged.

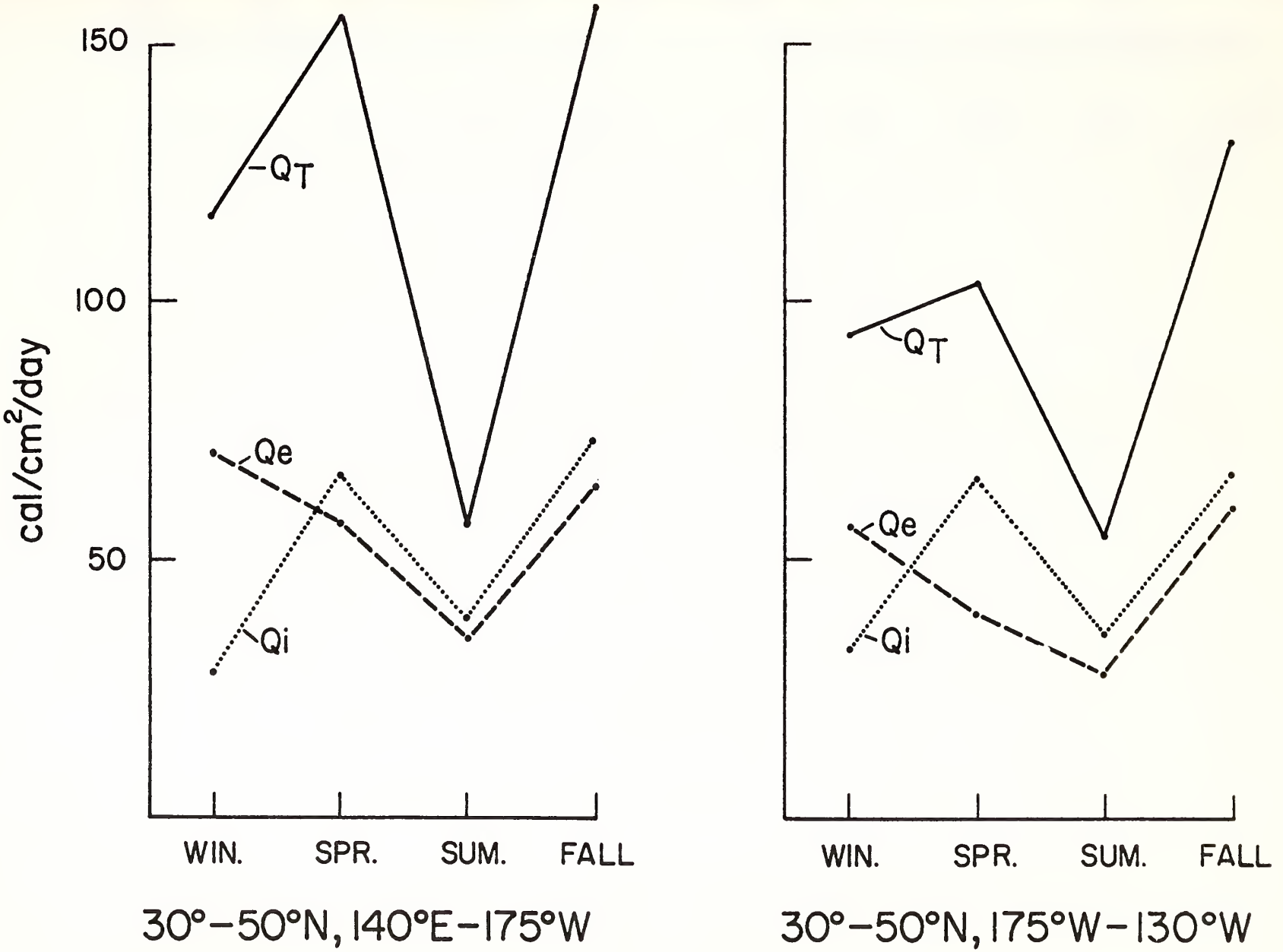
150
100
50
cal/cm²/day
QT
Qe
Qi
WIN.
SPR.
SUM.
FALL
30°–50°N, 140°E–175°W
QT
Qe
Qi
WIN.
SPR.
SUM.
FALL
30°–50°N, 175°W–130°W

Fig. 2

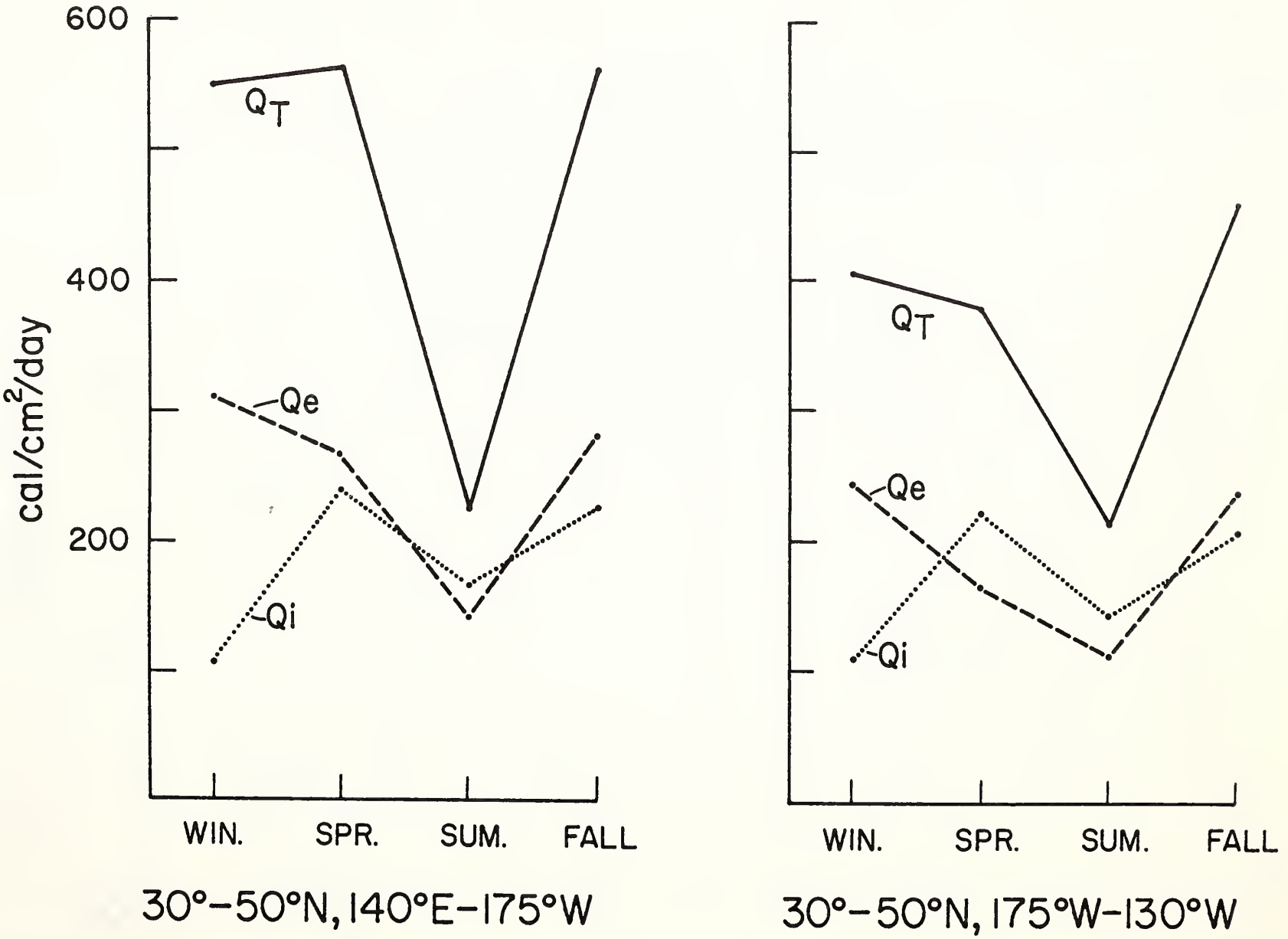
600
400
200
cal/cm²/day
Q_T
Qe
Qi
WIN.
SPR.
SUM.
FALL
30°–50°N, 140°E–175°W
Q_T
Qe
Qi
WIN.
SPR.
SUM.
FALL
30°–50°N, 175°W–130°W

FIG. 2

FIG. 3

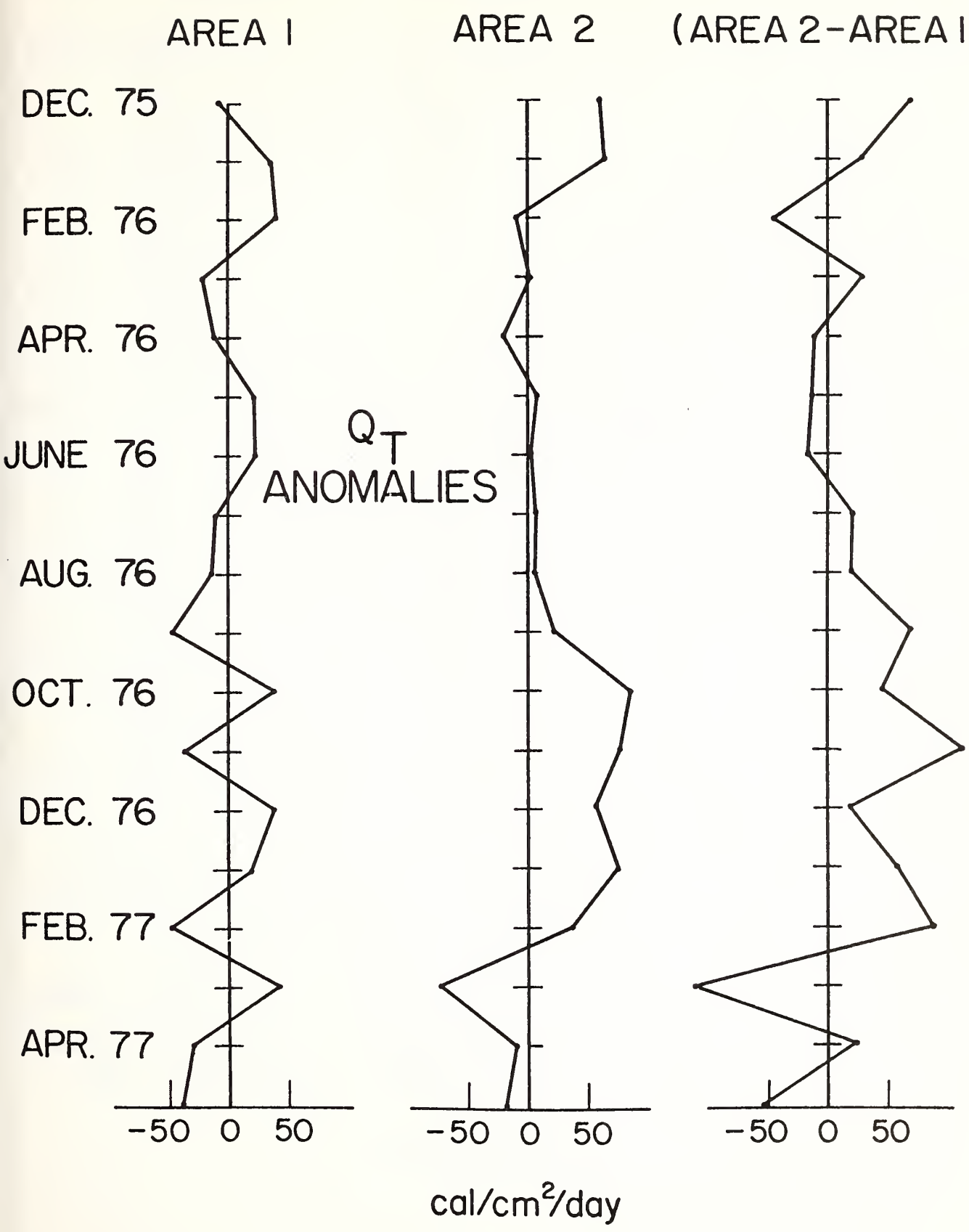
AREA 1
AREA 2
(AREA 2-AREA 1)
DEC. 75
FEB. 76
APR. 76
JUNE 76
AUG. 76
OCT. 76
DEC. 76
FEB. 77
APR. 77
Q_T
ANOMALIES
-50 0 50
-50 0 50
-50 0 50
cal/cm²/day

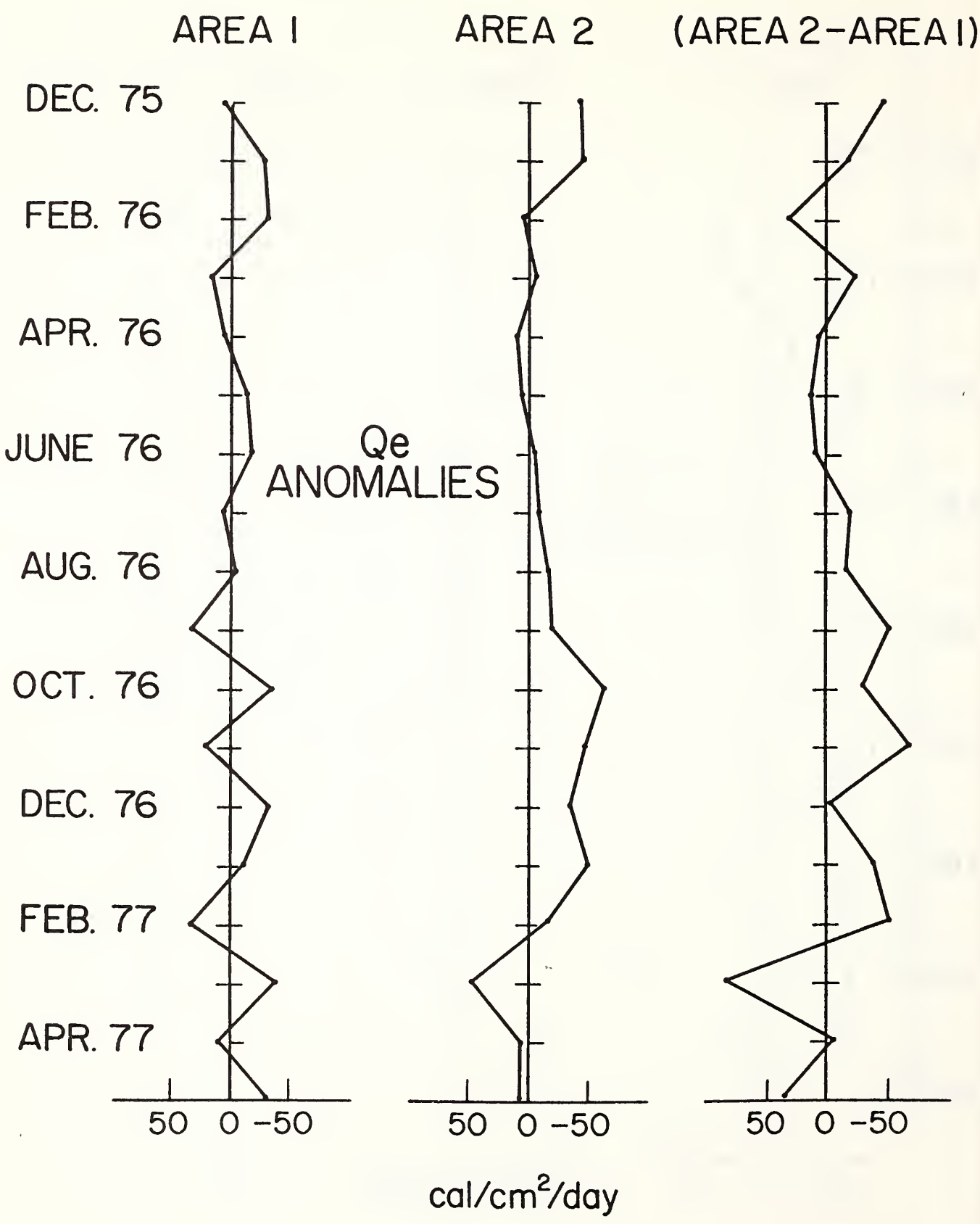
AREA 1
AREA 2
(AREA 2-AREA 1)
DEC. 75
FEB. 76
APR. 76
JUNE 76
AUG. 76
OCT. 76
DEC. 76
FEB. 77
APR. 77
Qe
ANOMALIES
50 0 -50
50 0 -50
50 0 -50
cal/cm²/day

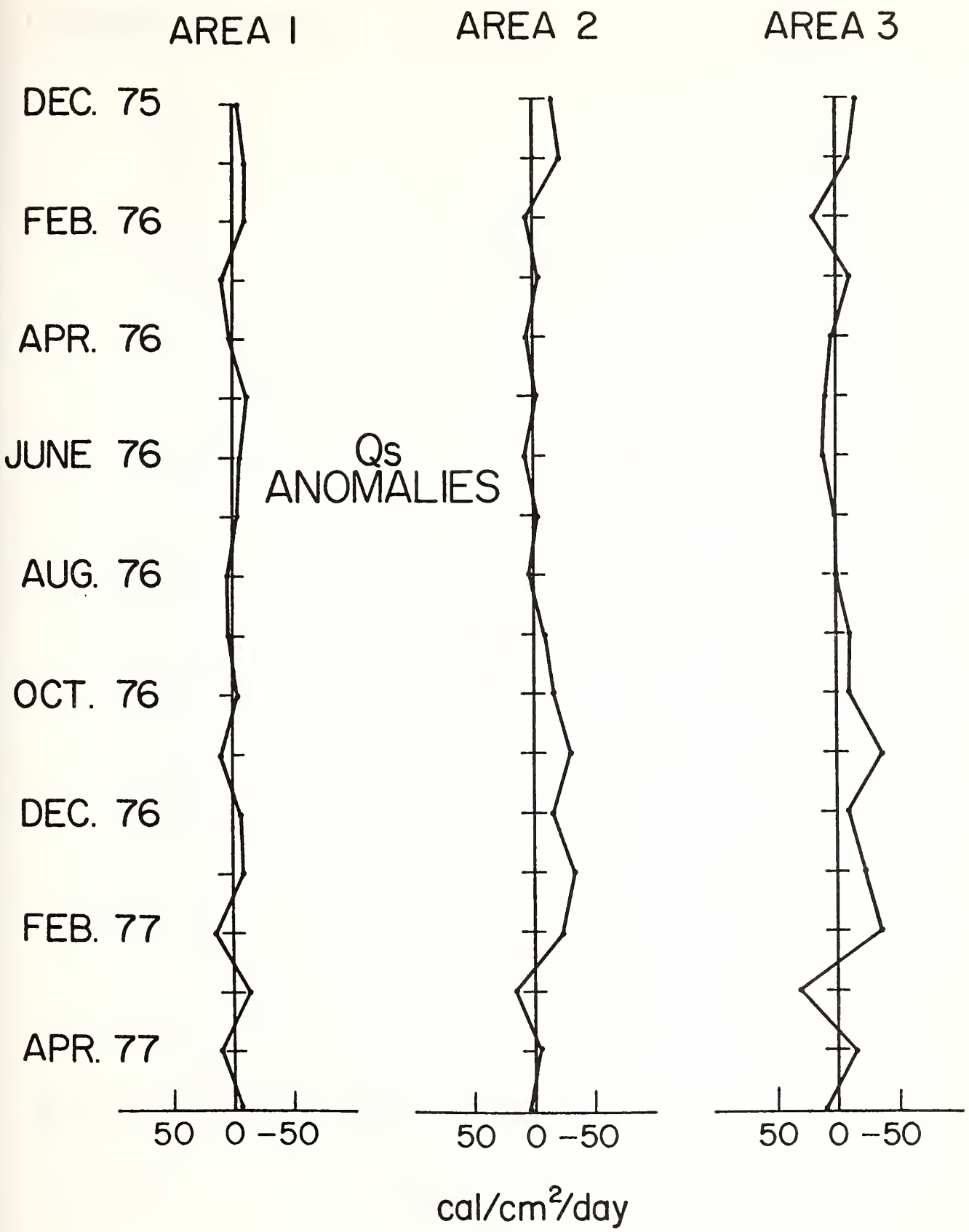
AREA 1
AREA 2
AREA 3
DEC. 75
FEB. 76
APR. 76
JUNE 76
AUG. 76
OCT. 76
DEC. 76
FEB. 77
APR. 77
Qs
ANOMALIES
50 0 -50
50 0 -50
50 0 -50
cal/cm²/day

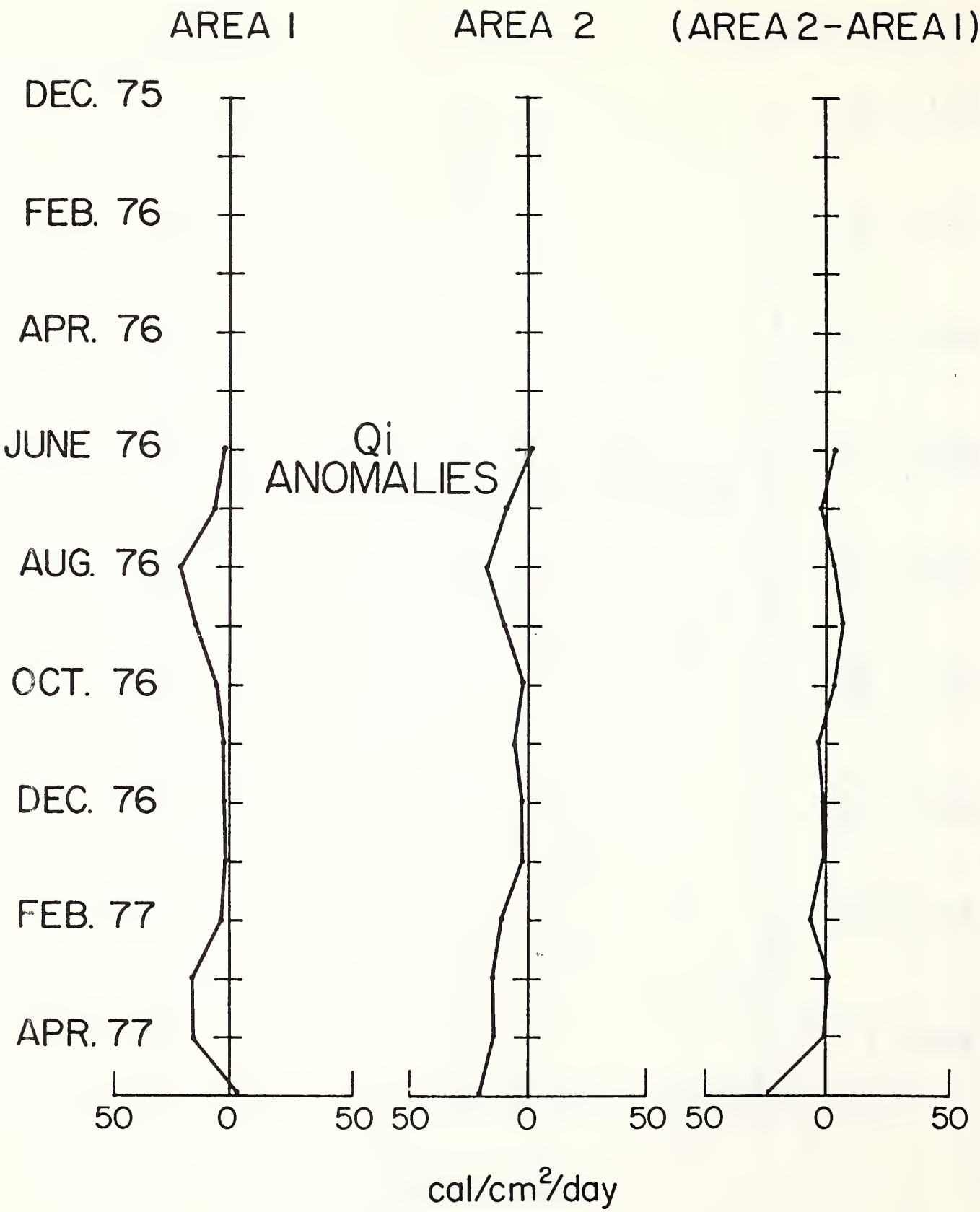
AREA 1
AREA 2
(AREA 2-AREA 1)
DEC. 75
FEB. 76
APR. 76
JUNE 76
AUG. 76
OCT. 76
DEC. 76
FEB. 77
APR. 77
Qi
ANOMALIES
50
0
50
50
0
50
50
0
50
cal/cm²/day

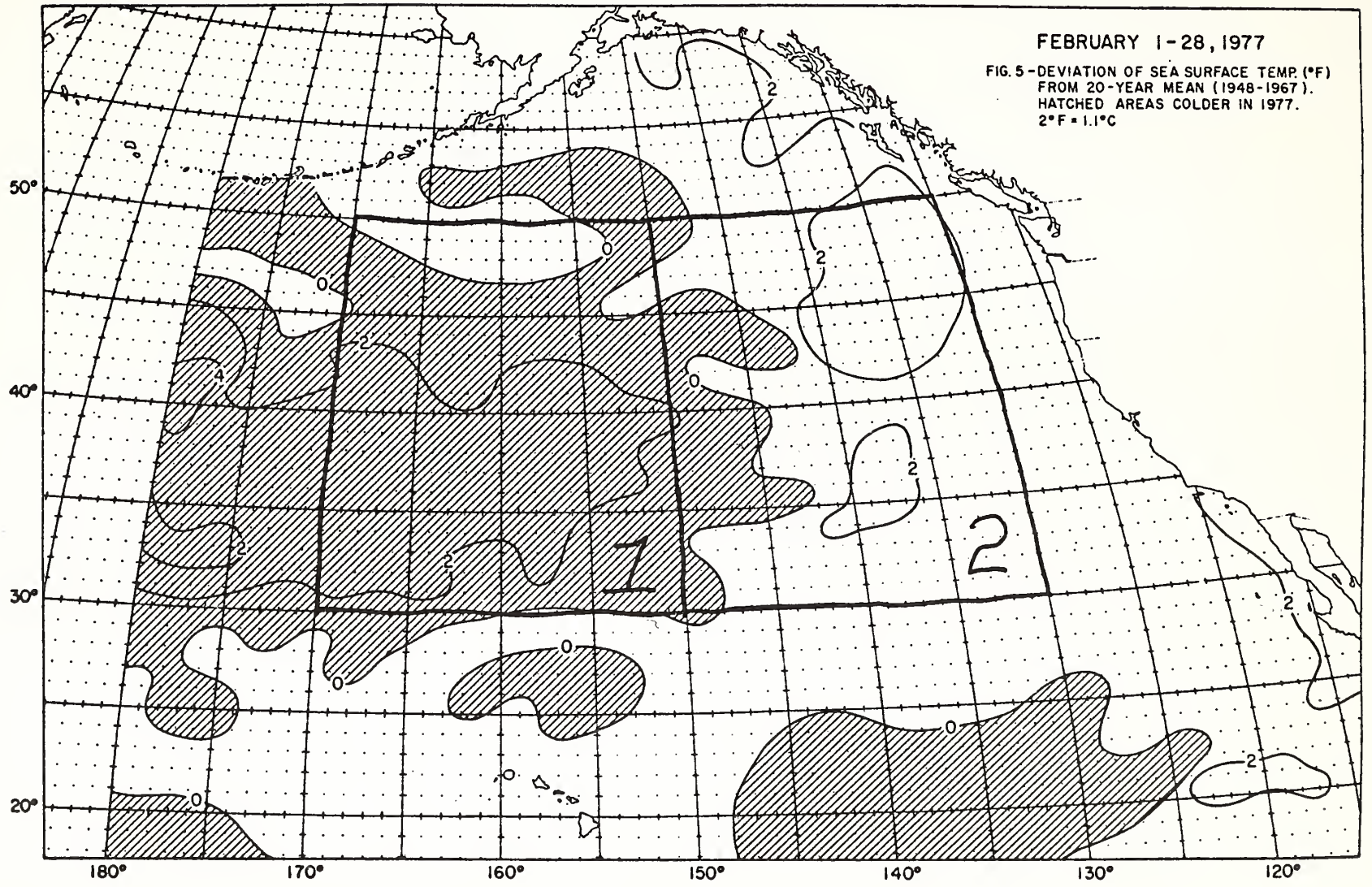
FEBRUARY 1-28, 1977
FIG. 5 - DEVIATION OF SEA SURFACE TEMP. (°F) FROM 20-YEAR MEAN (1948-1967). HATCHED AREAS COLDER IN 1977. 2°F = 1.1°C
50°
40°
30°
20°
180°
170°
160°
150°
140°
130°
120°
1
2

A 25-year Oceanic Flux Data Set of the Atlantic Ocean and Analyses

Andrew F. Bunker
Woods Hole Oceanographic Institution
Woods Hole, Massachusetts 02543

Energy fluxes at the surface of the Atlantic Ocean from 80°N to 60°S and averages of meteorological variables have been computed on a monthly basis for the 25-year period from 1948 through 1972. Fluxes of sensible, latent, and radiational heat and momentum were calculated using bulk aerodynamic equations with variable exchange coefficients and empirical radiation equations. The data used were the surface marine observations collected and recorded on magnetic tape by the National Climatic Center. Averages of fluxes and variables were formed over complete Marsden Squares (10×10 degree squares) for each month during the period. These averages together with identification and number of observations have been recorded on magnetic tape. The list of variables and fluxes is shown on Fig. 1. The tapes are available to all at cost of duplication. In addition to monthly averages other tapes contain statistics describing the data set. These include means, standard deviations, third order orthogonal polynomials, and other quantities by month, season, year, and entire set.

Exploratory analyses using various statistical techniques have been carried out in preparation for a systematic study of the data set. Figure 2 presents the 25-year average of the annual net heat gain by the ocean which depicts the energy exchange regimes of the ocean. The purpose of the study is to determine the physical processes producing the observed temporal and spatial variations of the fluxes and variables.

A survey of charts of standard deviations of fluxes and variables quickly pin-points regions in which the variability is large and suggests relations between components of the system. Figure 3 shows the variation of the oceanic heat gain during winter. A region of high variability extends from the Norwegian Sea southwestward to the Caribbean Sea. Much of this variability is caused by the variability of the meridional wind component as shown in Fig. 4. Variability of the meridional and zonal winds in the neighborhood of continents result in large air-sea temperature difference variability as shown in Fig. 5. Other charts available but not presented here show contributions by variability of cloud cover, pressure and sea temperature. In the tropics where the trade winds blow with little variation the heat exchange variation is produced primarily by variations in cloudiness and sea temperature variations presumably caused by upwelling and current variations. In the westerlies of South America during the southern hemisphere summer the largest variation appears in a region with few observations and hence is suspect. If the variation is real, other charts show that it is caused by greater variability in cloudiness, meridional winds and air-sea temperature differences.

Anomalies of the heat gain by the ocean during January 1950 are presented in Fig. 6 to show the large scale and continuity of patterns.

Charts for other months show similar large scale characteristics although the patterns are dissimilar. A mean sea level pressure chart has been inserted in the lower left to demonstrate the relationship between pressure pattern and heat gain through the advection of warm or cold air.

Time variations of fluxes have been explored by a) plotting the spatial distribution of linear trends, b) spectral and cospectral analyses of time series of heat gain and variables, and c) computing eigenvectors and plotting time series of their combination vectors. Fig. 7 exhibits the linear trend over the 25-year period of the oceanic heat gain by the ocean in W $m^{-2}yr^{-1}$. It is seen that most of the North and South Atlantic has a small negative trend. Only in the northwestern regions of the North Atlantic, regions off the west coast of Africa, and a small region inside the horn of South America is there a positive trend.

Many fluxes and variables have been analyzed to determine spectral and cospectral variations. Figure 8 presents the spectra of anomalies of oceanic heat gain, meridional winds, and latent heat flux in Marsden Square 115. The Gulf Stream flows eastward through the northern section of the square and the Sargasso Sea occupies the southern part. The energy density of heat gain and latent heat flux show little or no slope for periods from 2 months to 5 years but it increases toward longer periods. The meridional winds are quite variable throughout the spectral range and have a trend toward lower energy density in the long periods. In the 2 to 5 year period range the peaks and troughs of the heat gain and latent heat flux vary in unison while the meridional winds are out of phase. This negative covariance is shown more clearly in Fig. 9, the cospectrum of the meridional winds and the latent heat flux.

Several time series for a few areas which have the greatest variability have been analyzed by the empirical orthogonal function technique. Presented here are some results for January time series. In Fig. 10 the upper left-hand chart presents the covariance of the oceanic heat gain anomalies in Marsden Square 116 with the gain in other squares. It is seen that squares in the Gulf of Mexico and containing the Gulf Stream have high covariances. Cold shelf and slope water off Nova Scotia have a smaller covariance while squares in the eastern Atlantic have negative covariance values. The other charts show the first 5 eigenvectors. The percentages written to the upper right of each chart give the percentage of the variance explained by each eigenvector. A physical interpretation can be given to some of the eigenvectors. The first appears to be associated with the warm Gulf Stream and possibly the Brazil Current off Argentina. The second appears to be more regional than physical since it has high values in the northeastern Atlantic and the equatorial regions. The third eigenvector seems to be associated with the cold Labrador Current and cold water upwelling off West Africa, along the equator, and off Southwest Africa. The fourth eigenvector is puzzling in that it has large negative values over most of the South Atlantic.

Combination vectors associated with eigenvectors 1 and 3 are the only vectors which show any readily discernable trend patterns. In Fig. 11 it is seen that the first vector series is positive from the beginning until 1955, reaches a minimum in the mid-60's, then slowly rises. The third series starts positive, drops rapidly to a low in 1952, becomes positive in 1963, reaches a peak in 1967 and then decreases.

As noted earlier, a more systematic study of the data set will be carried out in the future.

KEY TO DATA RECORD FIELDS

NOTE: A VALUE OF -99.000 IN FIELDS 4 - 27 INDICATES THAT THERE WAS NO DATA FOR THAT MONTH.

FIELD	DESCRIPTION	UNITS
1	- MARSDEN SQUARE NUMBER	
2	- YEAR	
3	- MONTH	
4	- NUMBER OF OBSERVATIONS	
5	- AVERAGE AIR TEMPERATURE AT SURFACE	CENTIGRADE
6	- AVERAGE MIXING RATIO	G/KG
7	- AVERAGE SEA SURFACE TEMPERATURE	CENTIGRADE
8	- AVERAGE AIR-SEA TEMPERATURE DIFFERENCE	CENTIGRADE
9	- AVERAGE TOTAL CLOUD COVER	OKTAS
10	- AVERAGE WIND SPEED	M/SEC
11	- AVERAGE EAST-WIND VELOCITY	M/SEC
12	- AVERAGE NORTH WIND VELOCITY	M/SEC
13	- MEAN DIRECTION OF RESULTANT WIND	FROM 0 NORTH
14	- RATIO OF RAIN TO TOTAL OBSERVATIONS	
15	- AVERAGE PRESSURE	PASCALS/100
16	- RATIO OF SEA ICE COVERAGE '+' INDICATES OBSERVED COVERAGE ' ' INDICATES A CLIMATOLOGICAL MEAN	
	USING BUDYKO METHOD	
17	- AVERAGE RADIATION AT SURFACE	WATTS/METER**2
18	- AVERAGE EFFECTIVE INFRA-RED	WATTS/METER**2
19	- AVERAGE RADIATIONAL EXCHANGE	WATTS/METER**2
20	- AVERAGE LATENT HEAT FLUX	WATTS/METER**2
21	- AVERAGE SENSIBLE HEAT FLUX	WATTS/METER**2
22	- AVERAGE NET HEAT GAIN BY OCEAN	WATTS/METER**2
	USING OBSERVATIONS	
23	- AVERAGE LATENT HEAT FLUX	WATTS/METER**2
24	- AVERAGE SENSIBLE HEAT FLUX	WATTS/METER**2
25	- AVERAGE NET HEAT GAIN BY OCEAN	WATTS/METER**2
26	- AVERAGE WIND STRESS IN EAST DIRECTION	PASCALS
27	- AVERAGE WIND STRESS IN NORTH DIRECTION	PASCALS

Figure 1. Tabulation of meteorological variable and flux averages included in the oceanic data set.

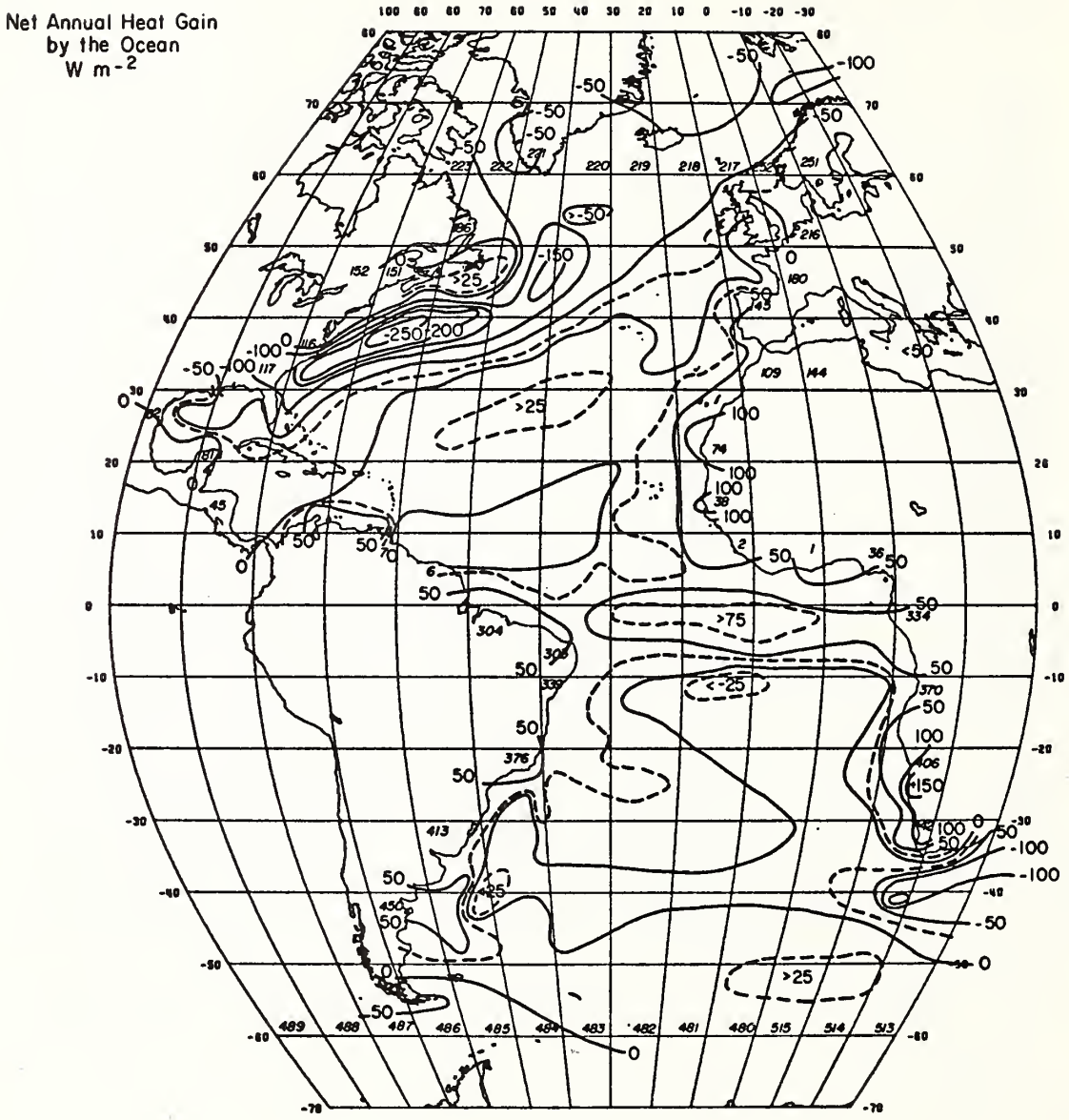

Figure 2. Net annual heat gain by the North and South Atlantic Ocean in Watta m^{-2}.

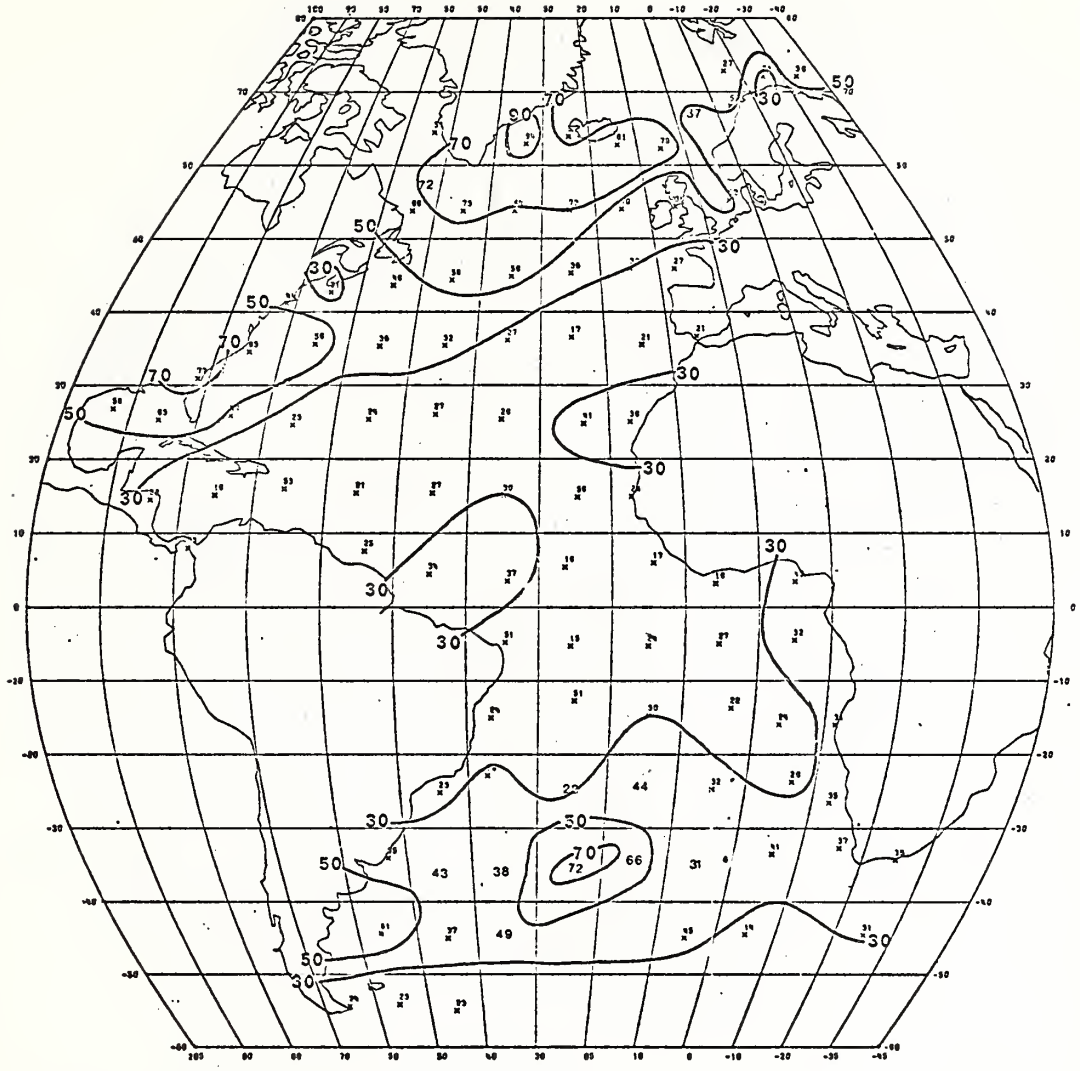

Figure 3. Standard deviation of net wintertime heat gain by the ocean in W m^{-2}.

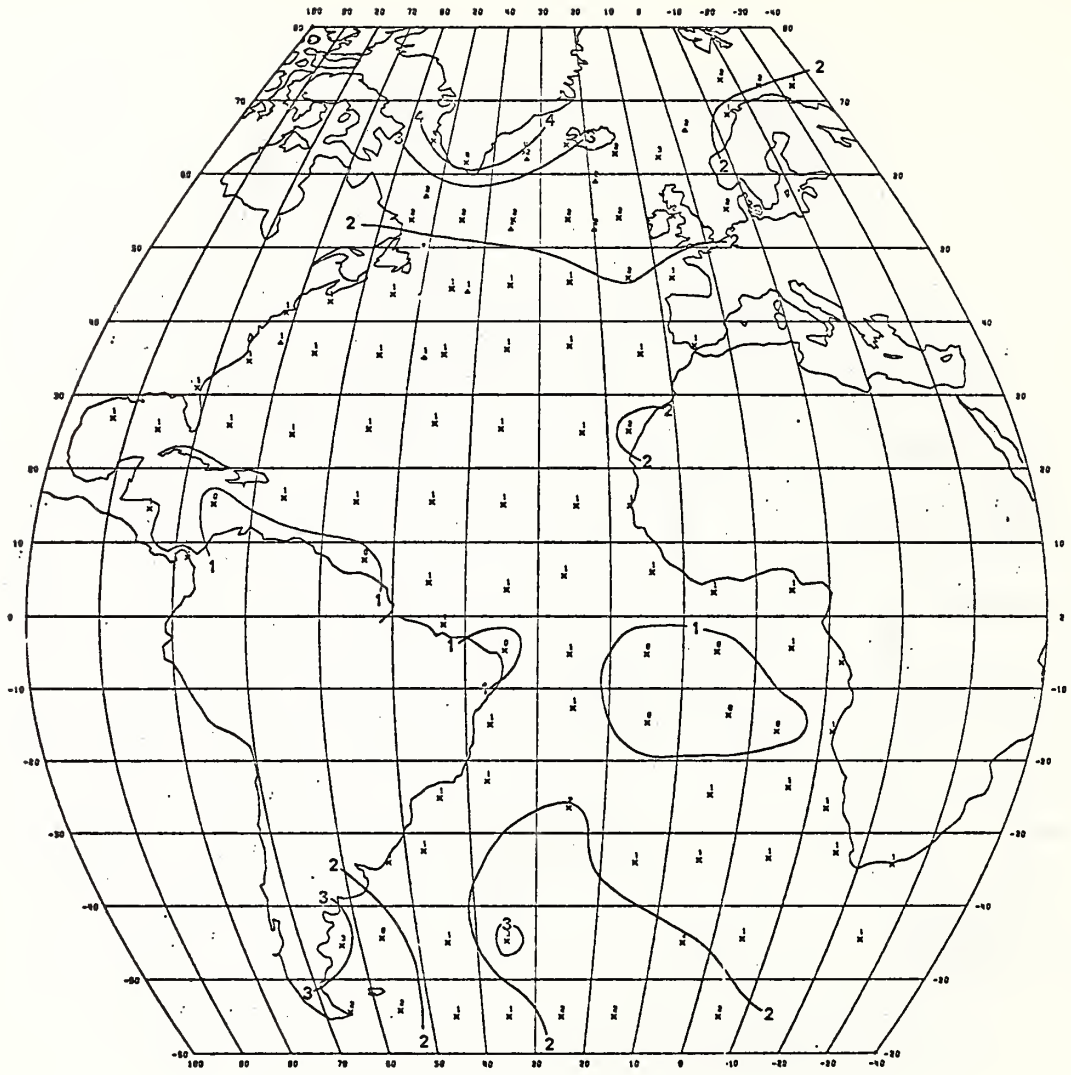

Figure 4. Standard deviation of meridional wind component in winter in m s^{-1}.

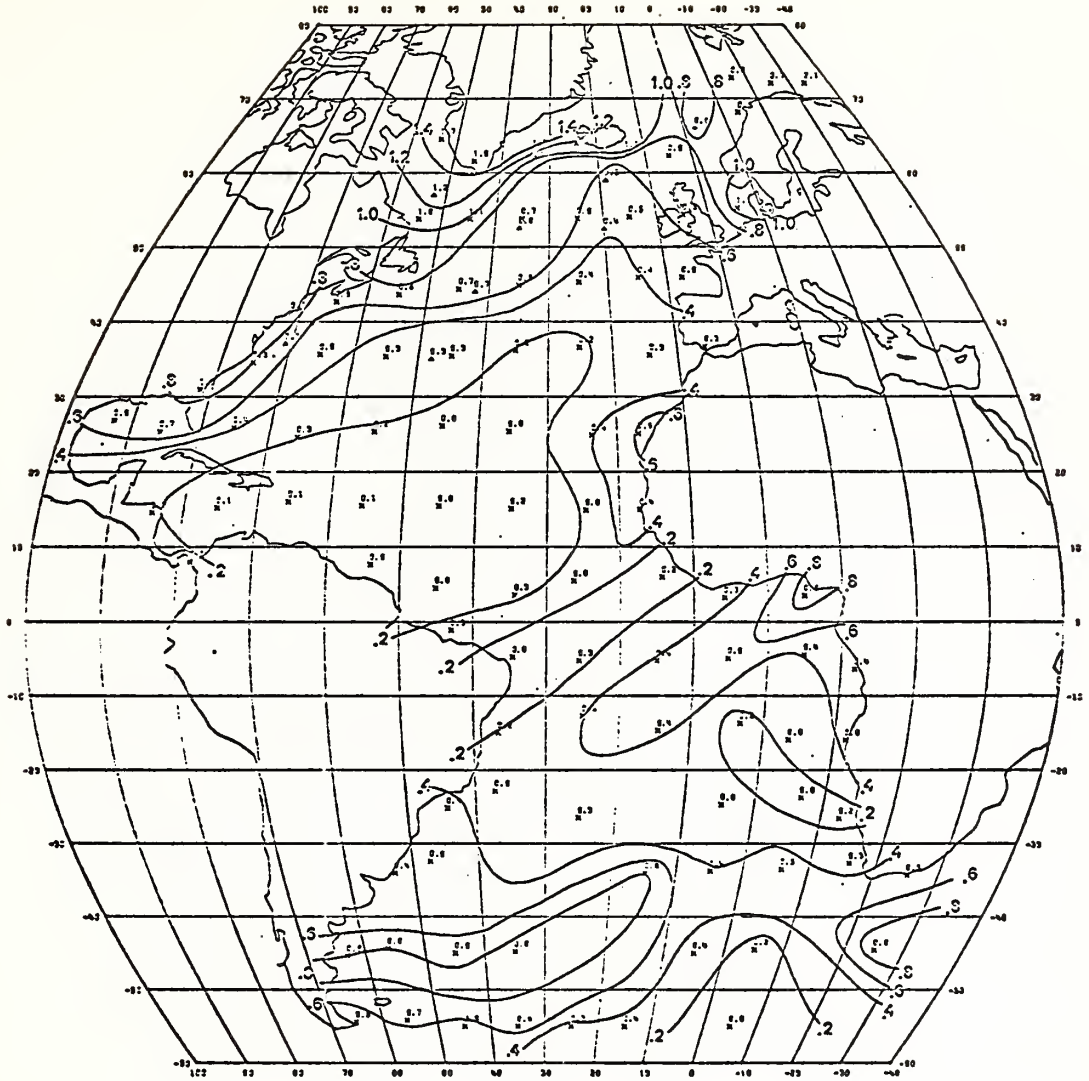

Figure 5. Standard deviation of wintertime air-sea temperature differance in ^{o}C.

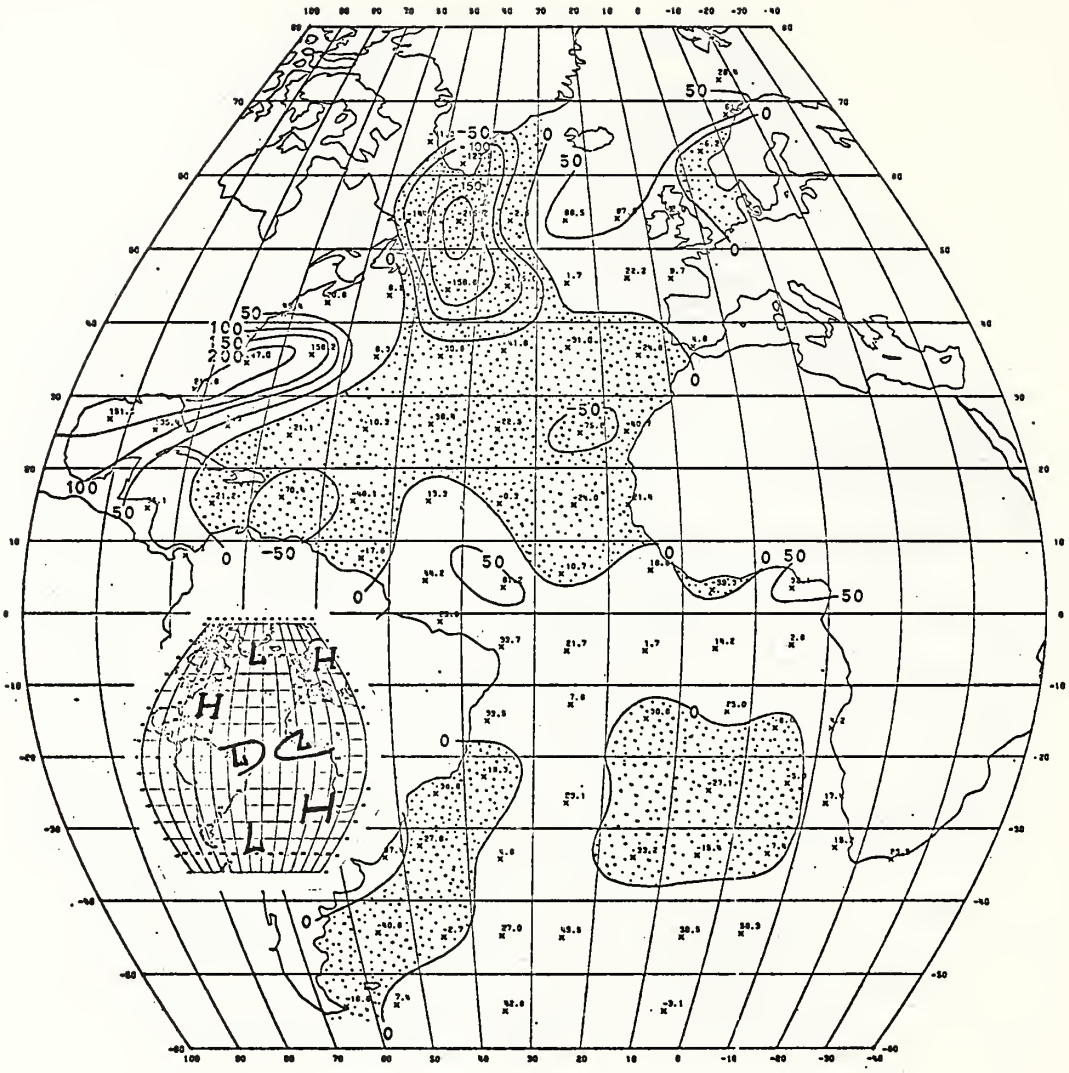

Figure 6. Anomaly of net heat gain by the Ocean, January 1950 in W m^{-2}.

Figure 7. Linear trends in oceanic heat gain in W m^{-2} yr^{-1}.

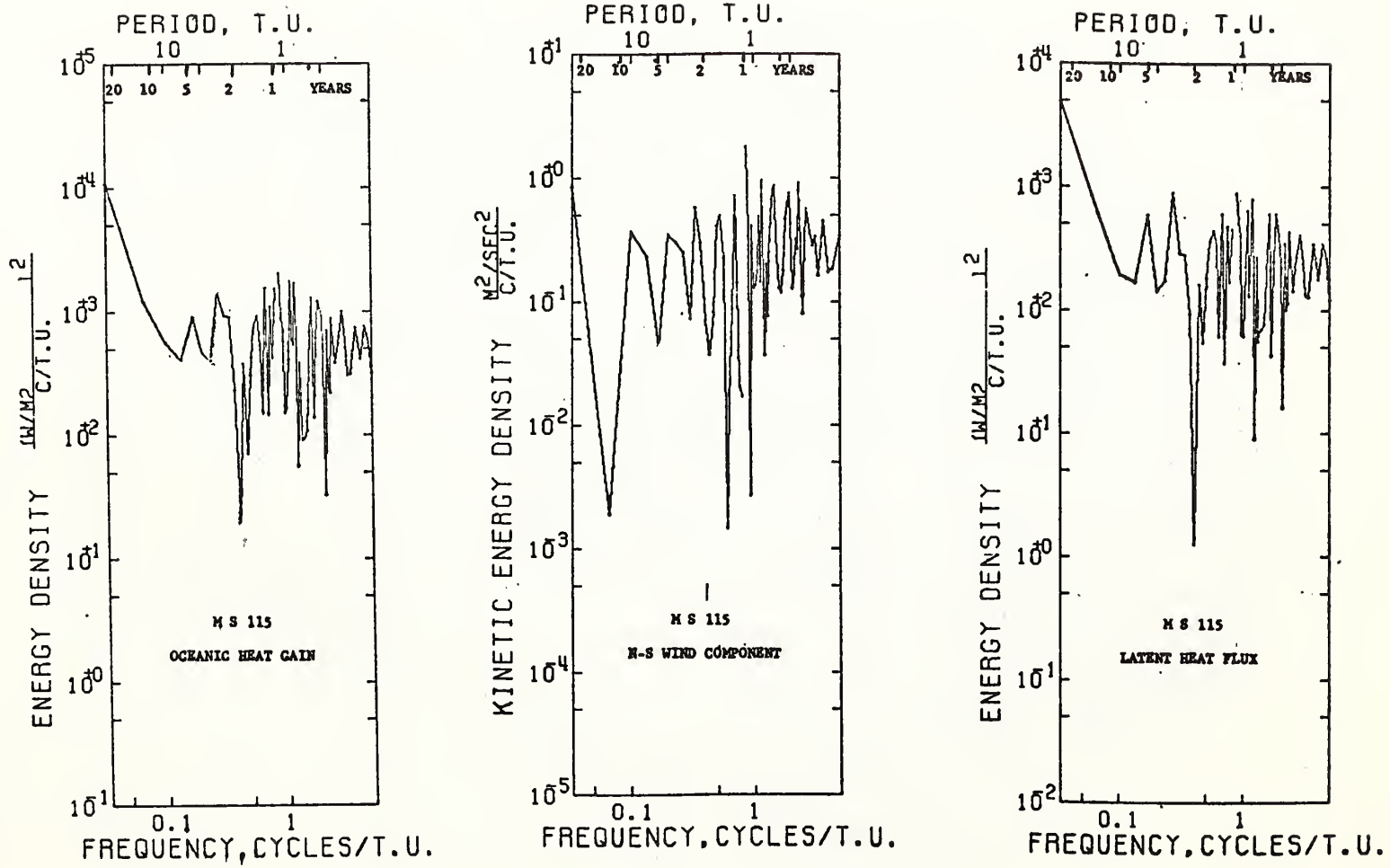

Figure 8. Spectral analyses of heat gain, meridional winds, and latent heat flux anomalies in Marsden Square (centered at 35°N, 65°W). 1 T.U. equals 10 months.

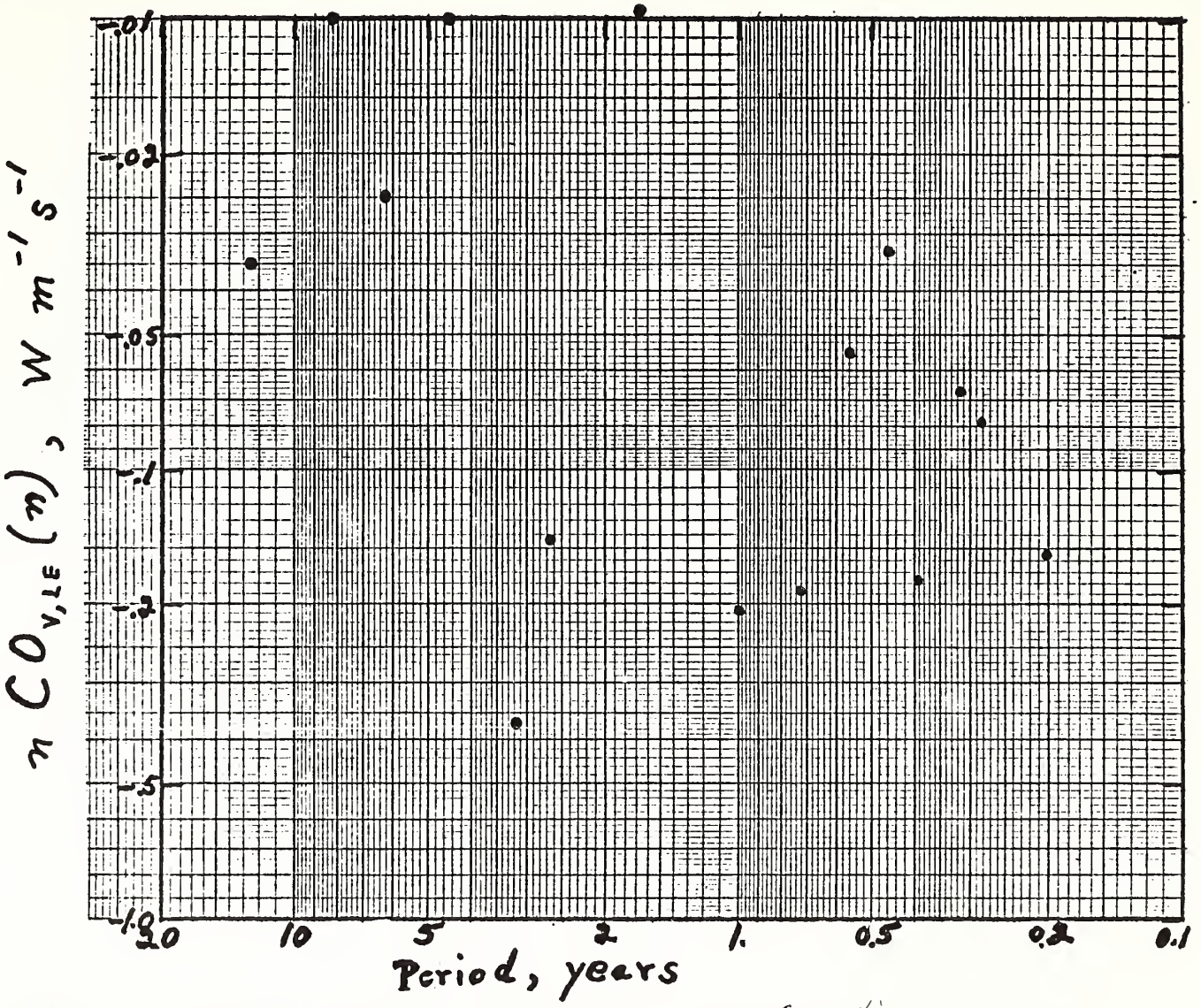

Figure 9. Cospectral analysis of latent heat flux and meridional wind anomalies in M.S. 115 (35N, 65W).

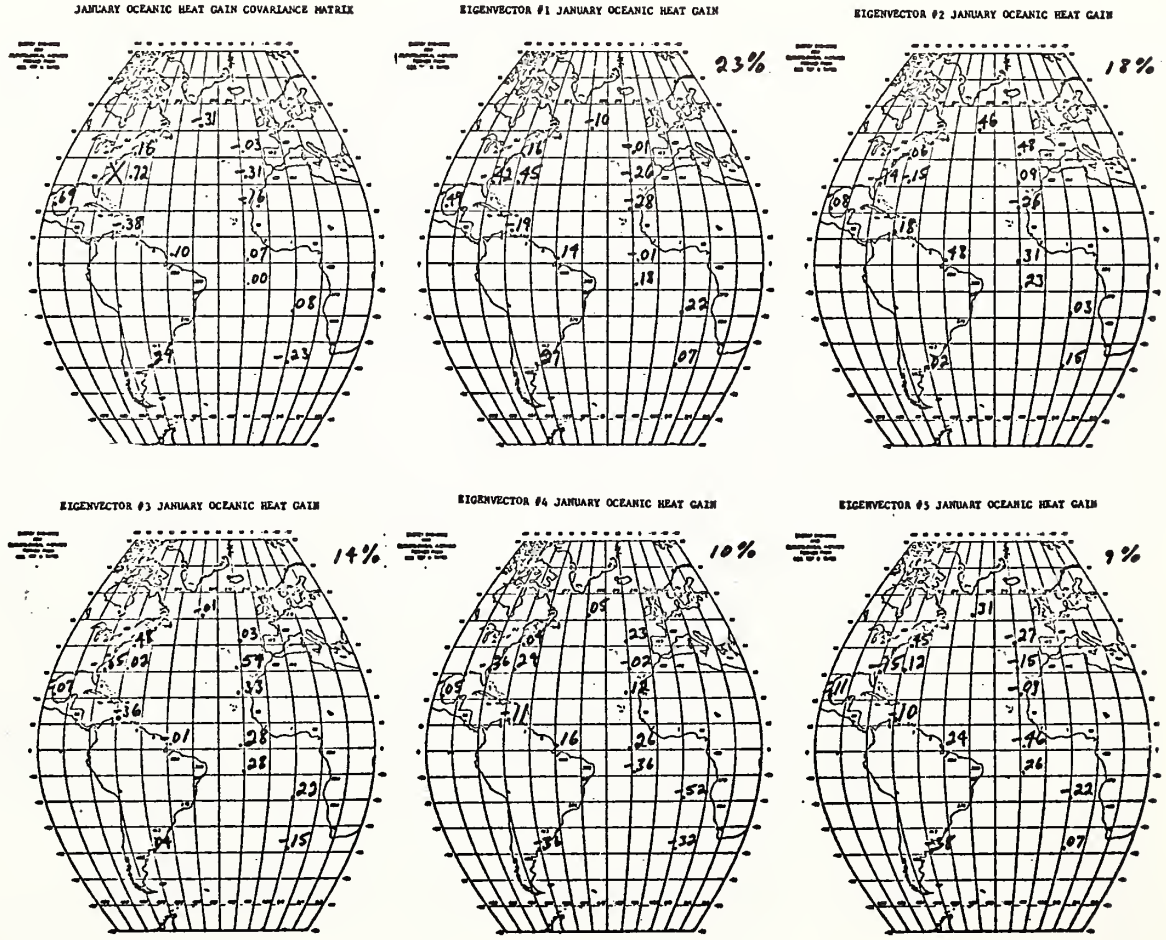

anomalies

Figure 10. Eigenvectors of the oceanic heat gain for January over 15 Marsden Squares. Top left chart gives covariances between M.S. 116 (marked X) and the indicated squares. Percentages denote amount of covariance accounted for by each eigenvector.

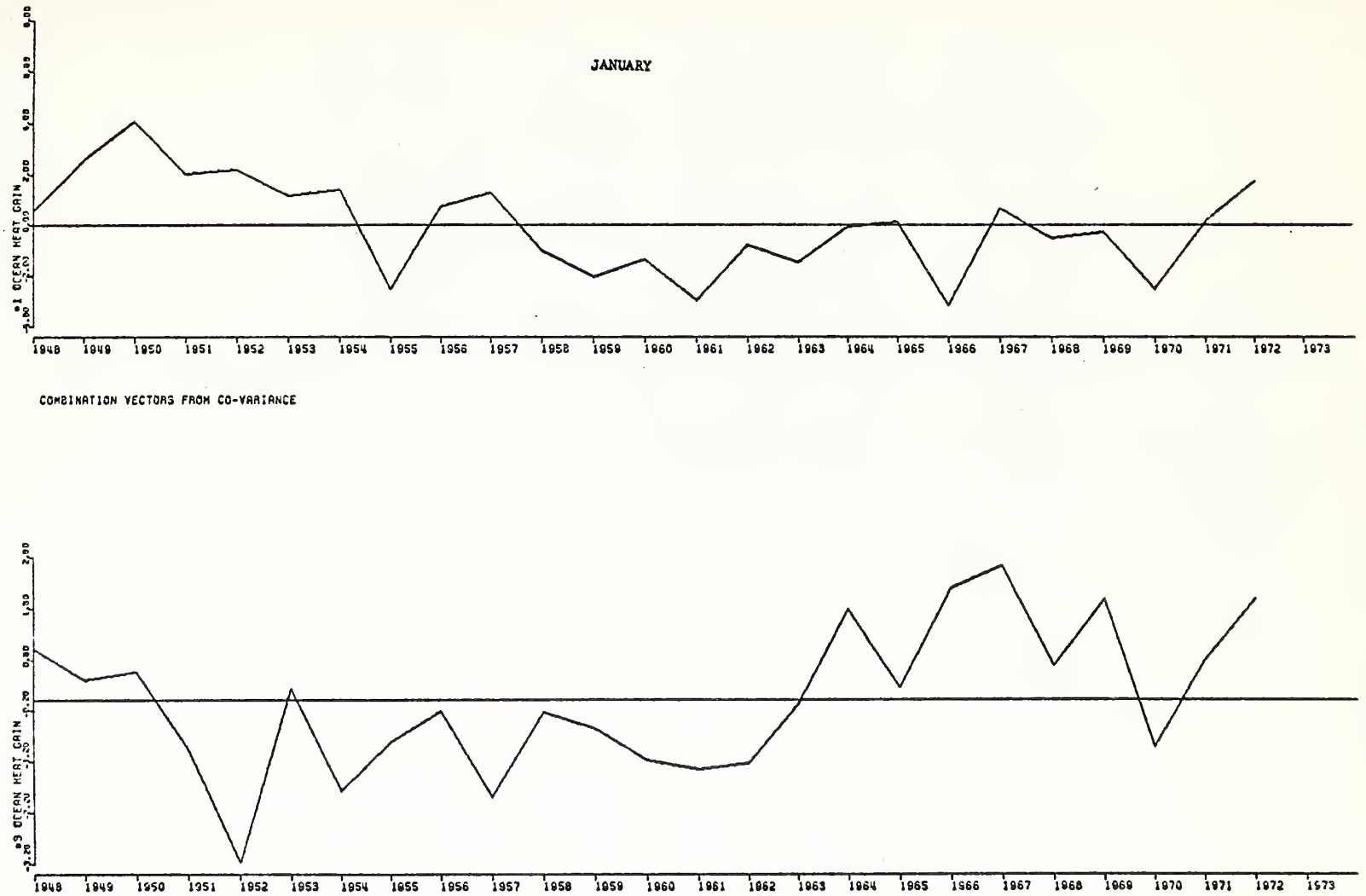

Figure 11. Combination vectors (eigenvector x coefficient) for eigenvectors 1 and 3.

Short Review of the Evidence for a Large Poleward Transport of Heat by the Oceans

Abraham H. Oort
Geophysical Fluid Dynamics Laboratory/NOAA
Princeton University
Princeton, New Jersey 08540

The various methods to determine the north-south oceanic heat flux can be grouped into four categories. They are (1) the direct method, (2) model methods, (3) the surface heat balance method, and (4) the planetary energy balance method. The characteristic features of each method are summarized in Table 1, and typical results can be found in Fig. 1.

Using each of the first three approaches transport values are found to range generally between 1 and 2 x 10^{15} watt in tropical latitudes. However, the fourth method (see Fig. 2) leads to much higher values of more than 3 x 10^{15} watt at low latitudes for the annual mean, and a seasonal amplitude variation of nearly 5 x 10^{15} watt. In the author's opinion, this serious discrepancy cannot be explained by errors in the planetary energy balance computations alone, and the first 3 methods probably underestimate the real transport. Some of the possible reasons are alluded to in Table 1 (see column labelled "difficulties").

Results from (still primitive) oceanic general circulation models (Bryan, 1978a) suggest the possible importance of zonal mean overturnings, often associated with Ekman drift. This gives some guidelines for a possible direct measurement program.

The time seems ripe to embark on pilot studies to directly measure *in situ* the oceanic heat flux. A good candidate project might be to sample the Atlantic Ocean intensively at a particular tropical latitude for an extended period of several years. Besides large seasonal, also sizeable interannual variations in the oceanic heat transport may be expected.

References

Baker, T. L., 1978: "Mass, salt, and heat transport across seven latitude circles in the North Atlantic Ocean: A description of the general circulation based on geostrophic calculations from International Geophysical Year and adjacent data." Report No. NPS68-78-004. M. S. Thesis, Naval Post-graduate School, Monterey, CA, 124 pp.

Bennett, A. F., 1978: "Poleward heat fluxes in the Southern Hemisphere oceans." J. Phys. Ocean., 8, 785-798.

Bryan, K., 1978a: "Models of the ocean circulation and the global heat balance." Proceedings of the JOC/GARP study conference on climate models, Washington, D. C., 3-7 April 1978. GARP Publications Series (in press).

Bryan, K., 1978b: personal communication on results of his diagnostic model computations using the observed density structure in the Atlantic Ocean.

Bryan, K. and L. J. Lewis, 1978: "A water mass model of the world ocean." J. Geophys. Res. (in press).

Budyko, M. I., 1963: "Atlas of the Heat Balance of the Earth." (In Russian.) Moscow, Globnaia Geofiz. Observ., 69 pp.

Bunker, A. F. and L. V. Worthington, 1976: "Energy Exchange Charts of the North Atlantic Ocean", Bulletin Am. Meteor. Soc., 57, pp. 670-678.

Düing, W. O., C. N. K. Mooers and T. N. Lee, 1977: "Low frequency variability in the Florida Current and relations to atmospheric forcing from 1972 to 1974." J. Marine Res., 35, 129-161.

Hastenrath, S., 1977: "Relative role of atmosphere and oceans in the global heat budget: tropical Atlantic and eastern Pacific." Quart. J. R. Met. Soc., 103, 519-526.

Holland, W. D., and A. Hirschman, 1972: "A numerical calculation of the circulation in the North Atlantic Ocean." J. Phys. Oceanogr. 2, 336-354.

Jung, G. H., 1955: "Heat transport in the North Atlantic Ocean," PhD Thesis, The A.& M. College of Texas, College Station, TX.

Manabe, S., K. Bryan and M. Spelman , 1978: "A global ocean-atmosphere climate model with seasonal variation - possible application to a study of climate sensitivity." Dynamics of Atm. and Oceans, (submitted for publication).

Oort, A. H., and T. H. Vonder Haar, 1976: "On the observed annual cycle in the ocean-atmosphere heat balance over the Northern Hemisphere." J. Phys. Oceanogr., 6, 781-800.

Sarkisyan, A. S. and V. P. Keonjiyan, 1975: "Review of numerical ocean circulation models using the observed density field." In Numerical Models of Ocean Circulation. Nat. Acad. of Sci., Washington, D. C., 116-124.

Schopf, P. S., 1977: " Numerical models of the oceanic heat transport." Ph.D. thesis, Princeton University, 248 pp.

Sellers, W. D., 1965: "Physical Climatology." The University of Chicago Press, 272 pp.

Takano, K., Y. Mintz and Y. Han, 1973: "Numerical simulation of the world ocean circulation." 2nd Conf. Numerical Prediction, AMS, Monterey, California, 1973.

Vonder Haar, T. H. and A. H. Oort, 1973: "New estimate of the annual poleward energy transport by Northern Hemisphere oceans." J. Phys. Ocean., 3, 169-172.

Voorhis, A. D., E. H. Schroeder, and A. Leetmaa, 1976: "The influence of the deep mesoscale eddies on sea surface temperature in the North Atlantic subtropical convergence." J. Phys. Ocean, 6, 953-961.

Worthington, V., 1976: "On the North Atlantic circulation." The John Hopkins University Press, Oceanographic Series, 6, 110 pp.

Table 1

Various methods to estimate poleward heat flux in the world oceans

Method	Investigators	difficulties	strength
1. Direct method			
From simultaneous direct in situ current and temperature observations	Düing et al. (1977) for Florida Current; Voorhis et al. (1976) for MODE eddies	presently only done for very limited regions; inertial oscillations, transient and possibly quasi-stationary eddies require extensive sampling	only direct method; should give definitive answer if properly planned and executed
2. Model methods			
a. From estimates of water mass exchange	Worthington (1976)	only gross numbers; no eddy effects included	compatible with independent oceanographic information (chemical tracers)
b. From in situ geostrophic calculations based on observed density structure in world oceans	Jung (1955); Bryan (1962) for Atlantic Ocean; Schopf (1977); Baker (1978); Bennett (1978).	assumption of no-motion level; transient eddy effects neglected; large uncertainty in flux calculations near continental shelves	fairly "direct" calculation
c. From observed density structure adjusted "somewhat" to numerical model characteristics	Sarkisyan and Keonjiyan (1975) for world oceans; Holland and Hirshman (1972) for Atlantic Ocean; Schopf (1977); Bryan (1978b)	includes only stationary component; somewhat model dependent; problems in continental shelf regions	non-geostrophic component included; dynamically consistent
d. From 3-dimensional general circulation model specifying only surface exchange of momentum, heat and water vapor (either as observed or from atmospheric general circulation model)	Manabe, et al.(1978), Bryan (1978a), Bryan and Lewis (1978)	model dependent; results contaminated by ad hoc parameterizations (e.g. in modeling subgrid-scale eddies)	consistent method; suggests contribution various transport mechanisms; promises possibility to study climate anomalies during recent as well as ancient climates
3. Surface heat balance method			
From surface heat balance estimates (net radiation, sensible and latent heat fluxes at ocean surface); the "classical" method	Budyko (1963), Bunker and Worthington (1976), Hastenrath (1977).	uncertainties in formulation air-sea exchange processes and in radiation parameterization	excellent global coverage by surface ship reports
4. Planetary energy balance method			
From heat balance estimates for entire climatic system (atmosphere, oceans, snow and ice, land) as a residual (net radiation from satellites, atmospheric storage and transports from rawinsonde network, oceanic storage from hydrographic and BT data)	Oort and Vonder Haar (1976)	data deficiencies in SH (mean meridional circulation transports in atmosphere cannot be measured reliably enough in SH); errors pile up in residual; perhaps most controversial method, because of very large oceanic transports found	unique in that, besides conservation of energy, no assumptions are needed; sum total of all components oceanic transport obtained

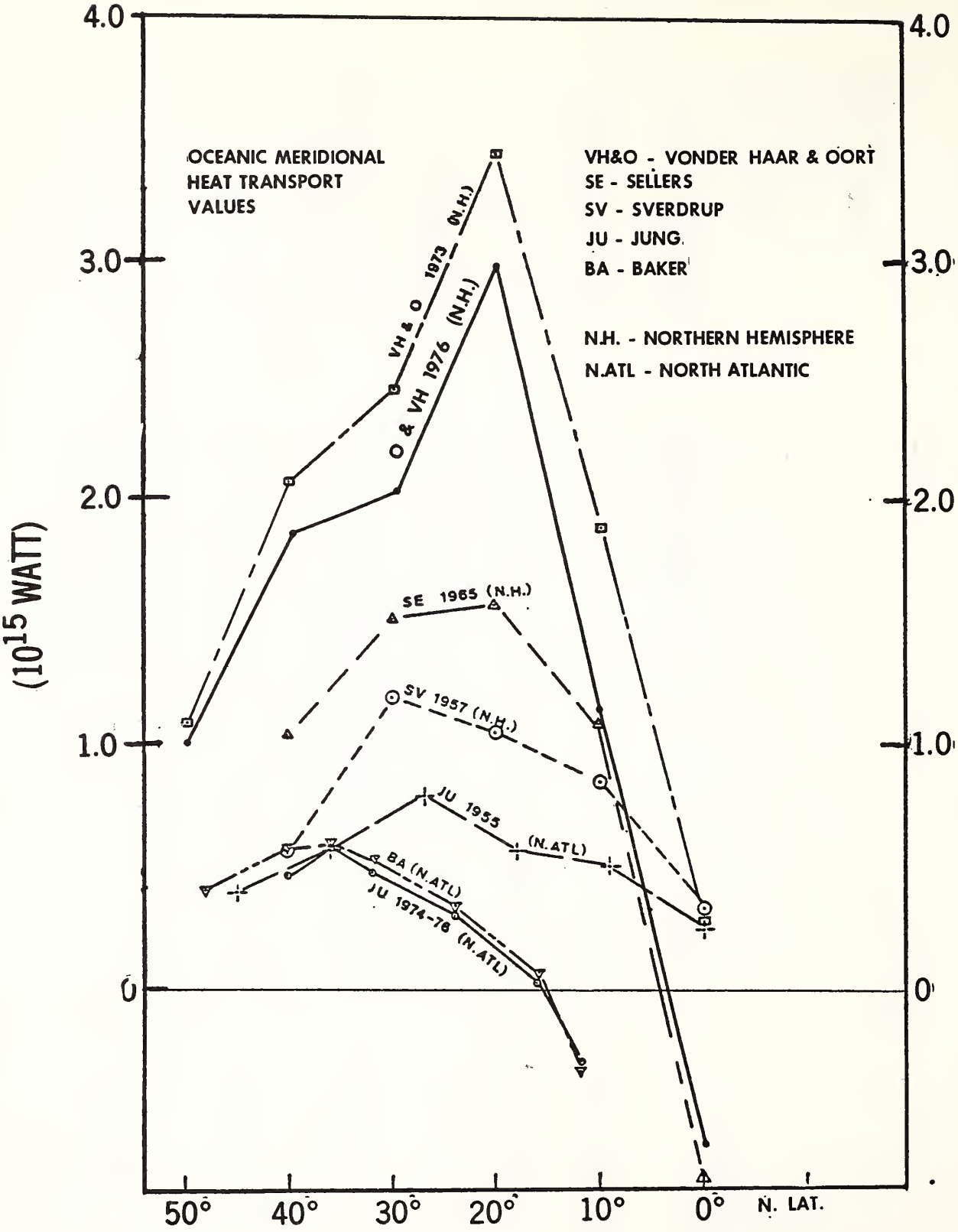

Fig. 1a. Various heat transport values for the North Atlantic Ocean and the Northern Hemisphere after Baker (1978). The lower four curves are based on model method 2b, the Sellers/ Budyko curve on the surface heat balance method 3, and the two upper curves on the planetary energy balance method 4. (The differences between the last 2 curves are mainly due to improvement of the satellite radiation estimates since 1973.)

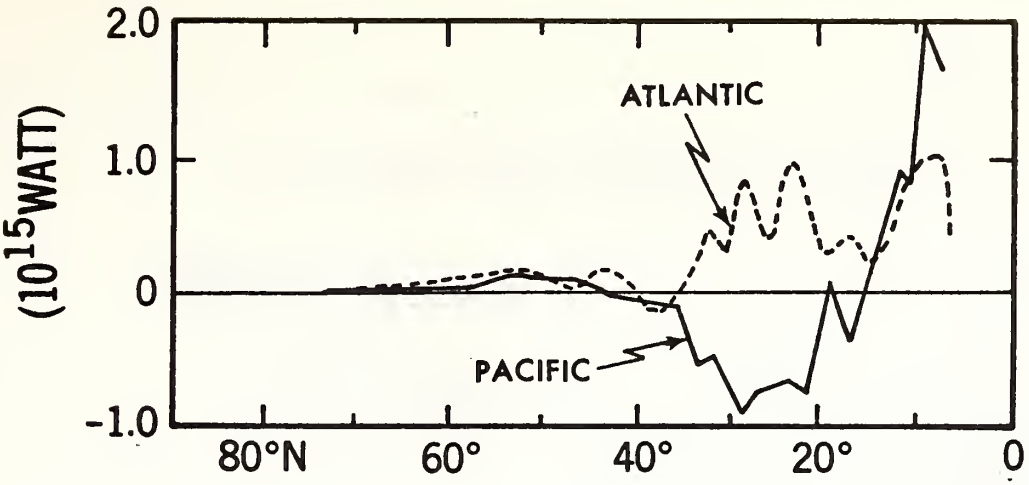

Fig. 1b. Northward heat transport in the North Atlantic and Pacific Oceans as calculated by Schopf (1977) using model method 2 c based on the observed 3-dimensional density structure. Geostrophic and Ekman fromulations are used to determine the shear flow component, and a barotropic model calculation to define the vertical mean flow component.

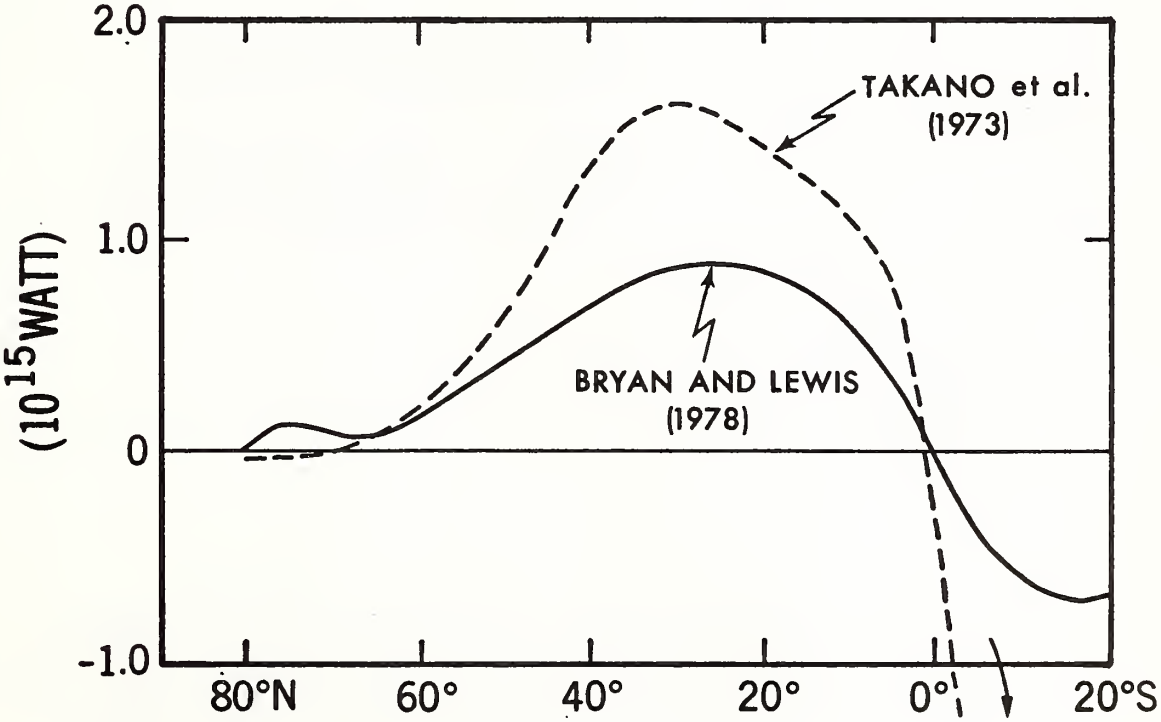

Fig. 1c. Northward heat transports as calculated by Takano et al. (1973) and by Bryan and Lewis (1978) using model method 2 c with only ocean surface conditions specified from observations. The curves represent average conditions for two steady-state (viscous - no transient eddies) January and July model runs.

ENERGY BALANCE FOR POLAR CAP

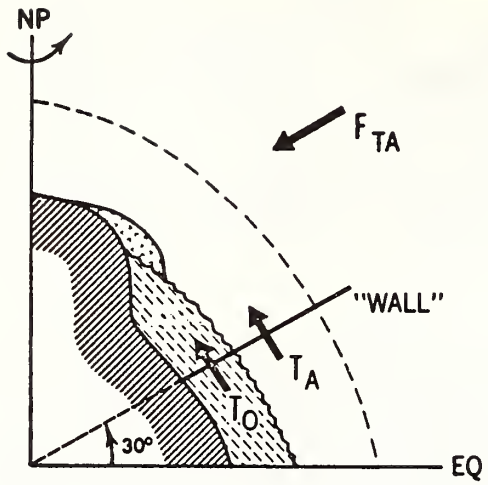

(a) ANNUAL MEAN CONDITIONS

$$T_O = -F_{TA} - T_A$$

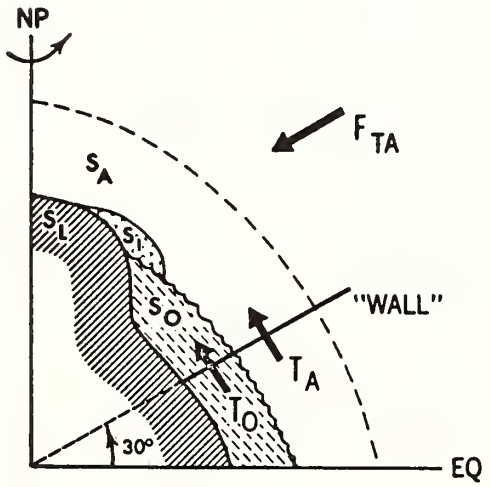

(b) SEASONAL MEAN CONDITIONS

$$T_O = -F_{TA} - T_A + (S_A + S_O + S_L + S_I)$$

Fig. 2. Schematic diagram of the energy flow in the Northern Hemisphere climate system for annual mean (a) and shorter time (b) averaged conditions. F_{TA} denotes the net radiative flux at top of the atmosphere, T_A and T_O the horizontal transports of energy in the atmosphere and oceans, resp., and S_A, S_I, S_L, S_O the rates of storage of energy in the atmosphere, cryosphere, land surface and oceans, resp.

THE HEAT BALANCE OF A DIAGNOSTIC MODEL OF THE NORTHERN ATLANTIC

Kirk Bryan

Geophysical Fluid Dynamics Laboratory/NOAA
Princeton University
Princeton, New Jersey 08540

Due to a lack of suitable data on ocean currents, the role of the ocean in the poleward transfer of heat is almost always estimated indirectly. Most estimates are carried out using the heat balance of the ocean surface. Recently, Vonder Haar and Oort (1973) and Oort and Vonder Haar (1976) have used the heat balance of the entire atmosphere and data on ocean heat storage to determine the transport of heat by ocean currents. Before planning new field studies to obtain the data needed for direct measurements of heat transport it is very important to make sure that all the information possible has been extracted from existing hydrographic data.

With this in mind a new diagnostic method has been developed for computing large scale ocean currents. Traditional methods for computing ocean circulation are based on geostrophic calculations from temperature and salinity measurements, and determining the total transport by choosing an arbitrary reference level or solving a vertically integrated vorticity equation. Diagnostic calculations of the latter type have been made by Sarkisyan (1971) and Holland and Hirschman (1972). The difficulty with such methods is that the velocity structure of the solution is not compatible with the conservation of heat and salinity as shown by Schopf (1977). Better success has been achieved with a new method which includes the conservation equations for potential temperature and salinity, as

well as the equations of motion. The solutions are constrained to be in the close neighborhood of observed values of temperature and salinity by adding a Newtonian damping term proportional to the local departure of the solution from data given by Levitus and Oort (1977).

Calculations are carried out on a $1.0^{o}x1.0^{o}$ grid for the North Atlantic with 12 levels in the vertical. Numerical integration with respect to time of the time-dependent model leads to a steady state in a relatively short period of time (one or two years). The following conclusions may be drawn about the heat and fresh water transport in the model.

a) Mesoscale eddies must have an effective diffusion of more then $10^3 m^2/S$ to be an important mechanism in poleward heat transport. At low latitudes the dominant effect is overturning in the meridional plane due to Ekman transport poleward below the trade winds.

b) Horizontal gyres due to the Gulf Stream and Norwegian Current are less effective in transporting heat. At high and middle latitudes mesoscale eddies are probably important.

c) The transport of fresh water amounts to $0.5x10^6$ metric tons/S, which is in rough agreement with atmospheric water balance data.

References

Holland, W. R. and A. Hirschman, A numerical calculation of the circulation of the North Atlantic Ocean. J. Phys. Ocean, 2, 336-352, 1972.

Levitus, S. and A. Oort, Global analysis of oceanographic data, Bull. Amer. Met. Soc., 58, 1270-84, 1977.

Oort, A. and T. Vonder Haar, On the observed annual cycle in the ocean-atmosphere heat balance over the Northern Hemisphere, J. Phys. Ocean., 6, 781-800, 1976.

Sarkisyan, A. and V. Ivanov, The combined effect of baroclinicity and bottom topography as an important factor in the dynamics of ocean currents, Izv. Acad. Nauk, USSR, Atmos. Ocean.Phys., 1, 173-188, 1971.

Schopf, P., Numerical Models of the Ocean Heat Transport, Ph.D. Thesis, Princeton University, 248 p, 1977.

Vonder Haar, T. and A. Oort, New estimate of annual poleward energy transport by Northern Hemisphere Oceans, J. Phys. Ocean., 2, 169-172, 1973.

Low-Latitude Seasonal Ocean Heat Transport

Paul S. Schopf
Laboratory for Atmospheric Sciences (GLAS)
Goddard Space Flight Center
National Aeronautics and Space Administration

In Hellerman's new compilation of global wind stress on a monthly basis, it is noticed that the annual cycle of mean zonal wind stress has a strong signal near the equator, which may be roughly approximated by:

$$\tau \sim A \sin(l_y \theta) \cos(-\omega t).$$

where $l_y = \pi/22^{\circ}$ and $\omega = 2\pi/1$ year. This reflects the strengthening of the low latitude easterlies in the winter hemisphere, and their weakening in the summer.

The oceanic response of this forcing consists of Ekman flow plus freely propagating planetary waves. The Ekman flow is symmetric about the equator, with:

$$V \sim B \frac{\sin(l_y \theta)}{\sin(\theta)} \cos(-\omega t)$$

showing a "sloshing" motion in the upper water column. Numerical model studies of a linear ocean circulation have included planetary waves with the Ekman flow. They show that the planetary waves do not significantly alter the net amount of heat transport, although they change the response locally.

A basin extending over 100° of longitude and from 50°N to 50°S was studied. The vertical temperature profile was chosen so as to agree with the mean values obtained from Levitus and Oort's (1977) data for the Pacific (over the same latitude span). The Ekman response of this basin indicated an annual cycle in heat transport of 1.5×10^{15} W across the equator.

Currently a three layer model is under construction at GLAS to enable us to include nonlinear effects and a thermodynamically active mixed layer. The above work carried heat adiabatically, and allowed no net heat exchange across the surface of the ocean (i.e., it ignores the dynamic effects of the surface heat flux on the flow). The new model will allow for rectification of the heat flux due to planetary waves, as well as the generation of more realistic boundary currents.

On the Heat Budget of the Tropical Atmosphere and Oceans

by

Stefan Hastenrath
University of Wisconsin

Abstract:

Heat budget estimates for the global tropics are derived from recent calculations of the oceanic heat budget and satellite measurements of net radiation at the top of the atmosphere. Annual mean heat export from the zone 30 N - 30 S, amounts to about 101 x 10^{14} W (= 100 units). Of this total 39 and 61 units are performed within the oceanic water body, and the atmospheric column over sea and land, respectively. In the zone 0 - 10 N, to which the planetary cloud band ("ITCZ") is essentially limited throughout the year, atmospheric heat export reaches only 13 units, as compared to an oceanic export of 18 units from the zone 0 - 10S. In particular, oceanic export in the belt 0 - 5 S alone contributes 11 units, being 90 percent of the net radiative heat gain at the top of the atmosphere in this latitude zone. Accordingly, atmospheric heat export from the realm of the "ITCZ" related to hot tower mechanisms seems to play a more modest role in the global heat budget than heretofore believed. By comparison, oceanic export from the cold water zones immediately to the South of the Atlantic and Pacific Equator emerges as an important factor in global energetics.

Oceanic meridional heat transport in the Pacific is directed from the tropics into either hemisphere; in the Atlantic it is northward from high Southern latitudes all the way to the Arctic; and it is directed southward in the Indian Ocean. Oceanic heat gain in the Pacific offsets dificits in the higher Southern latitudes of the Atlantic and Indian Ocean sectors, as well as in the Atlantic as a whole. Meridional heat transport for all oceans combined is largest around 30 N and 20 S, where it accounts for 53 and 35 percent of the total poleward transport. Atmospheric transport is largest and effects the bulk of the total transport in mid-latitudes.

Greatly different estimates of net radiation at the top of the atmosphere, and of oceanic and atmospheric heat export must be regarded as compatible within the broad error limits indicated at present for all three terms.

Biennial Variations in Surface Temperatures over the United States as Revealed by Singular Decomposition

Eugene M. Rasmusson, John B. Jalickee
Phillip A. Arkin and Wen-Yuan Chen

Center for Environmental Assessment Services
EDIS/NOAA

1. Introduction

The evidence for quasi-biennial variations in the surface air temperature derives mostly from single station analyses. In this study we examined these variations over the United States during the period 1931-75 using the dense array of mean monthly data from the 344 climate divisions which cover the conterminous 48 states. The method of analysis is known as singular decomposition (Lawson and Hansen, 1974). In the meteorological context it is often referred to as Empirical Orthogonal Function (EOF) Analysis (Lorenz, 1956). Our results will therefore be described in EOF terminology.

2. Basic EOF Analyses

Table 1 shows the variance explained by the EOF analyses.

Table 1

VARIANCE EXPLAINED BY THE 5 LEADING TERMS OF THE SINGULAR DECOMPOSITION

	TERM				
DATA SET	1	2	3	4	5
1. Departures from Monthly Means	47.7	23.8 (71.5)	8.9 (80.4)	4.5 (84.9)	2.6 (87.4)
2. Normalized Departures	45.2	20.8 (66.0)	10.0 (76.0)	5.3 (81.3)	3.6 (84.9)
3. Bandpass Filtered Normalized Departures	40.6	26.3 (66.9)	15.1 (82.0)	5.9 (88.1)	3.1 (91.2)
4. Hilbert Singular Decomposition of 3. Above	47.5	29.6 (76.1)			

Row 1 of Table 1 lists the explained variance for the EOF analysis of the non-seasonal departures. Similarly, the results for the EOF analysis of normalized non-seasonal departures are given in row 2. Row 3 shows the results for the data set which results from filtering the normalized non-seasonal departures using a band-pass filter with maximum response at 24 months, and half power points at 18 and 36 months (Landsberg et al., 1963).

We shall first summarize the results for the normalized departures (row 2). The 3 leading EOF's reflect the larger spatial scale variability. The smaller spatial scale variance (24 percent) is concentrated over the western U.S. and Florida (Fig. 1), and is mostly resolved by EOF's 4 and 5.

The spectra for the amplitude time series of EOF's 1, 2, and 3 are shown in Fig. 2. The dotted lines are the 5 and 95 percent confidence limits assuming the time series to be a first order Markov process (Gilman et al., 1962). These limits should be used only as a general guide.

Clearly evident in the EOF 3 time series is a quasi-biennial signal near a period of 26 months. The only other EOF 3 spectral estimate reaching the 95 percent confidence limit occurs at the third harmonic of a 26 month period. Similarly, the single EOF 2 spectral estimate which exceeds the 95% limit occurs at the fifth harmonic of a 26 month period. The spectrum for EOF 1 shows 5 peaks exceeding or nearly reaching the 95% confidence limit. Since the time series were not detrended, the very low frequency peak is probably not meaningful. The peaks at periods of 6.5 and 4.3 months again correspond to higher harmonics of a 26 month period. The remaining peaks at slightly more than 4 and 9 months are unexplained, and may be merely due to chance.

The quasi-biennial spike in the EOF 3 spectrum contains approximately 10 percent of the total variance of this time series. Since EOF 3 itself accounts for 10 percent of the total normalized non-seasonal variance, the biennial spike represents approximately 1 percent of the total non-seasonal variance.

Fig. 3 shows the EOF amplitude time series from which the spectrum was computed, with the solid line being a 12 month running mean. Quasi-biennial variations can easily be identified throughout almost the entire period of record.

The EOF 3 spatial field, also shown in Fig. 3, exhibits two out-of-phase areas of maximum variance. It should be noted that standard EOF analyses portray variations as either in phase or 180 degrees out of phase. Therefore, it is not possible to represent features with variable phase relationships, such as traveling waves, by a single EOF. The next section describes the results of analyses designed to more clearly reveal the phase relationships of the biennial signal.

3. Hilbert Singular Decomposition

The normalized non-seasonal departures were band-passed, as previously described, and the new data set subjected to an analysis which we refer to as Hilbert Singular Decomposition. The variance of the band-passed data set, represented in terms of the fraction of the original non-seasonal variance, is shown in Fig. 4. The values range between 4 and 11 percent, and average 6 percent. As might be expected, this value is considerably larger than the 1 percent of the total variance represented by the EOF 3 quasi-biennial spike. A reasonable estimate of the variance associated with quasi-biennial variations probably lies between these two values. EOF 3 (Fig. 3) and Fig. 4 show a general similarity, with maxima over the northeast U.S., minima from the northern plains to the south central Atlantic states, and a second maximum extending northwestward from Texas.

The Hilbert Singular Decomposition (HSD) analysis is similar to the method used by Wallace and Dickinson (1972) for analyzing the characteristics of tropical waves, and can be viewed as a complex form of EOF analysis. In order to perform this analysis an augmented matrix $A^+(x,t)$ is formed from the basic data matrix $A(x,t)$ by the following operation:

$$A^+(x,t) = A(x,t) + j \sum_{t'} W^H(t-t')A(x,t) \qquad (1)$$

where $j = \sqrt{-1}$

and $W^H(t-t')$ is the Discrete Hilbert Transform, with frequency response of unity magnitude and 90° phase shift.

Equation (1) follows directly from the basic theory of analytic functions.

Using the augmented matrix $A^+(x,t)$, a complex singular decomposition series can be computed in terms of phase and amplitude in both the time and space domains i.e.

$$A^+(x,t) = \rho_x^{(1)} e^{j\omega_x^{(1)}} \rho_t^{(1)} e^{j\omega_t^{1}} + \rho_x^{(2)} e^{j\omega_x^{(2)}} \rho_t e^{j\omega_t^{(2)}} + \cdots \qquad (2)$$

The amplitude at any point in space and time is then obtained by multiplying $\rho_x\rho_t$, while the phase is obtained by adding $\omega_x + \omega_t$.

The variance explained by the first two HSD components is listed in row 4 of Table 1. Only the spatial phase (ω_x) and amplitude (ρ_x) fields for the first component (Fig. 5) are presented. The amplitude field shows maxima over the northeastern and southwestern U.S. The phase varies little over the northeast, but shows a steady shift over the middle third of the nation, to variations over the southwestern states which are nearly 180° out of phase with those over the northeast.

4. Analysis of Selected Climate Division Time Series

It seems reasonable to return to the data from individual climate divisions in order to determine whether they exhibit the same features found in the large scale patterns of the EOF and HSD analyses. Accordingly, we examined the average values for the divisions covering the New England states (northeast) and those covering southwestern Wyoming, eastern Utah, western Colorado, and northwestern New Mexico (southwest).

Fig. 6 shows the autocorrelation functions for the non-seasonal departures for the two areas. Fig. 7 shows the same autocorrelation functions computed from band passed data. The unfiltered data show weak indications of quasi-biennial variations, and from the band passed data, the period is indicated to be around 25 months. The stronger quasi-biennial signal is indicated in the data from the northeast. This is confirmed by the spectra for the respective areas (Fig. 8). Although there is considerable power around 26 months in the spectrum for the southwest area, one would hardly attach significance to this period on the basis of data from that area alone.

The phase relationship between the two areas found in the HSD analyses is confirmed by the cross correlation analysis (Fig. 9) and cross spectrum analysis (Fig. 10). These analyses show the variations in each area with periods around 26 months to be almost 180 degrees out of phase.

5. Comparison with Tropical Stratospheric Wind Data

Without prejudging as to whether quasi-biennial variations found in the tropical stratosphere and those found in surface temperatures are related features, we performed preliminary comparisons between the phase of the quasi-biennial variations in surface temperature over the U.S. and variations in the Zonal Wind Component at 50 mb over Balboa, C.Z. The Balboa data were kindly supplied by Dr. James Angell. Initial results indicate an average phase difference of approximately 6 months between the EOF time series and the wind variations at 50 mb over Balboa. However, more detailed comparison failed to reveal any apparent correspondence between variations in the phase and amplitude of individual oscillations found in the two time series.

6. Conclusions

The analysis described in 2-5 were obtained from data covering the period 1931-1975, and strictly speaking, apply only for that period. However, the presence of quasi-biennial variations throughout the entire period, as illustrated in Fig. 5, suggest this to be a relatively stable climate feature. It might also be noted that we failed to find any convincing evidence of quasi-biennial oscillations in the corresponding precipitation data. We therefore draw the following conclusions:

(a) Quasi-biennial variations probably account for 1-5 percent of the total non-seasonal variance of surface temperature over the United States.

(b) By far the most pronounced spectral peak for periods from 2 months to 20 years, in the EOF amplitude time series, is associated with quasi-biennial variations. However, limited analyses suggest that the quasi-biennial oscillations may be masked by local effects in individual station data, particularly over the western United States.

(c) Both EOF analyses, and analysis of data from individual climate divisions indicates mean phase differences of the quasi-biennial oscillations over the United States of up to 180 degrees.

(d) During the period 1931-1975, there are indications of an average phase difference of around 6 months between the Balboa, C.Z. 50 mb west wind component and the EOF time series for the U.S. surface temperature data. However, little relationship was noted between variations in phase and amplitude of individual oscillations exhibited by the different time series.

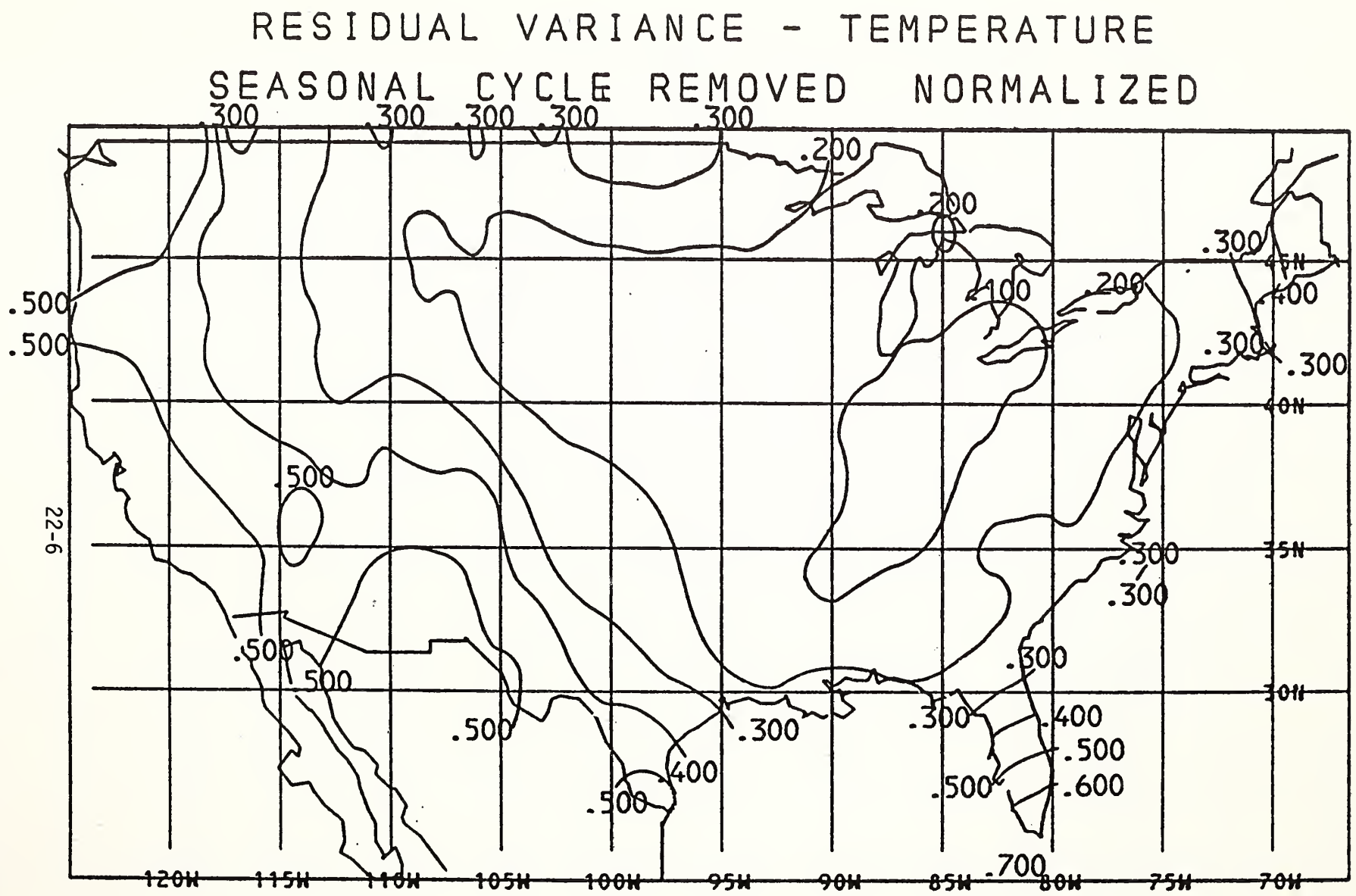

Fig. 1. Variance remaining after subtraction of EOF's 1, 2 and 3 from the normalized non-seasonal temperature departures.

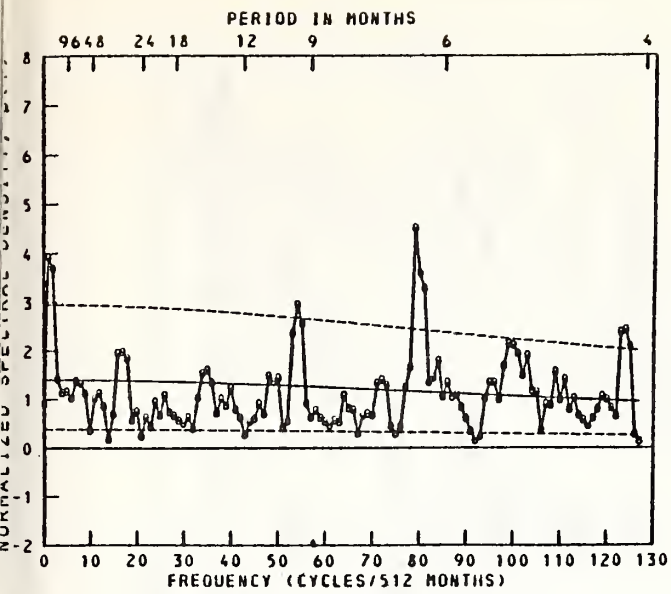

EOF 1

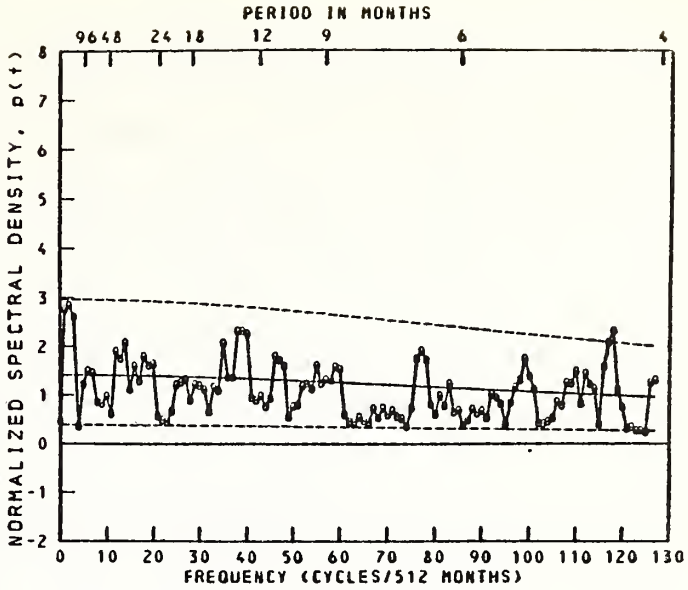

EOF 2

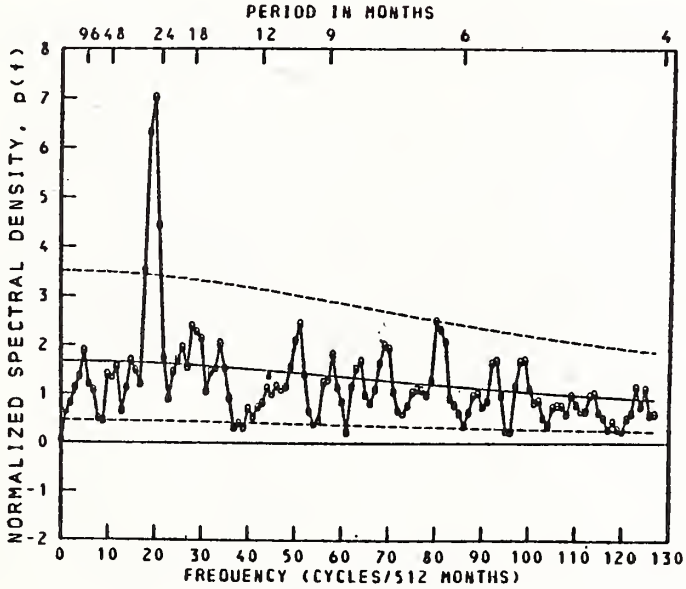

EOF 3

Fig. 2. Amplitude time series spectra for EOF's 1, 2 and 3.

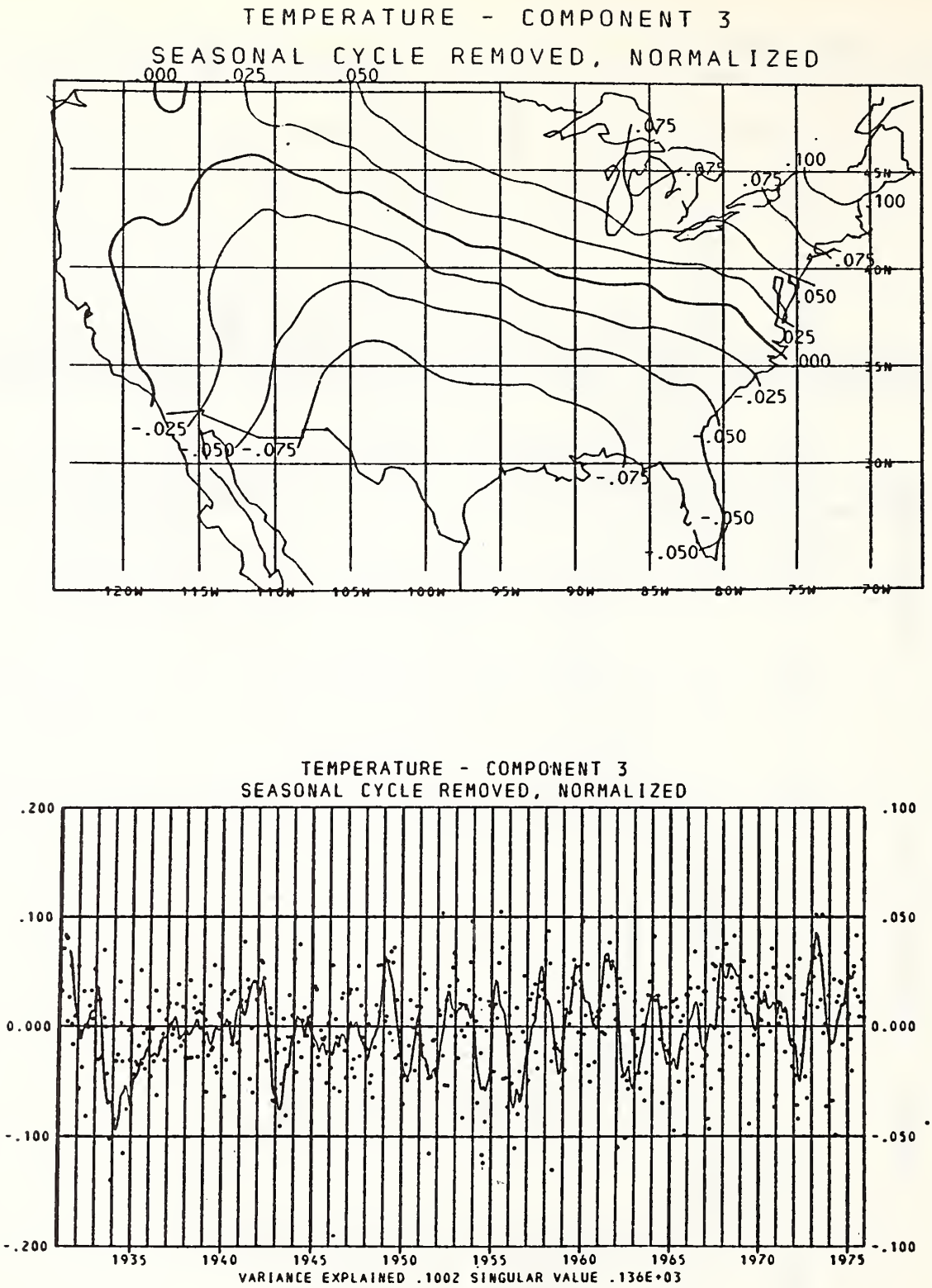

Fig. 3. EOF 3 and corresponding amplitude time series. Scale on right of amplitude time series is for 12 month running mean (solid line).

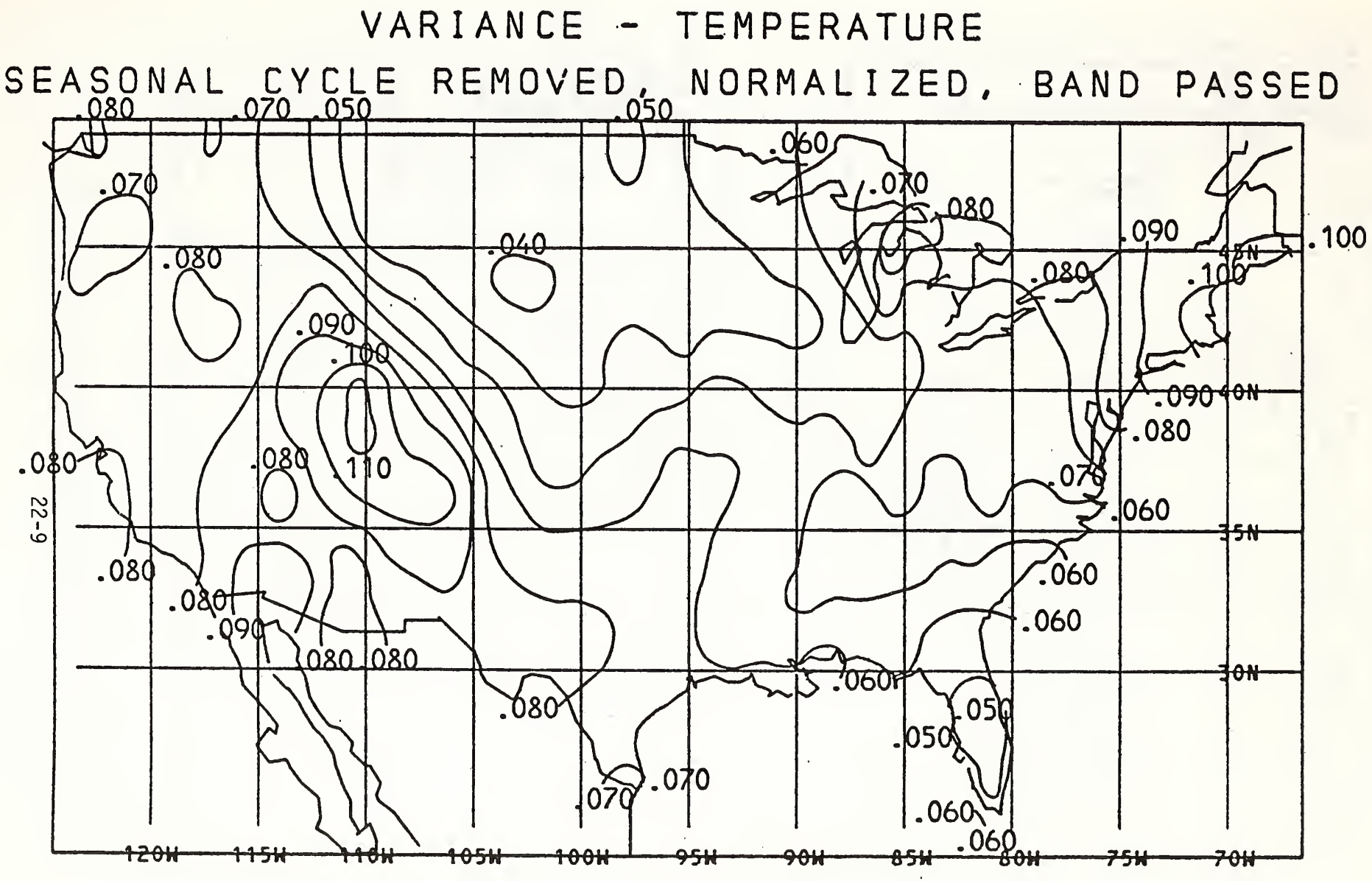

Fig. 4. Fraction of normalized non-seasonal variance remaining after band-pass filtering (see text).

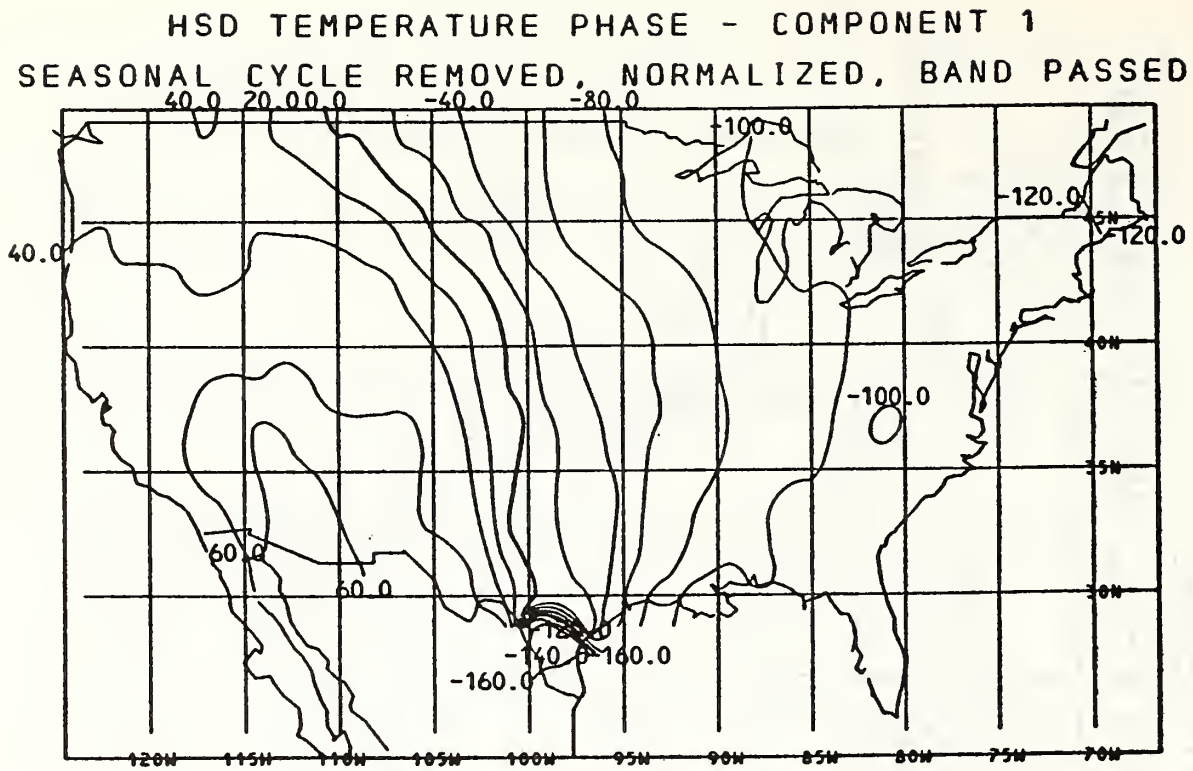

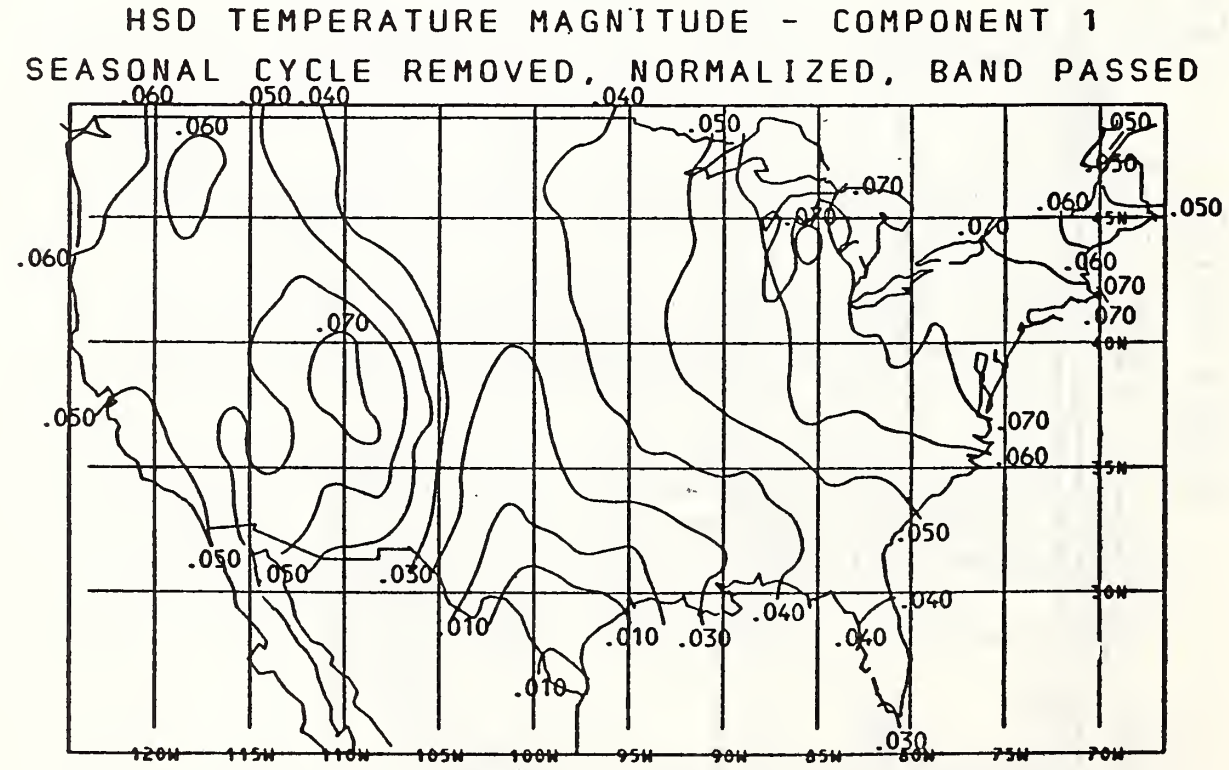

Fig. 5. HSD 1 phase and amplitude.

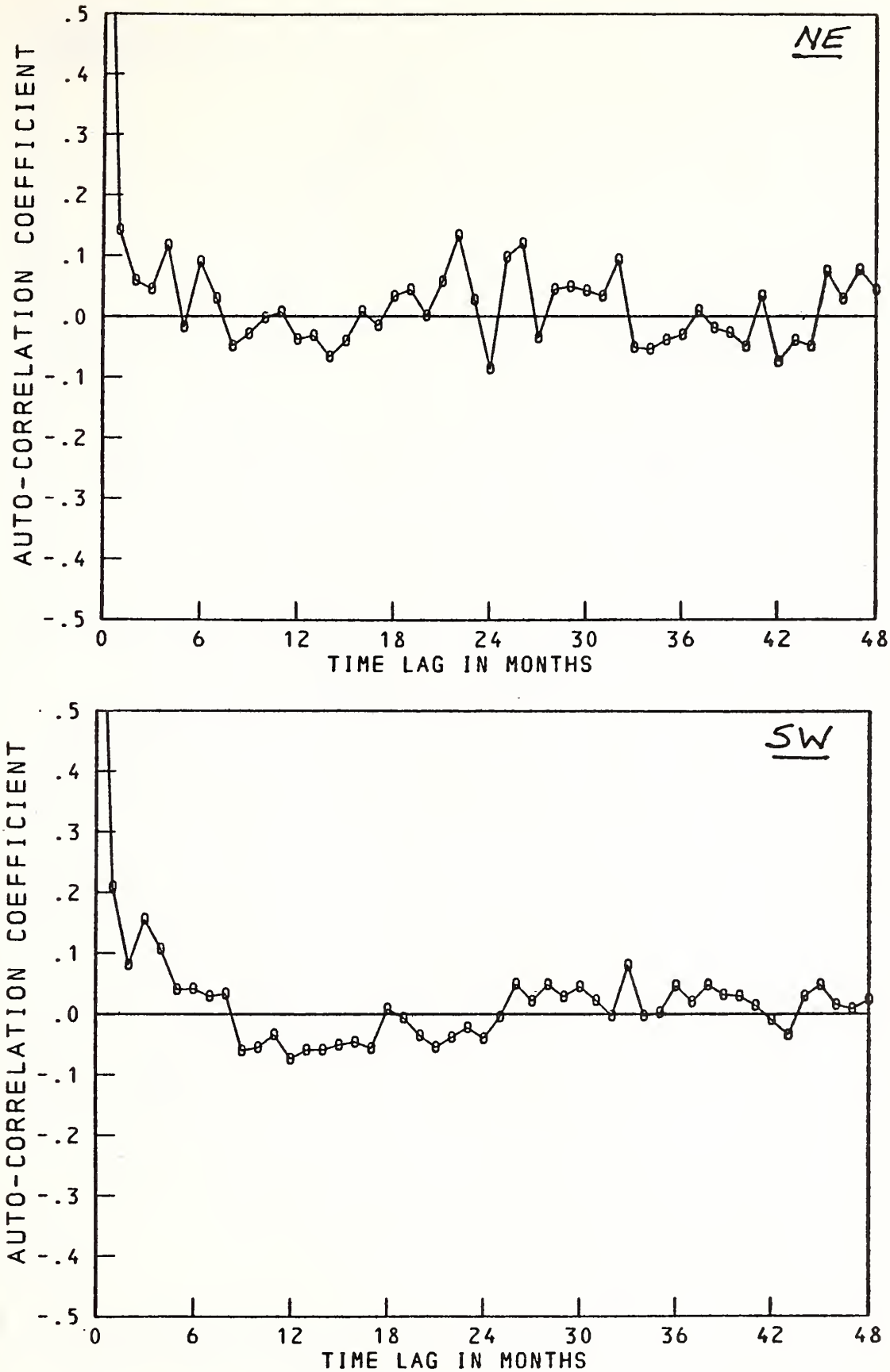

Fig. 6. Autocorrelation functions for average of climate zones over an area of the northeastern (above) and an area of the southwestern U.S. (see text).

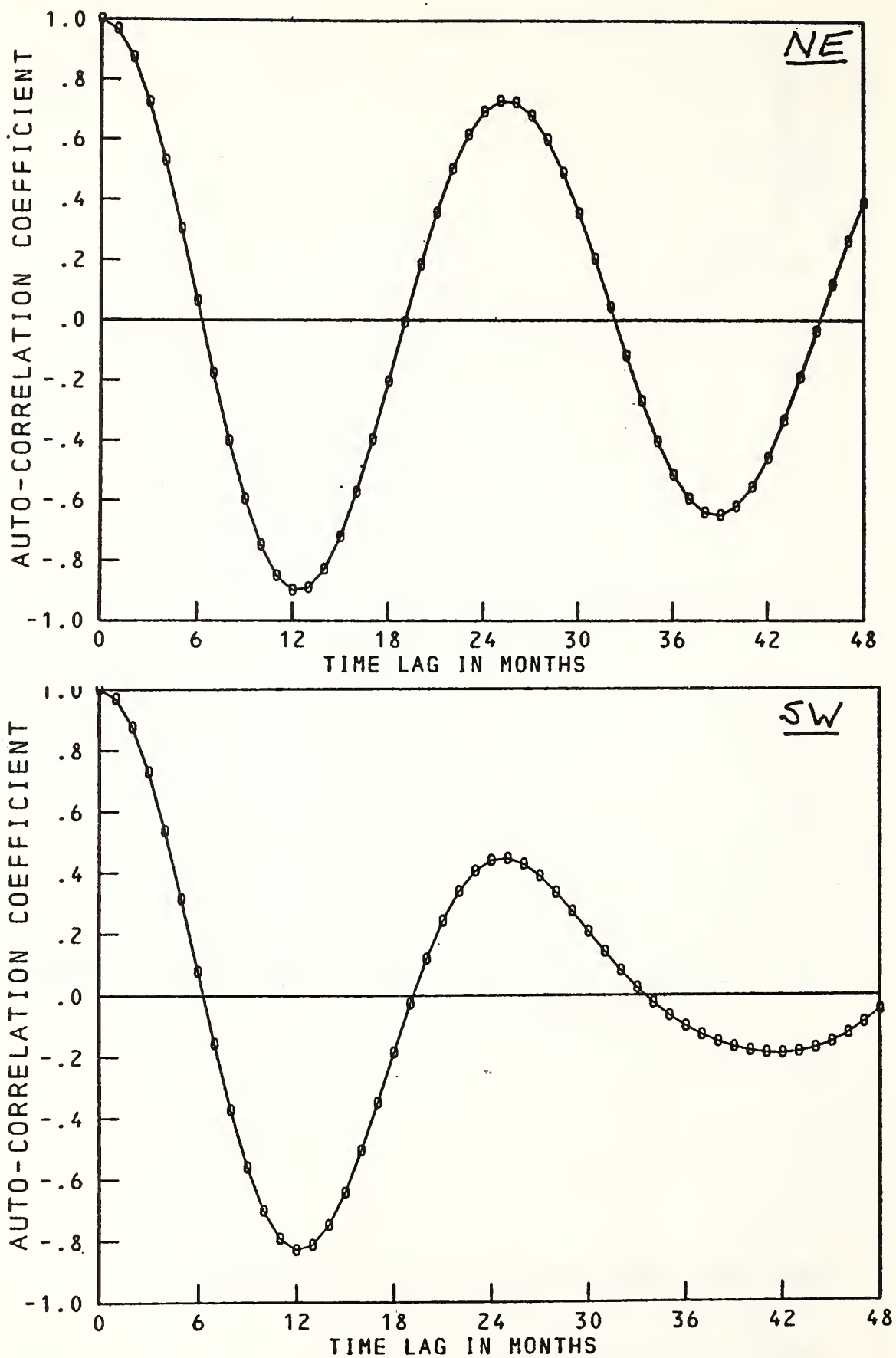

Fig. 7. Same as Fig. 6, except for band-passed data.

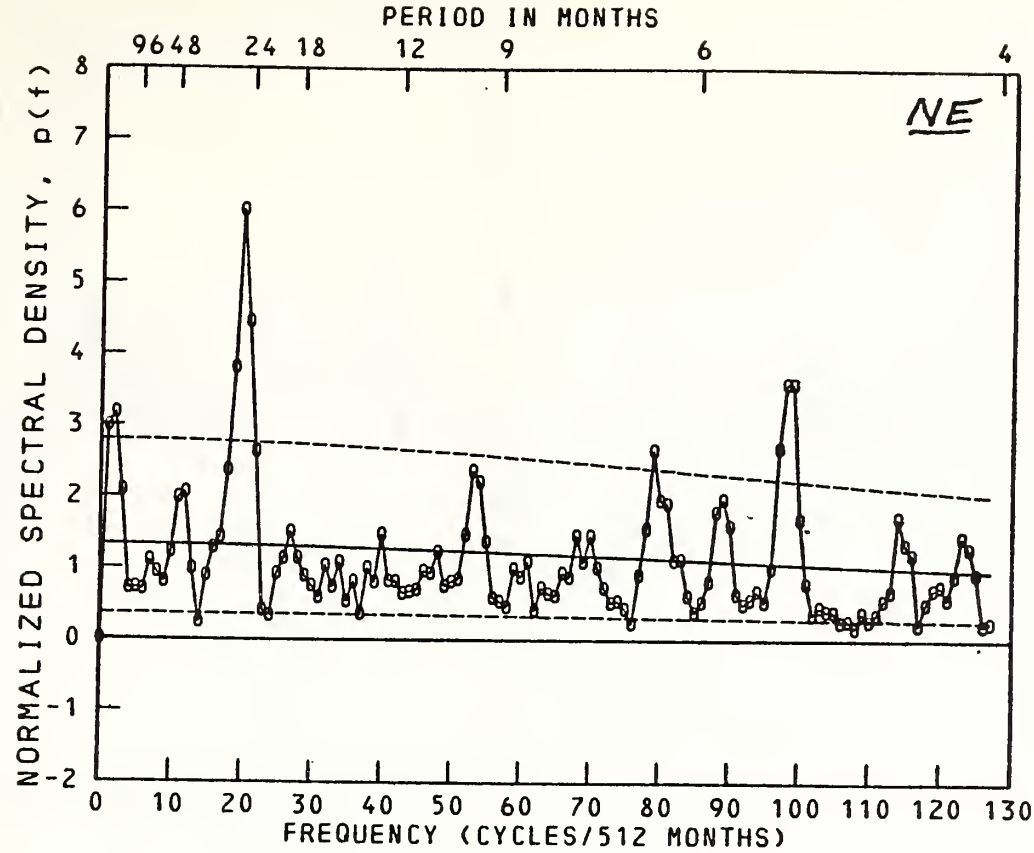
PERIOD IN MONTHS
96 48 24 18 12 9 6 4
NE
NORMALIZED SPECTRAL DENSITY, p(f)
8 7 6 5 4 3 2 1 0 -1 -2
0 10 20 30 40 50 60 70 80 90 100 110 120 130
FREQUENCY (CYCLES/512 MONTHS)

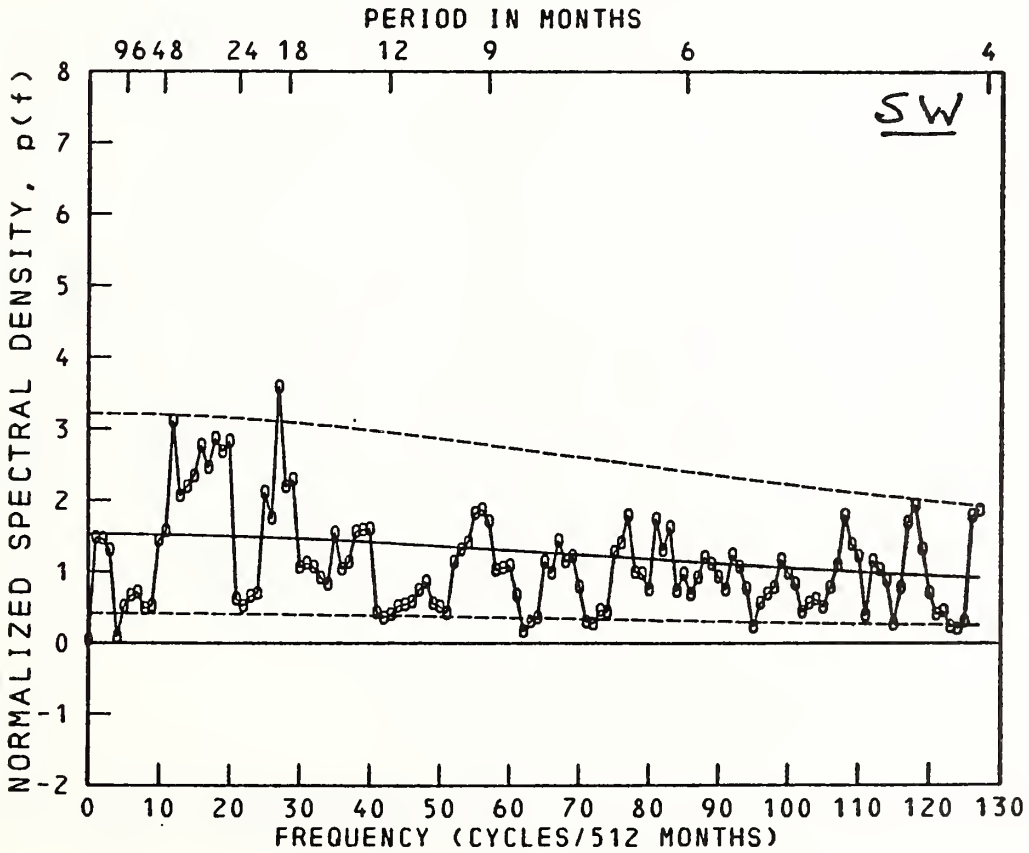
PERIOD IN MONTHS
96 48 24 18 12 9 6 4
SW
NORMALIZED SPECTRAL DENSITY, p(f)
8 7 6 5 4 3 2 1 0 -1 -2
0 10 20 30 40 50 60 70 80 90 100 110 120 130
FREQUENCY (CYCLES/512 MONTHS)

Fig. 8. Spectra for northeastern (above) and southwestern areas.

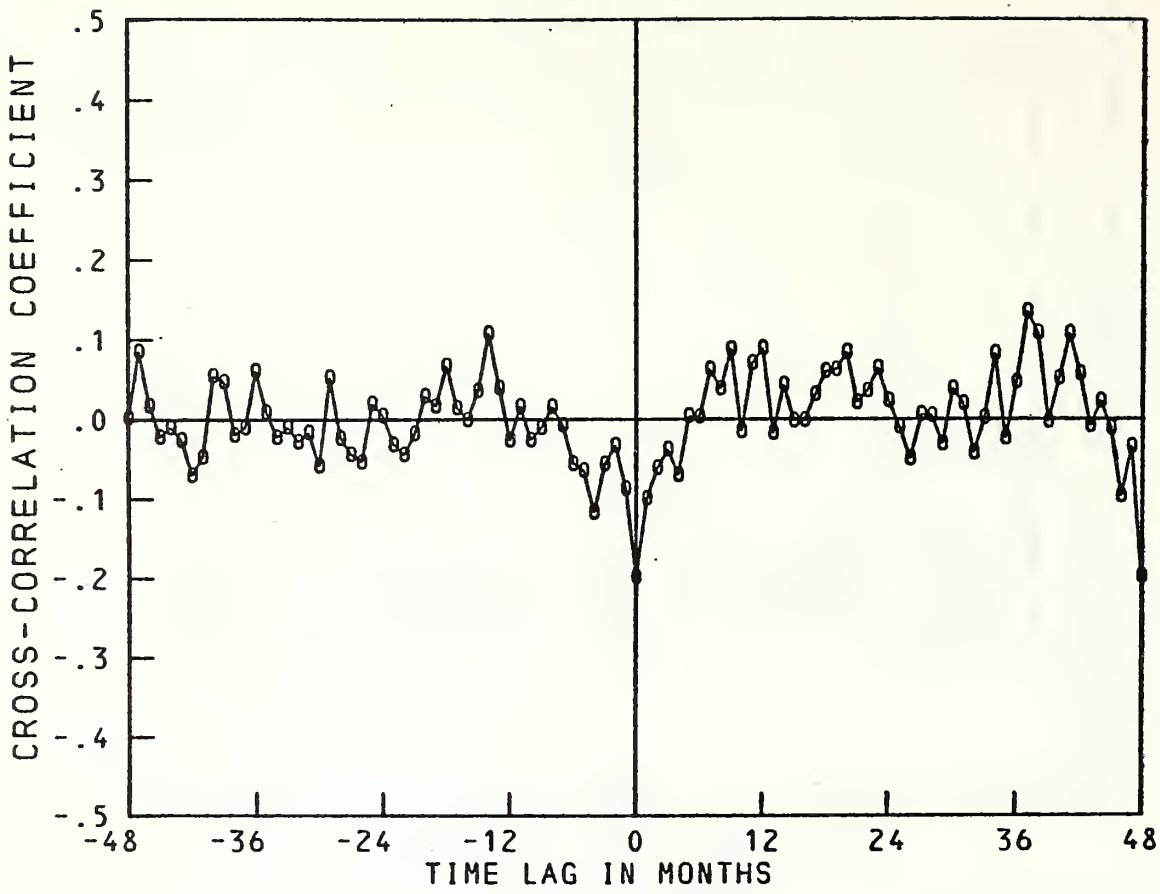

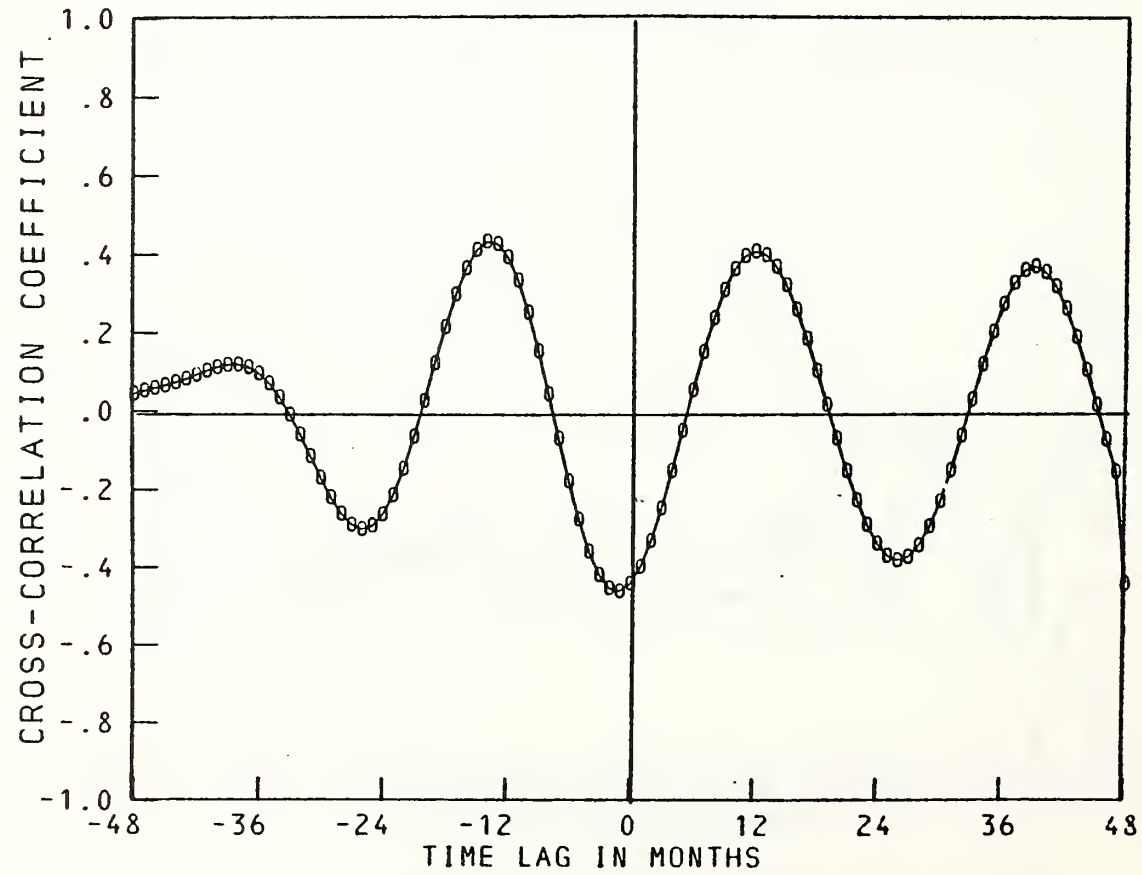

Fig. 9. Cross correlation functions for the northeast and southwest areas computed from unfiltered (above) and band-pass filtered data.

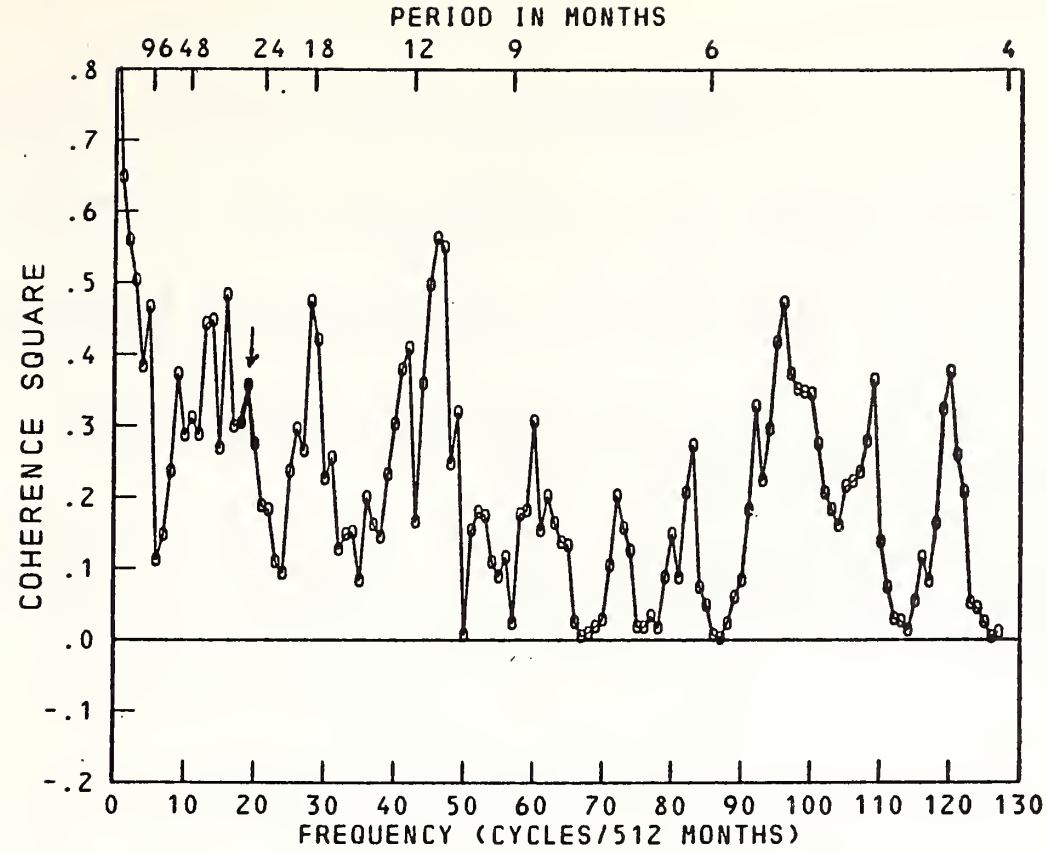

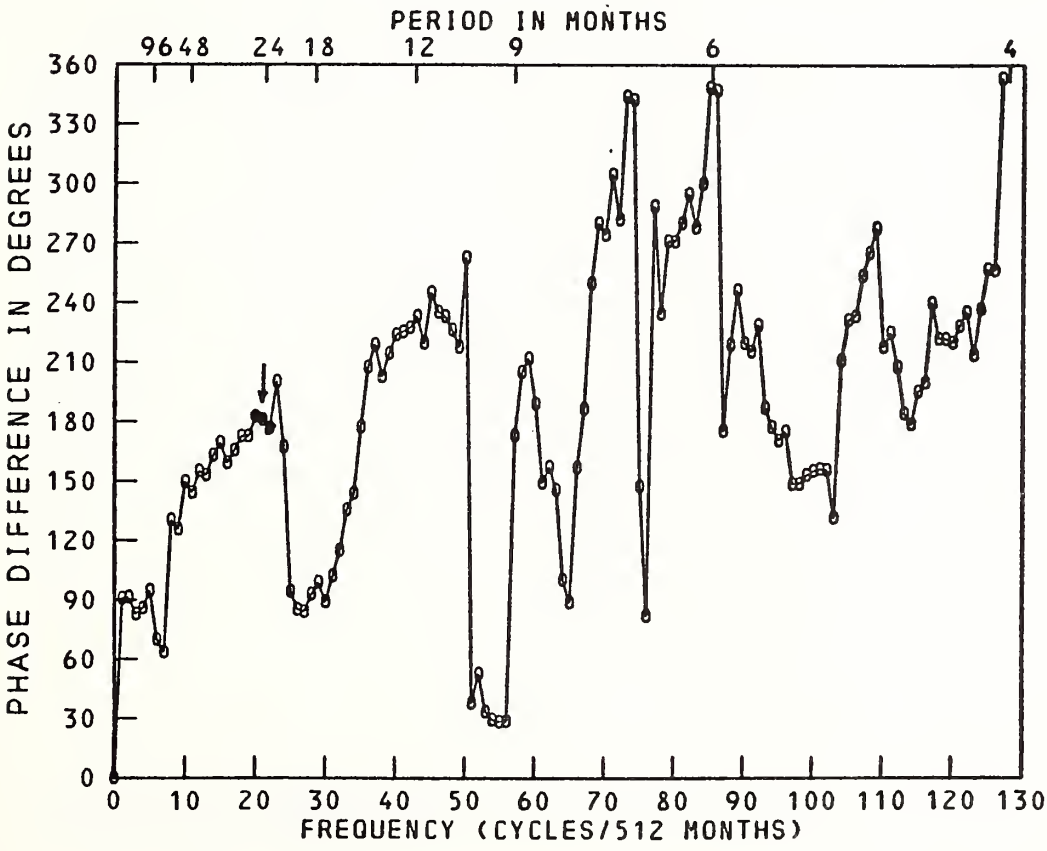

Fig. 10. Coherence squared and phase difference for the northeast and southwest areas computed from unfiltered, normalized non-seasonal departure data.

References

Gilman, D. L., F. J. Fuglister and J. M. Mitchell, Jr., 1963: "On the Power Spectrum of "Red Noise"," J. Atmos. Sci., 20, 182-184.

Landsberg, H. E., J. M. Mitchell, Jr., H. L. Crutcher and F. T. Quinlan, 1963: "Surface Signs of the Biennial Atmospheric Pulse," Mon. Weather Rev., 91, 549-556.

Lawson, C. L., and R. J. Hanson, 1974: Solving Least Squares Problems, Prentice-Hall, Inc., Englewood Cliffs, N. J.

Wallace, J.M. and R.E. Dickinson, 1972: Empirical Orthogonal Representation of Time Series in the Frequency Domain. Part I: Theoretical Considerations," J. Appl. Met., 11, 887-892.

SUMMARY OF NORTHERN HEMISPHERE 700 MB HEIGHT DEPARTURES FROM NORMAL, 1966-1969

By

Kirby J. Hanson
NOAA

Based on monthly 700 mb height departures from normal (DN) for the northern hemisphere from Gilman (1), zonal averages were calculated.* A 13-month running mean was applied to both the original monthly grid-point data and the monthly zonal values. Only 13-month running mean data are presented in this paper.

Zonal averages of 700 mb height DN for the period 1965-1970 are given in Figure 1. The continuity of the positive and negative anomalies with time and latitude is apparent.

Analysis of the regional distribution of 700 mb height DNs over the northern hemisphere during the portion of this period involving the first positive anomaly is given in Figures 2-4. A composite of the bi-monthly positions of the positive poleward moving anomalies is given in Figure 5.

The discussion at the workshop was centered on the possible significance (or insignificance)of these map features.

References

(1) Gilman, D., 1977, (private communication)

*A grid of 484 points north of 15°N having a separation of 5° latitude and 10° longitude.

Legends

Figure

1 Time variation of the zonal 700 mb height anomaly for 40°N. Lat., 1965-70.

2 Northern hemisphere distribution of 13-month mean 700 mb height anomalies centered on Jan. 1966.

3 Northern hemisphere distribution of 13-month mean 700 mb height anomalies centered on July, 1967.

4 Northern hemisphere distribution of 13-month mean 700 mb height anomalies centered on Jan. 1969.

5 Bi-monthly position of centers of positive 700 mb height anomalies, January, 1966- March,1969.

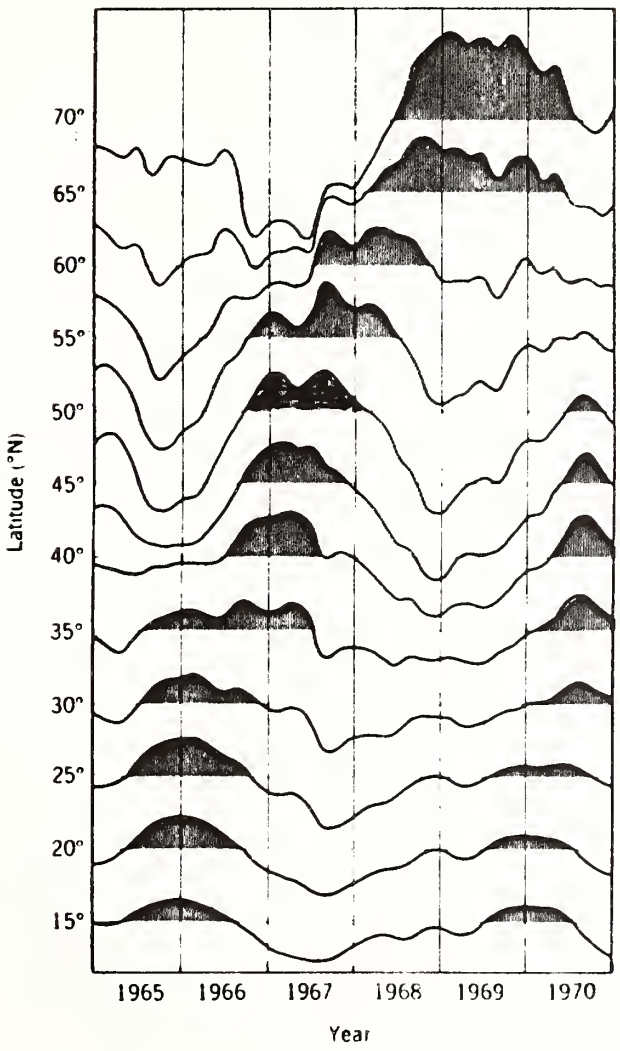
70°
65°
60°
55°
50°
45°
40°
35°
30°
25°
20°
15°
Latitude (°N)
1965
1966
1967
1968
1969
1970
Year

Figure 1.

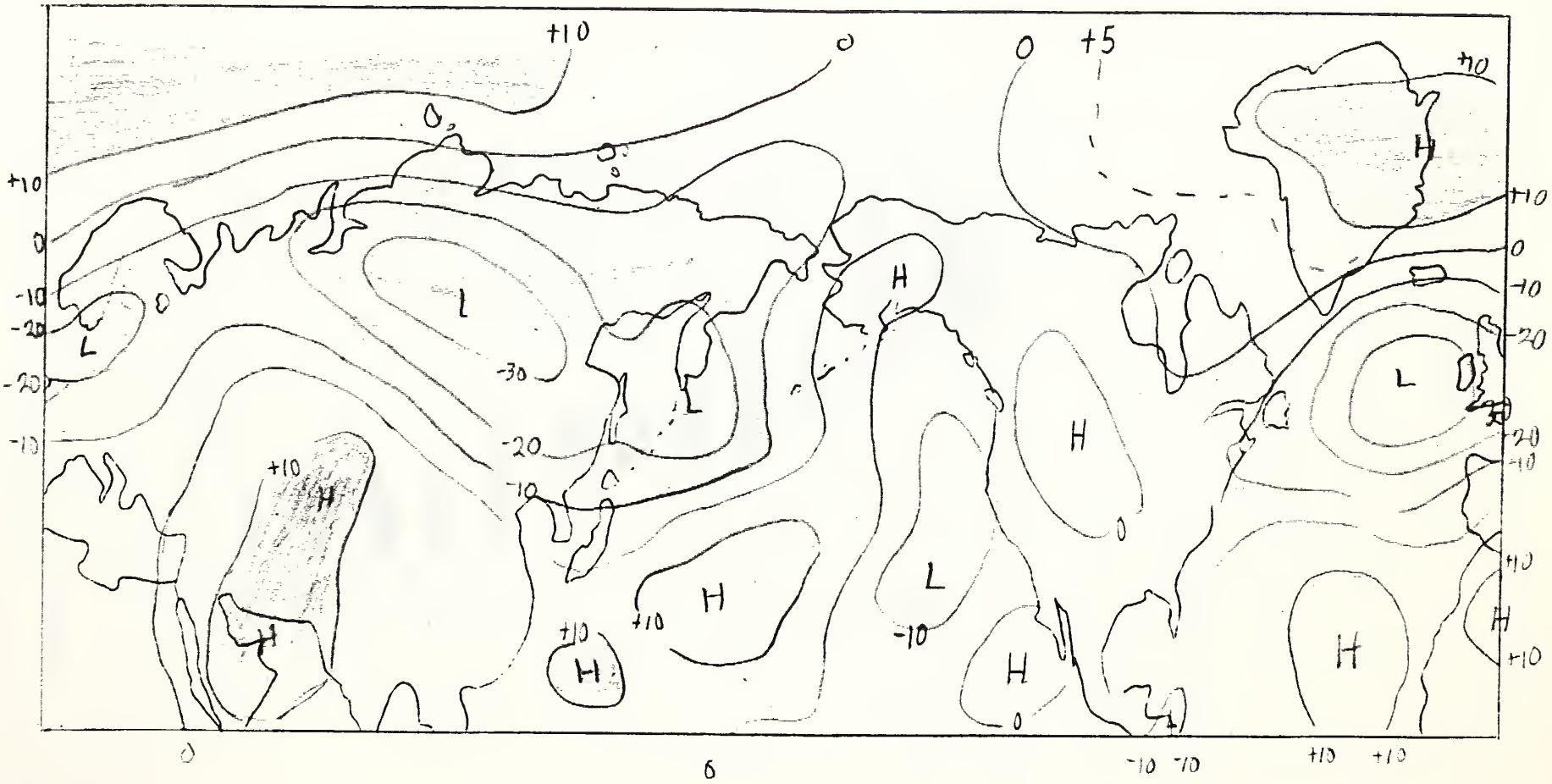

Fig. 2. Northern hemisphere distribution of 13-month mean 700 mb height anomalies centeres on Jan. 1966.

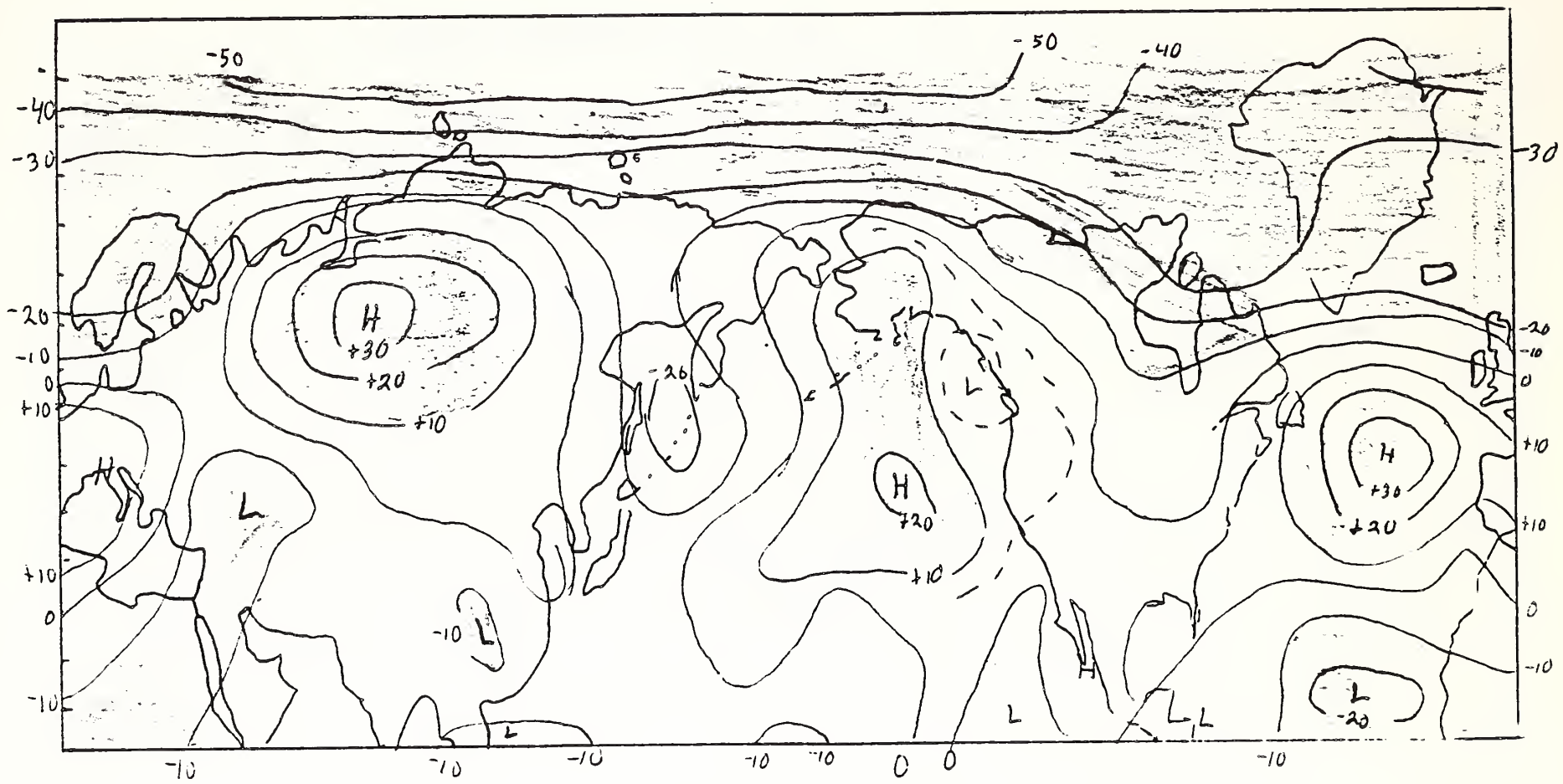

Fig. 3. Northern hemisphere distribution of 13-month mean 700 mb height anomalies centered on July, 1967.

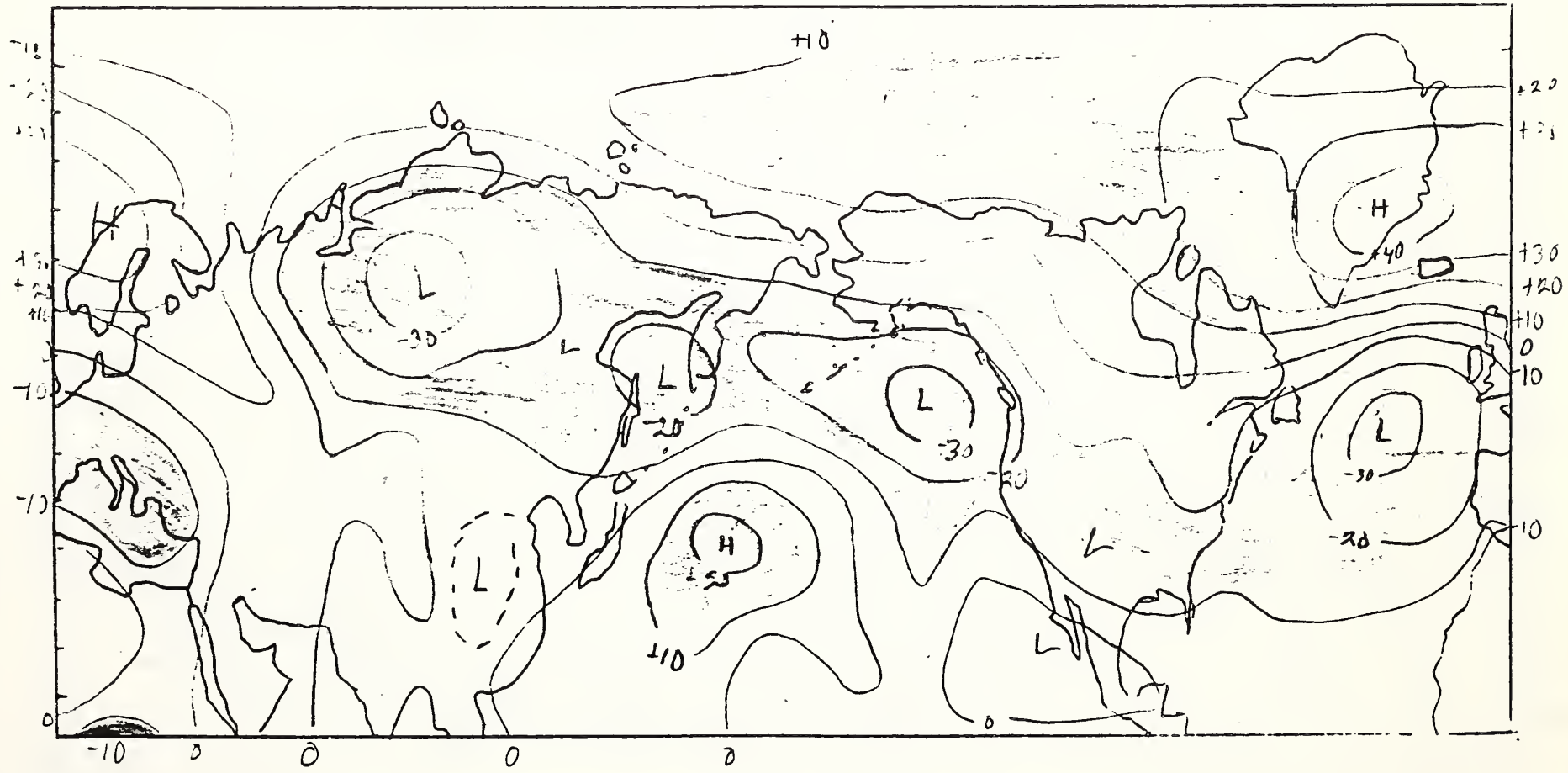

Fig.4. Northern hemisphere distribution of 13-month mean 700 mb height anomalies centered on Jan. 1969.

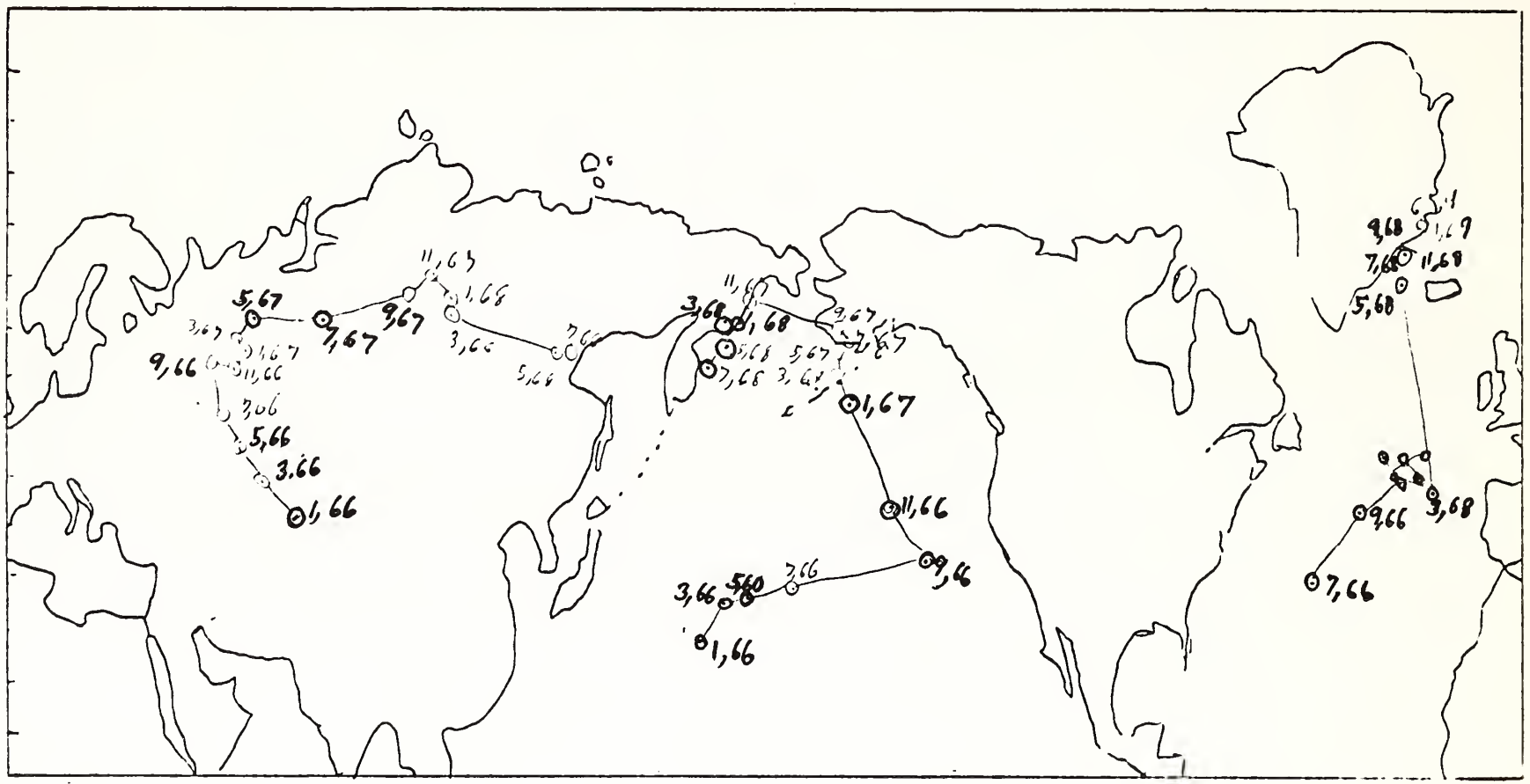

Fig. 5. bi-monthly position of centers of positive 700 mb height anomalies, january, 1966-march, 1969.

Variability in the Annual Fields of Large-Scale Atmospheric Water Vapor Transport

Richard D. Rosen
Environmental Research & Technology, Inc., Concord, Mass.

1. For the last several years, our studies at ERT have been aimed at diagnosing the interannual variability of the general circulation. Our data source has been the General Circulation Data Library, whose collection was begun at MIT under V.P. Starr and which has been added to in important ways by A. Oort at NOAA/GFDL.

2. One of our earliest studies along these lines included an evaluation of the annual mean meridional circulation patterns in the NH for each of 10 years (1958-1968). The results are shown in Fig. 1. Two features are immediately apparent: a 3-cell pattern in most years; and the existence of two regimes characterized by the relative strengths of the Hadley and Ferrel cells. During years 1-6, the Hadley cell is relatively weak, but during years 7-10 quite the opposite holds.

These results should be viewed with some skepticism, however. The mean circulation is one of the most difficult features of the general circulation to assess accurately. Moreover, the annual Hadley cell is the result of large cancellations between summer and winter. Nonetheless, we've used a consistent scheme throughout so that the changes from one year to the next may be realistic. If they are, then we have produced evidence that the "climate system" takes on discrete states that may persist for years and then change relatively quickly ("almost intransitivity"?).

3. Motivated in part by this result, we began a study of moisture fluxes in the atmosphere by looking at annual mean conditions for years drawn from both circulation regimes. Our interest in moisture fluxes derives from the important role water vapor plays in the energetics of the atmosphere.

4. Somewhat complicating the study of atmospheric water vapor are the problems involved in accurately sensing it. The bias discovered in the U.S. instrument during the mid to late 60's is a well-known example. These problems seem not to impact strongly on our results, however, as Fig. 2 shows. In it are displayed profiles of the vertically integrated amount of water vapor in the atmosphere for each of six years: years 1-5 from the first regime of meridional circulation patterns of Fig. 1, and year 10 from the second. Note that the profiles all lie fairly close to each other, although the decrease in moisture content between 1958 and 1963 first noted by Starr and Oort is visible, particularly in the region 10°-25°N.

5. Fig. 3 shows $\overline{Q}_\lambda = 1/g \int \overline{qu}\, dp$ for each of six years over the NH. Notice the mid-latitude westerly fluxes and the tropical easterly flow. The latter achieves a local maximum in the Pacific, which is well captured by the network of island stations. Although this center is fairly stable in years 1-5, it has shifted and weakened considerably in year 10. Indeed, as Fig. 4 shows, the $[\overline{Q}_\lambda] = 1/2\pi \int \overline{Q}_\lambda d_\lambda$ profile for year 10 is noticeably smaller in the tropics.

6. The contrasting behavior of year 10 in the tropical Pacific is also evident in the streamfunction field for moisture flow, the nature of which is largely determined by $\overline{Q}_\lambda$. Fig. 5 shows the streamfunction field for each of the six years. Note the large-scale organization of this field, the low wavenumber in its structure, and its reduced strength in the Pacific during year 10.

It is tempting to associate changes in the tropical circulation like the one we've depicted here to changes in oceanic forcing. The recent modeling study by Charney & Shukla tends to support this view, as well as the belief that year-to-year changes in mid-latitudes result from the natural evolution of a non-linear system.

7. Although the other component of moisture flow, $\overline{Q}_\phi = 1/g \int \overline{qv}\, dp$, is generally smaller than $\overline{Q}_\lambda$ locally, its zonal average is one of the major elements of the global energy cycle. The profiles of $[\overline{Q}_\phi]$ in Fig. 6 show once again a different character in year 10, in that the tropical southward fluxes extend over a greater latitude belt than in the other years. This supports our earlier finding of an expanded Hadley cell during year 10. The different behavior of $[\overline{Q}_\phi]$ in year 10 can be traced to strong southward fluxes which extend in a belt from the west coast of Africa to the east coast of Asia ($\overline{Q}_\phi$ values in the tropical Pacific are uncharacteristically small during year 10, just like $\overline{Q}_\lambda$).

Finally, it is worth noting that the range in $[\overline{Q}_\phi]$ is of considerable consequence for the workings of the energy cycle. For example, the difference in the moisture flux across 30°N between high and low values would, over a year imply a temperature change in the atmosphere north of this latitude of some 25°C. Certainly this was compensated for by other meridional energy exchange mechanisms, among which are oceanic heat fluxes. Vonder Haar and Oort have demonstrated that these fluxes are not small - we've shown here that there may in fact be enough freedom for them to vary considerably from one year to the next. (It must be borne in mind, of course, that there are other parts of the energy cycle besides ocean heat fluxes that could balance the variability in $[\overline{Q}_\phi]$.)

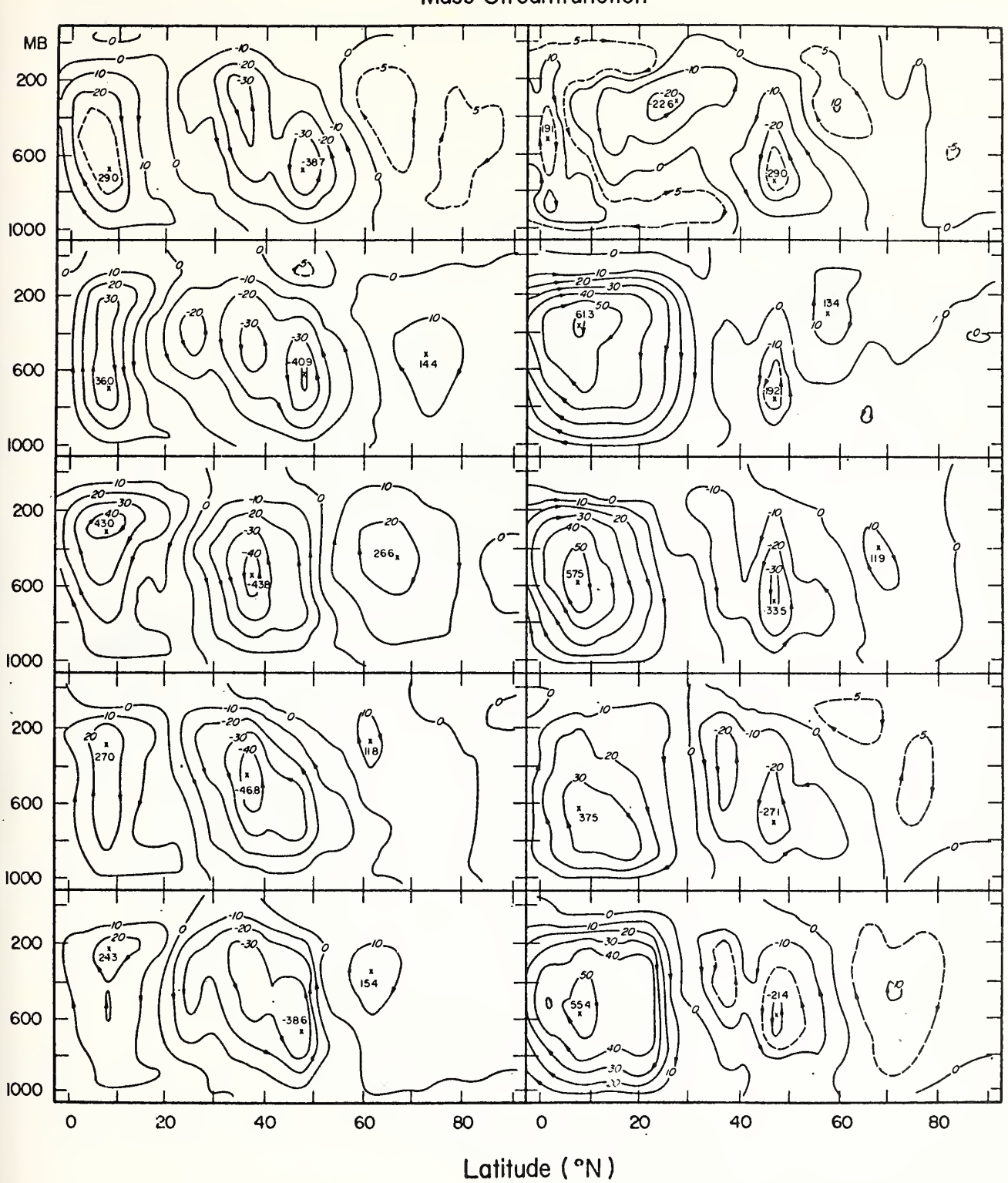

Fig. 1 Cross sections of the mass streamfunction for the mean meridional circulation for each of ten years. Year 1 refers to the period from May 1958 through April 1959, and so on for the other years. Units are 10^9 kg/s.

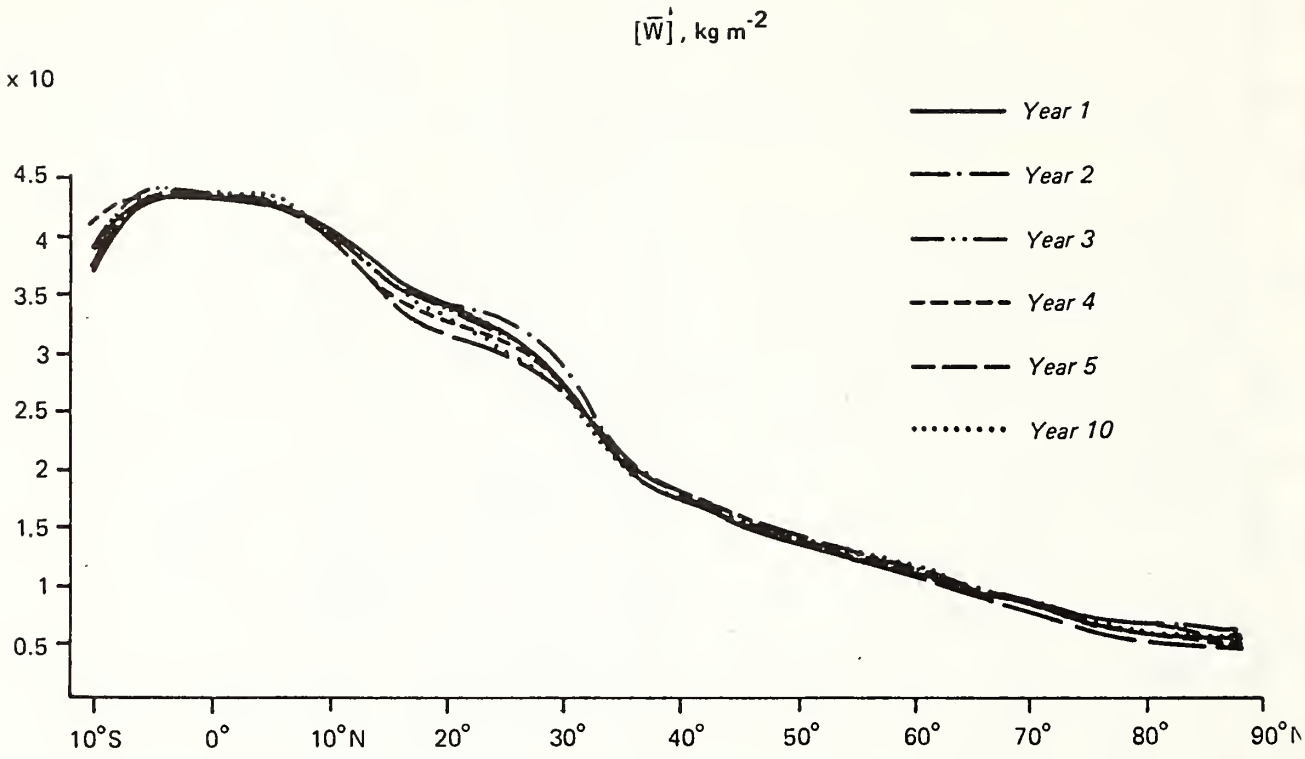

Fig. 2 Meridional profiles of the zonal mean of $\overline{W} = 1/g \int \overline{q}\, dp$ for each of six individual years.

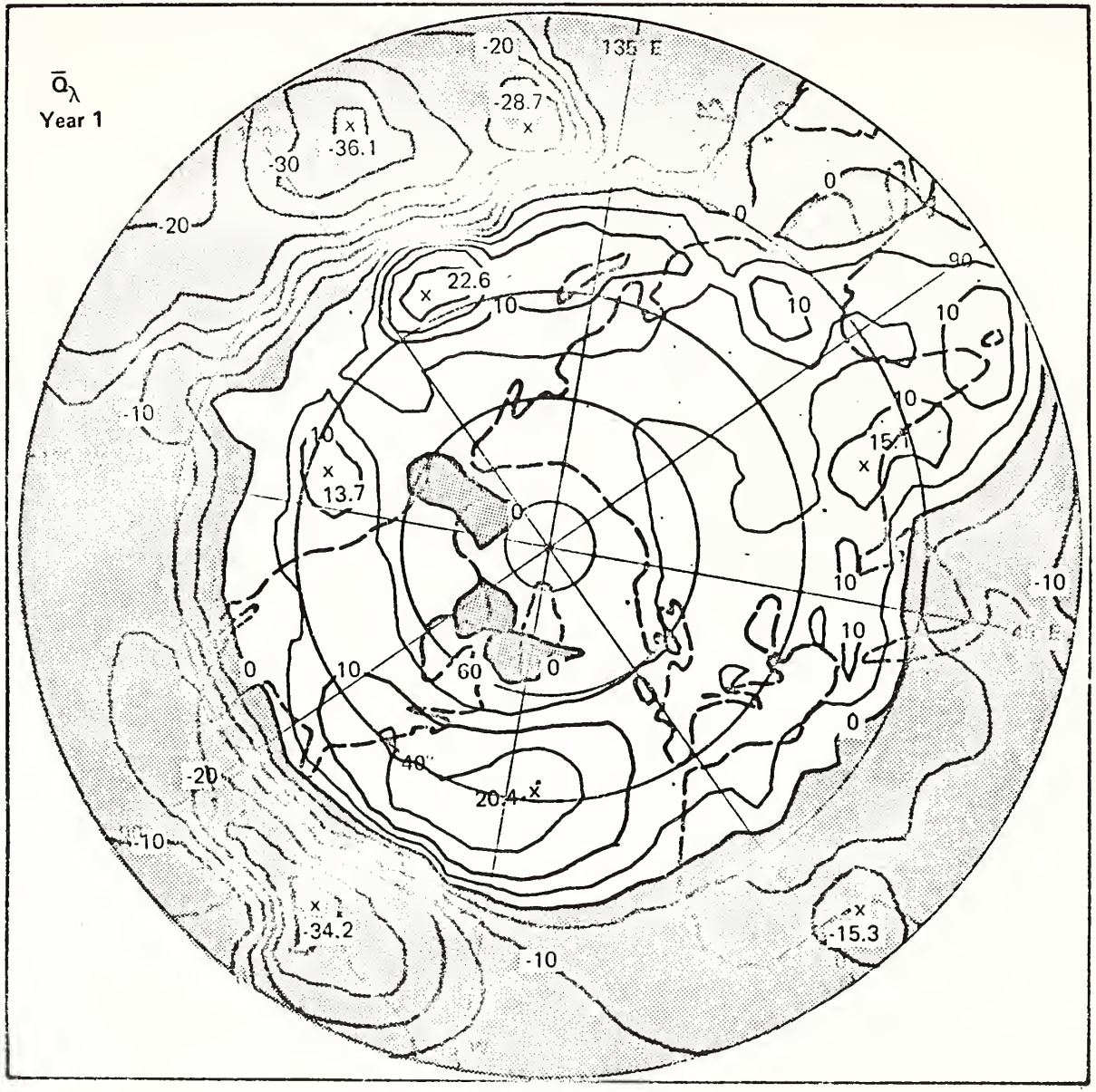
$\bar{Q}_\lambda$
Year 1
135 E
-20
-28.7
-36.1
-30
-20
0
0
90
22.6
10
10
10
10
-10
10
15.1
13.7
0
10
-10
10
60
0
0
-20
40
20.4
-10
-34.2
-15.3
-10

$\bar{Q}_\lambda$
Year 2
135 E
-20
180
x -34.0
-30
-10
0
x
20
27.6
10
10
10
90
-20
-10
0
10
x
13.0
10
0
0
60
10
10
45 E
10
10
40
x 19.8
-20
90
-10
0
x -32.9
-20
-10

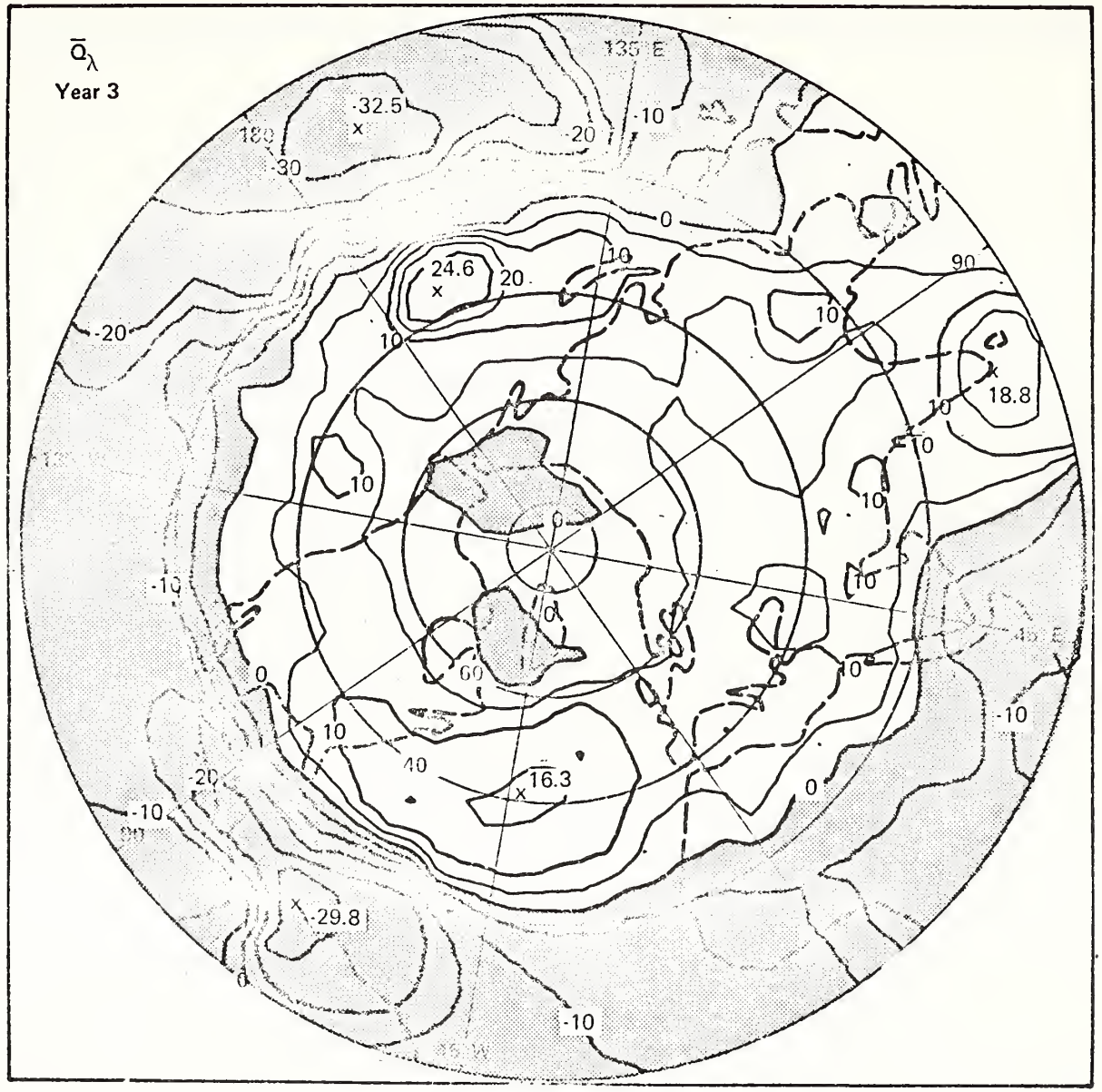
$\bar{Q}_\lambda$
Year 3
135 E
-32.5
-30
-20
-10
0
10
24.6
20
90
-20
10
10
18.8
10
10
10
10
10
0
0
-10
0
60
10
10
40
16.3
-10
-20
-10
-29.8
0
-10

$\bar{Q}_\lambda$
Year 4
-32.3
15.3
15.6
15.9
24.1
18.5
-28.6
-20
-10
0
10
20
40
15 E
45 W

$\bar{Q}_\lambda$
Year 5
-33.2
-30
-20
-10
0
20.6
10
17.4
60
16.4
16.2
-25.4
45 W
45 E

$\overline{Q}_\lambda$
Year 10
135 E
45 W
x -26.7
x 17.1
x -32.1
x 14.0
x -13.2
x 2.1
x 1.6
-10
0
10
-20
60
40
90

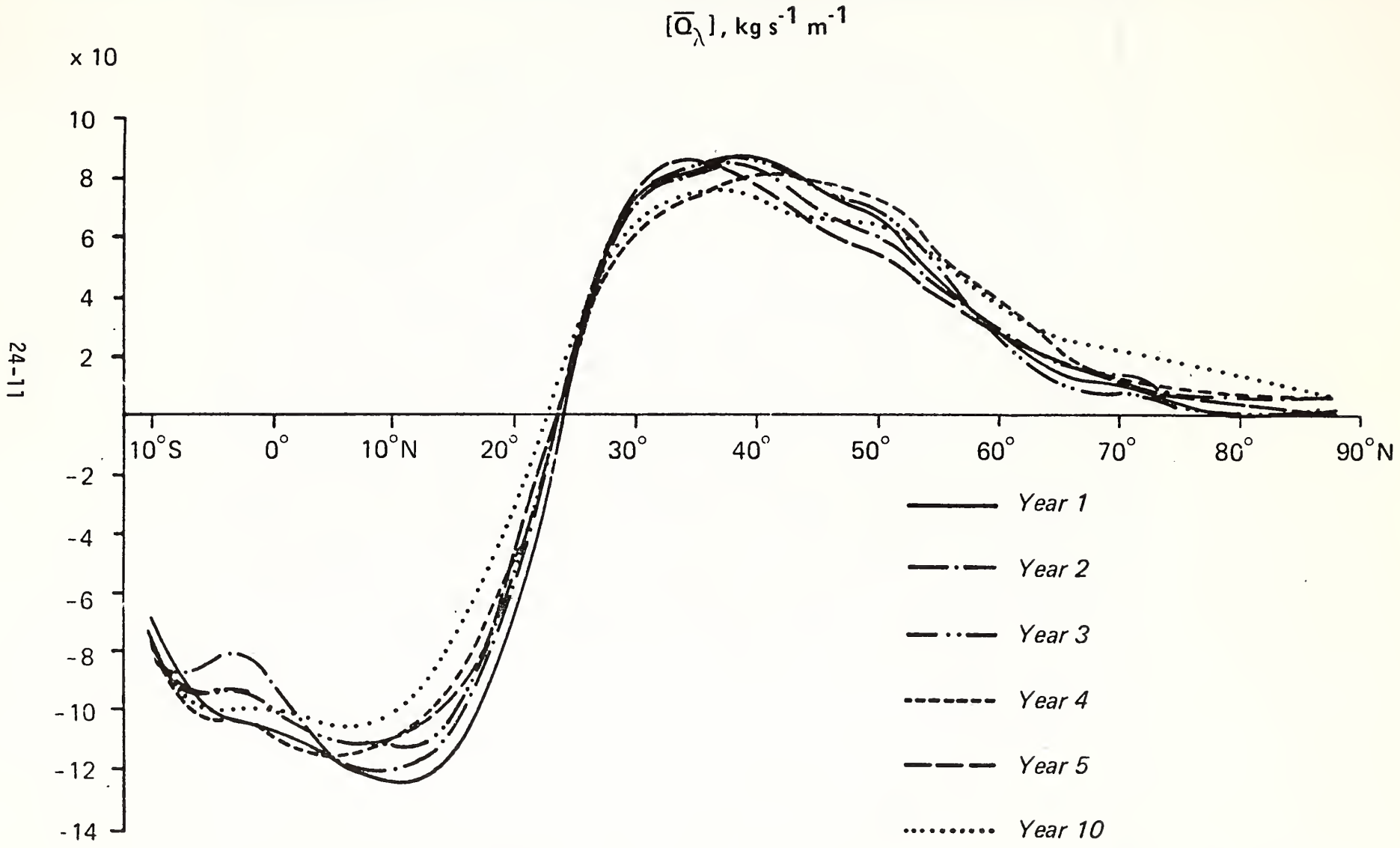

Fig. 4 Meridional profiles of the zonal mean of $\overline{Q}_\lambda = 1/g \int \overline{qu}\, dp$ for each of the years studied.

710205

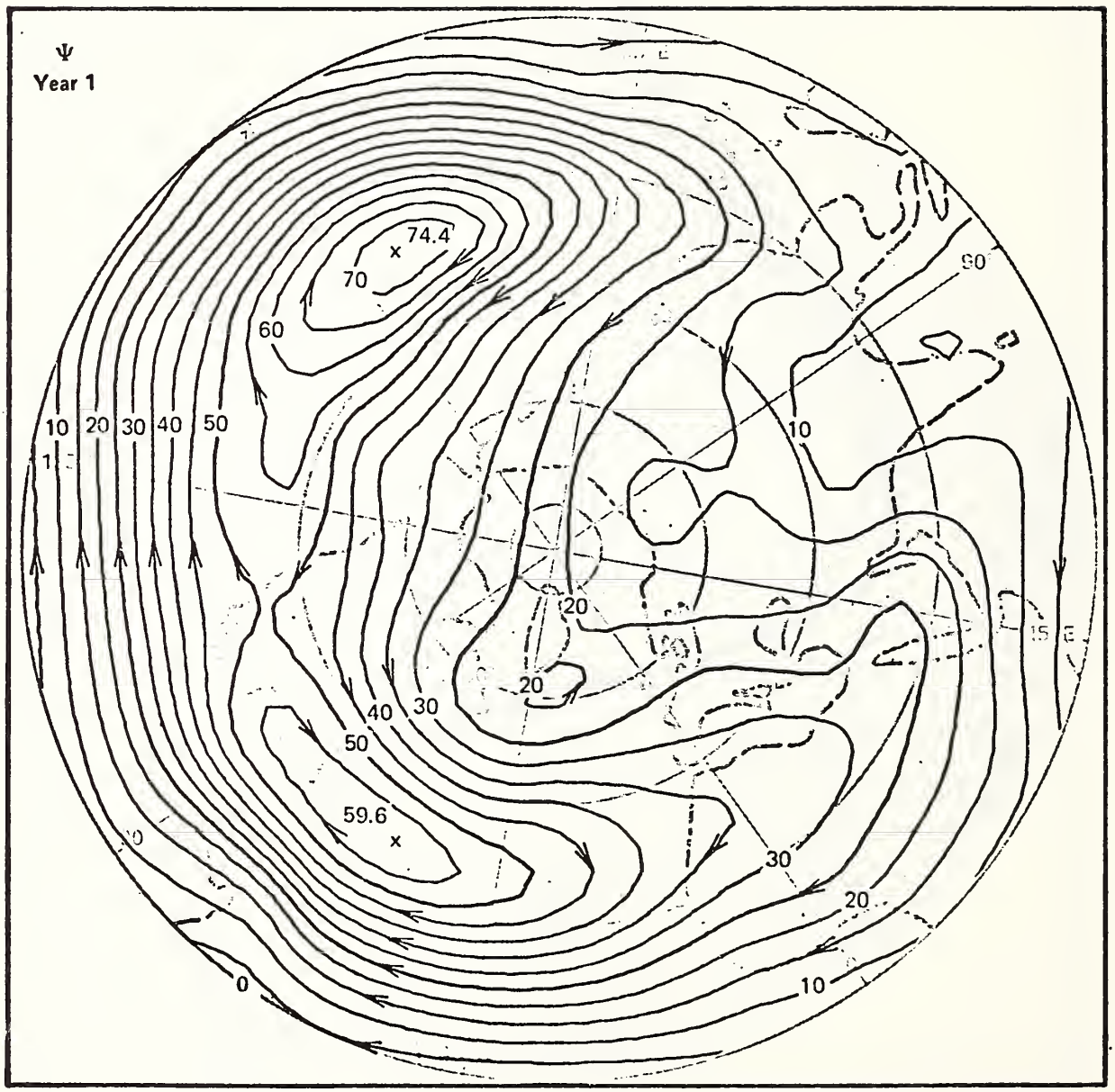

710206

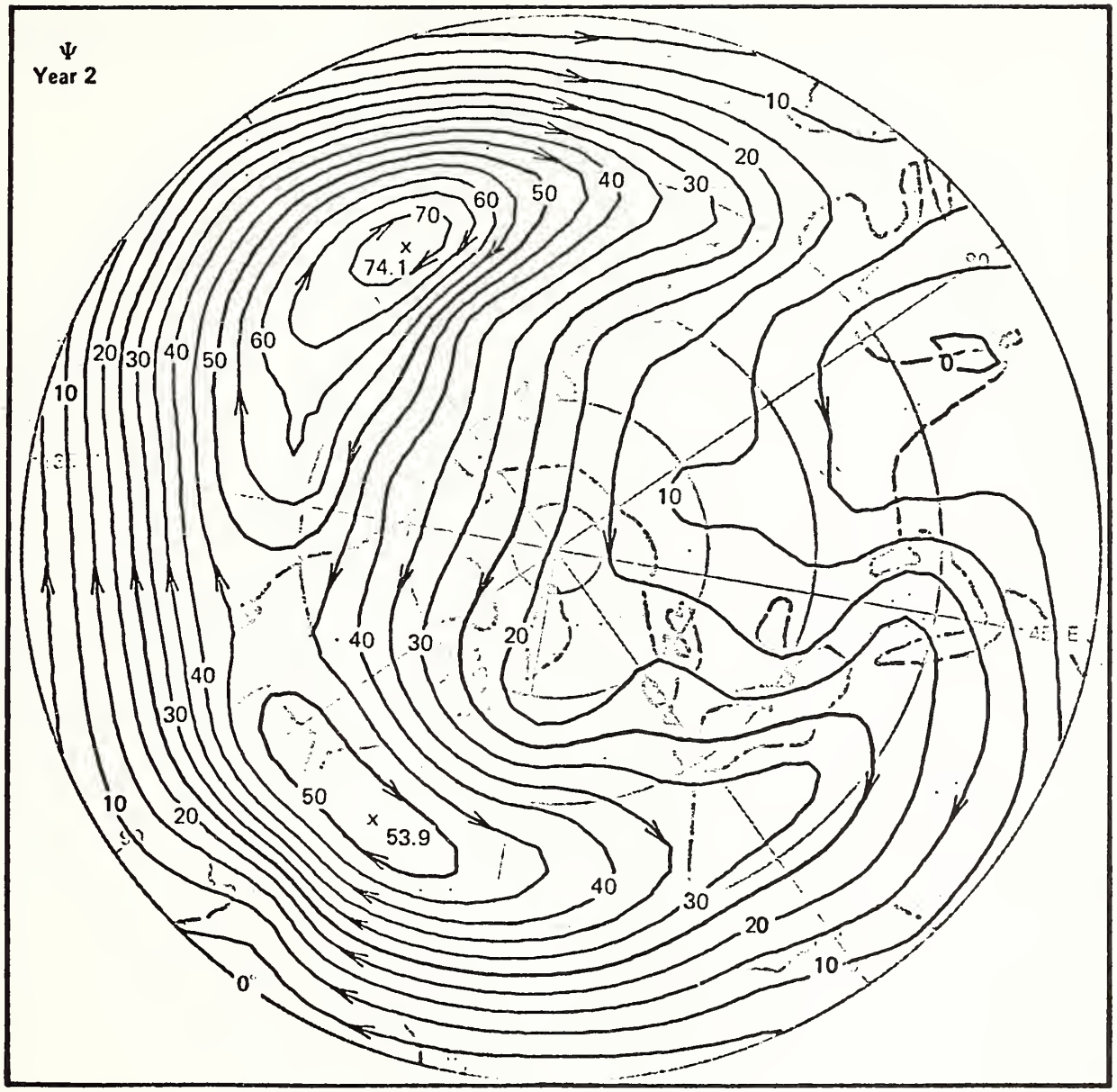

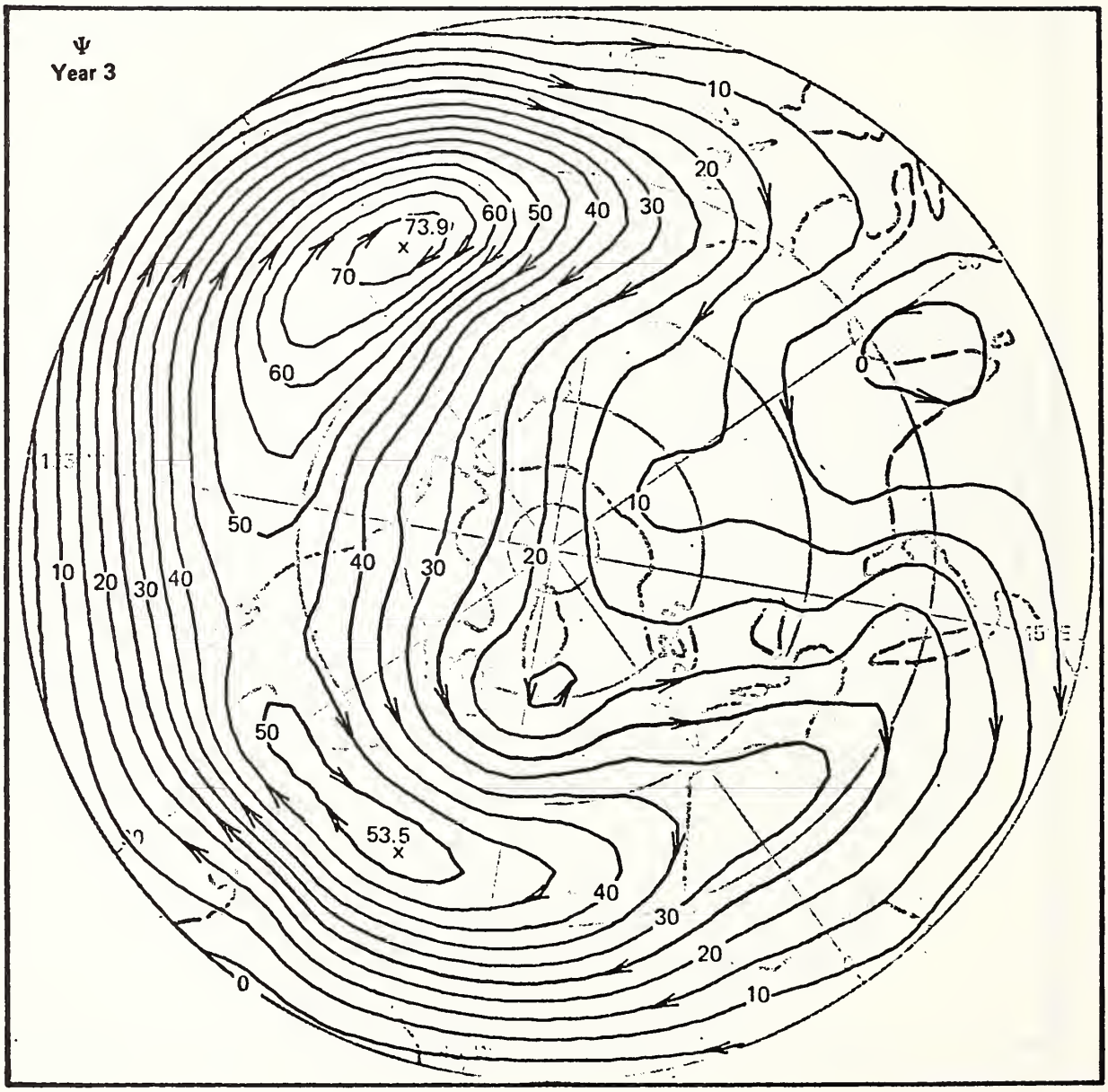
Ψ
Year 3
73.9
53.5
10
20
30
40
50
60
70
0

710175

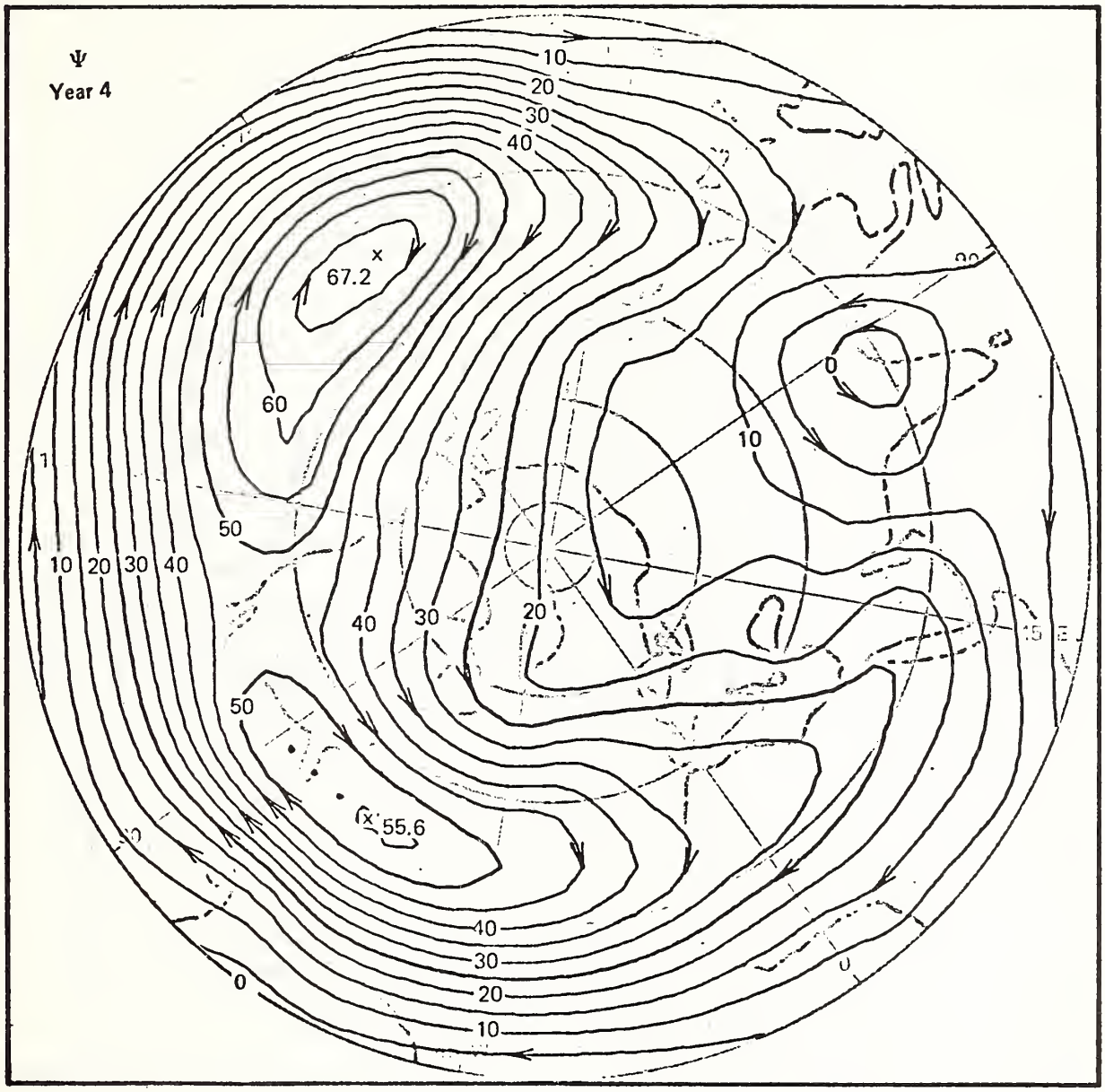

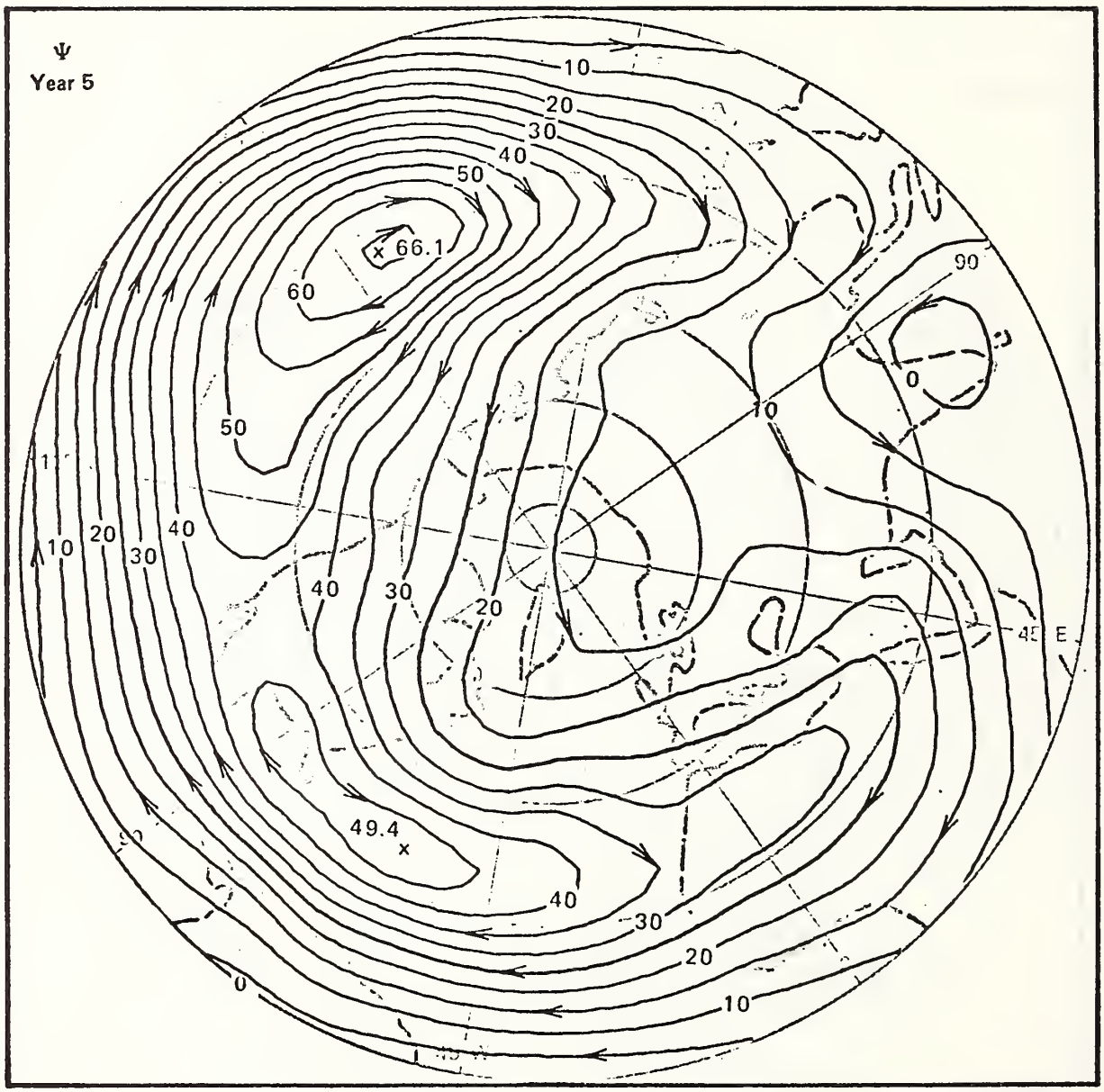
Ψ
Year 5
10
20
30
40
50
66.1
60
50
40
30
20
10
0
90
0
10
45 E
40
30
20
49.4
40
30
20
10
0

/710138

710239

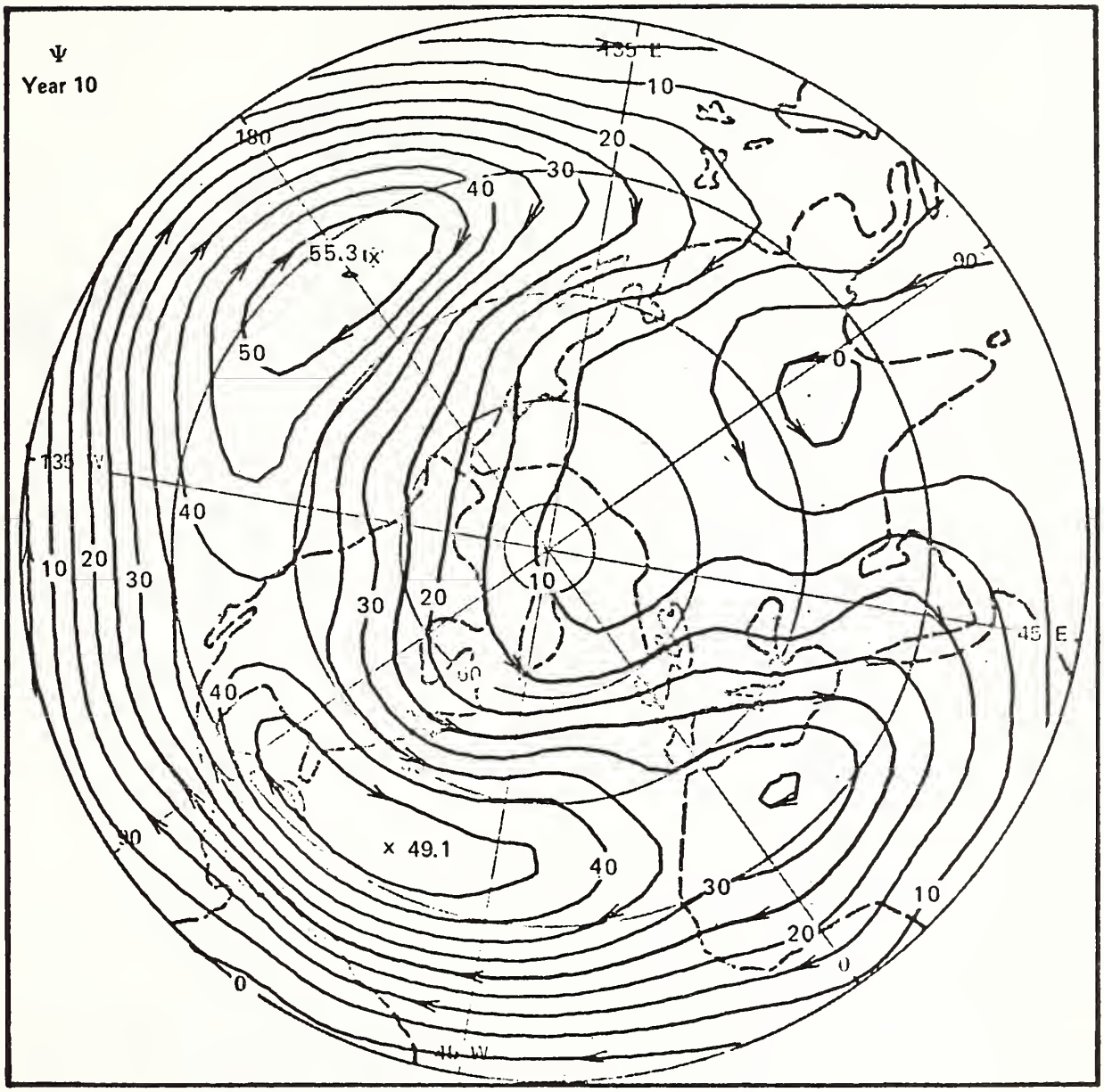

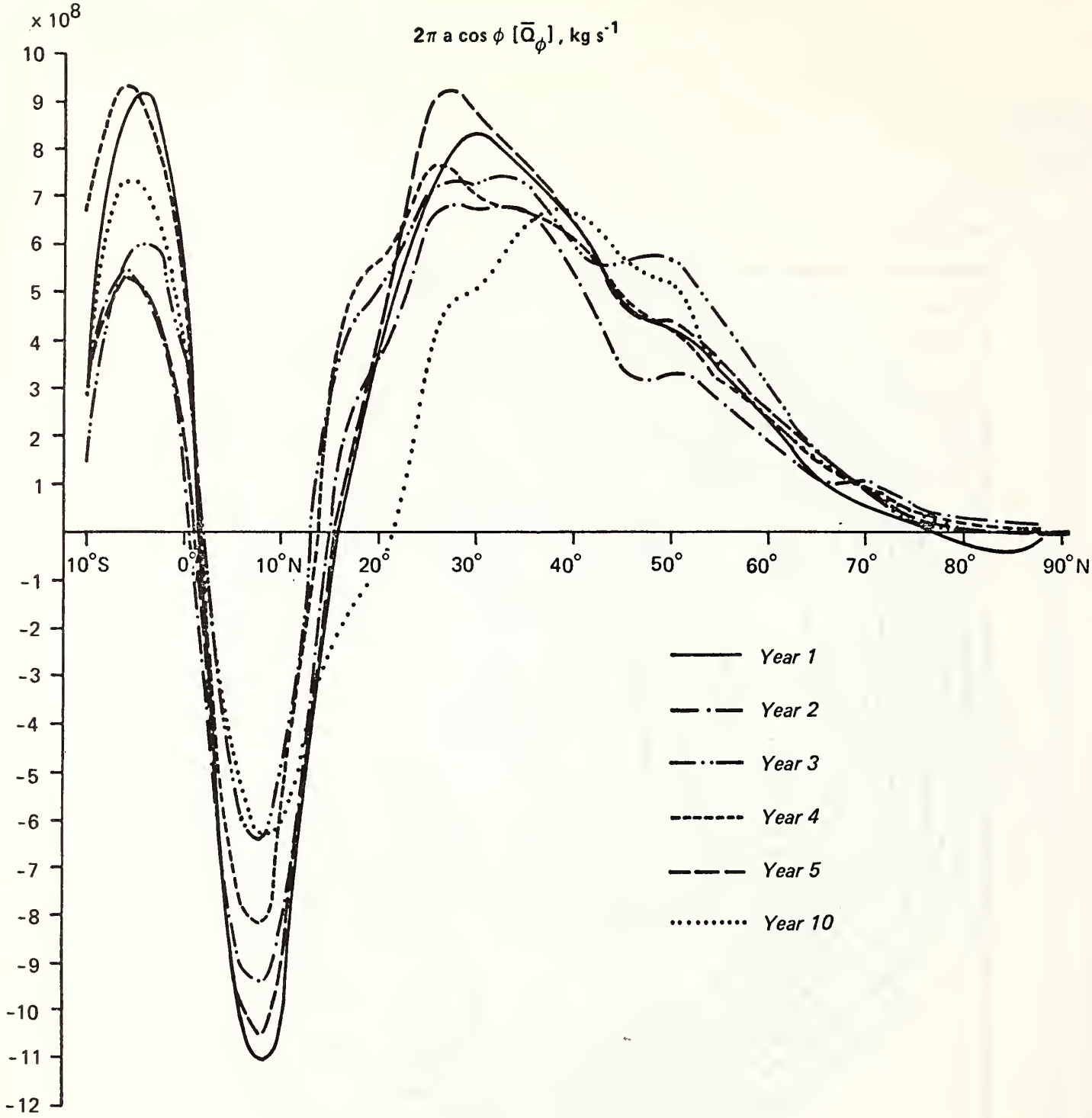

Fig. 6 Meridional profiles of the total moisture flow across latitude walls in the atmosphere for each of the years studied.

A COMPARISON OF SURFACE WIND PARAMETERS, CLOUD AMOUNT, AND SEA SURFACE TEMPERATURE IN THE TROPICAL PACIFIC

Ellen J. Steiner
CIRES, University of Colorado

Monthly means and monthly deviations from the mean of surface wind divergence, vorticity, wind speed, cloud amount, and sea surface temperature (SST) for the period 1965-1972 and the region 25°S-25°N, 130°-280° (190°-280° for the SSTs), were examined and compared. The reason for undertaking such a study is to determine the interactions between these variables. The ultimate purpose is to add to the understanding and aid in the forecasting of events such as El Nino.

The wind data used to compute the divergence and curl came from ship observations compiled by Wyrtki and Meyers (1975). The cloud data were from daily nephanalyses prepared from polar orbiting satellite data, and were averaged and gridded by Sadler (1969), and the SSTs were ship observations provided by Forrest Miller of the National Marine Fisheries Service.

Time series of correlation coefficients between the fields were computed, as well as maps of correlation coefficients over the entire time record and for winter and summer. For these calculations, the data were interpolated onto 5° latitude by 10° longitude grids. The high noise levels inherent in the data rendered the correlation coefficients systematically too low. However, their significance was confirmed through their consistency in time and their sampling distributions.

Several distinctive features were manifest in the mean fields (Figure 1). A region of strong convergence and cyclonic vorticity overlapped the deep near-equatorial cloudiness regime. A southern branch of convergence also coincided with a cloudiness maximum, and divergence in the northeastern and southeastern portions of the field were coincident with persistent stratocumulus. Both cloud and divergence fields were weakest in March and April. The SSTs predictably decreased polewards, with the isotherms shifting polewards in the summer.

The correlations in the time series between the cloud and surface divergence fields both in the mean and deviation cases were negative (Figures 2 and 3), demonstrating the relationship between subsidence and fewer clouds and convergence and more clouds. There was a striking hemispheric difference in the correlations between the mean cloud and divergence fields, with the southern hemisphere correlations far more irregular. Stratocumulus which exist in the face of divergence systematically reduce the negative correlations in the time series and emphasize the importance of knowing cloud type as well as cloud amount for future analyses.

The time series correlations between the other mean fields are not discussed because meridional gradients (especially in the SSTs) completely obscured the subtle relationships sought for here. Similarly, maps of the correlations between the

mean fields mainly reflected the seasonal oscillation. In some cases, the correlations were found to reverse sign once the seasonal trend was removed. The seasonal oscillation of the variables was in phase in the region of the near equatorial convergence and cloud bands; that is, warm SSTs occurred together with increased cloudiness, which in turn was concurrent with cyclonic vorticity and convergence. Other regions were more anomalous. An interesting example is the mean SST vs. cloud amount correlation field (Figure 4) which shows two large negatively correlated regions extending from the northwest and southeast.

Seasonal and meridional gradients do not appear in correlations between the deviation fields. These correlations will be discussed next.

Cloudiness was correlated with cyclonic vorticity (Figure 5). There were very weak positive correlations between anomalies of SST and vorticity when the SSTs were lagged by one, two, and four months. Also, the SSTs were very slightly negatively correlated with deviations of divergence and cloud amount. In the case of SST vs. cloud amount, two large negatively correlated regions (similar to those in the map of the mean field correlations) possibly dominate the signs of the correlations in the time series (Figure 6). Other correlation fields showed coherent regional differences as well. Anomalies of SST and wind speed were slightly negatively correlated, supporting the tenets that strong winds lead to upwelling, and also increase the depth of the oceanic mixed layer by generating turbulence. Anomalies of wind speed and cloud amount were positively correlated (Figure 7), perhaps because of an association between strong winds and sub-grid scale wind speed variability. Deviations of SST especially, and of cloud amount to a lesser extent, were found to be persistent in time. This may account for the persistence of the correlations when the sea surface temperatures were lagged against the other variables.

There were often regional differences between the winter and summer correlation fields. The most striking examples were the seasonal SST vs. cloud amount correlations (Figure 8). The winter correlation field shows substantial regions of positive correlations in the east and northwest. By summer, the positive correlations in the east had contracted and weakened while those in the west had intensified. Correspondingly, the winter minus summer correlation difference field was positive in the east and negative in the west.

The relatively small correlations and in some cases the weak relationships opposite to those expected (such as those between the divergence and SST, and vorticity and SST), while in part a function of the noise level of the data, may also point towards the existence of some large scale forcing which overrides local effects. The differences between correlations in the winter and summer fields suggest that this forcing is a function of both season and region. Though too small to be useful in forecasts, the correlations do attest to the existence of empirical relationships between the parameters. Better and more complete data for recent years will be used to resolve some of the questions left unanswered in this study.

REFERENCES

Elsberry, R.L., and R.W. Garwood, Jr., 1978: Sea surface temperature anomaly generation in relation to atmospheric storms. Bull. Amer. Meteor. Soc., 59, 786-789.

Reiter, E.R., 1978: The interannual variability of the ocean-atmosphere system. J. Atmos. Sci., 35, 349-370.

Reiter, E.R., 1978b: Long term variability in the tropical Pacific, its possible causes and effects. Mon. Wea. Rev., 106, 324-330.

Sadler, J.C., 1969: Average cloudiness in the tropics from satellite observations. International Indian Ocean Expedition Meteorological Monographs, No. 2, East-West Center Press, 22 pp and 12 plates.

Sadler, J.C., L. Oda, and B.J. Kilonsky, 1976: Pacific Ocean cloudiness from satellite observations. Rept. Meteor. Univ. Hawaii, 137 pp.

Wyrtki, K., and G. Meyers, 1975: The trade wind field over the Pacific Ocean, Part 1. The mean field and the mean annual variation. H16-75-1. Hawaii Institute of Geophysics, University of Hawaii, 55 pp.

JANUARY

a)

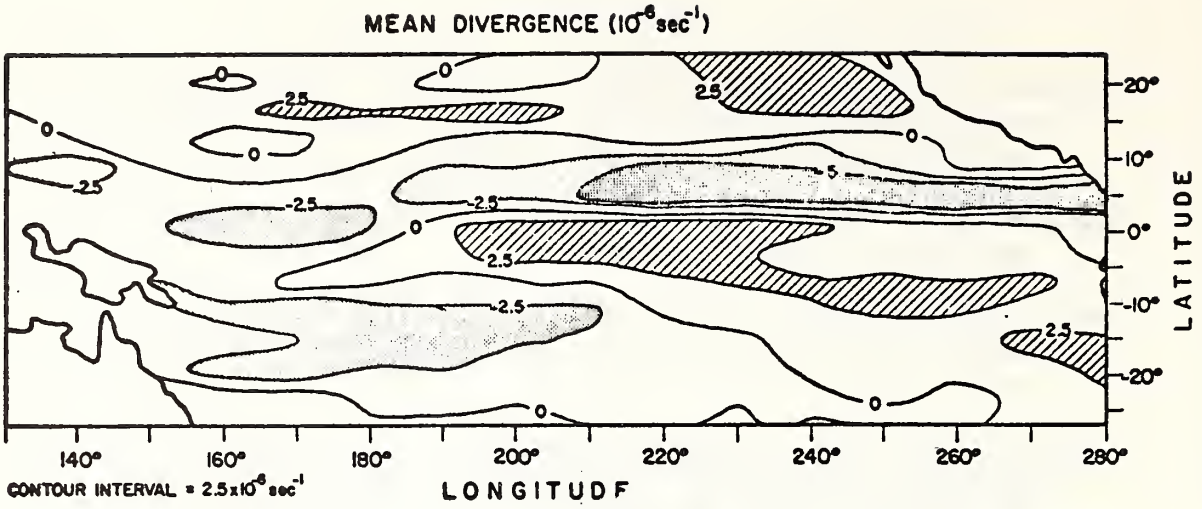

b)

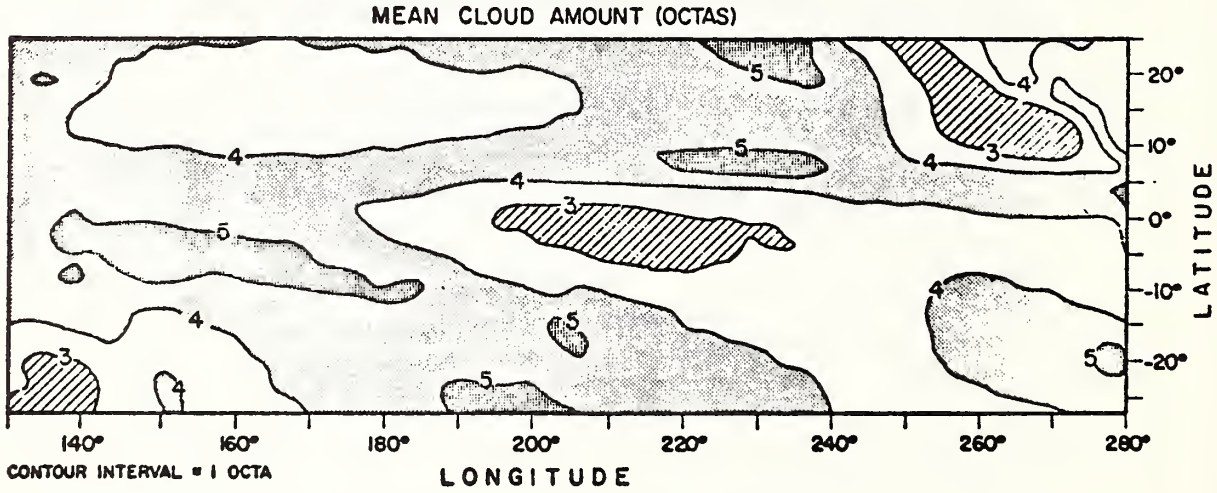

Light Shading: -5×10^{-6} sec^{-1} < Divergence < -2.5×10^{-6} sec^{-1}
4 octas < Cloud amount < 5 octas

Dark Shading: Divergence < -5×10^{-6} sec^{-1}
Cloud Amount > 5 octas

Hatched Shading: Divergence > 2.5×10^{-6} sec^{-1}
Cloud amount < 3 octas

Figure 1

JANUARY

c)

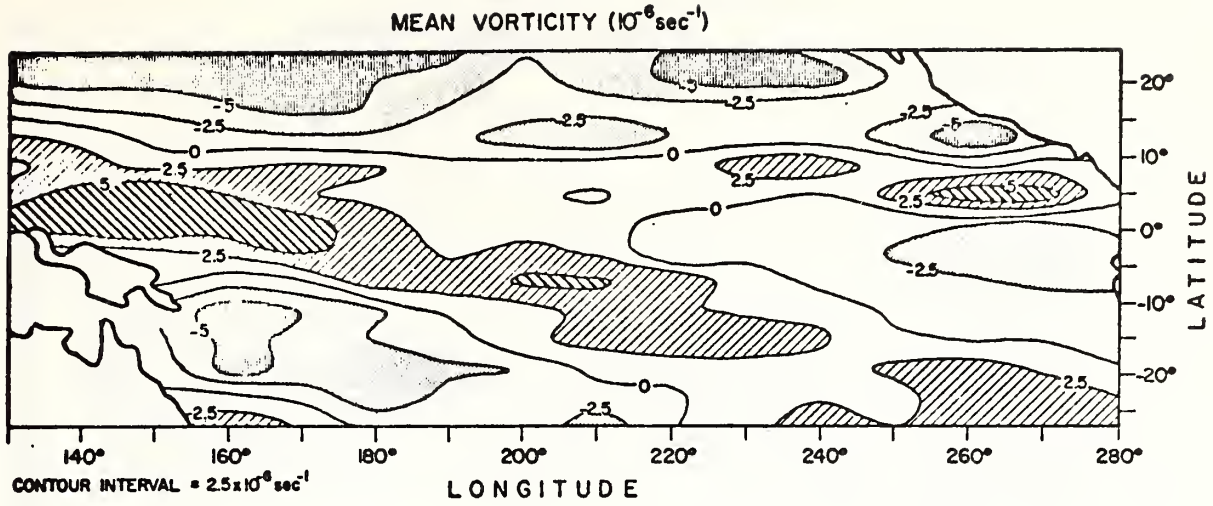

d)

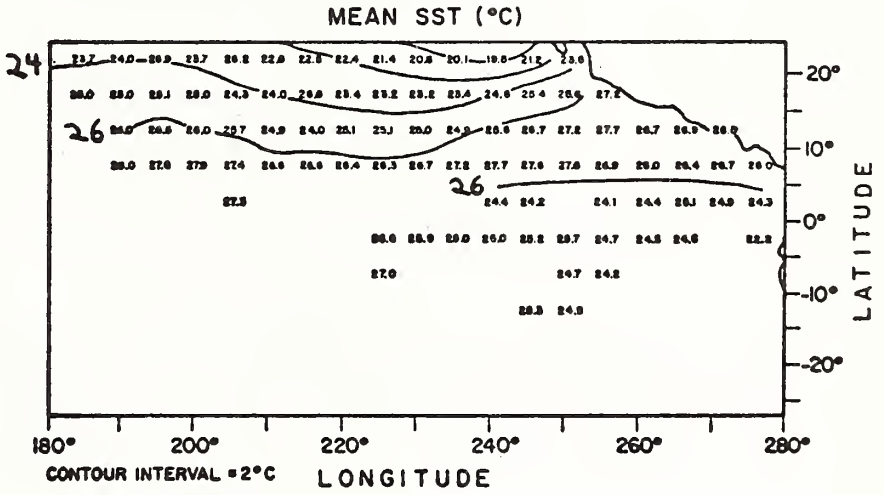

Light Shading $-5\text{x}10^{-6}$ sec^{-1} < Vorticity < $-2.5\text{x}10^{-6}$ sec

Dark Shading: Vorticity < $-5\text{x}10^{-6}$ sec^{-1}

Hatched Shading: $2.5\text{x}10^{-6}$ sec^{-1} < Vorticity < $5\text{x}10^{-6}$ sec^{-1}

Dark Hatched Shading: Vorticity > $5\text{x}10^{-6}$ sec^{-1}

(Hatched shading indicates cyclonic vorticity in northern hemisphere, anticyclonic vorticity in southern hemisphere)

Figure 1

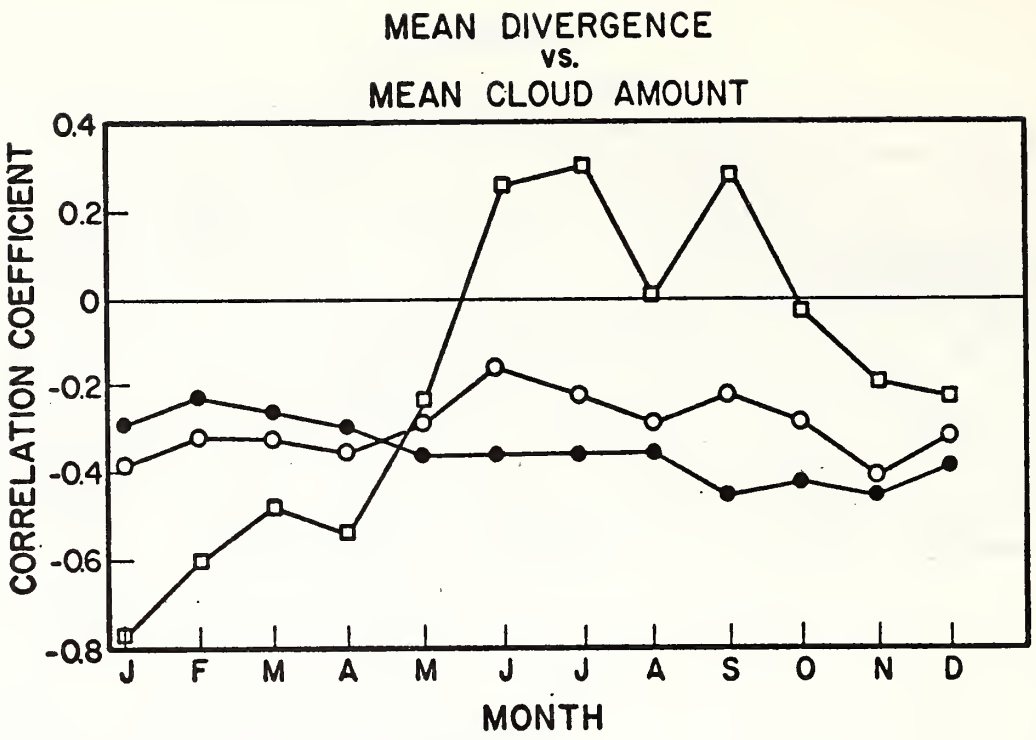

Open Circles: Entire region
Closed Circles: Northern Hemisphere
Squares: Southern Hemisphere

MEAN DIVERGENCE vs. MEAN CLOUD AMOUNT

Correlation Coefficients

Longitude

Latitude	130	140	150	160	170	180	190	200	210	220	230	240	250	260	270	280
25	.46	.70	.54	.37	.22	.48	.23	-.54	-.48	-.22	.16	.00				
20	-.22	-.13	-.58	-.67	-.19	.15	-.26	-.53	-.30	.07	-.10	.12				
15	.25	-.55	-.52	-.70	-.82	-.23	-.55	-.33	-.48	.21	.55	.16	-.89	-.94		
10		.32	.12	-.35				-.69	-.63	-.82	-.74	-.77	-.82	-.94		
5		-.34	.10					-.58	-.59	-.76	-.93	-.43		-.10	-.02	.11
0			-.42					-.71					.46	.63	.79	
-5							.41					-.70	-.31	.22	.49	
-10				.17			.48			.16	-.27	-.36	-.11	-.36	.47	
-15			.67	-.33			-.29	-.69	-.75	-.72	.39	-.18	.02			
-20				-.64	-.16	.27	-.39	-.28	.26		.03	.32				
-25				-.39	-.11	.27	-.23	-.14	-.19	.57	-.30	-.45				

Figure 2

CLOUD AMOUNT ANOMALIES
vs.
DIVERGENCE ANOMALIES

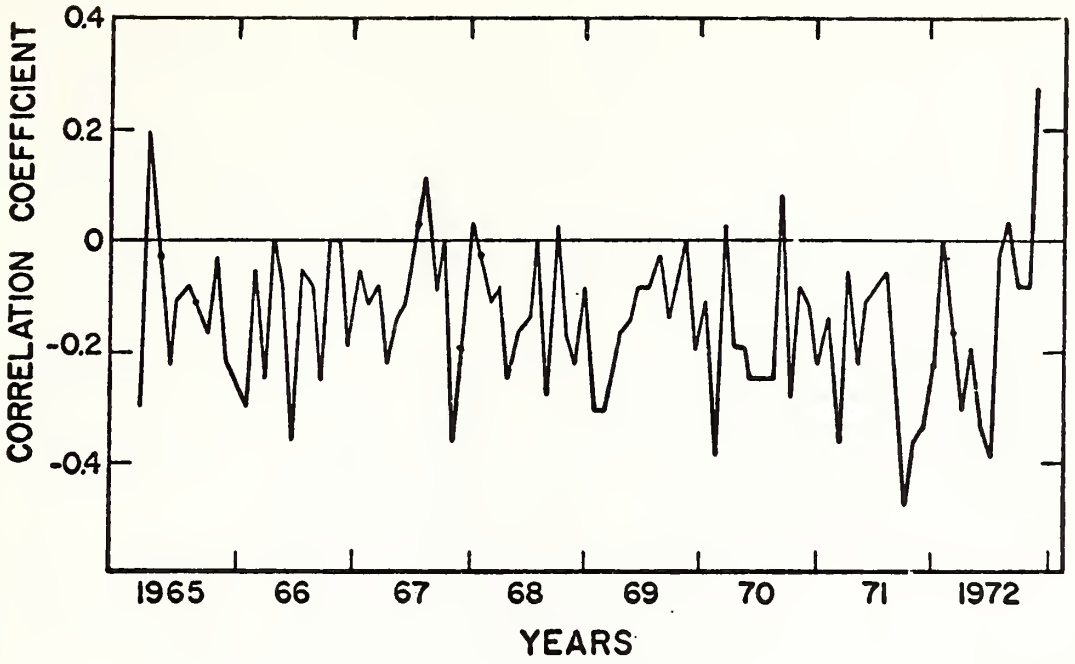

MEAN	σ	95% confidence interval for mean
-.14	.14	-.17 - -.12

CLOUD AMOUNT ANOMALIES vs. DIVERGENCE ANOMALIES

Correlation Coefficients

Longitude

Latitude	130	140	150	160	170	180	190	200	210	220	230	240	250	260	270	280
25	-.23	-.07	-.16	-.19	-.11	-.04	-.04	-.14	-.25	.01	-.13	.15				
20	-.15	-.27	-.30	-.22	-.02	.12	-.06	-.17	-.12	-.11	.12	.25				
15	-.02	-.23	-.07	.42	-.10	-.25	-.20	-.21	-.03	-.02	-.09	-.13	-.21	-.40		
10		-.33	.15	.06				-.38	-.31	-.23	.01	-.29	-.28	-.43		
5			-.26					-.22	-.34	-.42	-.24	-.36		-.20	-.09	-.14
0													-.05	-.10	-.12	
-5							-.20					-.33	-.21	.04	-.09	
-10				-.50			-.11			-.04	-.02	.01	.15	.22	.12	
-15			-.32	-.18			-.25	-.44	-.33	.03	-.08	-.08	-.15			
-20				-.20	-.17	-.16	-.02	.06	.01		-.20	-.27	.05			
-25				-.08	.11	-.09	-.07	-.02	-.01	-.18	-.06	-.18				

Figure 3

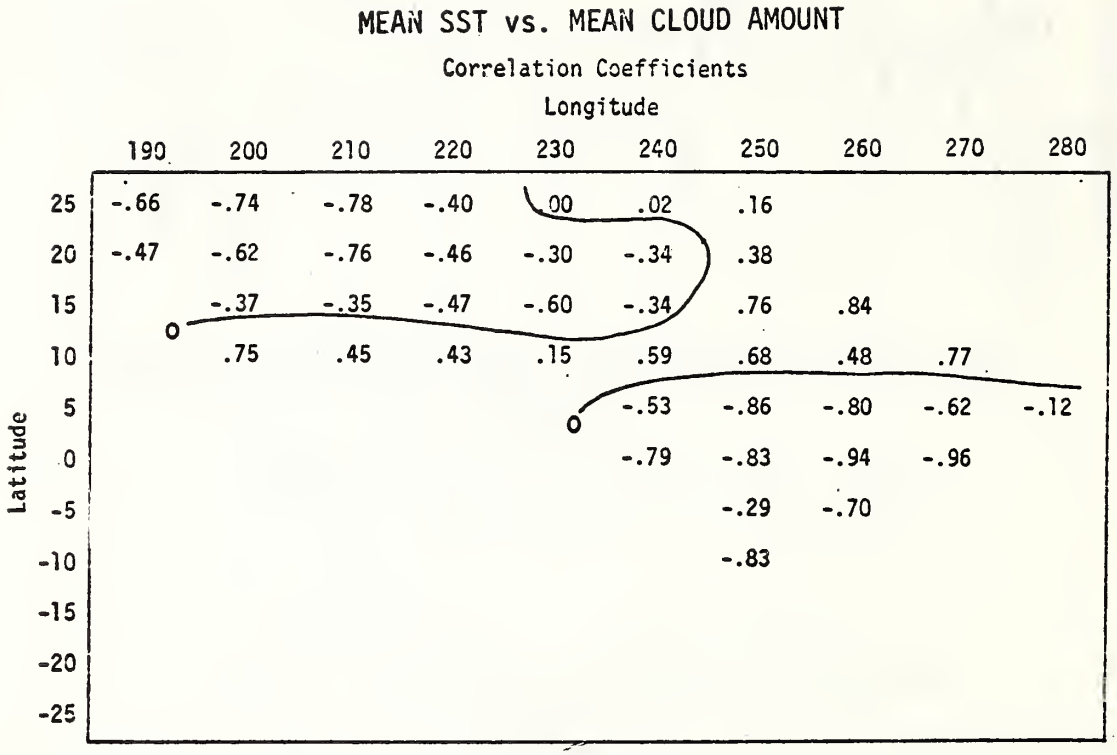
MEAN SST vs. MEAN CLOUD AMOUNT
Correlation Coefficients
Longitude
190 200 210 220 230 240 250 260 270 280
Latitude
25 -.66 -.74 -.78 -.40 .00 .02 .16
20 -.47 -.62 -.76 -.46 -.30 -.34 .38
15 -.37 -.35 -.47 -.60 -.34 .76 .84
10 .75 .45 .43 .15 .59 .68 .48 .77
5 -.53 -.86 -.80 -.62 -.12
0 -.79 -.83 -.94 -.96
-5 -.29 -.70
-10 -.83
-15
-20
-25

Figure 4

CLOUD AMOUNT ANOMALIES
vs.
VORTICITY ANOMALIES

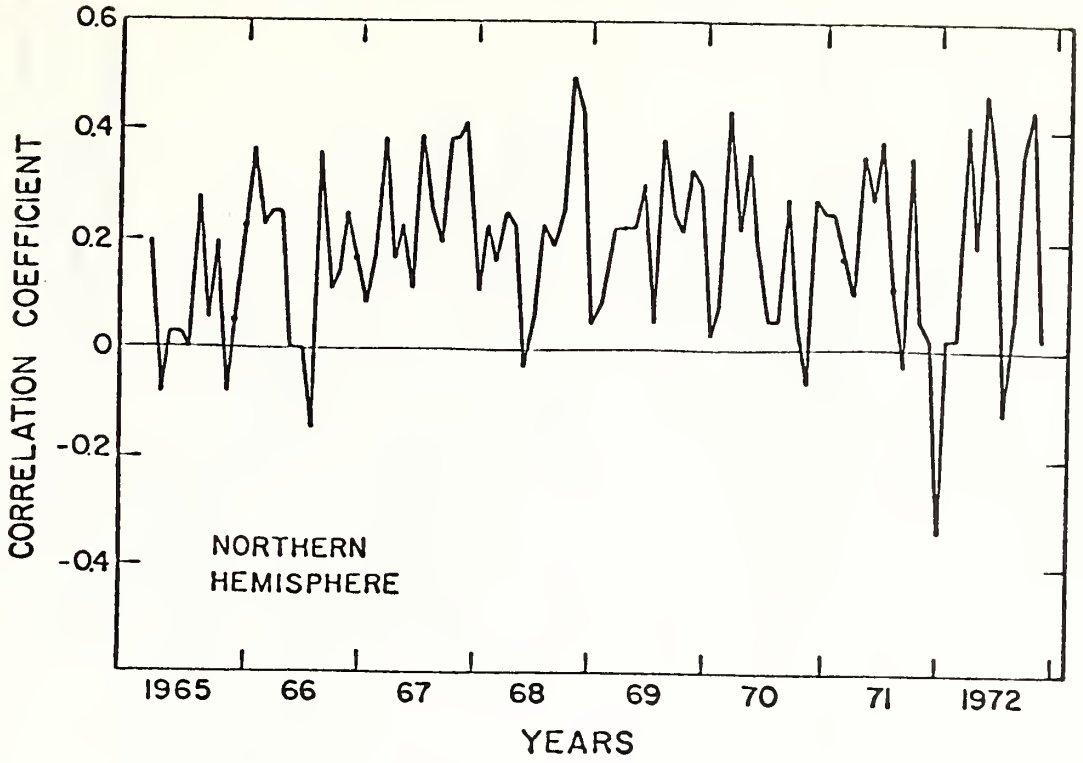

Mean	σ	95% confidence interval for mean
.19	.16	.15 - .22

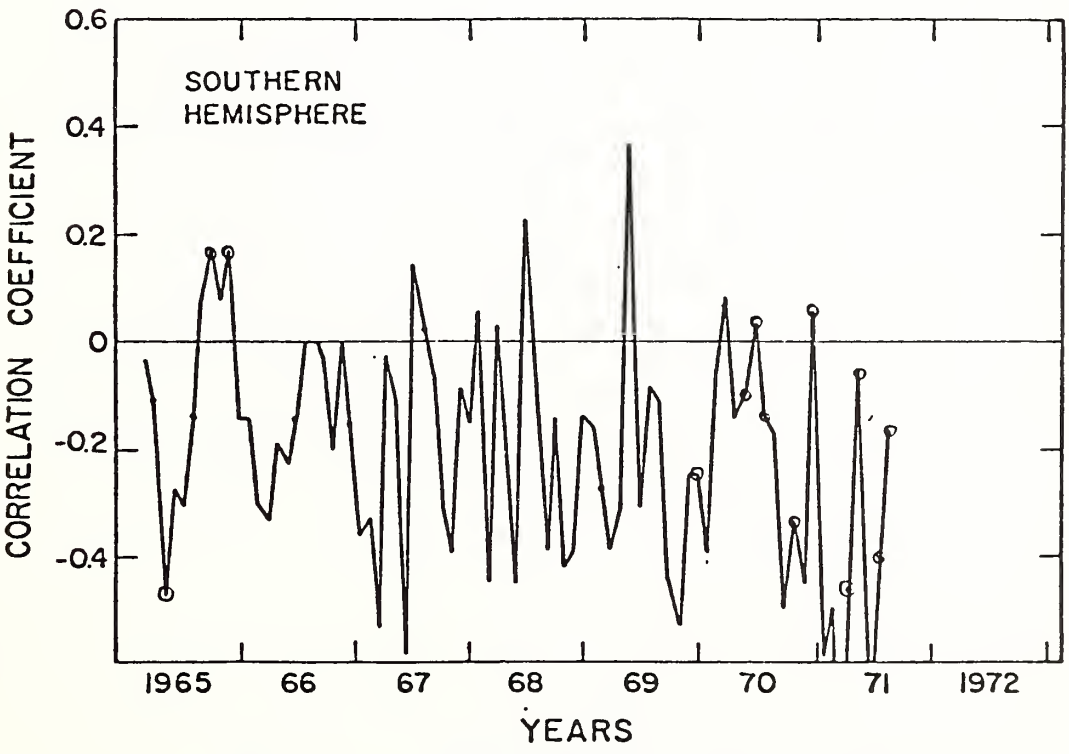

Mean	σ	95% confidence interval for mean
-.20	.22	-.25 - -.15

(Correlations using < 21 pairs are circled)

 Figure 5

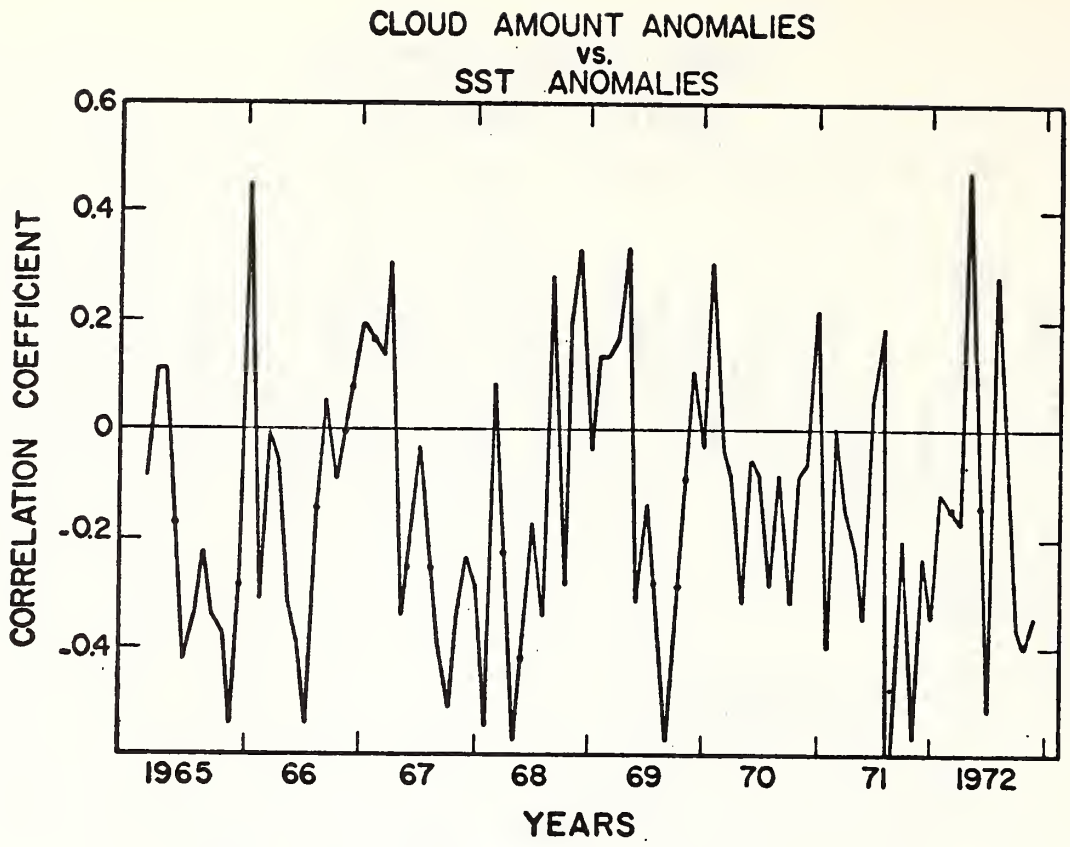

MEAN	σ	95% confidence interval for mean
-.10	.23	-.15 - -.04

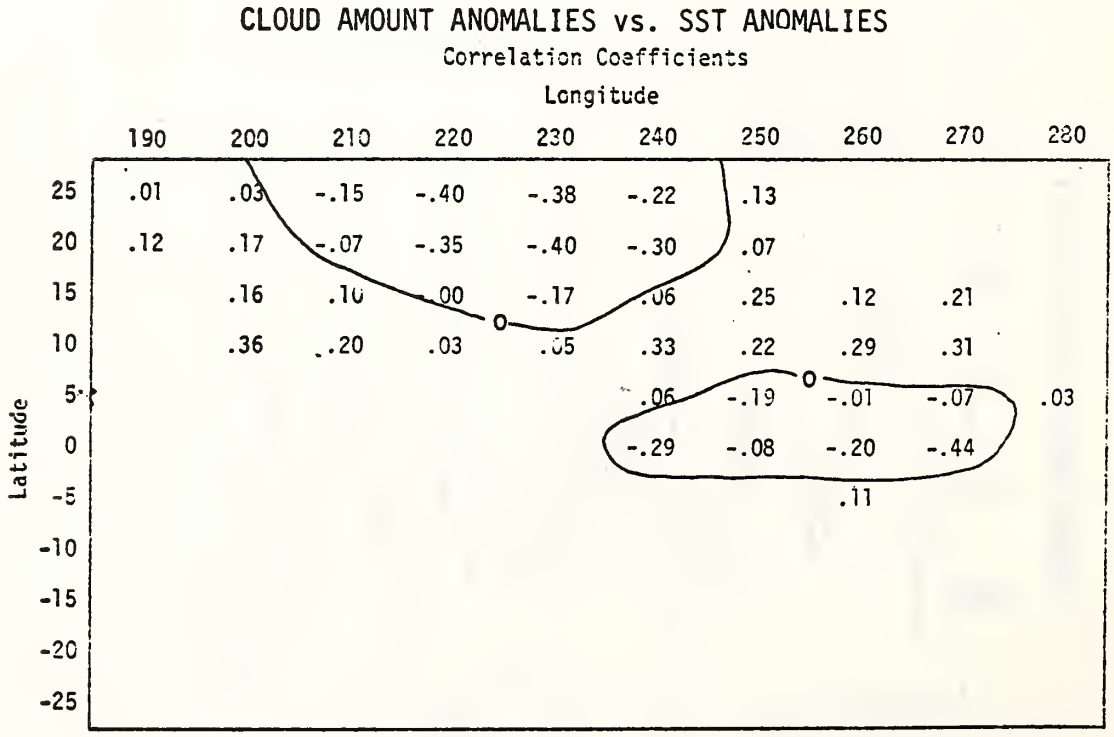

Figure 6

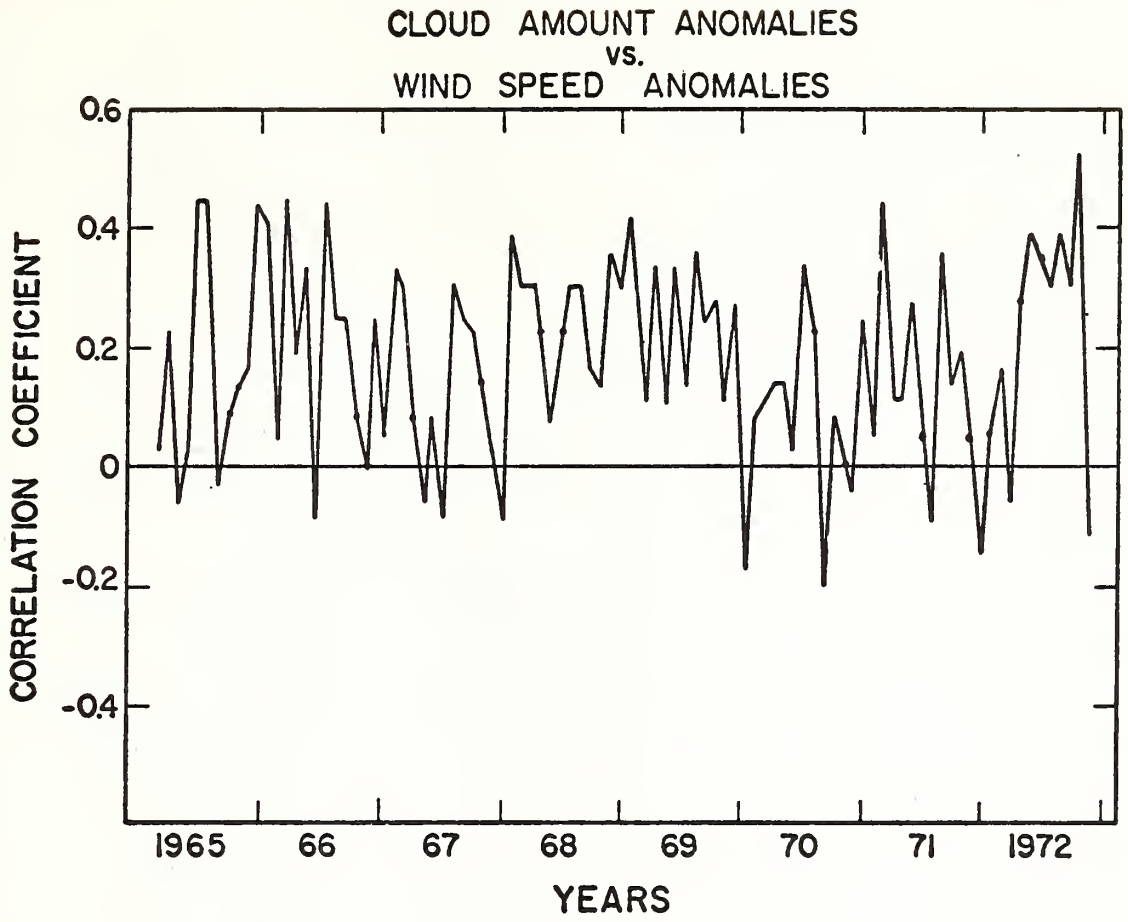

Mean	σ	95% confidence interval for mean
.18	.17	.15 - .21

Figure 7

a) WINTER DEVIATIONS OF SST V. DEVIATIONS OF CLOUD AMOUNT

Correlation Coefficients

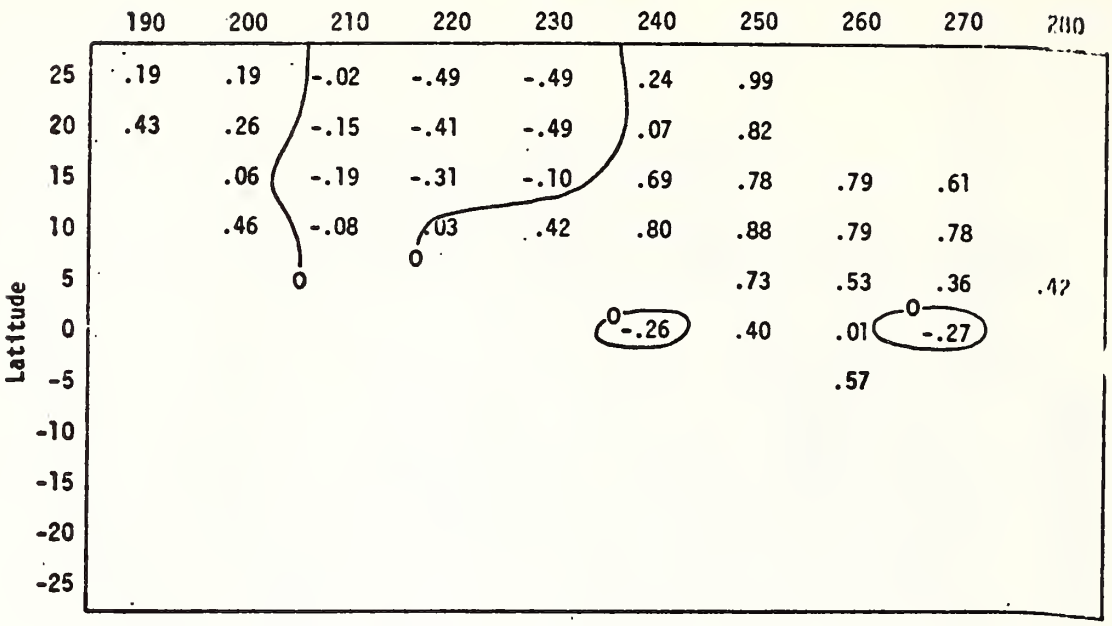

b) SUMMER DEVIATIONS OF SST V. DEVIATIONS OF CLOUD AMOUNT

Correlation Coefficients

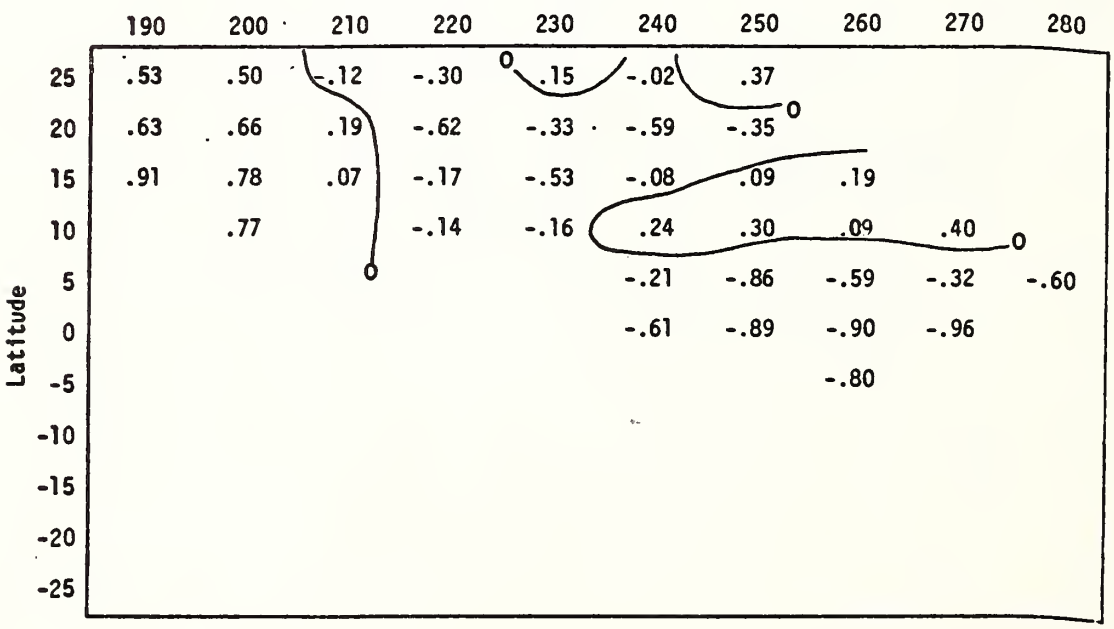

Figure 8

c)

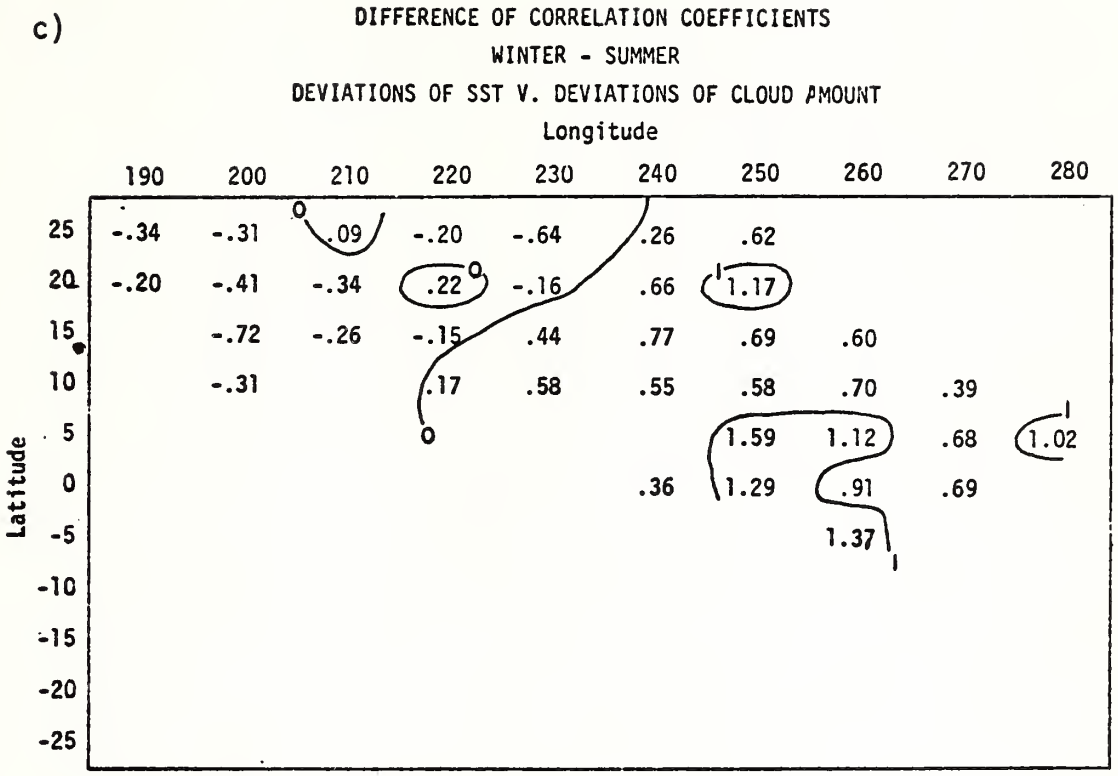
DIFFERENCE OF CORRELATION COEFFICIENTS
WINTER - SUMMER
DEVIATIONS OF SST V. DEVIATIONS OF CLOUD AMOUNT
Longitude
190 200 210 220 230 240 250 260 270 280
Latitude
25 -.34 -.31 .09 -.20 -.64 .26 .62
20 -.20 -.41 -.34 .22 -.16 .66 1.17
15 -.72 -.26 -.15 .44 .77 .69 .60
10 -.31 .17 .58 .55 .58 .70 .39
5 1.59 1.12 .68 1.02
0 .36 1.29 .91 .69
-5 1.37
-10
-15
-20
-25

Figure 8

Ocean Variability and Climate Change

J. O. Fletcher
NOAA/ERL, Boulder, Colorado

The ponderous ocean, integrator of atmospheric behavior, should reflect climatic behavior more coherently than does the atmosphere.

The 100 year marine data set (1861-1960) for the Pacific and Indian ocean areas is being examined to identify the nature of significant climatic changes and the coherence of related sea surface temperature (SST) anomalies in time and space. Highlights of preliminary findings are:

1. The SST field exhibits two main modes of fluctuation.

2. One mode is identified with short periods of anomalous warmth over the eastern equatorial pacific and occurs at irregular intervals (3-15 years). One manifestation of this recurring anomaly is the "El Nino" phenomenon but coherent behavior is apparent over the entire pacific basin and the central Indian ocean. Temporal coherence is strong from more than one year before the maximum to about a half year after.

3. The other mode of SST fluctuation appears to span more than a century so the inference that it is a recurring mode is drawn from proxy data spanning longer periods (such as runoff of the Nile river).

However, its remarkable coherence in space and time is reflected in the 1860-1960 data set as follows: Before 1870 SST was generally warmer than the century average over most of the oceans, especially the circumpolar current, eastern Pacific and North Pacific. In this generally warm ocean there appeared in 1870 a cold anomaly around southern New Zealand, which persisted and spread eastward and northward across the south Pacific during the following 45 years. Less distinct but similar anomaly patterns also developed in the north Pacific. This cooling trend intensified after 1900, reaching a climax about 1916, at which time warm anomalies suddenly appeared at the same locations and subsequently spread in the same patterns as did the previous cold anomalies. The warm anomalies appeared in 1916 (cold in 1870) intensified in 1940 (cold in 1900) and continued to the end of the data set (1960) averaged over the whole ocean, temperatures were warmer before 1900 and after 1940, cooler between 1900 and 1940. This cool ocean period coincides with the much discussed northern hemisphere "climatic warming". The two modes interact. During periods of cool ocean at 0-30^{0} lat (1900-1940) the El Nino mode anomaly occurs infrequently. During periods of warmer ocean it occurs more frequently. From Nile runoff data, the inferred counterpart of the 1900 change of climatic state is about 1780 (120 year). From SST

data through 1976 it appears that the cold anomaly originating in 1870 may be repeating in 1975 (105 year) but later data is needed to evaluate this.

The marine data set also includes wind direction and force. The following gross changes in the wind fields correspond to the SST changes described. Before 1870 wind was stronger (than the mean) nearly everywhere, about 20% in the circumpolar westerlies, over 50% in the western Pacific monsoon region. The main features of the circulation were farther north than normal in both hemispheres. After 1870 the stronger winds in the monsoon region but the westerlies and subtropical highs remained stronger than normal until about 1900. After 1900 the winds weakened generally, especially the southern hemisphere westerlies in the Indian ocean sector. The weakening of the wind field climaxed during the 1918-1938 period, with the westerlies 10-15% below normal in both hemispheres. In 1940-60 the wind field strengthened generally but the southern westerlies remained 10-15% down.

Sea-Air Interaction at the Pole-tide Frequency: A Preliminary Report

T.B. Starr, R.A. Bryson and J.E. Kutzbach
Center for Climatic Research, Institute for Environmental Studies
University of Wisconsin, Madison, Wisconsin 53706

Maximum monthly sea-level pressure anomalies at the pole-tide (Chandler) frequency have been found by Bryson and Starr (1977) to be at higher mid-latitudes in the eastern parts of the oceans, especially the North Sea-Scandinavia area. The work of Kutzbach, Chervin and Houghton (1977) suggests that large anomalies in those areas can be related to sea surface temperature anomalies in the western parts of the oceans. Assuming that this mechanism is operative at the pole-tide frequency, one might hypothesize that there should be a sea surface temperature variation at the same frequency. This report is on the preliminary results of an investigation of the hypothesized relation.

The raw material for the study was a long set of monthly mean sea surface temperature data by ocean squares.

Fourteen squares from the Pacific eastern and western edges were chosen on the basis of completeness and quantity of data (60 years), and fourteen more were chosen reaching across the North Atlantic from Labrador to the North Sea (72 years).

Fast fourier transform spectra were calculated for the 28 time series. Most of the spectra showed more-than-expected variance at both the a priori specified Chandler and Chandler alias frequency bands (Table 1). In a majority of the spectra these concentrations of variance were significant beyond the 95% level compared to a white noise hypothesis with "trend" frequencies longer than 1 cy/15 yrs excluded. This seemed to be true also when reddening of the spectra was accounted for by excluding intra-annual variance.

These results are consistent with the angular momentum conservation mechanism suggested by Bryson and Starr (op. cit.). If that mechanism is valid there should also be a strong phase shift across the oceans at the pole-tide frequencies for the mechanism requires lateral shifts of water masses. Such a phase shift was found. The amplitude of the thermal wave at the pole tide frequencies is also consistent in order of magnitude with the calculated lateral shifts and observed temperature gradients.

References

Bryson, R. A. and T. B. Starr, 1977: "Chandler Tides in the Atmosphere," J. Atm. Sci., 34:1975-1986.

Kutzbach, J. E., R. M. Chervin, and D. D. Houghton, 1977: "Response of the NCAR General Circulation Model to Prescribed Changes in Ocean Surface Temperature. Part I: Mid-Latitude Changes," J. Atm. Sci., 34:1200-1213.

Table 1. Chandler Band Signature in Monthly Sea Surface Temperatures 1900-1960

	AREA	LAT	Ratio of Chandler Band Variance to Expected Variance*	
			Fundamentals	Aliases
19	Off Honshu	30-40	4.0	10.0
18	Off Kyushu	30-40	2.7	4.5
16	Yellow Sea	30-40	2.2	17.8
29	Off Taiwan	20-30	4.4	7.8
42	S. China Sea-Central	10-20	1.7	5.0
52	S. China-Sulu-Celebes Seas	0-10	2.3	6.2
51	S. China Sea-Gulf of Siam	0-10	1.0	10.0
14	Wash-Ore--Offshore	40-50	4.2	8.3
15	Wash-Ore--Onshore	40-50	3.1	9.2
27	Calif--Offshore	30-40	1.5	7.7
28	Calif--Onshore	30-40	1.7	5.0
87	Great Austral Bight	30-40	1.0	3.8
88	Tasman Sea	30-40	1.4	1.7
79	Off Queensland	20-30	1.0	2.0

*Variance at periods of 20 y and longer removed.

Interannual Sea Surface Temperature Variations As Related to Severe North American Winters

by

Arthur V. Douglas

Climatology Program
Department of Geography
University of Nebraska
Lincoln, Nebraska 68588

The unusually cold winters of 1976-1977 and 1977-1978 in the central and eastern United States have been linked, inpart, to anomalous sea surface temperatures in the North Pacific. The purpose of this report is to demonstrate that most of the severe winters since 1904 have been associated with similar oceanic states.

In order to select winters with comparable conditions in the United States,separate eigenvector analyses were run on monthly temperature data for December, January, and February. In all cases the first eigenvector of monthly temperature contrasts conditions in the eastern United States with conditions along the west coast. This is illustrated in Figure 1. An examination of the time coefficients for the eigenvectors indicates that eigenvector 1 for December is poorly correlated with eigenvector 1 for subsequent months. As a result of this lack of persistence between December and subsequent winter months, it was decided to narrow this study to the months of January and February.

The past two winters were characterized by high time coefficients for eigenvector 1 in January, and the winter of 1977-1978 was also characterized by an equally high time coefficient for eigenvector 3. The seven highest time coefficients for eigenvector 1 (positive) in either January or February were in 1912, 1918, 1929, 1936, 1940, 1977, and 1978. Data presented at the last climate diagnostics workshop indicated 1905 may have been very similar to these seven years, and thus it is included in this analysis. The January through February air temperature anomalies for these 8 years are presented in Figures 2-9.

Sea surface temperature anomalies for the Novembers prior to these cold winters are shown in Figures 2-9. Anomalously cold sea surface temperatures are noted in the subtropical North Pacific prior to each of the eight cold winters in the central and eastern United States. These

cold water pools suggest enhanced sea surface temperature gradients over the subtropical central North Pacific and possible increased atmospheric baroclinicity, frontogenesis, and cyclogenesis.

The relationship between subtropical central North Pacific sea surface temperatures and 700 mb heights is illustrated in Figure 10. In January below normal temperatures are usually associated with below normal 700 mb heights downstream. In addition, apparently colder than normal sea surface temperatures in the subtropical central North Pacific are associated with above normal heights along the west coast of North America. Farther downstream, a deepened continental trough is implied during the cold water years. The suggested teleconnections in Figure 10 are very similar to the events observed during the past two winters.

A correlation of November sea surface temperatures for the same location with subsequent January through February air temperatures (Figure 10) shows a striking resemblance to eigenvector 1 (Figure 1). It is suggested that most of the cold winters in the central and eastern United States were a partial result of the above air-sea interactions and downstream teleconnections.

LEGENDS TO FIGURES

Figure 1. The first and third eigenvectors of January temperatures in the United States. Period of analysis 1906-1978 for 32 stations.

Figure 2. Eastern North Pacific sea surface temperature anomalies for November 1904 (upper) and United States air temperature anomalies for January through February 1905 (lower). Sea surface temperature anomalies are based on the 23 year period 1949-71, and air temperature anomalies are based on the 40 year period 1938-77.

Figure 3. Same as Figure 2 except sea surface temperature anomalies are for November 1911, and air temperature anomalies are for January through February 1912.

Figure 4. Same as Figure 2 except sea surface temperature anomalies are for November 1917, and air temperature anomalies are for January through February 1918.

Figure 5. Same as Figure 2 except sea surface temperature anomalies are for November 1928, and air temperature anomalies are for January through February 1929.

Figure 6. Same as Figure 2 except sea surface temperature anomalies are for November 1935, and air temperature anomalies are for January through February 1936.

Figure 7. Same as Figure 2 except sea surface temperature anomalies are for November 1939, and air temperature anomalies are for January through February 1940.

Figure 8. Same as Figure 2 except sea surface temperature anomalies are for November 1976, and air temperature anomalies are for January through February 1977.

Figure 9. Same as Figure 2 except sea surface temperature anomalies are for November 1977, and air temperature anomalies are for January through February 1978.

Figure 10. Upper map shows the correlation between central North Pacific sea surface temperatures and 700 mb heights. Lower map shows the correlation between November sea surface temperatures and January through February United States air temperatures.

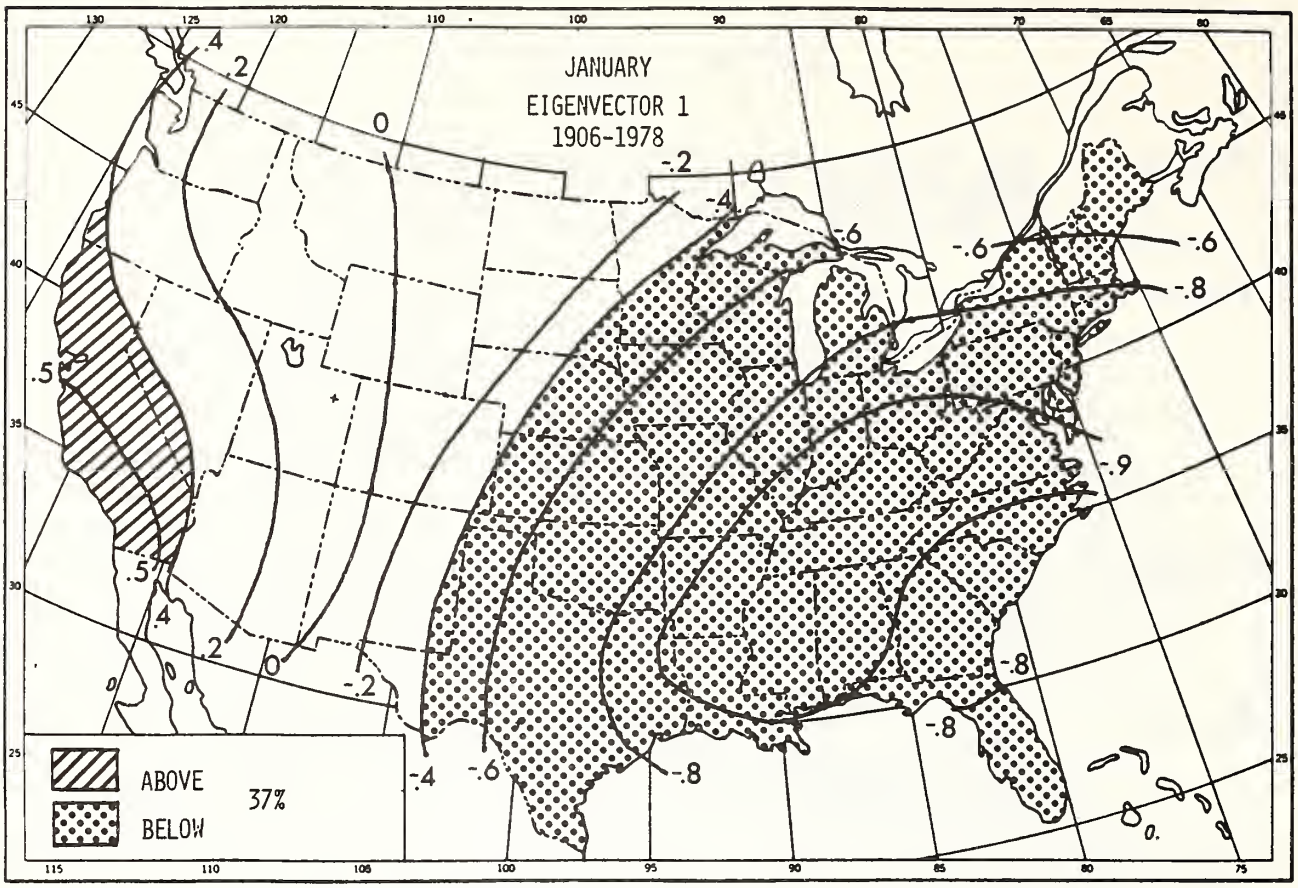
JANUARY
EIGENVECTOR 1
1906-1978
ABOVE
BELOW
37%

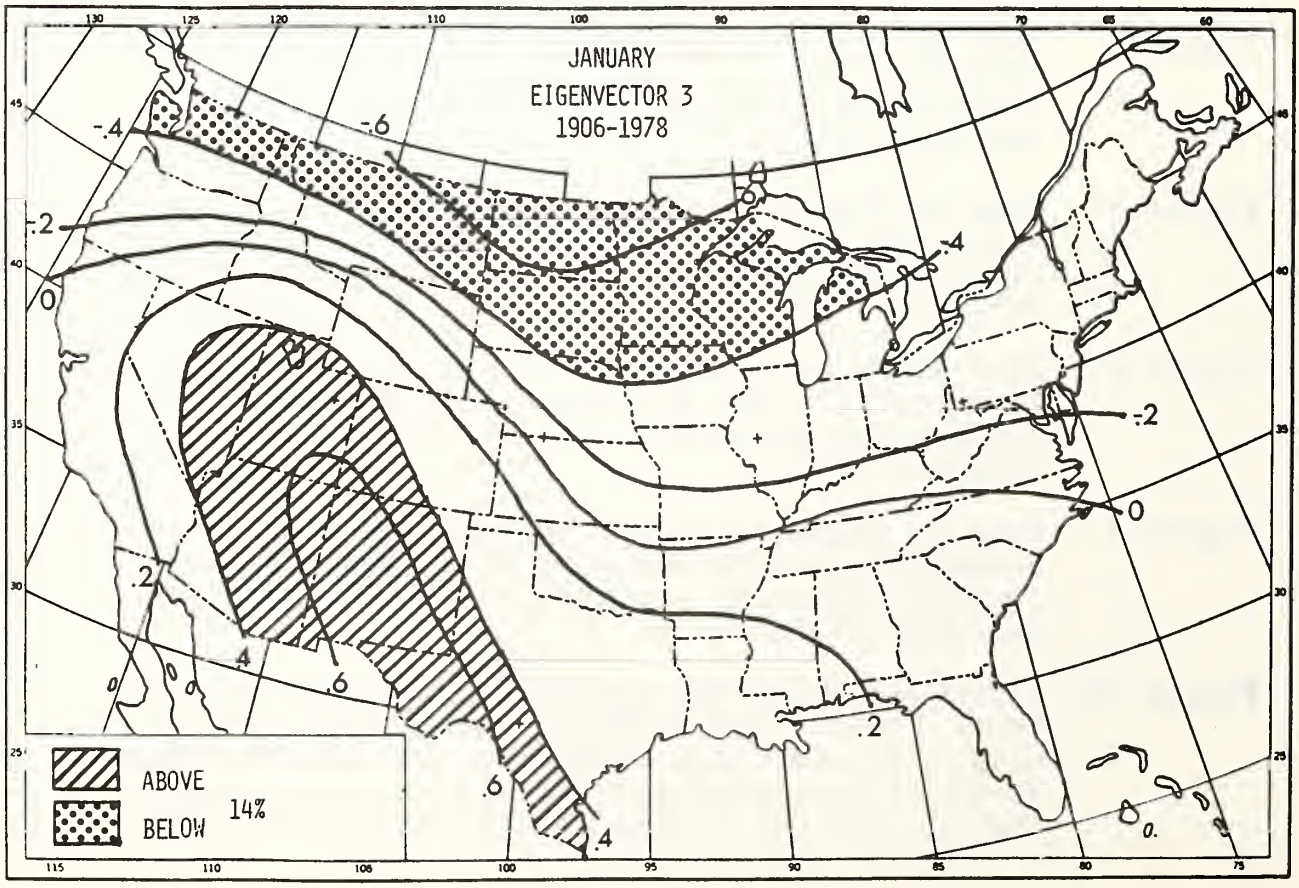
JANUARY
EIGENVECTOR 3
1906-1978
ABOVE
BELOW
14%

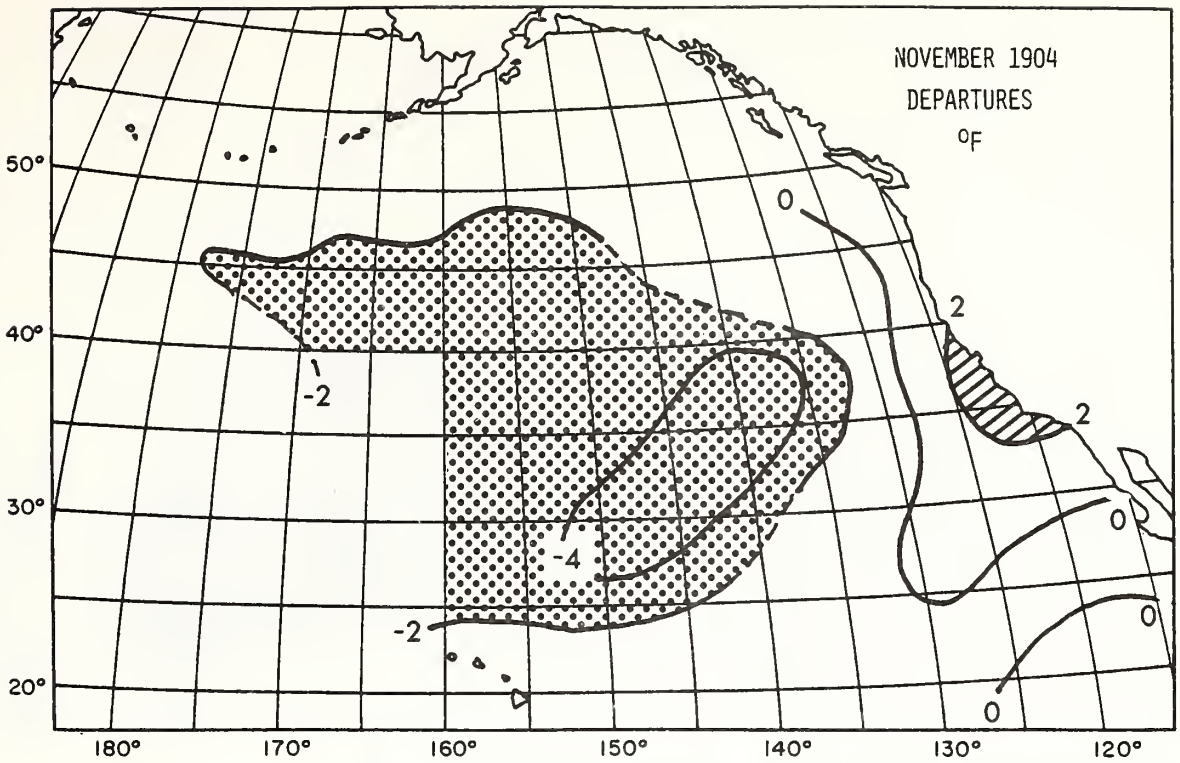
NOVEMBER 1904
DEPARTURES
°F
50°
40°
30°
20°
180°
170°
160°
150°
140°
130°
120°
0
2
2
-2
-4
-2
0
0
0

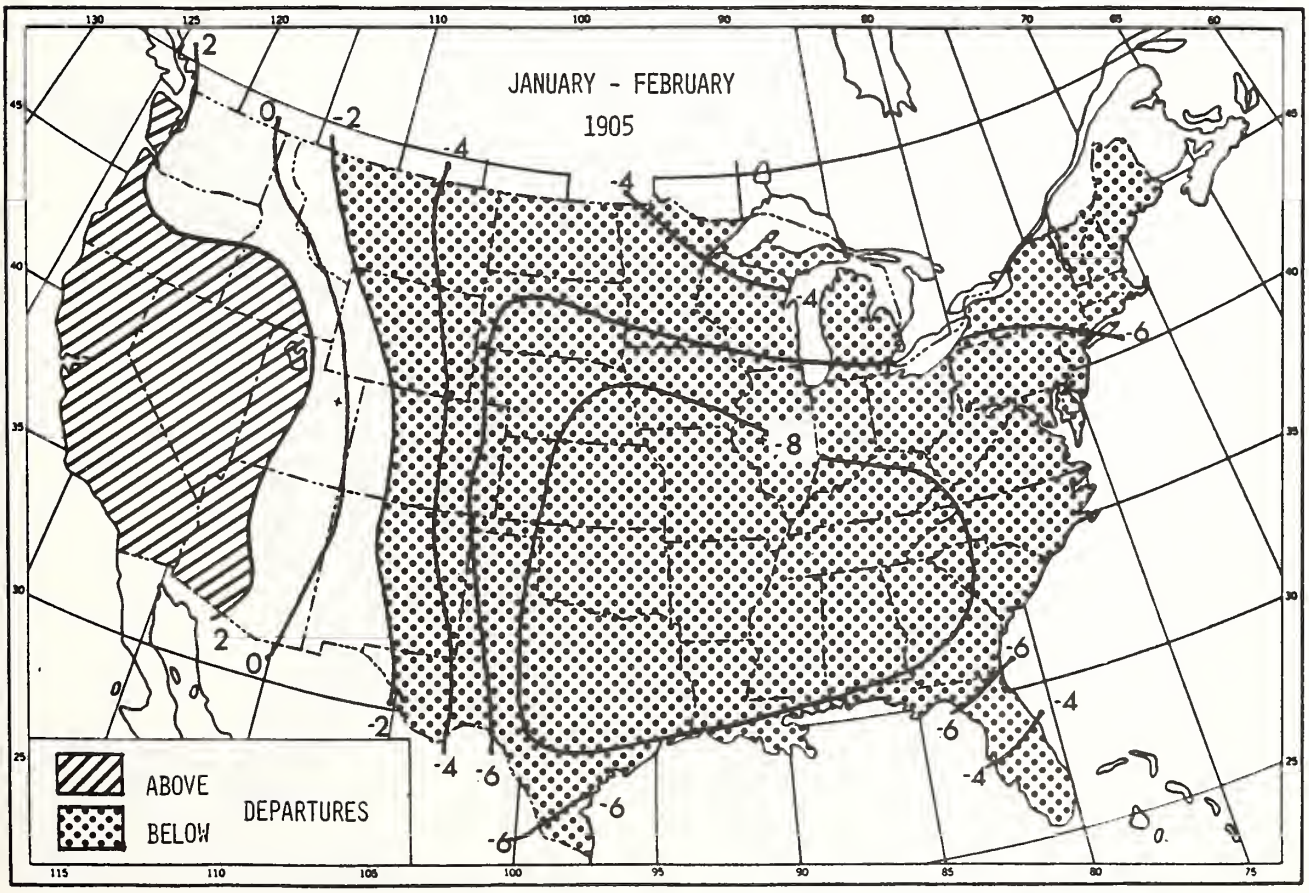
JANUARY - FEBRUARY
1905
ABOVE
BELOW
DEPARTURES
2
0
-2
-4
-4
-4
-6
-8
-6
-4
-6
-4
-6
-6
0.

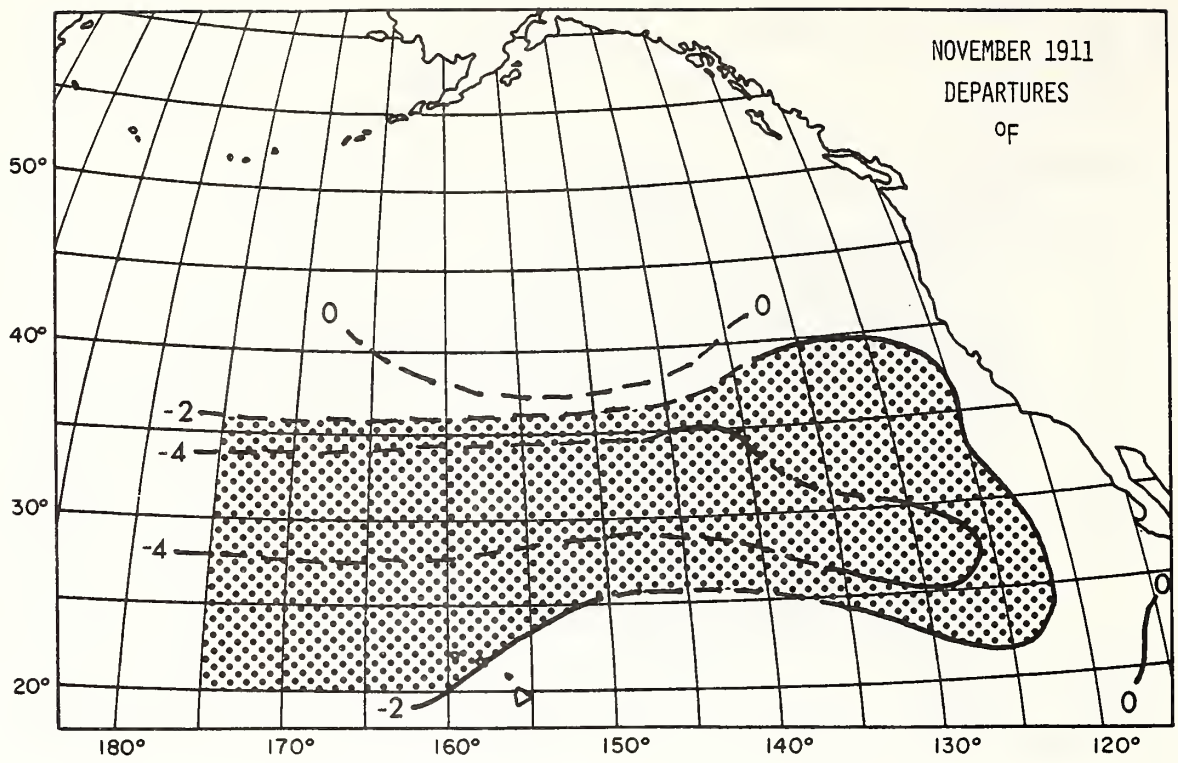
NOVEMBER 1911
DEPARTURES
°F
50°
40°
30°
20°
180°
170°
160°
150°
140°
130°
120°
0
-2
-4

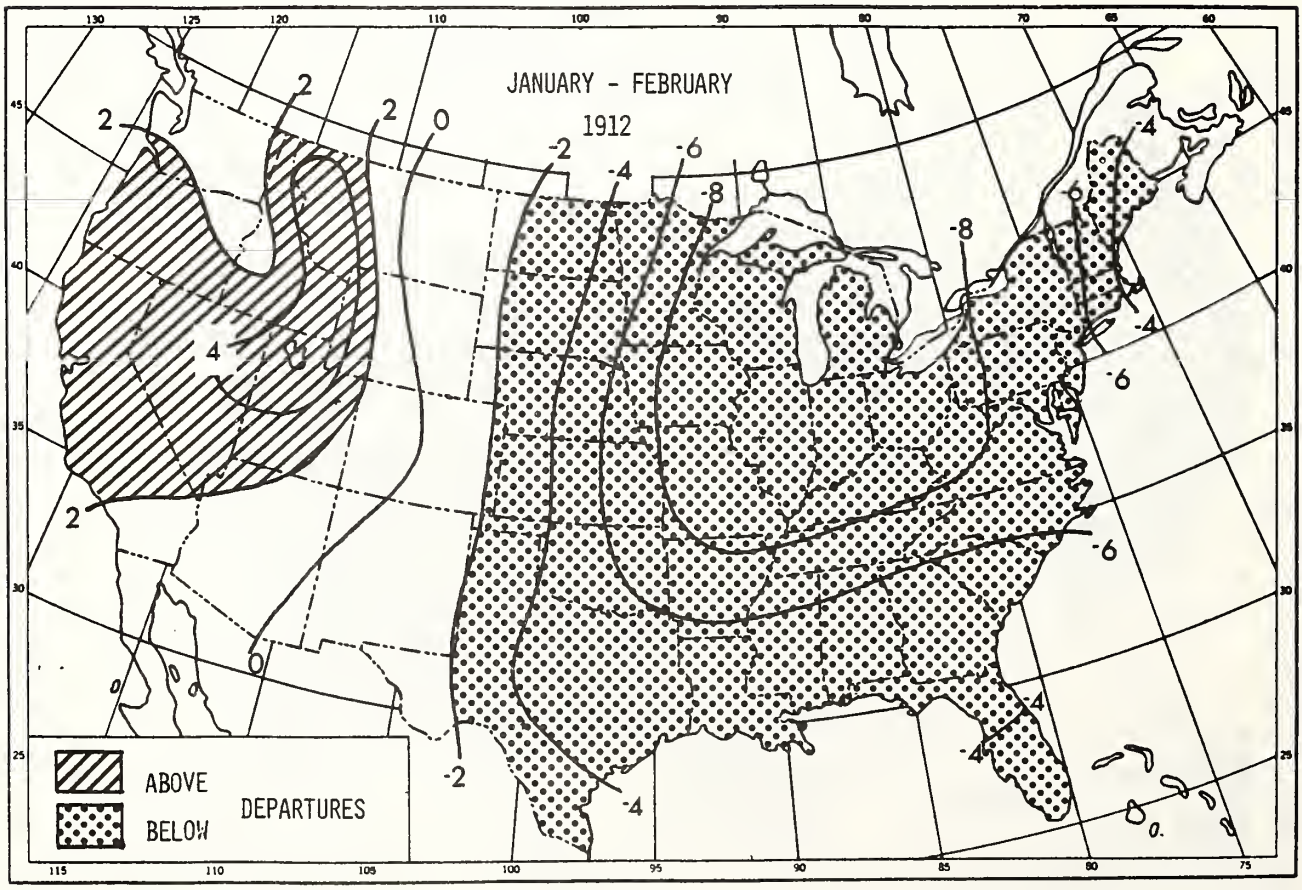
JANUARY - FEBRUARY
1912
ABOVE
BELOW
DEPARTURES

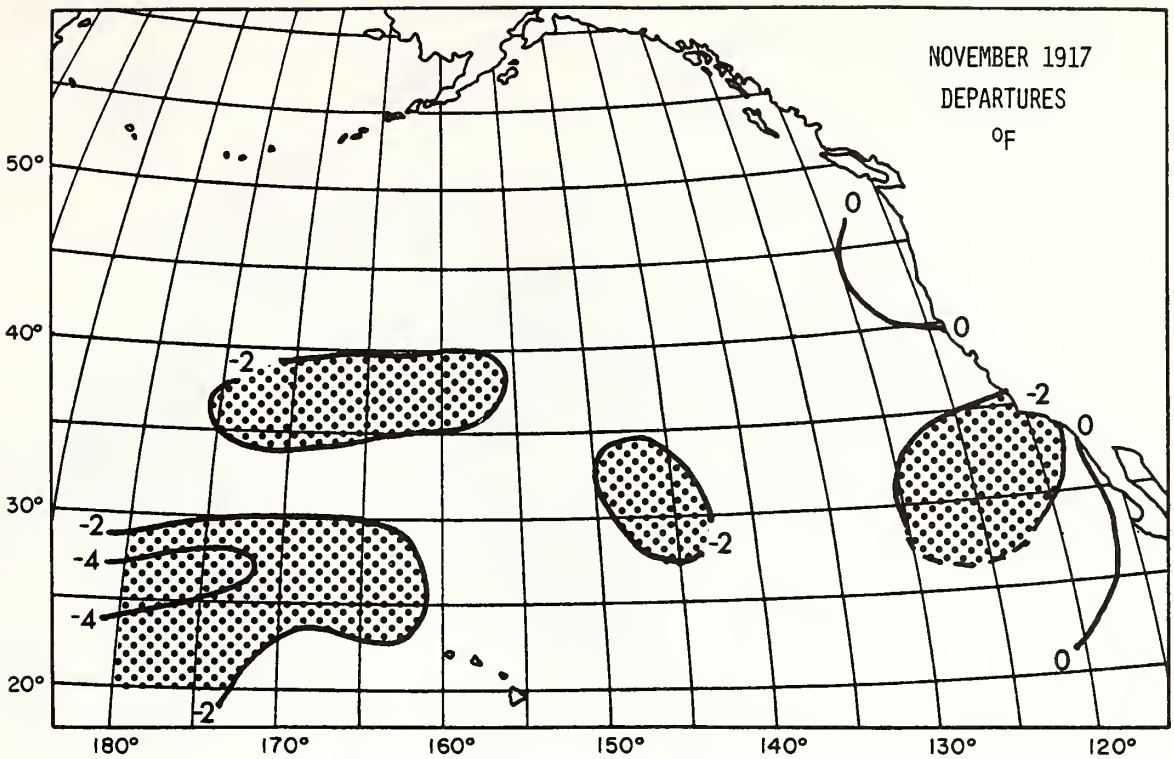
NOVEMBER 1917
DEPARTURES
°F
50°
40°
30°
20°
180°
170°
160°
150°
140°
130°
120°
0
-2
-4

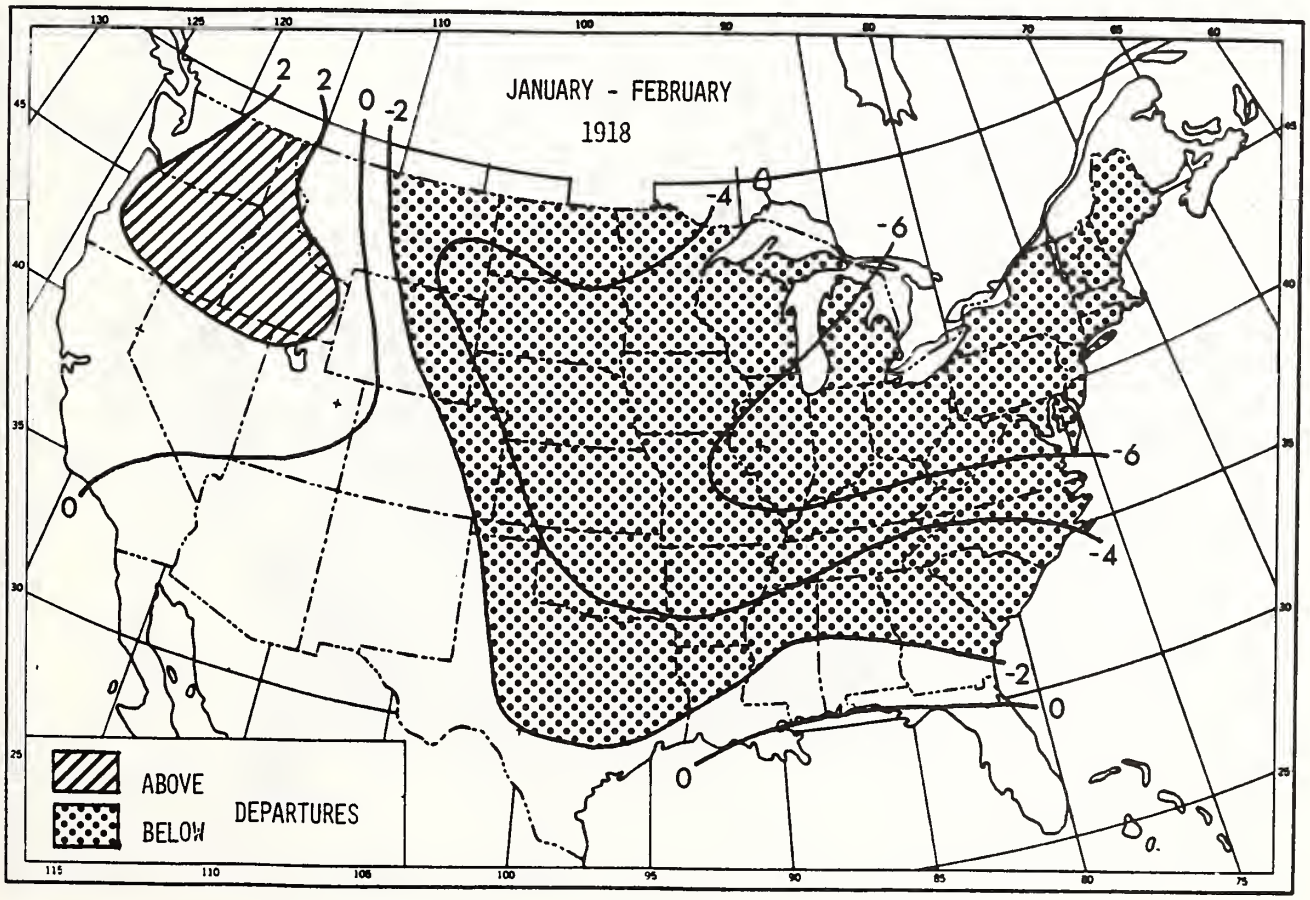
JANUARY - FEBRUARY
1918
2
0
-2
-4
-6
ABOVE
BELOW
DEPARTURES

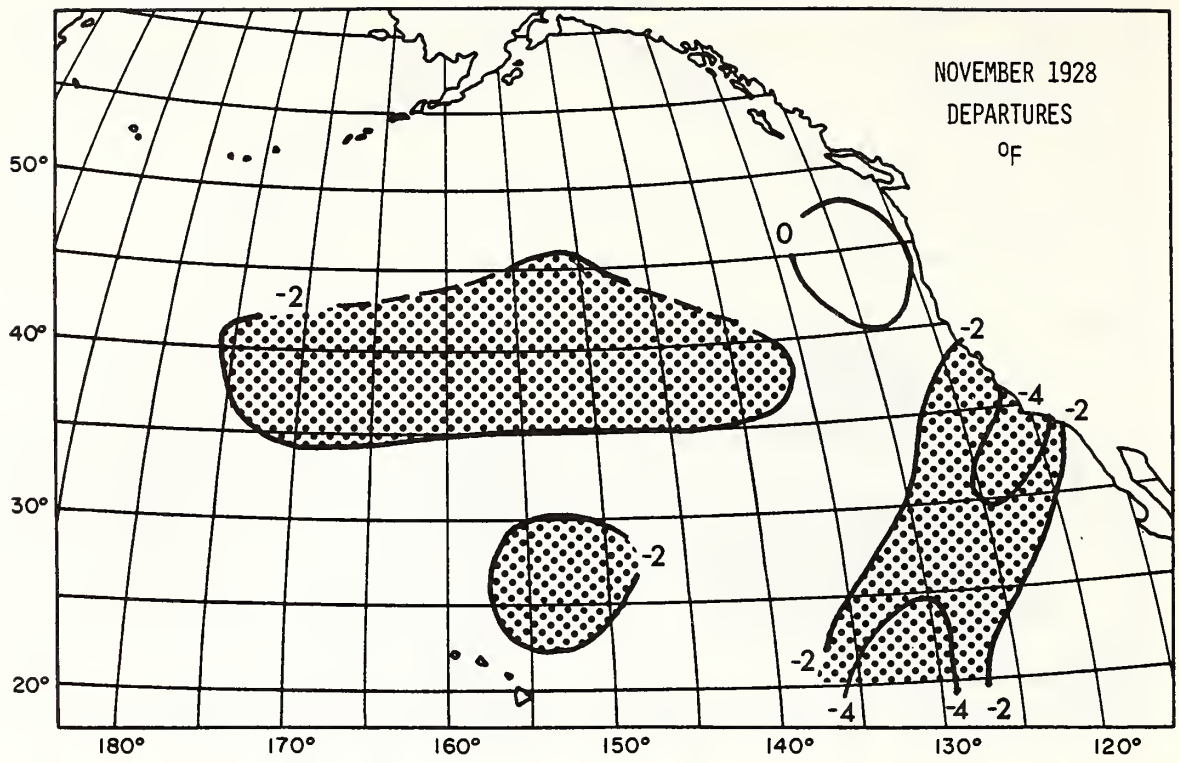
NOVEMBER 1928
DEPARTURES
°F
50°
40°
30°
20°
180°
170°
160°
150°
140°
130°
120°
0
-2
-2
-4
-2
-2
-2
-2
-4
-4
-2

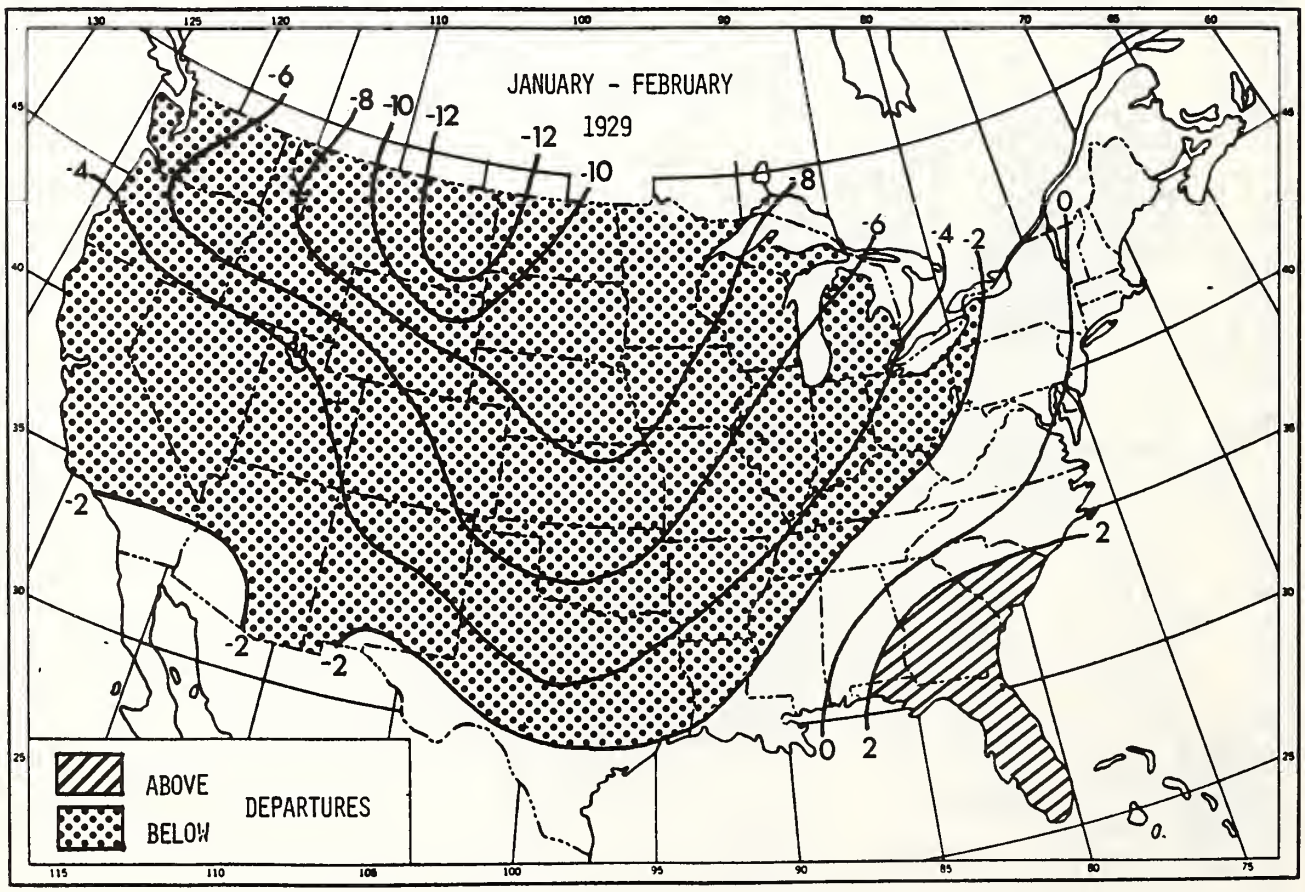
JANUARY - FEBRUARY
1929
-6
-8
-10
-12
-12
-10
-8
-4
-6
-4
-2
0
-2
-2
-2
2
0
2
ABOVE
BELOW
DEPARTURES

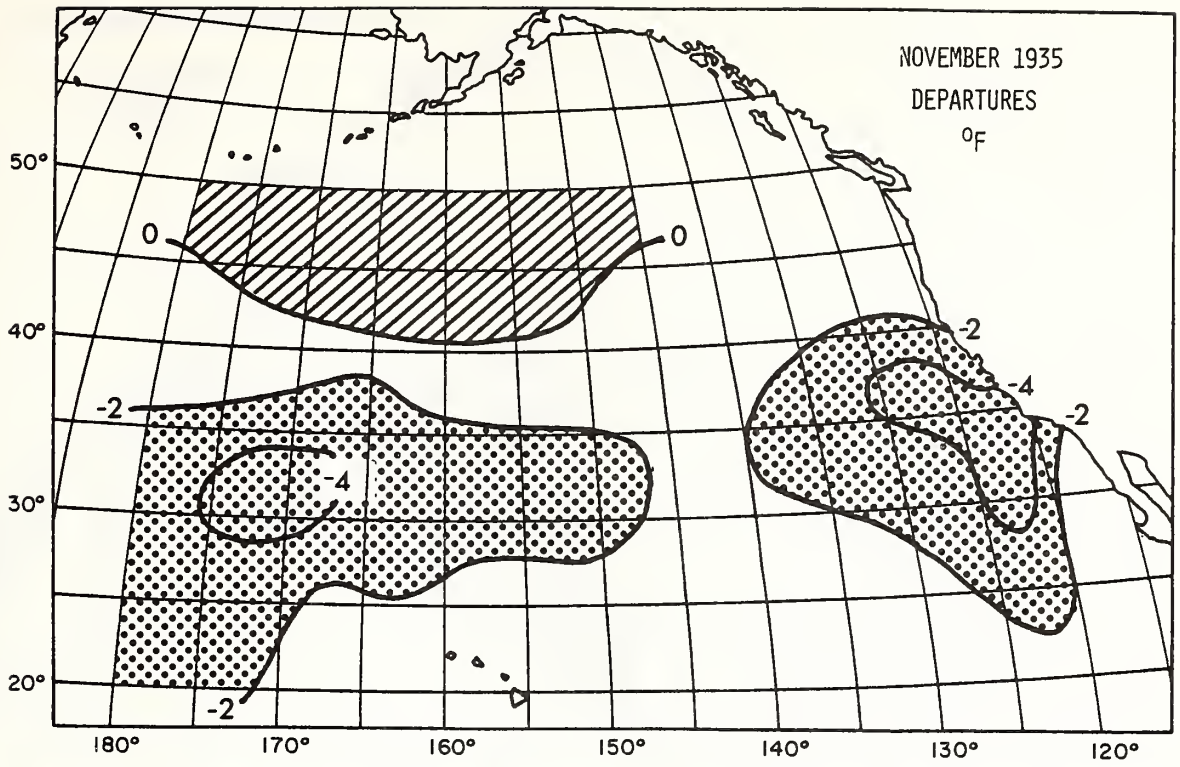
NOVEMBER 1935
DEPARTURES
°F
50°
40°
30°
20°
180°
170°
160°
150°
140°
130°
120°
0
0
-2
-4
-2
-4
-2
-2

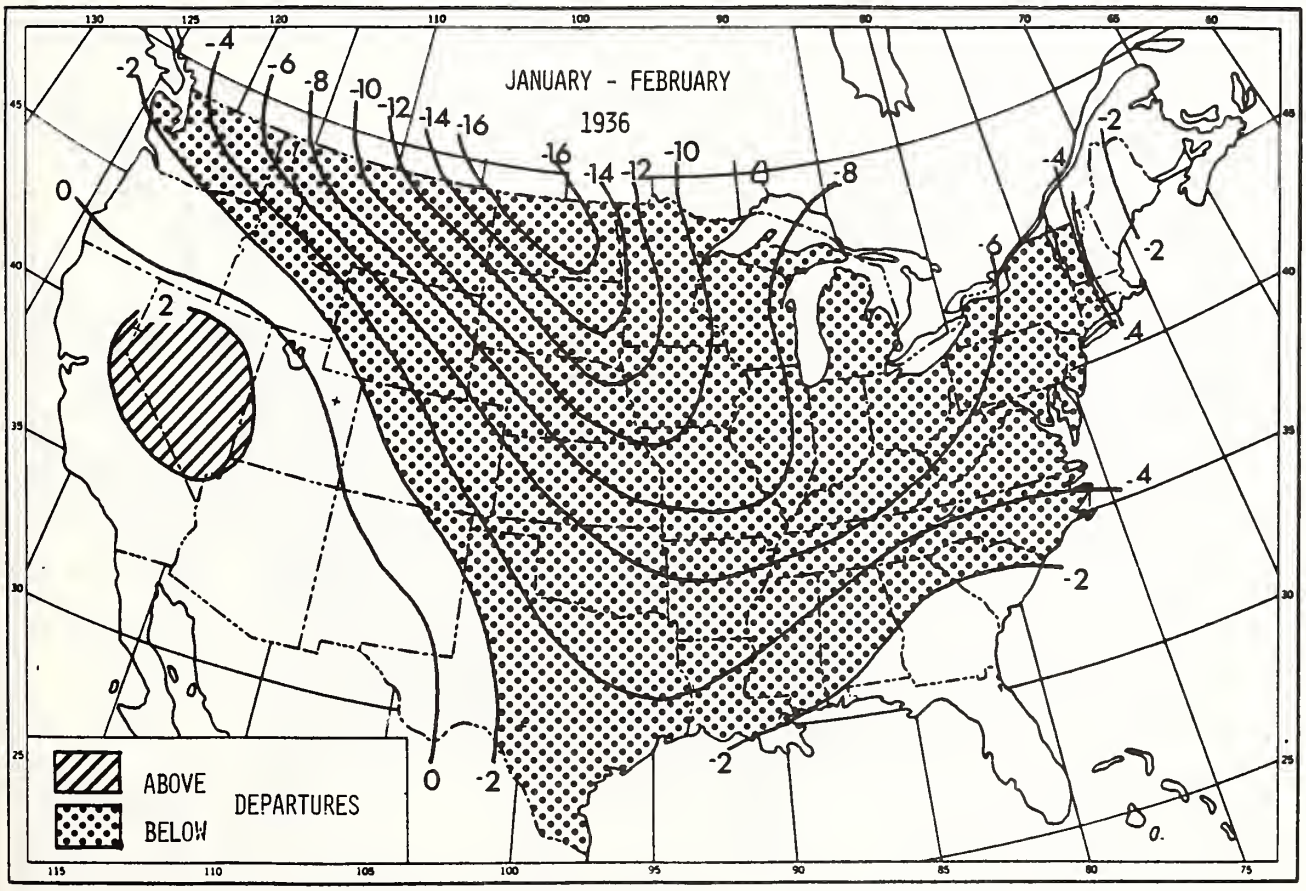
JANUARY - FEBRUARY
1936
ABOVE
BELOW
DEPARTURES
-2
-4
-6
-8
-10
-12
-14
-16
0
2

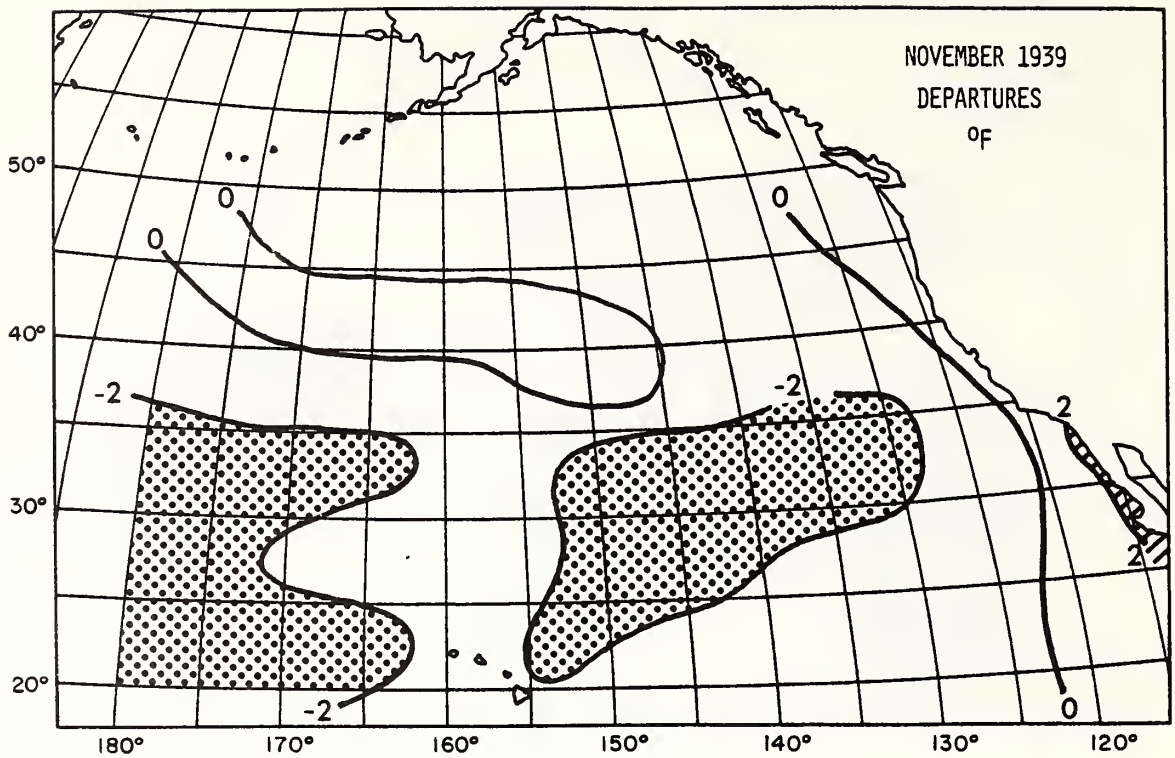
NOVEMBER 1939
DEPARTURES
°F
50°
40°
30°
20°
180°
170°
160°
150°
140°
130°
120°
0
-2
2

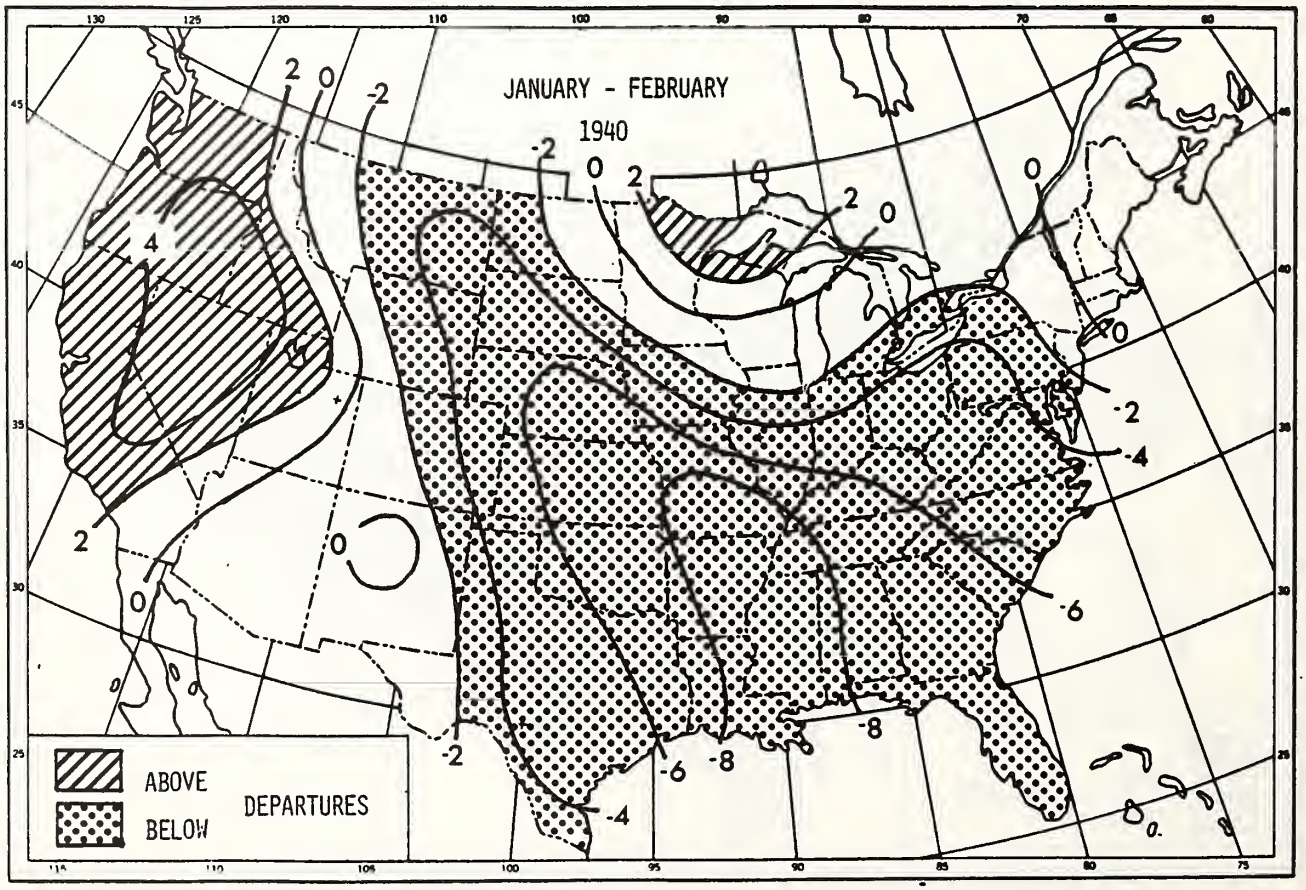
JANUARY - FEBRUARY
1940
ABOVE
BELOW
DEPARTURES
2
0
-2
4
-4
-6
-8

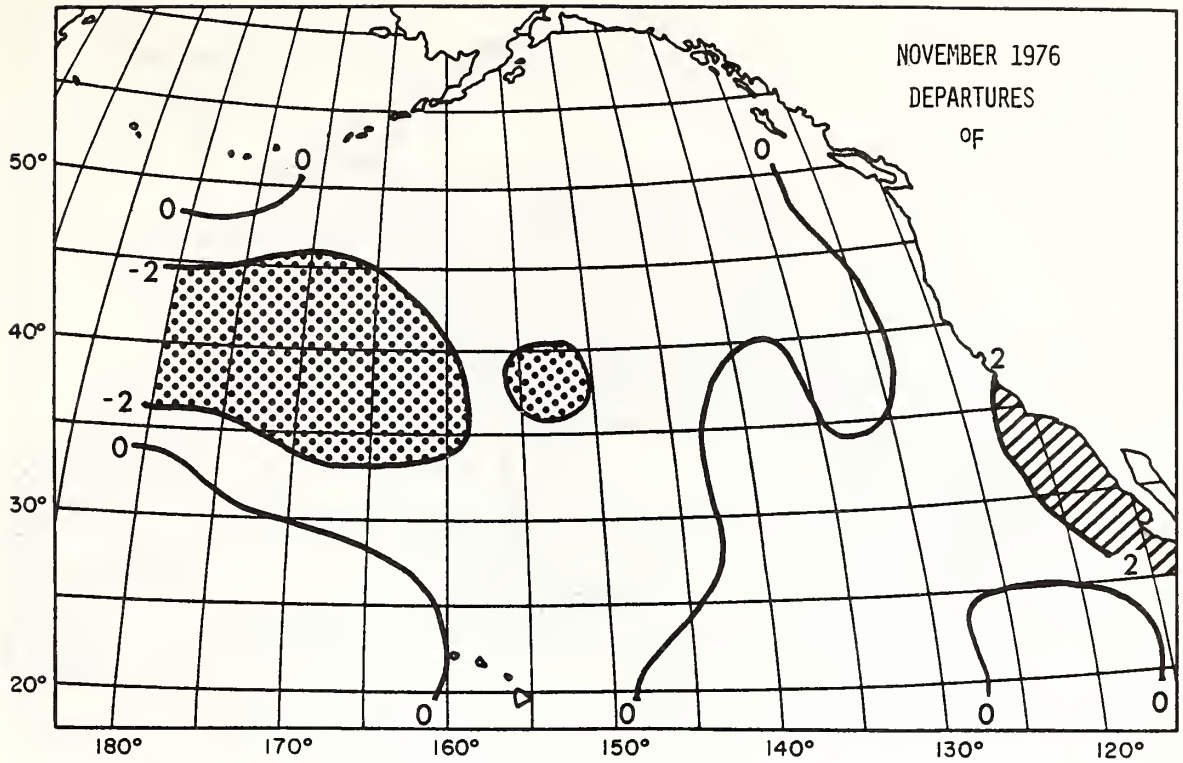
NOVEMBER 1976
DEPARTURES
°F
50°
40°
30°
20°
180°
170°
160°
150°
140°
130°
120°

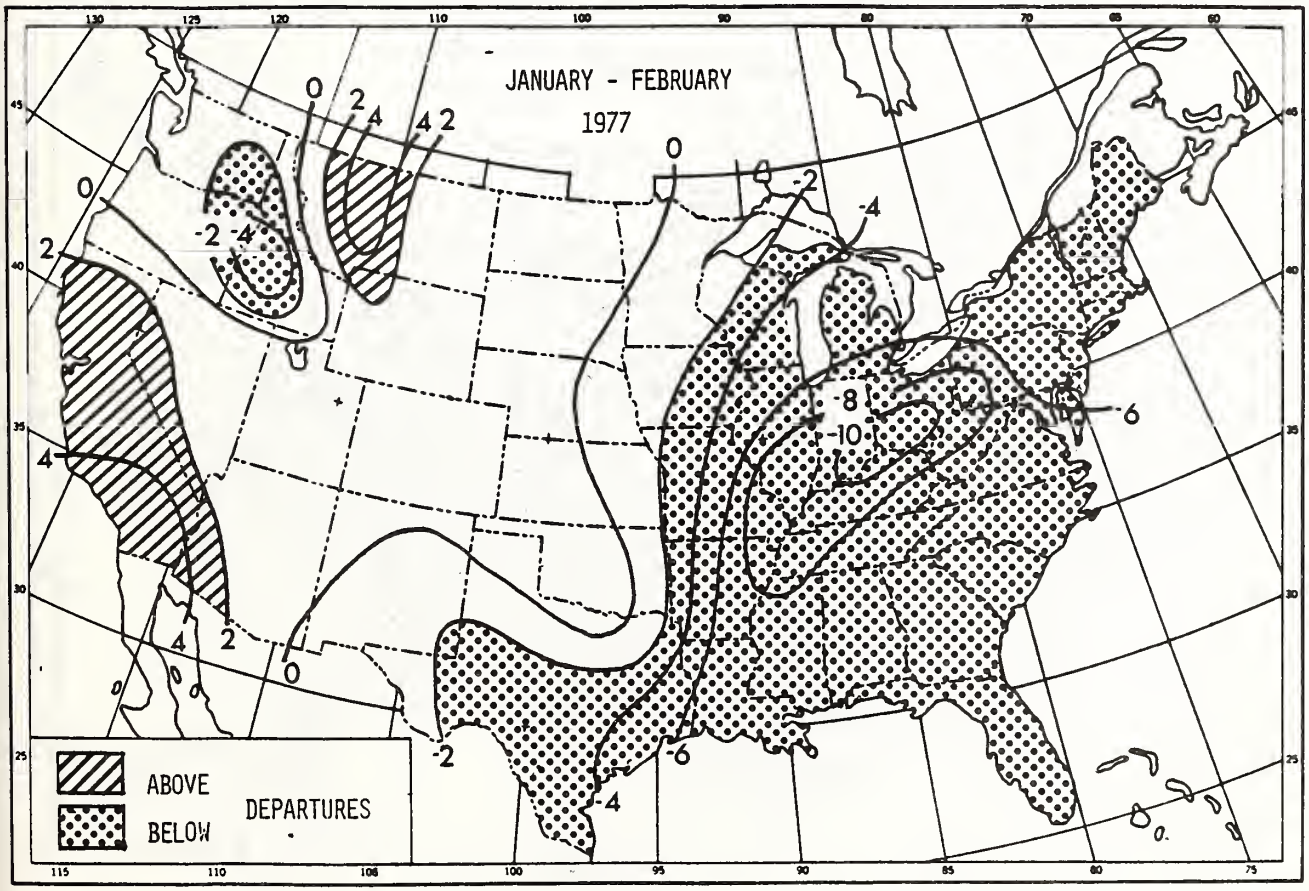
JANUARY - FEBRUARY
1977
ABOVE
BELOW
DEPARTURES

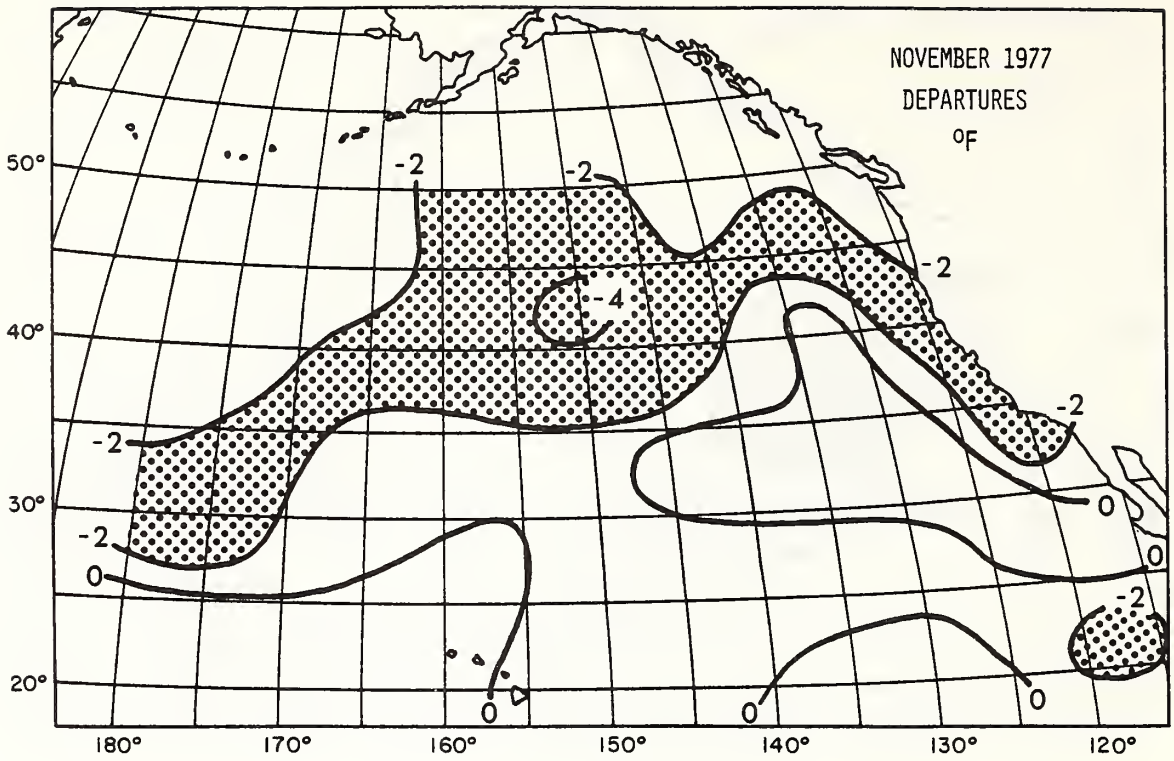
NOVEMBER 1977
DEPARTURES
°F
50°
40°
30°
20°
180°
170°
160°
150°
140°
130°
120°

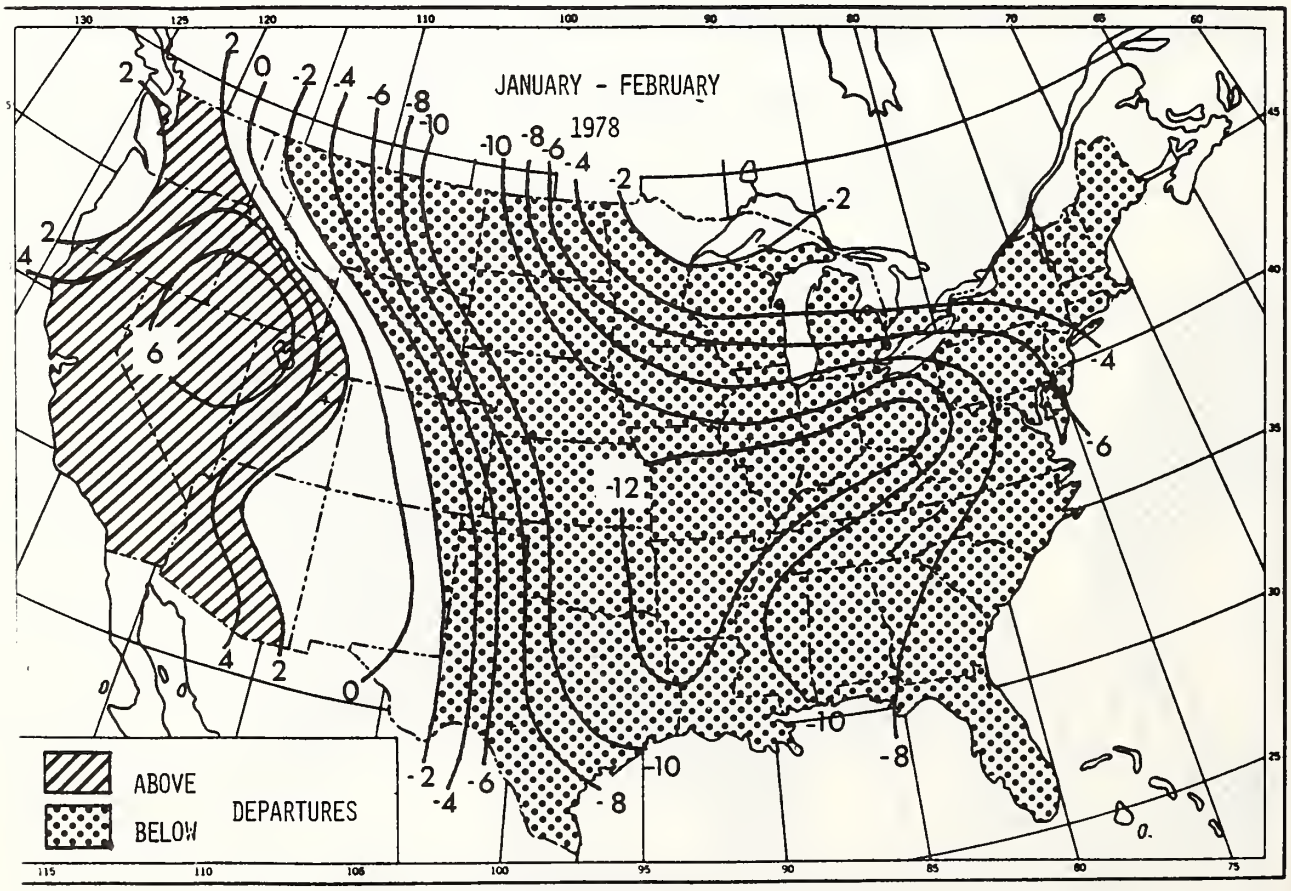
JANUARY - FEBRUARY
1978
ABOVE
BELOW
DEPARTURES

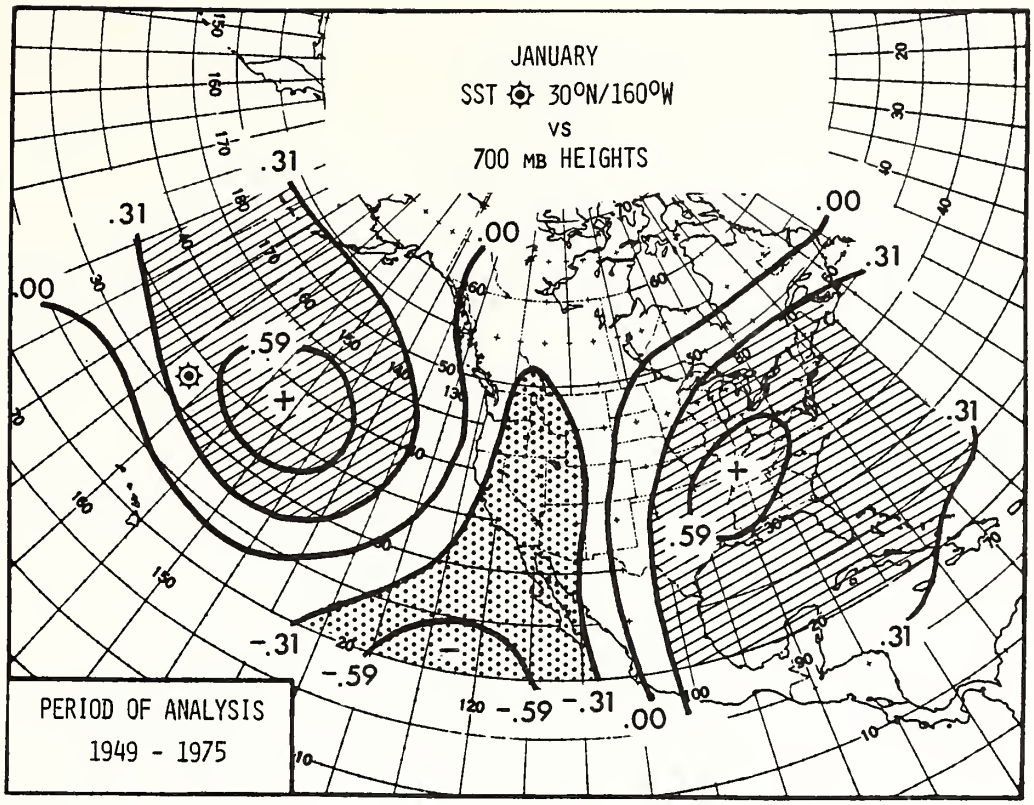
JANUARY
SST ☉ 30°N/160°W
vs
700 MB HEIGHTS
.31
.31
.00
.59
.00
.00
.31
.31
.59
.31
-.31
-.59
-.59
-.31
.00
PERIOD OF ANALYSIS
1949 - 1975

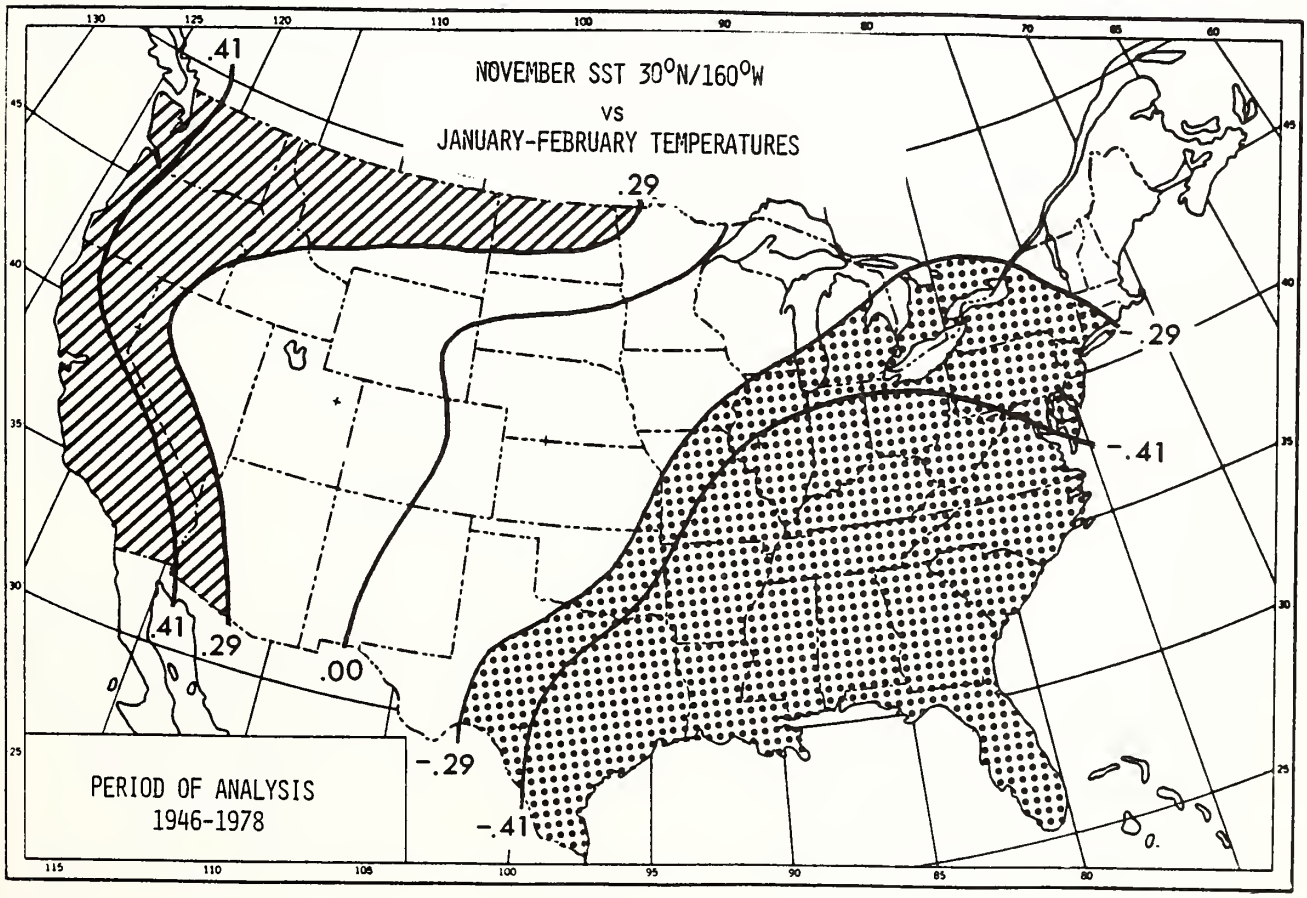
NOVEMBER SST 30°N/160°W
vs
JANUARY-FEBRUARY TEMPERATURES
.41
.29
.29
-.41
.41
.29
.00
-.29
-.41
PERIOD OF ANALYSIS
1946-1978

Sensitivity Study of the Annual Water Balance

Peter S. Eagleson
Massachusetts Institute of Technology
Cambridge, Massachusetts 02139

Soil moisture dynamics may be uncoupled from soil heat flow and from atmospheric dynamics by the expedient assumption that the land surface temperature, T_g, is an independent climatic variable. The instantaneous water balance is then governed by the conservation equation

$$i - e_T - y = \partial S/\partial t \tag{1}$$

and two soil moisture flux relations

$$y = y(s, t; \text{climate, soil}) \tag{2}$$

and

$$e_T = \begin{cases} e_T(s, t; \text{climate, soil, vegetation}), & e_T < e_p \\ e_p & \text{otherwise} \end{cases} \tag{3}$$

in which i = rainfall intensity; e_T = evapotranspiration rate; y = surface + groundwater runoff rate; S = water storage; t = time; s = moisture concentration in the soil boundary layer; e_p = potential evaporation rate.

Integrating Equations (2) and (3) over the respective storm and interstorm periods and using the probability density functions for the independent climatic variables allows estimation of the expected annual value of Eq. (1). This gives, for a <u>given climate, soil and vegetation</u>

$$E[P_A] = E[E_{T_A}(s_o)] + E[R_{s_A}(s_o)] + E[R_{g_A}(s_o)] \tag{4}$$

in which P_A = annual precipitation; E_{T_A} = annual evapotranspiration; R_{s_A} = annual surface runoff; R_{g_A} = annual groundwater runoff; and s_o = time average moisture concentration in the soil boundary layer.

In Figure 1, the bare soil evaporation (normalized by the potential evaporation) is presented as a function of the dimensionless climate-soil parameter

$$E = \frac{2\beta n K(1)\Psi(1)\phi_e}{\pi\, m\, \bar{e}_p^{\,2}}\, s_o^{(c+5)/2} \tag{5}$$

in which β = reciprocal of mean time between storms; n = effective soil porosity; K(1) = effective hydraulic conductivity of soil at saturation; $\Psi(1)$ = (extrapolated) soil moisture potential at saturation; ϕ_e = dimensionless diffusivity of soil; $m = -\, ds_o/d\Psi(s_o)$; $c = dK(s_o)/ds_o$.

Notice that as E gets large the evaporation, E_{T_A}, becomes climatically

limited by the potential evaporation, E_{p_A}, and is independent of the soil properties. On the other hand, when E gets small, E_{T_A} falls away from E_{p_A} due to limitations of water supply to the soil surface either by precipitation (small s_o as given by Eq. (4)) or by the inability of the soil to deliver moisture to the surface. For small E, evaporation is very sensitive to soil properties. This characteristic dominates water balance behavior as is illustrated in the following.

For a given set of climate, soil and vegetation parameters, Eq. (4) determines s_o which can then be reintroduced to evaluate each term of the water balance. In this way, the water balance sensitivity of bare soil (i.e., no vegetation) to changes in soil and climate parameters is explored as is illustrated in Figures 2 and 3. We will examine a sub-humid and an arid climate having the characteristics given in Table 1.

In Figure 2, the normalized water balance components of the two climates are compared for a range of saturated intrinsic soil permeabilities, k(1), and of soil pore disconnectedness, c. Moisture moves most easily for large k(1) and small c. Notice the insensitivity of E_{T_A} to soil properties in the sub-humid climate except where the soil is impermeable. In the arid case, E_{T_A} is extremely sensitive to the soil properties.

To illustrate the importance of the potential rate of evaporation, we have used the Santa Paula $\bar{e}_p$ with the rest of the Clinton parameters in Figure 3-b. Notice that this single change causes a large qualitative alteration in the Clinton water balance causing it to closely resemble the arid Santa Paula case.

This illustrates the important role played by soil properties in determining local recharge of atmospheric moisture and may help to explain why an increased albedo (such as accompanies overgrazing), through its reduction of $\bar{e}_p$, reduces the local recharge of atmospheric moisture.

REFERENCE

Eagleson, P. S., "Climate, Soil and Vegetation," Parts 1-7, Water Resources Research, Vol. 14, No. 5, Oct. 1978.

Table 1

COMPARATIVE CLIMATES

Clinton, Ma.	Characteristic	Santa Paula, Ca.
94.1 cm	$E[P_A]$	53.4 cm
0.15 cm/day	$\bar{e}_p$	0.27 cm/day
365 days	Season length, m_τ	212 days
109	Number of storms, m_ν	16
0.3 days	Storm duration, m_t	1.4 days
0.9 cm	Storm depth, m_H	3.4 cm

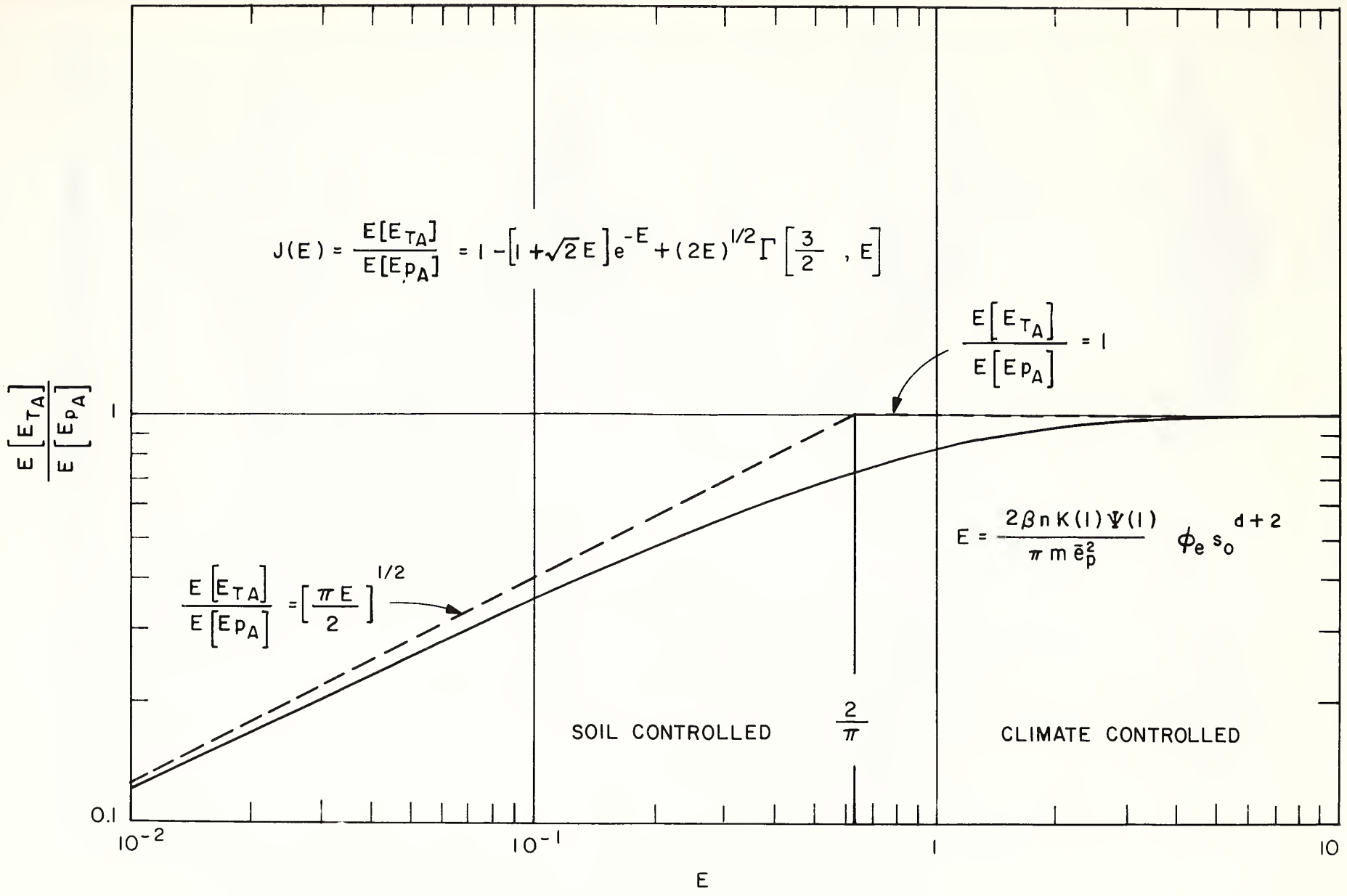

FIGURE 1 BARE SOIL EVAPORATION FUNCTION

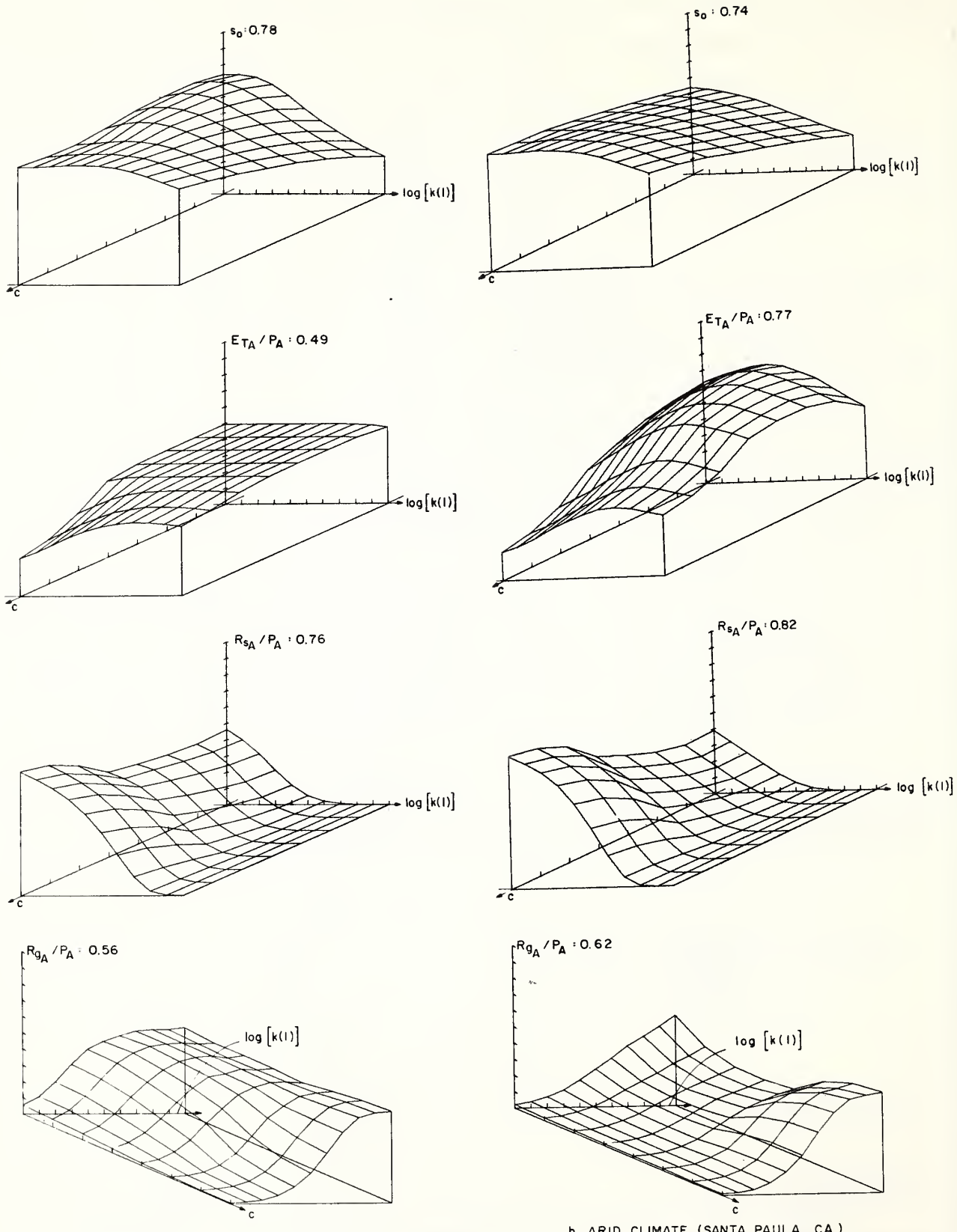

a. SUB-HUMID CLIMATE (CLINTON, MA.)

b. ARID CLIMATE (SANTA PAULA, CA.)

FIGURE 2 WATER BALANCE SENSITIVITY TO SOIL PROPERTIES

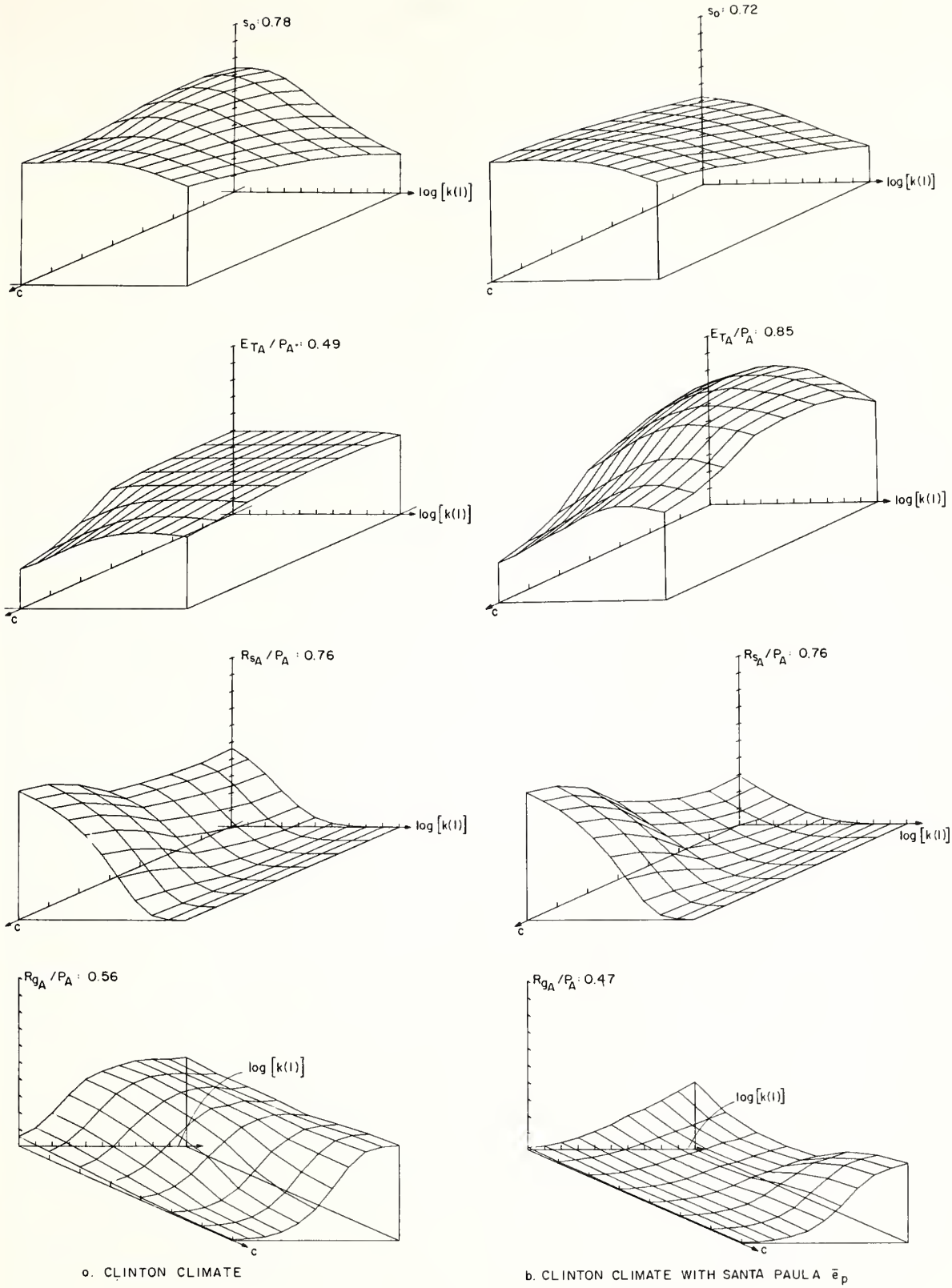

a. CLINTON CLIMATE

b. CLINTON CLIMATE WITH SANTA PAULA $\bar{e}_p$

EFFECT ON ANNUAL WATER BUDGET DUE TO INCREASING AVERAGE RATE OF POTENTIAL EVAPOTRANSPIRATION

FIGURE 3 WATER BALANCE SENSITIVITY TO RATE OF POTENTIAL EVAPORATION

STUDY OF THE HYDROLOGICAL CYCLE BASED ON SATELLITE AND SURFACE INFORMATION

by

Yu.V. Kurilova, P.A. Kolosov, E.L. Muzylev,

L.K. Poplavskaya

The study of real processes of moistening anomaly formation is possible only on the basis of full description of the water exchange processes and active parameterization of the hydrological cycle. Such a parameterization includes the following three steps: - (1) search for analytical or correlation relationships between internal parameters of the hydrological cycle and external parameters of large-scale atmospheric processes obtained from surface and satellite information; (2) formation of generalized informative parameters of the hydrological cycle having properties of spatial generalization; (3) consideration of regularities of real processes within the framework of space-time genetic boundaries. Natural temporal boundaries separate the main seasons in the hydrological cycle according to the relation between phase states of water and values of the radiation balance. The establishment of spatial natural boundaries is made taking into account the zones of different moistening, and amounts to isolating the anomalies or areas of uniform values of hydrometeorological fields and accounting for their total or mean characteristics via informative generalized parameters. The distribution of zones of different moistening is determined by the relation between heat and moisture

which is governed by large-scale atmospheric processes and defined from both the thermal characteristics, and subsequent precipitation and soil moisture storage.

Most suitable information for obtaining the necessary generalized characteristics of water exchange is satellite information due to its properties of generalization and global registration. In the proposed parameterization, global fields of cloudiness, snow cover, soil moistening and anomalies of ocean characteristics are used as initial information.

Being the link connecting all processes of the hydrological cycle, the moistening of the layer of soil thermal regulation $W(t)$ is chosen as the basic parameter for description of the hydrological cycle. Having more inertia than dry soil, moistened soil is functioning as a "memory" in the atmosphere – underlying-surface-of-the-continents system. The degree of inertia in heat absorption and release is proportional to soil moistening. Since soil moistening for a given moment is the result of the processes of heat and moisture exchange for a certain preceding period, it turns out to be able to affect the direction and character of subsequent processes, thus playing the role of a regulator for the processes of heat and moisture exchange between the atmosphere and the land surface.

Parameterization of the hydrological cycle is based on the water balance equation for the layer of thermal regulation

$$W(t) = W_c + W_{cH} + \int_0^t B(\tau)\, d\tau$$

$$B(\tau) = x(\tau) - y(\tau) - E(\tau), \qquad (1)$$

where W_c – is the initial soil moistening characterizing year-to-year changes of soil moisture; W_{cH} – is the water equivalent of snow cover; $x(\tau)$, $y(\tau)$, and $E(\tau)$ – describe the changes of precipitation, streamflow and evaporation respectively for the period under consideration. The thermal regulation layer is variable with time; for its description we used data on moisture storage in the one-meter layer, in accordance with measurements of the existing agrometeorological network. Dynamic components of the water balance $B(\tau)$ in equation (1) determine the processes of accumulation and discharge of soil moisture and form the most inertial water balance component, i.e. soil moistening $W(t)$. Its value for the given moment plays role of the initial condition for the subsequent stages of the hydrological cycle.

The hydrological cycle is different in various climatic zones. The principal distinctive features showing up in the inertia of processes are determined by the phase state of water in winter. They can be described by the following characteristics: the relation between liquid

and solid precipitation and duration of the seasonal snow cover. On the basis of these characteristics the following four zones are identified according to the annual distribution of surface albedo: a zone with settled snow cover; a zone where snow cover is absent; and two transitional zones with the prevalence of solid and liquid precipitation respectively. Parameterization of the hydrological cycle according to equation (1) was made for zones with settled and unsettled snow cover.

In accordance with seasonal variations of the radiation balance, two basic periods are isolated within the hydrological cycle - i.e. a warm period with the active turbulent heat and moisture exchange, and a cold passive period of the supressed exchange processes (Fig. Ia, Ib). The principles of estimating the water balance elements for these periods are different. In the former, the dynamic members of equation (1) are taken into account; in the latter, the resulting effect is estimated.

In the warm snowless period, according to the relation between accumulated heat and stored moisture, and consequently according to the character of the interaction of the processes with the underlying surface, the following three stages are isolated: -

(1) the initial stage of active evaporation in spring, with the unlimited soil moisture storage and sharp increase of the radiation balance;

(2) the summer proper, with the maximum radiation balance and prevalence of transpiration;

(3) the final stage of attenuation of evaporation when at the small radiation balance, conditions for autumn soil moistening are formed.

In the cold winter period, when the heat and moisture exchange between the atmosphere and land does not occur, due to heat-insulating properties of snow, and over ocean, it is more active, the relevant stage of hydrological cycle may amount to accumulating oceanic moisture in the continental snow cover.

A genetically transitional season preceding early winter (when snow is accumulated) and a pre-spring season (when snowmelt occurs) are characterized by the presence of two phase states of water fixed in satellite images by intermittent white and black patches. The physical meaning of the influence of these seasons amounts to including self-intensifying mechanisms with a positive feedback at the snowline, which were studied from satellite data by G. Kukla. The main point of such mechanisms in snowmelt is an approximately 4-fold increase of the radiation balance through an uneven decrease of albedo by 80 to 20 per cent. The intensity of inclusion of such mechanisms influencing the snowmelt rate, may be defined not only by atmospheric conditions but also by the water equivalent of the snow cover accumulated during the winter, i.e. the depth of

snow cover. Thus, the snow cover "keeps memories" of the character of the preceding winter. Similar, but weaker, feedback mechanisms can be observed in the period of maturation and harvesting, grass and leaves yellowing, when albedo increases by 5 to 15 per cent. Thus, for regions with the settled snow cover, six seasons of different duration with the prevalence of different physical processes are distinguished within the annual hydrological cycle (Fig. 2a). In regions with the settled snow cover, where the entire cold period represents an extended transitional season (Fig. 2b), only four genetic seasons are noted. The duration of these genetic seasons is subject to changes from to year depending on the peculiarities of circulation processes.

The transitional period of snow cover formation (season preceding early winter) may be considered as a passive period of the so-called suppressed processes of exchange with the underlying surface since the evaporation from snow cover $E(t)$ is close to zero, the precipitation $X(t)$ on snow cover is realized only in spring, and the runoff equal to 2 to 4 mm (as was approximately estimated by the authors for the Don catchment area) may be neglected. The downward flux from the thermal regulation layer may be not taken into account either since they participate in the active exchange only in the succeeding warm period. Therefore, by the end of the period preceding early winter the total value of soil moistening remains equal to W_0.

In the transitional snowmelt period (pre-spring season) evaporation participates unevenly, its value, at

first, being equal to zero (over the snow surface), and then climbing to the maximum (typical for the spring season) over extremely moistened snow-free areas. It should be noted that in this period evaporation increases through both the limiting value of soil moistening in the spring flood period and extention of snow-free area, and an increase of the radiation balance intensified by the climb of albedo during the snowmelt period. The part of water which was not evaporated distributes among the surface runoff $y(t)$ and ground-water storage in accordance with the runoff coefficient η .

Dynamic members of equation (1) $B(t)$ somewhat alter their contributions in spring and summer in connection with different relations between heat and moisture - in spring, the soil moisture storage is practically unlimited, at the relatively small radiation balance; and in summer, when the radiation balance is great, evaporation is limited by the soil moisture content. Transpiration becomes significant, its relation with evaporation being of the order of 4 : 1. The above explains the reason for a substantial excess of evaporation in summer over that in spring (Fig. 1).

At the moment, at which transpiration becomes prevalent over evaporation and excesses it significantly may be considered as the genetic boundary of the beginning of the summer proper. On a series of satellite images (especially multizonal ones), where vegetation and soil are distinguished, it is possible to identify the contours of the vegetation-covered areas, in accordance with the above criterium.

Parameterization of components of the hydrological equation (1))

1. Initial moistening W_{oc}

It is reasonable to begin the study of the hydrological cycle with the end of the summer season since under the conditions of due greatest evaporation rate in summer, the relationships with the antecedent processes fixed by the moistening of the active layer are broken to a great extent. The minimum soil moistening in the end of summer is assumed equal to W_{oc} and calculated using the same equation (1). As the zero approximation, it may be assessed using a map of soils taking into account their least water field capacity : $W_{oc.} = \alpha W_{нпв}$

2. The initial water equivalent of snow cover $W_{сн.}$

$W_{сн.}$ is determined for the moment of snow melting by tracing the snowmelt limit on a series of subsequent images. $W_{сн}$ is calculated from

$$W_{сн.} = \sum_{(i)} (F_{i+1} - F_i) k(F) \qquad (2)$$

where F_i and F_{i+1} - are areas where snowmelt occurred during successive periods; $k(F)$ - is a coefficient describing the snowmelt rate which may be considered proportional to the

changes of snow-free area ΔF ; $k \sim \Delta F$.

Temporal trend of values ΔF obtained from satellites is in a good agreement with the temporal trend of the averaged surface temperatures (Fig. 2). Then

$$W_{CH.} = k \sum_{i=1}^{n} \left(F_{i+1} - F_i \right)^2 \qquad (3)$$

From surface data on the water equivalent of snow cover and satellite data on the dynamics of areas where snowmelt had occurred, the map of the value k was prepared for the south of the European territory of the country (Fig. 3). The coefficient k varied within the range of the order increasing regularly in the direction from south-west to north-east, which conforms with the boundaries of physiographic zonality. Therefore, in remote determination of the water equivalent of snow cover using formula (3), zonation of the value k is taken into account.

3. Parameterization of the dynamic member $\chi(t)$ of equation (1) is aimed at reconstruction of precipitation fields in the standard grid square (2.5° x 2.5°) from cloud fields fixed in TV images. The calculation is made for the total daily, 10-day and monthly precipitation using formulae (4) and (5) respectively

$$X_{mm} = \sum_{(j)} P_j i_j S_j \qquad (4)$$

$$X_{mm_{дек.}} = \sum_{j} P_j i_j S_j N_j \qquad (5)$$

Here N_j denotes the indices of groups of large-scale and mesoscale cloud fields; S_j , P_j and i_j are the areas of cloud cover, probability and intensity of precipitation respectively, for each group. The selection of cloud groups and calculation of probabilities and mean intensity of their precipitation were made using prior sampling in the analysis of both the satellite information on clouds and surface rainfall data. The basic amount of precipitation is carried by the frontal cloudiness - though the amount of cyclonic clouds for 10 days is two times less than that of air-mass clouds, the former carries two-fold more precipitation than the latter. The averaged and reduced rainfall rates in different groups (Table 1) show that the air-mass cloud contribution to precipitation is almost an order less than that of frontal cloudiness. Therefore, the intensity of the former may be given by a constant. In case of large-scale cloudiness, different phases of the development of the cyclonic cloud system are identified, and in compliance with them the groups of large-scale cloudiness have been

assumed (Table 1).

4. Runoff $y(t)$

The methods of runoff parameterization are different for different seasons depending on characteric properties of its formation. For instance, low flow, summer flow and winter flow may be neglected since they are defined by deep groundwater formed during the hydrological cycle of the preceding years. Over the entire continents (including those with sparse data), the estimates of spring flow, the contribution of which to the hydrological cycle is great, may be made by the following two satellite methods. The first method is based on the relationship between the flow at the outlet and the portion of the catchment area where the snow had melted. Such relationships in relative units (runoff in per cent of the maximum value; snow coverage in per cent of the entire catchment area) were derived by the authors earlier for 22 catchments of the Don, Volga and Ob. Fig. 4 confirms such a relationship for the catchment of the Ob. A relative hydrograph may be transformed into an absolute hydrograph <u>via</u> the maximum flow determined from the nomogram of its dependency on the water equivalent of snow cover $W_{cr.}$ and soil moisture storage in the end of autumn $W_{oc.}$

The other method of streamflow routing uses the genetic formula of flow

$$y = \int_{c}^{t=\tau_{max}} \eta(\tau) F(\tau) k(\tau) P(t-\tau) d\tau \qquad (6)$$

where apart from the areas where snow had melted away $F(\tau)$ and the snowmelt rate $k(\tau) = k\Delta F$, one more characteristics is used, namely the runoff coefficient η, which may also be determined with the aid of satellite data. The authors made calculations of the runoff coefficient $\eta = \frac{y}{W_{сн}}$ as a relation between the depth of snowmelt runoff and water equivalent of snow cover estimated by the above diagnostic method $W_{сн.} = k(\Delta F)^2$. A map of the runoff coefficient was made for a part of the European territory of the country (Fig. 5c) on the basis of preliminarily prepared maps of the depth of snowmelt runoff for april and may 1972 (Fig. 5b), and the water equivalent of snow cover on 5 March 1972 (Fig. 5a). The calculated map of the runoff coefficient was then compared with the map of the depth of autumn runoff for September, October and November 1971 (Fig. 5d), which was assumed as an idex of the degree of autumn moistening since thellatter usually defines the runoff coefficient to a great extent. The coefficient of correlation of the value η with the value of the depth of autumn runoff, calculated from the values of η in the standard grid point taking into account two soil types (deep chernozem and leached podzolic chernozem) turned out to be equal to 0.9. Without taking into account the soil types, the correlation coefficient was substantially lower.

5. Estimation of evaporation from large territories for short intervals. Analysis of soil moisture movement

Evaporation for short intervals is usually estimated for a point, as the residual member of the water balance equation. Maps of climatic values of evaporation for large territories were prepared using formal interpolation of point data. To estimate evaporation for short intervals from large territories, the authors performed modification of Oldecop analytical relationship derived for conditions of climatic averaging

$$E = E_0 \, th \left(\frac{X - \Delta W}{E_0} \right), \qquad (7)$$

where $E_0 = f(R, d, U, t^\circ)$ is determined from Penman-Budagovsky formula through the radiational balance R, - moisture deficit d, air temperature t° and wind velocity U; X is precipitation; ΔW is the change of stored soil moisture in the one-meter layer.

Analysis of soil moisture movement at different levels up to 1 m, together with determination of evaporation from formula (7), has shown that the argument of equation (7) may be interpreted as a parameter as a parameter classifying the relation between heat and moisture and determining both the trend of the water exchange processes in the

evaporation system and the types of evaporation process. Algorithms of the computation of evaporation from formula (7) is presented in Table 2.

At $\eta \leq 0.5$, the conditions of insufficient moistening are realized. Under these conditions the evaporation process is described by a linear relationships (Fig. 6).

At $0.5 \leq \eta \leq \eta_{крит.}$, the conditions of optimal moistening are realized; the nonlinear portion of Oldecop curve complies with these conditions. And when the value approximates $\eta \approx \eta_{крит.}$, the deviations from linearity increase sharply (Fig. 6).

At $\eta \geq \eta_{крит.}$, the process tends to saturation, a attaining the maximum possible magnitude $E = E_0$ which results from the small radiation balance. Thus, at $\eta \geq \eta_{крит.}$, the conditions of excessive moistening, and evaporation is governed only by the complex of atmospheric conditions.

The values of parameter η also fix different movements of soil moisture (Table 3). Since at the insufficient moistening, the decrease of the value η from 0.5 to 0 (and even to negative values) is in line with the decrease of the downward moisture flux from the one-meter layer practically to zero and even to the occurrence of upward moisture fluxes from the lower layers, at the increase of the value η from 0.5 up to $\eta_{крит.}$, the increase of downward moisture flux is observed as compared with the case

of $\eta \leq 0.5$ which is mainly defined by an increase of precipitation (Table 3).

At the excessive moistening $\eta \geq \eta_{kpum.}$, the saturation of the one-meter layer and downward moisture flux to the lower layers takes place. Only the late autumn period with small radiation balance and abundant antecedent moistening, responsible for the saturation of the one-meter layer through the soil lens, presents an exception (Table 3).

Computation of evaporation from formula (7) is liable to have results similar to those obtained using the heat balance method. And the relative error for the conditions of optimal and excessive moistening is not more than 5 per cent. The difference amounts to 25 per cent only under the conditions of insufficient moistening for which the heat balance method proves inaccurate. Maps of the parameter η (Fig. 7) provide the patial zoning according to the types of evaporation processes and soil moisture flux.

Another parameter - Budyko radiation index $\frac{R}{Lx} = f(t)$ also takes into account (though more roughly) the relation between heat and water resources. This proves the similarity of maps of parameters η and $\frac{R}{Lx}$ (Figs. 7 and 8). Good agreement between the isolines of parameters η and $\frac{R}{Lx}$ with the precipitation isolines shows that basic deviations from the zonality in the character of moistening are defined by large-scale cyclonic cloud systems. Therefore parameter $\frac{R}{Lx}$, the numerator and denominator of

which may be expressed by the cloud field, can be determined only using satellite TV images. Then taking in account the similarity in the fields of parameters h and $\frac{R}{Lx}$, i.e. assuming that $h = f\left(\frac{R}{Lx}\right)$ come to the principle of satellite assessment of the fields of the parameter $\eta = \frac{x - \Delta W}{E_o}$, and consequently to the background assessment of soil moisture fields W; and using formula (7) we come to the background assessment of evaporation.

Conclusion

The proposed parameterization (1) describing the dynamics of the annual continental hydrological cycle was studied as applied to the zones of snowmelt feeding. The zone under consideration is in moderate latitudes. It is a zone of interaction between the equatorial and polar regions, and is characterized by a multiphase hydrological system. Therefore the hydrological cycle is formed here by the natural moisture integrators ($W_{\text{л}}$ and $W_{\text{сн}}$) during sharply distinguished genetic periods. These integrators define the prehistory of the cycle and become the initial conditions for the hydrological cycle of the succeeding year, thus relating the cycles of adjacent years. Dynamic parameters of equation (1) characterize the governing influence of the atmosphere upon and the role of soil moisture in the formation of the cycle and should be computed inde-

pendently. Physical regularities of the moisture exchange to be found out in a similar parameterization will prove essential for the study of year-to-year variations of the water exchange.

Table 1

Probabilities and intensity of precipitation for 9 groups of clouds obtained from a two-month sample

Groups of clouds	Probability of precipitation in the portions of a unit	Intensity of precipitation in mmd	Intensity of precipitation in mmd per 1 cloud ball
	Cyclonic formations		
1. Wave	1.0	12.3	1.0
2. Young cyclone	1.0	16.7	1.5 - 2.1
3. Front: -			
(a) continuous cloudiness	1.0	7.8	0.8 - 1.3
(b) broken cloudiness	0.9	3.7	0.2 - 1.0
(c) the ends of the front are broken	0.0	0.0	-
4. Point of occlusion	1.0	10.3	0.9 - 1.2
	Air-mass clouds		
5. Cumulonimbus clouds	0.8	0.22	0.16
6. Stratiform clouds	0.6	0.1	0.01
7. Cumuliform	0.4	0.1	0.01
8. Strato-cumuliform clouds	-	-	-
9. Cirrus	0.1	0.01	-

Table 2

Algorithm of computation of evaporation

Value n	Value R $\frac{\text{Kcal}}{\text{cm}^2\text{month}}$	Portion of Oldecop curve	Formula of calculation of evaporation	Formula of calculation of upward and downward moisture fluxes
1. $0 \le n \le 0.5$	any	linear	1. $E = x - \Delta W$ 2. $E = E_0 \text{th} \frac{x - \Delta W}{E_0}$	~ 0 (within the range of the measurement error)
2. (a) $0.5 \le n \le 1$	any	weak non-linearity	$E = E_0 \text{th} \frac{x - \Delta W}{E_0}$	$D = x - \Delta W - E$
(b) $1 \le n \le n_{kpum}$		strong non-linearity		
3. $n \ge n_{kpum}$	$R > 0.5$	strong non-linearity	$E = E_0 \text{th} \frac{x - \Delta W}{E_0}$	$D = x - \Delta W - E$
4. $n \ge n_{kp}$	$R < 0.5$	plateau	$E = E_0$	$D = x - \Delta W - E_0$
5. $n < 0$	$R < 0.5$	plateau	$E = E_0$	$U = -D = \Delta W + E_0 - x$
6. $n < 0$	$R > 0.5$	linear	$E = E_0 \text{th} \frac{x + \Delta W}{E_0}$	$U = -D = \Delta W + E - x$

Table 3

Examples of types of evaporation and soil moisture movement

	1	2(a)	2(b)	3	4	5	6
η	0.26	0.80	1.34	2.22	2.63	-1.22	-0.12
R $\frac{\text{Kcal}}{\text{cm}^2\text{month}}$	3.6	1.1	1.1	3.3	0.2	0	1.3
X mm	12.1	37.3	37.0	176.6	42.3	39.5	5.5
ΔW mm	-9	17	6	86	8	51	10
$X - \Delta W$ mm	21.1	20.3	31.0	90.6	34.3	-11.5	-4.5
E_o mm	79.7	25.5	23.2	40.7	13.0	9.4	38.0
E mm	20.6	16.9	20.2	39.7	13.0	9.4	14.8
U mm	0	0	0	0	0	20.9	19.3
From mm D	0.5	3.4	10.8	50.9	21.3	0	0
	Askaniya-Nova September Fall plowed land after winter wheat	Krasnoarmeisk October Winter wheat after winter wheat	Chernobyl October Winter wheat after flax	Lubny September Winter wheat after pea	Kherson November Winter wheat after corn	Poltava November Winter wheat after barley	Kherson October Winter wheat after corn

List of Figures

of the paper "Study of the Hydrological Cycle Based on Satellite and Surface Information" by Yu.V. Kurilova, P.A. Kolosov, E.L. Muzylev, L.K. Poplavskaya

Fig. 1. Scheme of the hydrological cycle for the zones of settled (a) and unsettled (b) snow cover. The dimensions of arrows corresponding to the components of the water balance are proportional to their values.

Fig. 2. Changes of snowmelt rate (a) and mean temperature (b) on the territory of the Don and the Volga in the pre-spring period. March 1972.
1. Snow patches, then snow-free area. 2. Continious snow cover, then snow patches. 3 Continious snow cover, then snow-free area. 4. The Don. 5. Prikaspy 6 The Middle Volga. 7. The Ural.

Fig. 3. Distribution of the coefficient (formula (3)) based on the series of the satellite snow cover maps (March 1972) for catchment areas 20000-60000 km^2.

Fig. 4. Relationship between the portion of the snow-free basin area F (in per cent) and runoff (in per cent of Q max) at the outlet for catchment areas of the Ob river.

(1) the Ishim; τ = 19 days;

(2) the Tobol, τ = 15 days

(3) the Iset, τ = 2 days

(4) the Tura, τ = 9 days

Fig. 5. Maps illustrated the calculation of the coefficient of the snowmelt depth:
(a) the water equivalent of snow cover W_{cn} on 5 March 1972; (b) snowmelt depth for April, May 1972; (c) coefficient of the runoff depth η ; (d) depth of the autumn runoff for September, October, November 1971.

Fig. 6. Set of Oldecop curves for different months and the different conditions of moistening.

Fig. 7. Maps of isolines of monthly total precipitation and values of the parameter n .

Fig. 8. Maps of isolines of the Budyko radiational index $\frac{R}{Lx}$

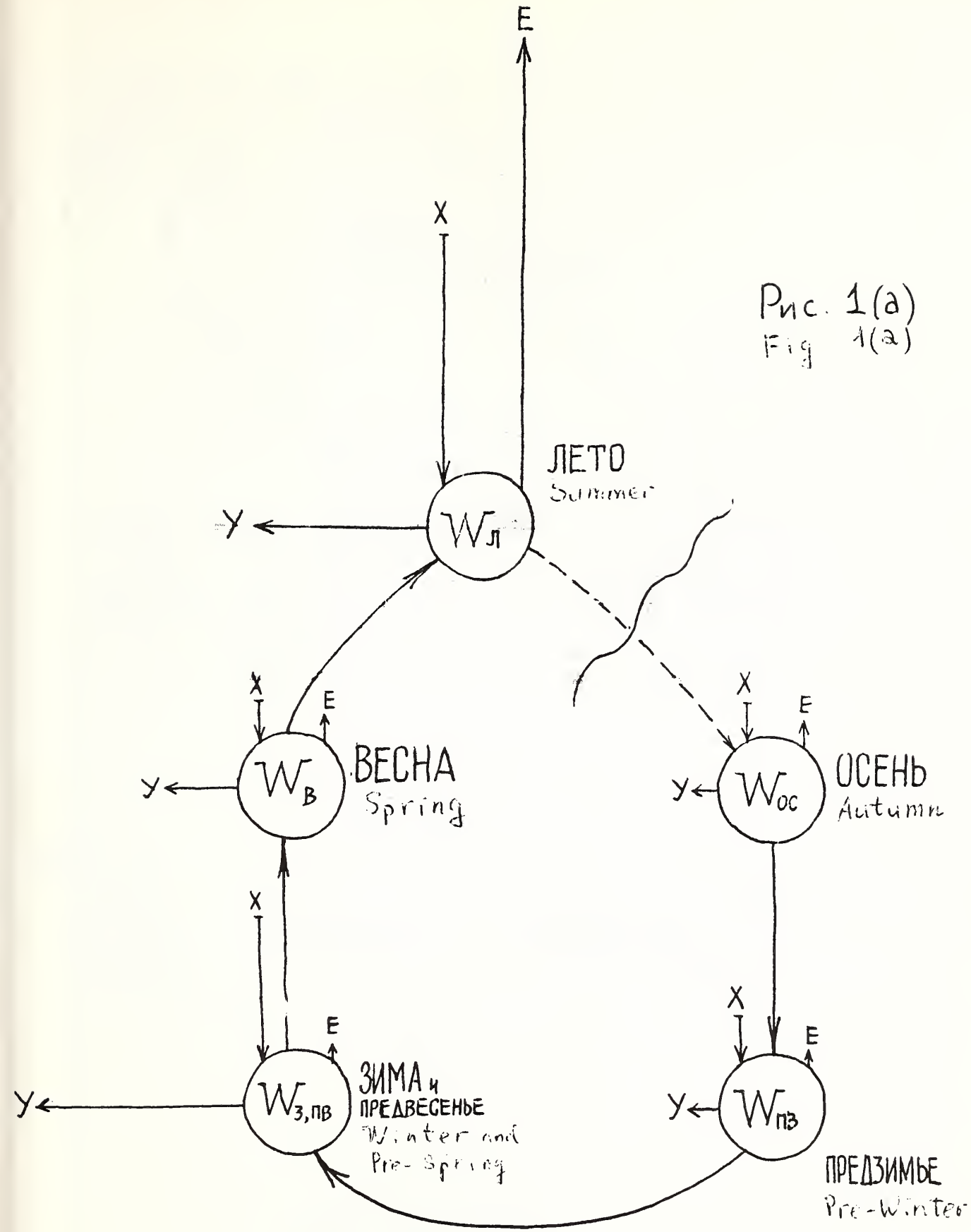
E
X
ЛЕТО
Summer
У
$W_Л$
X
E
$W_В$
ВЕСНА
Spring
У
X
E
$W_{ОС}$
ОСЕНЬ
Autumn
У
X
E
$W_{З,ПВ}$
ЗИМА и
ПРЕДВЕСЕНЬЕ
Winter and
Pre-Spring
У
X
E
$W_{ПЗ}$
ПРЕДЗИМЬЕ
Pre-Winter
У

Рис. 1(а)
Fig 1(a)

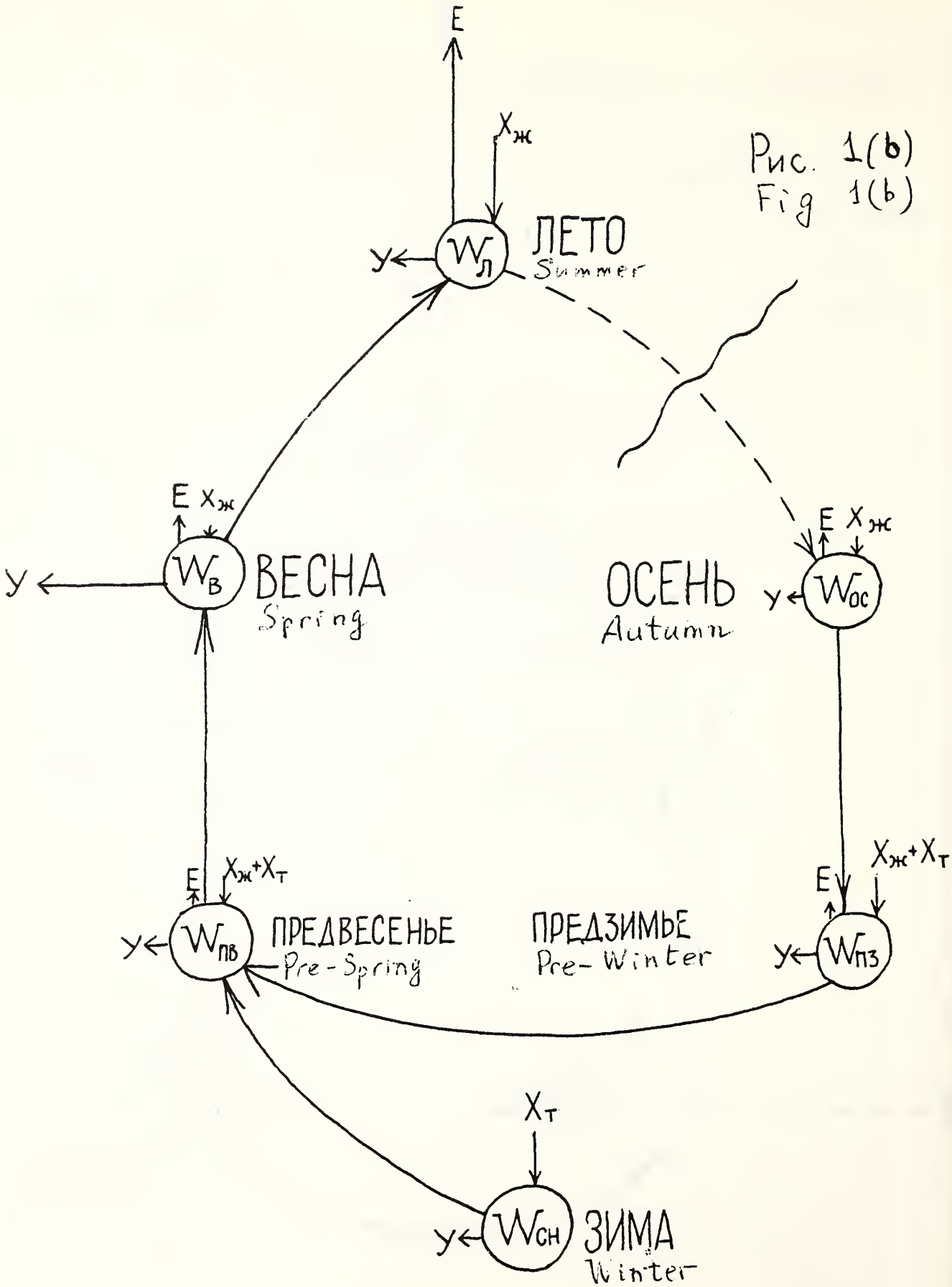
E
$X_ж$
$W_л$
ЛЕТО
Summer
У
E $X_ж$
$W_в$
ВЕСНА
Spring
У
E $X_ж$
$W_{ос}$
ОСЕНЬ
Autumn
У
E $X_ж+X_т$
$W_{пв}$
ПРЕДВЕСЕНЬЕ
Pre-Spring
У
ПРЕДЗИМЬЕ
Pre-Winter
E $X_ж+X_т$
$W_{пз}$
У
$X_т$
$W_{сн}$
ЗИМА
Winter
У

Рис. 1(b)
Fig 1(b)

ΔF_{cm} (thousands of km²)

ΔT (d)

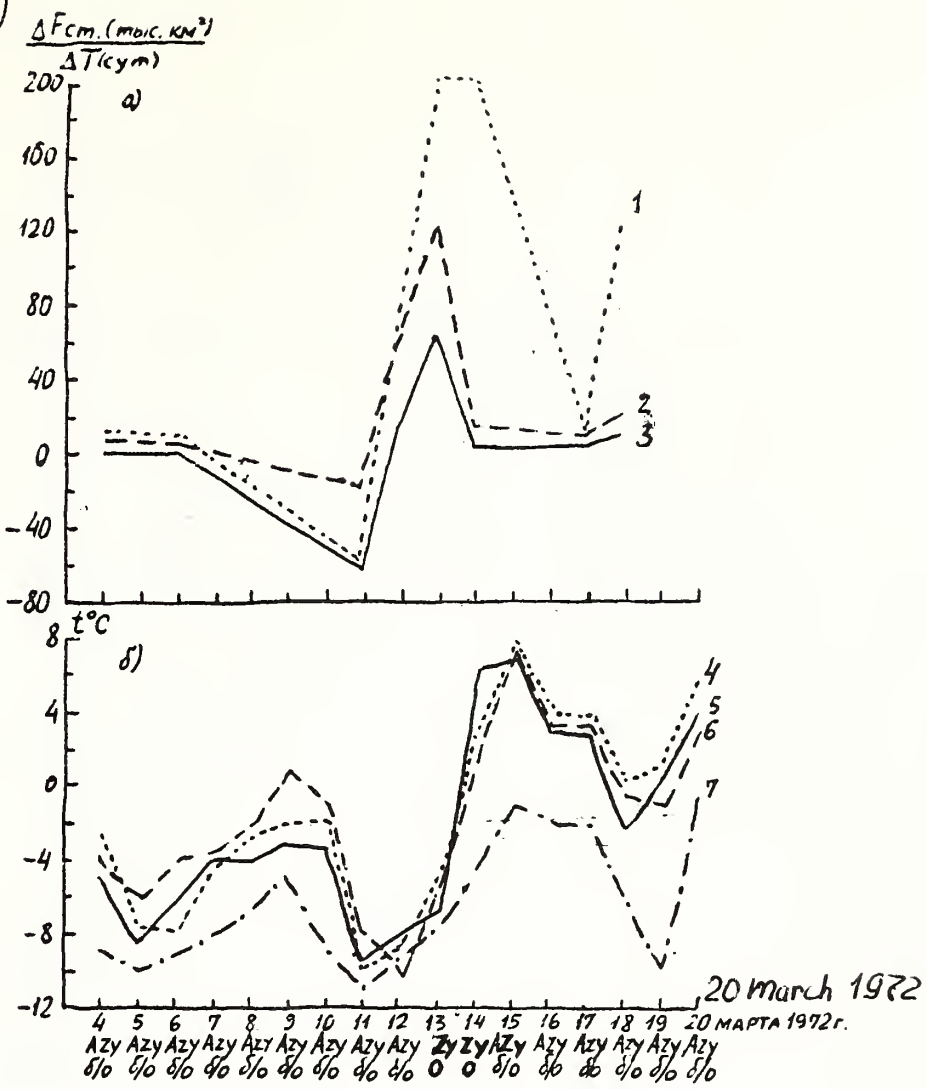

Рис. 2

Fig. 2

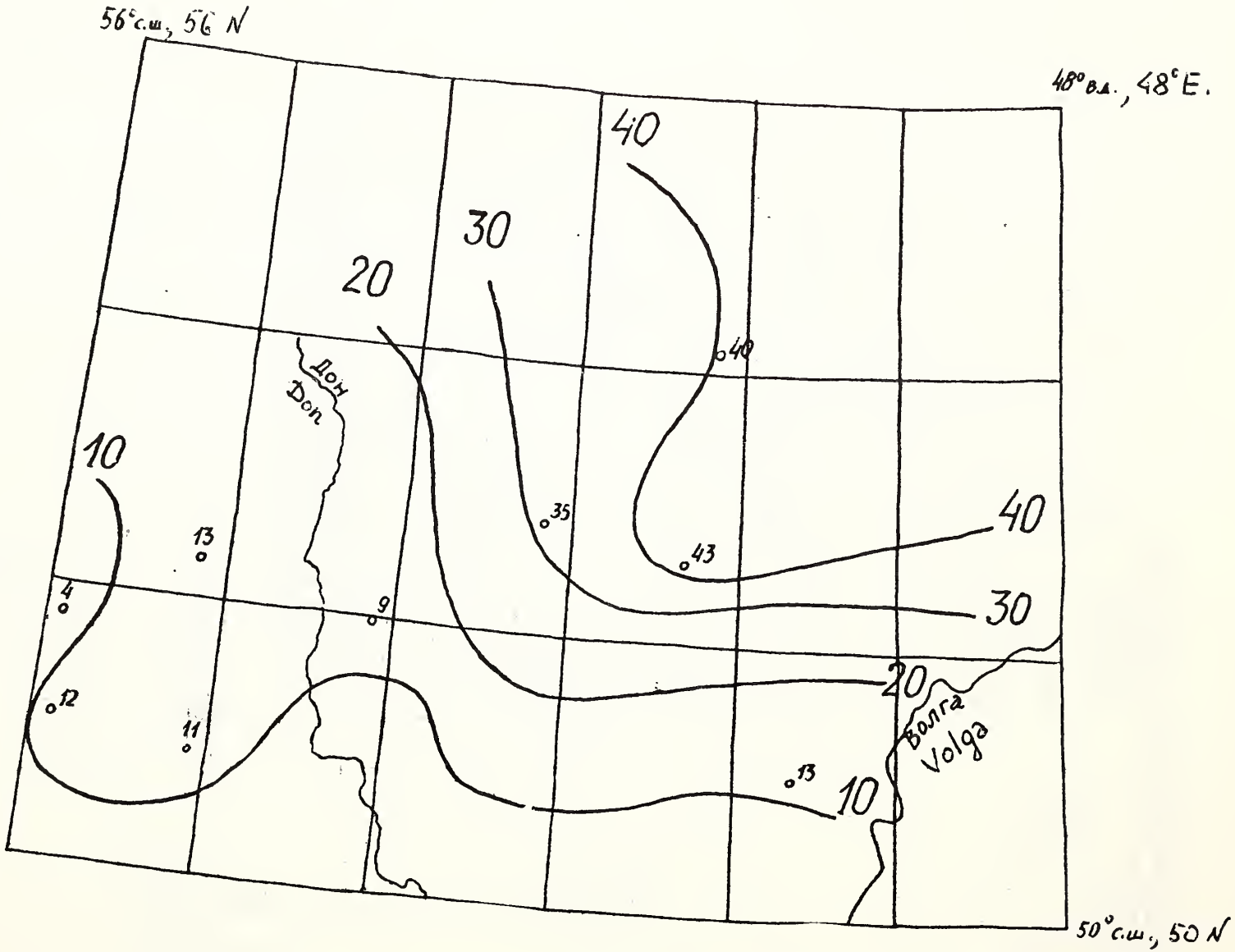

Рис. 3
Fig. 3

30-26.

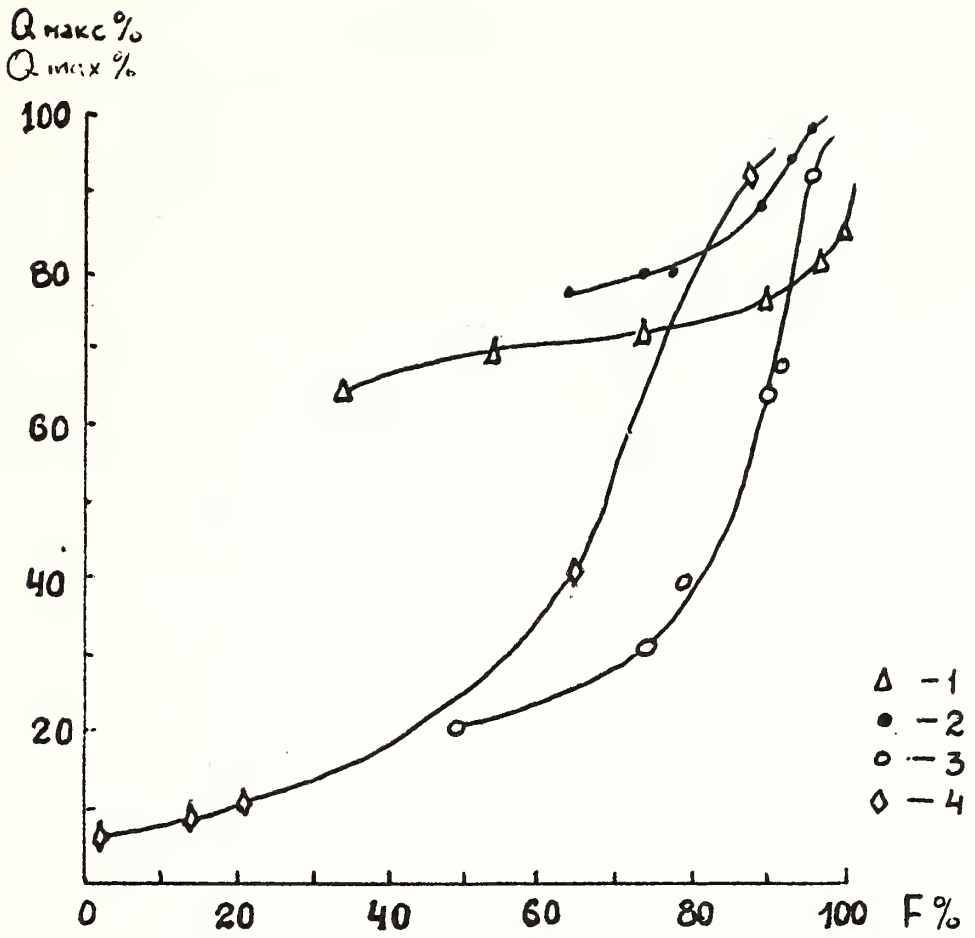

Рис 4
Fig 4

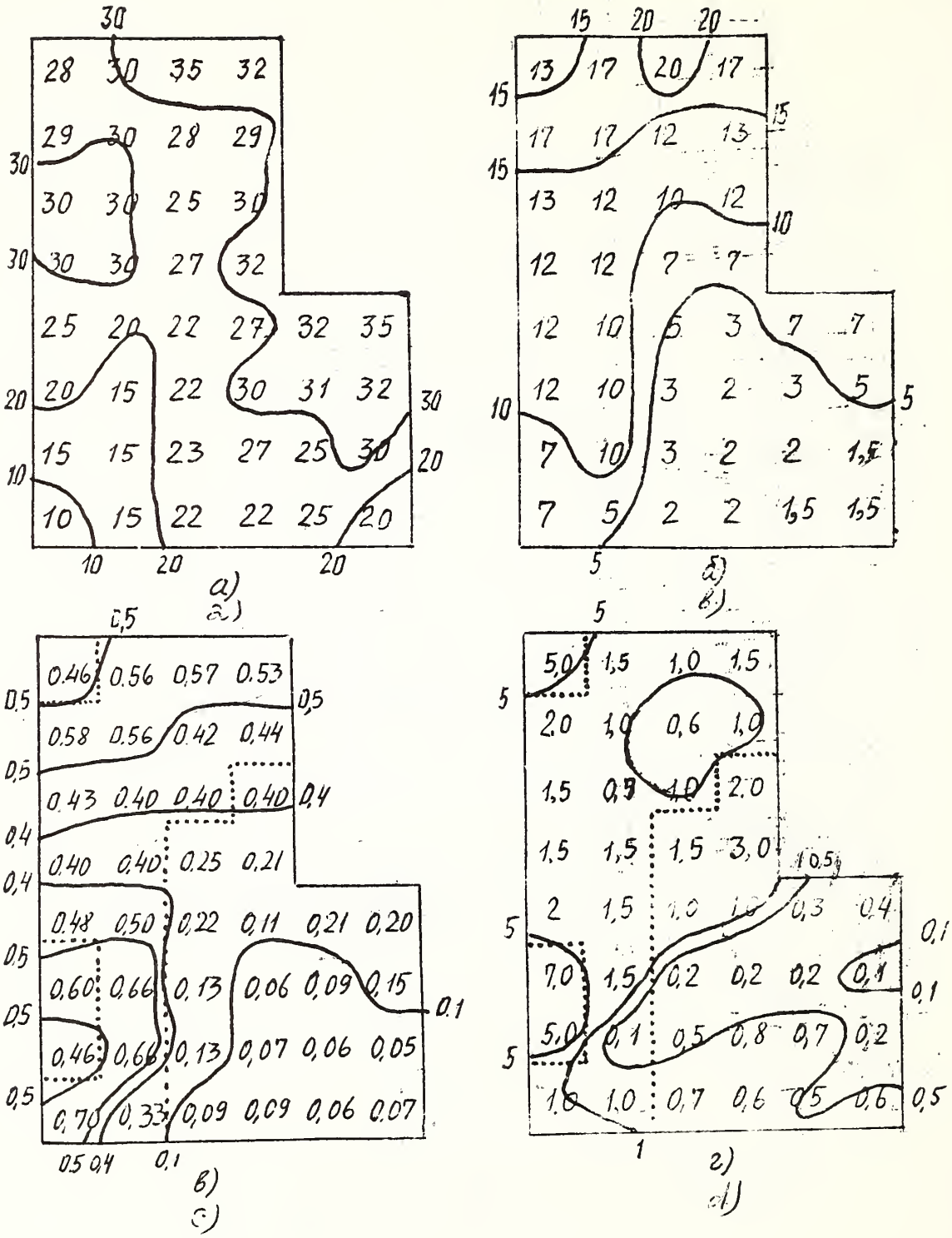

Рис 5
Fig 5

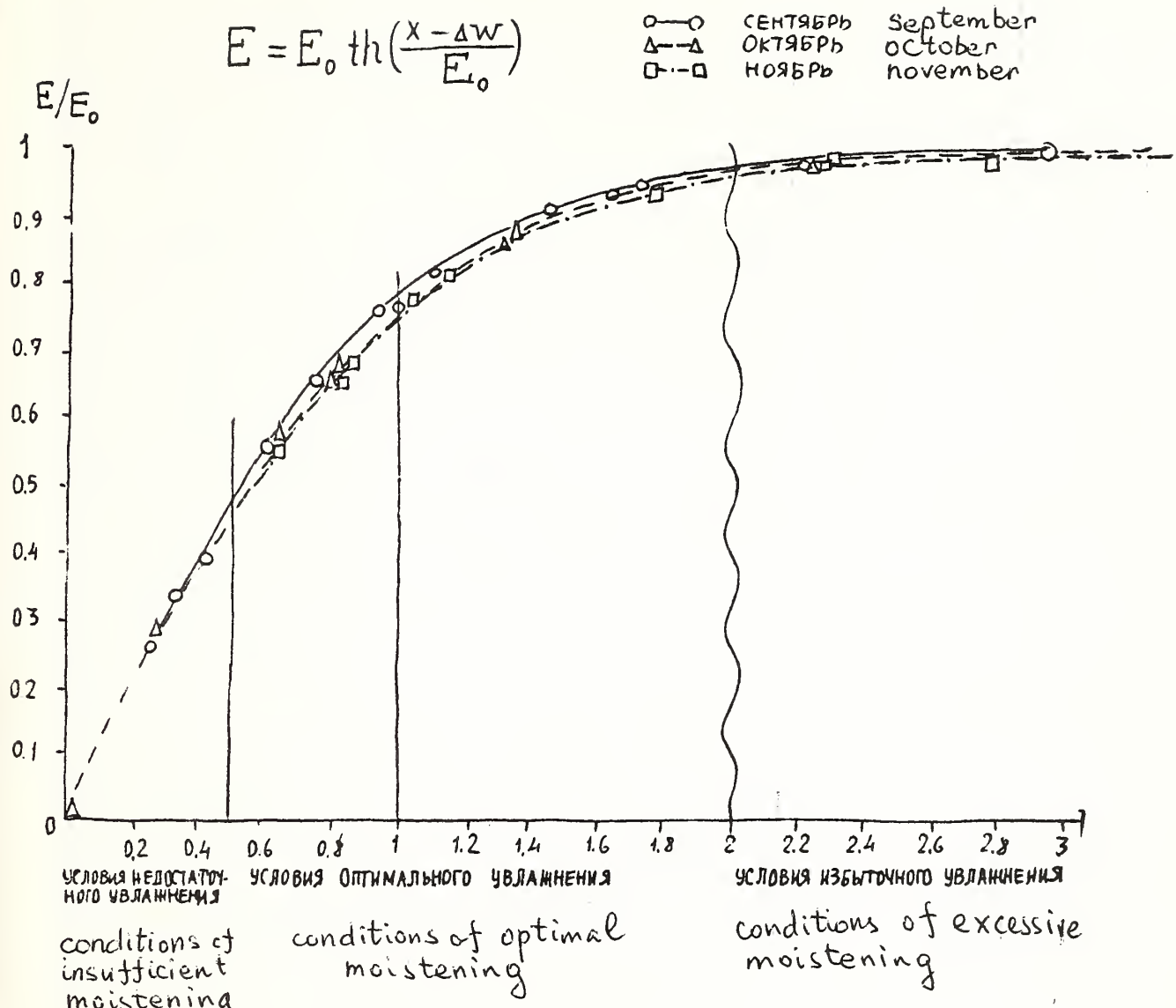
$E = E_0 th\left(\frac{X - \Delta W}{E_0}\right)$
сентябрь September
октябрь october
ноябрь november
E/E₀
1
0.9
0.8
0.7
0.6
0.5
0.4
0.3
0.2
0.1
0
0.2 0.4 0.6 0.8 1 1.2 1.4 1.6 1.8 2 2.2 2.4 2.6 2.8 3
УСЛОВИЯ НЕДОСТАТОЧНОГО УВЛАЖНЕНИЯ
УСЛОВИЯ ОПТИМАЛЬНОГО УВЛАЖНЕНИЯ
УСЛОВИЯ ИЗБЫТОЧНОГО УВЛАЖНЕНИЯ
conditions of insufficient moistening
conditions of optimal moistening
conditions of excessive moistening

Рис. 6
Fig. 6

The National Weather Service Extended Streamflow Prediction Techniques: Description and Applications During 1977

Dr. John C. Schaake, Jr., NOAA, NWS, W22
Silver Spring, Maryland 20910

Streamflow forecasts are needed for a variety of water resource management purposes. They are needed for future periods ranging from a few days to several months. As the duration of the forecast period increases so also does the uncertainty in the forecast. Recognizing this uncertainty, the National Weather Service has developed an extended streamflow prediction model (ESP) to produce probabilistic estimates of future streamflow.

The ESP forecast model includes within it a conceptual hydrologic model representing the movement of water through the hydrologic cycle. Inputs to the hydrologic model are climatic variables: precipitation, temperature, and potential evapotranspiration. The hydrologic model responds to these climatic inputs by accumulating and ablating snow cover during the winter months by simulating the movement of water through soil and ground water systems and by representing the flow of water in the surface, stream, and river systems. This hydrologic model must be calibrated for a specific location on the basis of historical climatic and streamflow data. Model calibration is needed because model parameters vary from place to place and can only be estimated on the basis of historical data.

To use the conceptual model in streamflow forecasting, the initial condition of the hydrologic system must be known and forecasts of the climatic variables are needed as well. Initial conditions can be known by operating the model continuously in time with observed data, using streamflow data to update model state variables so that the model is in tune with the most current data.

Since ESP uses a simulation approach, specific time series of future input climatic variables are needed. Since the future input series are unknown, it becomes necessary to work with a sample of equally likely input series. The ESP model must be operated starting from the same current initial condition for each of the input series in the sample and produces a streamflow output for each input series. These streamflow output series can then be used to derive the forecast probability distribution for the streamflow variables of interest.

If there were no skill in forecasts of precipitation, temperature, or evapotranspiration, an appropriate sample of climatic input time series would be offered by the historical record. In other words, historical series of precipitation, temperature, and evapotranspiration starting from the current day in each of the past years could be used as input to the hydrologic model. For each of these years the model would simulate the streamflow that would have occurred in those years if the current hydrologic conditions were to

have existed at that time. In the limit as the forecast period becomes long, the simulated streamflow will approach the observed streamflow because the effect of the initial conditions dissipates with time. It follows then that very long term streamflow forecasts from the ESP model will be the same as given by the historical streamflow records (within the limits of model error).

This approach was taken to forecast the lowest flows on record in the state of California during 1977. As an example, the American River natural inflow to Folsom Dam near Sacramento, California, for the month of May 1977, was predicted to be between 45,000 and 90,000 acre-feet with the most probable value of 60,000 acre-feet. The historical median flow for May is 540,000 acre-feet. This forecast was made on April 15, 1977. The main factor dominating this particular forecast was the initial condition of snow-water equivalent in the Sierra Nevada Mountains and depleted soil moisture as computed by the hydrologic model.

Following the western drought of 1977 and the application of ESP in California, another drought occurred in the east - - but on a much more limited spacial scale. This occurred in northern Virginia and the water supply for parts of the metropolitan Washington, D.C., area were severely threatened. This was the driest year in the last 27 years. The ESP model was used to assess the situation and to analyze alternative water conservation measures that would bring the risk within acceptable levels. The ESP application began late in September of 1977.

One of the significant problems in the northern Virginia case was the tremendous uncertainty in the future quantities of streamflow to be expected. The Occoquan Reservoir serving northern Virginia was almost empty. Inflow to the reservoir from natural ground water seepage was less than the rate water was being taken from the reservoir. Before runoff could occur from the land surface it was necessary for the soil moisture and ground water systems to be replenished by rainfall. At the same time, natural evapotranspiration was continuing to deplete the water remaining in the soil moisture and ground water systems. The soil moisture and ground water deficiencies totaled about 5.5 inches. This was of considerable concern because the mean October rainfall of 2.83 inches is much less than this moisture deficit. Preliminary studies had shown that the historical streamflow during the driest years in the past when combined with the depleted contents of the Occoquan Reservoir would not suffice to meet the needs for water at the current demand rate.

Applying the ESP technique to the northern Virginia case, it was important to consider if the future precipitation series were adequately represented by the historical series or if there were some information available in this particular year that would indicate the forthcoming October would be wetter or drier than normal. Therefore, we looked very carefully at the forecast information available from the National Weather Service long range prediction unit for October. Don Gilman did not believe that a very accurate quantitative precipitation forecast could be made for the month of October, but he did believe that the best possible way to use the available data was through an

anti-analog approach. According to this approach it would be possible to judge that certain of the historical years were not representative of the current year because the forecast of upper air circulation pattern for October was vastly different, in a sense opposite, from the historical upper air circulation patterns for October in a number of years. A total of 5 years were excluded from the historical record and the remaining record was judged to be representative of the type of precipitation pattern that might be expected in the current year. The mean of this conditional distribution was only about a tenth of an inch above the mean for the climatic distribution for October and the standard deviation of the condition of distribution was about 7% greater than the climatic distribution.

The ESP technique was applied in northern Virginia, using the complete historical precipitation series. It was found there is about a 10% chance that reservoir levels in the Occoquan Reservoir would fall below the threshold that would require the water authorities to declare a so-called stage three emergency which would prohibit all water use not essential for maintaining the health and safety of the community. Conversely there was a 90% chance of avoiding a stage three emergency and there was a considerable chance that the reservoir would refill before the end of the 1977 calendar year. But there was a 10% risk of reaching a stage three emergency. This was judged by the community to be unacceptable. Therefore, additional studies were made with the ESP technique to determine what conservation measures were required to reduce the risk to a more acceptable level. Although political representatives of the community were unable to define an unacceptable risk level, it was judged that a 20% reduction in withdrawal from the reservoir would reduce the risk level to about 2 or 3 percent. Plans were made, therefore, to reduce withdrawals until the reservoir had recovered to a normal level. Heavy rains began to occur in October and lasted through November. By mid-November the reservoir had refilled and the emergency was over. Analysis of the precipitation for October and November showed that there was only a five percent chance of having such a wet fall. Northern Virginia was indeed very lucky.

MODELS IN NWSRFS

- LAND PHASE
- SNOW ACCUMULATION AND ABLATION
- RESERVOIR OPERATION
- EXTENDED STREAMFLOW PREDICTION
- RIVER ROUTING
- DYNAMIC WAVE ROUTING
- DAM BREAK

A GENERALIZED
HYDROLOGIC MODEL
TENSION WATER STORAGE
FREE WATER STORAGE
TENSION WATER STORAGE
SUPPLEMENTARY FREE WATER STORAGE
TENSION WATER STORAGE
PRIMARY FREE WATER STORAGE
UPPER ZONE
LOWER ZONE
DIRECT RUNOFF
INTERFLOW
SURFACE RUNOFF
BASEFLOW
GROUNDFLOW
OUTFLOW

PECK (12)

PECK (13)

NWS APRIL 1977 FORECAST FOR INFLOW TO FOLSOM RESERVOIR

(100 Ac Ft)

	TOTAL APR-OCT	APR	MAY	JUN	JUL	AUG	SEP	OCT
FORECAST								
Minimum	116	55	45	10	1	1	1	3
Median	154	70	60	16	2	1	1	4
Maximum	300	100	90	35	15	10	20	30
OBSERVED	228	77	99	56	1	0	0	5
HISTORICAL								
Minimum	274							
Median	1407	480	540	280	59	17	12	19
Maximum	2964							

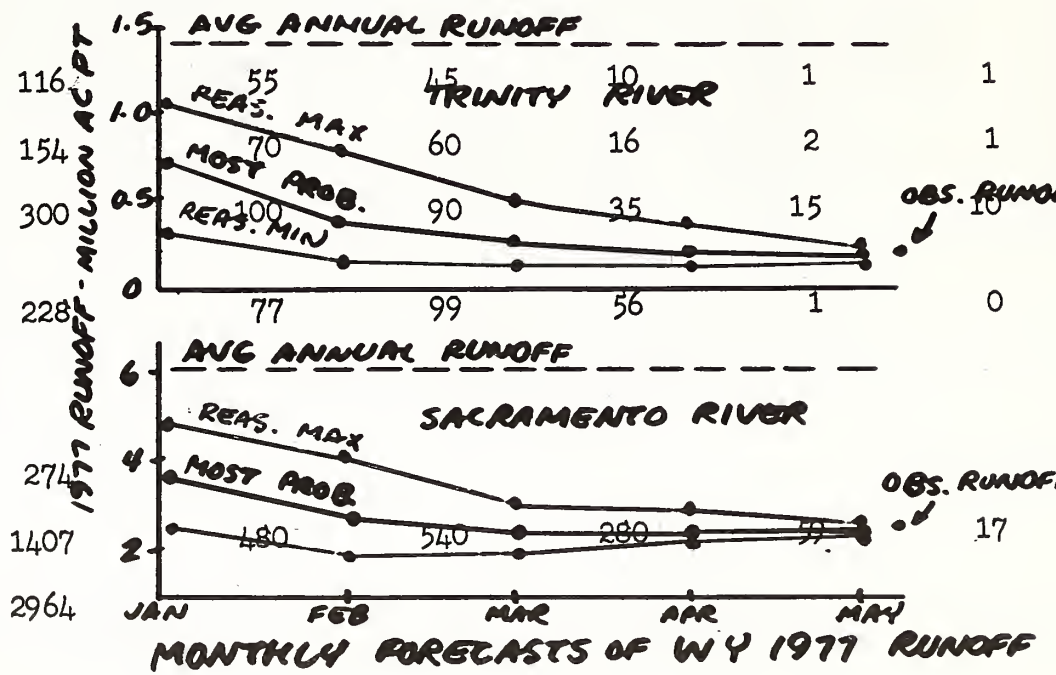

ISSUE DATE April 15, 1977

EXTENDED STREAMFLOW PREDICTIONS

The extremely dry winter throughout California is expected to result in the lowest flows of record through most of the state. Actual flows will be primarily dependent upon the variation from normal temperatures and precipitation.

2

BASIN	FORECAST PERIOD	.... FORECASTS .... MOST PROBABLE	REASONABLE MAXIMUM	REASONABLE MINIMUM	HISTORIC MEDIAN
CLEAR LAKE INFLOW Includes evaporation affects	April	-6	0	-7	
	May	-18	-8	-21	
	June	-25	-23	-28	
	July	-32	-25	-34	
	Aug	-31	-25	-34	
	Sept	-21	-14	-24	
	Oct	-12	1	-15	
	Nov	0	18	-8	
TRINITY RIVER Inflow to TRINITY DAM	April	35	50	28	210
	May	20	35	14	230
	June	5	20	4	100
	July	2	10	1	28
	Aug.	2	8	1	10
	Sept	2	8	1	8
	Oct	5	15	3	13
	Nov	6	30	4	29
SACRAMENTO RIVER Natural Inflow to SHASTA DAM	April	200	270	180	615
	May	175	220	160	462
	June	160	200	145	292
	July	155	195	140	224
	Aug	150	180	140	206
	Sept	145	175	135	200
	Oct	155	210	135	227
	Nov	160	280	140	274
FEATHER RIVER Natural Inflow to OROVILLE DAM	April	95	125	75	720
	May	80	125	70	580
	June	50	100	40	290
	July	45	90	35	135
	Aug	45	90	35	98
	Sept	45	95	35	86
	Oct	55	100	35	89
	Nov	65	150	35	126

.... FORECASTS ....

BASIN	FORECAST PERIOD	MOST PROBABLE	REASONABLE MAXIMUM	REASONABLE MINIMUM	HISTORIC MEDIAN
FEATHER RIVER North Fork - Inflow to LAKE ALMANOR	April	25	40	20	100
	May	25	40	20	105
	June	20	35	15	63
	July	20	35	15	48
	Aug	20	35	15	42
	Sept	20	40	10	38
	Oct	30	50	15	39
	Nov	35	60	20	43
YUBA RIVER Natural Inflow above SMARTVILLE	April	45	120	30	420
	May	45	80	20	440
	June	12	35	7	200
	July	4	15	2	45
	Aug	2	10	1	23
	Sept	3	20	3	20
	Oct	4	30	3	27
	Nov	10	50	5	48
AMERICAN RIVER Natural Inflow to FOLSOM DAM	April	70	100	55	480
	May	60	90	45	540
	June	16	35	10	280
	July	2	15	1	59
	Aug	1	10	1	17
	Sept	1	20	1	12
	Oct	4	30	3	19
	Nov	8	50	6	44
AMERICAN RIVER Middle Fork - Natural Inflow near AUBURN	April	34	50	27	205
	May	23	34	17	226
	June	4	10	3	105
	July	1	7	0	24
	Aug	0	5	0	7
	Sept	0	7	0	5
	Oct	2	15	1	6
	Nov	4	25	2	15
COSUMNES RIVER above MICHIGAN BAR	April	4	9	3	60
	May	2	6	1	39
	June	0	2	0	15
	July	0	1	0	2.6
	Aug	0	0	0	0.7
	Sept	0	0	0	0.4
	Oct	1	2	0	1.1
	Nov	3	5	0	3.4

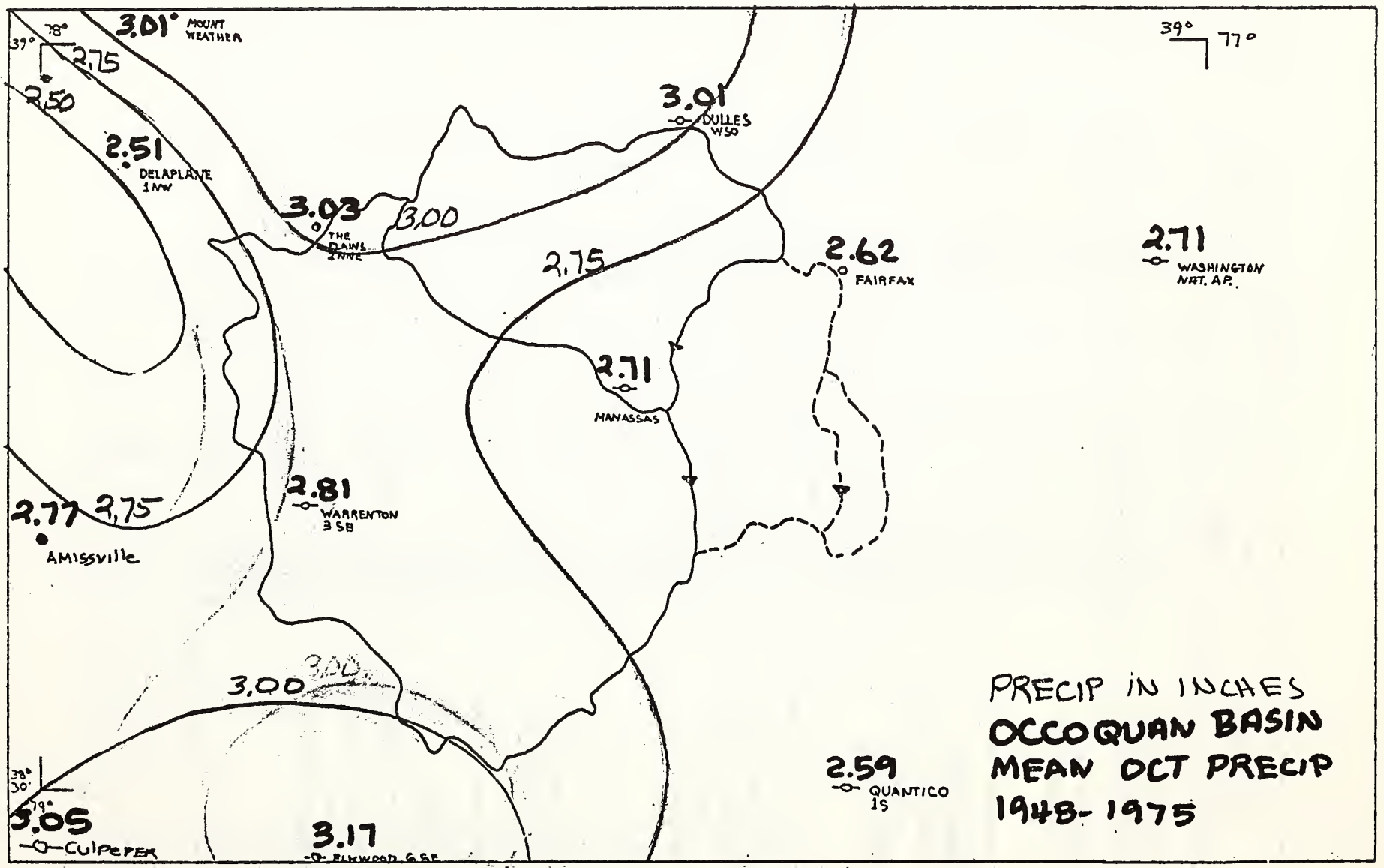
3.01 MOUNT WEATHER
78°
39°
2.75
2.50
2.51 DELAPLANE 1 NW
3.03 THE PLAINS 2 NNE
3.00
2.75
3.01 DULLES WSO
2.62 FAIRFAX
2.71 WASHINGTON NAT. AP.
39°
77°
2.71 MANASSAS
2.81 WARRENTON 3 SE
2.77
2.75
AMISSVILLE
3.00
3.00
2.59 QUANTICO 1S
PRECIP IN INCHES
OCCOQUAN BASIN
MEAN OCT PRECIP
1948-1975
38° 30'
3.05 CULPEPER
3.17 ELKWOOD 6 SE

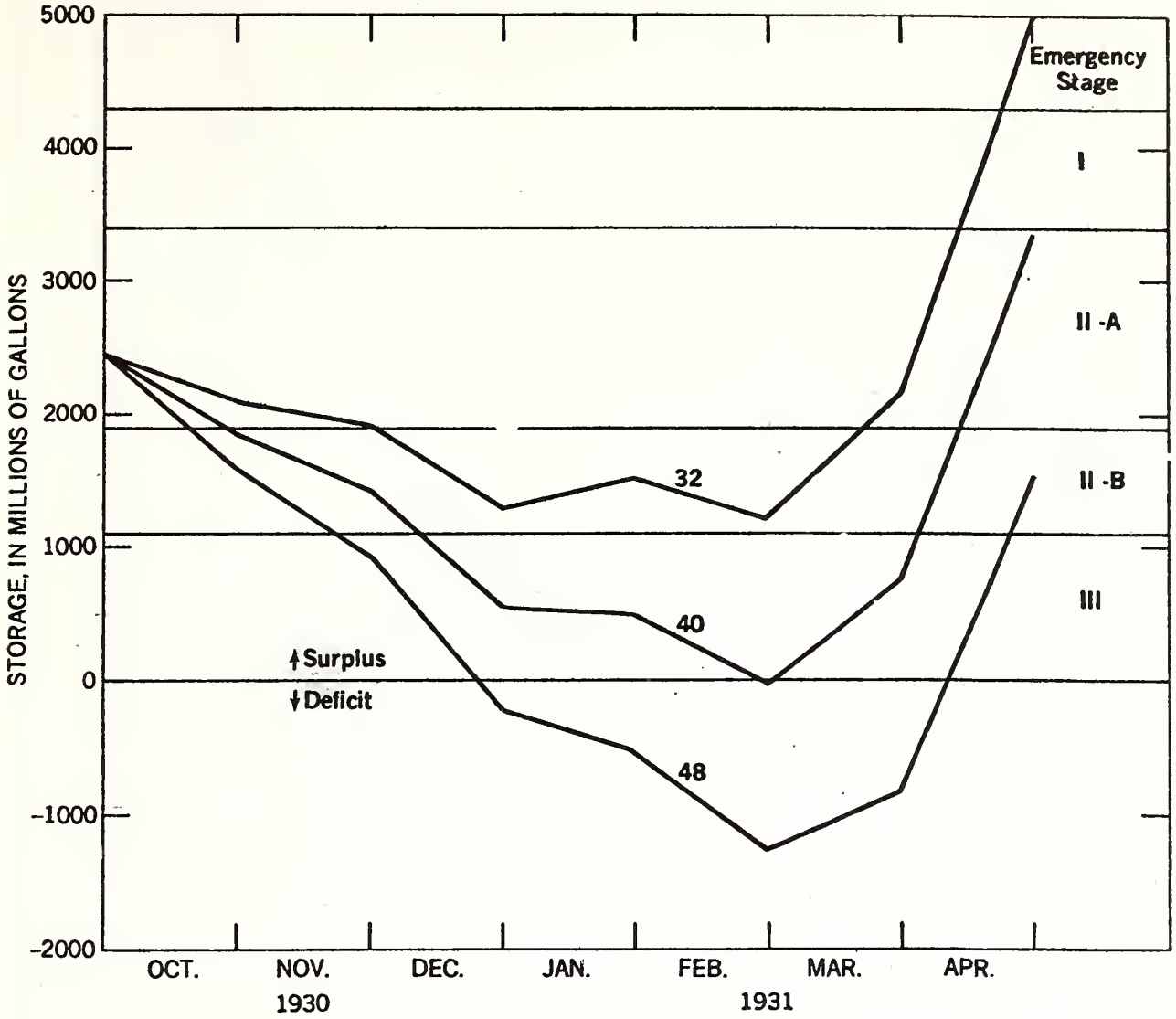

Figure 10.--Position Analysis: Simulated storages for the 1930-1931 drought, at production rates of 32, 40, and 48 Mgal/d.

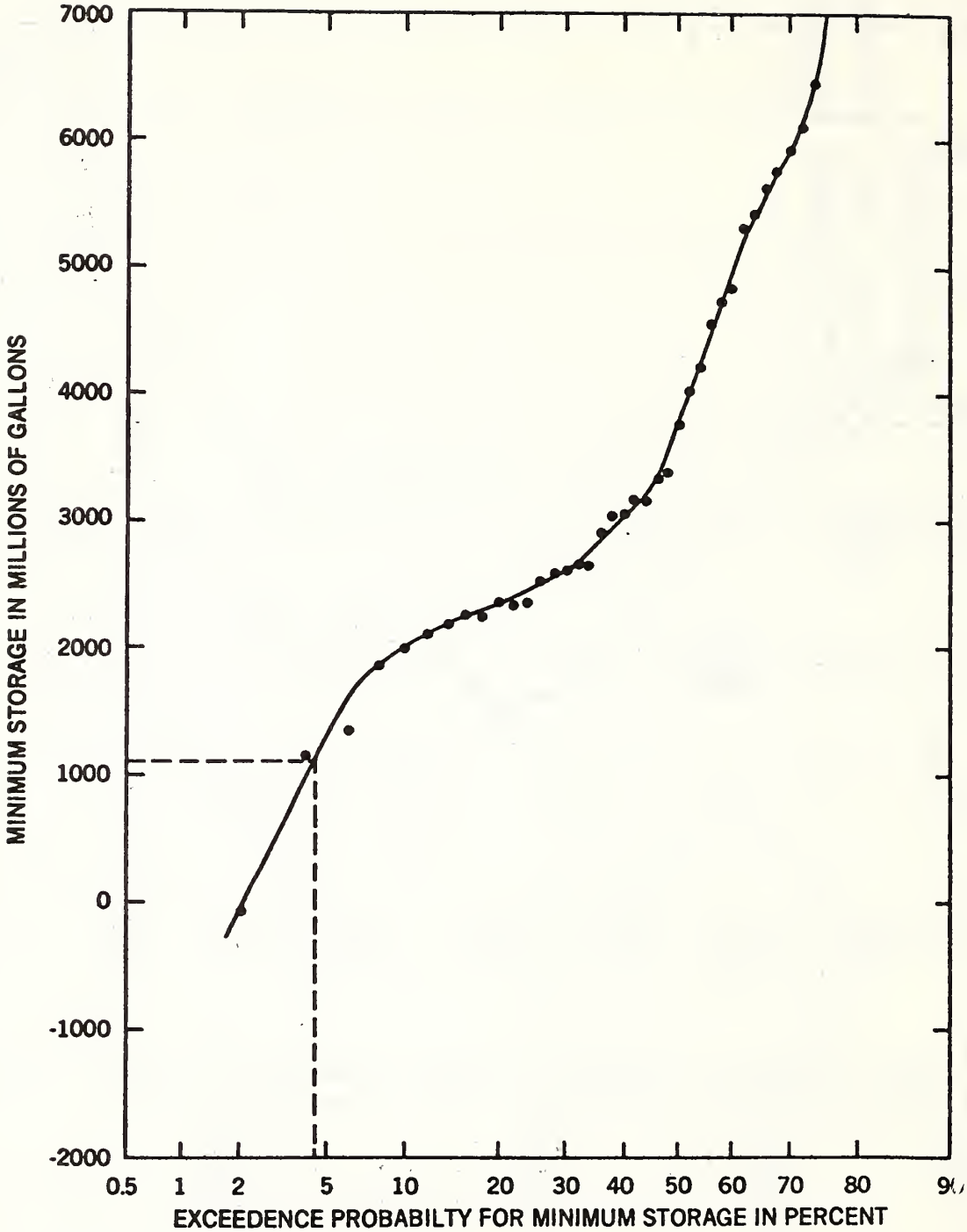

Figure 13.--Cumulative distribution function for S_{min}, 40 Mgal/d production rate, from Position Analysis based on 49 years of record.

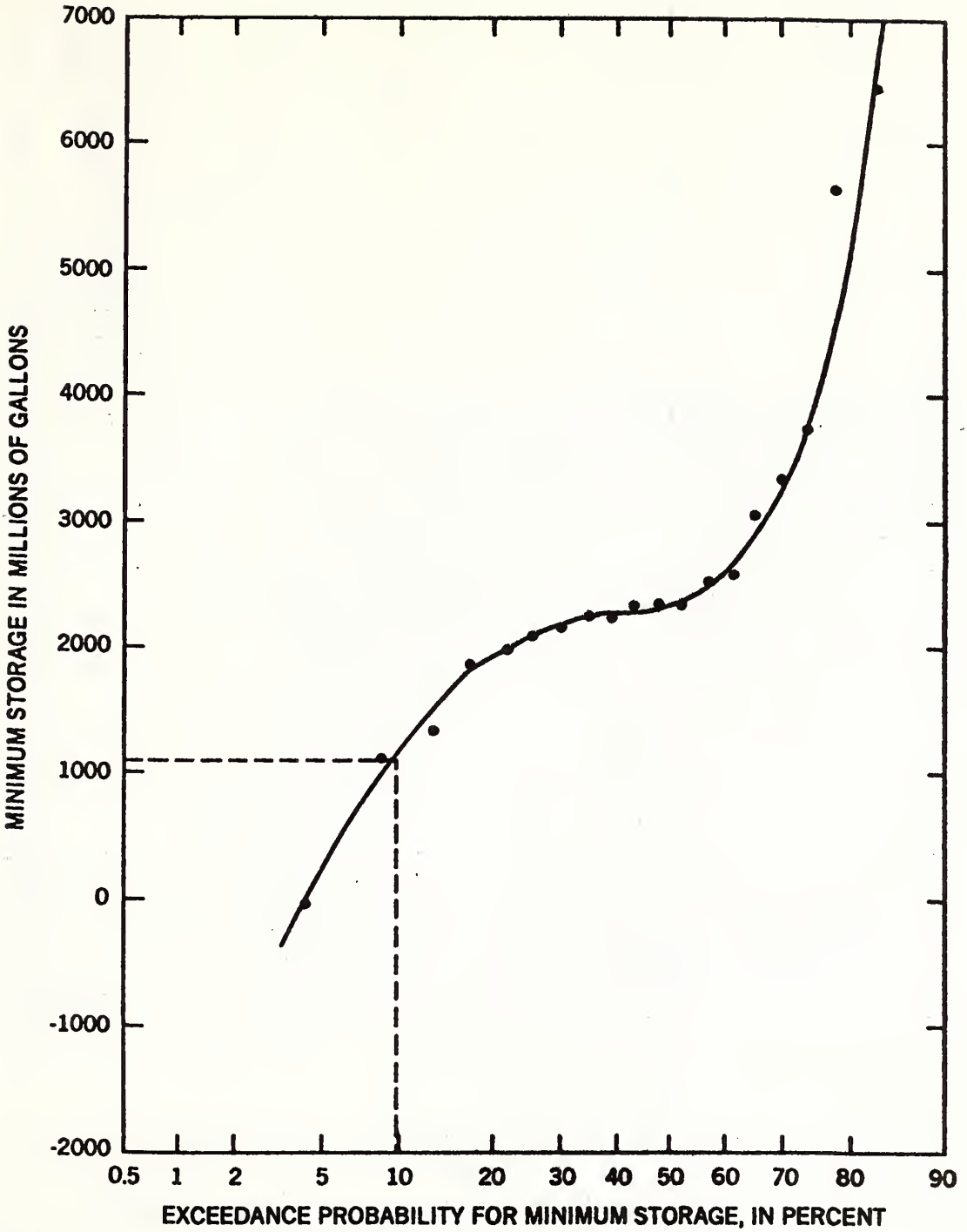

Figure 14.--Cumulative distribution function for S_{min}, 40 Mgal/d production rate, from Position Analysis based on 22 years with dry late-summer periods.

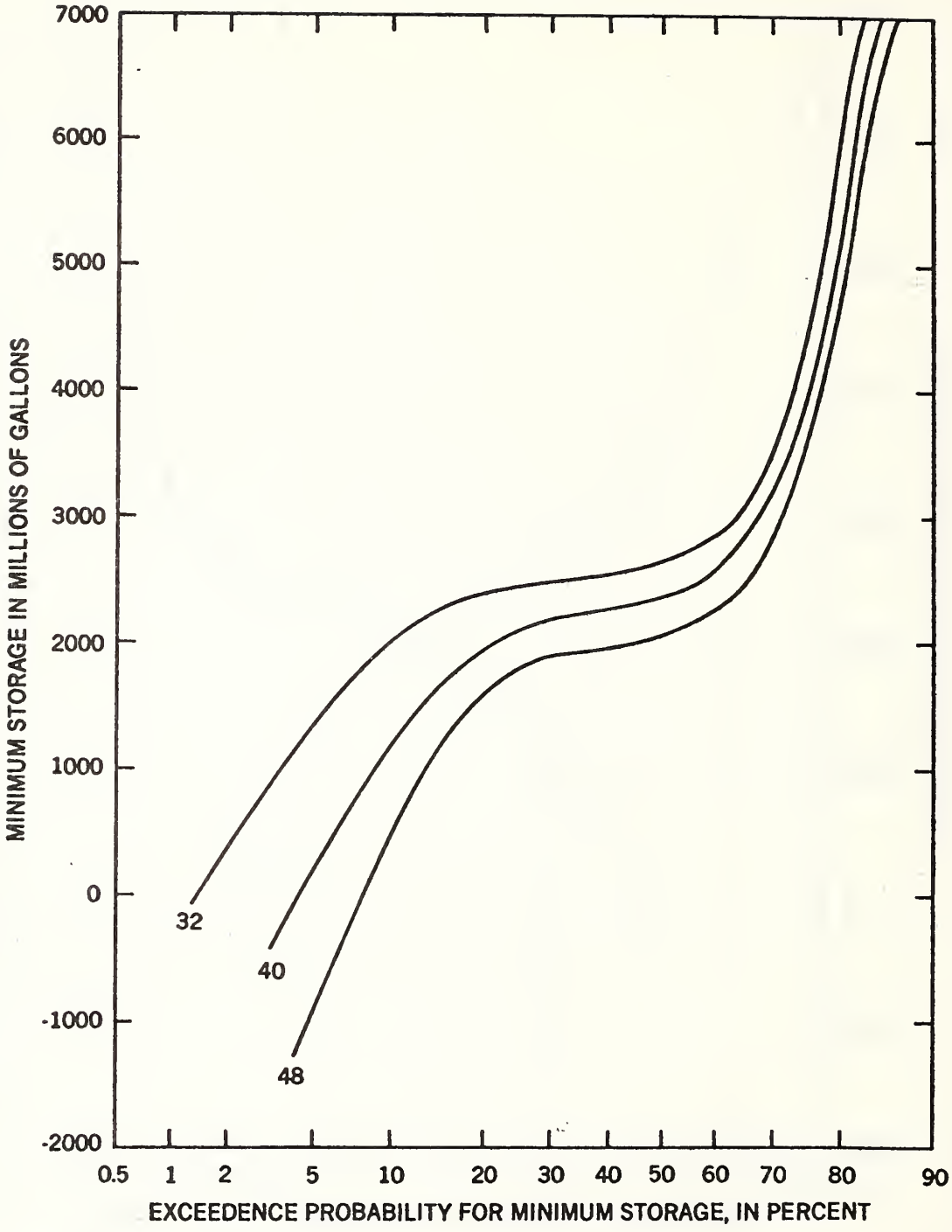

Figure 15.--Cumulative distribution functions for S_{min} at 32, 40, and 48 Mgal/d production rates, from Position Analysis based on 22 years with dry-late summer periods.

average monthly weather outlook

U.S. DEPARTMENT OF COMMERCE • National Oceanic and Atmospheric Administration • National Weather Service

FOR MID-OCTOBER TO MID-NOVEMBER 1977

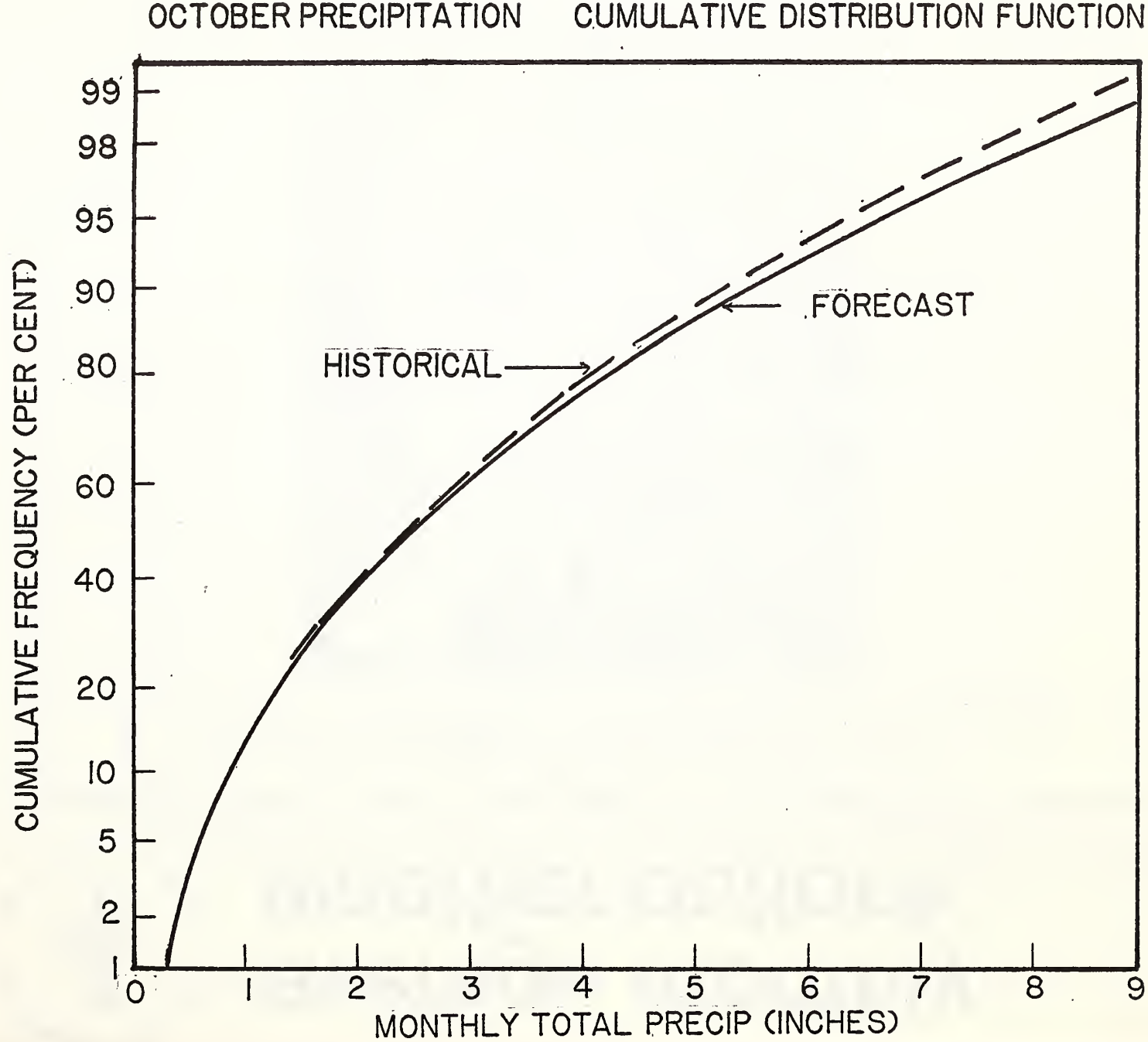
OCTOBER PRECIPITATION CUMULATIVE DISTRIBUTION FUNCTION
CUMULATIVE FREQUENCY (PER CENT)
99
98
95
90
80
60
40
20
10
5
2
1
HISTORICAL
FORECAST
0
1
2
3
4
5
6
7
8
9
MONTHLY TOTAL PRECIP (INCHES)

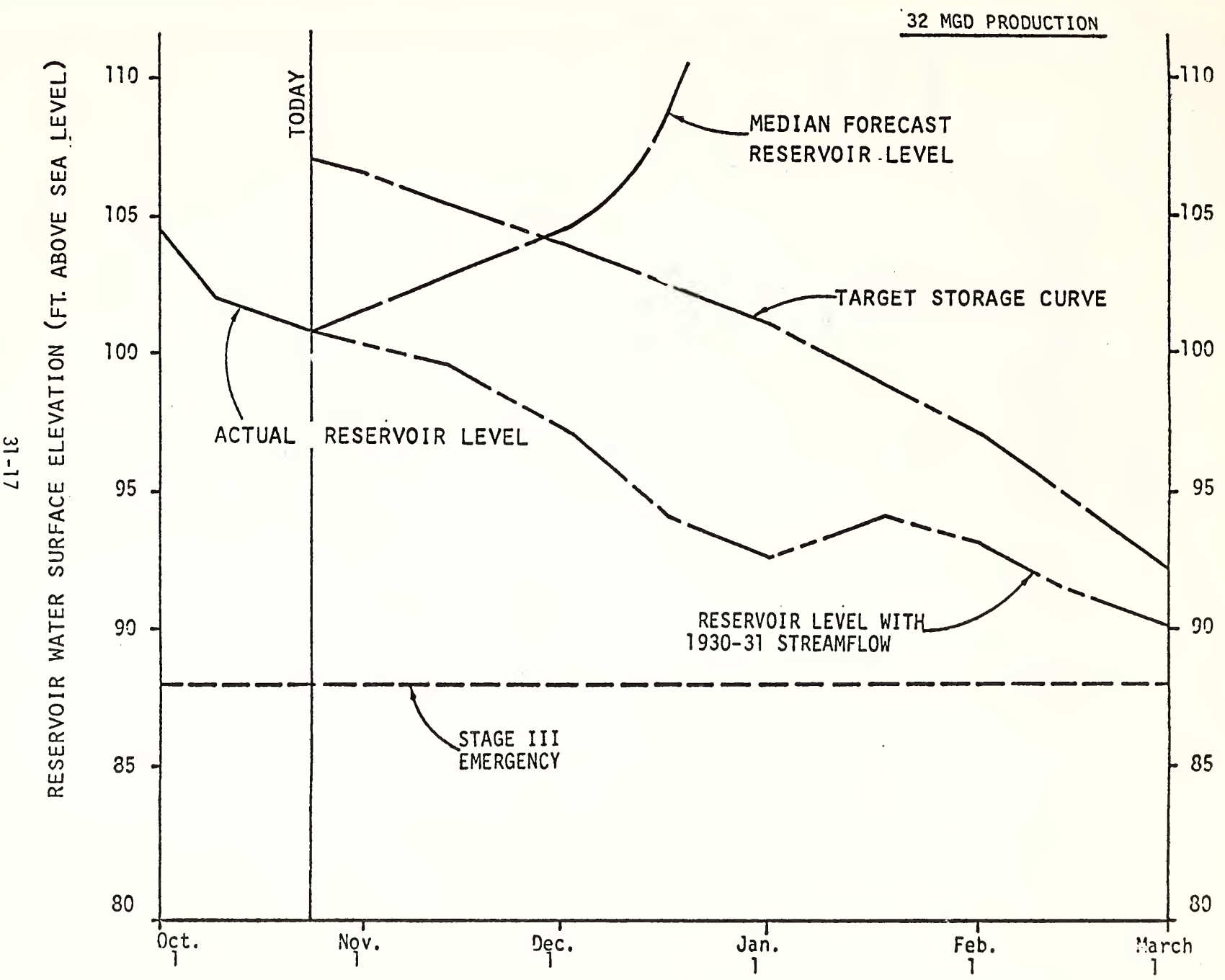
32 MGD PRODUCTION
RESERVOIR WATER SURFACE ELEVATION (FT. ABOVE SEA LEVEL)
110
105
100
95
90
85
80
TODAY
MEDIAN FORECAST
RESERVOIR LEVEL
TARGET STORAGE CURVE
ACTUAL RESERVOIR LEVEL
RESERVOIR LEVEL WITH
1930-31 STREAMFLOW
STAGE III
EMERGENCY
Oct. 1
Nov. 1
Dec. 1
Jan. 1
Feb. 1
March 1

FIGURE 2

TABLE 1

PROBABILITIES OF FALLING BELOW STORAGE LEVELS
AT 40 MGD (CURRENT PRODUCTION RATE) AT OCCOQUAN*

Storage Level	93 feet	88 feet	83 feet
Volume of Storage Remaining	1.7 B.G.	1.1 B.G.	0.7 B.G.
Probability	13%	10%	8%

* Purchase of 1.5 B.G. from Lake Manassas is assumed.

TABLE 2

PROBABILITY OF FALLING BELOW STORAGE LEVELS
AT 32 MGD PRODUCTION AT OCCOQUAN*

Storage Level	93 feet	88 feet	83 feet
Volume of Storage Remaining	1.7 B.G.	1.1 B.G.	0.7 B.G.
Probability	5%	3%	2%

* Purchase of 1.5 B.G. from Lake Manassas is assumed.

APPLICATION OF THE UNIVERSITY OF WISCONSIN MODEL TO CLIMATE PREDICTION

Gerald J. Dittberner
USAF Environmental Technical Applications Center
Scott AFB, IL 62225

Studies of past climates indicate that there is no single cause of climatic variation. Evolution of the atmosphere, variations of the earth's orbital parameters, solar variations, continental drift, volcanic activity variations, and still other causes are all thought to be important at different time scales. For scales such as the coming season and the coming year many of these potential causes of variation can be considered negligible.

The climate prediction model was constructed based on two sub-models. The low frequency sub-model (Bryson and Dittberner, 1976 and Dittberner, 1978) deals with trends and differences in decadal or pentadal means assuming until otherwise demonstrated that these variations are determined by extrinsic physical factors such as changes in volcanic activity, anthropogenic aerosols and carbon dioxide and assuming that there is no inherent random variation. Unexplained variance of the observed climate from the model was regarded as a shortcoming of the model or of the observations and not as a fundamentally unexplainable random variation in climate.

In the high frequency sub-model (Bryson and Starr, 1977) it was assumed that part of the interannual variation of monthly mean patterns of pressure, temperature and precipitation is associated with the complex set of atmospheric tidal oscillations related to the Chandler Motion of the earth's pole. Model construction uses regression to link these input factors to monthly mean temperature and monthly total precipitation at 21 stations in the United States.

The importance of estimating effectiveness in climate prediction methods cannot be overemphasized. Accordingly, a technique was developed, based primarily on that described in Barnett and Preisendorfer (1977) to estimate the effectiveness of the University of Wisconsin Model. For each station, regression coefficients were computed on a dependent data set (1882 - 1950) and used to calculate values for 1951 through 1955. The procedure was then repeated using data from 1883 - 1951 to calcuate values for 1952 through 1956. Repeating this procedure through 1974 produced 23 one year ahead calculations, 22 2-year ahead calculations, etc. Statistical significance was estimated for a three category (H,M,L) system (each category having a probability of one third) using the binomial distribution. Values of significance were determined as in the following example. For the case where there is a total of 11 correct categories out of 24 at-

tempts we find that the probability of 11 or more correct out of 24 is 0.14 (for a probability of occurrence by chance of 1/3). Subtracting this from unity gives a value of 0.86. This can be considered a measure of forecast significance, skill or confidence.

Analysis of the confidence values for 21 stations in the United States indicates the following:

1. There are indications that the confidence or skill of this model may not be primarily a function of forecast lead time.

2. This method may not be applicable to all stations in all months; however it is possible that for some stations in some months the method may demonstrate significant success.

3. The geographic distribution of calculated confidence values suggests that the method may be applicable to stations in the Dakotas for January mean temperature, the eastern United States for April mean temperatures, the southern and eastern United States for January total precipitation and Texas for April total monthly precipitation.

Intriguing relationships between the mapped confidence patterns and potentially related factors (e.g., airmass dominance, importance of local effects, possibilities for improving the forecast methods, etc.) provide fruitful ground for continued study

REFERENCES

Barnett, T.P., and R.W. Preisendorfer, 1977: Short-term prediction of global climate using multi-dimensional analog methods. Preprints, Amer. Meteor. Soc. Fifth Conference on Probability an Statistics in Atmospheric Sciences, 15-18 November 1977, Las Vegas, Nevada, 11-15.

Bryson, R.A., and G.J. Dittberner, 1976: A non-equilibrium model of hemispheric mean surface temperature. J. Atmos. Sci. 33, 2094-2106.

Bryson, R.A., and T.B. Starr, 1977: Chandler tides in the atmosphere. J. Atmos. Sci., 34, 1975-1986.

Dittberner, G.J., 1978: Climate projections based on volcanic activity, man-made pollution and carbon dioxide. Preprints, Amer. Meteor. Soc. Conference on Climate and Energy: Climatological Aspects and Industrial Operations, 8-12 May 1978, Asheville, N.C., 125-132.

WISCONSIN MODEL

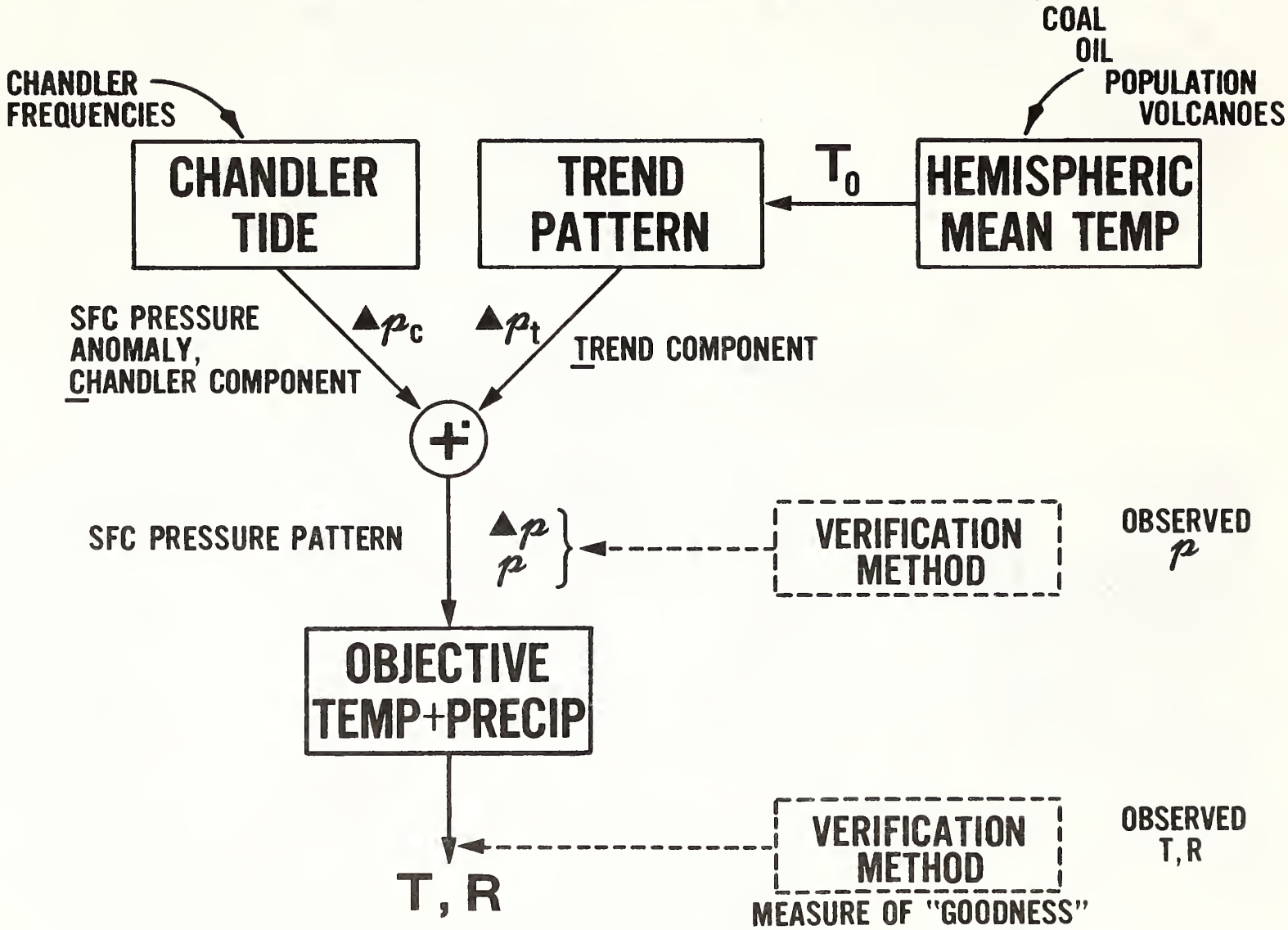

Monthly Mean Temperature

SIGNIFICANCE

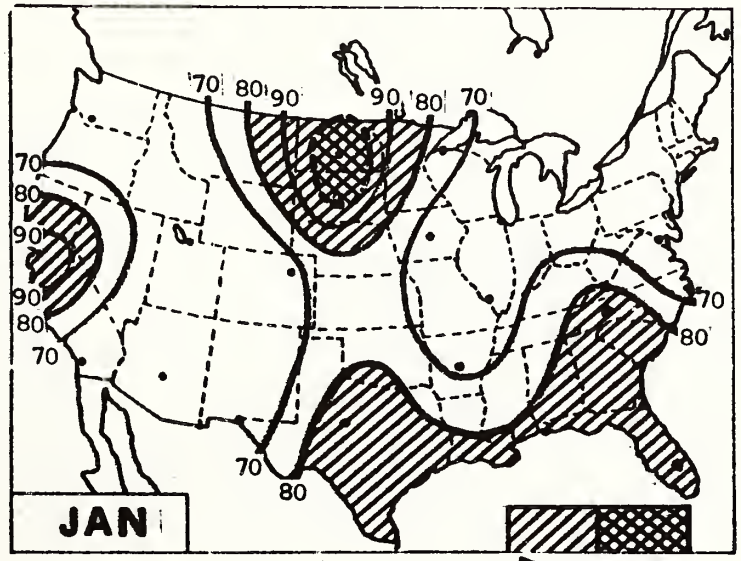

3 CATEGORY

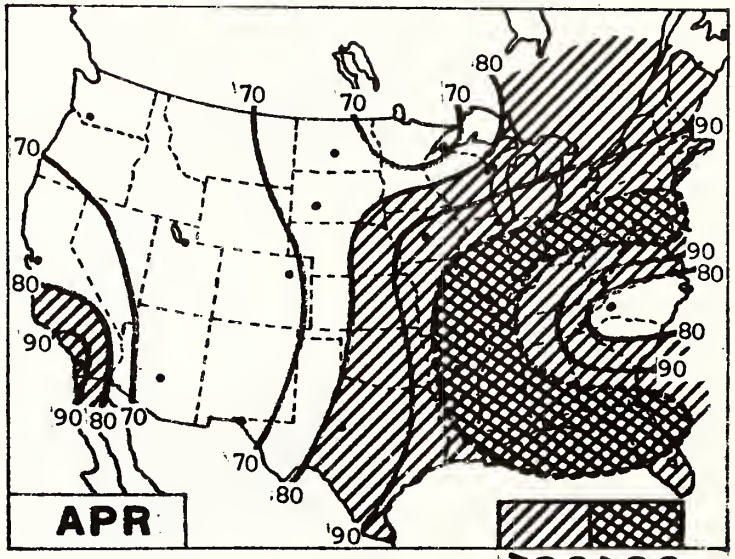

Monthly Total Precipitation

SIGNIFICANCE

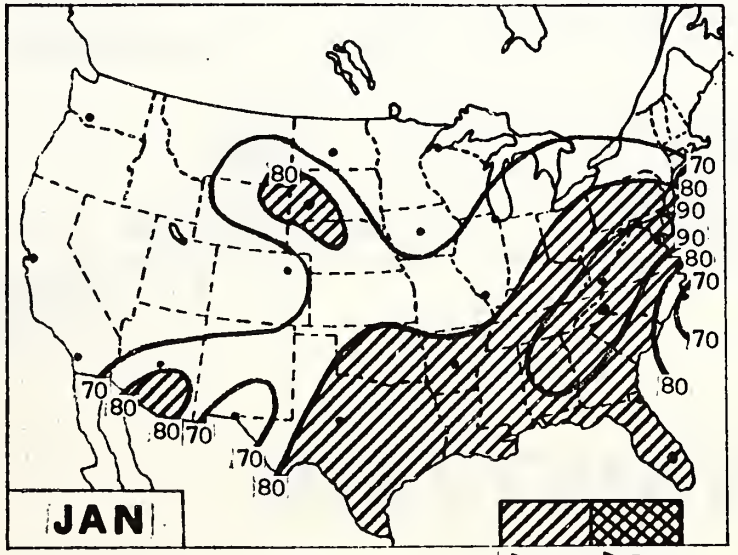

3 CATEGORY

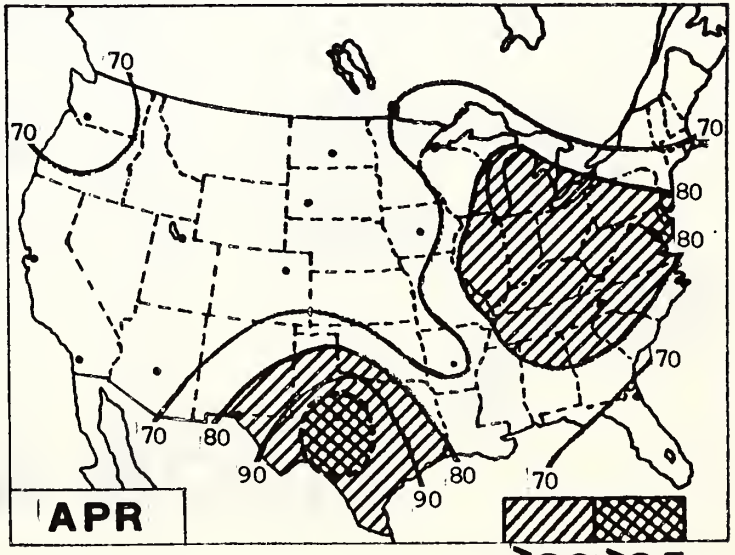

PREDICTABILITY OF AIR TEMPERATURE OVER NORTH AMERICA - A PROGRESS REPORT

T. P. Barnett

Introduction

It has often been stated that properties of the ocean and atmospheric field in the Pacific Ocean can be used to predict atmospheric variables over North America. This is a progress report on a quantitative attempt to verify such hypotheses.

The method of linear prediction has been used to test a variety of hypotheses. The details of the method, i.e., mathematics significance test, etc., are given in Barnett and Hasselmann (in press) and will not be repeated here. Suffice it to say, the technique attempts to take a series of specified predictors and see how well they can be used to forecast a given variable at different lead times. The crucial new element in the approach has been to balance predictive skill with statistical significance. Thus it is possible to make models with higher skill than those shown here. However, they will surely have less significance. In the following work we attempt to construct models that are significantly different from the null-hypothesis type model at the 90% confidence level.

The predictors used in this study are shown in Figures 1 and 2. Areal averages for the various regions have been constructed from the historical weather map series in the case of sea level pressure and from a recent updated version of the Marine Deck (TDF11) in the case of sea-surface temperature. Thus, for each of the index regions shown in Figures 1 and 2 we have developed a time series of either pressure or sea-surface temperature anomalies by season for the period 1899 through 1972. The regions over which the average were computed, by the way, were defined semi-objectively by methods of variance analysis and also on physical grounds. The time series from the index regions have been compared where possible with independent data sets. The cross comparisons have shown the long time histories to be surprisingly good in their

quality and continuity.

Specifications

Before trying to predict anything, it is first important to ask, given a set of information, can one use it to simultaneously specify the properties of the variable that eventually we want to predict. With this in mind, the sea level pressure variables in winter have been used to specify the corresponding winter air temperature anomalies at 42 stations over the North American continent. The results of this specification are shown in Figure 3. The numbers show the percent of variance accounted for in the specification (62% of the variance) leave a large measure of variation unaccounted for. The principal feature of the diagram is the region where skills of less than 30% were found in the Great Plains area. Based on this we might expect our ability to predict in these areas will be relatively small.

We have next taken the sea-surface temperature anomaly data (Figure 2) for winter and attempted to specify the winter air temperature over North America. The results are shown in Figure 4. It is seen that the large region of low specification ability is enhanced and deepened by using SST variables. Furthermore, the percent of variance accounted for throughout the continental United States is substantially lower using the sea-surface temperature. Thus it would appear the sea-surface temperature is not nearly as skillful at specifying air temperature anomalies as is sea level pressure.

One Season Predictability

At this early stage in the work we have considered only the situation of predicting winter air temperatures from fall sea-surface temperature and sea level pressure anomalies. Furthermore, we have only used the limited set of predictors shown in Figures 1 and 2. Thus the results of the following predictability experiment should be considered as very preliminary in nature.

Prior to computing the predictabilities, however, it is important to estimate the amount of skill that a prediction based solely on persistence would have. The results are shown in Figure 5 where it is seen that the amount of variance accounted for by persistence is generally less than 20% and then only significant at the 90% level in the extreme northwest part of the continental U.S. The apparent skills of 12 and 20 in the central and eastern U.S. respectively are almost certainly chance values (indeed at the 90% level we should expect at least 4 stations to be significant by chance).

We next attempted to predict the air temperature over North America during winter from the fall sea level pressure anomalies of the Pacific. The results are shown on Figure 6. It is seen that there is extremely low predictability over most of the continental U.S. A region of increasing predictability exists as one moves from the Dakotas into southern Canada. Also, as indicated in the upper left corner of Figure 6, substantial predictability exists at Nome and Juneau, Alaska. Thus while the results may be encouraging for those interested in Canadian winter forecasts they cannot be considered encouraging for those interested in predicting air temperatures over North America during the winter. Principal predictors responsible for the skill shown in Figure 6 come from the sub tropical ridge, specifically regions 6 and 8; although region 7 does contribute to the predictability also. Thus it appears a major part of the skill shown in Figure 6 is associated with tropical events during the preceding fall and summer (the time structure of the predictor field is also available through these studies [see cf Banrett and Hasselmann] but will only be mentioned briefly here).

We next used information on fall sea-surface temperature anomalies to try to predict winter air temperature anomalies over North America. The results are shown on Figure 7. Again we observe that over most of the continental United States there is little or no predictability. Low levels of predictability exist in the same region

as they did for sea level pressure, but again are generally smaller in magnitude than available from the pressure data. An interesting feature in the variance field shown in Figure 7 is the apparent existence of significant predictability along the west coast of the United States. In fact, study of predictors for this region showed that the skill was due to fall water temperatures immediately off the coast. Since these water temperatures persist for a period of seasons, we thus are seeing the effect of air blowing over warm or cold water and affecting the stations immediately at the coast. Note that the effect does not penetrate very far inland since both Sacramento and Spokane have no significant levels of predictability.

The principal predictors associated with the sea-surface temperature field come almost exclusively from regions 4 and 5, and to some extent region 6. The former regions are associated with tropical sea-surface temperature anomalies exclusively, and particularly those generally associated with El Niño. The importance of region 6 as a predictor and seems to imply land/sea contrast is of principal importance in determining the resulting predictability. It was clear that the often mentioned region of SST variability in the central Pacific, i.e., SST 1 on Figure 2, was not important as a predictor in the present study.

Conclusions

Preliminary results suggest there is very little skill in using Pacific predictors to forecast from fall to winter air temperatures over continental United States. Significant and substantial skill, however, does exist for forecasting this same variable in the region of southern Canada. What skill that was found came almost exclusively from the tropical regions of the Pacific Ocean, thus suggesting that there must be direct teleconnective effects between these areas and the high latitudes over North America. The mid-latitude regions of the central Pacific Ocean appear to play a minor role in the demonstrated abilities to predict from fall to winter.

Caveats

The above results must be considered as tentative for a variety of reasons which are listed below.

1. There may be other predictors that would have given better forecast skill. However, the predictor regions used are the ones most often described in the scientific literature as having importance and predictive ability over North America.

2. It may be argued that the linear model used here will fail in strongly nonlinear situations. However, work by a number of authors has shown that linear prediction models work well even for quasi-nonlinear systems. Furthermore, most workers seem to feel that quasi-linear models of climate are more than adequate to represent our current data set. Thus the linear model may not be as much of a limitation as one might imagine.

3. The skill scoring method used to estimate predictability was the amount of variance accounted for by the forecast model. This is a tough skill score and one that is unforgiving of large errors in model hindcast. A more lenient skill score could perhaps have produced a result that would have appeared more pleasing to the eye.

4. The significance test used to evaluate the models is a new approach to the significance problem (Banrett and Hasselmann). There are those that might argue that a significance test over a hindcast is not a true measure of model validity. In fact some might argue the only way significance can be demonstrated is making a model of half of a record and then using it to predict the independent part of the record. This becomes a matter of philosophy as to which way to proceed. At any rate, the same study as described above has been carried out over the 30-year data set, 1947 through 1976. The results are substantially the same.

5. The results indicated above are for only one season and one lag forecasts. Perhaps we will be more successful in other seasons or at other lags.

6. Other predictands, e.g., those from the Atlantic, may increase our abilities to predict air temperatures and other variables over North America. Certainly during

other seasons there is no reason to believe the Pacific is the sole source of all weather over North America.

7. The predictor data has been subjected to a variety of error checks. However there are some checks which it still must undergo and so we must assume that its quality is only reasonably well established. Thus unknown errors in the predictor data may be giving us lower levels of predictability than actually exist.

References

Barnett, T. P. and K. Hasselmann, 1978: Techniques of linear prediction with application to oceanic and atmospheric fields in the tropical Pacific. Submitted to Reviews of Geophysics and Space Physics.

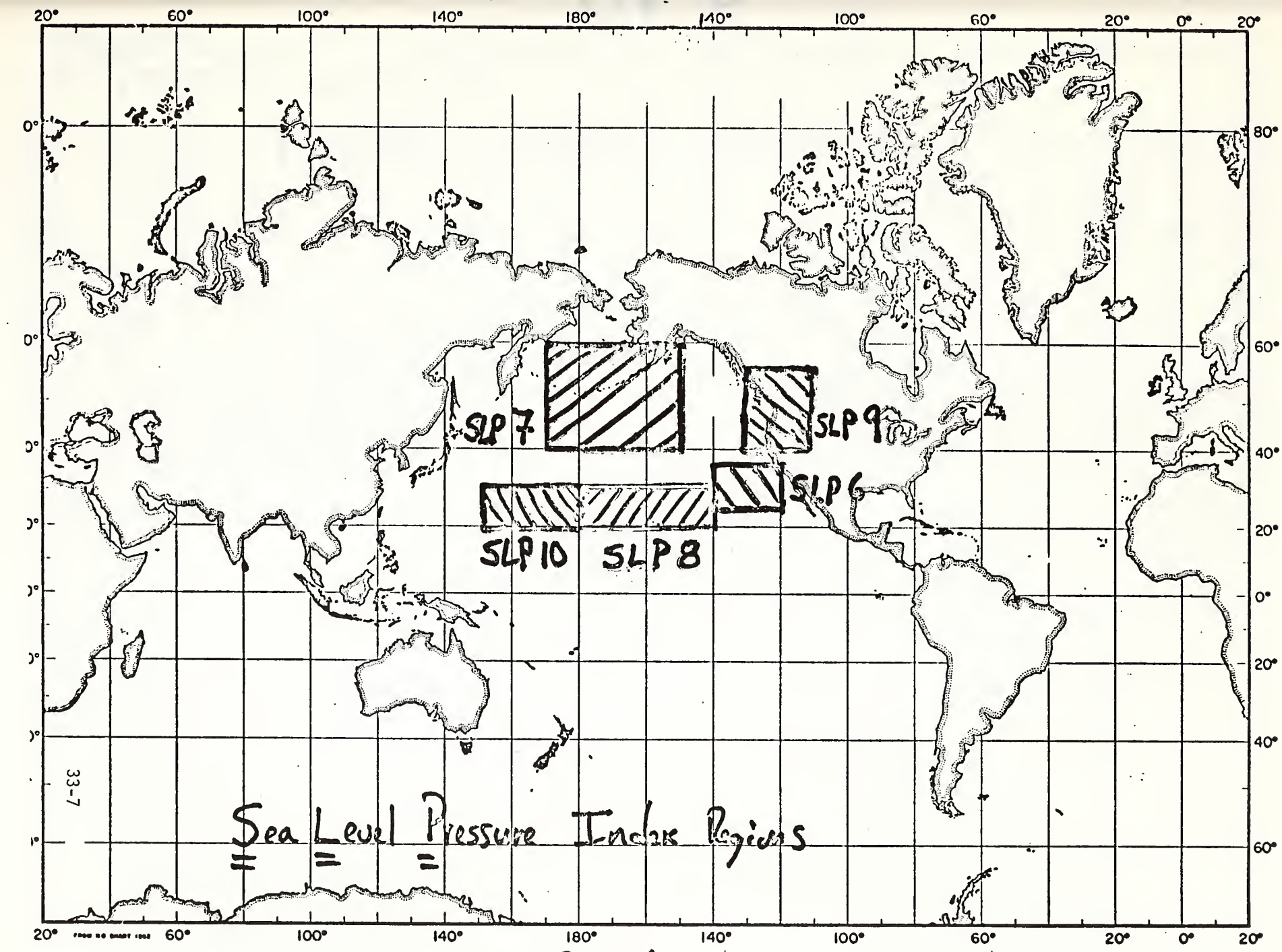
SLP 7
SLP 9
SLP 6
SLP 10
SLP 8
Sea Level Pressure Index Regions
33-7

FIG 1

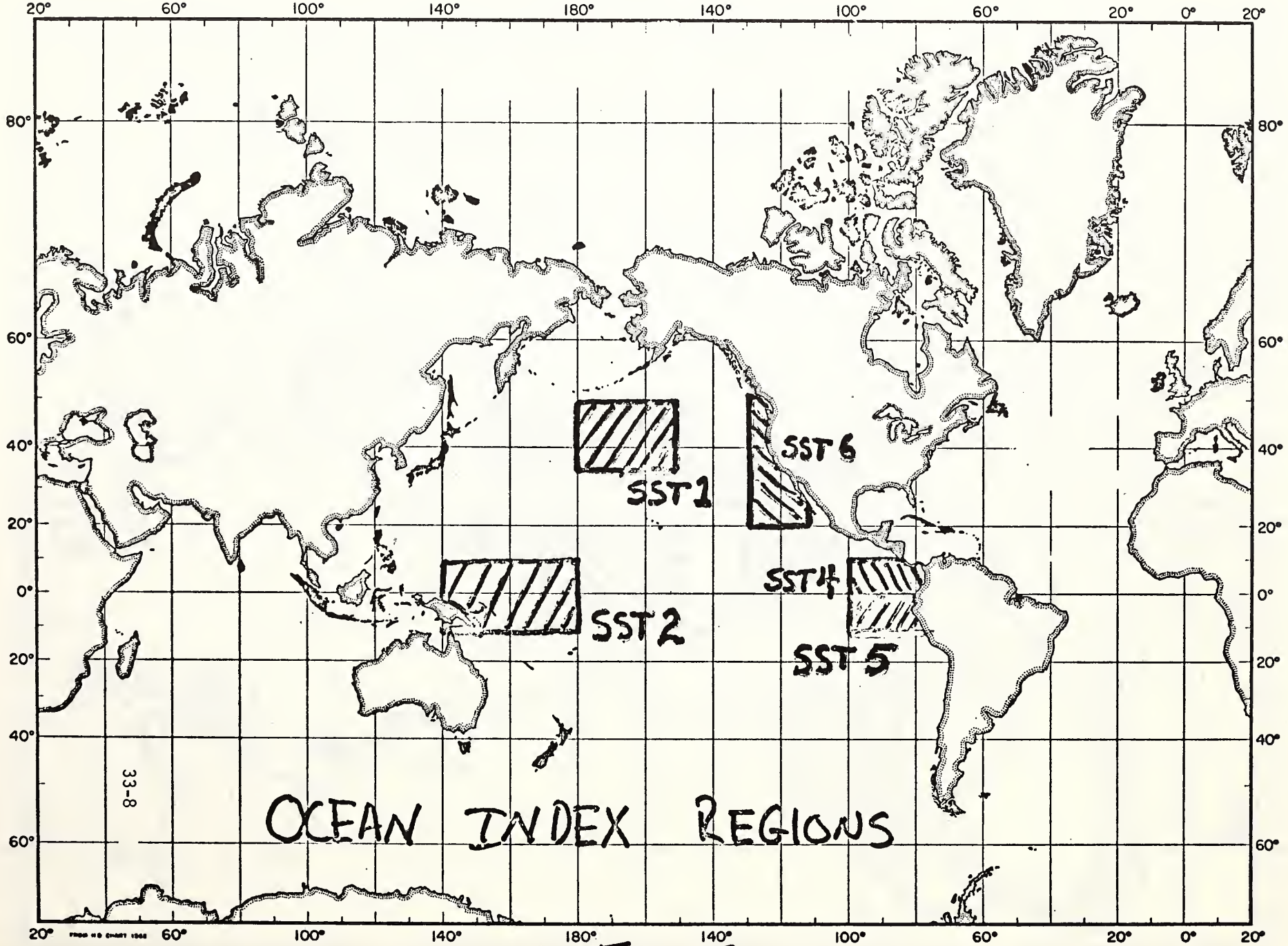

FIG 2

40 Nome
26 Juneau

Winter Air Temp
from Winter Pacific SLP

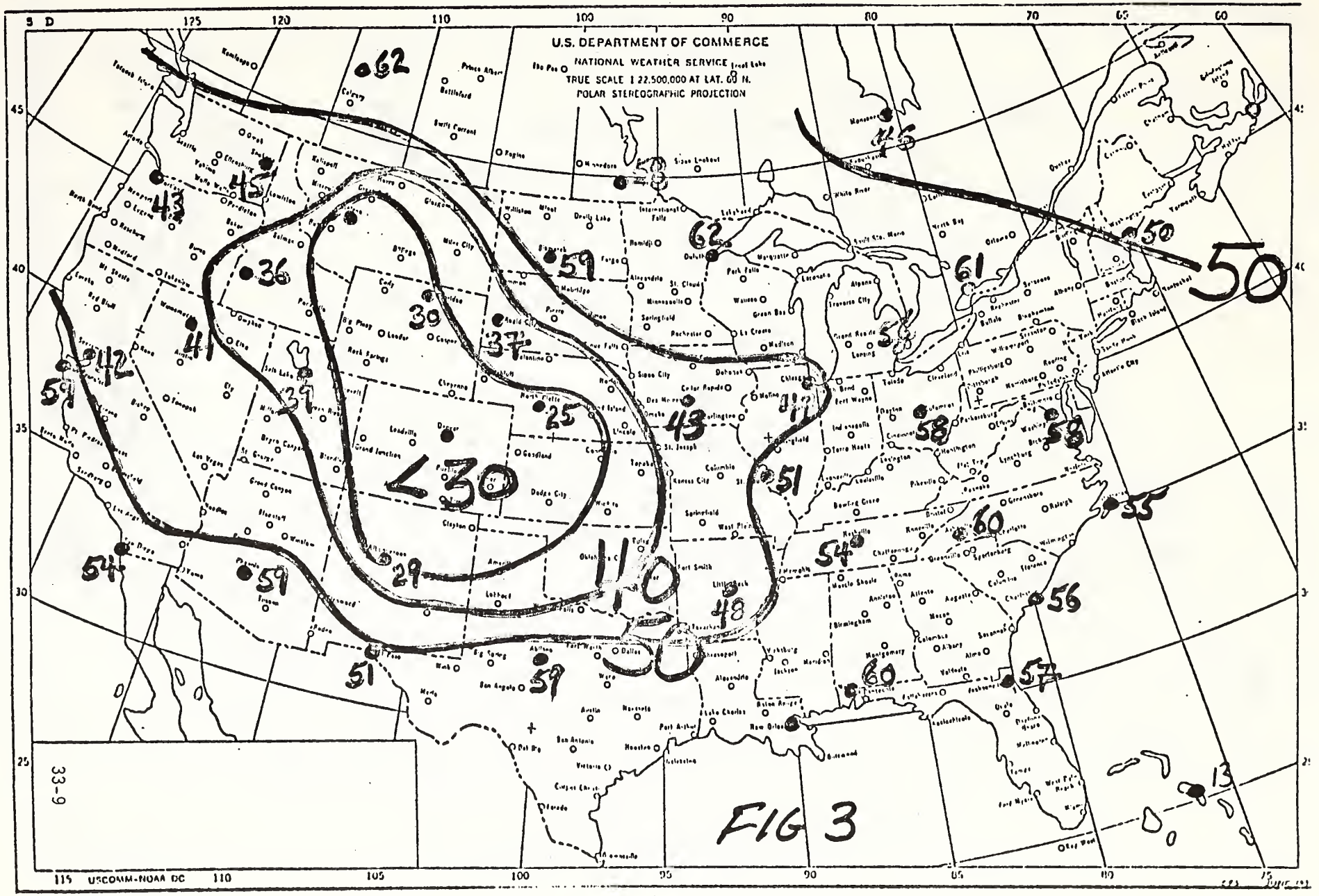

FIG 3

17 NOME
37 JUNEAU

WINTER AIR TEMP FROM WINTER PACIFIC SST

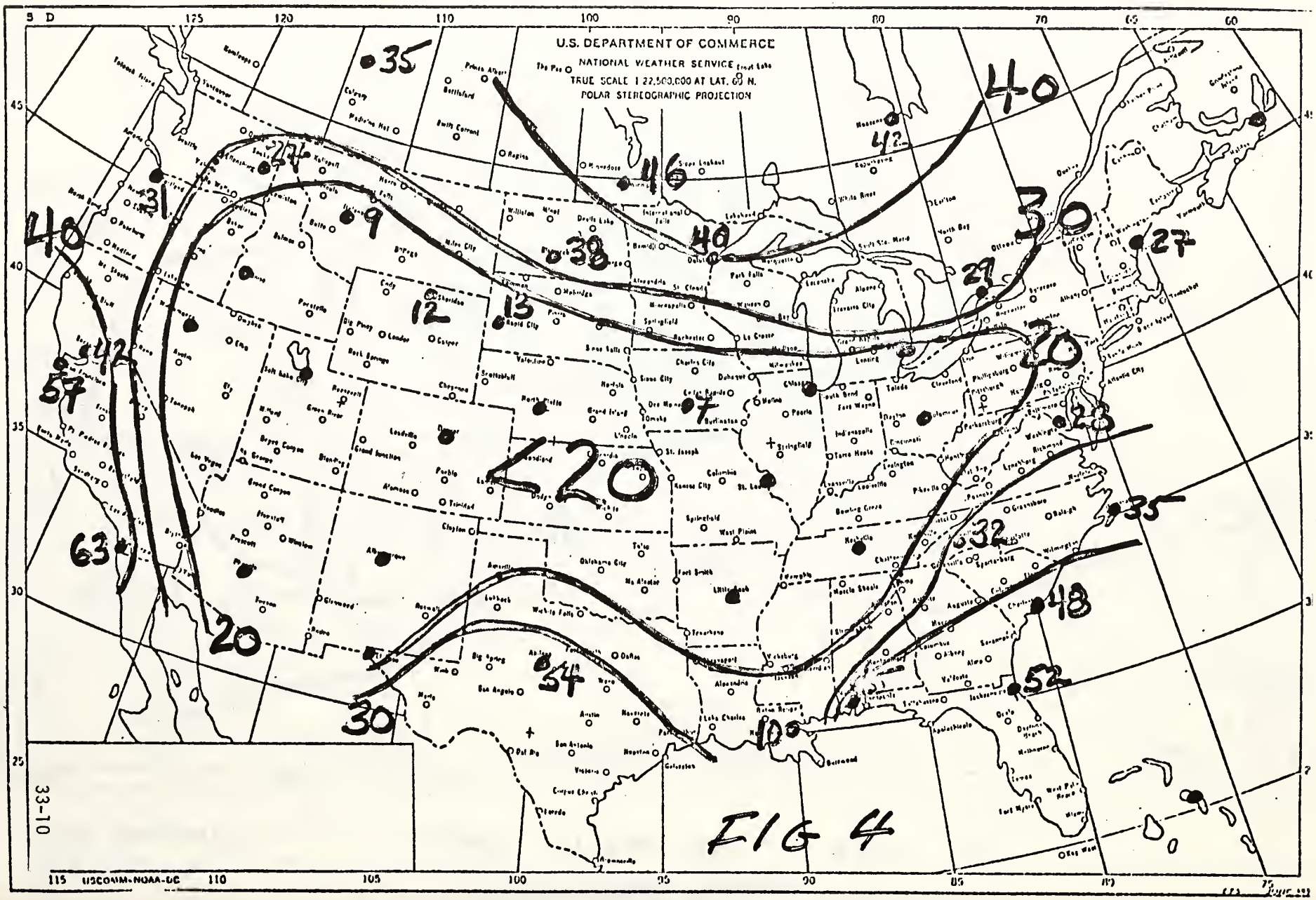

WINTER MAX TEMP.
from Fall PERSISTENCE

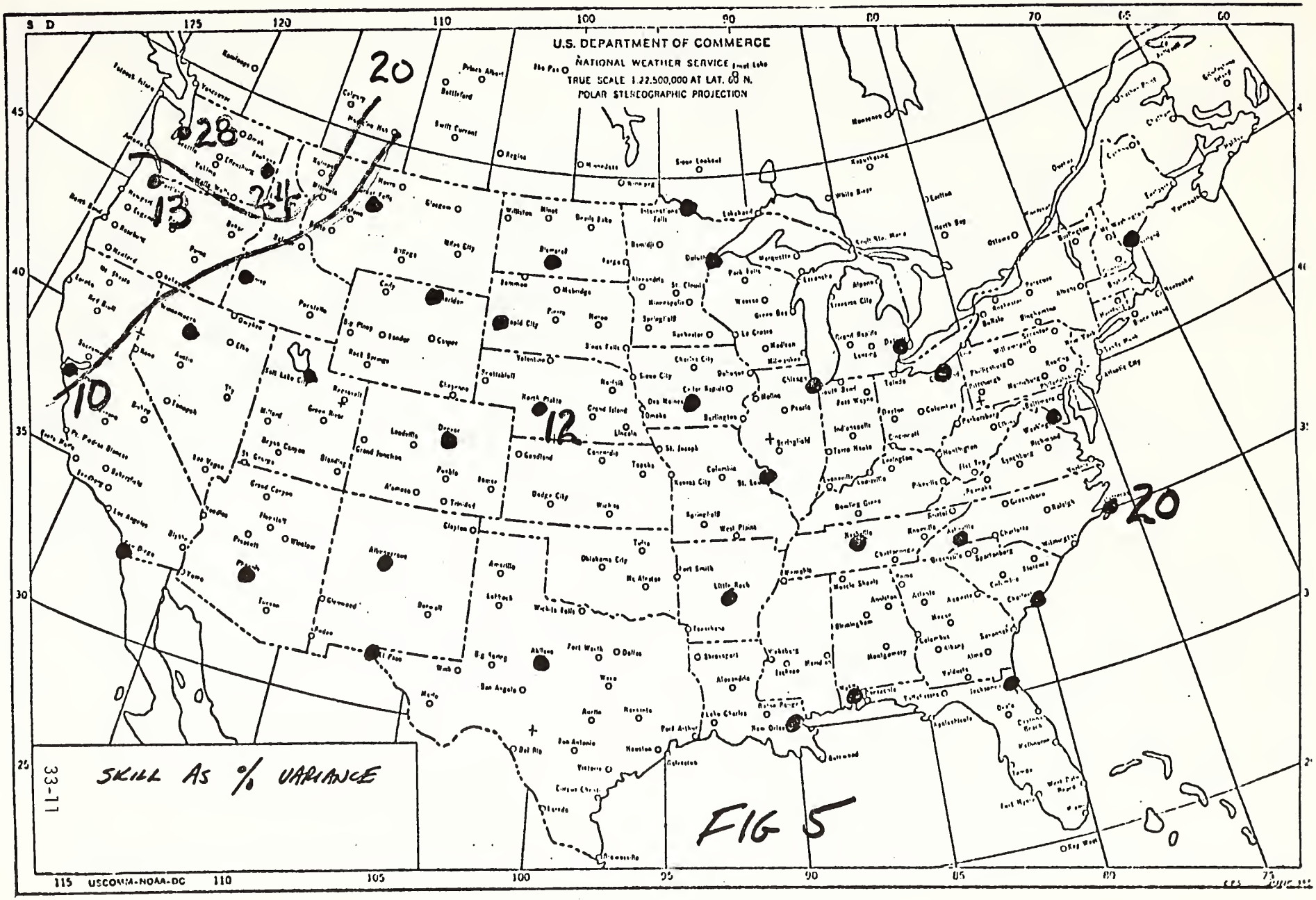

18 NOME
26 JUNEAU

WINTER AIR TEMP
from Fall Pacific SLP

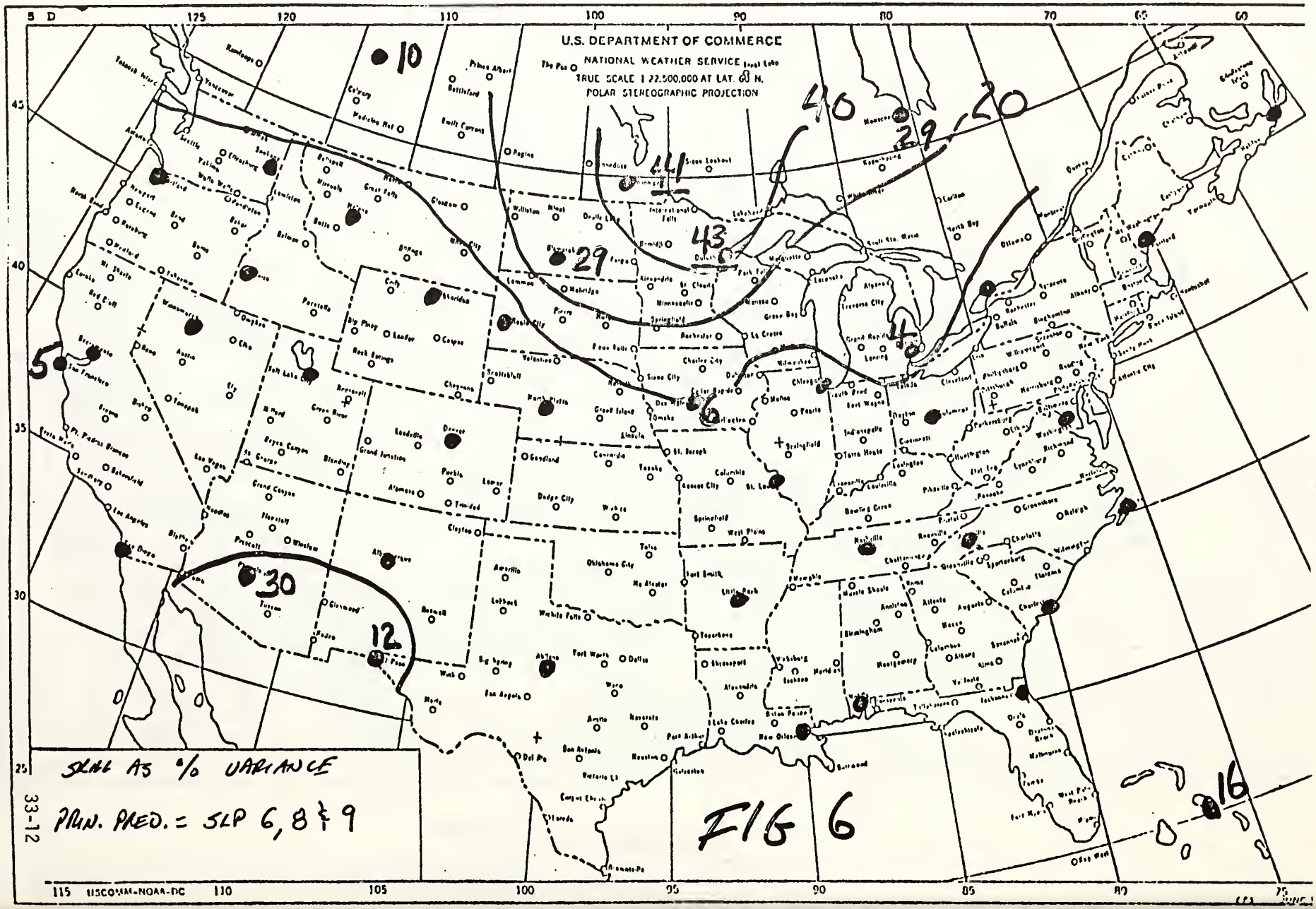

8 NOAA
18 JUNEAU

WINTER FOR TEMP
from Fall Pacific SST

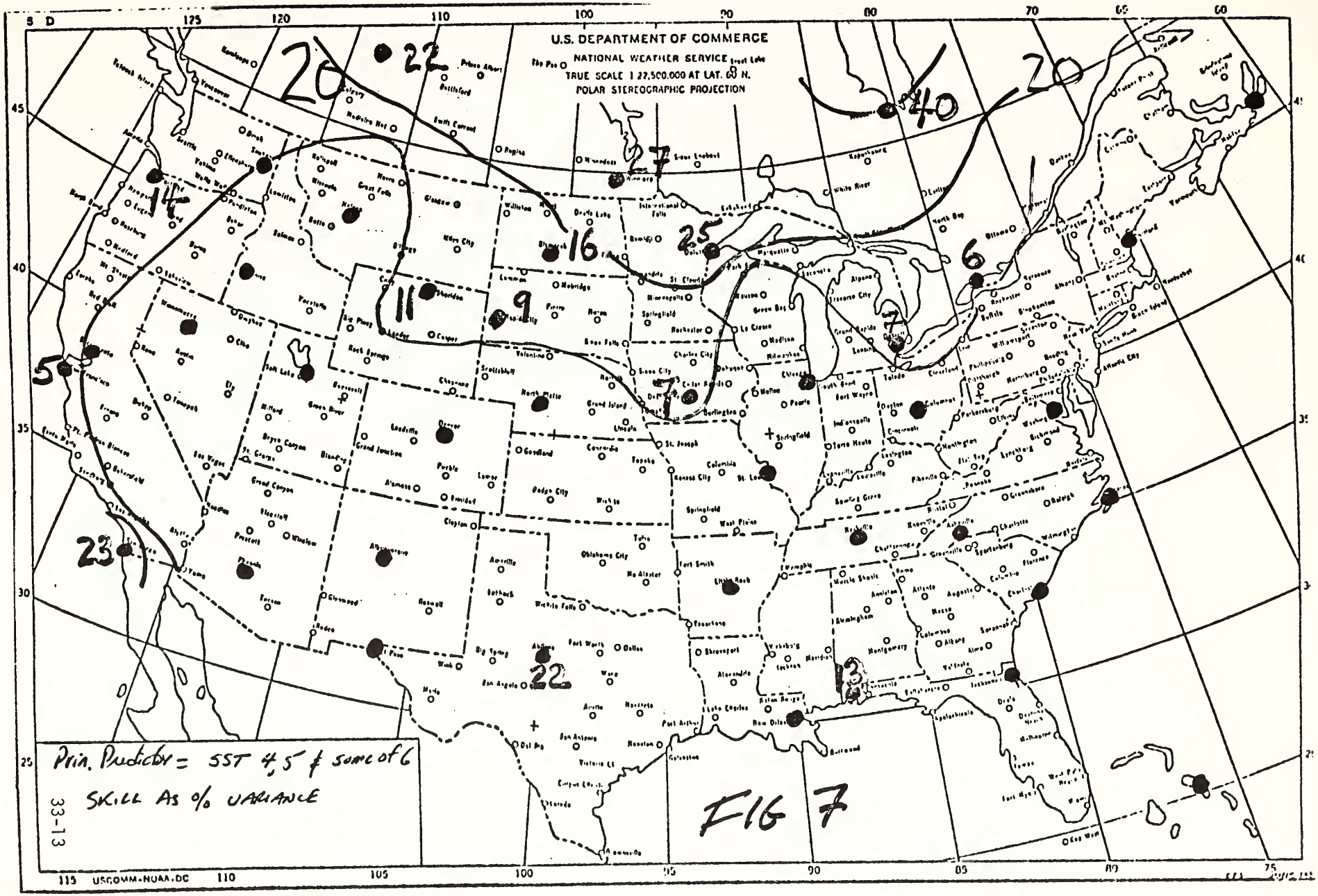

FIG 7

A Sea Level Pressure Analog Model for Predicting Temperature Over the Northern Hemisphere

J. G. Schofield
USAFETAC/DNC Scott AFB, Il. 62225

T. P. Barnett
Scripps Institution of Oceanography, La Jolla, Ca. 92093

Barnett and Preisendorfer introduced a new scheme for using analog methods in predicting climatic fluctuations at the October 1977 Climate Diagnostics Workshop. Their scheme involves the use of empirical orthogonal functions to represent data fields and defines a "climate state vector" that is described by the eigenvectors of the Northern Hemisphere climate field. Climatic analogs are chosen based on the behavior of this "climate state vector."

It was shown that the climate state vector idea resulted in statistically significant forecasting capabilities. However, the previous work did not make it clear which of the fields in the climate state vector was responsible for the predictability nor indicate what regions of the globe were the most sensitive predictors. In the present work we have tried to home in on the fields and geographic regions that might be responsible for predictability. As our first start we have considered only one field from which to make the analog forecast. That field was the hemispheric sea level pressure field extending from 1899 to present. We have developed a sequence of models using first the entire hemispheric field, then regional fields and finally weighted regional fields in order to determine the key predictor regions. Clearly this same type of analysis will have to be done with other fields used to define the climate state vector, e.g., sea-surface temperature.

A model based on the hemispheric pressure field was used to predict seasonal surface temperature anomalies for 42 North American stations over the 75 year period, 1902-1976. A similar analysis has been made for 81 stations in Eurasia. A regional model that uses spatially limited (150°E to 20°W) pressure field information was also developed for predicting temperature anomalies over the North American continent only. Finally, an attempt was made to find an "optimum" analog selection scheme.

A skill score was computed for the models by counting the number of correct predictions at each station. The temperature anomalies for each station [F(x,t)] were grouped into terciles, or groups of upper, middle, and lower thirds, denoted by Above normal, Normal, and Below normal. The two fields F(x,t) and F(x,t') match at station x if their numerical values fall into a common tercile. The total number of matches for a fixed forecast time t over each station (x) gives a measure of the skill of the model at forecast time t. The global skill is the average skill score over x for all forecast times t. The total number of matches for fixed x and all forecast times t gives the temporal, or local skill at each station x. Probability limits for the local skill scores are computed using the binomial distribution

$$p(r) = \frac{m!}{r!(m-r)!}\,\alpha^{r}(1-\alpha)^{m-r}$$

where r is the number of matches and m is the number of trials (75 in our example). A score of 29 matches over 75 years (38.7%) is significant at the 92% probability level.

Figure 1 shows the local skill scores for the hemispheric model. Shaded areas represent significant local skill. A comparison with the North American model (Figure 2) shows an increase in the areas of significant skill. For both models, the global skill score is relatively low. The fact that significant local skill can be obtained in certain areas, such as the East Coast, but not in others (the North Central U.S. for example) suggests that global skill scores may not be entirely representative of the model's capabilities.

An attempt was made to find an "optimum" method for selecting regional analogs. This scheme is based on the correlation between the sea level pressure EOF amplitudes (modes 1-6) and the North American temperature field EOF amplitudes (modes 1-6). Figure 3 shows the relationship between the winter pressure EOF amplitudes and the summer temperature EOF amplitudes. In this example, we selected modes 1, 2, and 4 for our "optimum" analog scheme and weighted the amplitudes according to their relative contributions in the pressure-temperature correlation. Mode 1, for example, is weighted more heavily than modes 2 and 4.

The results of the "optimum" selection model are depicted in Figure 4. Areas of significant local skill appear similar to the results obtained by the North American model (Figure 2), however the number of stations with significant local skill is slightly lower. The global skill score for the "optimum" analog scheme is considerably lower than the score for the North American model.

In summary, it was found that the regional analog model for North America showed a significant increase in skill over the Northern Hemisphere model. The attempt to find an "optimum" analog scheme did not meet with success, however research in this area is continuing.

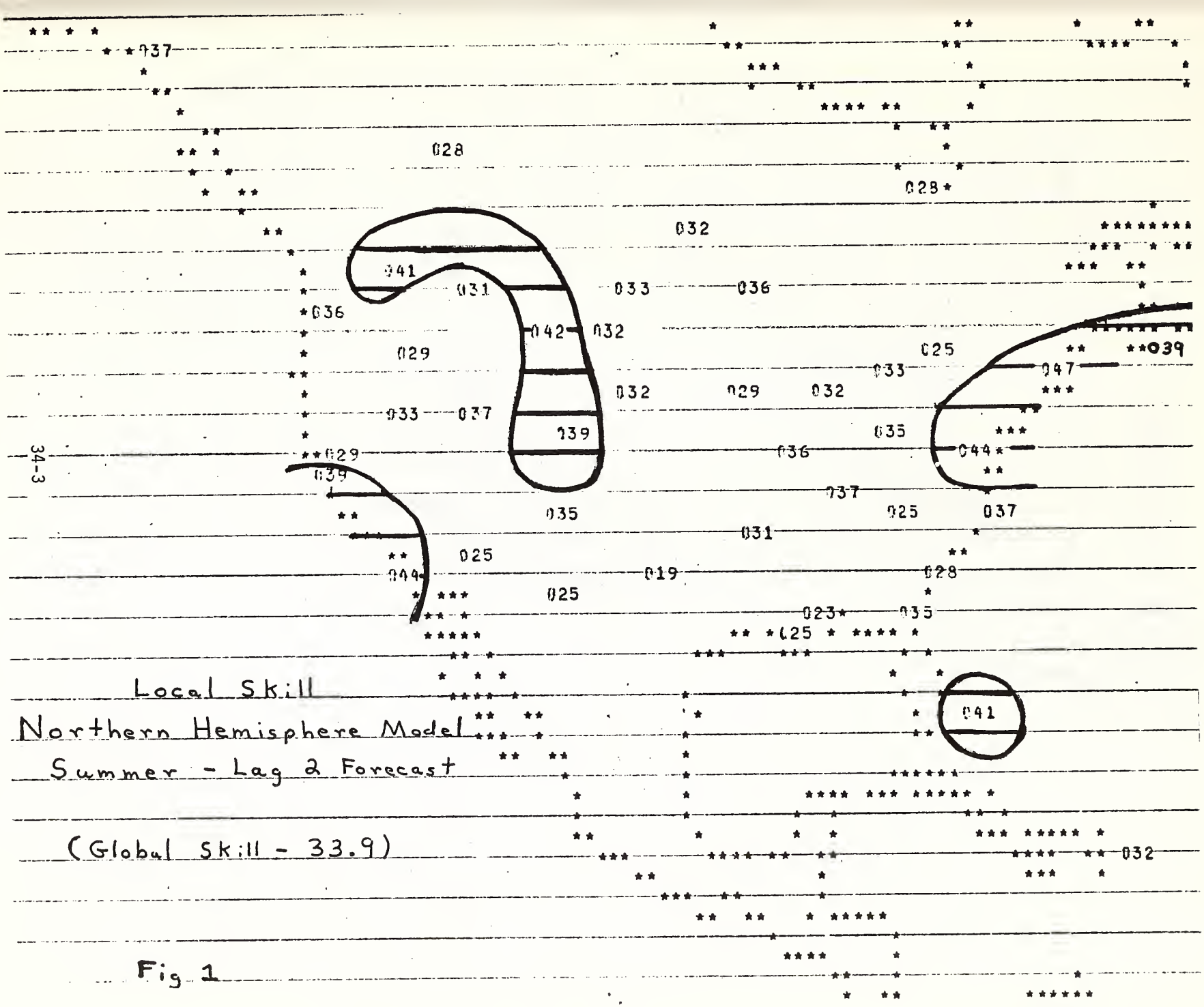

34-3

Local Skill

Northern Hemisphere Model

Summer - Lag 2 Forecast

(Global Skill - 33.9)

Fig 1

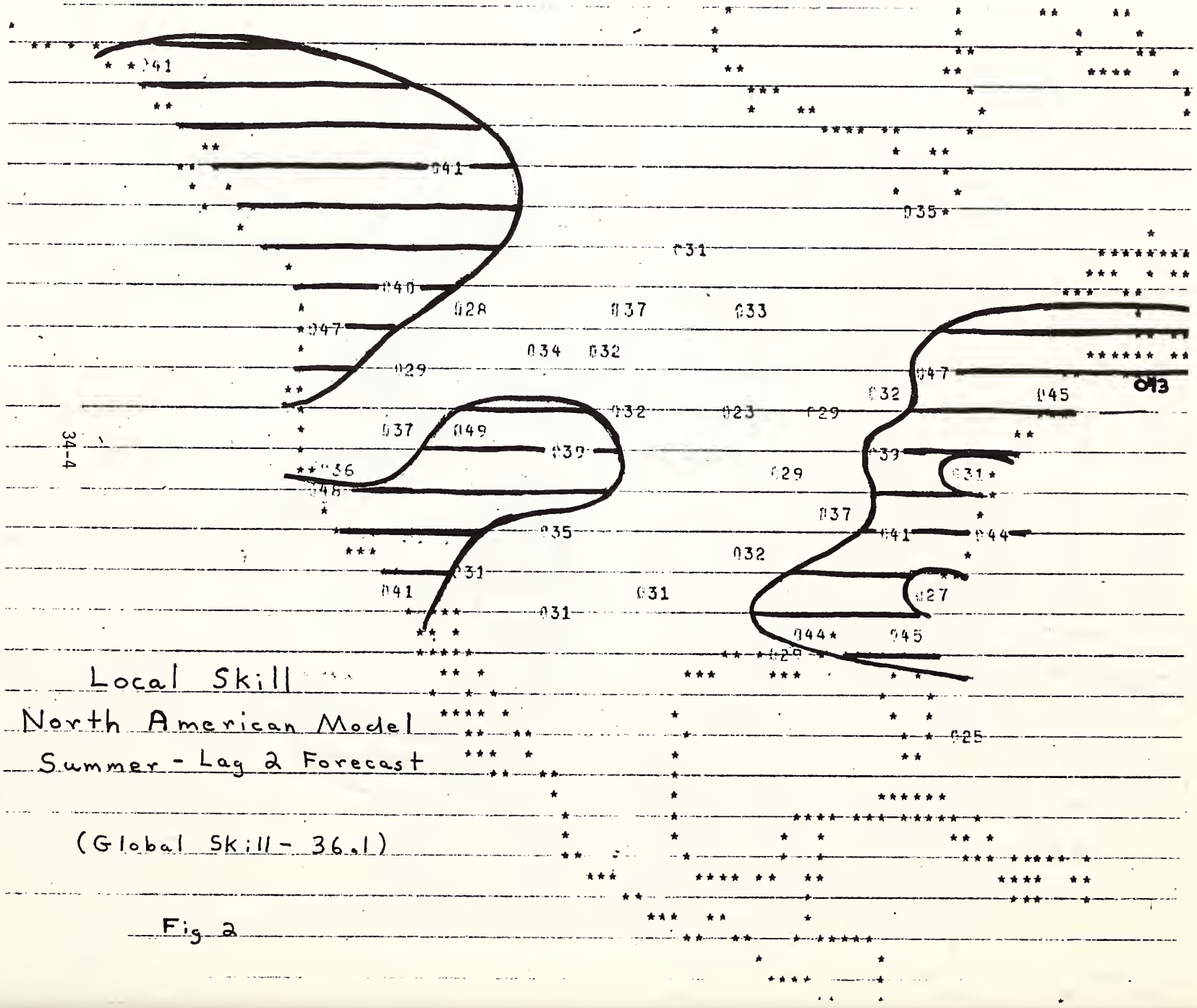

Local Skill

North American Model

Summer - Lag 2 Forecast

(Global Skill - 36.1)

Fig 2

Figure 3

"OPTIMUM" Analog Scheme

Based on correlation of pressure EOF amplitudes with temperature EOF amplitudes:

Winter Pressure EOF Amp. (modes 1-6) ↓	Summer Temperature EOF Amp. (modes 1-6) →					
	(.23)	(.25)	-.04	(.29)	.15	-.14
		-.11	(-.28)	.07	-.06	(-.29)
			-.02	-.01	.18	.04
				-.11	(-.32)	.18
					.17	.08
						-.02

Use pressure EOF modes 1, 2, 4 in analog model.

The optimum metric is

$$d^2(t,t') = w_1 (A_1(t)-A_1(t'))^2 + w_2 (A_2(t)-A_2(t'))^2 + w_3 (A_4(t)-A_4(t'))^2$$

min [d] at t,t* so t*+δt is forecast for t+δt

$w_1 = 0.6979$

$w_2 = 0.2337$

$w_3 = 0.0683$

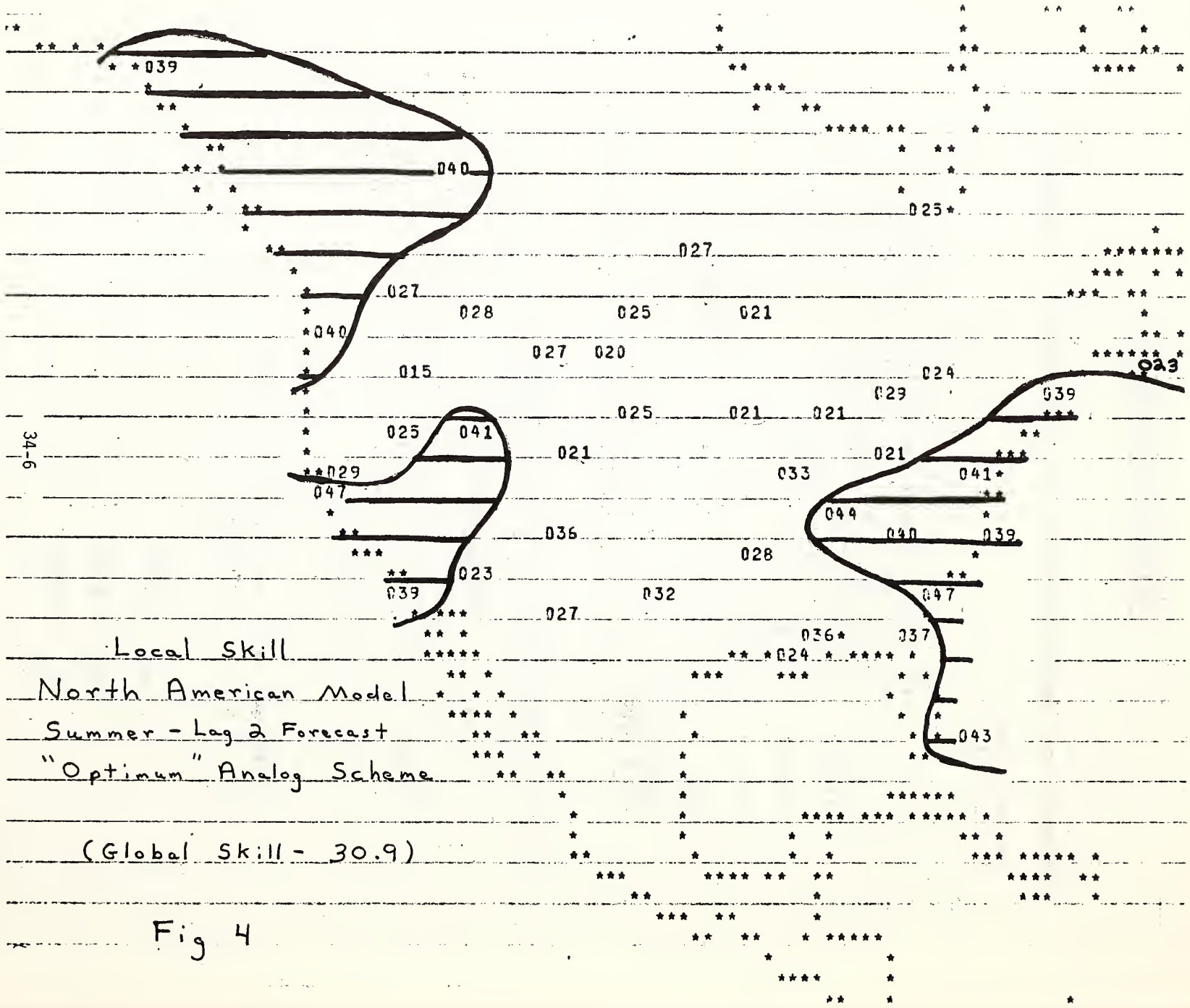
039
040
027
028
040
025
027
021
027
020
015
024
023
029
039
025
041
025
021
021
021
029
033
041
047
044
036
040
039
028
023
039
032
047
027
036
037
024
043
Local Skill
North American Model
Summer - Lag 2 Forecast
"Optimum" Analog Scheme
(Global Skill - 30.9)

Fig 4

Solar Variations and Weather/Climate

A. B. Pittock

Laboratory of Tree-Ring Research, University of Arizona, Tucson 85721
(On leave from CSIRO Atmospheric Physics, Victoria 3195, Australia)

In a recent more extensive review paper (Pittock 1978) I concluded that despite a massive literature on the subject, there is at present little or no convincing evidence of statistically significant or practically useful correlations between sunspot cycles (11- or 22-yr. periods) and the weather or climate. Further, that the evidence to hand suggests that if in the future more data and better analyses enable the detection of statistically significant relationships, these will account for so little of the total variance in the climatic record as to be of little practical value.

It is conceivable that a more complex hypothesis could be developed capable of accounting more subtly for a greater proportion of the variance, perhaps one which allows for climatic discontinuities or flips from one climatic state to another (suggested by data such as in figs. 1 and 2) such that solar influences have different effects in different epochs. Such a hypothesis would not be established as a viable theory, however, until it was used to make detailed predictions which were verified on independent data.

On shorter time scales, characterized by the period of solar rotation, the passage of solar magnetic sector boundaries, solar flares, and related events, there is again a voluminous and confusing literature. Many claimed relationships are again based on inadequate data and/or analysis but there appear to be some statistically significant results (Wilcox et al, 1976; Hines and Halevy, 1977). Other related studies, however, have drawn negative or inconclusive results, so that in the absence of detailed and testable physical hypotheses as to causal mechanisms the few statistically convincing results are not yet so persuasive as to enable us to dogmatically assert that solar-weather relationships on this time scale have been "proven" to exist.

Hope of progress is greater on the shorter time scale because it is much easier to gather independent data sets with which to establish more credible statistics and to test mechanisms and predictions. So far statistics on the skill of conventionally-based numerical weather forecasts following key days (Larsen and Kelley, 1977) show only a marginally significant drop in skill on days which might be related to solar-induced effects. More extensive testing might prove profitable here. Short-term transient effects seem to me intuitively more plausible than significant effects on the 11- and 22-yr. time scales.

On the longer time scales of centuries, where the possibility of physically significant changes in the solar "constant" exist, there is some evidence suggestive of a relationship between solar variations and climate (Eddy, 1977). Long proxy records of solar activity via carbon 14 in tree rings, and of climatic variables, exist or can be developed for some localities. These may lead to the establishment

of statistically significant relationships, but there is a danger of circularity in relating solar variations via C-14 variations to climate, since climatic change might affect C-14 concentrations.

The literature on solar cycle-weather/climate relationships displays a great lack of rigor and particularly of the "common-sense" application of relatively simple statistical considerations. The effects of auto-correlations, smoothing, and the a posteriori selection of data, on the statistical significance of results have very often been overlooked. Elaboration of hypotheses to fit the data, without testing on independent data, is not uncommon. Contradictory and sometimes incredible results have too often been uncritically accepted, and there has been a widespread lack of appreciation of the non-stationary behavior of climatic data series.

Many of these faults are evidently the result of over-enthusiasm and self-delusion, and the lack of inter-disciplinary communication and criticism. There is evidence (Gani, 1975) that these faults are widespread in the climatological literature where a frustratingly inadequate data base often raises the temptation to overstate the statistical or practical significance of a result. This may be particularly the case with unrepresentative or highly auto-correlated oceanic data and with short runs of upper atmospheric data. Comments and some gratuitous advice will be found in my published review.

References Cited

Bell, G. J., Changes in sign of the relationship between sunspots and pressure, rainfall and the monsoons, Weather 32, 26-32, 1977.

Eddy, J. A., Climate and the changing sun, Climatic Change 1, 173-190, 1977.

Gani, J., The use of statistics in climatological research, Search 6, 504-508, 1975.

Hines, C. O., and I. Halevy, On the reality and nature of a certain sun-weather correlation. J. Atmos. Sci. 34, 382-404, 1977.

Larsen, M. F., and M. C. Kelley, A study of an observed and forecasted meteorological index and its relation to the interplanetary magnetic field, Geophys. Res. Letters 4, 337-340, 1977.

Pittock, A. B., A critical look at long-term sun-weather relationships, Rev. Geophys. Space Physics, 16, 400-420, 1978.

Rodhe, H. and H. Virji, Trends and periodicities in East African rainfall data, Mon. Weather Rev. 104, 307-315, 1976.

Wilcox, J. M., L. Svalgaard, and P. H. Scherrer, On the reality of a sun-weather effect, J. Atmos. Sci. 33, 1113-1116, 1976.

Captions

Figure 1. Water level in Lake Victoria 1899-1973 as measured at the Jinja gauge (height in meters). Note the apparent nonstationarity of the data set, and see the discussion by Rodhe and Virji (1976).

Figure 2. Variations of the correlation coefficient, calculated over moving 15-year intervals, between the mean sea level pressure at the indicated stations in August and the mean annual sunspot relative number. In each case the 15-year correlation coefficient is for the 15 years following the indicated date (after Bell, 1977). Note that the correlation coefficients vary from +0.5 to -0.5 over different 15-year intervals.

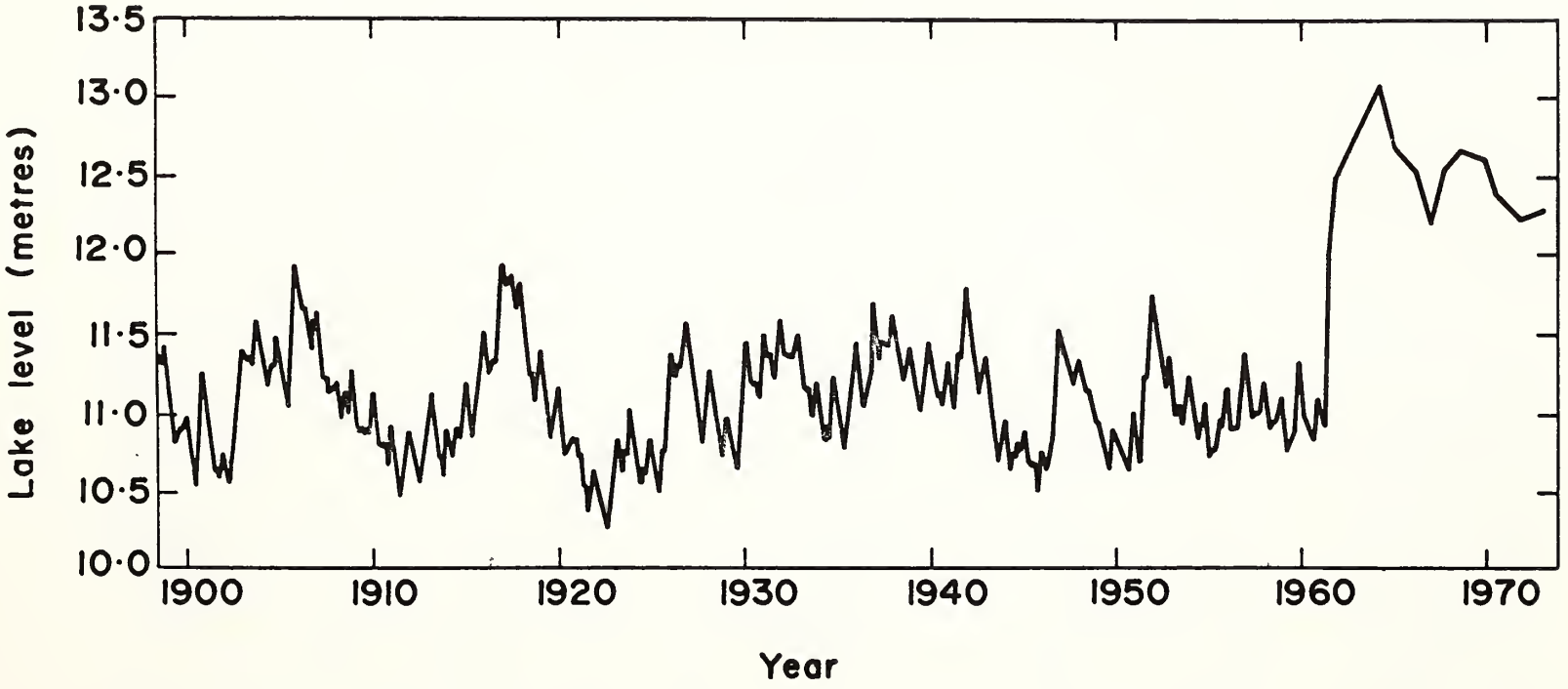

Figure 1. Water level in Lake Victoria 1899-1973 as measured at the Jinja gauge (height in meters). Note the apparent nonstationarity of the data set, and see the discussion by Rodhe and Virji (1976).

FIG. 1
PITTOCK

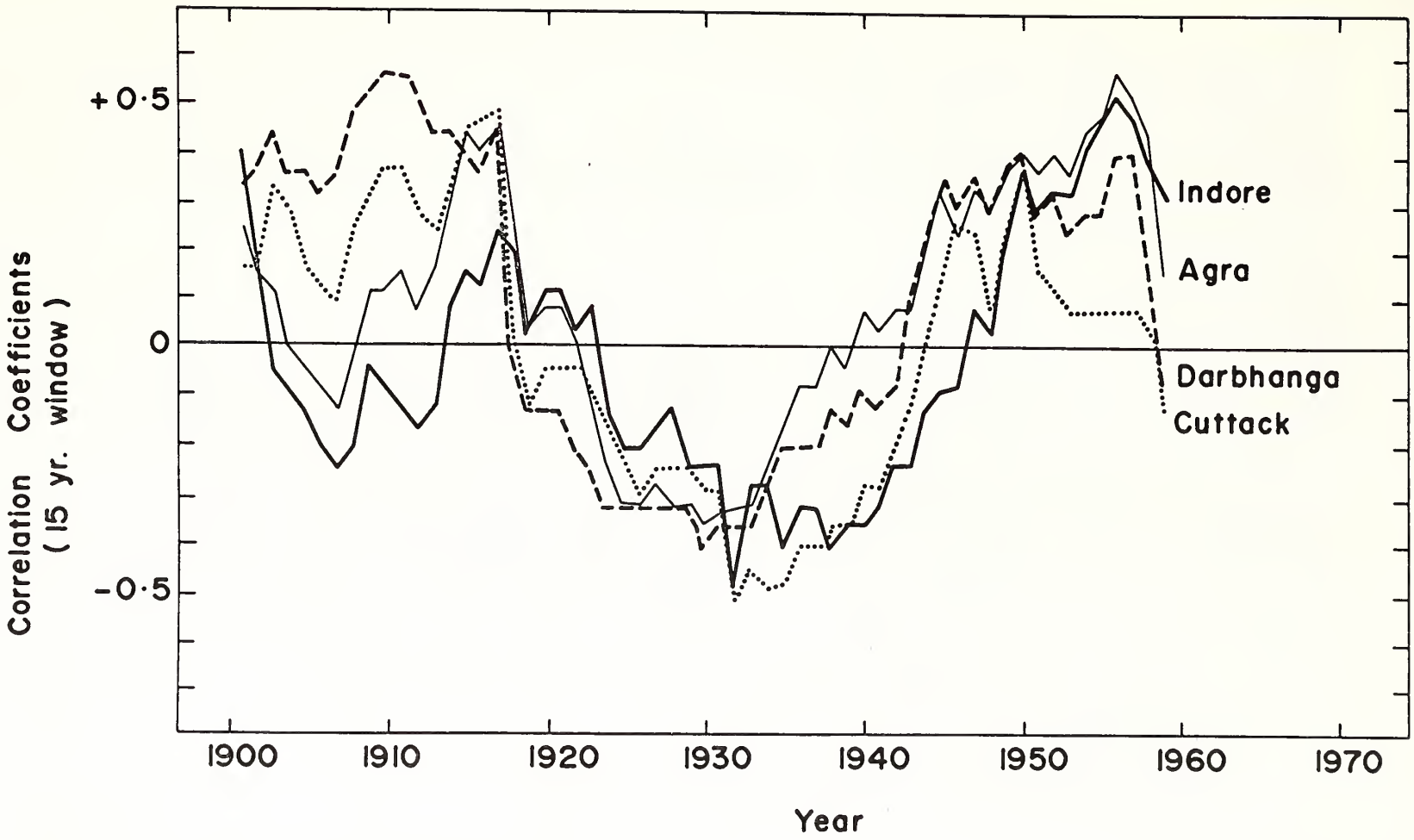

Figure 2. Variations of the correlation coefficient, calculated over moving 15-year intervals, between the mean sea level pressure at the indicated stations in August and the mean annual sunspot relative number. In each case the 15-year correlation coefficient is for the 15 years following the indicated date (after Bell, 1977). Note that the correlation coefficients vary from +0.5 to -0.5 over different 15-year intervals.

Additional comment

It may be worthwhile in the context of short-term climatic studies (which have a potential for forecasting which could be of great economic and social value) to remind ourselves of the traditional scientific attitude that a hypothesis is merely a hypothesis until it is proven beyond reasonable doubt. In contrast to this, there are undoubtedly situations of a practical nature involving decision-making under uncertainty in which one should act on a hypothesis as if it were true unless it is proven beyond reasonable doubt that it is false. Such decisions are properly made by estimating the consequences (or value) of a decision either way and weighting these by the statistical probabilities of what statisticians call a type I or type II error (see eg., Pittock, 1972). I suspect that some solar-cycle enthusiasts, convinced of the potential value of a solar activity-climate link in forecasting, have confused type I and type II errors in their eagerness to see the practical application of the solar activity hypothesis. As climatologists in general address themselves increasingly to the problem of climatic forecasting, our enthusiasm may well tempt us into a similar confusion. For the sake of our science the distinction must be consciously and rigorously maintained.

Additional reference:

Pittock, A. B., Evaluating the risk to society from the SST: some thoughts occasioned by the AAS report, Search 3, 285-289, 1972.

Status Report on the Geophysical Data Processing of the Seasat Microwave Sensors

John A. Ernst and John W. Sherman, III - NOAA/NESS

The Seasat spacecraft failed on the night of October 9, 1978 after approximately 100 days in orbit. During this period the four microwave sensors, consisting of an imaging radar, a scatterometer, a radar altimeter and a multichannel radiometer, collected data which will satisfy approximately 80% of the NOAA program objectives.

This status report represents only the initial findings on the sensor's ability to provide geophysical information on the ocean surface conditions. These data are essentially unvalidated at this juncture, although there are comparisons to surface data in several cases.

Hurricane Fico, which occurred in the mid-Pacific during July 1978, provided wind and wave extremes for early assessment of the scatterometer and radiometer, although the coverage was not simultaneous. The early results are consistent with the expectations of these instruments, with the initial scatterometer results more quantitative than the radiometer results. For the scatterometer pass over Fico on July 20, 1978, the winds ranged from several meters per sec to as great as about 50 m sec^{-1}. The Seasat data is shown in the sequenced figures attached. Subject to the atmospheric attenuation effects near the eye of Fico, the winds agree relatively well with surface measurements. The importance of making the atmospheric corrections are obvious.

The radiometer data has been processed for Hurricane Fico for July 12, 1978 in terms of antenna temperatures, not actual brightness temperatures or some other geophysical unit (wind speed, surface temperature, precipitation, etc.) Even with the modest resolution of this instrument, details of the eye can be readily seen and can be detected down to resolutions on the order of 50-60 km.

Data samples using the imaging radar information from Fico were processed from about 10 km x 10 km areas to establish the radar's ability to image waves. Such images are possible when there is a radial wave component of velocity with respect to the spaceborne radar. Under certain conditions, wave imaging is difficult when only an along-track wave component of velocity exists. The selected sample illustrated shows a successful case and the effects of special processing techniques.

Also shown for the radar is a sample showing internal waves off the Baja California Coast, the effects of a storm squall moving off the Florida Peninsula and sea

ice characteristics west of Banks Island.

Sea ice from Antarctica has also been imaged by the radiometer and a selected sample, again using antenna temperatures only, is illustrated.

Lastly, the radar altimeter is designed to measure precisely the displacement from the satellite to the ocean surface. GEOS-3 earlier had demonstrated the geodetic utility of such measurements with an rms precision of about 50 to 100 cm for its radar altimeter. The Seasat altimeter is expected to perform at a precision approaching 10 cm, and based on early noise analyses and the classic history of the Puerto Rica Trench results from SKYLAB, and GEOS-3, the Seasat altimeter appears intuitively to be near its goal. The set of three paired graphs compare three different algorithms to obtain significant wave height (SWH) from GEOS-3 altimetric data.

☆U.S. GOVERNMENT PRINTING OFFICE: 1979-281-067/101

PENN STATE UNIVERSITY LIBRARIES
A00007202245O